UCB/SEMM-93/09

STRUCTURAL ENGINEERING
MECHANICS AND MATERIALS

NONLINEAR GEOMETRIC, MATERIAL AND TIME DEPENDENT ANALYSIS OF SEGMENTALLY ERECTED, THREE DIMENSIONAL CABLE STAYED BRIDGES

by
Sajid Abbas

Faculty Supervisor: Prof. A. C. Scordelis

September 1993

DEPARTMENT OF CIVIL ENGINEERING
UNIVERSITY OF CALIFORNIA
BERKELEY, CALIFORNIA

TECHNICAL REPORT STANDARD TITLE PAGE

1. Report No.	2. Government Accession No.	3. Recipient's Catalog No.

4. Title and Subtitle	5. Report Date
NONLINEAR GEOMETRIC, MATERIAL AND TIME DEPENDENT ANALYSIS OF SEGMENTALLY ERECTED, THREE DIMENSIONAL CABLE STAYED BRIDGES.	September 1993
	6. Performing Organization Code

7. Author(s)	8. Performing Organization Report No.
Sajid Abbas	UCB/SEMM-93/09

9. Performing Organization Name and Address	10. Work Unit No.
Department of Civil Engineering University of California Berkeley, California 94720	11. Contract or Grant No.
	13. Type of Report and Period Covered
12. Sponsoring Agency Name and Address	Final Report
	14. Sponsoring Agency Code

15. Supplementary Notes

16. Abstract

A numerical method of analysis has been developed to trace the response of segmentally erected, three dimensional, reinforced and prestressed concrete cable stayed bridges due to either immediate or sustained loads. The analysis incorporates the effects of both material and geometric nonlinearity. Time dependent effects due to load history, creep, shrinkage and aging of concrete and relaxation of stress in the prestressing steel are included in the analysis. The response of concrete structures can be tracked both before and after cracking, through the inelastic range and past the peak resistance through strain softening behavior.

This numerical procedure can predict the response of the changing structural configuration as it evolves progressively through different phases of cantilever construction of cable-stayed bridges. Any statically feasible construction sequence may be considered, including the installation or removal of deck or tower elements, placement and stressing of prestressing tendons, installation, stressing, restressing or removal of permanent and auxiliary cable stays. In addition boundary restraints may be added or released at any point in time.

Tower and deck segments are modeled with multi-slice fiber beam-column elements with variable shape functions that are updated as the state of the element changes. Two different types of cable elements have been developed, a shallow cable element appropriate for modeling cable-stays and a general cable element which may be used for modeling large sag cables such as those used in suspension bridges. Nonlinear material constitutive models are used for concrete, reinforcing steel, prestressing steel and cable-stay steel. Refined creep models are used for concrete. Nonlinear geometric effects can be included in all structural elements.

This analytical method is incorporated into a computer program CALBRG. Results from a numerical example of a segmentally erected, cable stayed bridge, which is constructed sequentially using a cantilever erection scheme and then loaded to failure, are presented to demonstrate the application of the numerical procedure to an actual design.

17. Key Words	18. Distribution Statement
Structural Engineering, Cable Stayed Bridges, Cable Element, Fiber Beam-Column Element, Segmental Erection, Time Dependent Effects, Nonlinear Analysis, Computer Program.	Unlimited

19. Security Classif. (of this report)	20. Security Classif. (of this page)	21. No. of Pages	22. Price
Unclassified	Unclassified	467	

Form DOT F 1700.7 (8-69)

Nonlinear Geometric, Material and Time Dependent Analysis of Segmentally Erected, Three Dimensional Cable Stayed Bridges

by

Sajid Abbas

B.E. (N.E.D. University of Engineering and Technology, Karachi) 1982

M.S. (University of California, Berkeley) 1983

M.E. (University of California, Berkeley) 1988

A dissertation submitted in partial satisfaction of the

requirements for the degree of

Doctor of Philosophy

in

Engineering-Civil Engineering

in the

GRADUATE DIVISION

of the

UNIVERSITY of CALIFORNIA at BERKELEY

Committee in charge:

Professor Alexander C. Scordelis

Professor Edward L. Wilson

Professor Henry Helson

1993

ABSTRACT

NONLINEAR GEOMETRIC, MATERIAL AND TIME DEPENDENT ANALYSIS OF SEGMENTALLY ERECTED, THREE DIMENSIONAL CABLE STAYED BRIDGES

by
Sajid Abbas
Doctor of Philosophy in Civil Engineering
University of California at Berkeley

Professor Alexander C. Scordelis, Chair

A numerical method of analysis has been developed to trace the response of segmentally erected, three dimensional, reinforced and prestressed concrete cable stayed bridges due to either immediate or sustained loads. The analysis incorporates the effects of both material and geometric nonlinearity. Time dependent effects due to load history, creep, shrinkage and aging of concrete and relaxation of stress in the prestressing steel are included in the analysis. The response of concrete structures can be tracked both before and after cracking, through the inelastic range and past the peak resistance through strain softening behavior.

This numerical procedure can predict the response of the changing structural configuration as it evolves progressively through different phases of cantilever construction of cable-stayed bridges. Any statically feasible construction sequence may be considered, including the installation or removal of deck or tower elements, placement and stressing of prestressing tendons, installation, stressing, restressing or removal of permanent and auxiliary cable stays. In addition boundary restraints may be added or released at any point in time.

Tower and deck segments are modeled with multi-slice fiber beam-column elements with variable shape functions that are updated as the state of the element changes. Two different

types of cable elements have been developed, a shallow cable element appropriate for modeling cable-stays and a general cable element which may be used for modeling large sag cables such as those used in suspension bridges. Nonlinear material constitutive models are used for concrete, reinforcing steel, prestressing steel and cable-stay steel. Refined creep models are used for concrete. Nonlinear geometric effects can be included in all structural elements.

This analytical method is incorporated into a computer program CALBRG. Results from a numerical example of a segmentally erected, cable stayed bridge, which is constructed sequentially using a cantilever erection scheme and then loaded to failure, are presented to demonstrate the application of the numerical procedure to an actual design.

A. C. Scordelis

A. C. Scordelis

Chairman of Committee

TABLE OF CONTENTS

LIST OF FIGURES

LIST OF TABLES

ACKNOWLEDGEMENTS

I would like to express my sincere thanks to Prof. A. C. Scordelis. I am deeply indebted to him for his invaluable guidance and encouragement during the course of this dissertation. His advice, support and friendship through many a rough patch is greatly appreciated.

I am thankful to Prof. E. L. Wilson for his expert advice about programming techniques and to Prof. H. Helson for serving on my thesis committee.

Thanks is also due to my brother, Humayun Abbas, for many helpful discussions and ideas. I am grateful to my father Lt. Col. (retd.) Abbas Ali and my mother Fahmida Abbas for their love, understanding and prayers.

Last but not the least, special thanks to my wife Seerat for her love and encouragement which made this work possible.

1. INTRODUCTION

1.1. GENERAL

The evolution of the modern cable stayed bridge took place almost exclusively in postwar Germany in the early fifties. Since then it has become increasingly popular in many countries because of its remarkable structural efficiency as well as its aesthetically pleasing appearance.

As opposed to the classical suspension bridge, the cable-stays are directly connected to the bridge deck resulting in a much stiffer structure. A large number of closely spaced cable stays support the bridge deck throughout its length, reducing the required depth and bending stiffness of the longitudinal girder to a minimum thereby allowing the construction of relatively longer spans. The structural action is simple in concept; the deck loads are carried by the cables to the towers and from there to the foundation. The primary forces in the structure are tension in the cable stays and axial compression in the towers and deck; the effect of bending and shear is considered to be secondary.

The early designs of modern cable stayed bridges essentially consisted of a stiff girder supported by a few cables. The stay forces were rather large and consequently the anchorage design was excessively complex. Further development indicated that these problems could be remedied by increasing the number of stays. The multi cable arrangement has several advantages. First, the deck can be erected using a cantilever

erection sequence in conjunction with suspension by successive cable-stays. Secondly, the use of a large number of small cables reduces the concentrated forces at the anchorage points in the tower and the deck. Moreover, the deck bending moments between the points of suspension are reduced. Thirdly, a damaged or corroded cable-stay can be easily replaced without over stressing the bridge structure. Finally, excellent aerodynamic stability is obtained as the damping of the system is increased by adding a large number of cables of different lengths and hence different natural frequencies.

For a multi cable system, it is not necessary to have a stiff deck girder to carry the loads predominantly through a bending action. However, the girder still must have sufficient stiffness for safety against buckling due to the large longitudinal forces induced in the deck by the inclined stays and to limit local deformations under concentrated live loads.

The aerodynamic stability of the bridge deck is another important consideration. When the slender deck of a relatively flexible long span structure is exposed to cross winds, small variations in the angle of incidence of wind modify the lift on the section and tend to induce both torsional and flexural oscillations in the bridge deck. Under certain wind conditions these oscillations can build up to dangerous levels. This phenomenon known as flutter was first manifested in total collapse of the First Tacoma Narrows Suspension Bridge in 1940. A number of research studies carried out since then indicate that the incidence of flutter can be avoided in long span bridges by keeping the torsional and bending frequencies sufficiently apart. According to Mathivat [83] a ratio of frequencies higher than 2.5 seems to be adequate.

Another problem associated with air flow across the deck is the phenomenon of vortex shedding or Von Karman effect which can cause excessive vibrations in the structure and may initiate torsional vibrations or flutter. This effect can be minimized by streamlining the shape of deck cross section as on the Severn Bridge in Britain, or by adding deflectors to channel the air flow around sharp angles in the deck profile.

Both Leonhardt [67] and Menn [86] have noted that multiple cable bridges with slender girders are less susceptible to vibration build up as compared to conventional girder bridges or suspension bridges. Due the geometric non linearity of cables the frequency of free vibrations is a function of the amplitude. As the amplitude begins to build up due to an excitation of resonant frequency, the natural frequency of the structure shifts away from the frequency of excitation and the oscillations break down. Moreover, the natural frequencies of the lower modes are very close to each other and when excited tend to cancel out their mutual effect. It must be noted, however that this behavior is observed only in multi cable bridges and that bridges with a small number of stays have exhibited serious vibration problems.

Segmental or stage construction techniques are well suited for erecting cable stayed bridges and constitute the method of choice specially when the bridge spans deep valleys or the site conditions are such that the erection of temporary river piers is difficult.

Although, such construction techniques enhance the economic feasibility of the cable stayed bridge form, on the other hand they present the engineer with a substantial analysis problem. Segmental construction may involve cast-in-situ concrete or precast concrete of different ages and qualities, prestressing tendons installed at different construction stages, permanent and auxiliary cable-stays being installed and stressed and a changing structural form being subjected to permanent and time dependent loads.

In addition to these, cable-stayed bridges exhibit a nonlinear structural response, principally because of geometric nonlinearity of stay-cables and combined bending moment and axial load effect in the deck and towers. These considerations require relatively sophisticated analysis procedures.

The state of the art in the design and construction has changed immensely since the first cable-stayed bridge was built in Stormsund, Sweden in 1955. This can be gauged from the fact that the Stormsund Bridge had a span of 183 m. whereas Tatara Bridge which is under

construction in Japan will have a central span of 890 m. A list of long span cable stayed bridges arranged in descending order with respect to the span length is given in the table below:

Long Span Cable Stayed Bridges in the World [43]

Name	Center Span (m)	Country	Completion date
Tatara	890	Japan	1999
Normandie	856	France	1993
Meiko-Chuo	590	Japan	1997
Skarsundet	530	Norway	1991
Tsurumi-koro	510	Japan	1995
Ikuchi	490	Japan	1991
Higashi-kobe	485	Japan	1994
Alex Frazer	465	Canada	1986
Second Hoogly	457	India	

However the full potential of cable stayed bridge is yet to be realized. Leonhardt [67] notes that future spans of prestressed concrete bridges may reach up to 700 m. whereas in the case of steel bridges because their lower dead weight, span lengths of up to 1700 m. are possible. A case in point is the Messina Straits Bridge for which designs have been prepared with a main span of 1500 m; no structural difficulties were found.

The recent trend towards building longer span cable-stayed bridges raises new questions about the validity of linear analyses to predict the response of the bridge structure. The increase in the cable sag can lead to a substantial decrease in stiffness of the stay and subsequent nonlinear behavior of the entire bridge under live loads. As the spans have increased, the general trend amongst the designers is to use slender and streamlined bridge decks. With the lighter bridge deck, the live load became a larger percentage of the total load and hence fatigue has become an important question.

1.2. REVIEW OF LITERATURE

The main emphasis of this study is on the application of finite element method to the analysis of reinforced and prestressed concrete cable stayed bridges. The review of the literature will therefore be limited to the following topics:

- Finite element modeling of fiber beam columns.
- Analysis of cable-stays.
- Analysis procedures for cable stayed bridges.

FINITE ELEMENT MODELING OF FIBER BEAM-COLUMN MODELS

Since Ngo and Scordelis [94] published the first paper on the finite element analysis of reinforced concrete structures in 1967, an immense research effort has been made to develop sophisticated analysis procedures aimed at predicting the response of reinforced and prestressed structures through various limit states. Scordelis [115, 116, 117], Schnobrich [113] and Wegner [146] have presented comprehensive reviews of the application of finite element method to reinforced concrete structures. This discussion is therefore limited to fiber type beam-column elements which have been used in the present study to model tower and deck segments of a cable stayed bridge.

A beam element based on the fiber model for analyzing plane frames was introduced by Kang [49]. Material behavior is monitored at three sections placed at Gauss integration points. Each section is further divided into layers over its depth. Cubic Hermitian shape functions are used to relate element deformations to section curvature and strain.

Chan [19] used a similar formulation for a three dimensional beam element. The element has six degrees of freedom at each end and a mid length degree of freedom in the axial direction. Three control sections are placed at Gauss points. Each control section is discretized into fibers over both its width and height.

Later Mari [80] and Kasti [51] refined Chan's element and added prestressing to investigate the behavior of prestressed concrete elements subjected to biaxial bending.

Suharwardy and Pecknold [130] presented a procedure based on varying the shape function according to predetermined rules as the element yields. This allows long in-elastic beam columns to be modeled accurately using a single element.

Mahasuverachai and Powell [79] generalized the procedure of Suharwardy et al. by introducing a multi-slice element with variable shape functions, which are updated as the state of the element changes.

Kaba and Mahin [47] used a strategy similar to Mahasuverchai et al. [79] for concrete beam elements to investigate the dynamic response of concrete frames subjected to considerable levels of axial loads.

Zeris [150], and Zeris and Mahin [149] refined the model developed by Kaba et al. and enhanced the element to account for biaxial effects and anchorage zone deformations.

Lai, Will and Otani [55] suggested a relatively simple element that can simulate the stiffness degrading behavior of concrete members while avoiding the high computation effort associated with fiber models. An elastic element is connected in series to an inelastic element at each end. The inelastic element consists of four spring elements or mega fiber elements which are calibrated to simulate flexural yielding effects of the reinforcement and the compressive deformations of the concrete close to the end region.

ANALYSIS OF CABLES.

Analysis of cables freely suspended between two points are by no means a modern phenomenon; The original differential equation of equilibrium of a stretched cord is believed to have been derived by the brothers James and John Bernoulli in 1690. Leibnitz and

Huygens also discovered the catenary at about the same time through independent efforts. The solution of symmetrically suspended elastic catenary is due to Routh, 1891 [110].

More recently, Ernst (1965) [28] came up with a simplified formulation for low sag cable-stays. He postulated that cable could be considered as a truss bar with a modulus of elasticity which is a function of the cable stress. This formulation has been used extensively by several designers as it linearizes cable response for a given stress level and hence greatly simplifies analysis of cable-stayed structures.

O'Brien and Francis (1964) [95], and O'Brien (1967) [96] have presented a general solution to the suspended cable problem and have suggested an iterative flexibility procedure to solve cable systems.

Mollmän (1965) [89] has written extensively on the analysis procedures for suspension structures. He has also discussed analysis procedures regarding the analysis of shallow cables wherein the cable profile can be approximated by a parabola [90].

Baron and Venkatesan (1971) [6] have presented an iterative procedure for the analysis of cable and truss structures. The cable element is limited to low sag or shallow cables.

Peyrot and Goulois (1978) [101, 102] refined O'Brien's [96] method and presented a procedure for solving the highly nonlinear equilibrium equations based on a tangent stiffness formulation combined with an iterative solution. A numerical scheme to improve the convergence of solution is also discussed.

Irvine (1981) [45] has presented a comprehensive text dealing with statics and dynamics of suspended cables. He has discussed classical solutions to the problem of large sag catenary as well as engineering approximations to the solution of relatively flat cables such as those used in guyed masts, cable trusses and cable-stayed bridges.

Gimsing has written several papers on the analysis of suspension and cable-stayed bridges [33]. He has also authored a text book [32] in which he presents a detailed discussion of

design and analysis of suspension bridges; strong emphasis is placed on simple analytical techniques and on developing a broader perspective aimed at synthesis of the design process rather than obscure computational algorithms.

ANALYSIS PROCEDURES FOR CABLE STAYED BRIDGES.

It is difficult to chronicle the voluminous technical literature available on cable-stayed bridges in this brief survey. Extensive bibliographies about the design, analysis and construction aspects of cable stayed bridges have been presented by the subcommittee on cable-stayed bridges [135], and Narayanan et al. [93]. Some of these publication are discussed in this section and others will be referred to elsewhere as relevant.

A wealth of technical information about various aspects of cable stayed bridges is available in European Literature. One of the earliest papers about cable stayed bridges was published by Dischinger in 1949 in which he discussed the feasibility of cable stayed structures for rail road bridges.

Professor Fritz Leonhardt, a distinguished Bridge Engineer from Germany, has played a pioneering role in the development of cable stayed bridges and is well known for his several contributions to the design and analysis of cable stayed bridges; Leonhardt, Andra and Wintergrest on Knie Bridge in Dusseldorf [65], Leonhardt Zellner and Saul on Bridge over Parana River in Argentine [64], Leonhardt on areodynamic stability of suspended bridges [66]. Some of his more recent publications are discussed below.

Leonhardt and Zellener [68] have discussed the design, detailing and construction aspects of cable stayed bridges. Optimization of cable stayed bridge form through the use of large number of cables and slender aerodynamic bridge decks is described.

Leonhardt [61] has also published a state of the art report regarding latest developments in cable stayed bridges for long spans and the technical and economic feasibility of such structures.

Leonhardt, Zellner and Svensson [69] have discussed the design and construction of the Columbia River Bridge at Pasco-Kennewick. The authors have also reported the analysis procedures involved; the overall forces in the bridge were determined using a two dimensional elastic model wherein the cables were given the same constant elastic modulus because the change in sag under lived load was deemed to be negligible due to the small ratio of live to dead load. The stiffness of towers and beams were based on uncracked sections. The local forces in beams and towers were determined using space frame models of relevant components. Areas of heavy stress concentrations, such as tower heads were analyzed by using finite element models.

Professor Rene Walther has published a comprehensive text book [144] on the state of the art in the design and analysis of cable stayed bridges. He has presented detailed discussions on the European practice regarding the static and dynamic analysis of cable stayed bridges and deliberated on the various practical details involved.

Mathivat's [83] text book on the cantilever erection procedures used in prestressed concrete bridges devotes an entire section to cable stayed bridges.

Professor Christian Menn, the designer of Ganter Bridge in Switzerland, who has written a text on prestressed concrete bridges [86], also discusses some significant aspects pertaining to the design of cable stayed bridges.

Moving back to North American practice; Man-Chung Tang (1971) [133] presented a numerical procedure dealing with both linear and nonlinear analysis of cable-stayed bridges. Instead of stiffness corrections, the nonlinear force deformation relationship of cable-stays was accounted for by applying a pair of imaginary forces at the ends of each cable. Later in a

second paper, Tang (1972) [134] presented a review of the design and erection procedures for cable stayed bridges.

Lazar (1972) [59] has discussed direct stiffness analysis of cable stayed bridges wherein cable stiffness is based on the equivalent modulus concept of Ernst [28]. Subsequently, Lazar [60] has described the application of load balancing method to the design of cable stayed bridges.

Professor Baron of University of California at Berkeley was one of the first to investigate both the static and dynamic behavior of cable stayed bridges. Baron and Lien (1973) [7] published a report on the southern crossing of the San Francisco Bay using a cable stayed girder bridge. This bridge was not constructed due to environmental concerns. A static analysis including the effects of nonlinear geometry, was conducted to predict the response of the structure to dead loads. However, in the case of dynamic analysis linear behavior was assumed in order to use the modal superposition method. Element masses were lumped at the nodes and a tangent stiffness matrix corresponding to the deformed shape of the structure under dead load was used.

Troitsky [138] has presented a summary of classical analysis techniques and prevailing design procedures in his text which was first published in 1977.

Another pioneering effort was the design of proposed Ruck-a-Chucky Bridge over the American River in California by Professor T.Y. Lin; this structure was unique in that the cable stays were anchored on to rock faces of the river gorge instead of towers and supported an elegant bridge deck which was curved in plan. This bridge spurred a number of studies into the behavior of cable stayed bridges. Godden and Aslam [35] and Godden [34] conducted seismic model studies of this bridge. Shah [125] conducted a seismic risk analysis of the bridge site. Scanlan [111] looked into the aerodynamic aspects of the problem and performed a wind stability analysis.

Zung-An Lu (1979) [76] has discussed the dynamic analysis of Ruck-a Chucky bridge using the computer program SAP IV [9] and compared the analytical results with those obtained from the model studies conducted by Godden [35]. Straight stiff axial members were used to represent the cables. The nonlinear behavior of cables is accounted for by using an equivalent modulus of elasticity as defined by Ernst [28]. The deck was modeled with beam elements. Lu reports agreement with model results.

Hegab (1986) [39] has presented a method for the static analysis of cable stayed bridges based on the potential energy of the system. An improvement to this approach was later discussed by Aboul-ella (1988) [29]. Both methods assume linear cable behavior.

Podolny and Scalzi [103] have presented an in-depth survey of construction and design procedures of cable-stayed bridges in text book published in 1987.

Seif [124] and Seif and Dilger [123] have formulated a procedure for the nonlinear analysis and evaluation of ultimate strength of prestressed concrete cable stayed bridges. Both material and geometric nonlinearity are considered. The concrete beam element can model the cracking of concrete, yielding of steel and plastic hinge formation. Cables sag is accounted for by using a modified modulus of elasticity based on Ernst's equation. The procedure is limited to the analysis of two dimensional models.

Abdel-Ghaffar and Nazmy (1987) [2] have studied the seismic response of cable stayed bridges subjected to multiple support excitations. A tangent stiffness iterative procedure is used to predict the dynamic response of the structure to seismic excitation. The effects of geometric nonlinearity are included in the analysis. The cables are modeled as truss bars with a modified modulus of elasticity based on Ernst's equation [28].

1.3. OBJECTIVE AND SCOPE

The objective of the present study is to develop an efficient numerical analysis procedure for the material and geometric nonlinear, three dimensional analysis of segmentally erected reinforced and prestressed concrete or steel cable stayed bridges, including the time dependent effects due to load history, creep, shrinkage and aging of concrete and relaxation of stress in the prestressing steel.

The aim of the analysis is to trace the time dependent response of the structure through various construction stages; and following completion, through their service load history as well as through elastic, inelastic and ultimate ranges.

The analysis procedure should be able to predict the state of the forces and deformation in the structure caused by changes in the configuration of the structure during the construction sequence. Any statically feasible construction sequence may be considered for the three dimensional analytical model, including the installation or removal of deck or tower elements, placement and stressing of prestressing tendons, installation, stressing, restressing or removal of permanent or auxiliary cable-stays. In addition, boundary restraints may be added or released at any point in time.

The tower and deck segments are modeled with a multi slice fiber beam-column elements with variable shape functions which are updated as the state of the element changes. The element has three translational and three rotational degrees of displacement freedom at each end. Material behavior is monitored at two or more slices or control sections. Each slice is further divided into a number of sub elements or fibers. The location of the intermediate slices is selected in such a manner so as to closely approximate the actual variation of curvature over the length of the element. Element stiffness matrix is obtained by integrating the contribution of all slices over the length of the element.

The material constitutive relationship is introduced at the fiber level. The stress-strain behavior of concrete under uniaxial loading is modeled by the modified Kent-Park relationship which includes cracking at a limiting stress, strain softening after crossing the maximum compressive strength and enhancement in strength and ductility due to the confining effects of transverse reinforcement. Tension stiffening effects can also be included in the analysis. Variation of concrete strength with time is recognized. For steel a bilinear strain hardening model approximating the Bauschinger's effect is used.

Creep strain is evaluated using Kabir's algorithm [48]; this procedure is based on the principle of superposition and the use of a special form of creep compliance function which does not require the storage of entire stress history of the element. Refined creep integration schemes proposed by Ketchum [53] are also implemented.

Two different types of cable elements have been developed. The shallow cable element is used for modeling cables with a low sag to span ratio and is appropriate for the modeling of cable-stays. This element is based on a series model in which one component simulates the elastic behavior of the cable and the second models the sag effect. The other element is a general cable element whose formulation is based on the differential equation of an elastic catenary. This element can be used for modeling large sag cables such as those used in the large span suspension bridges.

Prestressing steel tendons are modeled as a series of piece wise linear prestressing steel segments each of which spans a frame element. Each tendon segment is modeled as an eccentric truss bar. The displacements of segment end points are slaved to that of the corresponding end nodes of the host frame element. Initial stress losses due to friction and anchorage slip are accounted for.

Cantilever erection procedures which are commonly used for rapid and cost effective construction of cable stayed bridges can be simulated numerically by keeping track of the state of the structure as its configuration changes progressively with time.

For a time dependent analysis, the time domain is divided into a discrete number of intervals. Next a time step integration is performed during which the state of the structure is updated continuously as the solution progresses in the time domain. At each time step, the changes in structural configuration and loading are accounted for, and a direct stiffness solution based on the displacement method is performed.

Ultimate load analysis can be carried out by either a load control or a displacement controlled solution strategy. The load control strategy is essentially a step-iterative method of solving nonlinear equilibrium equations; the load is divided into a number of small increments and during each load step the equilibrium equations are solved iteratively using the Newton-Raphson method. The displacement control strategy implemented in this study consists of applying controlled displacement increments to a selected degree of freedom and then solving for either increase or decrease in the load applied to the structure which will hold the new displaced configuration of the structure in equilibrium. This strategy is particularly useful for post buckling analyses and to track strain softening behavior of structures.

Several examples have been solved to confirm the validity and range of application of the present method of analysis. These examples may be divided into three categories. The first category consists of numerical examples pertaining to verification of certain procedure such as creep integration schemes. The second deals with the verification of individual elements developed in this study and is presented at the end of the chapter concerning that particular element. The last category deals with the analysis of complete cable stayed bridges; this includes the ultimate load response of a foot bridge and a complete analysis of the concrete and steel designs for the Ruck-a-Chucky Bridge by Professor T. Y. Lin [73].

2. CABLE STAYED BRIDGES

2.1. HISTORICAL REVIEW

Evolution of modern cable stayed bridges took place in post world war II Germany. The pioneering effort is attributed to Franz Dischinger, who found that the use of inclined cable stays in rail road bridges resulted in a much stiffer structure as compared with the classical suspension bridge. In 1955, the German Firm DEMAG, in collaboration with Dischinger designed the first modern cable stayed bridge at Störmsund in Sweden.

Driven by the need to replace the bridges destroyed in the war and a newly discovered emphasis on aesthetics, German bridge engineers were quick to appreciate the merits of this new bridge form and several cable-stayed designs were proposed. However it was not until 1958 that the first cable stayed bridge was built in Germany over the Rhine in Dusseldorf. The North bridge which was designed by Karl Schaechterle, Friderich Tamms and Leonhardt, had a main span of 260 m., two free standing cantilever towers and a lateral suspension system with a harp arrangement of cable stays.

Later, two more cable-stayed bridges were designed in vicinity of the North bridge. These were Knie Bridge (1969) and Oberkassel Bridge (1973). Together, the three bridges form an exciting display of the new structural form.

The popularity of this new type of structure slowly extended to other countries and it became the dominant bridge type in the span ranges from 150 to 600 meters and by 1987 more than

eighty five had been built in Europe, Japan, United States and elsewhere, Billington [12]. For the sake of brevity, the remainder of this discussion is confined to the cable-stayed bridges constructed in North America.

Cable-stayed bridges did not become popular in North America until the early seventies. Sitka Harbor Bridge in Alaska was the first cable-stayed bridge in America; it was completed in 1973. This bridge has a center span of 450 ft. and side spans of 150 ft. each.; the main span is supported by one pair of cables from each tower, the towers are free standing steel cantilevers which are held in position by back stays.

The Pasco-Kennewick Bridge over river Columbia in Washington was completed in 1978. This bridge was designed by the firm of Arvid Grant and Associates in collaboration with the famous German firm, Leonhardt und Andrä. The bridge has a main span of 981 ft. and two side spans of 413 ft. each. The deck is built of precast concrete elements, which consist of two triangular box beams at the edges connected by transverse girders and the roadway slab. A double plane lateral suspension system with the cables arranged in a radial pattern is used. The portal frame shaped concrete towers have a specially designed steel tower heads for anchoring the stay cables.

These early designs captured the attention of American bridge engineers and a series of major works followed. The Luling Bridge was first in this list; Designed by the firm of Modjeski and Masters, it crosses the Mississippi just above New Orleans and has a central span of 1235 ft, and two side spans of 495 each. It has an orthotropic steel deck and modified *A* frame towers. The cables are arranged in a radial pattern in two converging inclined planes. Construction began in 1975 and was completed in 1983 at which time it replaced the Pasco-Kennewick Bridge as the longest span cable stayed bridge in North America.

The next major project was the East Huntington Bridge in Ohio, which was built in 1985. This bridge was also designed by the Pasco-Kennewick team, namely Arvid Grant and

Associates in collaboration with Leonhardt und Andrä . It is an asymmetric structure having a major span of 900 feet and a side span of 608 feet. The bridge deck consists of two solid rectangular concrete edge beams with transverse structural steel floor beams and a composite concrete deck. The single tower has a delta shape in the transverse direction and semi harp cable arrangement is used. Professor Billington considers this to be one of the most striking bridges of any type built in the United States [12].

Sunshine Skyway Bridge over Tampa Bay in Florida was completed in 1986. Similar in concept to the Brotonne bridge in France, it was designed by Figg and Muller with a strong emphasis on aesthetics. The bridge has a main span of 1200 ft. which is supported by a single plane of cables fanning out along the longitudinal center line of the bridge. The cross section of the deck consists of a single cell concrete box girder, which provides the necessary torsional stiffness required for single plane cable systems. This is presently the largest precast concrete segmental bridge in the world.

The Anacis Island Bridge (presently known as the Alex Fraser Bridge) over the Fraser River near Vancouver in British Columbia was also completed in 1986. The bridge has a center span of 1525 ft. and side spans of 599 ft. The reinforced concrete towers are H-shaped and support a double plane of cables arranged in a semi harp pattern. The deck cross section consists of two steel edge girders, connected by transverse ribs and overlaid by a concrete roadway slab. This structure was designed by CBA Engineering and the firm of Buckland and Taylor, both of Vancouver Canada.

Next came the Dame Point Bridge over the St. John's River in Jacksonville, Florida. This was completed in 1987. This bridge has a concrete deck with a main span of 1300 feet and side spans of 650 feet. The towers are H-shaped and built of reinforced concrete from which two planes of cable stays in harp configuration support the reinforced concrete deck girders. This structure was designed by the firm of Howard, Needles, Tammen and Bergendoff.

The Quincy Bridge over the Mississippi between Illinois and Missouri, designed by Modjeski and Masters was completed in 1987. The center span is 900 ft. and side spans are 440 ft each. It has H shaped concrete towers and a lateral suspension system with cables arranged in a semi-harp pattern. The deck consists of steel edge girders and cross beams topped with a composite concrete roadway slab.

The number of cable stayed bridges has gone up dramatically in the last decade. Structures are being built with ever increasing spans and even more notable architectural effect.

The Japanese are presently working on the Tatara Bridge, which when completed in 1999 will be the longest span cable stayed bridge in the world. The proposed bridge has a center span of 2920 ft. which is about 100 ft. longer than the Normandie Bridge in France. Tatara Bridge is an all steel structure. It has two A shaped towers and employs a lateral suspension system which consists of two sloping cable planes arranged in a semi-harp pattern. The deck consists of a steel box girder.

Another interesting example is the proposed Messina Straits Bridge linking Sicily and the Italian peninsula. Designed by Prof. Leonhardt, it will have a main span of 5900 feet for six lanes of road traffic and two railway tracks.

2.2. GEOMETRICAL CONFIGURATION

The cable stayed bridge can have a large variety of geometrical configurations; limited only by the creativity of the designer. The layout of the cable stays, the style of the pylons and the type of the super structure can be easily adjusted to suit the engineering requirements and enhance architectural beauty. A discussion of the various geometrical arrangements and structural forms is presented in this section.

2.2.1. CABLE SYSTEM.

The arrangement of cable stays is of crucial importance in the design of cable stayed bridges because of its strong influence on the structural performance of the bridge. For example arranging the cables into two planes, or the so called lateral suspension system, results in a torsionally stiff structural system permitting the use of a slender bridge deck. In contrast to this a single plane, or central suspension system, needs a relatively heavy box girder as the torsional stiffness of the system has to be supplied by the girder alone.

Furthermore, the spacing of the cables on the deck determines the type of the construction procedure to be used. For example, for a cost effective cantilever construction sequence which does not involve the use of temporary stays, the spacing of the cables at the deck should not exceed the length of deck segments. Also to facilitate the removal of a damaged or corroded cable, the cable spacing at the deck should be such that a single cable may be removed and replaced without the use of false work and without overstressing the system.

Various transverse and longitudinal arrangements of the cable stays, which are commonly used in practice are discussed in the subsequent sections.

TRANSVERSE CABLE ARRANGEMENT.

The basic cable arrangements transverse to the longitudinal axis of the bridge are shown in Fig. 2.01, [144].

SINGLE PLANE OR CENTRAL SUSPENSION SYSTEM.

The main advantage of a central suspension system are its aesthetic qualities; the motorist driving over the bridge has a clear view looking outward from the deck and the bystander looking diagonally at the bridge does not see a double line of cables. A slender central pylon,

although requiring an increased width of the carriage way, further enhances the architectural beauty of the bridge.

A relatively heavier box girder section with considerable torsional stiffness is required for the deck in order to resist asymmetric vehicle loading. On the other hand, a torsionally stiff deck reduces second order moments and contributes to the aerodynamic stability of the structure.

DOUBLE PLANE OR LATERAL SUSPENSION SYSTEM:

Most of the cable stayed bridges built to date use lateral suspension systems, which consist of two cable planes which may be parallel and vertical or inclined towards each other and intersecting above the longitudinal axis of the bridge at the top of an A frame tower.

Lateral suspension increases the torsional stiffness of the structural system and hence improves the aerodynamic stability of the cable stayed bridge and optimizes the static and dynamic behavior of the bridge. This effect is even more pronounced in the case of A frame towers in which differential movement of the anchorage of the two cable planes is not possible.

However, inclined cable planes can give rise to vertical clearance problems for vehicular traffic and may therefore require either an increase in the tower height or extension of the transverse dimension of the deck.

This problem is not encountered in the case of vertical double planes for obvious reasons. Moreover the construction of vertical H shaped towers is relatively simpler and more economical as compared to A frame towers.

In a double plane system the cable anchorages at the deck end can be placed either inside or outside the bridge railing. If they are placed inside, a dead space is created which can not be used to carry traffic. In the latter case, auxiliary construction is needed to transfer the cable force from outside the railing onto the load bearing portions of the cross section.

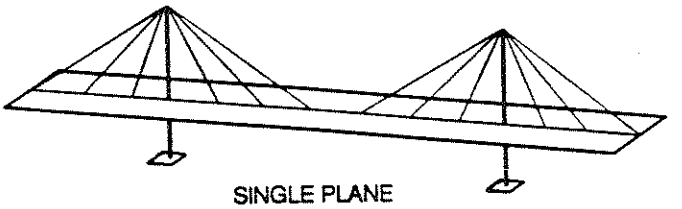

SINGLE PLANE

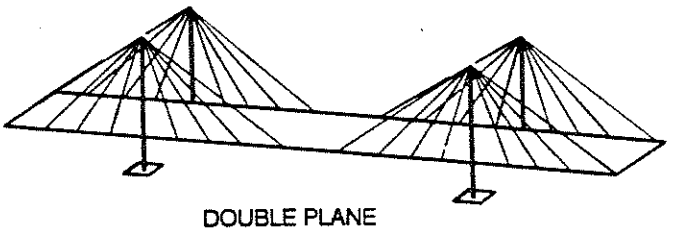

DOUBLE PLANE

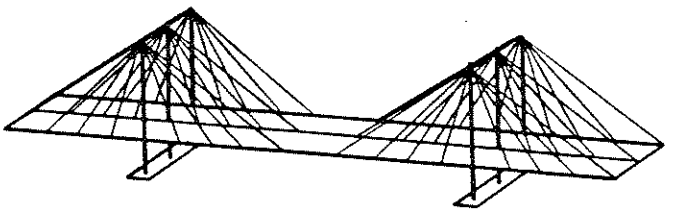

TRIPLE PLANE

FIG. 2.01 TRANSVERSE CABLE ARRANGEMENTS.

Walther, 1988.

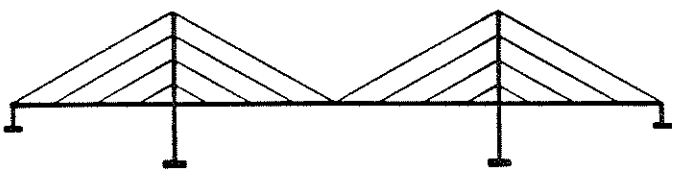

HARP PATTERN

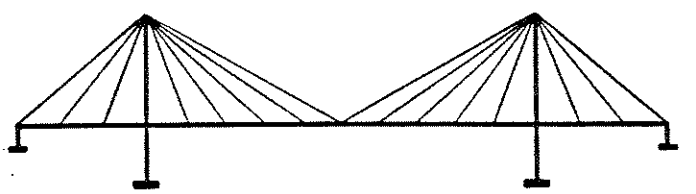

FAN PATTERN

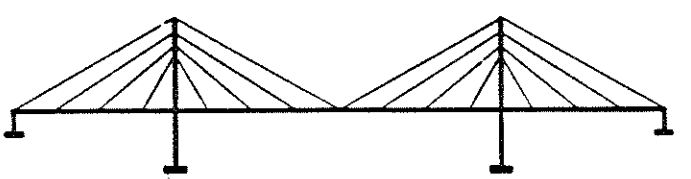

SEMI-HARP PATTERN

FIG. 2.02 LONGITUDINAL CABLE ARRANGEMENTS.

Walther, 1988.

THREE PLANE SYSTEM.

If the deck of a cable stayed bridge carries a very wide roadway, then the transverse bending moments may exceed the longitudinal bending moments. In such a situation, a costly deck can be avoided by using a three plane system of suspension. However, to date, despite a number of proposals, no such bridge has been built.

LONGITUDINAL CABLE ARRANGEMENT.

The basic cable arrangements in the longitudinal direction are shown in the Fig. 2.02 [144].

HARP PATTERN

In a harp layout the cables are parallel to each other and hence the cable anchors are distributed uniformly both along the height of the tower and along the bridge deck. This simplifies the detailing of the anchors at both ends of the cable and results in ease of installation of cable stays during the construction of the bridge as well as any future replacement of damaged stays.

Although from a structural standpoint, the harp pattern is the least efficient, from an aesthetic point of view it is the most elegant solution because of the harmonious and uncluttered appearance of cables running parallel to each other.

The three bridges over Rhine in Dusseldorf, namely the Knie Bridge, the Oberkassel Bridge and the Theodore Heuss Bridge are all built with cables in the harp pattern and form a unique ensemble of striking beauty defined by strong parallel lines.

FAN PATTERN

The fan pattern which concentrates the cable anchorages at the top of the tower is considered to be the most efficient structurally. The slope of the cable stays is maximized, increasing the load balancing component of the cable tension and at the same time

decreasing the horizontal axial force transferred to the bridge deck. As the primary force in the tower is axial compression, longitudinal bending of the towers is minimized.

On the negative side, the fan pattern is less attractive architecturally than the harp pattern discussed earlier. Moreover, the concentration of cable anchorages at the top of the tower results in a highly stressed zone whose construction can be rather complicated and costly.

SEMI HARP PATTERN

A combination of harp and fan patterns avoiding the individual pitfalls of both the systems, can be an ideal solution. By spreading the stays in the upper part of the pylon, anchorage details can be simplified; whereas those in the lower part of the pylon can be more steeply inclined resulting in a more efficient load carrying mechanism.

2.2.2. TOWERS

The shape of the towers used in cable stayed bridges is strongly influenced by the choice of the suspension system, site conditions and aesthetic considerations.

In the longitudinal direction, the tower configurations range from relatively flexible vertical elements to very stiff A frame towers.

When the cable stays are arranged in a harp pattern, non symmetrical traffic loads induce considerable longitudinal bending in the tower, which should therefore have adequate bending resistance as well as sufficient stiffness to reduce deformability of the deck.

On the other hand in the case of a fan pattern, back stays which connect the top of the tower to the rigid points at the ends of the span, restrain the movement of the top of the tower and hence increase the longitudinal stiffness of the whole system. This prevents large bending moments in the tower; in such cases the tower can be relatively flexible. It must, however, have sufficient stiffness to ensure an adequate margin of safety against buckling.

Leonhardt [68] recommends that towers should be slender in the longitudinal direction so that the unbalanced horizontal cable components caused by any live loads in the center span are transmitted to the ground through the back stays rather than through bending of the towers.

The transverse configuration of the tower depends on the type of the suspension system used. Some of these configurations are as follows (shaded boxes):

Type of Suspension	Single Cantilever	Twin Cantilevers	A-frame	Portal frame
Central	■		■	
Double Plane Inclined			■	
Double Plane Vertical		■		■

The towers are subject to bending in a plane transverse to the bridge axis due to wind loads. Menn [86] recommends that towers should be stiff transverse to the axis of the bridge. When the tower consists of two isolated cantilevers, the designer should carefully evaluate the possibility of geometric instability in the transverse direction. A-frame towers do not have such problems due to their high transverse stiffness. Moreover, the structural system defined by A-frame towers, stay-cables and the deck form a space truss which has a high torsional stiffness about the longitudinal axis of the bridge. The torsional and flexural frequencies of this system are well apart thereby increasing the aerodynamic stability of the structure. The A-frame pylon is usually used for long span bridges, where the tower has sufficient height and the sloping cable planes do not interfere with the required vertical clearance above the deck.

The height of the tower is determined from several considerations such as cable arrangement, visual appearance, economics etc. The recommended height of the tower is between 20 to 25 percent of the length of the main span, Leonhardt [68], Menn [86]. Increasing the height of the towers decreases the steel consumption of the cables as well as

the longitudinal compressive force in the deck; however, it increases the cost of the tower itself.

It is preferable to keep the towers vertical. Inclined towers, such as that used in the Bratislava Bridge over Danube, are aesthetically daring but difficult to construct and uneconomical, [74].

2.2.3. GIRDER CROSS SECTION

The deck girder is designed to be as slender as possible without compromising its safety against geometric stability. Other design considerations include aerodynamic behavior and ease of cable anchorage. The shape of the cross section depends on the type of suspension system used.

In the case of double plane suspension, hollow or solid slabs with stiffened edges are most economical for deck widths up to 15 m., Leonhardt [68]. The deck does not need to furnish any torsional stiffness; any loads that are unsymmetric with respect to the center line of the bridge are picked up by the cables which provide a stiff support along the edges. Cable anchors are usually placed outside the deck or within the side walks. An example is the Diepoldsou Bridge in Switzerland where a 0.55 m. thick concrete slab is hung by double cable planes.

For decks of larger width, double T girders with diaphragms are recommended, Menn [86]. Other innovative solutions are possible; for Pasco-Kennewick Bridge over the Columbia river in USA which has a deck width of 24.4 m., the transverse cross section consists of two triangular box beams placed at the sides and joined by a top slab with transverse ribs positioned every 2.7 meters. The triangular box beams pick up the axial force in the deck and provide anchorage for the stay cables.

In the case of axial suspension, box sections must be used to ensure adequate torsional stiffness. Consider the example of Brotonne Bridge in France, Mathivat [83], where a single cell concrete box girder section, stiffened internally by inclined braces placed every three meters is used. The cable is anchored at the point of intersection of the two braces in the top flange; the braces which pick up the cable force are subject to very heavy tension and have to be prestressed.

2.3. CONSTRUCTION METHODS

The various methods of construction of cable stayed bridges are broadly classified as follows:

- The staging method.
- The push out method.
- The cantilever method.

The choice of the construction technique has significant influence on the cost of the project as well as on the final profile of the bridge deck and the distribution of stresses in the structure. The cantilever method is by far the most versatile technique and is commonly used in the construction of cable stayed bridges. The other two procedures are used only under special circumstances and are presented here for the sake of completeness.

The present trend is to prefabricate components as large as possible in the controlled environment of a shop thereby simplifying the fabrication process as well improving the overall quality of construction.

2.3.1. STAGING METHOD

The staging method of erection is used where the clearance to the underside of the structure is low and temporary bents used for supporting the superstructure will not interfere with any traffic passing underneath the bridge. This method was used in the construction of Rhine Bridge at Maxau in Germany, Podolny [103].

2.3.2. PUSH OUT METHOD

The push out method is used in those cases where care must be taken not to interfere with the traffic below the bridge. In this method large sections of bridge deck are pushed out over the piers on roller bearings. The deck is pushed out either from both abutments towards the center or in some instances from one abutment all the way to the other abutment.

An assembly line is set up in a yard on one end of the bridge, the components are fabricated or cast, put together and then gradually rolled out over the span in a process somewhat similar to a mass production facility, ensuring the quality as well as the low cost inherent in a mass production process.

As an example, consider the Julicher Strasse Bridge in Germany. This structure is a highway overpass which crosses a railroad installation in an urban area of Dusseldorf. The bridge has a central span of 324 ft. and equal side spans of 104 ft. each. The railway tracks passing underneath were not to be interrupted. The designers therefore decided to use the push out method. The erection procedure used by the contractor is described in detail by Podolny [103].

2.3.3. CANTILEVER METHOD

The cantilever erection method is employed in cable stayed bridge construction where temporary supports are not possible. The principal advantages are:

- It does not interfere with the traffic below the bridge.
- It is more economical when the bridge spans deep valleys or the site conditions are such that the erection of temporary river piers is difficult or costly.

This method was employed in the construction of the Pasco-Kennewick Bridge over Columbia river, Podolny [103], Leonhardt et al. [69]. The bridge has a center span of 981 ft. and two side spans of 413 ft. each. Portal frame concrete towers support a double plane of

cable-stays arranged in a fan pattern. The deck consists of triangular concrete box beams connected by transverse beams and a roadway slab.

The deck segments were cast in a yard near the river bank. The segments were prestressed in the transverse direction and then moved to the bridge site on a barge. Each segment was lifted in position by the erection traveler, epoxy mortar was applied to the joint and the new segment pressed against the previously installed segment by longitudinal prestressing. After overnight curing , the cables were installed, one pair for each element.

3. NONLINEAR CONSTITUTIVE MODELS FOR REINFORCED CONCRETE

3.1. GENERAL

The material models used in the beam-column element developed in the present study are discussed in this chapter. These include material constitutive relations for concrete and steel in a state of uniaxial stress. Different approaches used to model the phenomenon of tension stiffening are also discussed.

The tri-linear torque-twist relationship used for concrete elements in the present study is also discussed in this chapter. The various strength and geometry parameters which affect this relationship are described.

Finally, an algorithm for state determination procedures is presented. This algorithm describes a generic procedure which may be employed for any type of stress-strain relationship, cyclic or otherwise.

3.2. CONCRETE

The mathematical model used in this study is a modification of the Kent-Park model shown in Fig. 3.01. This formulation can be used to model concrete confined by rectangular hoops. The mathematical model is completely described by defining the 28 day concrete strength f_c', the coordinates of the point at the end of the falling branch (ε_1,σ_1) and the ultimate

concrete strain at failure by crushing ε_u. The characteristics of this model are described by the following states:

State 1: The ascending portion of the compressive stress-strain curve is described by the following equation.

$$\sigma_c = f_c' \frac{\varepsilon_c}{\varepsilon_o} (2 - \frac{\varepsilon_c}{\varepsilon_o}) \tag{3.1}$$

$$\varepsilon_o = 2 \frac{f_c'}{E_{ci}} \tag{3.2}$$

$$E_{ci} = 33 (w)^{1.5} \sqrt{f_c'} \tag{3.3}$$

$$E_{ct} = E_{ci} (1 - \frac{\varepsilon_c}{\varepsilon_o}) \tag{3.4}$$

Where ε_o is the concrete strain corresponding to the maximum stress f_c', E_{ci} is the initial modulus for a concrete of unit weight w and having a 28 day strength of f_c' and E_{ct} is the tangent modulus of concrete at a strain of ε_c.

State 2: The descending part of the stress strain curve is defined by the following equations.

$$f_c = f_c [1 - Z (\varepsilon_c - 0.002)] \tag{3.5}$$

$$Z = \frac{0.5}{\varepsilon_{50u} + \varepsilon_{50h} - 0.002} \tag{3.6}$$

$$\varepsilon_{50u} = \frac{3 + .002 f_c'}{f_c' - 1000} \tag{3.7}$$

$$\varepsilon_{50h} = \frac{3}{4} \rho_s \sqrt{\frac{b'}{s_h}} \tag{3.8}$$

The parameter Z defines the slope of the falling line, ε_{50u} is a measure of the effect of concrete strength on the slope of the falling branch of unconfined concrete and ε_{50h} gives the additional ductility due to rectangular hoops . ρ_s is the ratio of volume of transverse

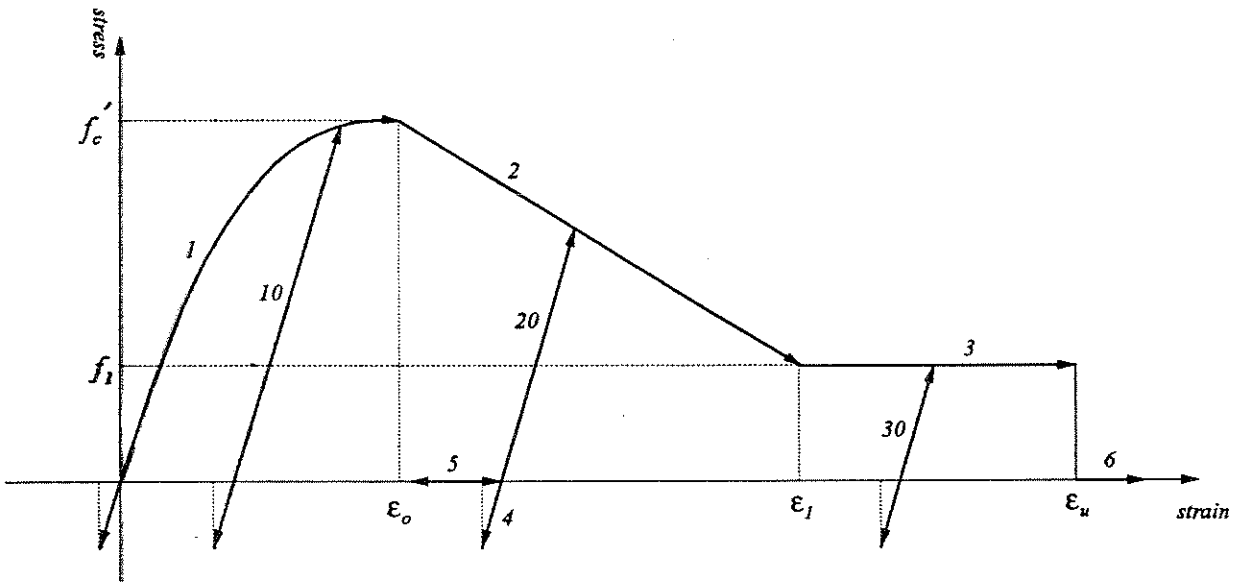

FIG. 3.01 CONCRETE MODEL; MATERIAL STATE CODES

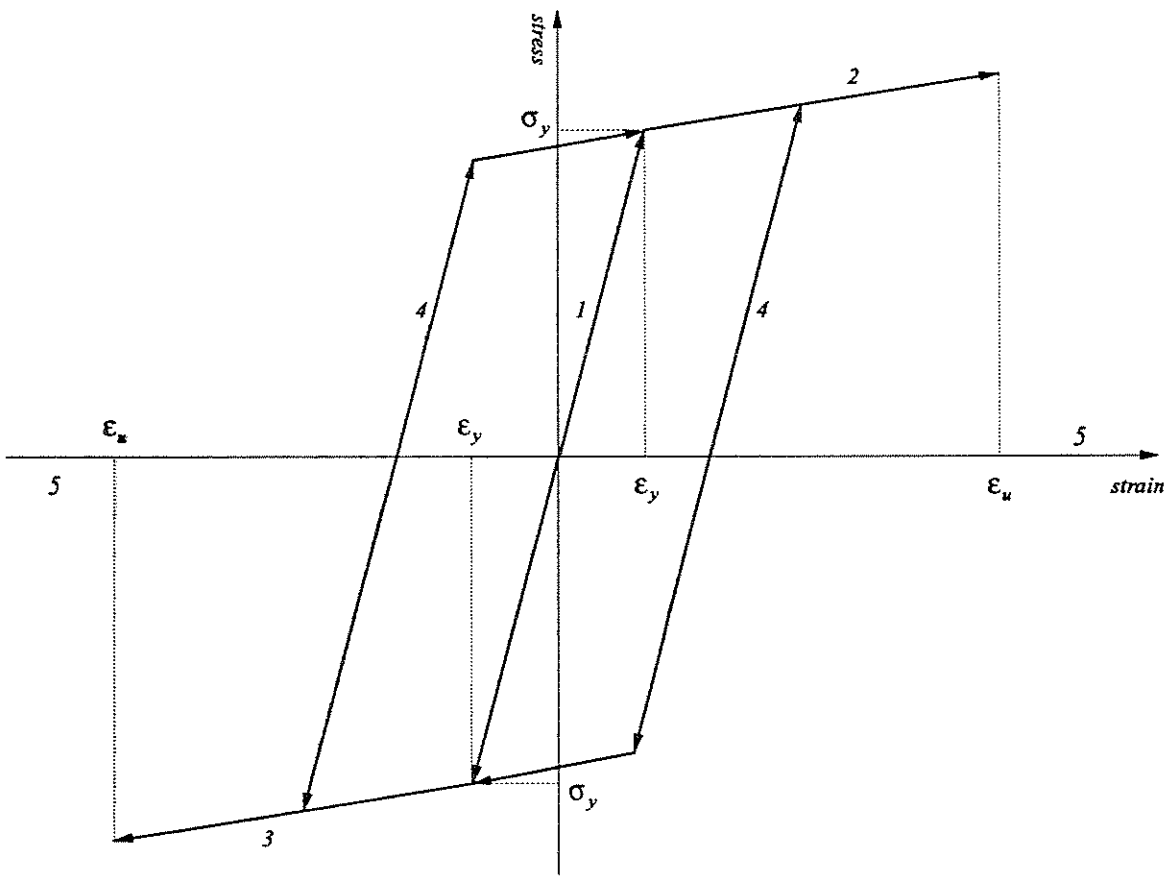

FIG. 3.02 STEEL MODEL; MATERIAL STATE CODES

reinforcement to volume of concrete core measured to outside of hoops, b' is the width of confined core to outside of hoops and s_h the spacing of hoops.

State 3: This region accounts for the ability of the concrete to sustain some stress at very large strains.

$$f_c = 0.2\, f_c' \tag{3.9}$$

State 6: This state defines the crushing failure of concrete.

State 10: This state describes load-unload from state 1. The unloading is assumed to be linear with a slope equal to the initial concrete modulus E_{ci}. The coordinates of the point on the virgin compression curve where the unloading commences are stored and in case of reloading beyond the upper bound of state 10, the virgin curve is traced starting from the original unloading point.

State 20: This state describes load-unload from state 2.

State 30: This state describes load-unload from state 3.

3.2.1. TENSION STIFFENING

The tensile strength of concrete is about 10% of its compressive strength, which is relatively low and cracking may occur in the tension zone of the members subjected to flexure or to axial tension. Cracking reduces the stiffness of concrete members and is therefore an important consideration in the analysis of reinforced concrete members.

The presence of reinforcement complicates this phenomenon. Goto 1971 [36], investigated the manner in which the axial load is shared between the concrete and the reinforcement along the length of the member. He showed that the forces are transferred from the bar to the concrete by inclined compressive forces radiating out from the bar and that internal secondary cracks are formed in addition to the primary cracks visible on the surface.

Refer to Fig. 3.03; consider an axially loaded concrete prism reinforced with a steel bar. Cracking starts when the tensile stress in the concrete reaches the tensile strength in the concrete at some point in the bar. At the crack the stress in the concrete drops to zero and the entire load is carried by the steel. Between the cracks, however, concrete still carries some tensile stress because of the bond between concrete and reinforcing steel. This phenomenon is referred to as the tension stiffening effect. As the load is further increased, stress builds up in the concrete on either side of the crack; at the primary cracks the concrete will be unstressed and at a certain distance (transfer length) from the cracks the stress will build up to the cracking stress and new cracks will form. This process continues until the distance between the adjacent primary cracks is not large enough to build up to the cracking load. Any loading beyond this stage simply widens the existing cracks.

If the variation of the tensile force in the steel bar along the length of the member is known then the corresponding steel strains can be calculated and the deformation of the member can be calculated by integration of these strains over the length. The total axial extension of the member divided by its length yields an average strain in the steel bar. Thus it may be possible to devise a relation between average steel stress and strain which accounts for the phenomenon of tension stiffening. The average steel strain is less than the maximum strain in steel which occurs at the cracks; this results in an increased stiffness for the reinforcing steel. A number of researchers, Gilbert [31], Van Zyl [141], Choudhury [20] have chosen to ignore the concrete after cracking and have used variously enhanced stiffness of reinforcing steel.

On the other hand, the tensile force in the concrete can be worked out by subtracting the force carried by the steel bar from the total force and a relation obtained between average concrete stress and average strain. When the first crack forms, the average stress in the concrete will be equal to the cracking stress. After the formation of the first crack the average stress in the concrete will be reduced and as further cracks develop, the average stress will

be further reduced. This results in an unloading stress-strain curve for reinforced concrete in tension. Scanlon [112] used a stepped piecewise linear unloading relationship to model this behavior. A similar approach using a smooth unloading curve was used by Lin and Scordelis [71].

In this study, the latter approach based on the average stress-strain curve for reinforced concrete is used. A modification of the model suggested by Vecchio and Collins [142] is employed, Fig. 3.04. The characteristics of this model are described by the following states:

State 4: The behavior in primary tension is assumed to be linear; the slope of the line is equal to the initial modulus of concrete at 28 days.

$$\sigma_c = \varepsilon_c E_{ci} \tag{3.10}$$

State 5: This state defines the failure of concrete by cracking in tension and is active only when tension stiffening model is not operative.

State 7: This defines the unloading relation between the average stress and strain of cracked reinforced concrete as defined by Vecchio and Collins [142] and later modified by Collins and Mitchell [22].

$$f_c = \frac{\alpha_1 \alpha_2 f_{cr}}{1 + \sqrt{500\,\varepsilon_c}} \tag{3.11}$$

$$E_{ct} = 0 \tag{3.12}$$

where α_1 is the factor accounting for bond characteristics of reinforcement; it is equal to 1.0 for deformed bars, 0.7 for plain bars and 0.0 for unbonded reinforcement. α_2 is a factor for loading rate; it is equal to 1.0 for short term monotonic loadings and 0.7 for sustained loading.

State 70: This state defines the load-unload path from state 7. The path is described by a straight line which connects the unloading point on the virgin curve with the point of zero crossing.

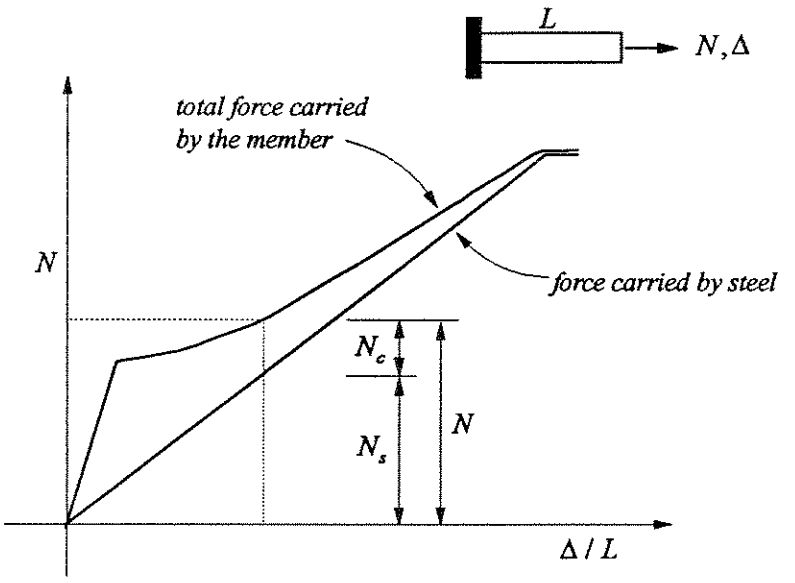

FIG. 3.03 LOAD DEFORMATION RESPONSE OF A REINFORCED CONCRETE MEMBER SUBJECT TO AXIAL LOAD

Adapted from Collins & Mitchell, 1991

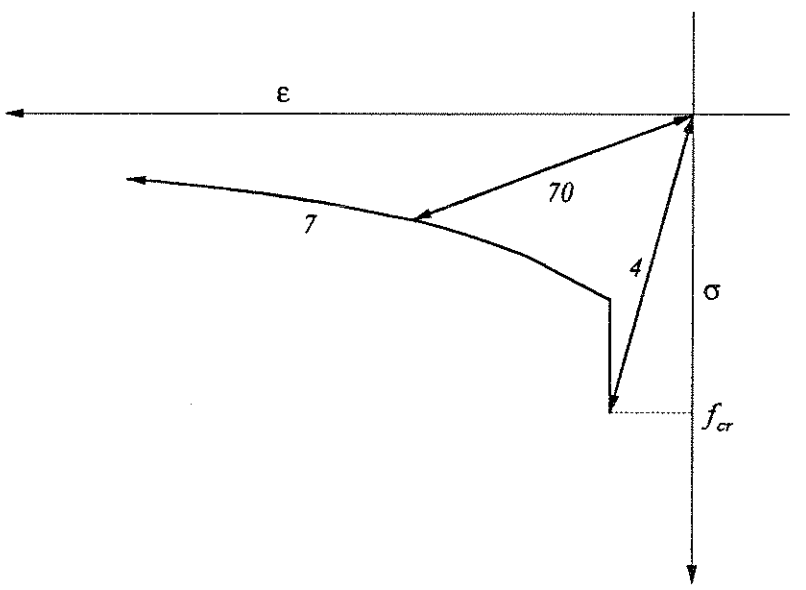

FIG. 3.04 TENSION STIFFENING MODEL; MATERIAL STATE CODES

3.3. STEEL

A bi-linear strain hardening model is used for steel. The model includes simulation of stress reversal and Bauschinger effect. The basic characteristics of the model are shown in Fig. 3.02.

The model is defined by the following parameters:

σ_y, yield strength of steel.

ε_u, ultimate strain at failure.

E, initial modulus.

E_{sh}, strain hardening modulus.

A description of various material states as shown in Fig. 3.02 is as follows:

State 1: Initial elastic state (modulus E).

State 2: Tension yield (modulus E_{sh}).

State 3: Compression yield (modulus E_{sh}).

State 4: Unload and reload from the strain hardening branch (modulus E).

State 5: Failure in tension or compression ($|\varepsilon_s| \geq |\varepsilon_y|$).

3.4. TORSION MODEL

The torque-twist model used in the present study is adapted from Chan, 1982 [19]. It is assumed that the bending and torsional actions are completely uncoupled. A tri-linear torque-twist relationship is used to model the response of reinforced concrete beams subjected to torsion alone, as shown in Fig. 3.05. The model is defined completely by the following parameters:

(α_{cr}, T_{cr}) The twist at first cracking and the corresponding torque.

(α_{yp}, T_{yp}) The twist and torque at full yielding of all reinforcement.

(α_u, T_{yp}) The twist at ultimate failure.

The tri-linear torque-twist relationship is modeled by two components, Fig. 3.06, each exhibiting elasto-perfectly plastic behavior. These components are defined by the following parameters

(α_{cr}, T_{y1}) and (α_{yp}, T_{y2}); the twist and torque at yield for components 1 and 2.

α_u the ultimate twist at failure for both components.

Elastic torsional stiffness for each component is given by

$$GJ_1 = \frac{T_{y1}}{\alpha_{cr}} \tag{3.13}$$

$$GJ_2 = \frac{T_{y2}}{\alpha_{yp}} \tag{3.14}$$

The results from the two components are directly added to yield the total torque and the torsional stiffness of the concrete beam.

$$T = T_1 + T_2$$
$$GJ = GJ_1 + GJ_2 \tag{3.15}$$

The two stiffnesses GJ_1 and GJ_2 and hence the two yield torques T_{y1} and T_{y2} are obtained by solving the following simultaneous equations:

$$GJ_1\,\alpha_{cr} + GJ_2\,\alpha_{cr} = T_{cr} \tag{3.16}$$

$$GJ_1\,\alpha_{yp} + GJ_2\,\alpha_{yp} = T_{yp} \tag{3.17}$$

The solution is given by:

$$GJ_1 = \frac{T_{cr}}{\alpha_{cr}} - \left(\frac{T_{yp} - T_{cr}}{\alpha_{yp} - \alpha_{cr}}\right) \tag{3.18}$$

$$GJ_2 = \left(\frac{T_{yp} - T_{cr}}{\alpha_{yp} - \alpha_{cr}}\right) \tag{3.19}$$

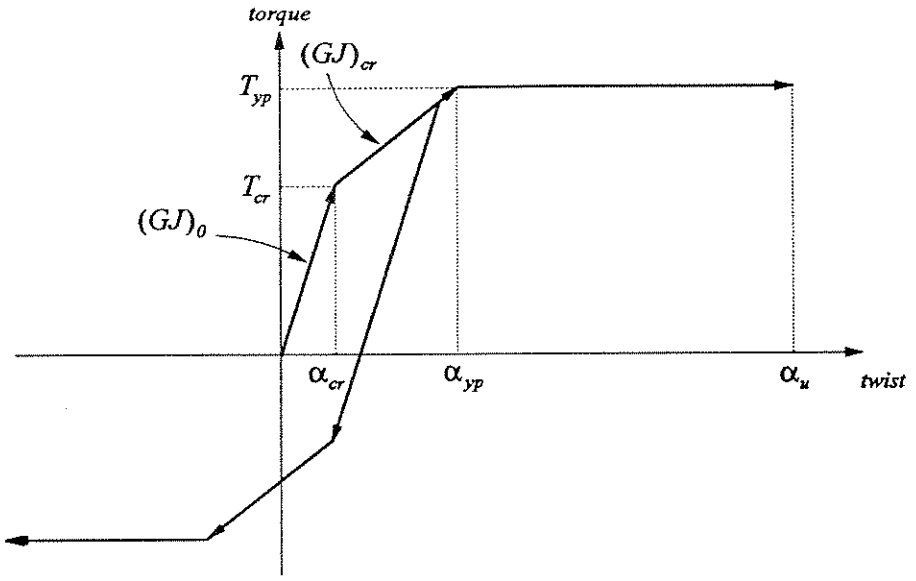

FIG. 3.05 ASSUMED TORQUE-TWIST RESPONSE

Chan, 1982

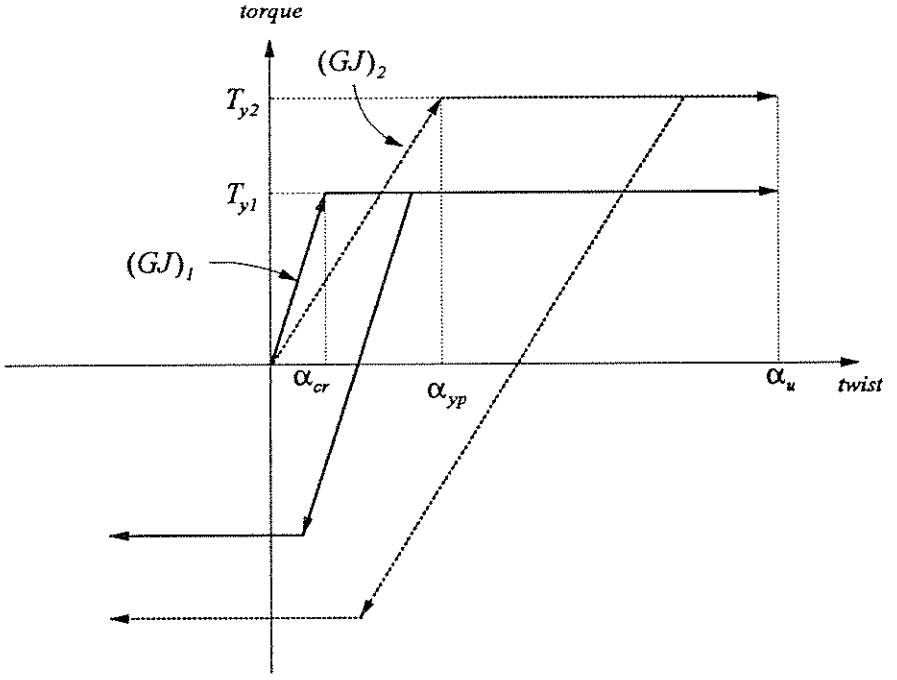

FIG. 3.06 MODELING OF TRI-LINEAR RESPONSE WITH TWO EPP ELEMENTS CONNECTED IN PARALLEL

3.4.1. TORSIONAL RESPONSE PRIOR TO CRACKING

The torsional response of concrete members prior to cracking is almost linear. The torsional response of solid non-circular members is complex, St. Venant [26] was the first to develop a solution for such problems based on the theory of elasticity in 1853. Analytical solutions for torsion of solid rectangular members have been presented by Timoshenko [137] using the classical theory for unrestrained warping torsion. The maximum shear stress, the angle of twist and the torsion stiffness is given by

$$\tau_{max} = \frac{T}{\kappa b t^2} \tag{3.20}$$

$$\phi = \frac{TL}{(\beta b t^3)\, G} \tag{3.21}$$

$$k = \frac{(\beta b t^3)\, G}{L} \tag{3.22}$$

T is the torque applied to member of length L and a cross sectional are of $b \times t$ where $t \leq b$, κ and β are functions of the ratio b/t and k is the torsional stiffness of the member.

For a thin walled hollow member

$$T = 2A_0\, q \tag{3.23}$$

$$q = t\,\tau \tag{3.24}$$

$$(GJ_o)\oint \frac{ds}{t} = 4A_0^2 G \tag{3.25}$$

where A_o is the area enclosed by the center line of the wall, q is the shear flow, t is the average thickness of the wall, τ is the shear stress and s is measured along the centerline of the thin wall.

If f_{cr} is uniaxial tensile strength of concrete then the torsional moment at first cracking and the corresponding twist per unit length is given by

$$T_{cr} = 2A_o\, t\, f_{cr} \tag{3.26}$$

$$\alpha_{cr} = \frac{T_{cr}}{GJ_o} \tag{3.27}$$

3.4.2. TORSIONAL RESPONSE AFTER CRACKING

Torsional stiffness is reduced substantially after cracking. Two major theories are used to explain the torsional strength of concrete. The first theory is known as the skew bending theory; this was developed by Lessig [70]. This theory, which forms the basis of torsion design provisions in the ACI code assumes that the mode of failure involves bending on a skew section resulting from the crack spiraling around three of the four sides of the member. All sections, hollow or solid are considered as solid sections.

The second theory presented by Lampert [57] and Lampert and Thurliman [56] is based on the assumption that a cracked concrete member subjected to torsion behaves in a manner similar to a plastic space truss. All sections, hollow or solid are considered to be hollow sections. After the concrete cracks in torsion, the concrete in the center of the member has little effect on the torsional strength of the member. Torsion is transmitted by inclined compressive stresses in the walls of the tube and transverse stirrups and longitudinal reinforcement are required for equilibrium. This theory forms the basis of the torsion provisions in the Comite Euro-International du Beton Model Code [87].

This study uses the space truss theory. The yielding torque obtained by Lampert [58] is given as

$$T_{yp} = 2\frac{A_h f_{hy}}{s \tan\alpha_c} A_o \tag{3.28}$$

$$T_{yp} = 2\frac{A_h f_{hy}}{s \tan\alpha_c} A_o \tag{3.29}$$

A_h, f_{hy} and A_l, f_{ly} are the area and the yield stress of hoop reinforcement and longitudinal reinforcement respectively, A_o is the area enclosed by the centerline of the hoop, p_o is the hoop centerline perimeter, s is the spacing of hoops and α_c is the inclination of the diagonal crack lines. The post cracking stiffness is given by

$$GJ_{cr} = \frac{4E_s A_o^3}{p_o^2} \quad \frac{1}{\frac{1}{\sigma_h} + (\frac{1}{2\sigma_s} + \frac{1}{2\sigma_s'})} \tag{3.30}$$

$$\sigma_h = \frac{2A_h}{A_o} \qquad \sigma_s = \frac{2A_{sb}}{A_o} \qquad \sigma_s' = \frac{2A_{st}}{A_o}$$

where A_h, A_{sb} and A_{st} is the steel area for hoops, longitudinal reinforcement at bottom and top of beam respectively.

The torsional deformation corresponding to the yielding torque is given by

$$\alpha_{yp} = \frac{T_{yp}}{GJ_{cr}} \tag{3.31}$$

Failure is assumed to occur when the maximum shearing strain in the concrete extreme fibers reaches an ultimate value of γ_u. This value usually lies in the range of .01 and .02.

3.5. A GENERIC ALGORITHM FOR STATE DETERMINATION

The state of material is defined by a set of parameters which uniquely determine the stress in that material. Consider a material fiber of known current state, which is subjected to a given strain increment. The process of computing the new state is known as the state determination.

A general algorithm for state determination is presented. The algorithm is best explained by means of an example. The concrete material model used in CALBRG will be used as the demonstration example. Tension stiffening is ignored in order to maintain clarity of presentation. The reference state of a concrete fiber is described by the following parameters:

- *EPS* concrete strain
- *SIG* concrete stress
- *EMOD* tangent modulus

- *KEY* material state code
- *CRACK* true if previously cracked else false
- *EPSV* strain at virgin curve on unload

The total current strain in concrete *EPSN* is given. It is required to find the current state of the concrete fiber.

The basic step is to set up a path diagram; such a diagram displays the path to be traced on

Path Diagram

EPSN < EPS			*KEY*	*EPSN > EPS*				
5	[4]	10	1	1	2	3	6	
5	[4]	20	2	2	3	6		
5	[4]	30	3	3	6			
	5	4	4	4	1	2	3	6
	5	4	4 (10)	10	1	2	3	6
	5	4	4 (20)	20	2	3	6	
	5	4	4 (30)	30	3	6		
		5	5	1	2	3	6	
		5	5 (10)	10	1	2	3	6
		5	5 (20)	20	2	3	6	
		5	5 (30)	30	3	6		
		6	6	6				
5	[4]	10	10	10	1	2	3	6
5	[4]	20	20	20	2	3	6	
5	[4]	30	30	30	3	6		

the stress-strain diagram from a given state to the ultimate failure state.

Note:

- Integers within circular brackets ( ) indicate the previous load-unload path.
- Skip state 4 if enclosed in square brackets [ ]; indicates previous cracking.

Using the path diagram such as that shown above, a path vector is set up. The dimension of the path vector is equal to the maximum possible number of states in any path. For example, let the reference state be state 10 and the current total strain be greater than the reference strain. Then the path vector is given by:

$$P = \begin{bmatrix} 10 \\ 1 \\ 2 \\ 3 \\ 6 \end{bmatrix}$$

Next, the path vector is processed. This can be done in two ways:

1. Tracing
2. Bracketing

Each method is described in detail in the following sections.

3.5.1. TRACING

The path is traced on the stress-strain diagram from state to state in a manner analogous to the actual physical behavior of the material. One subroutine is written for each state. These subroutines are called in the sequence dictated by the path vector. The input information to the first subroutine is the reference state and the current strain. If the current strain falls within the strain domain of the subroutine then the corresponding stress, the state is updated and the tracing process exited. However, if the current strain falls outside the domain of the processing subroutine then the stress at the upper or lower boundary of the state is computed depending on whether strain is increasing or decreasing and the output state is handed over to the next subroutine as required by the path vector. The pseudo code for the example being considered above is as follows:

```
eps=eps_ref
sig=sig_ref

do 10 n=1,5
        k=kpath(n)
        select case (k)
                case (0)
                        exit
                case (1)
                        call c_mode_1 (eps,sig)
                case (2)
```

```
                    call c_mode_2 (eps,sig)
                case (3)
                    call c_mode_3 (eps,sig)
                case (4)
                    call c_mode_4 (eps,sig)
                case (5)
                    call c_mode_5 (eps,sig)
                case (6)
                    call c_mode_6 (eps,sig)
                case (10)
                    call c_mode_10 (eps,sig)
                case (11)
                    call c_mode_11 (eps,sig)
                case (12)
                    call c_mode_12 (eps,sig)
            end select
            if (eps=epsn) exit
10      continue
```

The array *KPATH* stores the path vector. If the terminal state is state 3, then case 10, 1, 2 and 3 will be processed in sequence. At this stage, *EPS*, the strain at exit from case 3 must equal the given current strain *EPSN*. When this condition is detected then the state determination is complete and the process is exited.

3.5.2. BRACKETING

The strain limits, that is the upper and lower boundaries of each state are calculated. The known current strain is compared with the strain limits of each state as dictated by the path vector and the terminal state is identified. The strain limits of the terminal state must bracket the given value of current strain. Only one processing subroutine corresponding to the terminal state is used to calculate the fresh state.

```
        do 10 n=1,5
            k=kpath(n)
            up=limit_up (k)
            dn=limit_dn (k)
            if (dn <= epsn <= up) then
                terminal_case=k
                exit
            end if
10      continue
```

```
eps=eps_ref
sig=sig_ref
m=terminal_case
select case (m)
        case (1)
                call c_mode_1 (eps,sig)
        case (2)
                call c_mode_2 (eps,sig)
        case (3)
                call c_mode_3 (eps,sig)
        case (4)
                call c_mode_4 (eps,sig)
        case (5)
                call c_mode_5 (eps,sig)
        case (6)
                call c_mode_6 (eps,sig)
        case (10)
                call c_mode_10 (eps,sig)
        case (11)
                call c_mode_11 (eps,sig)
        case (12)
                call c_mode_12 (eps,sig)
end select
```

The arrays *LIMIT_UP* and *LIMIT_DN* store the upper and lower strain limits of various material states.

The tracing approach may seem to be computationally inefficient; however, if the load or displacement steps are small, which is generally the case, then the path may span at the most two states and computational efficiency is maintained.

The bracketing approach requires evaluation of upper and lower strain limits for each mode. If the material model is time dependent or if the material is on a load reversal path then new limits have to be evaluated thereby imposing a considerable computational overhead.

4. TIME DEPENDENT EFFECTS OF CONCRETE

4.1. GENERAL

Shrinkage of concrete is defined as the change in the volume of concrete with time , independent of any external loads or thermal effects. It is caused by the loss of water as the concrete dries and volume changes due to carbonation. The magnitude of shrinkage strains is strongly influenced by the water cement ratio of the concrete, increasing sharply for larger ratios. Shrinkage strains are also affected by the type of aggregate used in the concrete; hard aggregates with low absorption result in lower shrinkage. Other significant factors include relative humidity and size of concrete member.

Creep of concrete is defined as the increase in strain with time due to a sustained load. When concrete is loaded, an instantaneous elastic strain is developed, Fig. 4.01. If the load remains, additional creep strains develop with time. The final creep strain may be of the order of two to three times the instantaneous elastic strain. If the load is removed, elastic strain is recovered instantaneously. This is followed by a gradual recovery of only a portion of the original creep strain.

In general creep has little effect on the strength of the structure; however it leads to an increase in deflections with time and may lead to a redistribution of stresses. It is also one of the major causes of stress loss in prestressed tendons.

The creep strain developed in the concrete is influenced by a number of factors listed below.

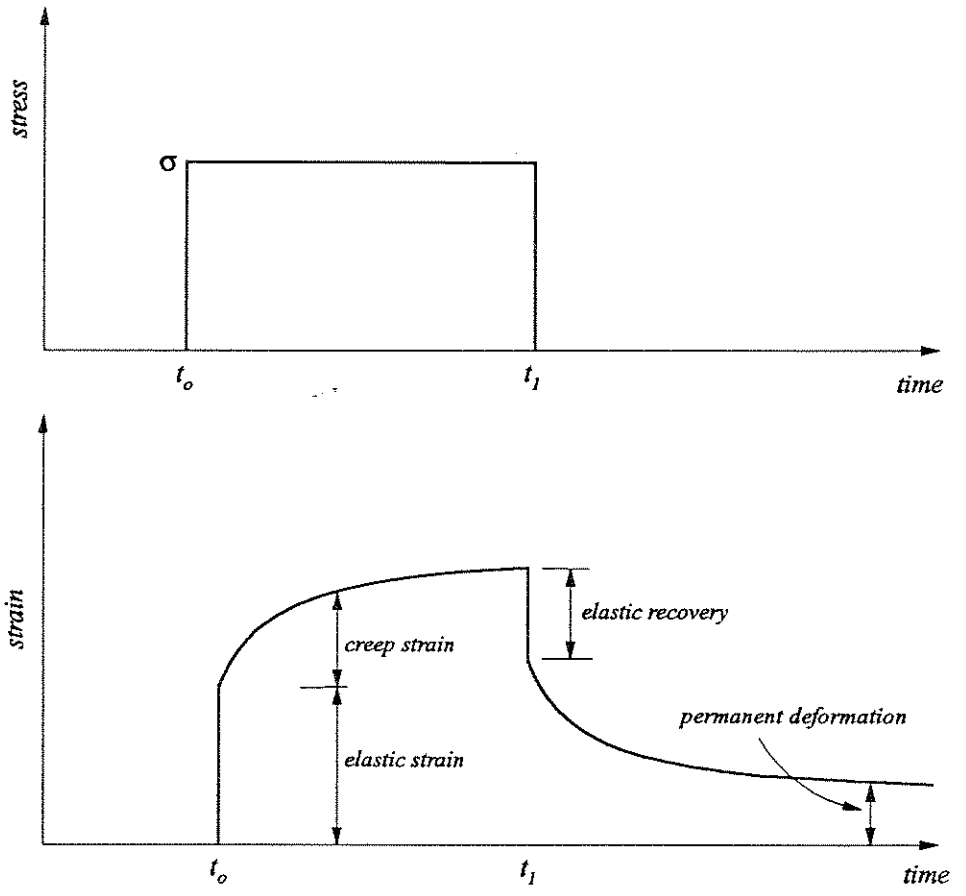

FIG. 4.01 ELASTIC AND CREEP STRAINS AT LOADING AND UNLOADING.

- Stress; creep strain occurring over a given period of time is proportional to the applied stress, provided that the stress level does not exceed about 40% of the compressive strength of concrete, CEB-FIP code 1990 [88].
- Temperature; For a temperature range between $0^{O}F$ and $180^{O}F$ creep deformation is directly proportional to temperature, Bresler [15].
- Age of concrete at loading; mature concrete develops smaller creep strains.
- Ambient relative humidity; Larger creep strains develop in dry conditions. For samples submerged in water, creep strains vary from small to none, Kristek [128].
- Thickness of concrete specimen; Structural members of smaller dimensions develop higher creep strains as compared to larger members. This difference is attributed to more intensive moisture exchange in the smaller members.
- Concrete mix; Creep strains are affected by the type of cement, aggregate and the water cement ratio used in designing the mix. An aggregate with a lower modulus of elasticity will develop higher creep strains. Water cement ratio strongly affects the magnitude of the creep strains; for example the ultimate creep strain for a water cement ratio of 0.65 is three times that corresponding to a ratio of 0.40, Kristek [128].

Mathematically, the creep strain ε^c at time t due to a stress σ applied at time τ is given by:

$$\varepsilon^c(t) = C(t,\tau)\,\sigma \tag{4.1}$$

$$\varepsilon^c(t) = \varphi(t,\tau)\,\varepsilon_e \tag{4.2}$$

where $C(t,\tau)$ is defined as the specific creep and gives the creep strain at time t caused by a unit sustained stress applied at time τ. $\varphi(t,\tau)$ is defined as the creep coefficient and expresses the ratio of creep strain to instantaneous elastic strain.

Accurate formulation of time dependent material behavior is essential for predicting the stresses and deflections in a structure at various stages through its life. The numerical method used in this study to evaluate creep strain in a reinforced concrete member at any

given instant of time is based on the procedure used by Kabir [48], Kang [49], Van Zyl [141], Van Gruenen [140], Chan [19] and Ketchum [53].

This procedure is based on the assumption that the principle of superposition is valid in the sense that the strain response due to the sum of stress histories is equal to the sum of individual strain responses. The basis of this technique may be described with reference to an example.

- Assume that an element of concrete is subject to a uniform stress σ_1 at a time t_1, Fig. 4.02 (a). The application of this load leads to creep and elastic strains shown.
- Consider a second element that is subjected to a stress σ_2 at time t_2 which generates the strains shown in Fig. 4.02 (b).
- Principle of superposition dictates that the strains in a third concrete element subject to a stress history of σ_1 from t_1 to t_2 and $(\sigma_1+\sigma_2)$ from t_2 to t_3 is given by adding the elastic and creep curve in Fig 4.02 (a) and (b).The resultant conditions are indicated in Fig. 4.02 (c).

Any stress history can be built up by adding additional load cases. However, such an integration, if carried out directly would require a large data storage capacity on a computer and is quite impractical. The technique developed by Kabir [48], explained in detail in later sections, avoids this problem by storing the effect of all previous stress histories in a so called hidden state variable.

4.2. Prediction of Creep and Shrinkage Strains

Creep and shrinkage strains that will develop over time in a given specimen of concrete subject to known environmental conditions and loads can be predicted from available experimental data.

When such data is not available, empirical models may be used to predict these strains. Several such models have been suggested, ACI-Committee 209, Comite Euro Beton

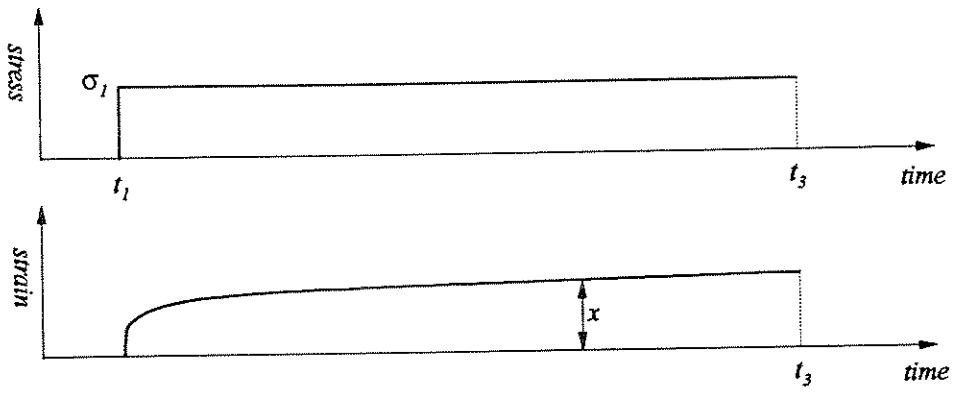

(a) Element 1, Stress and Creep Strain History

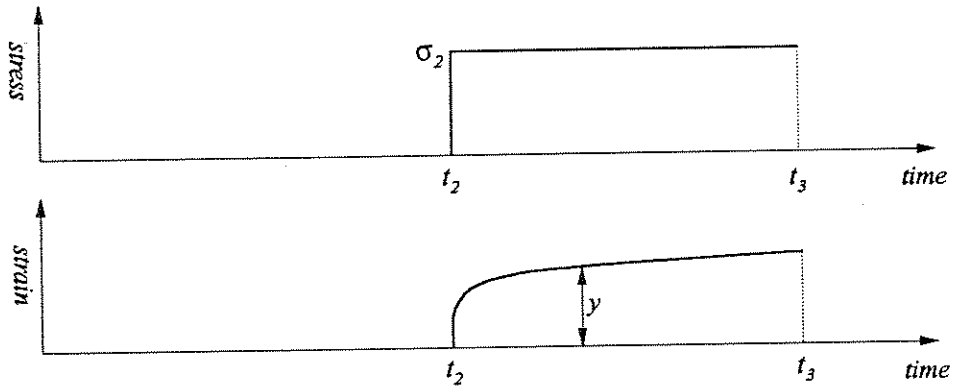

(b) Element 2, Stress and Creep Strain History

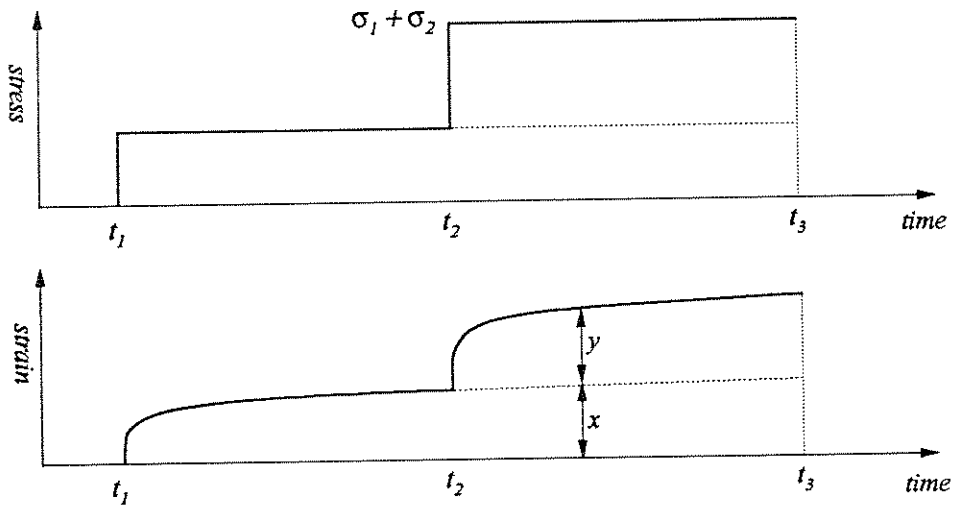

(c) Element 3, Stress and Creep Strain History

FIG. 4.02 METHOD OF SUPERPOSITION

(1978), Bazant-Panula (BP II), Comite Euro Beton (1990), etc. These models differ in their degree of accuracy and complexity. ACI-209 model is the easiest to use whereas BP II is considered by many to be the state of the art.

The CEB-FIP model was not originally designed for use with computers as data has to be taken off several graphs. Kristek et al. [128] have proposed analytical expressions to approximate these graphs, hence increasing the versatility of the model.

Two of the methods mentioned above, namely ACI-209 and CEB (1978) have been used in the present study and implemented in the computer program CALBRG. These are discussed in more detail in the subsequent sections.

4.2.1. ACI-COMMITTEE 209 RECOMMENDATIONS

The recommendations of committee 209 are based on the studies of Branson et al. [14].

4.2.1.1. SHRINKAGE

Shrinkage strain is given by the following equation:

$$\varepsilon^s(t) = K_S\, K_h\, K_H \quad \frac{(t-t_0)^e}{f+(t-t_0)^e}\, \varepsilon_u{}^s \tag{4.3}$$

where

t is the observation time.

t_o is the age of concrete at end of curing.

$\varepsilon^s(t)$ is the shrinkage strain at observation time (t).

$\varepsilon_u{}^s$ is the ultimate shrinkage strain to be determined from experiment.

f, e constants to be determined by experiments.

K_S is the slump correction factor.

K_h is the size correction factor.

K_H is the relative humidity correction factor.

The ACI Committee 209 recommends the following standard equation for concrete which is moist cured for 7 days:

$$\varepsilon^s(t) = K_S\, K_h\, K_H \quad \frac{(t-7)}{35+(t-7)}\, 800\times 10^{-6} \tag{4.4}$$

In the case of concrete which is steam cured for three days

$$\varepsilon^s(t) = K_S\, K_h\, K_H \quad \frac{(t-3)}{55+(t-3)}\, 730\times 10^{-6} \tag{4.5}$$

The correction factors are provided to take into account variations in field conditions:

1. Slump:

   $K_S = 0.89 + 0.041S$

   where S is slump in inches.

2. Humidity:

   $K_H = 1.4 - 0.01H \qquad 40 \le H \le 80$
   $K_H = 3.0 - 0.03H \qquad 80 \le H \le 100$

   where H is percent relative ambient humidity.

3. Thickness:

   The linearized analytical version of graphical relationship suggested by ACI-209 is as follows:

   $K_h = 1.14 - 0.023h$ $\le$ 1 year of drying.

   $K_h = 1.10 - 0.017h$ for ultimate drying.

   where h is the minimum thickness in inches.

4.2.1.2. CREEP

According to ACI committee 209 the creep coefficient $C(t,\tau)$ is given by

$$C(t,\tau) = K_S\, K_H\, K_h\, K_\tau \quad \frac{(t-\tau)^{0.6}}{10+(t-\tau)^{0.6}}\, C_U \tag{4.6}$$

where

t is the observation time in days.

τ is the age of concrete at loading in days .

C_u is the ultimate creep coefficient.

K_S is the slump correction factor.

K_h is the size correction factor.

K_H is the relative humidity correction factor.

K_τ is the age at loading correction factor.

The correction factors are determined as follows:

1. Slump:

   $K_S = 0.81 + 0.07S$

   where S is slump in inches.

2. Humidity:

   $K_H = 1.27 - 0.0067H \qquad H \geq 40$

   where H is percent relative ambient humidity.

3. Size:

   $K_h = 1.0 - 0.0167(sz - 6.0) \quad sz > 6.0$
   $K_h = 1.0 \quad sz \leq 6$

   where sz is the minimum thickness of the member in inches.

4. Age at loading:

   $K_\tau = 1.25\ \tau^{-0.118}$ for concrete which is moist cured for 7 days.

The standard conditions for which all the correction factors are assumed to 1.0 are as follows:

- Slump of 2.7 in.

- Ambient relative humidity of 40% or less.
- Minimum thickness of 6 in. or less.
- Loading age of 7 days for moist cured concrete.

4.2.1.3. STRENGTH

Compressive strength of concrete as a function of time is given by the following expression:

$$f_c'(t) = \frac{t}{a + bt} f_c'(28) \qquad (4.7)$$

where

t is the observation time in days.

a and b are constants.

$f_c'(28)$ is the cylinder strength of concrete at 28 days.

The ranges of a and b for the normal weight, sand light weight, and all light weight concretes (using both moist and steam curing and types I and III cement) are :

$a=0.50$ *to* 9.25

$b=0.67$ *to* 0.98

The modulus of elasticity of concrete is given by:

$$E_c(t) = 33\, w^{1.5} \sqrt{f_c'(t)} \quad psi \qquad (4.8)$$

where w is the weight density of concrete in pounds per cubic feet.

4.2.2. CEB-FIP RECOMMENDATIONS (1978)

The CEB-FIP procedure for evaluating creep and shrinkage strains in conjunction with the analytical expressions developed by Kristek et al. is described in the following sections.

Note that the method for evaluation of creep strain was revised in the new CEB-FIP model code released in 1990.

4.2.2.1. CREEP

The creep coefficient for plain concrete is given by:

$$\varphi(t,t_o) = \beta_a(t_o) + \varphi_d \beta_d(t - t_o) + \varphi_f \left[\beta_f(t) - \beta_f(t_o)\right] \tag{4.9}$$

where

t is the observation time.

t_o is the age of concrete at loading.

β_a is a function which represents initial irreversible creep strain.

β_d is a function expressing the development of delayed elasticity with time.

β_f is a function expressing the development of delayed plasticity with time.

φ_d is a coefficient representing delayed elasticity taken equal to 0.4.

φ_f is a coefficient representing the delayed plasticity.

If the ambient temperature differs greatly from 20^oC then the time is corrected for ambient temperature; each actual period of time Δt_m during which the average ambient temperature is T_m is converted into a fictitious period Δt

$$\Delta t = \frac{\alpha}{30} \sum_{0}^{m} (T_m + 10) \Delta t_m \tag{4.10}$$

where α is equal to 1.0 normal cement, 2.0 for rapid hardening and 3.0 for rapid hardening and high strength cement.

The function $\beta_a(t_o)$ is given by:

$$\beta_a(t_o) = 0.8 \ (1 - \frac{f_c'(t_o)}{f_c'(28)}) \tag{4.11}$$

$R_c(t_o)$ and $R_c(\infty)$ are the compressive strengths of concrete at times t_o and as $t \to \infty$ respectively. Kristek [128] gives the following expression for $\beta_a(t_o)$:

$$\beta_a(t_o) = 0.95\, t_o^{-0.3} - 0.1 \tag{4.12}$$

The coefficient of delayed plasticity φ_f is expressed as a product of two other coefficients.

$$\varphi_f = \varphi_{f1}\,\varphi_{f2} \tag{4.13}$$

$\varphi_f = \varphi_{f1}\,\varphi_{f2}\varphi_{f1}$ is a function of ambient humidity and ranges from 0.8 for concrete submerged in water to 3.0 for concrete exposed to very dry air , and φ_{f2} is a function of notional thickness d_f.

$$d_f = \lambda\frac{2A_c}{U_c} \quad mm \tag{4.14}$$

where A_c is the area of cross section of concrete and U_c is the perimeter length of cross section and λ is a humidity factor which varies from 30.0 for concrete submerged in water to 1.0 for concrete exposed to dry air. Kristek [128] provides the following functions for φ_{f2} and β_d.

$$\varphi_{f2} = 1.1089 + 0.8469e^{-.0027\,d_f} \tag{4.15}$$

$$\beta_d(t-t_o) = 0.28 + 0.5\tan^{-1}\left[0.011\,(t-t_o)^{\frac{2}{3}}\right] \tag{4.16}$$

Similarly the function for β_f is given by:

$$\beta_f(t) = 1 - e^{-(A_f\,t)^{B_f}} \tag{4.17}$$

$$A_f = 0.078e^{-1.22\log d_f} \tag{4.18}$$

$$B_f = 0.528e^{-0.13\log d_f} \tag{4.19}$$

4.2.2.2. SHRINKAGE

The shrinkage strain over the time interval $(t-\tau)$ is given by the following formula:

$$\varepsilon_s(t,\tau) = \varepsilon_{so}\left[\beta_s(t) - \beta_s(\tau)\right] \tag{4.20}$$

where

t is the age of concrete at observation time.

τ is the age of concrete at the beginning of time interval.

$\varepsilon_{so} = \varepsilon_{s1}\,\varepsilon_{s2}$

ε_{s1} depends on the ambient humidity.

ε_{s2} depends on the fictitious depth d_f.

β_s is a function of time and of fictitious depth d_f.

Again Kristek [128] has provided a set of analytical expressions to evaluate the above functions:

$$\varepsilon_{s2} = 0.7001 + 0.6292\ e^{-0.0046 d_f} \tag{4.21}$$

$$\beta_s(t) = 1 - e^{-(A_s t)^{B_s}} \tag{4.22}$$

$$A_s = 3.16 e^{-2.98 \log d_f} \tag{4.23}$$

$$B_s = 0.18 e^{0.49 \log d_f} \tag{4.24}$$

4.3. MATHEMATICAL FORMULATION OF CREEP

The constitutive relationship for a linear viscoelastic, aging material subject to a uniaxial stress is given by Volterra [143], as follows:

$$\varepsilon(t) = \int_0^t J(\tau, t-\tau) \frac{\partial \sigma(\tau)}{\partial \tau}\ d\tau \tag{4.25}$$

where $\varepsilon(t)$ is the strain at time t and $J(\tau, t-\tau)$ is the compliance function which represents the strain at time t caused by a unit constant stress that has been acting since time τ.

$$J(\tau, t-\tau) = \frac{\varepsilon^e + \varepsilon^c}{\sigma} = \frac{1}{E(\tau)} + C(\tau, t-\tau) \tag{4.26}$$

where $E(\tau)$ is the modulus of elasticity at age τ and $C(\tau, t-\tau)$ is the creep compliance function or specific creep. The creep strain at any time may therefore be expressed as

$$\varepsilon^c(t) = \int_0^t C(\tau, t-\tau) \frac{\partial \sigma(\tau)}{\partial \tau}\ d\tau \tag{4.27}$$

Direct evaluation of the above equation involves integration over the entire previous stress history. Such a solution is not feasible numerically as it requires a large data storage capacity on the computer.

It has been found that certain forms of mathematical approximations for the specific creep compliance function, while representing the creep curves accurately, do not need to store the entire stress history of the element. A formulation of this type based on expressing the creep compliance function as a Dirichlet series was developed by Kabir [48] based on the work of Zienkiewicz and Watson [151]. The creep compliance function given by Kabir is as follows:

$$C(\tau, t-\tau) = \sum_{i=1}^{m} a_i(\tau)\left(1 - e^{-(t-\tau)\lambda_i}\right) \tag{4.28}$$

Where $a_i(\tau)$ are scale factors depending on the age of loading τ and λ_i are exponential constants which control the shape of the logarithmic decaying creep curve. Note that Kabir also used a temperature shift function which is not included in the present formulation. The total creep strain at any time t is then given by:

$$\varepsilon^c(t) = \int_0^t \sum_{i=1}^{m} a_i(\tau)\left(1 - e^{-(t-\tau)\lambda_i}\right)\frac{\partial\sigma(\tau)}{\partial\tau}\, d\tau \tag{4.29}$$

Using a numerical integration scheme, the above equation is then developed into a recursive relation of the form given below:

$$\varepsilon^c(t_j) = \varepsilon^c(t_{j-1}) + \Delta\varepsilon^c(t_j) \tag{4.30}$$

The creep strain increment $\Delta\varepsilon^c(t_j)$ from time t_{j-1} to t_j can be evaluated by assuming that stress and material parameters do not change over the time interval Δt_j as described by Kabir [48].

Bazant and Wu [11] have described a scheme based on linear variation of stress and constant material properties. Ketchum [53] proposed a third scheme based on linear variation of both stress and material properties. All three schemes were implemented by Ketchum in the computer program SFRAME [53].

4.3.1. Determination of Coefficients to the Creep Compliance Function

As discussed earlier the Dirichlet series representation of the creep compliance function is given by:

$$C(\tau,t-\tau)=\sum_{i=1}^{m}a_i(\tau)\left(1-e^{-(t-\tau)\lambda_i}\right)$$

This function is completely defined after the constants m, $a_i(\tau)$ and λ_i have been determined. These constants are evaluated by the following procedure wherein the analytical expression given above is "fitted" to a creep curve which has been previously defined by experiment or predicted by a model such as that given by ACI-209 for a concrete loaded at age τ.

1. m and λ_i, $i=1,\ldots m$ are chosen on a trial basis.
2. Various times t_j, $j=1\ldots n$ are chosen such that $t_j \geq \tau$.
3. Values of the creep compliance function are read from the target curve $\tilde{C}(\tau,t_j-\tau)$ at times t_j.
4. The analytical expression of Dirichlet series is set equal to $\tilde{C}(\tau,t_j-\tau)$ at times t_j.

$$\sum_{i=1}^{m}a_i(\tau)\left(1-e^{-(t_j-\tau)\lambda_i}\right)=\tilde{C}(\tau,t_j-\tau) \tag{4.31}$$

This results in the following over determined system of equations:

$$\begin{bmatrix}\left(1-e^{-(t_1-\tau)\lambda_1}\right) & \cdots & \left(1-e^{-(t_1-\tau)\lambda_m}\right)\\ \vdots & & \vdots\\ \left(1-e^{-(t_n-\tau)\lambda_1}\right) & \cdots & \left(1-e^{-(t_n-\tau)\lambda_m}\right)\end{bmatrix}\begin{bmatrix}a_1(\tau)\\ \vdots\\ a_m(\tau)\end{bmatrix}=\begin{bmatrix}\tilde{C}(\tau,t_1-\tau)\\ \vdots\\ \tilde{C}(\tau,t_n-\tau)\end{bmatrix}$$

$$\mathbf{A}_{n\times m}\mathbf{a}_{m\times 1}=\mathbf{b}_{n\times 1} \tag{4.32}$$

These equations are solved for the $a_i(\tau)$ so that a least squares fit is obtained to the target curve.

$$\mathbf{A}^{\mathrm{T}}(\mathbf{Aa}) = \mathbf{A}^{\mathrm{T}}(\mathbf{b})$$

$$\mathbf{a} = (\mathbf{A}^{\mathrm{T}}\mathbf{A})^{-1}(\mathbf{A}^{\mathrm{T}}\mathbf{b}) \tag{4.33}$$

5. A different set of m and λ_i are chosen and steps 1 through 4 are repeated until the following criteria are satisfied.

   (a) The least squares error is minimized.

   (b) $a_i(\tau)$ for which the ultimate creep strain is about 4/3 of the 1 year creep strain.

   (c) The contribution of all $a_i(\tau)\left(1-e^{-(t_j-\tau)\lambda_i}\right)$ are nearly equal.

6. Repeat the process for several values of τ and determine corresponding sets of $a_i(\tau)$. Linear interpolation is used to determine $a_i(\tau)$ for any intermediate age.

4.4. NUMERICAL EXAMPLES

The creep strain integration schemes used in the present study are based on the work of Kabir [48] and Ketchum [53]. However the numerical procedure has been modified to work for a three dimensional fiber beam-column element. Furthermore a new convergence acceleration scheme based on Steffenson's method [18] has been added. This made it necessary that each of the three integration schemes be tested numerically against previous work. These are as follows:

- Integration type 1: Stress and material properties constant over each time step.
- Integration type 2: Linear variation of stress and constant material properties over each time step.
- Integration type 3: Linear variation of stress and material properties over the time step.

These schemes were tested on three different examples after Ketchum [53]. The test structure consists of a cantilever beam, 120" long, 9" wide and 22" deep. The fiber beam-column element described in Chapter 6. is used to model the beam. The element has two controls sections, one at each end. The cross section is divided into 44 concrete fibers over its depth and width. The concrete strength at 28 days is taken as 5000 psi and the ultimate

creep coefficient is assumed to be 3.0. The beam is loaded 30 days after casting and its response is tracked upto 1230 days. The three analysis models are described below:

4.4.1. BEAM A; PURE CREEP; FIG. 4.03

A load of 10000 lb. is applied at the free end of the cantilever on day 30 and then removed on day 630. During this period the beam is subjected to a constant state of stress and all three integration schemes should give the same results.

The variation of cantilever tip displacement over time is shown in Fig 4.03. As expected all three integration schemes yield same results.

4.4.2. BEAM B; PURE RELAXATION; FIG. 4.04

The vertical displacement of the free end of the cantilever is controlled; it is subjected to an imposed displacement of 0.1 in. upward on day 30 and held in this position until day 630, when the applied displacement is reversed. The total strain remains constant during each time step.

The bending moment at support A is plotted against time in Fig. 4.04. Note that integration schemes 2 and 3 give slightly higher results (3%) during the period stretching from day 30 to 630. More importantly, integration scheme 1 does not oscillate as reported earlier by Ketchum.

4.4.3. BEAM C; MOMENT REDISTRIBUTION; FIG. 4.05

A 10000 lb. load is applied to end B of the beam as shown in Fig. 4.05 on day 30. Immediately after the application of load, the rotation at end B is locked. The load is removed on day 30.

The variation of the bending moment at the support section A is shown in Fig. 4.05. Same results are obtained by all three schemes and agree with the results reported by Ketchum.

In addition the vertical displacement at the cantilever tip B is plotted versus time in Fig. 4.06. Note that results obtained from scheme 1 are close to the other two schemes and do not show any oscillations as reported earlier by Ketchum.

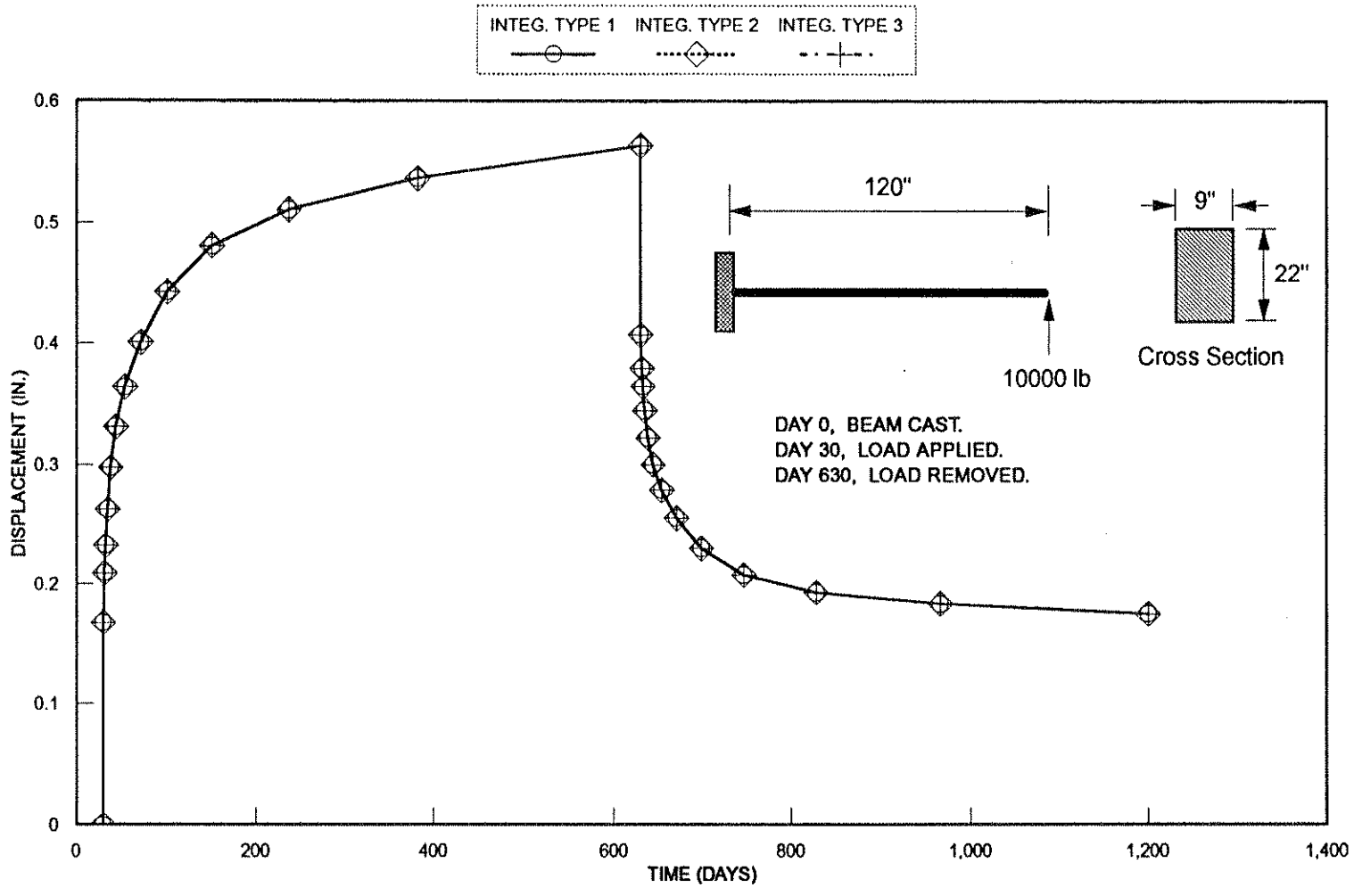

FIG. 4.03 COMPARISON OF VARIOUS CREEP INTEGRATION SCHEMES
PURE CREEP; BEAM MODEL A, KETCHUM 1986 .

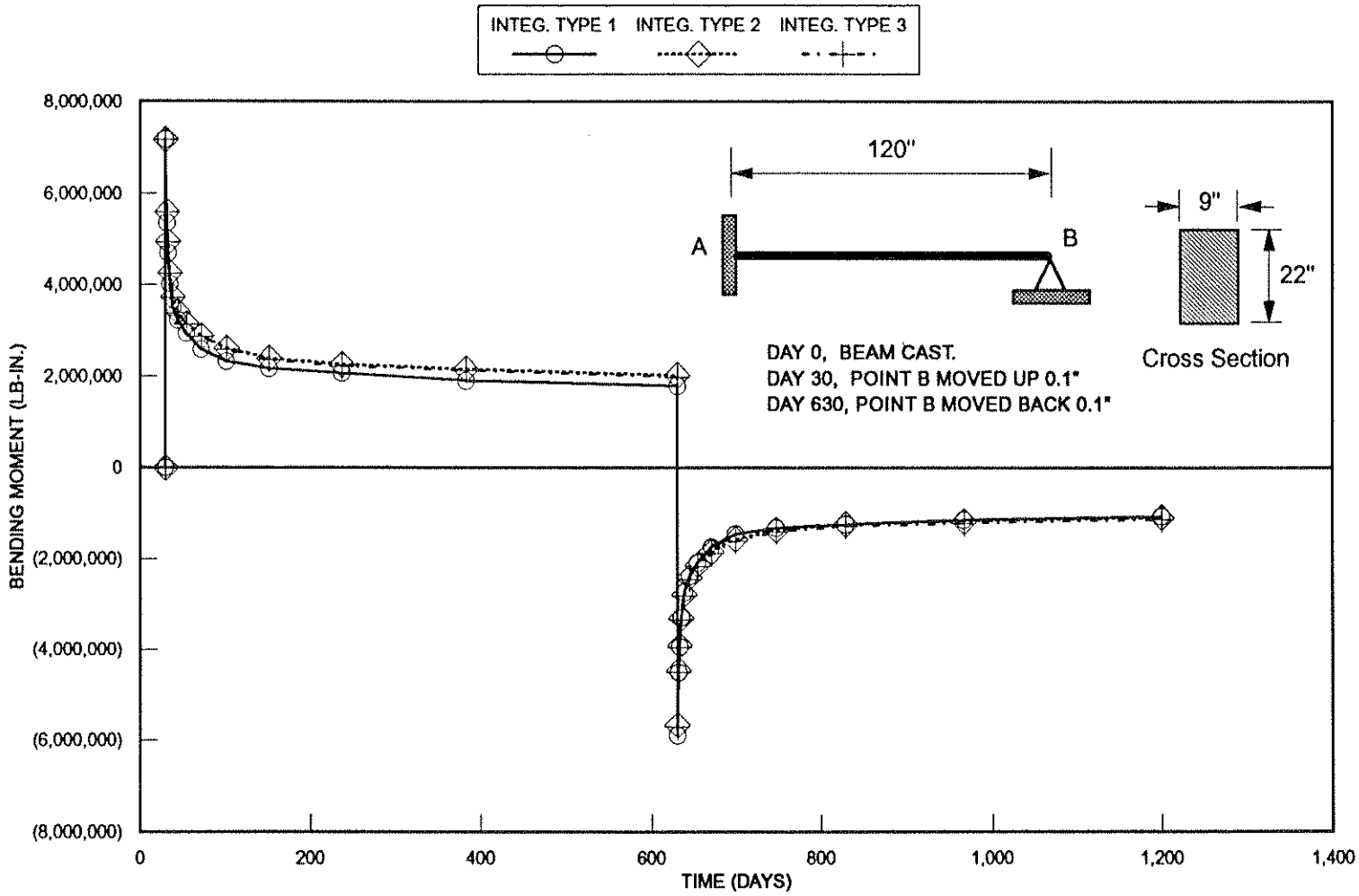

FIG. 4.04 COMPARISON OF VARIOUS CREEP INTEGRATION SCHEMES
PURE RELAXATION; BEAM MODEL B, KETCHUM 1986 .

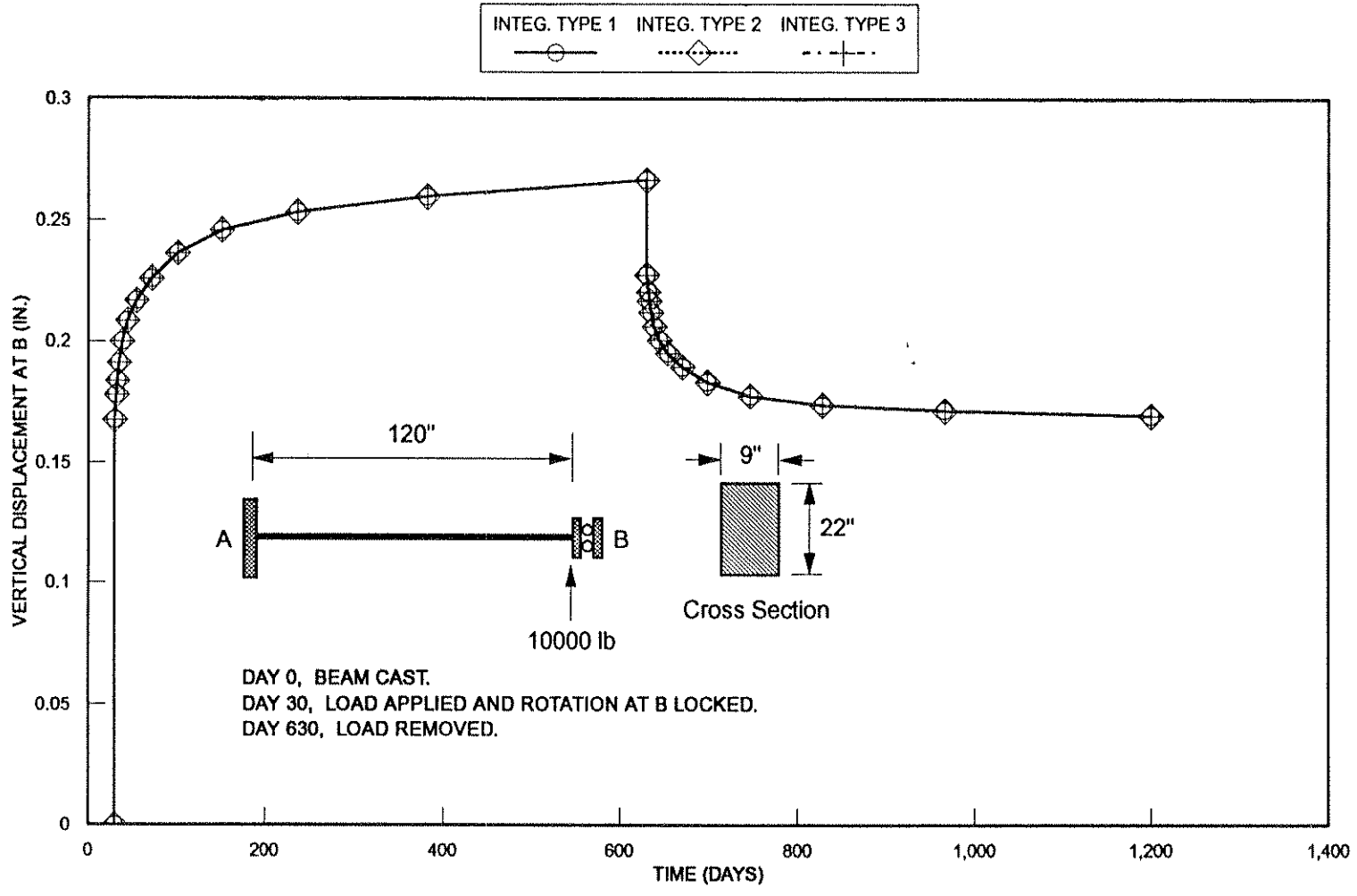

FIG. 4.05 COMPARISON OF VARIOUS CREEP INTEGRATION SCHEMES
MOMENT REDISTRIBUTION; BEAM MODEL C, KETCHUM 1986.

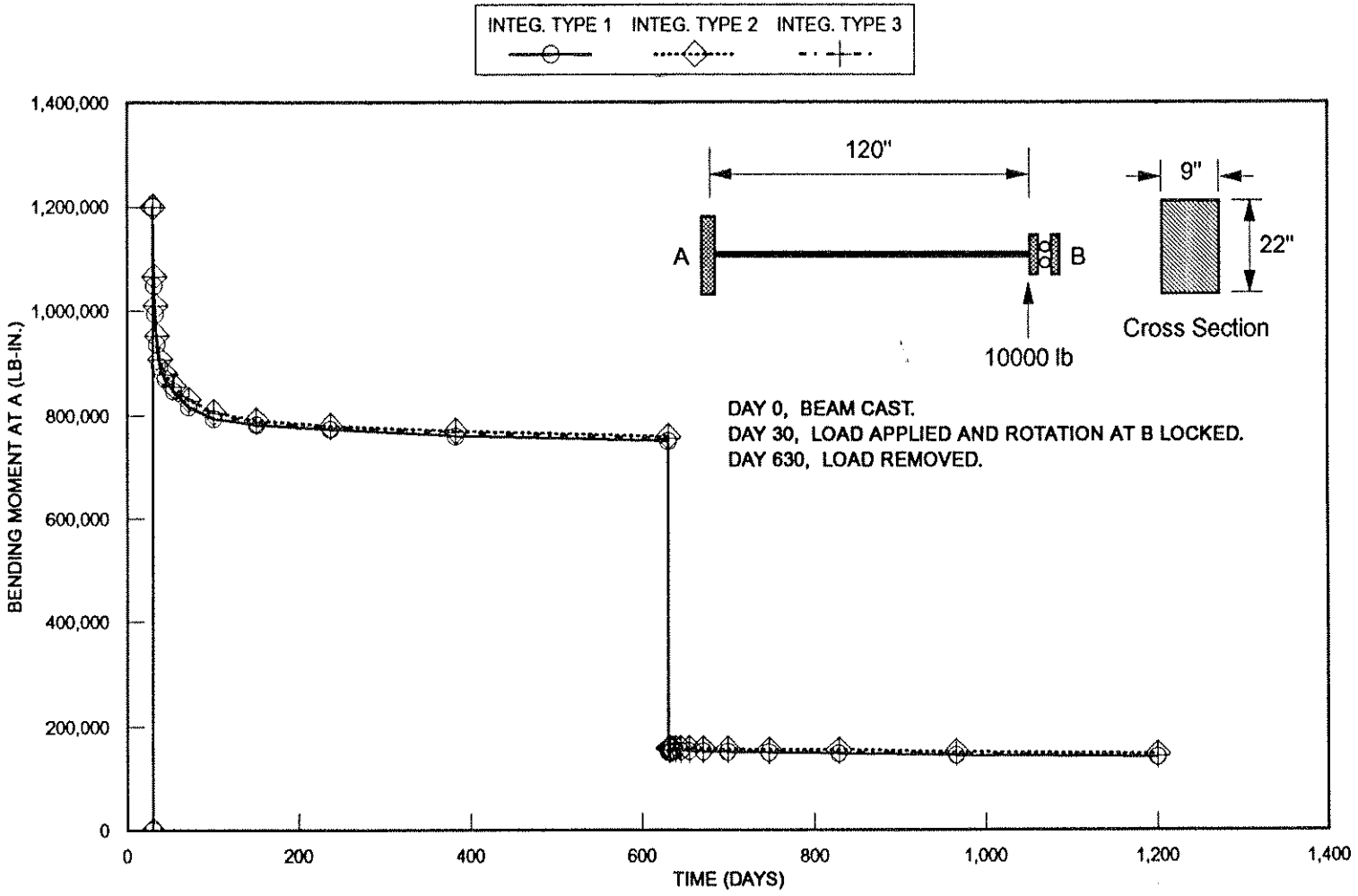

FIG. 4.06 COMPARISON OF VARIOUS CREEP INTEGRATION SCHEMES
MOMENT REDISTRIBUTION; BEAM MODEL C, KETCHUM 1986 .

5. SOLUTION STRATEGIES FOR NONLINEAR AND TIME DEPENDENT ANALYSIS

5.1. GENERAL

One of the major objectives of this study was to develop procedures for the analysis of segmentally erected cable stayed bridges with steel or prestressed concrete decks through the construction sequence and at various stages of load up to the ultimate state.

The procedure must be able to account for time dependent effects of creep and shrinkage in concrete and relaxation of prestressing tendons. In addition, it should be able to keep track of the response of a changing structural configuration which may include addition or removal of deck segments, installation and stressing of prestressing tendons, placement or removal and tensioning or re tensioning of both permanent and auxiliary cable-stays.

Further the analytical technique should allow for a material and geometry nonlinear analysis of the structure through various loading stages. The inclusion of geometric nonlinearity is required since cable stayed bridges exhibit geometric nonlinearity even at service load level.

The analysis techniques and the corresponding numerical algorithms presented in this chapter are directed at achieving the above mentioned objectives.

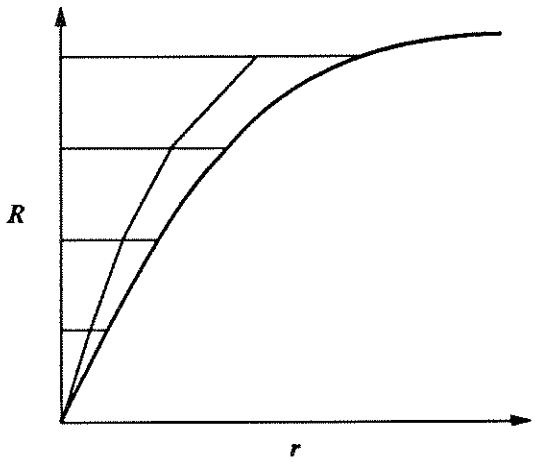

INCREMENTAL LOAD METHOD; NO EQUILIBRIUM CORRECTIONS.

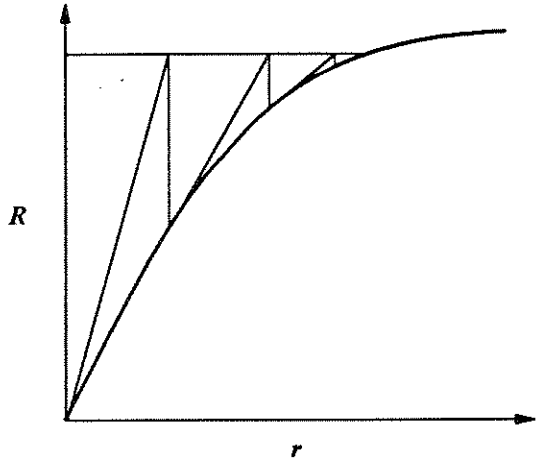

ITERATIVE METHOD; TANGENT STIFFNESS.

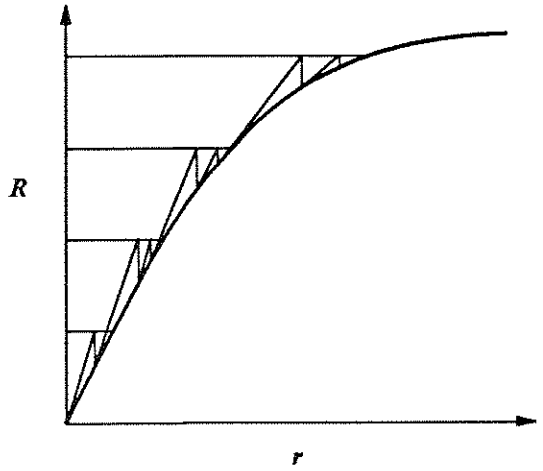

STEP-ITERATIVE METHOD.

FIG. 5.01 SOLUTION METHODS FOR NONLINEAR EQUILIBRIUM EQUATIONS.

5.2. NONLINEAR ANALYSIS

The available solution strategies for nonlinear analysis can be divided into three main categories.

- Step by step methods.
- Iterative methods.
- Step-iterative methods.

Each of these techniques and its relative merits or shortcomings are described at length in the succeeding sections and illustrated in Fig. 5.01.

5.2.1. STEP BY STEP METHODS

In this method the external load is applied in several small steps. The stiffness matrix is re-formed at each load step and the response is obtained *without iteration*. The solution sequence is as follows:

1. Divide the external load into n load increments

   $$\Delta \mathbf{R} = \frac{1}{n} \mathbf{R}$$

2. For each load step, form the tangent stiffness matrix $\mathbf{K}_T^j$.

3. Find the displacement increment

   $$\Delta \mathbf{r}^j = (\mathbf{K}_T^j)^{-1} \Delta \mathbf{R}$$

   where j is the load step count.

4. Update the current displacement.

   $$\mathbf{r}^j = \mathbf{r}^{j-1} + \Delta \mathbf{r}^j$$

5. Repeat steps 2 to 3 n times.

Note that equilibrium is not necessarily satisfied at the end of each step and the computed response may deviate considerably from the true response. This problem can be remedied to some degree by selecting smaller load steps.

The solution can be further improved by adding a state determination phase at the end of each load step and hence calculating the unbalanced load for that step.

$$\Delta \mathbf{R}_u^{\,j} = j\Delta \mathbf{R} - \mathbf{R}_i^{\,j} \tag{5.1}$$

where $\mathbf{R}_i$ is the internal resisting load vector. The unbalanced load or residual is then added to the load increment to be applied in the next step.

$$\Delta \mathbf{r}^j = (\mathbf{K}_T^{\,j})^{-1} (\Delta \mathbf{R} + \Delta \mathbf{R}_u^{\,j-1}) \tag{5.2}$$

5.2.2. ITERATIVE METHODS

Iterative methods may be classified as Newton-Raphson, modified Newton-Raphson and Quasi Newton methods.

NEWTON-RAPHSON METHOD

The Newton-Raphson scheme for solution of nonlinear problems is well known. The method converges rapidly at a quadratic rate provided the initial solution is within the zone of attraction. The total external load is applied in one step and the solution is obtained iteratively by solving a series of linear problems. The iterative sequence is as follows:

1. Form tangent stiffness $\mathbf{K}_T^{\,j}$ in the current state.
2. Find displacement increment by solving equilibrium equations

   $\Delta \mathbf{r}^j = (\mathbf{K}_T^{\,j})^{-1}(\mathbf{R}_e - \mathbf{R}_i^{\,j})$

   $\mathbf{r}^{j+1} = \mathbf{r}^j + \Delta \mathbf{r}^j$

   $\mathbf{R}_e$ is the total external nodal load vector, $\mathbf{R}_i$ is the internal resisting load vector and j is the iteration number.
3. Determine new state of the structure. The new internal resisting load vector is a function of the current displaced state of the structure.

   $\mathbf{R}^{j+1} = \lambda(\mathbf{r}^{j+1})$
4. Calculate the unbalanced load vector. Check convergence by comparing some norm of the unbalanced load vector with a given tolerance. If converged stop iteration.

$$\left\|\mathbf{R}_e - \mathbf{R}^{j+1}\right\| \leq \varepsilon$$

5. If not converged then repeat steps 1 to 4.

The Newton-Raphson process, despite its rapid convergence has some serious shortcomings. For example a new stiffness matrix has to be formed and refactored at each iteration step. In addition, the load is kept constant during the iteration and if the strength of the structure is less than that required by the applied load then the solution will never converge.

MODIFIED NEWTON-RAPHSON METHODS

Some of the drawbacks of the Newton-Raphson method can be avoided by using a constant stiffness matrix. Variations on the NR scheme that do not refresh the stiffness matrix at each iteration are known as modified Newton methods, Powell and Simons [107]. The variable tangent stiffness matrix is replaced by a constant approximation.

$$\mathbf{K}^i_T \approx \overline{\mathbf{K}}_T \tag{5.3}$$

A number of choices exist here. For example in the initial stiffness iteration, the initial stiffness matrix $\mathbf{K}_T^0$ is used for all displacement increment calculations.

$$\overline{\mathbf{K}}_T = \mathbf{K}^0_T \tag{5.4}$$

In constant stiffness iteration the stiffness matrix is updated only at the beginning of each load increment and then kept constant during the iteration.

In general, modified Newton-Raphson methods have a relatively slower convergence rate, Zienkiewicz and Taylor [152], and are not recommended for highly nonlinear structures.

QUASI-NEWTON METHODS

Quasi-Newton methods are based on the idea the stiffness matrix should be modified at each step so that it is the secant stiffness matrix for displacements calculated in the previous step.

$$\Delta \mathbf{r}^j = (\mathbf{K}_s^j)^{-1} \mathbf{R}_u^j \tag{5.5}$$

where $\mathbf{K}_s^j$ is such that

$$\Delta \mathbf{r}_{j-1} = (\mathbf{K}_s^j)^{-1}(\mathbf{R}_u^{j-1} - \mathbf{R}_u^j) \tag{5.6}$$

$\mathbf{R}_u^{j-1}$ and $\mathbf{R}_u^j$ are the unbalanced forces at the beginning of step $j-1$ and j.

Note that for systems with more than one degree of freedom the determination of the stiffness matrix $\mathbf{K}_s^j$ is not unique. Many different forms of $\mathbf{K}_s^j$ can satisfy the Eq. 5.6 and a number of alternatives are used in practice.

The BFGS method (Broyden-Fletcher-Goldfarb-Shanno) [17] is widely used in practice. The updated matrix is symmetric and positive definite, Zienkiewicz [152], and can be inverted by applying the Shermann-Morrison formula, Dennis and More [27].

The stiffness matrix is modified by the addition of a rank two matrix, Simons [127].

$$\mathbf{K}_s^j = \mathbf{K}_s^{j-1} + G_1 \mathbf{u}_1 \mathbf{u}_1^T - G_2 \mathbf{u}_2 \mathbf{u}_2^T \tag{5.7}$$

where

$$\mathbf{u}_1 = \frac{(\mathbf{R}_u^{j-1} - \mathbf{R}_u^j)}{\sqrt{(\mathbf{R}_u^{j-1} - \mathbf{R}_u^j)^T (\mathbf{R}_u^{j-1} - \mathbf{R}_u^j)}}$$

$$G_1 = \frac{(\mathbf{R}_u^{j-1} - \mathbf{R}_u^j)^T (\mathbf{R}_u^{j-1} - \mathbf{R}_u^j)}{(\mathbf{R}_u^{j-1} - \mathbf{R}_u^j)^T \Delta \mathbf{r}^{j-1}}$$

A stiffness of magnitude G_1 is added in the direction $\mathbf{u}_1$, which is the change in the resisting force over the last iteration.

Similarly

$$\mathbf{u}_2 = \frac{(\mathbf{R}_u^{j-1})}{\sqrt{(\mathbf{R}_u^{j-1})^T (\mathbf{R}_u^{j-1})}}$$

$$G_2 = \frac{(\mathbf{R}_u^{j-1})^T (\mathbf{R}_u^{j-1})}{(\mathbf{R}_u^{j-1})^T \Delta \mathbf{r}^{j-1}}$$

A stiffness of magnitude G_2 is subtracted from the direction of vector $\mathbf{u}_2$ which is the direction of unbalanced force in the previous iteration.

5.2.3. STEP-ITERATIVE METHODS

The step by step and iterative methods described above may be combined to yield an improved algorithm. The total external load is divided into load increments. For each load increment a solution is obtained by iteration. If the solution converges then the unbalance is reduced to zero at the end of the load step and the computed response is exact.

5.3. PRESENT STUDY

Three different solution schemes based on the step-iterative method were used in the present study.

- Load control wherein load increments are applied to the structure and its displacement response evaluated.
- Displacement control in which there is a progressive increase in the displacement at a specified degree of freedom and the corresponding change in the load applied to the structure is determined.
- Time control or time step analysis involves determining the response of a concrete structure as time marches forward through predetermined intervals.

This allows the engineer considerable flexibility in the choice of analytical tools for solving the usual type of problems encountered in the design and analysis of cable-stayed bridges.

5.3.1. LOAD CONTROL

A typical load control strategy works by applying known or controlled increments of load to the structure and solving for the displaced configuration of the structure which will hold the external loads in equilibrium.

The strategy used in the present study is a combination of incremental and iterative methods discussed earlier. The algorithm used in the computer program CALBRG is as follows:

Given:

- An equilibrium or converged state of the structure. This includes structure displacements, element deformations, element actions and structure resisting forces.
- External load pattern vector $\mathbf{R}_{ptn}$.
- A load pattern multiplier m.
- Number of load steps *numstp*.

  Thus the total load applied to the structure is $numstp(m\mathbf{R}_{ptn})$.
- Convergence tolerances:

  Force tolerance for each solution step *tolf*.

  Force tolerance for stiffness update *tolk*.
- Maximum number of iterations allowed in each load step, *numit*.

Solution Procedure

- Set flags.

  converge=.true.

  revise=.true.

Start load step loop

- For k=1,2,.....*numstp*
- Update the current load vector

  $\mathbf{R}_e^{\,k} = m\mathbf{R}_{ptn} + \mathbf{R}_e^{\,k-1}$

Start iteration loop

- For j=1,2,.....*maxit*
- If (*revise=.true.*) then

  Form tangent stiffness matrix $\mathbf{K}_T^{\,j}$.

  end if
- Solve for incremental displacements

  $(\mathbf{K}_T^{\,j})\Delta\mathbf{r}^j = (\mathbf{R}_e^{\,k} - \mathbf{R}_i^{\,j-1})$

- Update current displacements

  $\mathbf{r}^j = \mathbf{r}^{j-1} + \Delta\mathbf{r}^j$

- Determine new state of the structure.

  Path dependent $\mathbf{R}_i^{\ j} = \lambda(\mathbf{r}^{j-1}, \mathbf{r}^j)$

  Path independent $\mathbf{R}_i^{\ j} = \lambda(\mathbf{r}^k, \mathbf{r}^j)$

- Find unbalanced load vector

  $\mathbf{R}_u^{\ j} = \mathbf{R}_e^{\ k} - \mathbf{R}_i^{\ j}$

- Check for convergence:

  if $\left(\left\|\mathbf{R}_u^{\ j}\right\| \le tolf\right)$ then

  set $converge =. true.$

  save current state as converged state

  exit iteration loop

  else

  set $converge =. false.$

  end if

- Check if stiffness refresh is required in next cycle

  if $\left(\left\|\mathbf{R}_u^{\ j}\right\| \le tolk\right)$ then

  set $revise =. false.$

  end if

End iteration loop

- if $(converge =. false.)$ then

  print " maximum number of iteration exceeded, no convergence"

  stop program

  end if

End load loop

5.3.2. DISPLACEMENT CONTROL

The basic idea behind displacement controlled solution strategies is to specify some measure of displacement increments and then to solve for the magnitude of the external load whose pattern is previously defined. Displacement control procedures are very effective for solution of structures which exhibit strain softening.

Haisler and Stricklin [38] describe a step by step displacement controlled solution strategy, Fig. 5.02. The displacement is increased by a specified amount in each step. The magnitude of load required to reach this displacement is initially unknown. In each solution step the unbalanced load is applied first and then the external load pattern is scaled to reach the specified displacement. Since no iterations are carried out, a substantial unbalance may be carried forward from one step to the other. Mathematically the problem may be expressed as n x n system of equations.

$$\mathbf{K}\,\Delta\mathbf{r} = \alpha\,\Delta\mathbf{R}_e + \Delta\mathbf{R}_u \tag{5.8}$$

The incremental displacement vector $\Delta\mathbf{r}$ consists of a specified displacement increment Δr_a and (n-1) unknown displacements $\Delta\mathbf{r}_b$.

$$\Delta\mathbf{r} = \begin{bmatrix} \Delta r_a \\ \Delta\mathbf{r}_b \end{bmatrix} \tag{5.9}$$

Eq. 5.8 is partitioned as follows:

$$\begin{bmatrix} k_{aa} & \mathbf{k}_{ab} \\ \mathbf{k}_{ba} & \mathbf{k}_{bb} \end{bmatrix} \begin{bmatrix} \Delta r_a \\ \Delta\mathbf{r}_b \end{bmatrix} = \alpha \begin{bmatrix} \Delta R_{ea} \\ \Delta\mathbf{R}_{eb} \end{bmatrix} + \begin{bmatrix} \Delta R_{ua} \\ \Delta\mathbf{R}_{ub} \end{bmatrix}$$

Rearranging we have:

$$\begin{bmatrix} \mathbf{k}_{ab} & -\Delta R_{ea} \\ \mathbf{k}_{bb} & -\Delta\mathbf{R}_{eb} \end{bmatrix} \begin{bmatrix} \Delta\mathbf{r}_b \\ \alpha \end{bmatrix} = \begin{bmatrix} \Delta R_{ua} \\ \Delta\mathbf{R}_{ub} \end{bmatrix} - \Delta r_a \begin{bmatrix} k_{aa} \\ \mathbf{k}_{ba} \end{bmatrix} \tag{5.10}$$

This equation is then solved for α and $\Delta\mathbf{r}_b$.

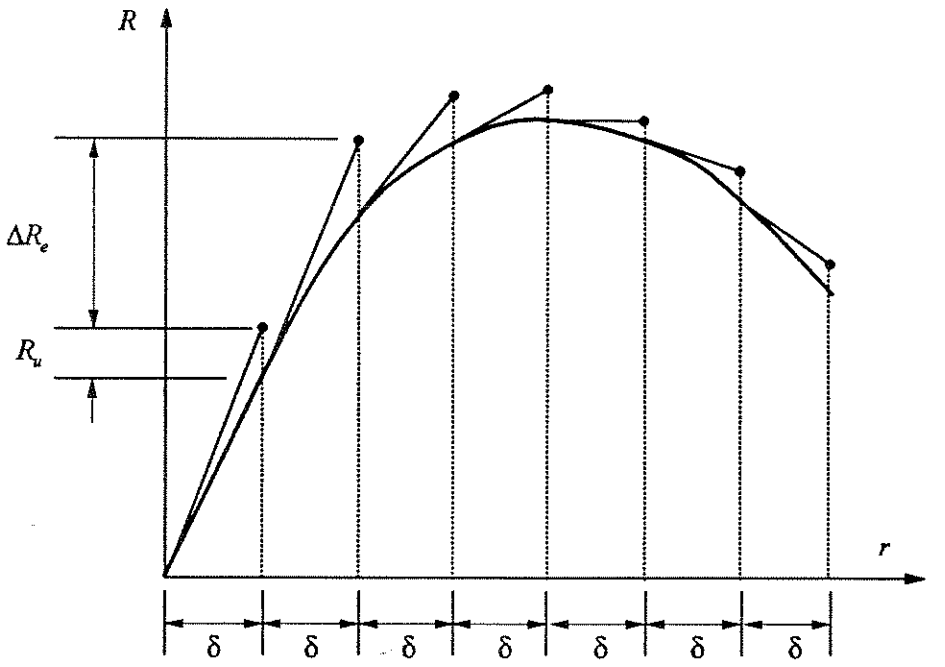

FIG. 5.02 DISPLACEMENT CONTROL STRATEGY OF HAISLER & STRICKLEN, 1977.

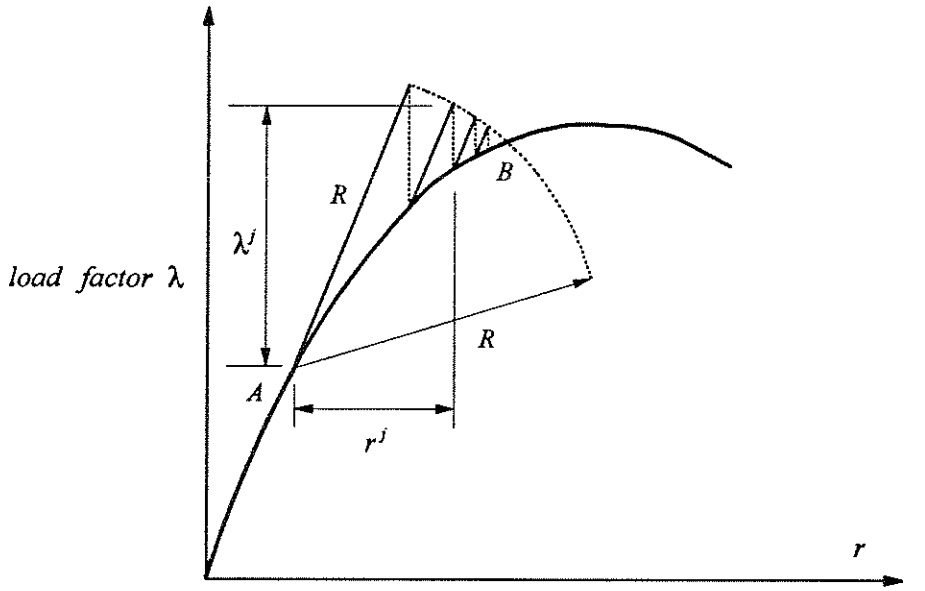

FIG. 5.03 ARC LENGTH METHOD.
RIK'S METHOD WITH MODIFIED NEWTON-RAPHSON TECHNIQUE; CRISFIELD, 1981.

Batoz and Dahtt [10] provided a more elegant solution of Eq. 5.8. They solved the equilibrium equations independently for displacements due to the unbalanced load and due to an arbitrary magnitude of the external load.

$$\Delta \mathbf{r}_u = \mathbf{K}^{-1}\Delta \mathbf{R}_u$$
$$\Delta \mathbf{r}_e = \mathbf{K}^{-1}\Delta \mathbf{R}_e \tag{5.11}$$

The displacement due to external loads is scaled such that when combined with the displacement caused by unbalanced load, it satisfies the following equation.

$$\Delta \mathbf{r} = \Delta \mathbf{r}_u + \alpha \Delta \mathbf{r}_e$$

$$\begin{bmatrix} \Delta r_a \\ \Delta \mathbf{r}_b \end{bmatrix} = \begin{bmatrix} \Delta r_{ua} \\ \Delta \mathbf{r}_{ub} \end{bmatrix} + \alpha \begin{bmatrix} \Delta r_{ea} \\ \Delta \mathbf{r}_{eb} \end{bmatrix} \tag{5.12}$$

The load factor α is then simply given by:

$$\alpha = \frac{\Delta r_a - \Delta r_{ua}}{\Delta r_{ea}} \tag{5.13}$$

Batoz and Dhatt further note that it is not necessary for the tangent stiffness matrix to be positive definite, provided it is not singular.

Powell and Simons [107] presented a general form of the Batoz and Dhatt procedure wherein they introduced the idea of a generalized scalar displacement which is controlled during the solution process. They also demonstrated that Haisler and Stricklen procedure is a special case of this general formulation.

The arc length method of Riks [109] shown in Fig. 5.03, which was later modified and improved by Crisfield [25] is a special of type of displacement control method wherein the Euclidean norm or magnitude of the displacement vector is kept constant during a step.

$$(\Delta \mathbf{r}^T \Delta \mathbf{r})^{1/2} = \Delta l \tag{5.14}$$

The scalar quantity Δl defines the arc length. This method is equally effective for structures which exhibit a snap through or a snap back buckling phenomenon, Fig. 5.04. Note that a

single degree of freedom displacement control strategy will not work for snap back type of response.

The present study uses the displacement control strategy described by Powell et al. as applied to a single degree of freedom, Fig. 5.05. The procedure is described in some detail in the next sections.

A solution strategy may be divided into two distinct phases:

- Advancing Phase: An initial load increment is selected.
- Correction Phase: Iteration until the unbalances are sufficiently reduced.

ADVANCING PHASE:

Solve for displacement increments due to unbalanced load $\Delta \mathbf{R}_{uo}$ leftover from previous iteration sequences and due to an arbitrary magnitude of external load vector $\Delta \mathbf{R}_e$.

$$\begin{aligned} \Delta \mathbf{r}_u &= \mathbf{K}_T^{-1} \Delta \mathbf{R}_{uo} \\ \Delta \mathbf{r}_e &= \mathbf{K}_T^{-1} \Delta \mathbf{R}_e \end{aligned} \tag{5.15}$$

The two displacements are combined to give

$$\Delta \mathbf{r} = \Delta \mathbf{r}_u + \alpha \, \Delta \mathbf{r}_e \tag{5.16}$$

Define a vector $\mathbf{b}_a$ such that

$$\begin{aligned} \Delta r_a &= \mathbf{b}_a^T \Delta \mathbf{r} \\ &= \delta \end{aligned} \tag{5.17}$$

Where δ is the magnitude of controlled displacement increment. Note that $\mathbf{b}_a$ contains zeros except for unity at location a. Multiply both sides of Eq. 5.16 by $\mathbf{b}_a^T$.

$$\begin{aligned} \mathbf{b}_a^T \Delta \mathbf{r} &= \mathbf{b}_a^T (\Delta \mathbf{r}_u + \alpha \, \Delta \mathbf{r}_e) \\ \delta &= \mathbf{b}_a^T (\Delta \mathbf{r}_u + \alpha \, \Delta \mathbf{r}_e) \end{aligned} \tag{5.18}$$

Solving for α we have:

$$\alpha = \frac{\delta - \mathbf{b}_a^T \Delta \mathbf{r}_u}{\mathbf{b}_a^T \Delta \mathbf{r}_e} \tag{5.19}$$

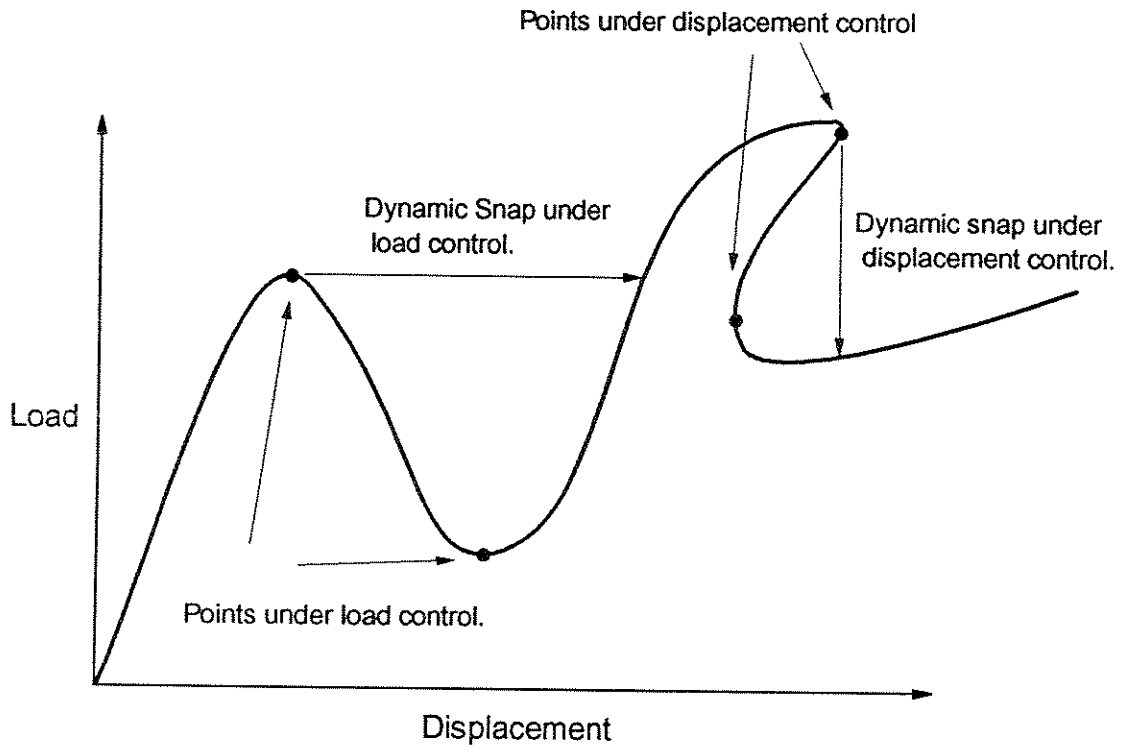

FIG. 5.04 SNAP BUCKLING; CRISFIELD, 1981.

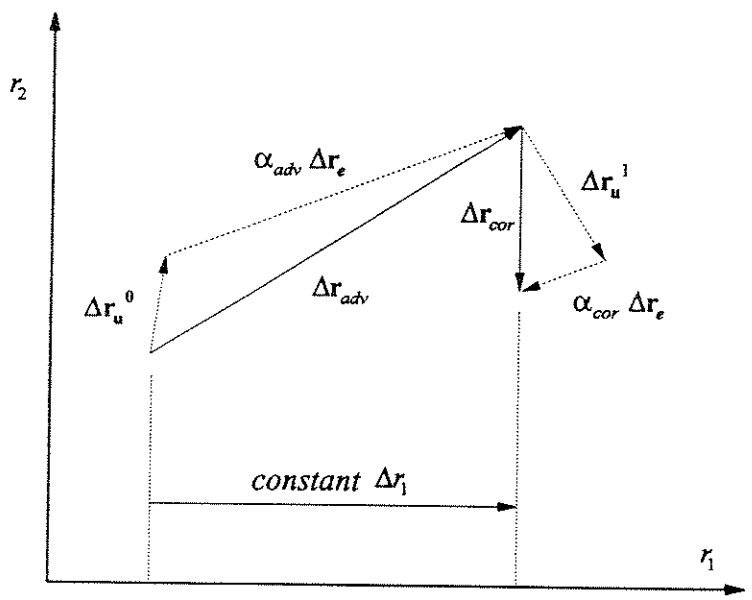

FIG. 5.05 DISPLACEMENT CONTROL STRATEGY OF POWELL AND SIMONS, 1981.
ADVANCING AND CORRECTING PHASES IN THE DISPLACEMENT SPACE.
FOR A TWO DEGREE OF FREEDOM SYSTEM.

CORRECTING PHASE:

Again determine the two displacement increments.

$$\Delta \mathbf{r}_u = \mathbf{K}_T^{-1} \Delta \mathbf{R}_u$$
$$\Delta \mathbf{r}_e = \mathbf{K}_T^{-1} \Delta \mathbf{R}_e \tag{5.20}$$

However, in the correcting phase, in order to keep the controlled displacement constant, the following condition is imposed.

$$\Delta r_a = \mathbf{b}_a^T \Delta \mathbf{r}$$
$$= 0 \tag{5.21}$$

Hence the scaling factor for adjusting the external load vector is given by:

$$\alpha = -\frac{\mathbf{b}_a^T \Delta \mathbf{r}_u}{\mathbf{b}_a^T \Delta \mathbf{r}_e} \tag{5.22}$$

Iteration continues until the unbalances are substantially reduced.

ALGORITHM FOR DISPLACEMENT CONTROL STRATEGY

The algorithm used in the computer program CALBRG is as follows:

GIVEN:

- An equilibrium or converged state of the structure. This includes structure displacements, element deformations, element actions and structure resisting forces.
- External load pattern vector $\mathbf{R}_{ptn}$.
- Number of displacement steps *numstp*.
- Controlled degree of freedom defined by node number and degree of freedom number.
- Magnitude of displacement increment δ
- Convergence tolerances:

  Force tolerance for each solution step *tolf*.

  Force tolerance for stiffness update *tolk*.
- Maximum number of iterations allowed in each load step, *numit*.

SOLUTION PROCEDURE

- Set flags.

  converge=.true.

  revise=.true.

- Generate the vector $\mathbf{b}_a$, it contains zeroes except unity at location a.

- Generate external load vector of arbitrary magnitude

  $\Delta \mathbf{R}_e = \mu \mathbf{R}_{ptn}$

  where μ is a small number

Start displacement step loop

- For k=1,2,.....*numstp*

Start iteration loop

- For j=1,2,.....*maxit*
- If (*revise=.true.*) then

  Form tangent stiffness matrix $\mathbf{K}_T{}^j$.

  end if
- Solve for incremental displacements due to unbalanced loads

  $\Delta \mathbf{r}_u{}^j = (\mathbf{K}_T{}^j)^{-1}(\mathbf{R}_u{}^{j-1})$
- Solve for incremental displacements due to external load pattern.

  $\Delta \mathbf{r}_e{}^j = (\mathbf{K}_T{}^j)^{-1}(\Delta \mathbf{R}_e)$
- If (*j=1*) then

  $\Delta = \delta$

  else

  $\Delta = 0$

  end if
- Calculate scaling factor.

$$\alpha = \frac{\Delta - \mathbf{b}_a^T \Delta \mathbf{r}_u^j}{\mathbf{b}_a^T \Delta \mathbf{r}_e^j}$$

- Determine total incremental displacements.

  $$\Delta \mathbf{r}^j = \Delta \mathbf{r}_u^j + \alpha \, \Delta \mathbf{r}_e^j$$

- Update current displacements.

  $$\mathbf{r}^j = \mathbf{r}^{j-1} + \Delta \mathbf{r}^j$$

- Update current displacements and external nodal loads

  $$\mathbf{R}_e^j = \mathbf{R}_e^{j-1} + \alpha \, \Delta \mathbf{R}_e$$

- Determine new state of the structure.

  Path dependent $\mathbf{R}_i^j = \lambda(\mathbf{r}^{j-1}, \mathbf{r}^j)$

  Path independent $\mathbf{R}_i^j = \lambda(\mathbf{r}^k, \mathbf{r}^j)$

- Find unbalanced load vector

  $$\mathbf{R}_u^j = \mathbf{R}_e^j - \mathbf{R}_i^j$$

- Check for convergence:

  if $\left(\left\|\mathbf{R}_u^j\right\| \le tolf\right)$ then

  set $converge = .true.$

  save current state as converged state

  exit iteration loop

  else

  set $converge = .false.$

  end if

- Check if stiffness refresh is required in next cycle

  if $\left(\left\|\mathbf{R}_u^j\right\| \le tolk\right)$ then

  set $revise = .false.$

  end if

End iteration loop

- if $(converge =. false.)$ then

    print " maximum number of iteration exceeded, no convergence"

    stop program

  end if

End displacement loop

5.3.3. TIME STEP ANALYSIS

The state of a concrete structure changes with time because of creep and shrinkage strains and due to the relaxation of stress in prestressing tendons if any. Deflections may increase and bending moments are redistributed. The purpose of time step analysis is to predict the state of the structure at any given time during the life of the structure, both during construction and after completion.

This type of analysis carries special significance for segmentally erected prestressed concrete box girder bridges, where segments are cast and integrated into the structure at different times, tendons are installed and stressed as segments are added to the structure and the load applied to different parts of the structure changes considerably. Ketchum [53] developed a numerical procedure for a time dependent analysis of two dimensional linear elastic segmentally erected prestressed concrete frames. Later Kang [50] adapted the procedure for non linear material and geometry and Mari [80] extended it to three dimensional frames. The present study has extended the domain of this series of analyses to three dimensional, non linear and time dependent analysis of segmentally erected cable stayed bridges.

The evaluation of creep strain over a period of time depends on the level of stress in concrete among other parameters. Since the variation of stress over the time interval is not known, creep integration schemes generally assume a constant or linear variation of stress during the time interval. In order to improve the accuracy of solution, the time domain is divided into

a number of steps. Since most of the creep and shrinkage strains occur early in the life of the structure these steps are not of equal length and in general a log-linear distribution is assumed.

The procedure used in time dependent analysis is essentially similar to load control method discussed earlier except that instead of load steps, time steps are used and that the load increment in each step consists of an equivalent load vector corresponding to the creep and shrinkage strain increments in the concrete.

At the beginning of each time step, the complete state of the structure is known. The nonlinear material constitutive model for concrete is adjusted for the age of concrete at the beginning of time step. The increment in creep and shrinkage strains over the time step is evaluated and expressed as an equivalent incremental load vector.

Next, the displacement increments are obtained using the tangent stiffness matrix at the beginning of the time step. The current displacements are updated and the new state of the structure is determined using a concrete model adjusted for age at end of time step.

At this stage the state of stress at the end of the time step is defined. If these stresses are considerably different from those at the beginning of time step, the creep strains may be in error as these were calculated on the basis of a constant stress over the time step. Ketchum [53] has suggested alternate creep integration schemes which assume a linear variation of stress and material properties over time. The numerical procedure used in the present study allows for three different schemes of creep strain integration.

- constant stress and constant material parameters.
- linear stress and constant material parameters.
- linear stress and linear material parameters.

If the latter of the two schemes is being used then an additional initial strain load vector is generated to account for linear variation of stresses and/or material parameters and iterations

are continued until the unbalanced load is reduced to desirable tolerances. A step by step procedure is described systematically in the following algorithm.

ALGORITHM FOR TIME STEP ANALYSIS

GIVEN:

- An equilibrium or converged state of the structure.
- External load vector $\mathbf{R}_e$.
- Time at start and end of solution t_{cur} and t_{end}.
- Number of time steps $numstp$.
- A vector $\mathbf{T}(numstep+1)$ with a log linear distribution of solution times

$$T(k) = t_{cur} + e^m$$
$$m = (k-1)\frac{\ln(t_{end} - t_{cur})}{numstep}$$

- Convergence tolerances:

  Force tolerance for each solution step $tolf$.

  Force tolerance for stiffness update $tolk$.

- Maximum number of iterations allowed in each time step $numit$.

SOLUTION PROCEDURE

- Set flags.

  converge=.true.

  revise=.true.

Start time step loop

- For k=1,2,.....*numstp*
- Get time step increment

$t_{prv} = T(k) \qquad t_{cur} = T(k+1)$

$\Delta t^k = t_{cur} - t_{prv}$

- Evaluate the equivalent load vector $\Delta \mathbf{R}_t^{\,k}$ due to time dependent effects over the time step. For a given creep model this is a function of fiber stress, concrete age t_{prv} and time step increment Δt^k. Since the fiber stresses at the end of the step is not known at this stage, it is assumed that the stress remains constant over the time step.
- If $(k = 1)$ then update current load vector $\mathbf{R}_e = \Delta \mathbf{R}_e + \mathbf{R}_e^{\,0}$

Start iteration loop

- For j=1,2,.....*maxit*
- If (*revise=.true.*) then form tangent stiffness matrix $\mathbf{K}_T^{\,j}$.
- Solve for incremental displacements

  $(\mathbf{K}_T^{\,j})\Delta \mathbf{r}^j = \mathbf{R}_e - (\mathbf{R}_i^{\,j-1} - \Delta \mathbf{R}_t^{\,j-1})$

  Note that $\mathbf{R}_i^{\,0} = \mathbf{R}_i^{\,k}$ and $\Delta \mathbf{R}_t^{\,0} = \Delta \mathbf{R}_t^{\,k}$.
- Update current displacements

  $\mathbf{r}^j = \mathbf{r}^{j-1} + \Delta \mathbf{r}^j$
- Determine new state of the structure.

  Path dependent $\mathbf{R}_i^{\,j} = \lambda(\mathbf{r}^{j-1}, \mathbf{r}^j)$

  Path independent $\mathbf{R}_i^{\,j} = \lambda(\mathbf{r}^k, \mathbf{r}^j)$
- Calculate additional creep strain caused by stress change during iteration and the corresponding equivalent load vector $\Delta \mathbf{R}_t^{\,j}$. This step is not required if the creep integration scheme being used assumes constant stress over the time step.
- Find unbalanced load vector

  $\mathbf{R}_u^{\,j} = \mathbf{R}_e - (\mathbf{R}_i^{\,j} - \Delta \mathbf{R}_t^{\,j})$
- Check for convergence:

  if $\left(\left\|\mathbf{R}_u^{\,j}\right\| \le tolf\right)$ then

  set *converge =.true.*

save current state as converged state

exit iteration loop

else

set $converge =. false.$

end if

- Check if stiffness refresh is required in next cycle

if $\left(\left\|\mathbf{R}_u^j\right\| \leq tolk\right)$ then

set $revise =. false.$

end if

End iteration loop

- if $(converge =. false.)$ then

print " maximum number of iteration exceeded, no convergence"

stop program

end if

End time step loop

5.3.4. A NOTE ON STATE DETERMINATION PROCEDURES

The process of calculating the state of the structure corresponding to the current displaced shape of the structure is known as state determination.

In an inelastic structure, the current state of any element will depend on the strain path that has been followed. Let S_{cvg} be a previously converged state at the beginning of the iteration sequence and let S^{j-1} be the state at the end of previous iteration. It is desired to find the current state S^j. The computation for state determination depends as to which of the two previous states is used as a reference state in the process

PATH DEPENDENT

If the state at the end of previous iteration S^{j-1} is used as the reference state, the state determination process is termed as path dependent. The final state S^j thus depends on the path followed during the iteration.

PATH INDEPENDENT

If the converged state at beginning of the iteration sequence S_{cvg} is used as the reference state, the state determination process is path independent. The final state S^j thus determined is dependent only on the beginning state and the sum of all displacement increments during the iteration sequence and is quite independent of the iteration path.

Consider a softening structural system subjected to a constant load iteration sequence. In general, the element strains will increase steadily during each iteration and either of the two state determination schemes will give the same solution. However, if the same system is subjected to a constant displacement iteration sequence, the strains may increase in the earlier iterations and then decrease, causing a path dependent scheme to incorrectly predict unloading. Therefore it is recommended that path independent state determination procedures be used for displacement controlled schemes, Simons [127].

6. BEAM-COLUMN ELEMENT

6.1. GENERAL

The prediction of nonlinear behavior of reinforced concrete is complicated by a number of phenomenon such as cracking and crushing of concrete, yielding of reinforcement, deterioration of bond between concrete and steel and consequent slipping of bars, time dependent effects of creep and shrinkage of concrete etc.

Various analytical models have been proposed for the nonlinear analysis of reinforced concrete members. We shall consider two main types in this section; namely elements based on the finite element method which treat the reinforced concrete member as a continuum by monitoring the internal stress state at selected points and the discrete element model which attempts to model the overall behavior of the member without consideration of the interior stress state of the element.

For a discrete element model, material nonlinearity is introduced at section level as a moment curvature relationship or some other phenomenon based relationship. Finite element based fiber elements usually employ stress-strain relationship at the fiber level and hence tend to be more rational.

A two component model was introduced by Clough, Benuska and Wilson [21]. The element consists of an elastic element and an elasto-perfectly plastic element connected in parallel. The stiffness of the two components can be added directly to obtain the total stiffness of the

element. The resulting element has a bilinear strain hardening moment curvature relationship.

Otani and Sozen [98] suggested a series model, in which an elastic element is connected in series with inelastic springs at each end. Since the elements are in series, the component flexibilities can be added directly to get the element flexibility matrix. The flexibility matrix is inverted to get the stiffness matrix and the two internal degrees of freedom are condensed out. The inelastic springs simulate the moment rotation behavior of the end sections of the member.

An improved multiple spring model has been suggested by Takayangi and Schnobrich [132], which consists of a series of springs interconnected by rigid links. The flexural rigidity of each spring is assumed to be spread uniformly over half the length of adjacent rigid link thereby approximating the curvature distribution over the entire length of the member.

Most of the models discussed above require a prior determination of moment-curvature or moment-rotation relationships for the actual reinforced concrete member. In addition, discrete models either do not account for the interaction of axial load and bending moment or use phenomenon based models to capture this effect. In contrast, the fiber beam-column elements avoid these difficulties by introducing the material properties at the fiber level in the form a stress-strain relationship instead of a moment curvature relationship at the section level. A brief discussion of past developments in the theory of fiber elements is presented in the subsequent paragraphs.

In general, fiber elements are based on the displacement formulation of the finite element method. Material behavior is monitored at two or more "control sections". Each section is discretized into a number of sub-elements or fibers. The stress-strain relationship of the material is defined at the fiber level. The cross section deformations, curvatures and strain at the reference axis, are defined by shape functions. The fiber strains are based on the

assumption of plane sections remaining plane. Element tangent stiffness matrix is obtained by integrating the contribution of beam slices over the length of the beam.

$$\mathbf{K}_T = \int_L [\mathbf{B}(x)]^T [\mathbf{K}_S(x)][\mathbf{B}(x)]\ dx \tag{6.1}$$

where $\mathbf{B}(x)$ is the shape function matrix relating element end deformations to section deformations of a section located at a distance x from one end of the element. The internal resisting loads are given by

$$\mathbf{R}_i = \int_L [\mathbf{B}(x)]^T [\mathbf{S}_S(x)]\ dx \tag{6.2}$$

where $\mathbf{S}_S(x)$ is the slice action vector.

A two-dimensional beam element based on the fiber model was introduced by Kang [49] for the nonlinear analysis of reinforced and presstressed concrete frames. The element has three degrees of freedom at each end. Material behavior is monitored at three sections placed at the integration points for a three point guass quadrature. Each section is divided into layers over its depth and the stress-strain response of each layer is tracked as the solution proceeds. Cubic Hermitian shape functions are used to relate element deformations to section curvature and strain. Kang derives the tangent stiffness matrix by setting $\mathbf{K}_S(x) = \mathbf{K}_S(L/2)$.

$$\mathbf{K}_T = \int_L [\mathbf{B}(x)]^T [\mathbf{K}_S(\tfrac{L}{2})][\mathbf{B}(x)]\ dx \tag{6.3}$$

The resulting expression is then evaluated by closed form integration. In contrast to this the internal resisting loads are evaluated by sampling section state at three sections located at guass points.

$$\mathbf{R}_i = \frac{L}{2} \sum_{i=1}^{3} w_i \left\{ [\mathbf{B}(\xi_i)]^T [\mathbf{S}_S(\xi_i)] \right\} \tag{6.4}$$

where ξ_i are the guass points and w_i are the corresponding weights. Initial strain effects due to creep and shrinkage were accounted for by including the effect of equivalent clamping forces in the load vector.

$$\mathbf{S}_M{}^0 = \int_L [\mathbf{B}(x)]^T \left[\mathbf{S}_S{}^0(x)\right] d \tag{6.5}$$

$$\mathbf{S}_S{}^0 = \sum_{k=1}^{N} \left\{ [\mathbf{A}_{FS}]^T (E_t \, \varepsilon^0) \right\}_k \tag{6.6}$$

where $\mathbf{S}_S{}^0(x)$ are the clamping forces at the section level, $\mathbf{A}_{FS}$ is a transformation matrix from section deformations to fiber strain, E_t is the tangent modulus and ε^0 is the initial strain in the *kth* fiber and N is the total number of fibers.

Chan [19] extended Kang's formulation to a three dimensional frame element of rectangular cross-section. The element has six degrees of freedom at each end and a mid length degree of freedom in the axial direction. The mid length DOF is required to allow for linear variation of axial strain; it is condensed out at the element level. In order to simplify the solution, torsion and flexural effects are assumed to be uncoupled. Chan also employed three control sections in his element model, one at mid length and the remaining two at the guass point locations corresponding to a two point guass quadrature. The section is discretized into fibers over its width and height. The state of the mid length control section is used to estimate an approximate tangent stiffness matrix for the element. Element internal loads are evaluated using a two point guass quadrature. Again the initial strain effects due to creep and shrinkage were accounted for in a manner similar to that employed by Kang. Later Mari [80] refined Chan's element by adding prestressing to investigate the behavior of reinforced and prestressed concrete elements of arbitrary cross-section.

Although these elements have been used successfully to solve a large variety of nonlinear problems, some shortcomings have been observed. For example consider a beam element subject to anti-symmetrical bending and let the end moments be larger than the yield

moments. The stiffness matrix which is based on the state of the mid length section does not represent the exact tangent stiffness of the element and may lead to erroneous solutions. If the shape of the moment diagram is known in advance then it may be possible to get around this problem by using smaller elements so that each element is subjected to bending of a single curvature.

Numerical problems may also be encountered in capturing post yield or strain softening behavior. Hellesland [40, 41] who used Kang's element to study the behavior of reinforced concrete bridge columns under imposed deformations, notes that such elements have difficulty in capturing softening behavior past the point of peak resistance. This problem arises from the fact that cubic shape functions used for these elements are derived for linear elastic beams and their use implies linear variation of curvature over the length of the element which is a poor representation of the nonlinear curvature existing in the yield zones of actual concrete members.

Hellesland also notes that the prediction of ultimate deflections is very sensitive to the size of elements used in and adjacent to the zone of potential yield. Very short elements in the plastic hinge zone underestimate the ultimate deflections of concrete members whereas elements covering the yield zone and extending well into the elastic zone have shown to produce good estimates of the same.

Suharwardy and Pecknold [130] presented a procedure based on varying the shape function according to predetermined rules as the element yields. This allows long in-elastic beam columns to be modeled accurately using a single element. However, this procedure is applicable only for those cases where the deformation modes of the element are well established and known in advance.

Mahasuverachai and Powell [79] generalized the procedure of Suharwardy et al. by introducing a multi-slice element with variable shape functions, which are updated as the state of the element changes. The material behavior is monitored at each slice. The element

has one slice at each end and up to seven intermediate slices. The location of the intermediate slices is selected in such a manner so as to closely approximate the actual curvature variation. At the beginning of a solution step the state of stress, strain and modulus of each fiber in each section is known. This information is used to form a tangent flexibility matrix for each slice. A linear variation of flexibility is assumed between the adjacent slices. Next a member flexibility matrix is formed by integrating the contribution of all slices over the length of the member. The member flexibility matrix is used to construct the shape functions which relate the element end deformations to slice deformations. This shape function is then used to evaluate the element tangent stiffness matrix and later during the state determination phase to determine the slice deformation increment.

Mahasuverachai and Powell [79], who used this element for analysis of piping systems, also report equilibrium violations at intermediate sections at or near peak resistance of the element. Numerical problems were also encountered for very low strain hardening ratios in the steel models.

Kaba and Mahin [47] used a strategy similar to Mahasuverachai et al. [79] for concrete elements to investigate the dynamic response of planar concrete frames subject to considerable axial loads. Numerical studies showed that this element could account for the interaction of axial load and bending moment and simulate the pinching of hysteresis loops due to the presence of axial loads on the element.

Zeris and Mahin [149] and Zeris [150] refined the model developed by Kaba et al. and enhanced the element to account for biaxial effects and anchorage zone deformations. Zeris also attempted to remedy the numerical difficulties encountered with softening systems. He suggested a "double-nested regula falsi" scheme to search for a deformation pattern to satisfy equilibrium at each of the intermediate sections.

Lai, Will and Otani [55] suggested a relatively simple analytical model that can simulate the stiffness degrading behavior of concrete members. The model consists of an elastic element

connected in series to an inelastic element at each end. The inelastic element consists of four spring elements which are calibrated to simulate the Bauschinger effect and flexural yielding of the reinforcement and the compressive deformations of the concrete close to the end region. In addition the element can also account for the anchorage slip of the reinforcing bars at the face of the joint. This element may be classified as falling between the sophisticated finite element based fiber models and the rather crude discrete models with constant axial load assumptions.

6.2. PRESENT STUDY

A multi-slice, fiber beam-column with six degrees of displacement freedom at each end is used in the present study to model the deck and tower segments in a three dimensional cable-stayed bridge, Fig. 6.01.

Because of its rational formulation the element can automatically account for the interaction of axial load and biaxial bending moments. Torsional and flexural effects are assumed to be uncoupled.

The element can account for moderately large deflections as an updated Lagrangian formulation is used in the host program.

GEOMETRY

The element is straight and may have an arbitrary orientation in space. The element geometry and coordinate axes are shown in Fig. 6.01. The local x-axis is defined by the two end nodes i and j. The y-axis lies in the plane defined by the k node. Note that x-axis or the reference axis does not have to be located at the centroidal axis of the member.

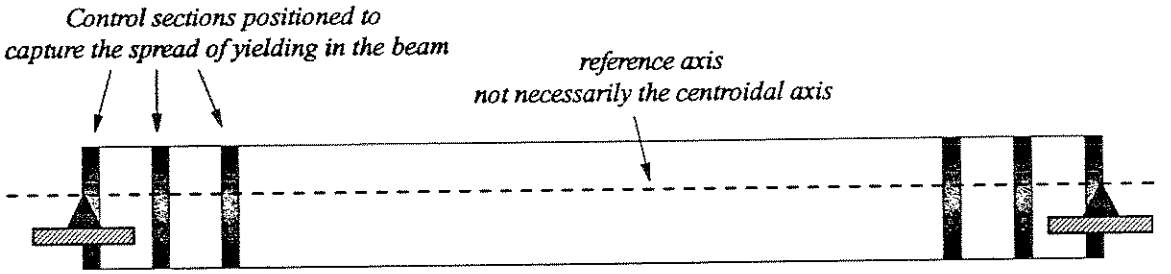

Beam Column Element

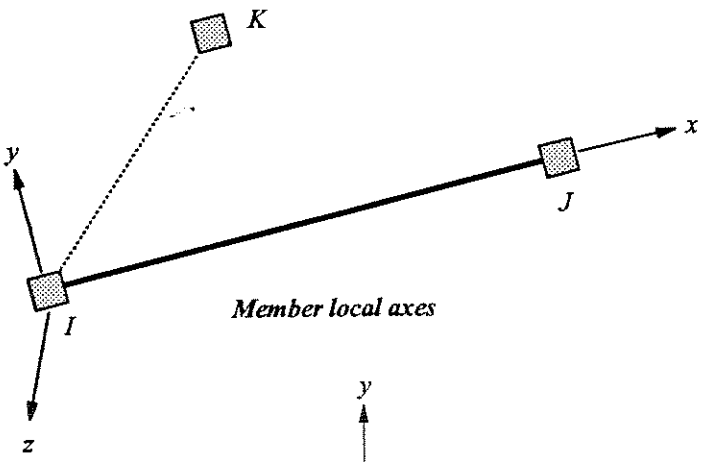

Member local axes

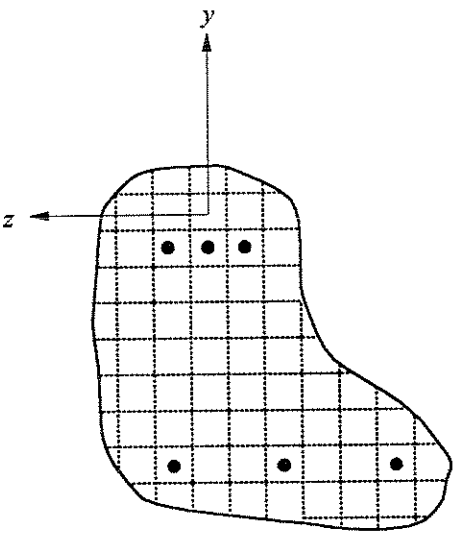

Discretization of section into concrete and steel fibers

FIG. 6.01 VARIABLE SHAPE FUNCTION, MULTI SLICE FIBER BEAM-COLUMN ELEMENT

The material behavior is monitored at up to six slices or control sections; one at each end of the element and the rest at appropriate locations within the element as selected by the analyst.

Each slice is divided into fibers or sub-elements. The geometry of a fiber is completely defined by its area A and its position coordinates (y,z). Note that member cross section may have an arbitrary shape and does not have to symmetric about either axis.

MATERIAL MODELS

The material model is introduced at the fiber level as a stress-strain relationship. The nonlinear stress-strain curve used for concrete is based on the modified Kent Park model, discussed in detail in chapter 4. This model can also predict the response of concrete confined by transverse hoops. Tension stiffening effects based on the model of Vecchio and Collins [142] can also be included.

A bilinear strain hardening model is used for steel which can account for load and reload from the strain hardening branch.

TIME DEPENDENT EFFECTS

The element can account for initial strain effects due to creep and shrinkage of concrete. The material model for concrete is updated continuously as the concrete ages. Basic creep curves are determined using ACI committee 209 model, CEB-FIP model or directly from laboratory data.

To account for variable stress levels and time dependent concrete properties, creep strain increments are determined using an integral formulation based on the method of superposition. The time domain is divided into a number of small steps and depending on the type of integration scheme used, Ketchum [53], concrete stress and material parameters are either assumed to remain constant or vary linearly over a time step. To avoid storage of

the entire stress history of a concrete fiber, a special type of exponential function based on the Dirichlet series is used in the superposition integral. This function is fitted to the basic creep curves using a least squares approach. The subsequent numerical integration scheme is essentially a recursive equation wherein only the previous state of the concrete fiber defined by a so called "hidden state variable" is required. Creep integration schemes are discussed in Chapter 4.

FORMULATION

A brief overview of the fundamental concepts is given here. The formulation is based on two key assumptions.

- Plane sections remain plane.
- The variation of slice flexibility between adjacent control sections is linear.

The element stiffness matrix is built by considering the behavior of the element at three different levels; fiber (F), slice (S) and member (M). The notation for actions, deformations, flexibility, etc. at each of these levels is shown in the table below:

	Actions	Deformations	transformation	Stiffness	Flexibility
Fiber	$\mathbf{S}_F$ (1x1)	$\mathbf{v}_F$ (1x1)		$\mathbf{K}_F$ (1x1)	
			$\mathbf{A}_{FS}$ (1x3)		
Slice	$\mathbf{S}_S$ (3x1)	$\mathbf{v}_S$ (3x1)		$\mathbf{K}_S$ (3x3)	$\mathbf{F}_S$ (3x3)
			$\mathbf{B}_{SM}$ (3x5)		
Member	$\mathbf{S}_M$ (5x1)	$\mathbf{v}_M$ (5x1)		$\mathbf{K}_M$ (5x5)	$\mathbf{F}_M$ (5x5)

1. The action deformation relationship at fiber level is given by

$$\mathbf{dS}_F = \mathbf{K}_F \mathbf{dv}_F \tag{6.7}$$

which is really equivalent to

$$d\sigma = E\, d\varepsilon$$

2. Next the slice stiffness matrix is built by summing the contribution of all fibers.

$$\mathbf{dS}_S = \{\sum_{k=1}^{N} [\mathbf{A}_{FS}{}^T \mathbf{K}_F \mathbf{A}_{FS}]_i\}\, \mathbf{dv}_S \tag{6.8}$$

where the transformation matrix $\mathbf{A}_{FS}$ is based on the assumption of plane sections remaining plane.

3. The slice stiffness matrix is inverted to get the slice flexibility matrix.

$$\mathbf{F}_S = \mathbf{K}_S{}^{-1} \tag{6.9}$$

4. The member stiffness matrix is then derived using the principle of virtual forces.

$$\mathbf{dv}_M = \{\int_L [\mathbf{B}_{SM}{}^T(x)][\mathbf{F}_S(x)][\mathbf{B}_{SM}{}^T(x)]dx\}\ \mathbf{dS}_M \tag{6.10}$$

where $\mathbf{B}_{SM}$ is a force transformation matrix. Note that the slice flexibility is only sampled at certain discrete sections and its actual variation along the length of the member is not known. However an approximation to the above integral can be evaluated by assuming a linear variation of slice flexibility between adjacent control sections.

5. Furthermore, the shape functions are constructed at this stage.

$$d\mathbf{v}_S = \{\mathbf{F}_S(x)\mathbf{B}_{SM}(x)\mathbf{F}_M{}^{-1}\}\ d\mathbf{v}_M \tag{6.11}$$

These are later used in the state determination phase to recover fiber strain increments.

The formulation of element stiffness and state determination is described in detail in the subsequent sections.

TORSION

Concrete members are rarely subjected to pure torsion. The presence of flexural moments decreases the torsional capacity of a concrete member. Both the truss analogy and skew bending theories indicate a parabolic interaction between flexure and torsion, Park [99].

The interaction of torsion and flexure is a complex phenomenon and is difficult to capture analytically. Future research using 3D brick elements along the length of the member or lumped plasticity approach may yield a solution to this complex problem.

In the present study, torsion and flexural effects are assumed to be uncoupled, Chan [19]. Torsional plasticity is accounted for by adding on a lumped plasticity torsional element in parallel with the fiber element.

A trilinear model is used to represent the torsional response of a reinforced concrete beam. The model is completely defined by three points.

1. The torque at first cracking T_{cr} and the corresponding twist α_{cr}.
2. The torque at complete yield of all reinforcement T_{yp} and the corresponding twist α_{yp}.
3. The twist at ultimate failure α_u.

The influence of member geometry and strength on these parameters is discussed in detail in Chapter 4.

6.3. Element Stiffness Matrix

The development of element stiffness matrix is explained sequentially in the following sections. Consider Fig. 6.02 and 6.03. Member action-deformation relations are considered at several levels to simplify the derivation and to develop a better physical feel for the process.

- Fiber level.
- Slice level.
- Member level. M-coordinate system. This consists of five deformation modes with respect to member coordinate system.
- Member level, M' coordinate system. The torsional deformations are included at this level, increasing the number of deformation modes to six.

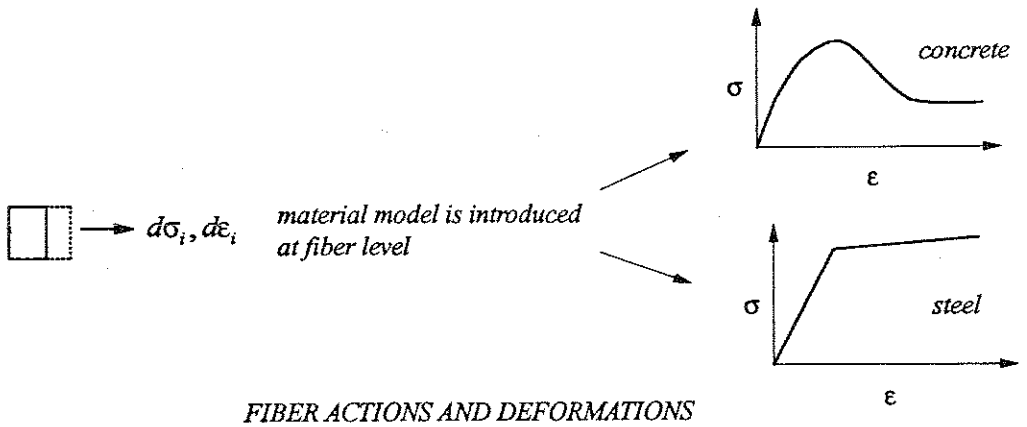

FIBER ACTIONS AND DEFORMATIONS

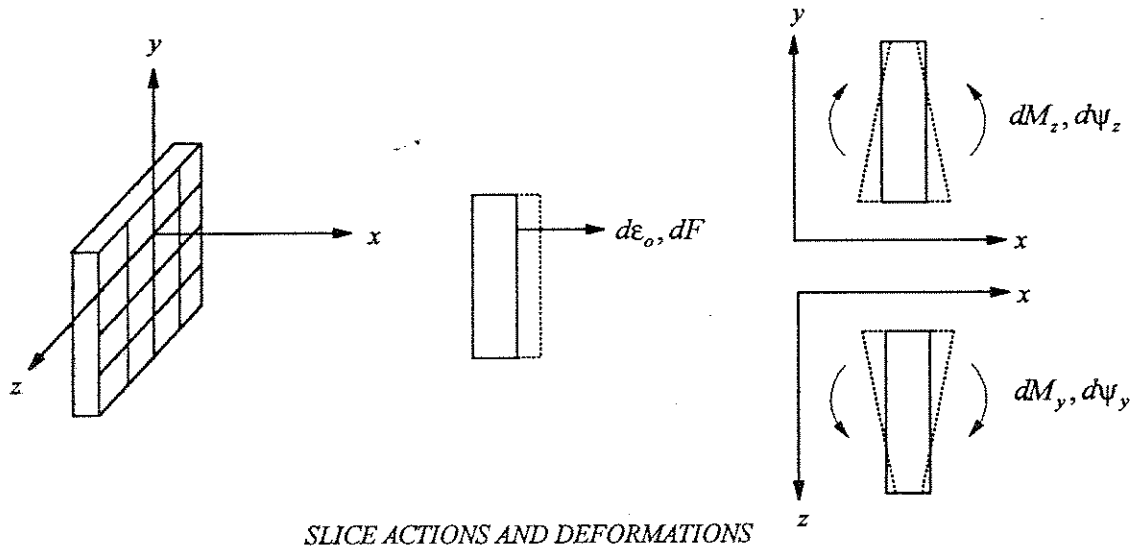

SLICE ACTIONS AND DEFORMATIONS

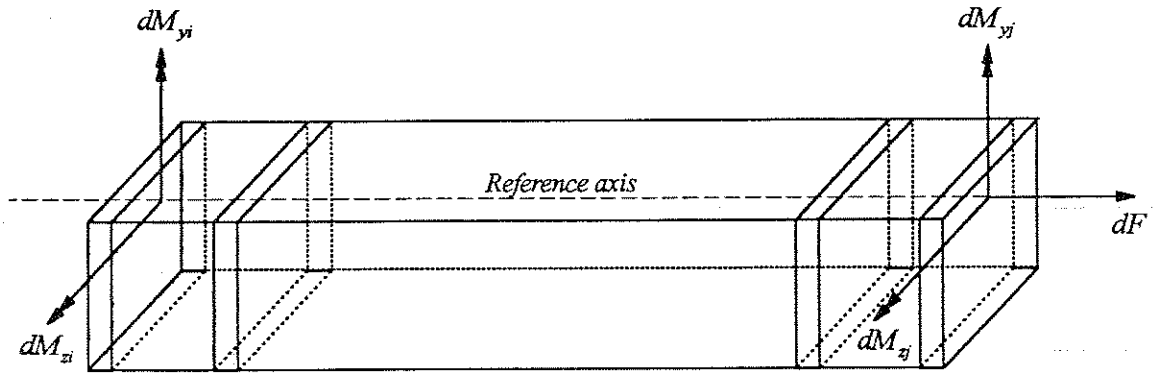

MEMBER ACTIONS AND DEFORMATIONS

FIG. 6.02 FIBER BEAM-COLUMN ELEMENT

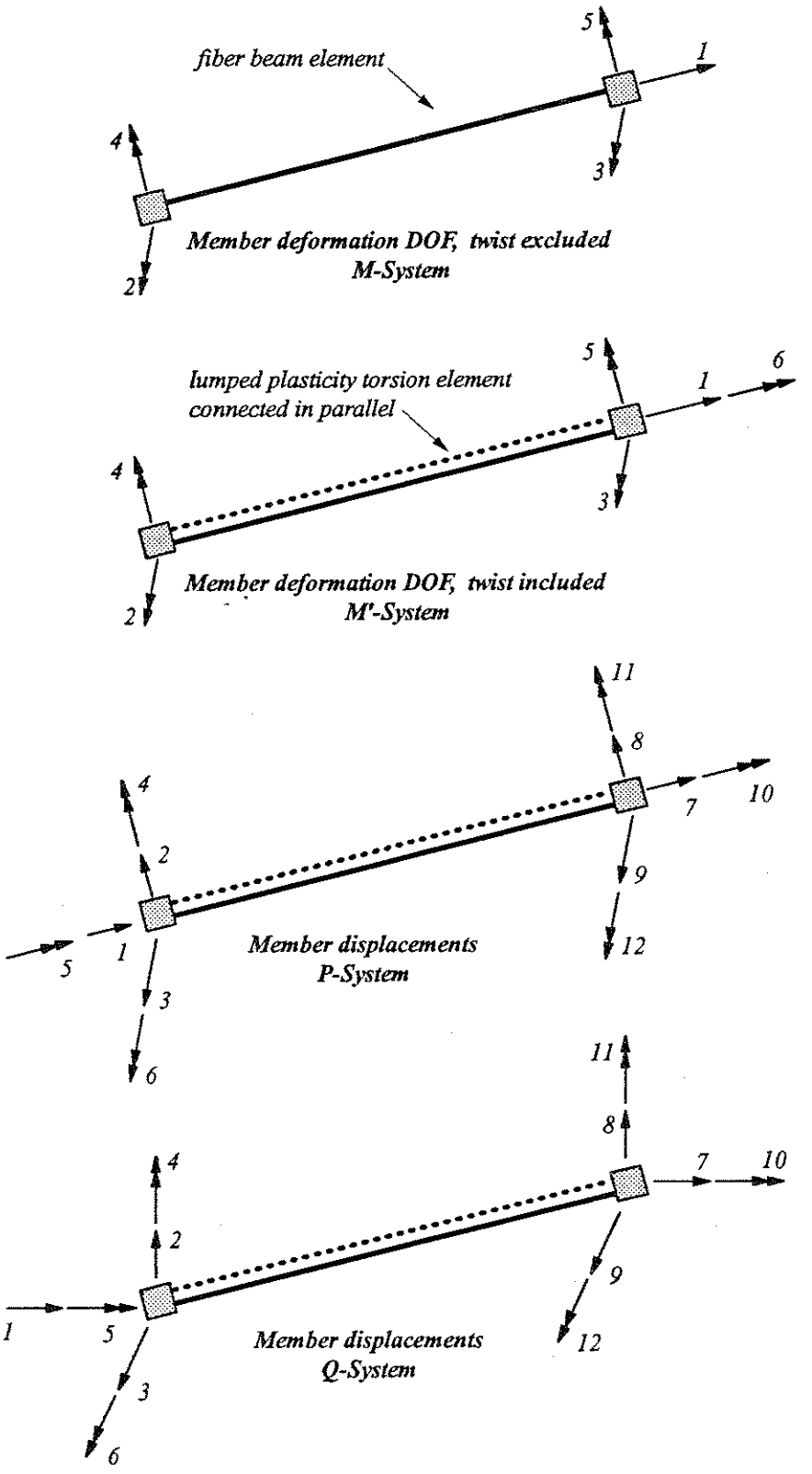

FIG. 6.03 BEAM ELEMENT; COORDINATE SYSTEMS

- Member level, P coordinate system. Member displacements; these consist of six deformation modes and six rigid body motions.
- Member level, Q coordinate system. Global displacements.

6.3.1. FIBER

Fiber action-deformation relationship is given by

$$d\sigma_i = \frac{1}{E_{ti}} d\varepsilon_i \tag{6.12}$$

where $d\sigma_i$ is the change in stress, $d\varepsilon_i$ is corresponding change in strain and E_{ti} is the tangent modulus of the *ith* fiber in the cross section.

6.3.2. SLICE

Slice deformation vector $\mathbf{dv}_S$ are defined as:

$$\mathbf{dv}_s = \begin{bmatrix} d\varepsilon_o \\ d\psi_z \\ d\psi_y \end{bmatrix} \tag{6.13}$$

where

$d\varepsilon_0$ axial strain increment at reference axis.

$d\psi_z$ curvature increment about Z axis.

$d\psi_y$ curvature increment about Y axis.

The corresponding vector $\mathbf{dS}_S$ defining slice actions is given by:

$$\mathbf{dS}_s = \begin{bmatrix} dF \\ dM_z \\ dM_y \end{bmatrix} \tag{6.14}$$

where

dF axial force increment.

dM_z bending moment increment about Z axis.

dM_y bending moment increment about Y axis.

The matrix $\mathbf{A}_{FS}$, transforming slice deformations to fiber deformations is given by:

$$d\varepsilon_i = \begin{bmatrix} 1 & -y_i & -z_i \end{bmatrix} \begin{bmatrix} d\varepsilon_o \\ d\psi_z \\ d\psi_y \end{bmatrix} \tag{6.15}$$

$$\mathbf{A}_{FS} = \begin{bmatrix} 1 & -y_i & -z_i \end{bmatrix} \tag{6.16}$$

where y_i and z_i are the position coordinates of the ith fiber with respect to member local coordinates. The slice stiffness matrix $\mathbf{K}_S$ can be derived by using the principle of virtual displacements and is given by:

$$\mathbf{K}_S = \sum_{i=1}^{n} [\mathbf{A}_{FS}]_i^T [E_t A]_i [\mathbf{A}_{FS}]_i$$

$$\mathbf{K}_S = \sum_{i=1}^{n} (E_t A)_i \begin{bmatrix} 1 & -y_i & -z_i \\ -y_i & y_i^2 & y_i z_i \\ -z_i & y_i z_i & z_i^2 \end{bmatrix} \tag{6.17}$$

where $(E_t A)_i$ is product of the tangent modulus and the area of cross section of the ith fiber.

The slice flexibility matrix is obtained by inverting the stiffness matrix.

$$\mathbf{F}_S = \mathbf{K}_S^{-1} \tag{6.18}$$

6.3.3. MEMBER M-COORDINATES

Member end actions $\mathbf{dS}_M$ with respect to M-coordinates are defined as:

$$\mathbf{dS}_M = \begin{bmatrix} dF \\ dM_{zi} \\ dM_{zj} \\ dM_{yi} \\ dM_{yj} \end{bmatrix} \tag{6.19}$$

where

dF axial force at the level of reference axis.

dM_{zi} bending moment at node i about z axis.

dM_{yj} bending moment at node i about y axis.

dM_{zj} bending moment at node j about z axis.

dM_{yj} bending moment at node j about y axis.

The corresponding member end displacement vector $\mathbf{dv}_M$ is defined as:

$$\mathbf{dv}_M = \begin{bmatrix} d\delta \\ d\theta_{zi} \\ d\theta_{zj} \\ d\theta_{yi} \\ d\theta_{yi} \end{bmatrix} \tag{6.20}$$

where

$d\delta$ displacement in the axial direction at node j.

$d\theta_{zi}$ rotation at i about z axis.

$d\theta_{yj}$ rotation at i about y axis.

$d\theta_{zj}$ rotation at j about z axis.

$d\theta_{yj}$ rotation at j about y axis.

The force transformation matrix $\mathbf{B}_{SM}$ relating slice and member end actions is given as

$$\mathbf{dS}_S = \mathbf{B}_{SM}\,\mathbf{dS}_M$$

$$\begin{bmatrix} dF \\ dM_z \\ dM_y \end{bmatrix} = \begin{bmatrix} 1 & 0 & 0 & 0 & 0 \\ 0 & -A(x) & B(x) & 0 & 0 \\ 0 & 0 & 0 & A(x) & -B(x) \end{bmatrix} \begin{bmatrix} dF \\ dM_{zi} \\ dM_{zj} \\ dM_{yi} \\ dM_{yj} \end{bmatrix} \tag{6.21}$$

where

$$A(x) = 1 - \frac{x}{l}$$

$$B(x) = \frac{x}{l}$$

l is the length of the element and x defines the position of the slice along the member axis.

Member flexibility matrix can be derived using the principle of virtual force. External work done by virtual forces moving through real displacements is equal to the internal work done by internal virtual forces multiplied by real deformations.

$$\begin{aligned}
\mathbf{d\bar{S}}_M{}^T\,\mathbf{dv}_M &= \int_0^l \mathbf{d\bar{S}}_S{}^T\,\mathbf{dv}_S\,dx \\
&= \int_0^l \mathbf{d\bar{S}}_M{}^T\mathbf{B}_{SM}{}^T\mathbf{dv}_S\,dx \\
&= \int_0^l \mathbf{d\bar{S}}_M{}^T\mathbf{B}_{SM}{}^T(\mathbf{F}_s\mathbf{B}_{SM}\,\mathbf{dS}_M)\,dx \\
\mathbf{dv}_M &= (\int_0^l \mathbf{B}_{SM}{}^T\mathbf{F}_s\mathbf{B}_{SM}\,dx)\quad \mathbf{dS}_M
\end{aligned}$$

(6.22)

$$\mathbf{F}_M = \int_0^l [\mathbf{B}_{SM}(x)]^T[\mathbf{F}_S(x)][\mathbf{B}_{SM}(x)]\,dx \tag{6.23}$$

In the numerical scheme the number of control sections is limited to improve the efficiency of the algorithm. Let a member segment be defined as the length of the member bounded by a control section at each end. It is assumed that the section flexibility varies linearly over the segment. If the integration is carried out over the segments then the above equation can be rearranged as follows

$$\begin{aligned}
\mathbf{F}_M &= \sum_{i=1}^{n-1}\int_{x_i}^{x_{i+1}} \mathbf{f}(x)\,dx \\
\mathbf{f}(x) &= [\mathbf{B}_{SM}(x)]^T[\mathbf{F}_S(x)][\mathbf{B}_{SM}(x)]
\end{aligned} \tag{6.24}$$

Where n is the total number of control sections. Integration is carried out using two point guass quadrature. Transforming from x to ξ coordinates we have

$$x = \frac{1}{2}\{(1-\xi)x_i + (1+\xi)x_{i+1}\}$$

$$dx = \frac{(x_{i+1}-x_i)}{2}\,d\xi$$

$$\mathbf{g}(\xi) = \left[\mathbf{B}_{SM}(\xi)\right]^T \left[\mathbf{F}_S(\xi)\right] \left[\mathbf{B}_{SM}(\xi)\right]$$

$$\lambda_i = \frac{(x_{i+1} - x_i)}{2}$$

$$\mathbf{F}_M = \sum_{i=1}^{n-1} \lambda_i \int_{-1}^{1} \mathbf{g}(\xi)\, d\xi$$

$$\mathbf{F}_M = \sum_{i=1}^{n-1} \lambda_i \left[\mathbf{g}\left(\tfrac{-1}{\sqrt{3}}\right) + \mathbf{g}\left(\tfrac{1}{\sqrt{3}}\right)\right] \tag{6.25}$$

The member flexibility matrix $\mathbf{F}_M$ (5x5) is then inverted to get the member stiffness matrix.

$$\mathbf{K}_M = \mathbf{F}_M^{-1} \tag{6.26}$$

6.3.4. MEMBER M'-COORDINATES

It is assumed that torsion and bending stiffness are uncoupled. The stiffness matrix $\mathbf{K}_M$ (5x5) is augmented to $\mathbf{K}_M'$ (6,6); this allows for including a torsional degree of freedom at member level.

$$\mathbf{K}_M' = \left[\begin{array}{ccccc|c} & & \mathbf{K}_M & & & \begin{matrix}0\\0\\0\\0\\0\end{matrix} \\ \hline 0 & 0 & 0 & 0 & 0 & \frac{GJ}{L} \end{array}\right] \tag{6.27}$$

The force displacement relationship at member level is given by

$$\mathbf{S}_M' = \mathbf{K}_M' \mathbf{v}_M'$$

$$\begin{bmatrix} dF_x \\ dM_{zi} \\ dM_{zj} \\ dM_{yi} \\ dM_{yj} \\ dT_x \end{bmatrix} = \mathbf{K}_M' \begin{bmatrix} d\delta \\ d\theta_{zi} \\ d\theta_{zj} \\ d\theta_{yi} \\ d\theta_{yj} \\ d\theta_x \end{bmatrix} \tag{6.28}$$

6.3.5. MEMBER P-COORDINATES

The displacement transformation matrix $\mathbf{A}_{MP}'$ (6x12) is given as follows

$$\mathbf{v}_M' = \mathbf{A}_{MP}' \mathbf{v}_P'$$

$$\mathbf{A}_{MP}' = \begin{bmatrix} -1 & 0 & 0 & 0 & 0 & 0 & 1 & 0 & 0 & 0 & 0 & 0 \\ 0 & \alpha & 0 & 0 & 0 & 1 & 0 & -\alpha & 0 & 0 & 0 & 0 \\ 0 & \alpha & 0 & 0 & 0 & 0 & 0 & -\alpha & 0 & 0 & 0 & 1 \\ 0 & 0 & -\alpha & 0 & 1 & 0 & 0 & 0 & \alpha & 0 & 0 & 0 \\ 0 & 0 & -\alpha & 0 & 0 & 0 & 0 & 0 & \alpha & 0 & 1 & 0 \\ 0 & 0 & 0 & -1 & 0 & 0 & 0 & 0 & 0 & 1 & 0 & 0 \end{bmatrix} \tag{6.29}$$

where $\alpha = \frac{1}{l}$. The structure stiffness matrix in P-system is given as

$$[\mathbf{K}_P] = \left[\mathbf{A}_{MP}'\right]^T \left[\mathbf{K}_M'\right] \left[\mathbf{A}_{MP}'\right] \tag{6.30}$$

6.3.6. MEMBER Q-COORDINATES

The displacement transformation matrix $\mathbf{A}_{PQ}$ (12x12) is given as follows

$$\mathbf{A}_{PQ} = \begin{bmatrix} \mathbf{A}_{\cos} & & & \\ & \mathbf{A}_{\cos} & & \\ & & \mathbf{A}_{\cos} & \\ & & & \mathbf{A}_{\cos} \end{bmatrix} \tag{6.31}$$

where $\mathbf{A}_{\cos}$ is 3x3 matrix of direction cosines of the member local axes (*M* system)

$$\begin{bmatrix} X_M \\ Y_M \\ Z_M \end{bmatrix} = \begin{bmatrix} x_1 & x_2 & x_3 \\ y_1 & y_2 & y_3 \\ z_1 & z_2 & z_3 \end{bmatrix} \begin{bmatrix} X_Q \\ Y_Q \\ Z_Q \end{bmatrix}$$

$$\mathbf{A}_{\cos} = \begin{bmatrix} x_1 & x_2 & x_3 \\ y_1 & y_2 & y_3 \\ z_1 & z_2 & z_3 \end{bmatrix} \tag{6.32}$$

where $(x_1 \quad x_2 \quad x_3)$ are the direction cosines for the member local X-axis etc. The stiffness matrix $\mathbf{K}_Q$ (12x12), in the global coordinates is given by

$$[\mathbf{K}_Q] = [\mathbf{A}_{PQ}]^T [\mathbf{K}_P][\mathbf{A}_{PQ}] \tag{6.33}$$

6.3.7. SHAPE FUNCTIONS

The shape function matrix $\mathbf{A}_{SM}$ relating section deformations to member displacement increments can be derived as follows:

$$\begin{aligned} \mathbf{dv}_s(x) &= \mathbf{F}_S(x)\, \mathbf{dS}_S \\ &= \mathbf{F}_S(x)\, \mathbf{B}_{SM}(x)\, \mathbf{dS}_{SM} \\ &= \left[\mathbf{F}_S(x)\, \mathbf{B}_{SM}(x)\, \mathbf{F}_M{}^{-1}\right] \quad \mathbf{dv}_M \end{aligned} \tag{6.34}$$

Hence

$$\mathbf{A}_{SM}(x) = \mathbf{F}_S(x)\, \mathbf{B}_{SM}(x)\, \mathbf{F}_M{}^{-1} \tag{6.35}$$

The shape functions thus generated are used in the state determination phase.

6.3.8. ELEMENT GEOMETRIC STIFFNESS

Kang [49] and Aldstedt [4] have derived exact geometric stiffness matrix using nonlinear terms in the strain-displacement relationship and based on cubic Hermitian shape functions.

Chan [19] used the geometric stiffness of a truss bar to approximate the geometric stiffness of a beam. He based his argument on the assumption that a beam subjected to a constant axial load carries it in a manner similar to that of a truss bar. Furthermore, when the equilibrium correction is performed on the solution, exact tangent stiffness need not be formed.

The formulation used in the present study is similar to that of Chan [19] because of its relative simplicity. Hence the geometric stiffness matrix is given by:

$$\mathbf{K}_g = \begin{bmatrix} 1 & -1 & 0 & 0 & 0 & 0 & 0 & 0 & 0 & 0 & 0 & 0 \\ & 1 & 0 & 0 & 0 & 0 & 0 & 0 & 0 & 0 & 0 & 0 \\ & & 1 & -1 & 0 & 0 & 0 & 0 & 0 & 0 & 0 & 0 \\ & & & 1 & 0 & 0 & 0 & 0 & 0 & 0 & 0 & 0 \\ & & & & 0 & 0 & 0 & 0 & 0 & 0 & 0 & 0 \\ & & & & & 0 & 0 & 0 & 0 & 0 & 0 & 0 \\ & & & & & & 1 & -1 & 0 & 0 & 0 & 0 \\ & & & & & & & 1 & 0 & 0 & 0 & 0 \\ & & & & & & & & 0 & 0 & 0 & 0 \\ & & & & & & & & & 0 & 0 & 0 \\ & & & & & & & & & & 0 & 0 \\ & & & & & & & & & & & 0 \end{bmatrix} \tag{6.36}$$

Note that $\mathbf{K}_g$ is a symmetric matrix.

6.4. STATE DETERMINATION

Given the member end displacement increment, the state determination process involves the evaluation of element resisting forces in the current displaced state. The process has two components

- Updating member, slice and fiber deformations.
- Determination of current fiber stresses, section forces and finally member end internal resisting forces.

6.4.1. UPDATING DEFORMATIONS

The step by step procedure is as follows:

1. Determine member deformations

$$\Delta \mathbf{v}_M = \left[\mathbf{A}_{MQ}\mathbf{A}_{PQ}\right]\Delta \mathbf{r}_Q \tag{6.37}$$

2. Calculate slice deformation increments using shape functions corresponding to previous state.

$$\Delta \mathbf{v}_S(x) = \left[\mathbf{F}_S(x)\mathbf{B}_{SM}(x)\mathbf{F}_M^{-1}\right]\Delta \mathbf{v}_M \tag{6.38}$$

3. Determine fiber strain increments

$$\Delta\varepsilon_i = \begin{bmatrix} 1 & -y_i & -z_i \end{bmatrix} \quad \Delta \mathbf{v}_S \tag{6.39}$$

4. Update current fiber strains. The fiber state is defined by its position on the stress-strain curve. The current fiber state is determined based on a reference state and the current fiber strain. The reference state may be the state saved at the end of the previous iteration or it may be an equilibrium state saved earlier.

6.4.2. ELEMENT RESISTING FORCES

1. Determine slice actions

$$\begin{bmatrix} F_x \\ M_z \\ M_y \end{bmatrix} = \sum_{i=1}^{n} \sigma_i \begin{bmatrix} 1 \\ -y_i \\ -z_i \end{bmatrix} \tag{6.40}$$

2. Member end forces may be obtained by applying the principle of virtual displacement.

$$\mathbf{S}_M = \int_0^l \left[\mathbf{A}_{SM}(x)\right]^T \left[\mathbf{S}_S(x)\right] dx \tag{6.41}$$

This integral can be evaluated by summing the contribution from each segment.

$$\mathbf{S}_M = \sum_{i=1}^{n-1} \int_{x_i}^{x_{i+1}} \left[\alpha(x)\right] dx \tag{6.42}$$

Using two point guass quadrature; transforming from x to ξ coordinates we have

$$\lambda_i = \frac{(x_{i+1} - x_i)}{2}$$

$$\mathbf{S}_M = \sum_{i=1}^{n-1} \lambda_i \int_{-1}^{1} \left[\beta(\xi)\right] d\xi$$

$$\mathbf{S}_M = \sum_{i=1}^{n-1} \lambda_i \left[\beta\left(\tfrac{-1}{\sqrt{3}}\right) + \beta\left(\tfrac{1}{\sqrt{3}}\right)\right] \tag{6.43}$$

3. The member end force vector $\mathbf{S}_M$ (5x1) is augmented to $\mathbf{S}_{\hat{M}}$ (6x1) to include the torsional moment.

4. The member end forces are then transformed to P-coordinates.

$$\mathbf{S}_P = \mathbf{A}_{\hat{M}P}{}^T \mathbf{S}_{\hat{M}} \tag{6.44}$$

5. Next, the member end forces are transformed to global coordinates.

$$\mathbf{S}_Q = \mathbf{A}_{PQ}{}^T \mathbf{S}_P \tag{6.45}$$

6.5. ELEMENT LOAD DUE TO INITIAL STRAIN

The initial axial strains $\varepsilon_c{}^o$ in the concrete filament due to the time dependent effects of creep and shrinkage give rise to clamping forces $\mathbf{R}^o$. The clamping forces at section level are given by:

$$\mathbf{S}_S{}^o = \sum_{i=1}^{n} E_i \, \varepsilon_{ci}{}^o \begin{bmatrix} 1 \\ -y_i \\ -z_i \end{bmatrix} \tag{6.46}$$

The clamping forces at member level are obtained by applying the principle of virtual displacement.

$$\mathbf{S}_M{}^o = \int_0^l \left[\mathbf{A}_{SM}(x)\right]^T \left[\mathbf{S}_S{}^o(x)\right] dx \tag{6.47}$$

The integral can be evaluated by summing the contribution from each segment using a two point guass quadrature as described earlier. The member end clamping forces thus obtained are transformed to the global coordinates and then added to the external load vector.

6.6. LARGE DISPLACEMENT ANALYSIS

The numerical scheme implemented in the present study is based on an updated Lagrangian formulation for moderately large deflections. The geometry of the beam and the direction of its local axes are continuously updated.

To update the local axes of the beam element, a procedure based on the average rotation of the beam's axes is adopted, Chan [19]. This procedure is restricted to large displacements and small incremental rigid body rotations.

Refer to Fig. 6.04; it is assumed that the geometry of the beam at solution step $(k-1)$ is known. The position of the beam axes is defined by a matrix of direction cosines.

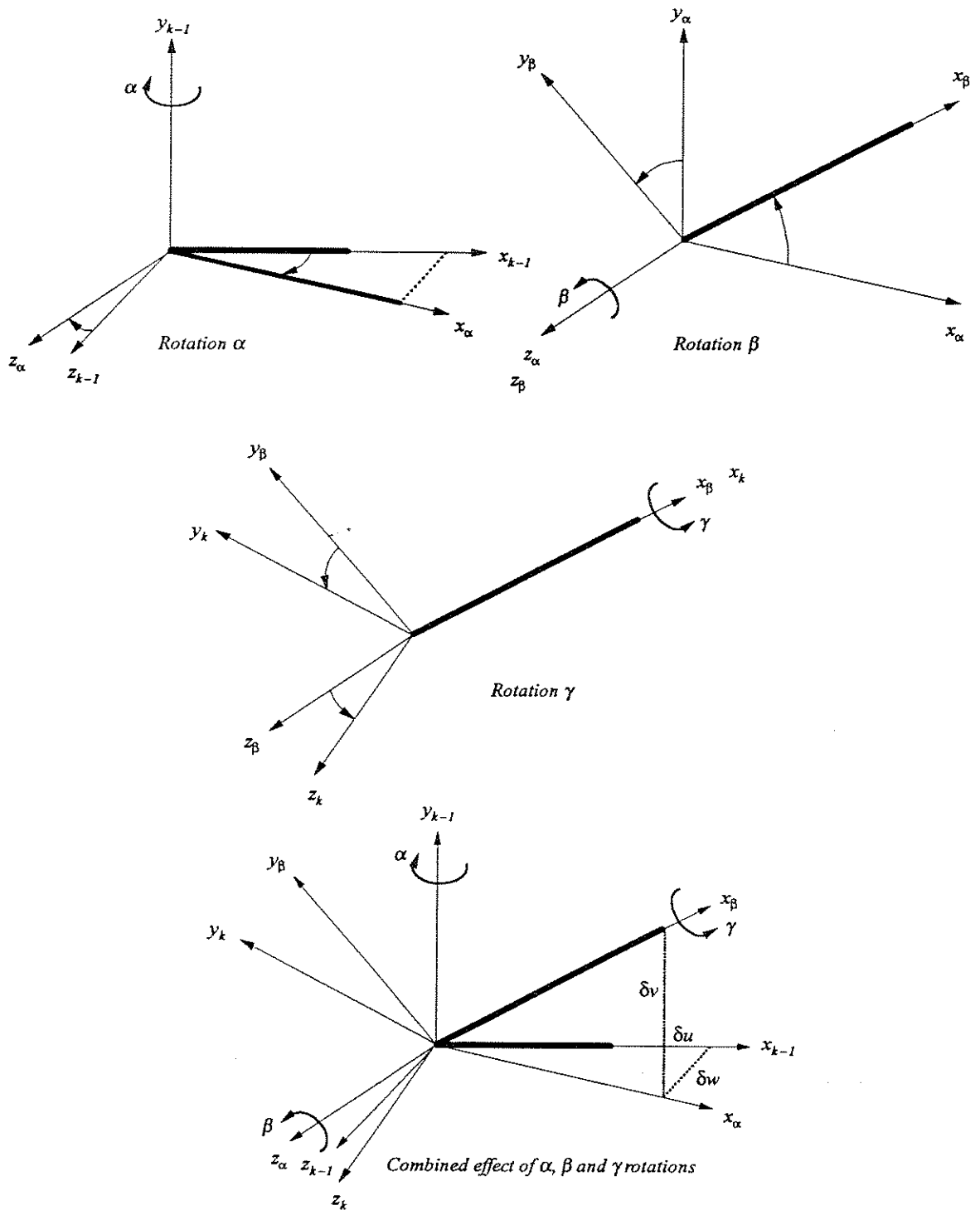

FIG. 6.04 TRANSFORMATION OF BEAM LOCAL AXES

$$\begin{bmatrix} \hat{\mathbf{x}}^T \\ \hat{\mathbf{y}}^T \\ \hat{\mathbf{z}}^T \end{bmatrix}_{k-1} = \begin{bmatrix} x_1 & x_2 & x_3 \\ y_1 & y_2 & y_3 \\ z_1 & z_2 & z_3 \end{bmatrix}_{k-1} \tag{6.48}$$

where $\hat{\mathbf{x}}$, $\hat{\mathbf{y}}$ and $\hat{\mathbf{z}}$ are unit vectors which define the coordinate system at step $(k-1)$ and $(x_1 \quad x_2 \quad x_3)$ etc. are the direction cosines of $\hat{\mathbf{x}}$ with respect to the fixed global coordinate system.

The incremental nodal displacements leading to the new position at the current step (k) are known. It is required to find the matrix of direction cosines for the current position of beam axes.

The relative displacement of one end j of the beam with respect to other end i in the $(k-1)$ coordinate system are given by:

$$\begin{bmatrix} \delta u \\ \delta v \\ \delta w \end{bmatrix} = \begin{bmatrix} \Delta u_j \\ \Delta v_j \\ \Delta w_j \end{bmatrix} + \begin{bmatrix} \Delta u_i \\ \Delta v_i \\ \Delta w_i \end{bmatrix} \tag{6.49}$$

The new coordinate axes at step (k) are obtained as a result of a series of movements.

1. The rotation α about the y axis in $(k-1)$ configuration. Let the new configuration be defined as α.
2. The rotation β about the z axis in α configuration. Let the new configuration be defined as β.
3. The rotation γ about the x axis in β configuration. This moves the beam at the final configuration at step (k).

The angles α, β and γ are given by the following equations:

$$\cos\alpha = \frac{(L_{i-1} + \delta u)}{\sqrt{(L_{i-1} + \delta u)^2 + (\delta w)^2}} \tag{6.50}$$

$$\sin\alpha = \frac{(\delta w)}{\sqrt{(L_{i-1} + \delta u)^2 + (\delta w)^2}} \tag{6.51}$$

$$\cos\beta = \frac{\sqrt{(L_{i-1}+\delta u)^2 + (\delta w)^2}}{\sqrt{(L_{i-1}+\delta u)^2 + (\delta v)^2 + (\delta w)^2}} \tag{6.52}$$

$$\sin\beta = \frac{\delta v}{\sqrt{(L_{i-1}+\delta u)^2 + (\delta v)^2 + (\delta w)^2}} \tag{6.53}$$

$$\gamma = \frac{1}{2}\left(\theta_{xi} + \theta_{xj}\right) \tag{6.54}$$

The transformation $\mathbf{A}_{(k)(k-1)}$ is given by a matrix triple product.

$$\begin{bmatrix} \hat{\mathbf{x}}^T \\ \hat{\mathbf{y}}^T \\ \hat{\mathbf{z}}^T \end{bmatrix}_{(k)} = \left[\mathbf{A}_{(k)(k-1)}\right] \begin{bmatrix} \hat{\mathbf{x}}^T \\ \hat{\mathbf{y}}^T \\ \hat{\mathbf{z}}^T \end{bmatrix}_{(k-1)}$$

$$\mathbf{A}_{(k)(k-1)} = \left[\mathbf{A}_{(k)(\beta)}\right]\left[\mathbf{A}_{(\beta)(\alpha)}\right]\left[\mathbf{A}_{(\alpha)(k-1)}\right] \tag{6.55}$$

Where the component matrices of the triple product are defined below:

$$\mathbf{A}_{(k)(\beta)} = \begin{bmatrix} 1 & 0 & 0 \\ 0 & \cos\gamma & \sin\gamma \\ 0 & -\sin\gamma & \cos\gamma \end{bmatrix} \quad \mathbf{A}_{(\beta)(\alpha)} = \begin{bmatrix} \cos\beta & \sin\beta & 0 \\ -\sin\beta & \cos\beta & 0 \\ 0 & 0 & 1 \end{bmatrix} \quad \mathbf{A}_{(\alpha)(k-1)} = \begin{bmatrix} \cos\alpha & 0 & \sin\alpha \\ 0 & 1 & 0 \\ -\sin\alpha & 0 & \cos\alpha \end{bmatrix}$$

and the triple product itself is given by:

$$\mathbf{A}_{(k)(\beta)} = \begin{bmatrix} (\cos\alpha\cos\beta) & (\sin\beta) & (\cos\beta\sin\alpha) \\ (-\cos\gamma\sin\beta\cos\alpha - \sin\gamma\sin\alpha) & (\cos\gamma\cos\beta) & (-\cos\gamma\sin\beta\sin\alpha + \sin\gamma\cos\alpha) \\ (\sin\gamma\sin\beta\cos\alpha - \cos\gamma\sin\alpha) & (-\sin\gamma\cos\beta) & (\sin\gamma\sin\beta\sin\alpha - \cos\gamma\cos\alpha) \end{bmatrix}$$

The global coordinates of each end of the beam are updated at the end of each solution step.

$$\begin{bmatrix} x \\ y \\ x \end{bmatrix}_{(k)} = \begin{bmatrix} x \\ y \\ x \end{bmatrix}_{(k-1)} + \begin{bmatrix} \Delta x \\ \Delta y \\ \Delta z \end{bmatrix} \tag{6.56}$$

Hence the new position of the beam element is completely defined in space by the following data:

- The updated global position coordinates of the end nodes of the beam.
- The updated position of the beam local axes defined by a direction cosine matrix.

6.7. NUMERICAL PROBLEMS ASSOCIATED WITH SOFTENING BEHAVIOR

Hellesland et al. [40] have reported numerical difficulties associated with the softening behavior of two slice fixed shape function fiber element developed by Kang [49]. Zeris and Mahin [149] have also reported problems encountered at or near the maximum resistance of the multi slice variable shape function elements.

The problem can be best described by first discussing the actual physical response of a reinforced concrete cantilever subjected to controlled displacement increments at its free end and then comparing that with the response of the numerical model.

Consider the cantilever beam shown in Fig. 6.05; the cross section and reinforcement are uniform over the length of the beam. Consider the moment curvature response of the beam section; note that the bending moment rapidly reaches a peak value and then drops gradually.

The beam is subjected to controlled displacement increments in the transverse direction and the corresponding changes in the load applied to the structure are recorded. The bending moment diagram at peak resistance and the corresponding curvature resistance is shown by lines ABC in the bending moments and curvature diagrams respectively in Fig. 6.05. As the tip displacement is increased further, the bending resistance at the base section decreases from point C to E. This is accompanied by a curvature increase at the base section. However, at section 2 the bending moment must decrease in order to satisfy equilibrium and this can only happen if the section unloads along line BD in the moment curvature diagram. This implies a decrease in curvature at section 2. The final curvature distribution is shown by line ADE in the curvature diagram.

Now consider the response of a multi slice, variable shape function element. As the tip displacement is increased past the point of maximum resistance, the shape functions being used are based on the previous state of the element which incorrectly predicts increase in

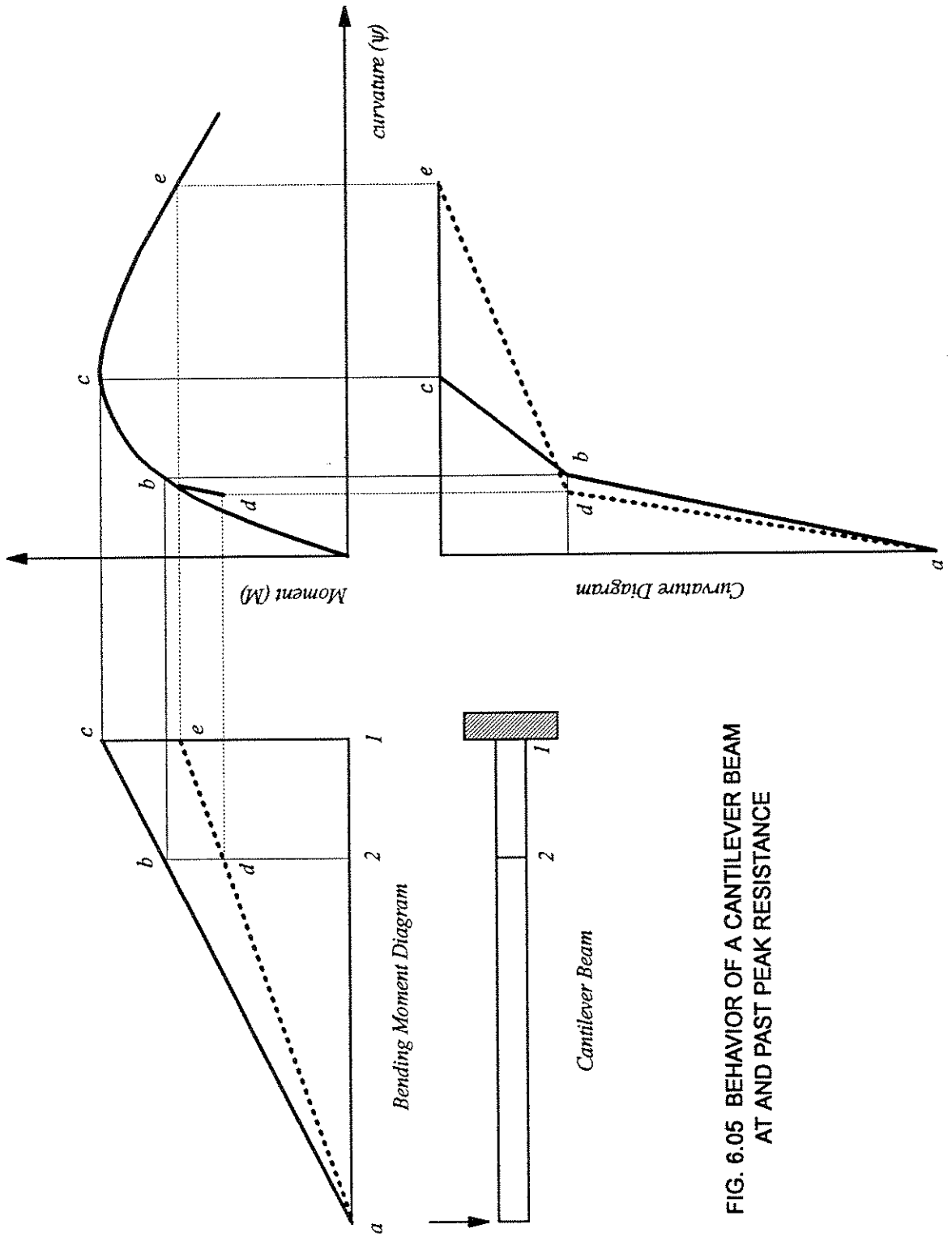

FIG. 6.05 BEHAVIOR OF A CANTILEVER BEAM AT AND PAST PEAK RESISTANCE

curvature at intermediate sections. This in turn results in equilibrium errors at intermediate sections and in some situations may cause convergence problems. Similar problems are encountered by two slice, fixed shape function elements.

6.7.1. PROPOSED SOLUTION

The present study attempts to solve the above mentioned problems by enforcing equilibrium at intermediate sections. However instead of using complex numerical methods based on "double nested regula falsi schemes" as suggested in an earlier study by Zeris and Mahin [149], a simple modification of the state determination procedure is proposed.

At the start of any solution step, the internal state of an element is completely defined by the stress, strain and material state code of each fiber. Refer to Fig. 6.06; in the regular procedure after the element end displacement increments are obtained, increments in slice curvatures are obtained both for the end and intermediate slices using the shape function defined at the beginning of the step. The slice curvatures are then translated into fiber strain increments, which are then use to determine the new stress and material state code of each fiber.

In the modified procedure illustrated in Fig. 6.06, at first, only the state of the end sections is updated. Since the bending moments and axial force at the end sections is known, the required actions at the intermediate sections can be determined from equilibrium conditions. This leaves us with the problem of updating the fiber state at the intermediate section. This is done simply by solving the following equation using the Newton-Raphson procedure.

$$\mathbf{K}_S \, \Delta \mathbf{v}_S = (\mathbf{S}_{eqm} - \mathbf{S}_i) \tag{6.57}$$

If the unbalance is large, it may be divided into smaller increments and the standard step iterative solution scheme is used. Since the unbalance is relatively small, the solution converges quickly.

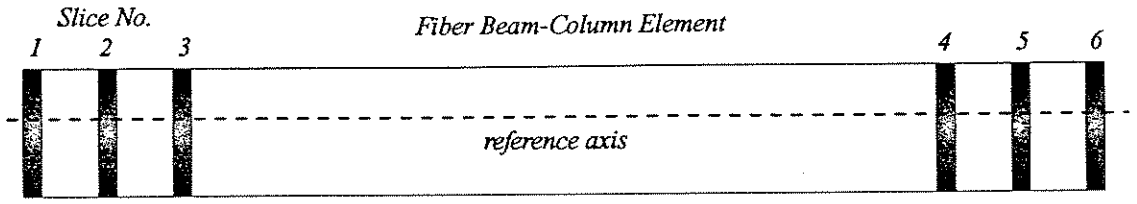

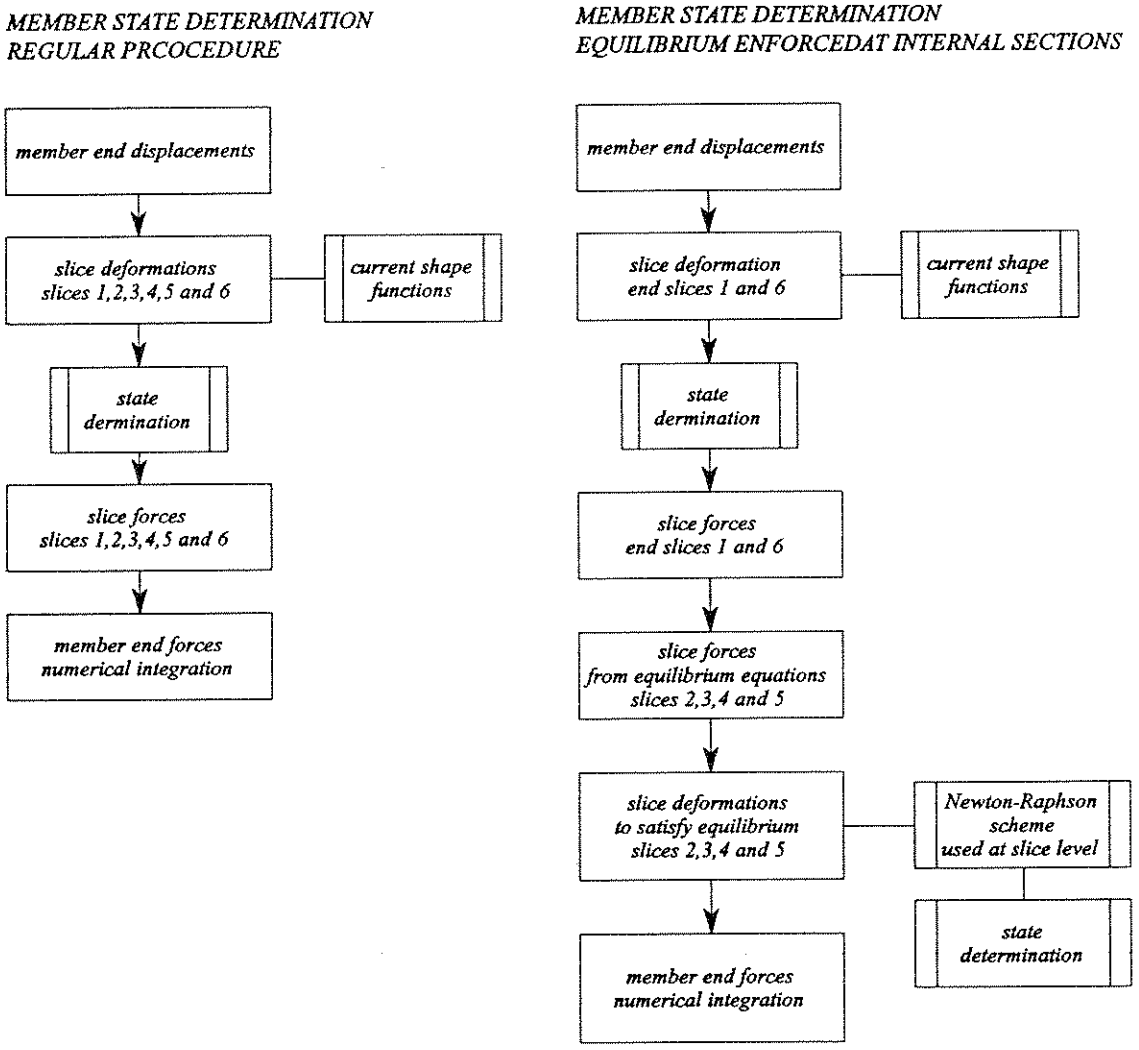

FIG. 6.06 MODIFIED STATE DETERMINATION PROCESS
EQUILIBRIUM ENFORCED AT INTERNAL SECTIONS

6.7.2. NUMERICAL TESTS

The computer program CALBRG developed in the present study allows for either the standard scheme for state determination or the one which enforces equilibrium at internal sections.

A cantilever column shown in Fig. 6.07 is subjected to a controlled displacement increment in the transverse direction and analyzed using both types of state update procedures described above.

The column is modeled with a single element with four control sections. The control sections are placed at *0, 0.2 L, 0.8 L* and *L*. Each section is descritized into 100 concrete fibers and 4 steel fibers. The concrete strength is assumed to be 3000 psi and the strain at the end of the descending branch was set to .004. The steel properties are as follows:

$$f_y = 40000 psi$$
$$E = 29 \times 10^6 psi$$
$$E_{sh} = 29 \times 10^4 psi$$
$$\varepsilon_u = 0.12$$

The load versus tip displacement plots are shown in Fig. 6.07. There is a marked difference in the response predicted by the standard state determination scheme (SSD) and the equilibrium state determination scheme (ESD). The SSD scheme shows a drastic change in the stiffness of member at a displacement of about 3 in., thereafter the curve stays nearly flat, exhibiting elasto plastic type of behavior. Compared to that, the ESD scheme shows a gradual softening after the initial yield of the steel, reaches a well defined peak, successfully unloads and then exhibits constant resistance. Fiber states were monitored at the critical section at various points marked along the load deflection path shown in Fig. 6.07 and the data obtained is summarized in the following table.

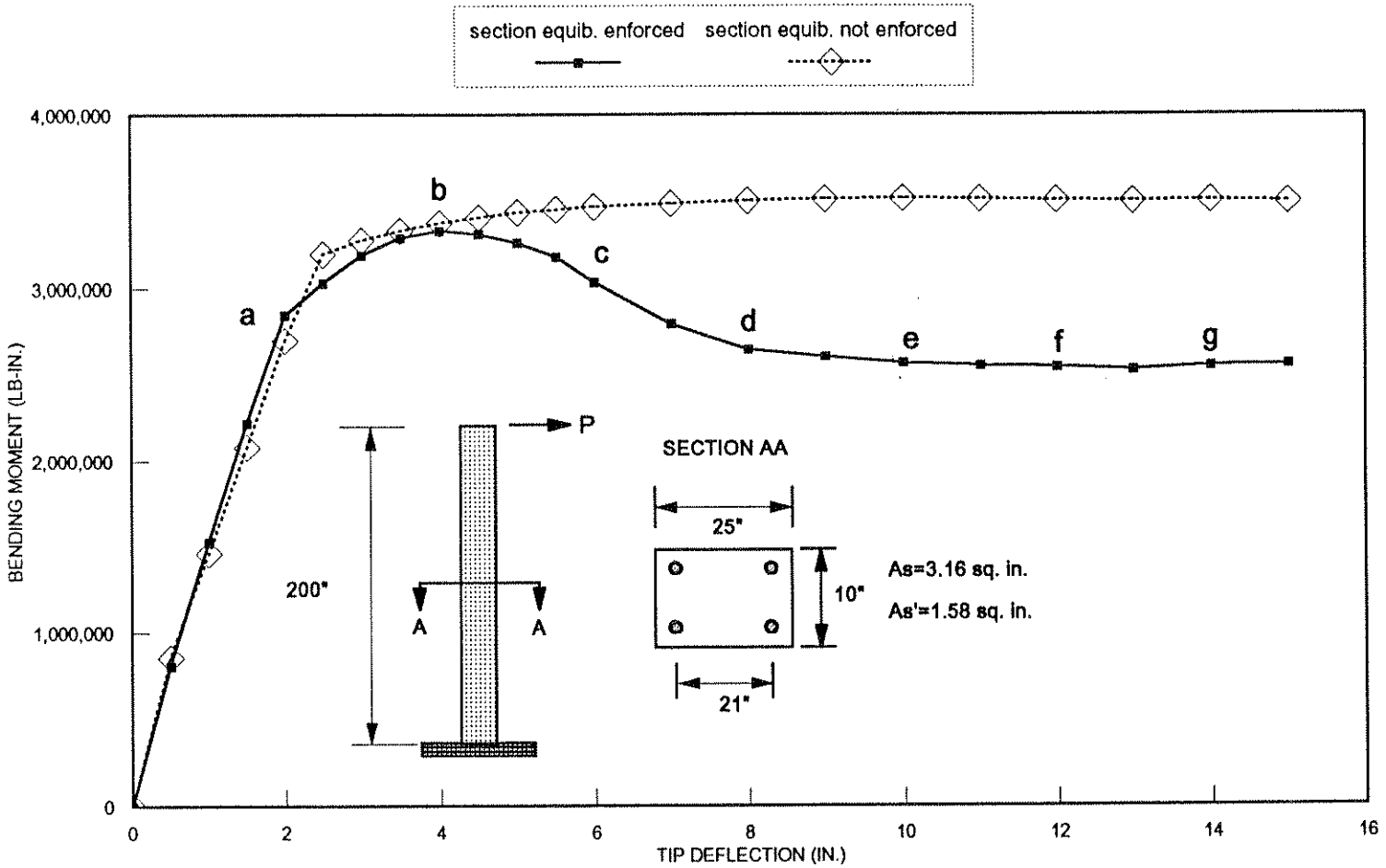

FIG. 6.07 BENDING MOMENT VS TIP DEFLECTION
EFFECT OF ENFORCING EQUILIBRIUM AT INTERMEDIATE SECTIONS.

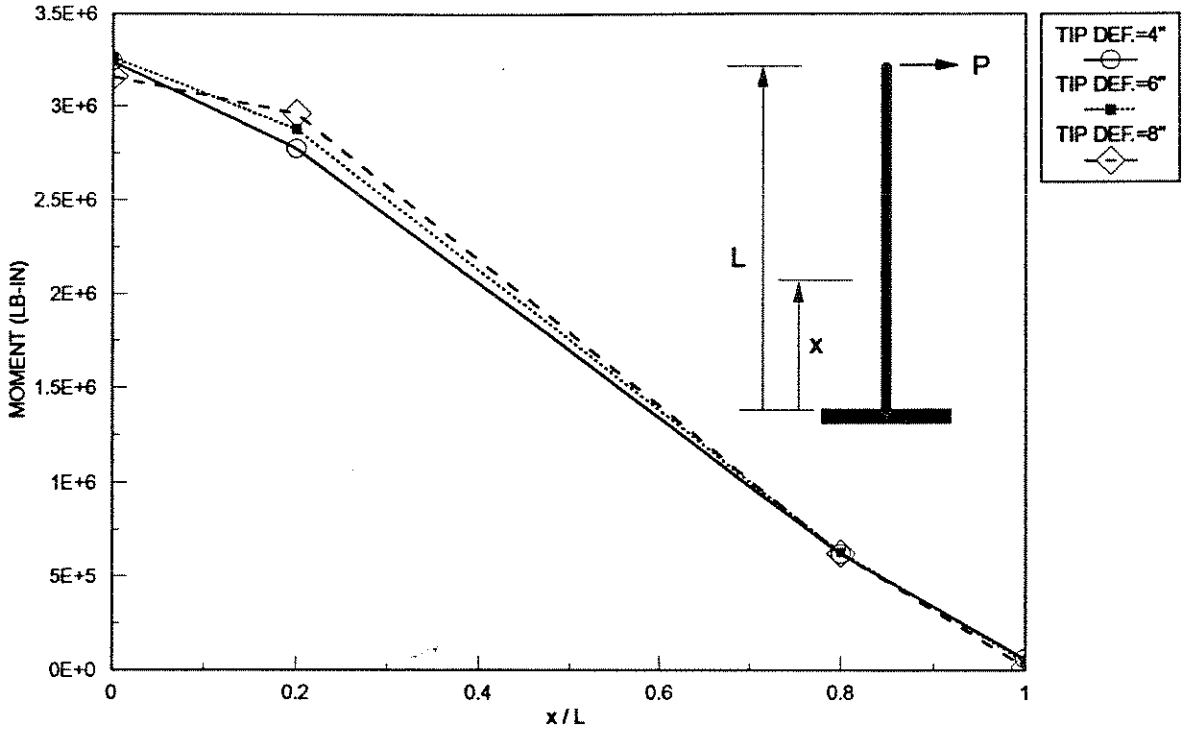

FIG. 6.08 BENDING MOMENT DISTRIBUTION ALONG COLUMN LENGTH
SECTION EQUILIBRIUM NOT ENFORCED

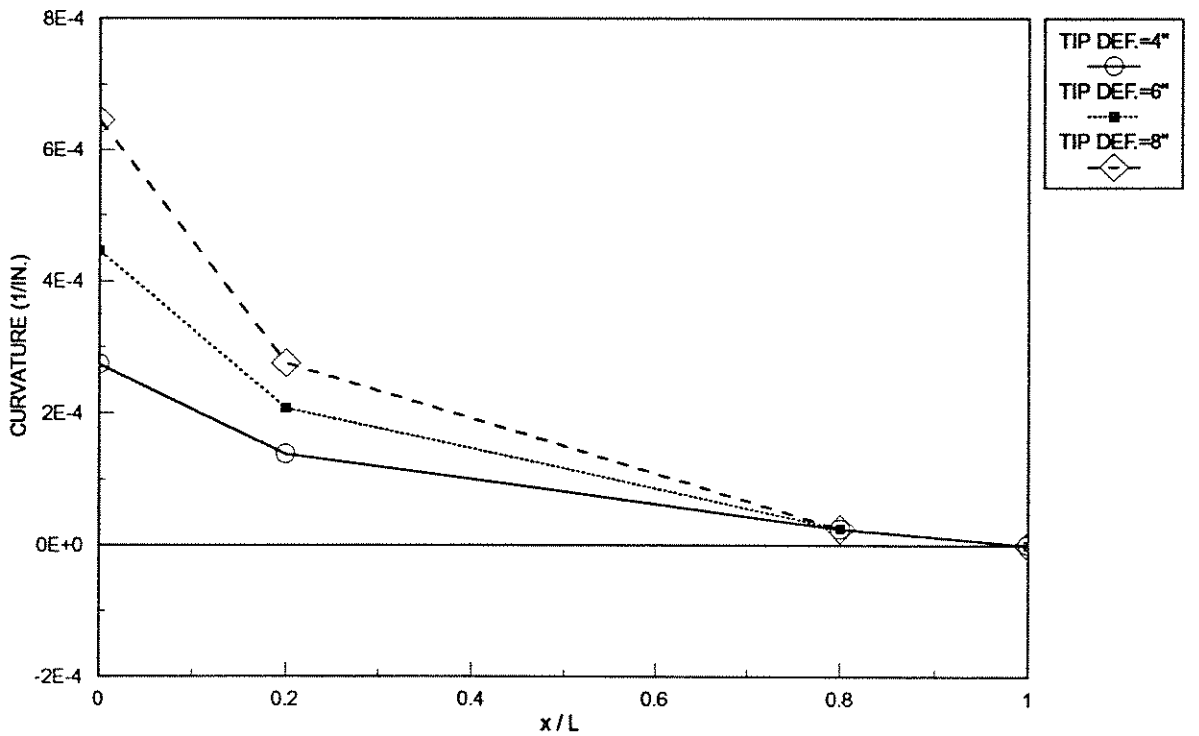

FIG. 6.09 CURVATURE DISTRIBUTION ALONG COLUMN LENGTH
SECTION EQUILIBRIUM NOT ENFORCED

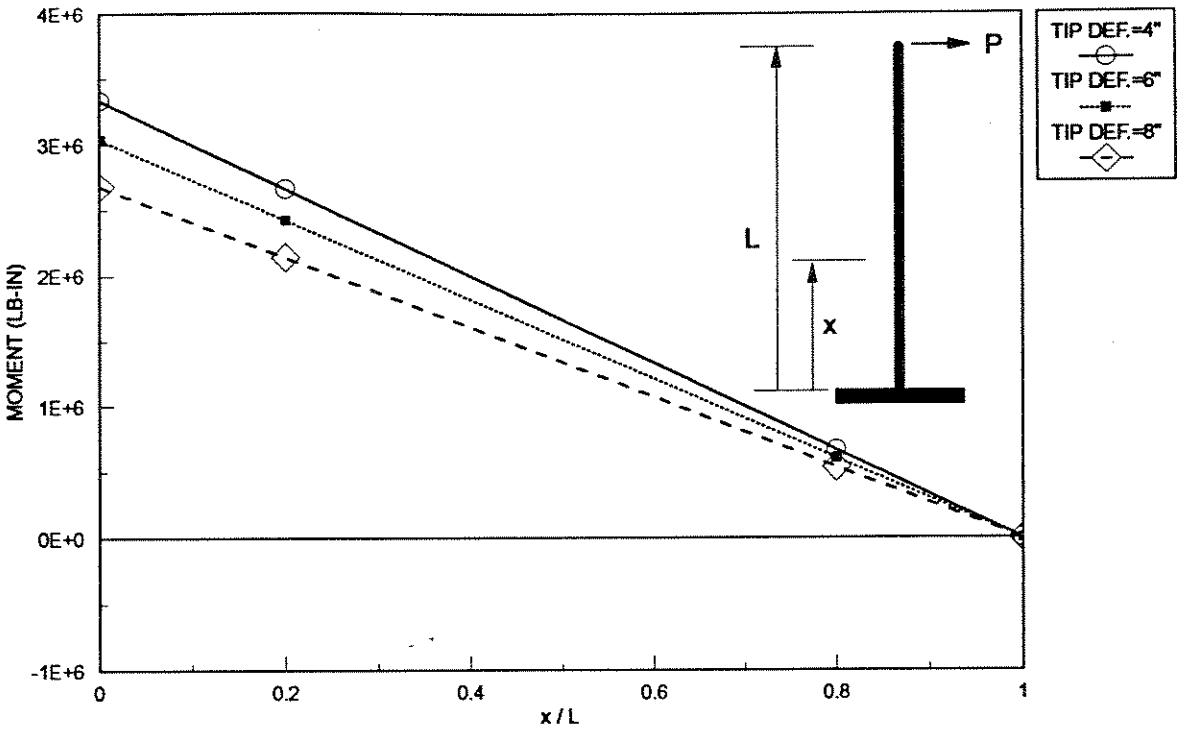

FIG. 6.10 BENDING MOMENT DISTRIBUTION ALONG COLUMN LENGTH
SECTION EQUILIBRIUM ENFORCED

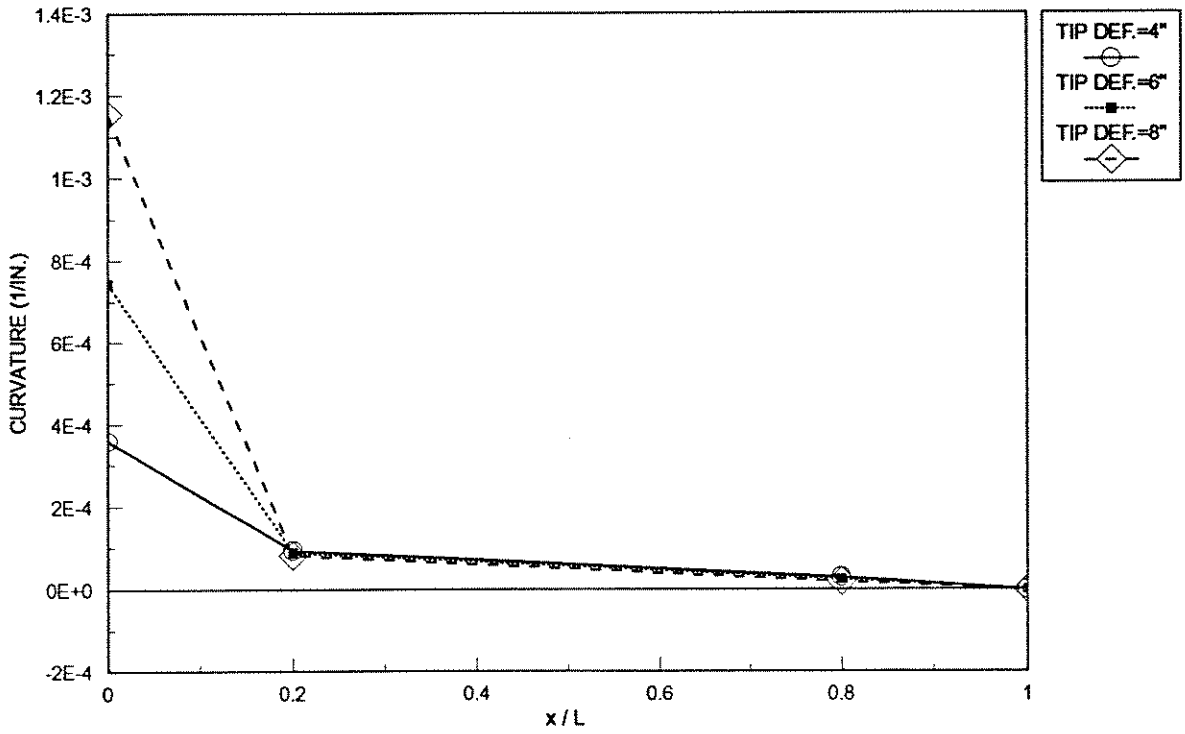

FIG. 6.11 CURVATURE DISTRIBUTION ALONG COLUMN LENGTH
SECTION EQUILIBRIUM ENFORCED

Fiber States at the Critical Section (ESD)

KEY	Fibers cracked %	Fibers crushed %	comments
a	58	0	tension steel yields
b	76	0	compression steel yields
c	76	2	
d	72	13	
e	72	17	
f	70	21	
g	68	23	

Further clues as to the differences between the two schemes are highlighted by looking at the slice moment and curvature plots along the length of the member at various values of tip deflection for both ESD and SSD schemes.

The SSD scheme, shown in Fig. 6.08 shows equilibrium violations at the intermediate section nearest to the critical section. As the bending moment at the end section pushes past peak resistance, it begins to decrease. Simultaneously, the corresponding moment at the intermediate section, begins to increase instead of decreasing.

This can be explained in conjunction with the slice curvature plot for SSD scheme shown in Fig. 6.09. Note that as the curvature at the end section increases past the point of maximum resistance, the curvature at the nearest intermediate section continues to increase thereby resulting in a higher moment and consequent equilibrium violation at the intermediate section.

In contrast, the results from the ESD scheme show that the bending moment variation stays linear at all stages, Fig. 6.10. As the bending moment at the critical section crosses the point of maximum resistance, it decreases, the bending moments at internal sections also decrease and equilibrium is satisfied at all sections.

Further, refer to Fig. 6.11, the curvature plots corresponding to the ESD scheme show that as the curvature at the critical section increases past the point of maximum resistance, the internal sections begin to unload and the curvature decreases slightly.

6.8. LOCATION OF SLICES ALONG ELEMENT LENGTH

The basic idea of the fiber beam-column element is to be able to capture the inelastic behavior of the complete element by monitoring the inelastic behavior of a finite number of slices and assuming linear variation of flexibility between the slices. The number and location of these slices is decided by the analyst, who must position them in such a manner that the actual behavior of the element is approximated.

In this section, the actual physical behavior of beam elements at or near the ultimate state is examined and numerical studies using several different slice location patterns are conducted. The results are then correlated with the actual behavior of the beam and recommendations made as to the optimum number and location of the slices. The organization is as follows:

- The actual response of the beam at ultimate limit state is discussed.
- Previous mathematical models used to predict the response of the beam at ultimate state are discussed.
- Solutions obtained with fixed shape function elements developed by Kang [49] are compared with the variable shape function element used in the present study.
- A simple equation relating the section location to the actual plastic hinge length in the element is derived.

PHYSICAL BEHAVIOR

Consider the actual behavior of a cantilever beam shown in Fig. 6.12, Park and Pauley [99], which has reached the ultimate curvature and bending moment at the critical section. The region of inelastic curvature is spread over a length of beam which is at least equal to or more than the length in which the bending moment exceeds the yield moment. The curvature fluctuations are due the increased rigidity of the member between the cracks, Fig. 6.12 (c).

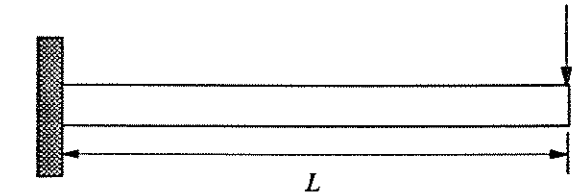

a. Cantilever Beam

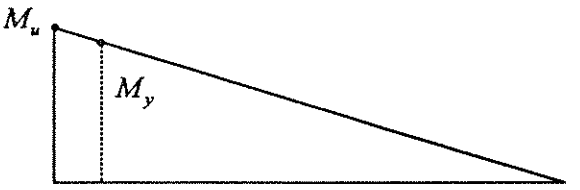

b. Bending Moment Diagram

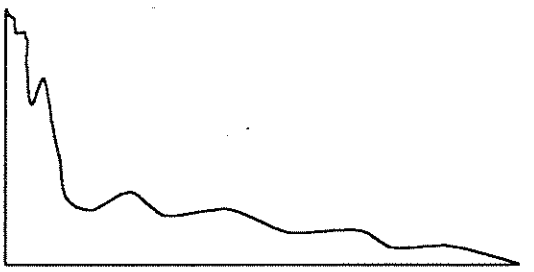

c. Curvature Distribution at Ultimate Load

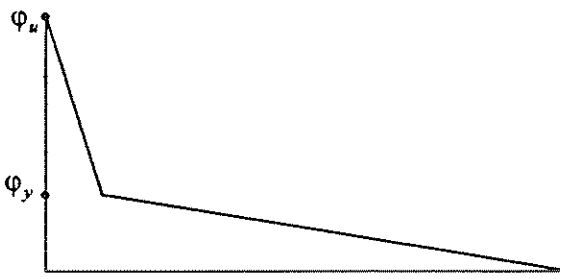

d. Idealized Curvature Distribution No Diagonal Cracks

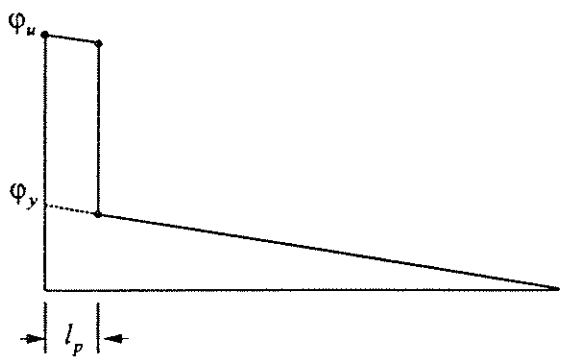

e. Idealized Curvature Distribution With Diagonal Cracks

FIG. 6.12 SPREAD OF PLASTICITY ALONG A CONCRETE MEMBER AT ULTIMATE LOAD

Adapted From Park & Pauley, 1975.

The curvature distribution may be idealized as shown by Fig. 6.12 (d). This type of distribution corresponds to a concrete member without diagonal tension cracks. The tip deflection at ultimate is approximated by the following expression:

$$\delta_u = \frac{l}{2}(\varphi_u - \varphi_y)(L - \frac{2l}{3}) + \varphi_y \frac{L^2}{3} \tag{6.58}$$

$$l = L\left(\frac{M_u}{M_y} - 1\right) \tag{6.59}$$

If diagonal tension cracks are present in the vicinity of the critical section, which is usually the case, a more realistic distribution of curvature is represented by Fig. 6.12 (e). The corresponding tip displacement is given by:

$$\delta_u = l_p(\varphi_u - \varphi_y)(L - \frac{l_p}{2}) + \varphi_y \frac{L^2}{3} \tag{6.60}$$

Several empirical expressions have been developed for the plastic hinge length l_p. Corley [24] has proposed the following expression for the length of a plastic hinge.

$$l_p = 0.5d + 0.2\sqrt{d}\left(\frac{z}{d}\right) \tag{6.61}$$

where d is the effective depth of the member and z is the distance from the critical section to the point of contraflexure. Later Mattock [84] simplified Corley's equation to the following expression.

$$l_p = 0.5d + 0.05z \tag{6.62}$$

PREVIOUS STUDIES

Mahasuverachai and Powell [79] have discussed the positioning of slices for an elasto-perfectly plastic material. Consider an element subjected to anti symmetric bending as shown in Fig. 6.13. If the end rotations are less than that causing yield $\theta \leq \theta_y$ then the variation of curvature along the element is linear and exact response can be predicted even with two slices, one at each end of the element. However if the end rotations exceed those

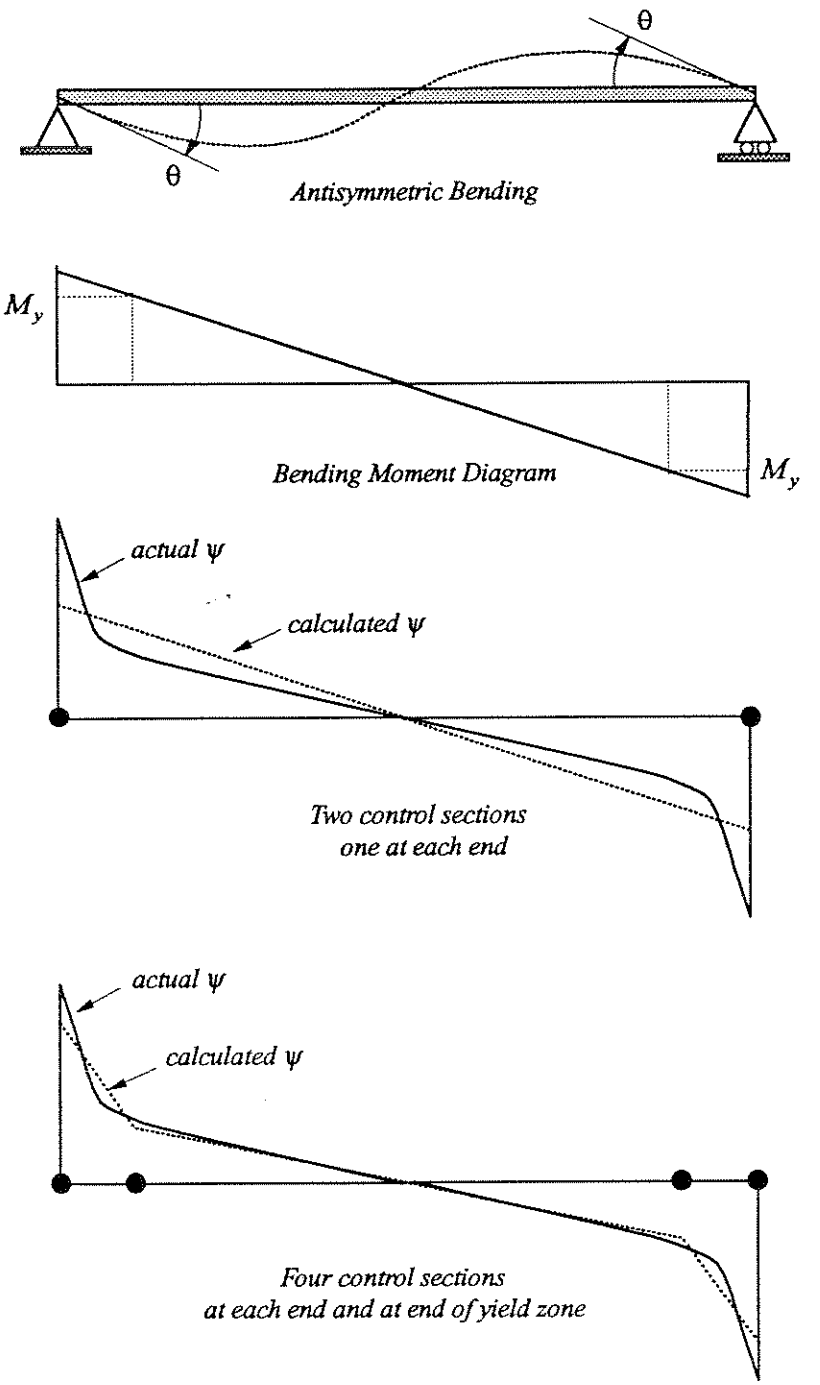

FIG. 6.13 LOCATION OF CONTROL SECTIONS
ANTISYMMETRICAL BENDING

Adapted from Mahasuverachai & Powell, 1982

Actual Variation of Flexibility

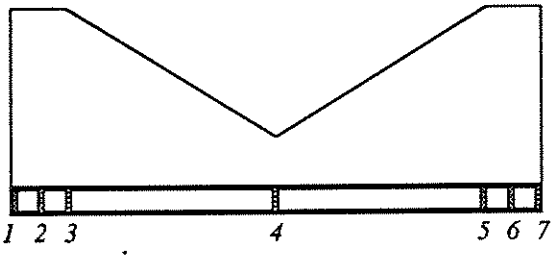

Flexibilty Variation Using 7 Slices

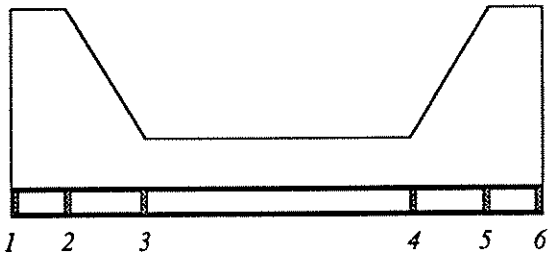

Flexibilty Variation Using 6 Slices
Adapted From Kaba & Mahin, 1982.

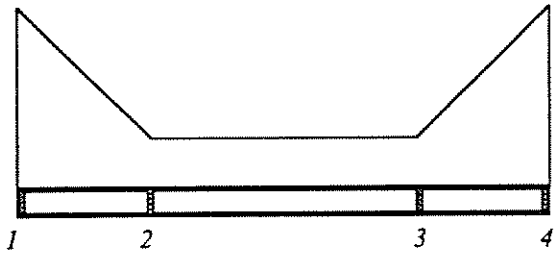

Flexibilty Variation Using 4 Slices
Present Study

FIG. 6.14 SLICE LOCATIONS TO CAPTURE ACTUAL BEHAVIOR OF BEAM

causing yield $\theta > \theta_y$ the curvature variation becomes nonlinear and at least four slices are needed to approximate the exact variation of curvature, at each end of the element and at the maximum extent of yield as shown in Fig. 6.13.

Moreover, Mahasuverachai and Powell [79] have also reported numerical tests in which they have tried two, four, seven and nine slices with a strain hardening material. For practical computation, they recommend the use of a seven slice model.

Kaba and Mahin [47] tested the effect of varying the number of slices on a two dimensional reinforced concrete fiber element. They tried five and nine slice element models wherein the slice spacing was non uniform with closer spacing in the potential yield zones. They reported that the five slice non uniformly spaced model performed as well as the 20 slice uniformly spaced model of Mark and Roesset [81].

Zeris and Mahin [149], recommended the use of six slices as shown in Fig. 6.14 to capture the behavior of concrete element subjected to symmetric or anti symmetric bending.

Hellesland and Scordelis [40] approached the problem in a different manner. They used a two slice element model with fixed cubic Hermitian shape function developed earlier by Kang [49]. Hence in order to approximate the nonlinear variation of curvature they had to resort to discretization at structure level.

FIXED AND VARIABLE SHAPE FUNCTION MODELS

The response computed with a variable shape function model (VS) with several different slice location patterns is compared with that of a fixed shape function element (FS) with several corresponding structure discretization levels.

In the case of the fixed shape function element, the results reported by Hellesland and Scordelis [41] are used. Hellesland considered the analysis of a cantilever column subject to a constant axial load and increasing lateral displacements at the free end as shown in Fig.

6.15. He considered two different types of element subdivisions and computed the tip displacement in the column as the maximum concrete strain at the base of the column reached a value of .0035.

Hellesland divided the cantilever column into 3 or 4 elements and defined the structure nodes according to the following two schemes.

(1) 0, L/60, L/6.67, L/2, L

(2) 0, L/6, 2L/3, L

In the present study, the same cantilever column is modeled as a single VS element and slices are positioned according to the following three schemes.

(1) 0, L/60, L/6.67, L/2, L

(2) 0, L/6, 2L/3, L

(3) 0, L/4, 3L/4, L

Note that the first two slice location patterns correspond to Hellesland's subdivisions 1 and 2. The use of the third scheme will be justified later. The concrete and steel properties are as follows:

$$f_c^{'} = 3320 psi$$
$$\varepsilon_u = 0.0038$$
$$f_y = 60000 psi$$
$$E = 29 \times 10^6 psi$$
$$E_{sh} = 0$$

A constant axial load is applied to the column such that $N = 0.165 f_c^{'} bd$. This is equal to about 35% of the so called balanced load. The transverse displacement at the free end of the column is incremented in steps until the maximum concrete strain reaches about .0035. The resulting load displacement plots are shown in Fig. 6.15.

KEY	PRESENT STUDY Variable Shape Functions		HELLESLAND Fixed Shape Functions	
	$\bar{r}$	$\overline{m}$	$\bar{r}$	$\overline{m}$
Type 1	1.74	.253	1.49	.250
Type 2	2.24	.251	2.62	.267
Type 3	2.49	.252		
Conventional			1.5	.248

where $\bar{r}$ and $\overline{m}$ are normalized transverse displacements at the top of the cantilever and normalized bending moment at the base of the cantilever respectively.

$$\bar{r} = \frac{\Delta h}{L^2} \times 10^3 \qquad \overline{m} = \frac{M}{f_c' bh}$$

Where Δh is the tip deflection, L is the span of the beam, b and h are cross section dimensions and M is the bending moment at the root of the cantilever,.

In the case of multi slice VS elements developed in the present study, curvatures at each control section corresponding to the ultimate state are plotted in Fig. 6.16.

In order to assess the relative merits of each of these analyses, the tip displacements must be compared with actual values. Using Mattock's equation for equivalent length of plastic hinge, the normalized tip displacements, corresponding to curvature distribution given in Fig. 6.12 (e), using a semi graphical integration scheme is given by:

$$\bar{\delta}_u = 2.44$$

Note that the results obtained by conventional type of analysis, Fig. 6.12 (d), are in good agreement with results obtained by both type 1 FS and VS elements. These are, however, theoretical values and are not of much practical use for actual concrete members.

The results computed with type 3 VS element closely approximate the tip deflection obtained by semi-graphical integration of curvatures shown in Fig. 6.12 (e).

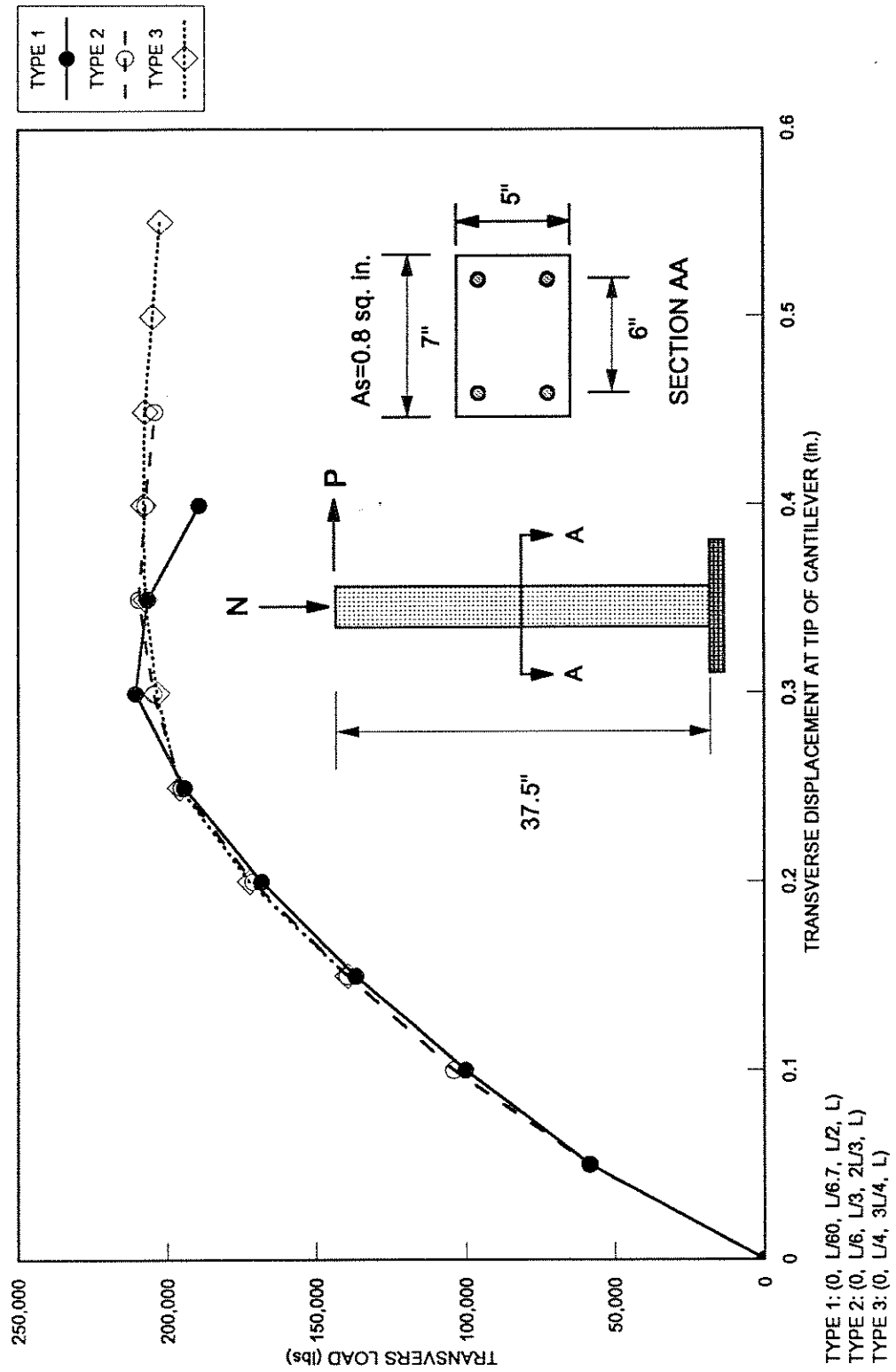

FIG. 6.15 EFFECT OF SLICE POSITION ON TRANSVERSE DISPLACEMENT AT TOP OF CANTILEVER COLUMN.

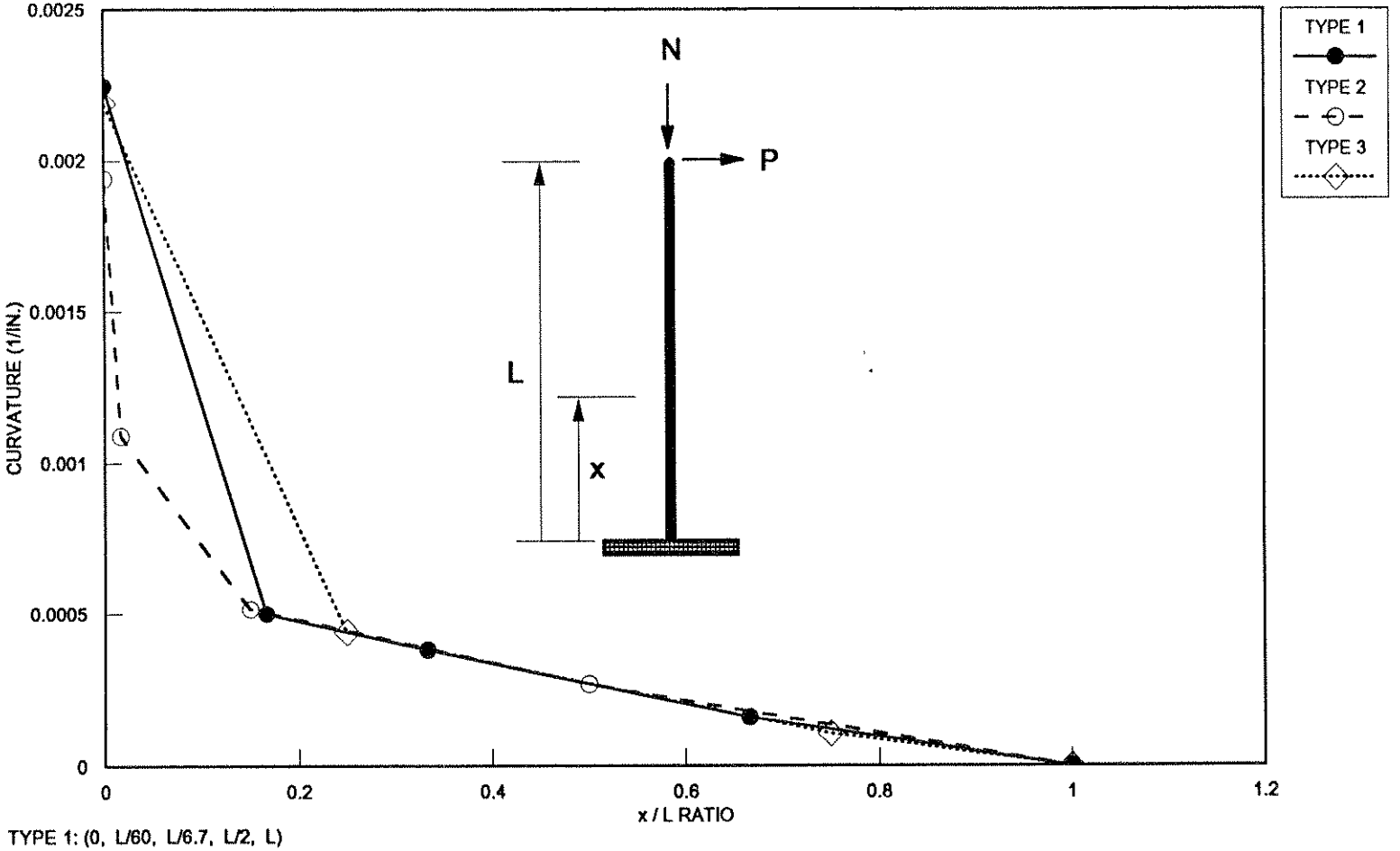

TYPE 1: (0, L/60, L/6.7, L/2, L)
TYPE 2: (0, L/6, L/3, 2L/3, L)
TYPE 3: (0, L/4, 3L/4, L)

FIG. 6.16 EFFECT OF SLICE POSITION ON CURVATURE DISTRIBUTION AT A MAXIMUM CONCRETE STRAIN OF .0035 .

Hence, it is suggested that a four slice VS element can capture the essential behavior of a concrete element in a relatively efficient manner provided that control sections are placed at appropriate positions.

RELATION BETWEEN SLICE LOCATION AND PLASTIC HINGE LENGTH

Numerical tests, in addition to those reported above, indicate that intermediate control sections when placed at about $2\,l_p$ from the end section, furnish satisfactory results. This statement can also be justified theoretically albeit not rigorously. Consider a four slice VS element as shown in Fig. 6.17. The curvature distribution captured by the element and its linear approximation is shown by the solid line and dotted lines respectively. The tip deflection at ultimate is given by:

$$\delta_u = \frac{x}{2}(\varphi_u - \varphi_y)(L - \frac{2x}{3}) + \frac{\varphi_y L^2}{3} \tag{6.63}$$

Setting Eq 6.62 equal to Eq. 6.59 and solving for x we have:

$$\frac{x}{L} = \frac{3 - \sqrt{9 - 8(6k - 3k^2)}}{4} \tag{6.64}$$

where $k = \frac{l_p}{L}$. Expanding the solution in a series and ignoring terms of third order and higher we have:

$$\frac{x}{L} = 2k + \frac{5}{3}k^2 + O(3) \tag{6.65}$$

Hence, in the case of the cantilever beam being considered, a control section placed at about twice the plastic hinge length will give a good estimate of the ultimate deflection.

The above discussion highlights the fact that in order to get reasonable estimates of ultimate deflections, intermediate control sections must be positioned to approximate the curvature distribution at ultimate load. This requires a prior knowledge of the physical plastic hinge length, which in turn is a function of the parameter z, the distance from the critical section to

the point of contraflexure. Hence depending on the degree of accuracy desired, the analysis model may be refined in an iterative manner.

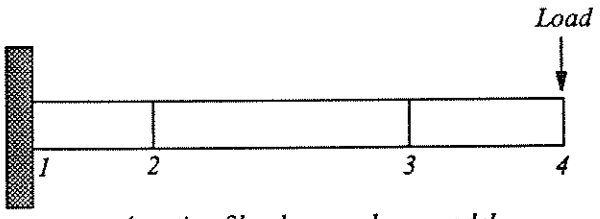

4 section fiber beam-column model

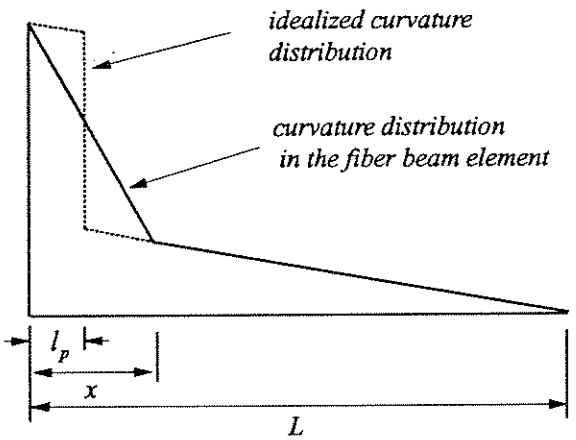

FIG. 6.17 SLICE LOCATION TO CAPTURE BEAM RESPONSE AT ULTIMATE

6.9. NUMERICAL EXAMPLES

The fiber beam-column element discussed above was implemented in the computer program CALBRG, which was developed as a part of this study. Several numerical examples were solved to test the accuracy of the element. A brief discussion of the results obtained in each case is presented in the next sections.

6.9.1. SNAP THROUGH OF A TWO-BAR TRUSS

A 2-bar truss, shown in Fig. 6.18 is subjected to a vertical load at node 2. A nonlinear geometry, large displacement analysis is performed.

The truss bars are modeled with beam elements of linear elastic material. The vertical displacement of node 2 is incremented in 13 equal steps of 1.5 units each. The resulting load displacement plot is shown in Fig. 6.18.

This example demonstrates the ability of the program CALBRG to solve a large displacement problem involving a snap through phenomenon. Note that the load carrying capacity of the structure drops to zero at two points; when the displacement of node 2 reaches 8 units and all three nodes are collinear and at a displacement of 16 inches when the structure has inverted completely.

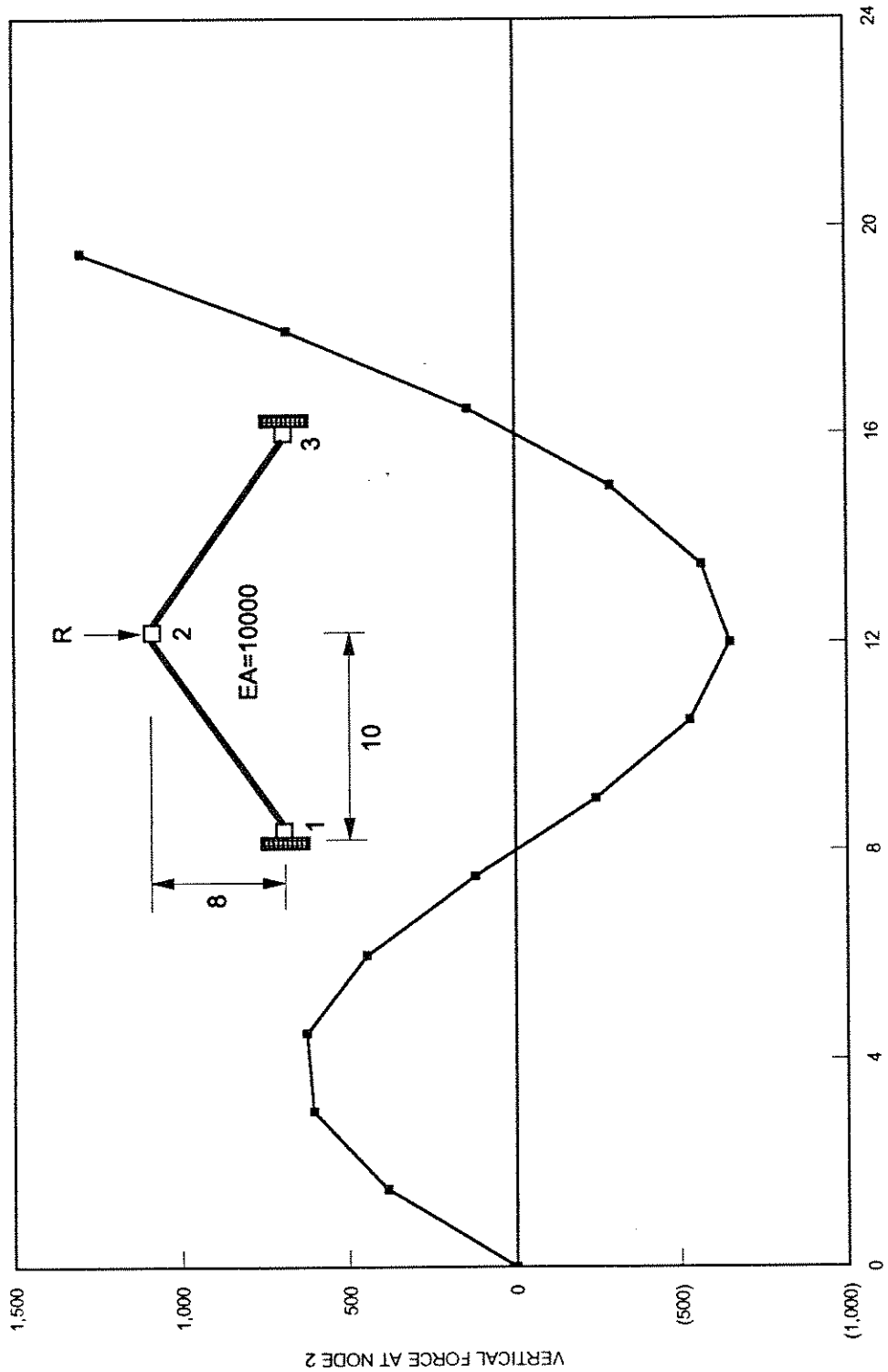

FIG. 6.18 SNAP-THROUGH OF A TWO-BAR TRUSS
DISPLACEMNT CONTROL SOLUTION

6.9.2. SYMMETRICAL BUCKLING OF A CIRCULAR ARCH DUE TO UNIFORM PRESSURE

The analysis of a fixed end shallow circular arch subjected to a uniform pressure is presented in this section to verify the capability of the program to solve a large displacement snap-through type of problem. Nonlinear geometry is enforced and the material is assumed to behave in a linear elastic manner.

The geometry and the material properties are shown in Fig. 6.19. Due to the symmetry of the structure, one half of the arch is modeled with ten equal sized beam elements. Each beam element has two control sections, one at each end. The cross section is divided into 20 fibers each having an area of 0.1 $in.^2$.

A displacement controlled analysis is performed. The vertical translation at the crown is selected as the degree of freedom to be controlled and the displacement is incremented in 10 equal steps of 0.5 in. each. The pressures-displacement response of the structure is shown in Fig. 6.19. The solution obtained by CALBRG is in good agreement with the analytical solution of Schreyer [114].

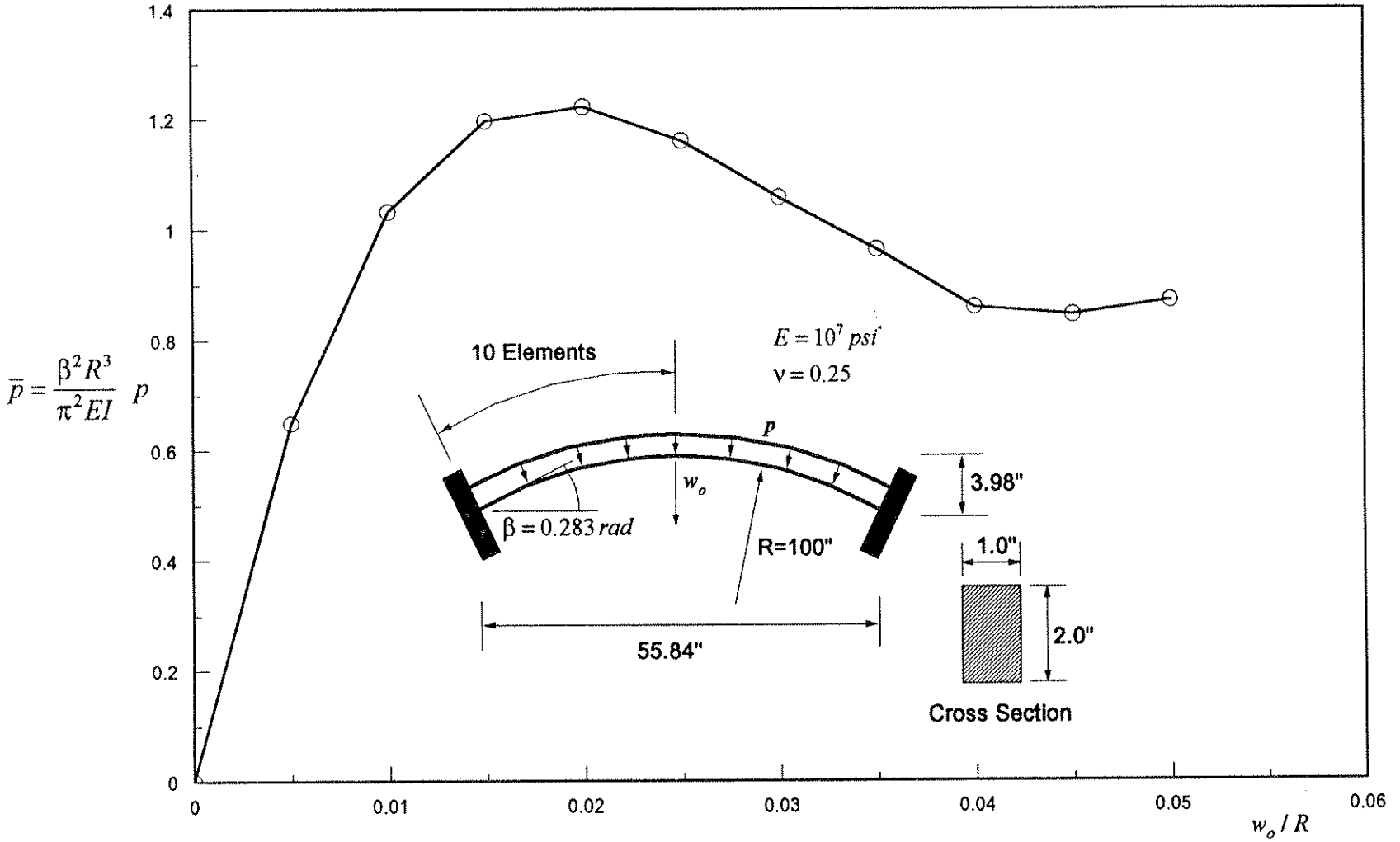

FIG. 6.19 SYMMETRICAL BUCKLING OF A CIRCULAR ARCH.
LOAD VS CENTRAL VERTICAL DISPLACEMENT.

6.9.3. BIAXIAL BENDING OF A REINFORCED CONCRETE COLUMN

The purpose of this example is to demonstrate the ability of the beam column element to handle problems in biaxial bending and to study the effect of slenderness ratio on the response of the column.

The geometry and material properties of the column are shown in Fig. 6.20. The column is fixed at the base and is subjected to an eccentric load at the top.

Two different cases are considered.

1. Column A, with a length of 100 inches.
2. Column B, with a length of 200 inches.

Both columns have the same cross section and reinforcement.

The cantilever column is modeled by 8 equal size beam-column elements. Each element had 6 evenly spaced control sections or slice locations. The cross section was discretized into 36 concrete and 16 steel fibers. The column was then analyzed by displacement control strategy; the vertical displacement at the top of the column was gradually incremented and the corresponding increase in the eccentric axial load noted. The solution included the effects of nonlinear material and geometry. The resulting load-displacement plots for both columns are shown in Fig. 6.21.

Column A was also analyzed by Warner [145] who assumes a cosine function for the deformed shape. Good agreement exists between the two solutions. Analysis results show that the column fails by yielding of reinforcement and cracking and yielding of concrete.

For further verification the results of column B were compared with a previous solution by Chan [19]. Again the two solutions are in good agreement and almost identical results are obtained.

Note that doubling the slenderness ratio results in almost a 50% decrease in the carrying capacity of the column whereas the ductility increases to more than four times that of column A.

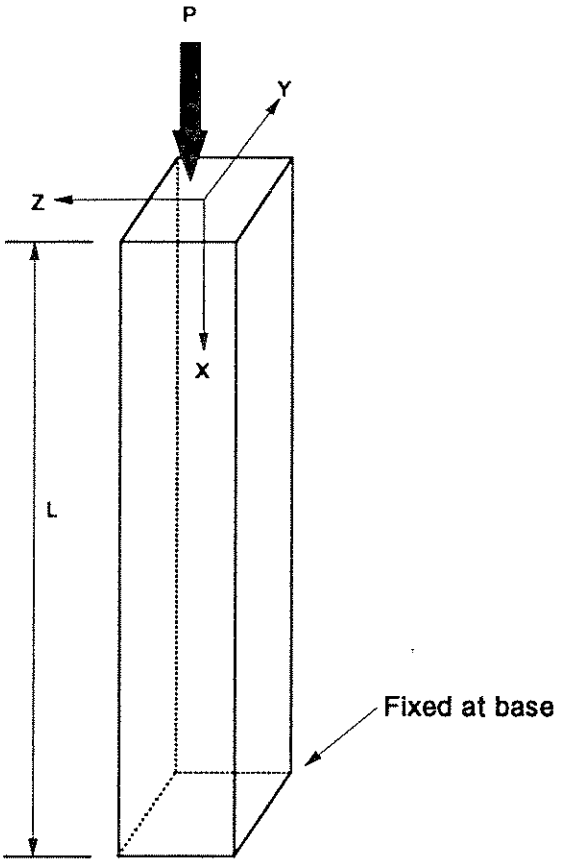

ISOMETRIC VIEW OF CANTILEVER COLUMN
FIXED AT BASE

Total area of Steel =5.46 sq. in.

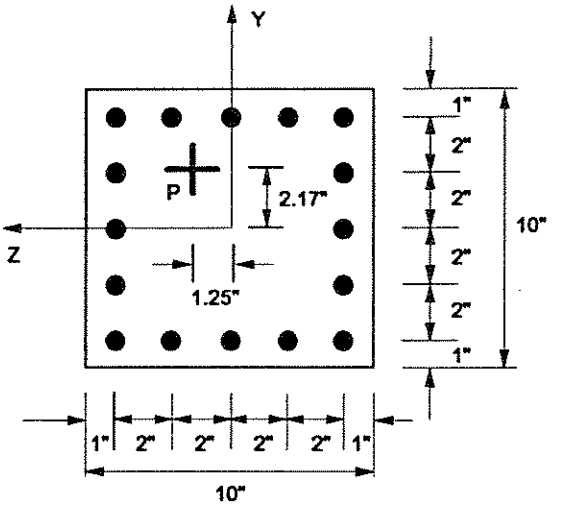

CROSS SECTION

CONCRETE PROPERTIES

$f_c^{'} = 4000\ psi$

$f_t = 10\ psi$

$E = 3.6 \times 10^6\ psi$

STEEL PROPERTIES

$f_y = 36600\ psi$

$E = 30 \times 10^6\ psi$

$E_{sh} = 0$

FIG. 6.20 BIAXIAL BENDING OF A REINFORCED CONCRETE COLUMN
GEOMETRY

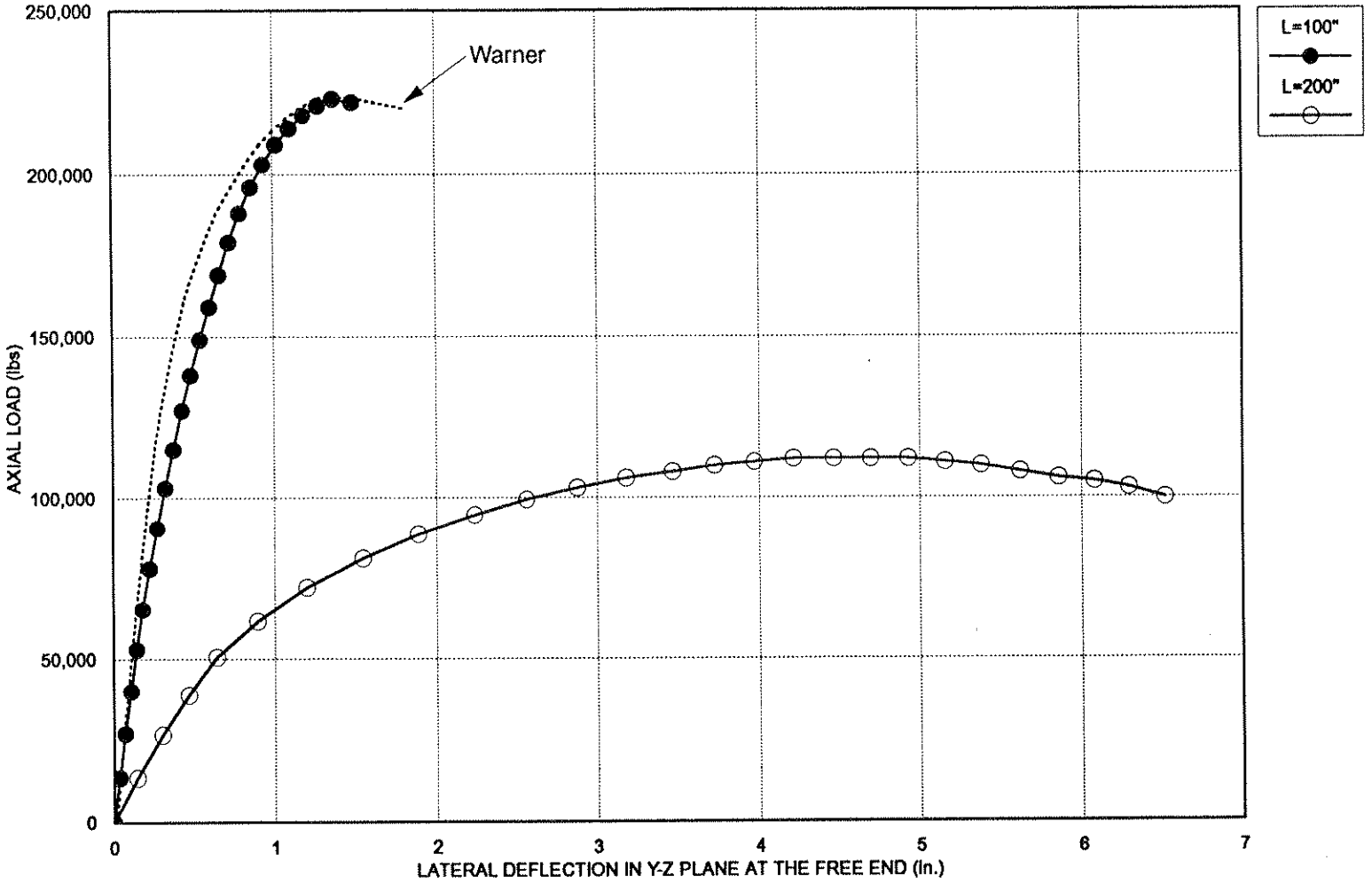

FIG. 6.21 BIAXIAL BENDING OF A REINFORCED CONCRETE COLUMN
LOAD VS LATERAL DISPLACEMENT IN THE Y-Z PLANE

6.9.4. REINFORCED CONCRETE TIMOSHENKO BEAM.

This problem was originally analyzed by Timoshenko who treated it as an elemental strip cut from a long rectangular elastic plate bending into a cylindrical surface. Later various researchers Aldstedt [4], Kang [49], Van Greunen [140], and Chan [19] used Timoshenko's solution as a bench mark to verify their analytical solutions for a reinforced concrete beam.

The reinforced concrete beam is simply supported and restrained against horizontal movement at the two ends and subjected to a uniformly distributed load over its length. The geometry of the beam, loading and material properties are shown in Fig. 6.22. Due to symmetry only one half of the structure is modeled with 10 beam-column elements as shown in Fig. 6.22. Note that in order to capture the behavior of relatively highly stressed mid span zone, element subdivision is refined in the middle third of the beam. Each element has two control sections or slices, one at each end. The cross section is descritized into 28 concrete fibers, the steel bars are represented by two appropriately placed steel fibers. Four different types of analyses were conducted:

1. Material linear, geometry linear.
2. Material linear, geometry nonlinear.
3. Material nonlinear, geometry linear.
4. Material nonlinear, geometry nonlinear.

The purpose of these analyses was to study the influence of each type of nonlineraity on the load-deflection response of the beam. The beam was analyzed by load control strategy wherein the load was gradually increased in equal steps of 14 lb./in. each. Fig. 6.23 shows the load versus deflection plot at mid span for each of the four cases listed above.

For case 1, with linear material and geometry, the equilibrium equations are solved in undeformed state. The load carried by the beam is directly proportional to the bending moment at mid span.

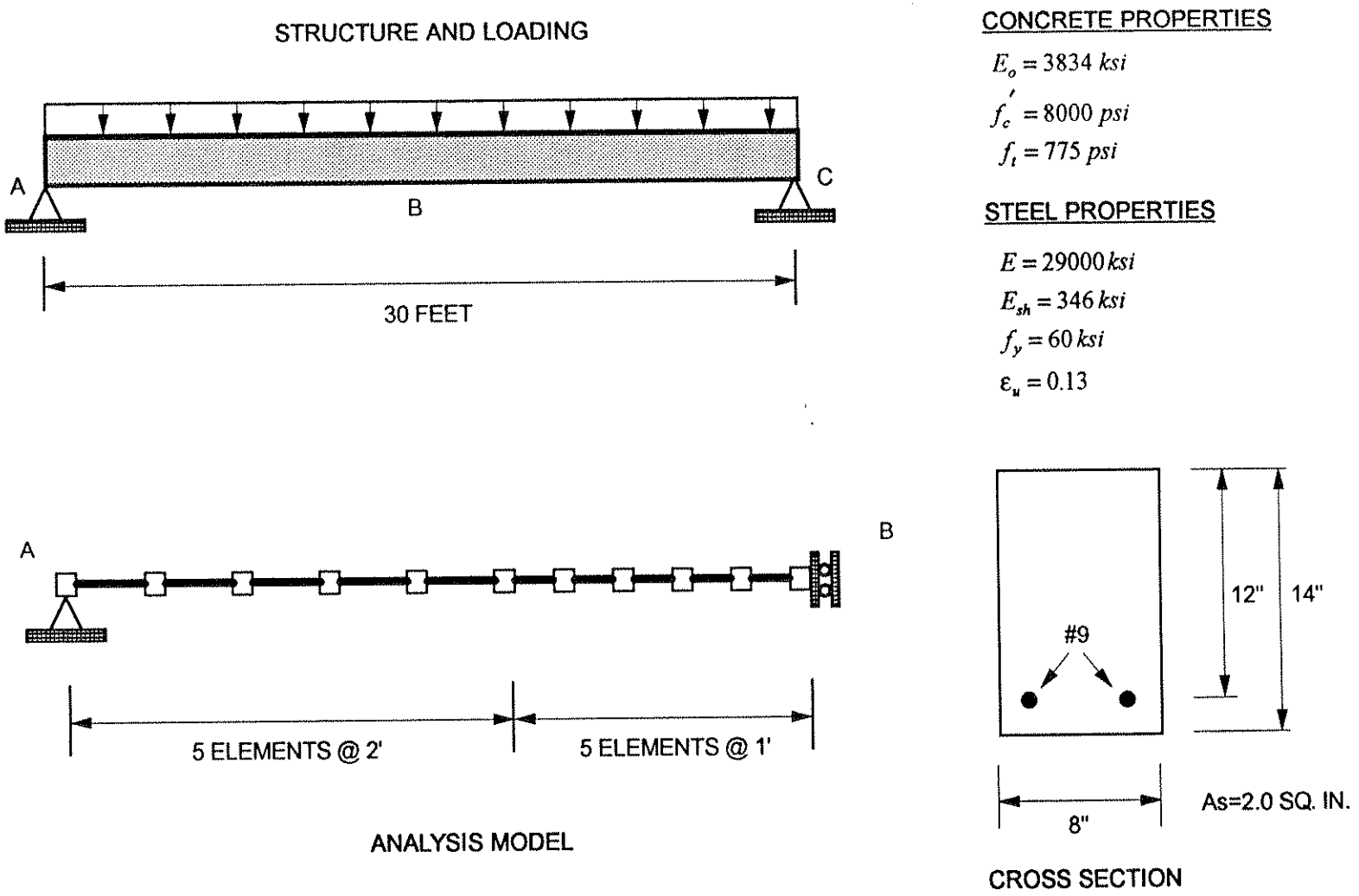

FIG. 6.22 REINFORCED CONCRETE BEAM; GEOMETRY & MATERIAL PROPERTIES.

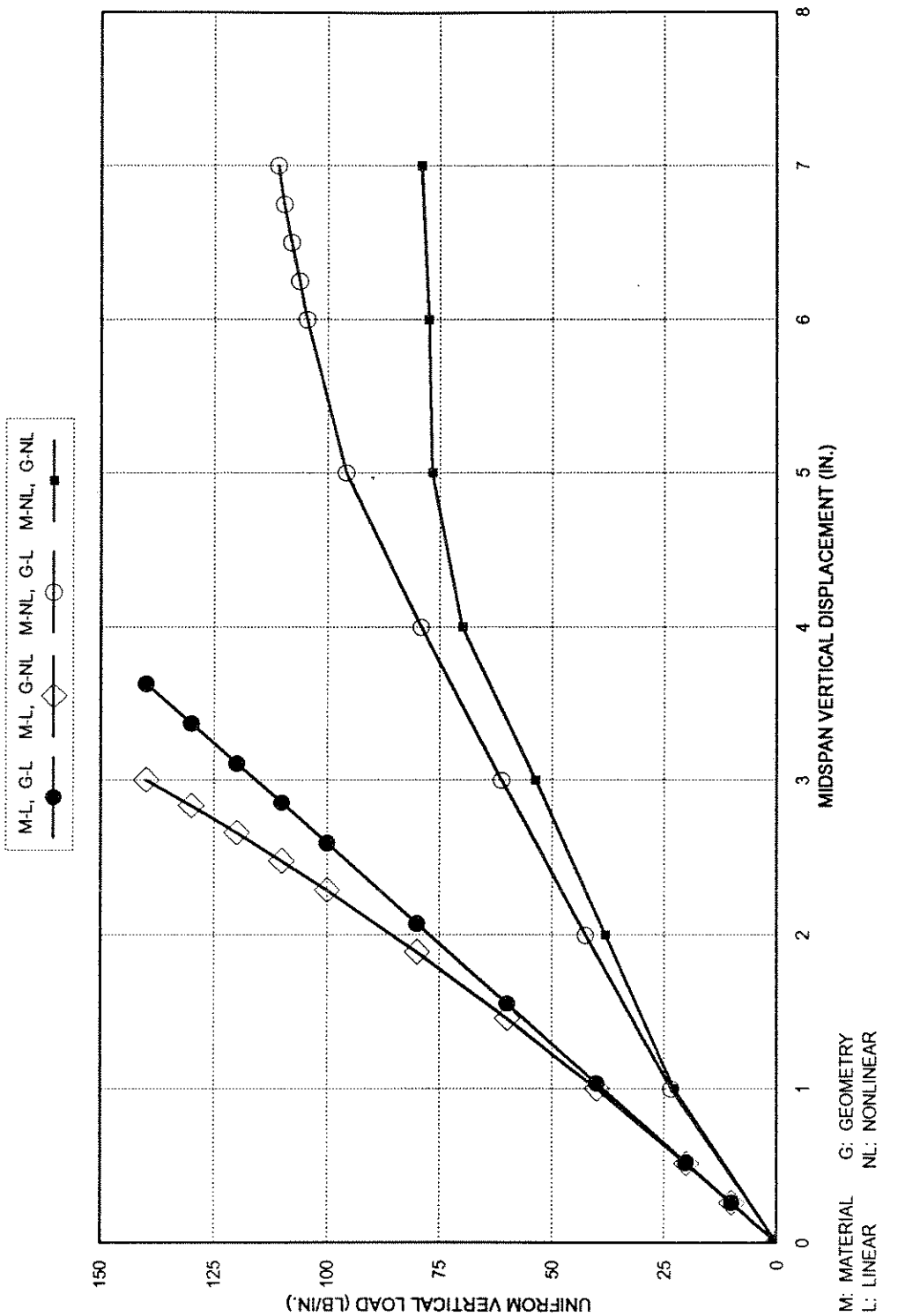

FIG. 6.23 REINFORCED CONCRETE BEAM
LOAD VS VERTICAL MIDSPAN DISPLACEMENT.

$$M = q\left(\frac{8}{l^2}\right)$$

In case 2, with nonlinear geometry, the equilibrium equations are solved in the displaced configuration. The moment equilibrium equation at mid span is given by:

$$(M + P\Delta) = q\left(\frac{8}{l^2}\right)$$

Note that the internal bending resistance is enhanced due to the $P-\Delta$ effect and the load-displacement plot exhibits a distinct stiffening effect due to the development of the in plane tensile forces in the beam

For case 3, which considers only material nonlinearity, there is gradual degradation in stiffness due to cracking of concrete fibers in tension and due to decrease in the modulus of concrete fibers in compression.

In contrast, case 4 which addresses both geometric and material nonlinearity shows a sudden softening of the structure at about 70 lb./in. due to yielding of steel probably due to the presence of in-plane tensile forces. The beam ultimately fails in a ductile manner at a load of about 80 lb./in.

7. PRESTRESSING

7.1. GENERAL

Prestressing is induced in concrete members to improve structural behavior. Structures can be prestressed either by pre-tensioning or by post-tensioning. Pre-tensioning is normally used for prefabricated concrete components whereas post-tensioned construction is more commonly used for bridge structures. In post-tensioned concrete structures, tendons are stressed after the concrete has been cast and hardened. The tendons are generally enclosed in metal ducts embedded in concrete and anchored at the ends using special anchoring devices. The ducts are usually grouted after the tensioning operation to protect the tendon from any corrosion.

Prestressing is used in bridges for a number of reasons.

- The same load can be carried by lighter structure.
- Improves service load behavior by control of cracking and limiting deflections.
- Enhances ultimate strength of the structure.
- Limits long term deflections.
- Allows for longer maximum spans.

The force carried by a prestressing tendon is affected by both short term and long term losses. Short term losses take place at the time of stressing and include friction losses, anchorage slip losses and any losses due to deformations of the concrete member. Long

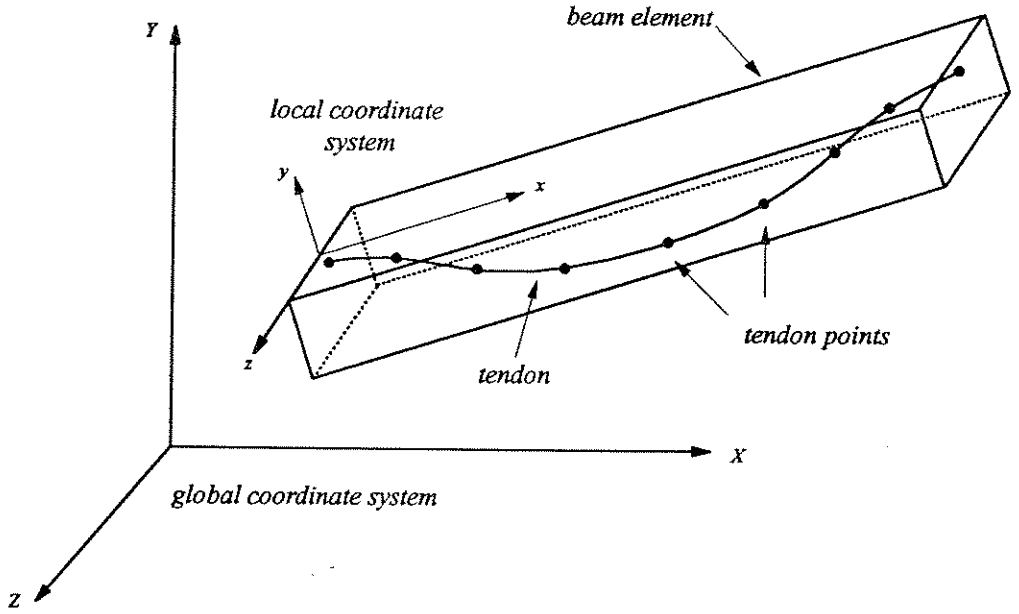

FIG. 7.01 TENDON COORDINATE SYSTEM AND GEOMETRY.

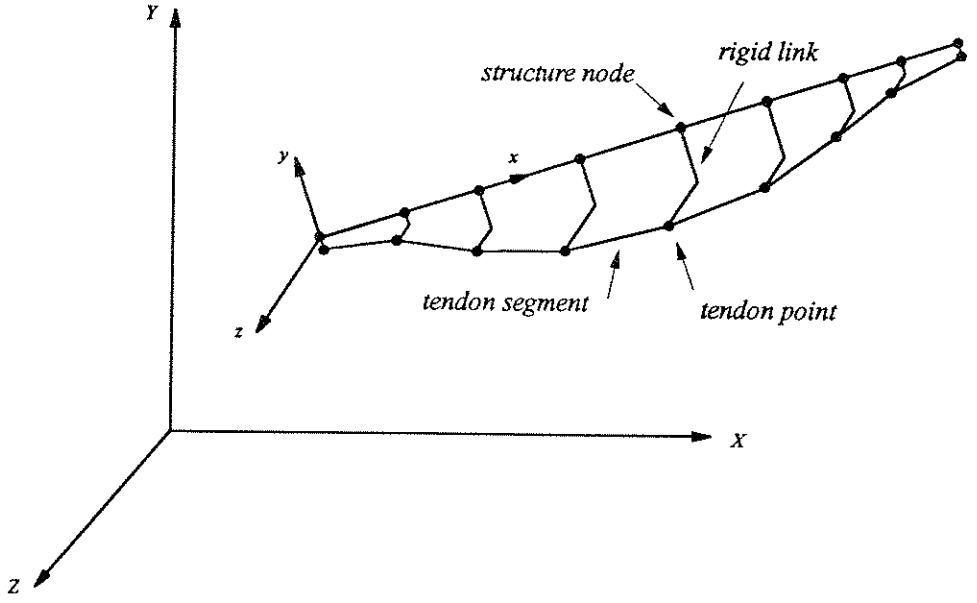

FIG. 7.02 PIECE WISE LINEAR DISCRETIZATION OF TENDON.

term losses take place during the life of the structure and are due to creep and shrinkage of concrete and relaxation of prestressing steel.

In addition, the force in the tendon is also affected by changes in the configuration of structure and the loads applied to it. The determination of these force changes which usually occur during cantilever construction of box girder bridges is a complex procedure and necessitates the use of special purpose computer programs which can keep track of tendon stress changes during a segmental construction sequence, Ketchum [53], Kang [50], Abbas [1].

Prestressing tendons are laid out in concrete box girders along pre defined profiles. These profiles may consist of a combination of parabolas or straight lines. In order to define the profile numerically for input to a computer program, it is discretized into a series of linear segments, Scordelis et al. [120]. The point of intersection of adjacent segments is known as a tendon point and it must lie on the original profile of the tendon. Tendon profiles may be specified either by direct input of tendon points along the length of the tendon or in the case of some commonly used standard profiles by specifying certain geometric parameters which are then used by the computer program to generate tendon point coordinates.

Scordelis et al. [120] accounted for prestressing in their analysis procedures by considering it as set of equivalent nodal loads. Tendon forces were first evaluated at the tendon points along the length of the tendon and then converted to statically equivalent nodal forces. The load vector thus obtained was combined with other load cases to determine the total stresses and displacements in the structure. This approach was used in computer programs MUPDI4, CURDI4 and CELL4 [120]. The numerical procedure implemented in these program was able to account for short term prestress losses due to friction and anchorage slip. However it could not account for long term losses caused by creep and shrinkage of concrete and due to relaxation of prestressing steel and these had to be simply specified as a fraction of initial prestressing force.

Later Ketchum [53] enhanced this formulation to account for long term losses. He assumed that a tendon segment behaved like a pre-strained eccentric truss bar whose ends were rigidly connected to appropriate structure nodes. This allowed him to keep track of changes in tendon force due to time dependent effects as well as due to changes in structural configuration. These procedures were implemented in the computer program SFRAME.

Kang [50] used a nonlinear material model for prestressing steel and was thus able to predict the ultimate strength of prestressed concrete bridges using the program SPCFRAME. However, both SFRAME and SPCFRAME were designed for two dimensional planar analysis.

The present study extends the formulation given by Scordelis et al. [120] and Ketchum [53] to a three dimensional case and takes into account both short and long term prestress losses. In addition, it also considers the effect of changing loads and structural configuration on the state of a stress in a prestressing tendon.

This chapter describes discretization of a tendon into a series of linear segments, definition of tendon profile and parametric generation of tendon point coordinates, computation of short term force losses due to friction and anchorage slip, improved algorithm for computation of tendon stress loss due to relaxation, equivalent nodal loads, stiffness formulation and state determination procedures involved in a non-linear solution.

7.2. TENDON DISCRETIZATION

Consider an actual tendon which follows a pre defined three dimensional curve in a box girder bridge as shown in Fig. 7.01. This tendon is modeled as a series of linear segments interconnected at tendon points which lie on the actual curve, Fig. 7.02. Thus there would be n tendon points in a tendon discretized into $(n-1)$ linear segments. Each tendon point is located at the same cross section as a structure node and the displacements of the tendon point are slaved to that of the node.

Note that the slaving of each tendon point to its corresponding structure node implies that displacement compatibility between the tendon and the surrounding concrete is enforced only at the tendon points. In the case of an actual unbonded post-tensioned tendon, displacement compatibility exists only at the end anchor points of the tendon. However, after the tendon is grouted, it is assumed that perfect bond exists between concrete and prestressing steel, which in turn implies displacement compatibility at every point along the length of the tendon. In this case modeling accuracy can be increased to any desired degree by a finer discretization of the tendon, however, a penalty must then be paid in terms of increased computational effort.

Piece wise linear discretization enables the analyst to describe a wide range of commonly used tendon profiles as well as relatively complex space curves. In addition, since each linear tendon segment is modeled as an eccentric truss bar whose ends are connected by rigid links to the member nodes, the effect of creep and shrinkage displacements at the member nodes is felt by the tendon as well.

Each tendon segment is assumed to have a constant force. The initial force in each tendon after short term losses is calculated by methods presented in Section 7.4. The evaluation of equivalent nodal loads and stiffness contribution of each tendon segment is decribed in Section 7.7.

7.3. DEFINITION OF TENDON PROFILE

To start with, we shall define some terms that will be frequently used in subsequent discussion.

- A tendon is a prestressing steel strand laid out on a pre-defined three dimensional path inside a concrete member and extends from one anchor to the other.

- A span is section of tendon which follows a standard geometric profile, this may or may not correspond to the actual physical spans of a bridge. Each tendon may have multiple spans.
- Each span is divided into a series of linear tendon segments inter connected at tendon points.

A tendon profile is said to be completely defined if the global position coordinates *(Xg, Yg, Zg)* of each tendon point are known. This may be done by direct input of tendon coordinates or by parametric generation of the profile.

The degree of discretization required in a tendon depends to a certain extent on the curvature of the tendon. For example, a parabolic profile requires a considerably finer subdivision into segments as compared to a linear profile. Care should be taken in discretizing straight tendons in a curved bridge as the tendon exerts radial forces on the structure along its length. Use of relatively shorter tendon segments is recommended in such cases.

7.3.1. DIRECT DEFINITION OF TENDON PROFILE

This method is generally used when non standard tendon profiles are used. It is a direct input method which although simple conceptually, may require a colossal effort on the part of the engineer to prepare the input data.

The direct definition of tendon profile involves the following steps:

- The engineer manually selects the tendon points on the tendon corresponding to structure nodes as specified earlier on an analysis model.
- The global coordinates of these tendon points are then directly input to the analysis program.
- The computer program developed in the present study CALBRG also allows for a direct input of the tendon point coordinates with respect to a local coordinate system. This coordinate system is defined by specifying a set of I, J and K nodes, where IJ

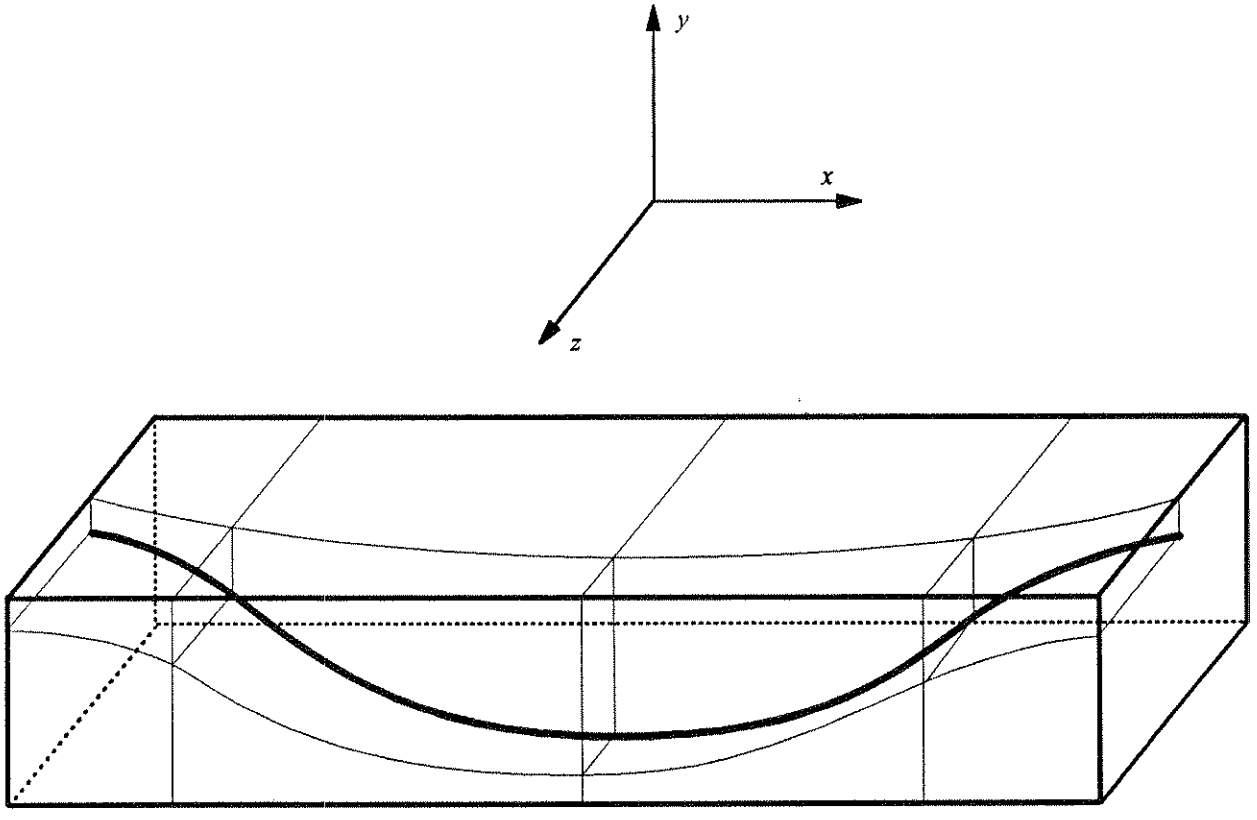

FIG. 7.03 TENDON PROFILE IN THREE DIMENSIONS
SIMPLE PARABOLA IN XZ PLANE
PARABOLAS CONNECTED IN SERIES IN XY PLANE

defines the local X-axis and IK lies in the local XY plane. For sake of convenience, this coordinate system usually coincides with the local coordinate system of the concrete member. Thus the engineer has to specify only the local coordinates Y and Z at each tendon point, these are then transformed internally by the computer program to global coordinates.

7.3.2. PARAMETRIC DEFINITION OF TENDON PROFILE

In general, certain standard tendon profiles are used in prestressed concrete bridges. For example, in the case of deck girders, a commonly used tendon profile consists of a combination of parabolas draped between pier supports. It is possible to generate tendon point coordinates for such profiles by specifying certain parameters. The procedures developed in the present study allow for the generation of parabolic profiles which are draped in both XY and XZ plane as shown in Fig. 7.03.

The nomenclature used to define a standardized tendon profile is shown in Fig. 7.04. The profile definition parameters used in the generation algorithms both in the XY plane and the XZ plane are shown in Fig. 7.05 and 7.06 Consider the profile in XY plane. It has a span length of L and is defined by a series of four parabolas, AB, BC, CD and DE. To ensure a smooth transition, the parabolas have common slope at the points of intersection B and D, point C has zero slope. In addition, the end points A and E also have zero slope to guarantee tangent connections with adjacent spans. Note that if the points A, B and E are the same level then the curve degenerates into a level straight line.

The tendon profile is completely defined by the following parameters. Note that all coordinates are referred to a local coordinate system selected by the analyst and described earlier.

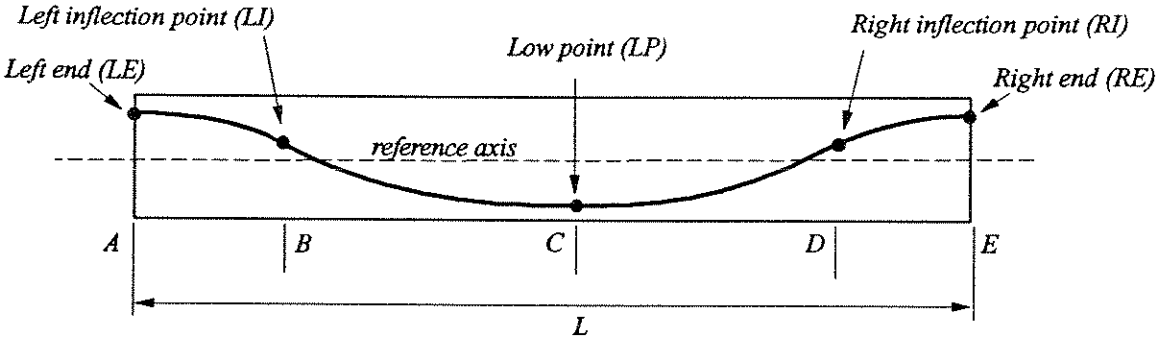

$$RLI = \frac{AB}{L} \qquad RLP = \frac{AC}{L} \qquad RRI = \frac{DE}{L}$$

FIG. 7.04 TENDON GEOMETRY; NOMENCLATURE.

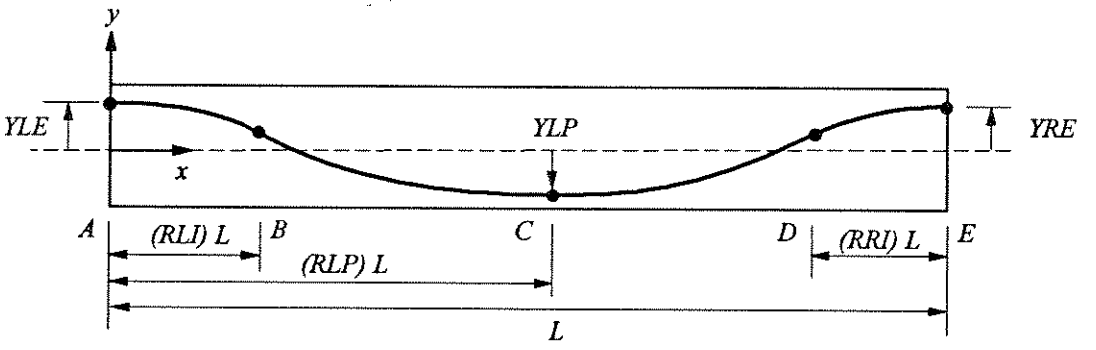

FIG. 7.05 PROFILE DEFINITION PARAMETERS; XY PLANE.

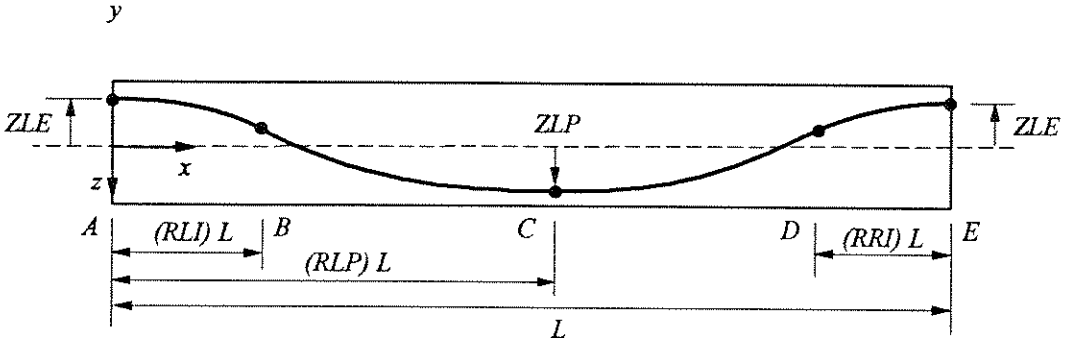

FIG. 7.06 PROFILE DEFINITION PARAMETERS; XZ PLANE.

XY PLANE

Y_LE	*Y coordinate of left end span.*
Y_LP	*Y coordinate of low point of span.*
Y_RE	*Y coordinate of right end of span.*
XY_RLI	*AB/AE; length ratio, left inflection point to span*
XY_RLP	*AC/AE; length ratio, low point to span*
XY_RRI	*ED/AE; length ratio, right inflection point to span*

XZ PLANE

Z_LE	*Z coordinate of left end span.*
Z_LP	*Z coordinate of low point of span.*
Z_RE	*Z coordinate of right end of span.*
XZ_LI	*AB/AE; length ratio, left inflection point to span*
XZ_LP	*AC/AE; length ratio, low point to span*
XZ_RI	*ED/AE; length ratio, right inflection point to span*

A number of other profiles can be generated by manipulation of the parameters listed above. Some of these are shown in Fig. 7.07.

If the tendon is curved in one plane but has a linear profile in the other orthogonal plane then the generation algorithm requires the following input.

IF LINEAR IN XY PLANE

Y_LE	*Y coordinate of left end of span.*
Y_RE	*Y coordinate of right end of span.*

IF LINEAR IN XZ PLANE

Z_LE	*Z coordinate of left end span.*
Z_RE	*Z coordinate of right end of span.*

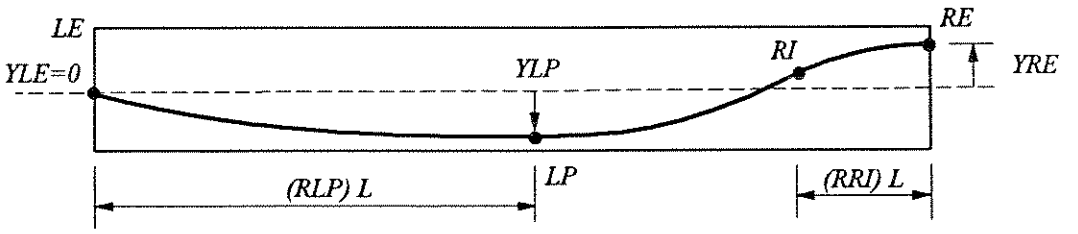

1. LEFT SPAN OF A TWO SPAN BRIDGE; RLI=0.

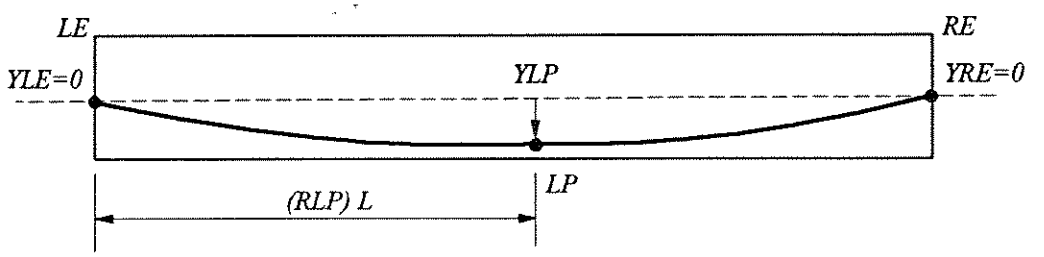

2. SIMPLE SPAN; RLI=0, RRI=0.

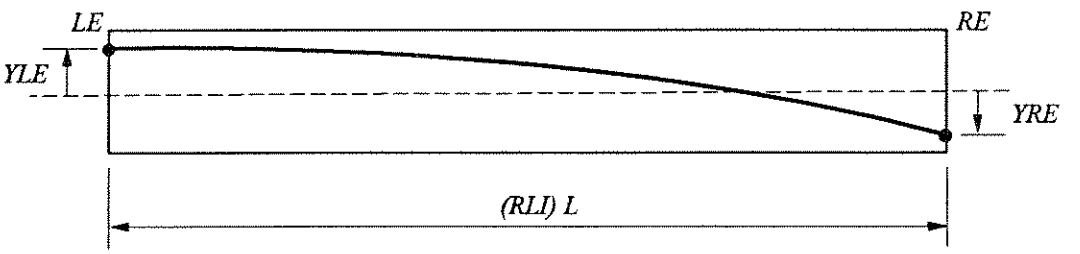

3. CANTILEVER SPAN; RLI=1.

FIG. 7.07 PARAMETRIC GENERATION OF TENDON PROFILE.
ADAPTED FROM SCORDELIS ET AL., 1985.

This procedure is repeated for each span until the entire tendon is defined. This technique allows for generation of very complex tendon geometries.

7.4. TENDON FORCE AFTER SHORT TERM LOSSES

When a tendon is being stressed by jacking, the force produced in the tendon is not constant along the length of the tendon due to friction between the tendon and the surrounding metal duct. Also at the time of transfer of prestressing force from the jack to the anchoring device, some slippage of the anchorage assembly is inevitable. This results in a further drop of prestressing force in the tendon.

Both these losses in the prestress force, namely friction and anchor slip are known as short term losses and may be substantial depending on the type of prestressing system involved.

7.4.1. FRICTION LOSSES

During the jacking operation, due to friction between the tendon and the metal duct surrounding it, the tendon force at the jacking end is greater than the force at some distance further along the tendon.

It is customary to consider the friction loss as consisting of two components:

1. Curvature friction results from the intended change of angle of tendon profile and its value depends on the coefficient of friction and the total angle change from the jacking end to the point under consideration.
2. Wobble friction is caused by unintended angle changes in the tendon along its length due to duct imperfections and construction practices. The magnitude of the wobble losses depends upon the rigidity of the duct, the diameter of duct. the spacing of duct supports, the tendon type and the duct type as well as the form of construction, Collins & Mitchell [22].

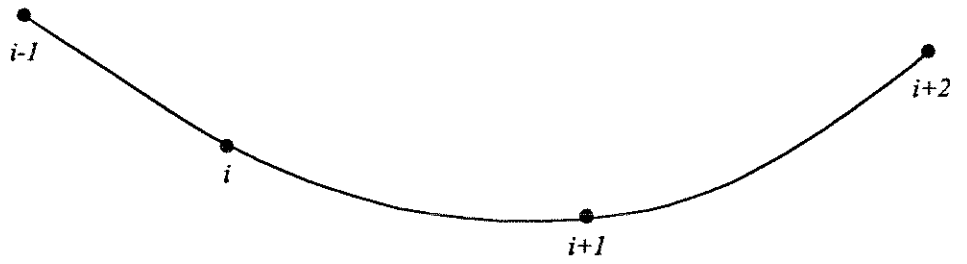

ACTUAL TENDON PROFILE

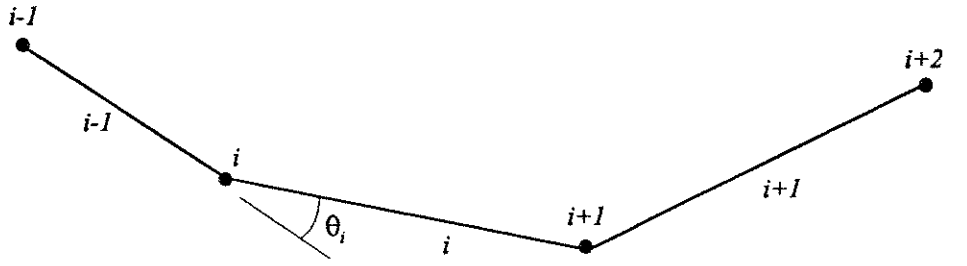

DISCRETIZED TENDON PROFILE

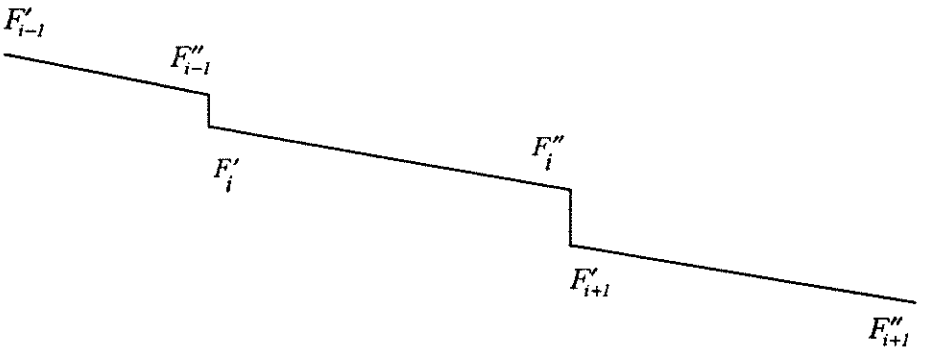

SEGMENT END FORCES AFTER FRICTION AND ANCHOR SET LOSSES.

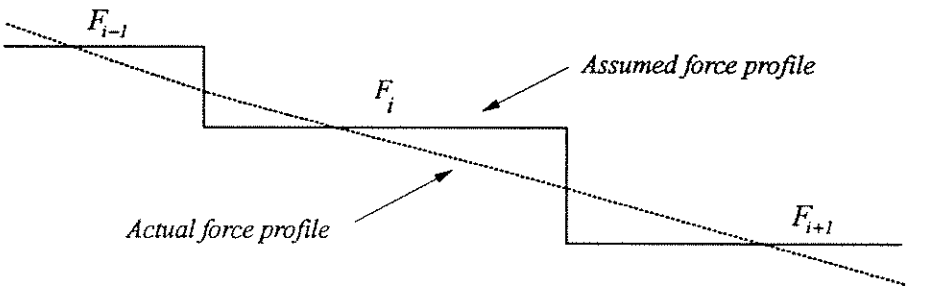

FORCE PROFILE BASED ON AVERAGE SEGMENT FORCE.

FIG. 7.08 CALCULATION OF SEGMENT FORCES.

The tendon force at distance x from the jacking end is given by the following equation.

$$P_x = P_0 \ e^{-(\mu\alpha + kx)} \tag{7.1}$$

where

P_0 is tendon force at the jacking end

μ is curvature friction coefficient.

α is cumulative angle change in radians between the jacking end and the point under consideration at a distance x.

K is the wobble friction coefficient per foot length of tendon.

x is the distance along the tendon from the jacking end to the point considered.

Consider the discretized tendon model as shown in Fig. 7.08. The angle changes are concentrated at the interior tendon points. Thus it may be surmised that curvature losses are lumped at interior tendon points whereas friction losses are distributed over each tendon segment.

Consider tendon segments $i-1$ and i as shown in Fig. 7.08. Given F_{i-1}, the force at the beginning of tendon segment $i-1$, it is required to find F'_{i-1} the force at the end of segment $i-1$ and F_i the force at the beginning of segment i. The required procedure is outlined below:

1. Define a vector $\mathbf{V}_{i-1}$ from tendon point $i-1$ to i.

$$\mathbf{V}_{i-1} = \begin{bmatrix} x_i - x_{i-1} \\ y_i - y_{i-1} \\ z_i - z_{i-1} \end{bmatrix} \tag{7.2}$$

where the length of this vector is given by:

$$|\mathbf{V}_{i-1}| = \sqrt{(x_i - x_{i-1})^2 + (y_i - y_{i-1})^2 + (z_i - z_{i-1})^2} \tag{7.3}$$

2. Define a vector $\mathbf{V}_i$ from tendon point i to $i+1$.

$$\mathbf{V_i} = \begin{bmatrix} x_{i+1} - x_i \\ y_{i+1} - y_i \\ z_{i+1} - z_i \end{bmatrix} \tag{7.4}$$

where the length of this vector is given by:

$$|\mathbf{V_i}| = \sqrt{(x_{i+1} - x_i)^2 + (y_{i+1} - y_i)^2 + (z_{i+1} - z_i)^2} \tag{7.5}$$

3. The angle between the segments i and $i-1$ is given by the following vector dot product

$$\mathbf{V_{i-1}} \bullet \mathbf{V_i} = |\mathbf{V_{i-1}}||\mathbf{V_i}| \cos\theta_i \tag{7.6}$$

$$\theta_i = \cos^{-1}\left(\frac{\mathbf{V_{i-1}} \bullet \mathbf{V_i}}{|\mathbf{V_{i-1}}||\mathbf{V_i}|}\right) \tag{7.7}$$

4. Force at the end of segment $i-1$ is given by

$$F''_{i-1} = F'_{i-1}\ e^{-Kx} \tag{7.8}$$

where x is the length of segment $i-1$.

$$x = |V_{i-1}| \tag{7.9}$$

5. Force at the beginning of segment i is given by

$$F'_i = F''_{i-1}\ e^{-\mu\theta_i} \tag{7.10}$$

This procedure is repeated for each tendon segment.

7.4.2. ANCHORAGE SLIP LOSS

After the jacking operation is complete the tendons have to be anchored. The anchoring operation will usually result in an additional loss of tendon force due either to seating of wedges or due to the deformation of shims. The anchorage set for strand tendons anchored by wedges is usually about 0.25 inches.

Fig. 7.09 shows the influence of anchorage set on the force variation near the jacking end. The length of the tendon affected by anchorage slip is a function of the frictional losses, the length being large for low friction losses. When the anchor slips, the direction of the frictional force is reversed and since the reversed frictional force depends on the same frictional

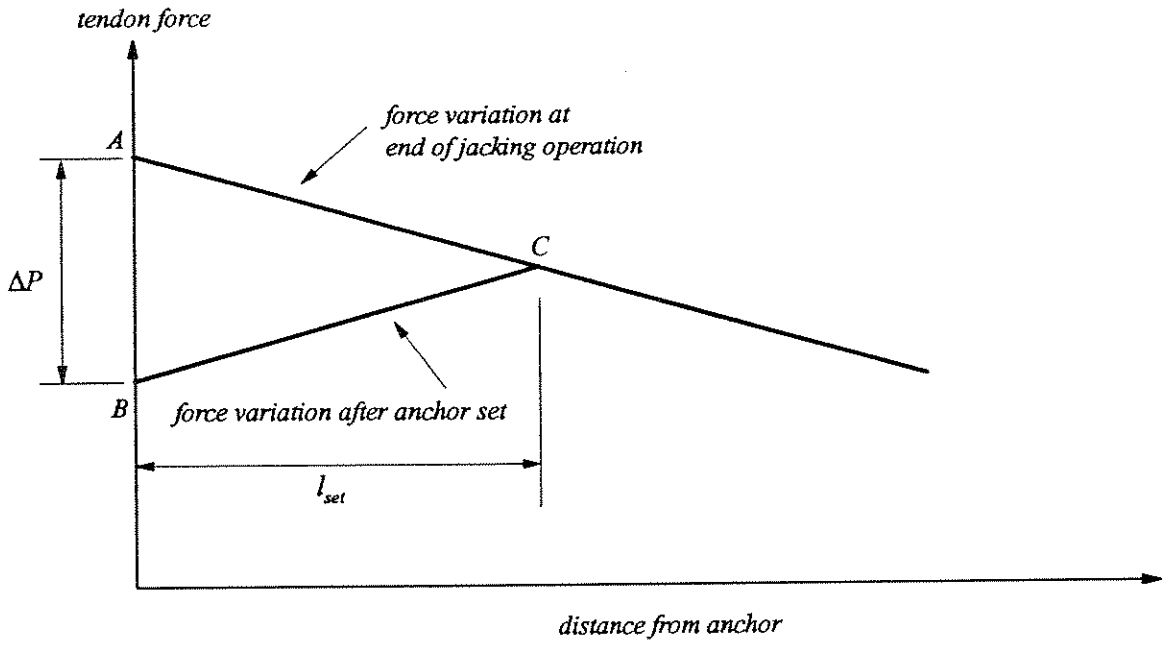

FIG. 7.09 ANCHOR SLIP LOSSES.

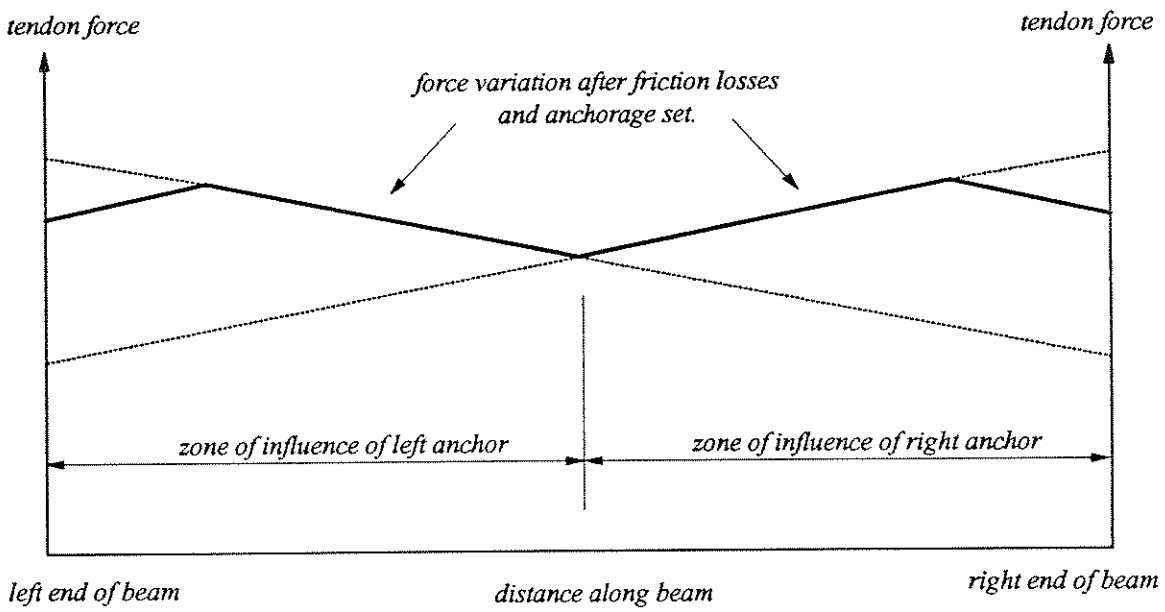

FIG. 7.10 INFLUENCE OF JACKING FROM BOTH ENDS ON THE VARIATION OF PRESTRESS FORCE.

coefficients as the initial force, the slopes of the lines AC and BC representing the force variations in the tendon just before and after the anchor set are equal and opposite. This results in the so called "mirrored" force profile near the anchorage zone.

The change in stress and the length over which it is effective may be derived from fundamental principles. The slip displacement must equal the shortening of the tendon which is caused by the drop in the tendon force and is given by the following expression, Collins and Mitchell [22].

$$\Delta_{set} = 0.5\Delta P \frac{l_{set}}{AE} \tag{7.11}$$

where $0.5\,\Delta P$ is the average drop in tendon force, l_{set} is the length of the tendon over which slippage is felt, A and E are the area of cross section and modulus of elasticity, respectively, of the prestressing tendon.

We can arrive at a graphical interpretation of the above equation by rearranging it as follows:

$$\begin{aligned} \Delta_{set} AE &= 0.5\,\Delta P l_{set} \\ \Delta_{set} AE &= area\ \ ABC \end{aligned} \tag{7.12}$$

The algorithm used in the present study to evaluate anchor slip losses scans each tendon segment starting at the jacking end in order to locate the position of point C in Fig. 7.09, which satisfies the above equality. After this point is located, all tendon forces between the jacking end and point C are modified to reflect the "mirrored" force profile.

7.4.3. Effect of Jacking Procedure

Two different types of jacking procedures are used in actual practice.

1. The tendon is jacked from one end. The other end has a passive or dead anchor.
2. The tendon is jacked from both ends, the resulting force profile is shown in Fig. 7.10.

The procedure for determination of tendon segment forces are similar for both cases except that in the case of two-end jacking the controlling anchorage must be determined for each tendon point. The procedure is as follows.

- Determine segment end forces under jacking from end A.
- Repeat step 1 with jacking from end B.
- Compare segment end forces due to the two procedures. The larger of the two forces controls.

This method is a close approximation of the actual physical situation.

7.4.4. SEGMENT FORCES

As mentioned earlier, it is assumed that the initial force in each tendon segment is constant. This force can be determined at this stage by taking the average of the two segment end forces.

The accuracy of the resulting force profile depends on:

- Degree of discretization.
- Tendon profile.

A better agreement is obtained for a harped tendon profile as compared to a draped profile because of the assumption made regarding the lumping of curvature friction losses at the tendon points.

Choudhury [20] has discussed relative merits of different averaging methods to improve the accuracy of results. Refer to Fig. 7.08, let the end forces in segments $i-1$, i and $i+1$ be given by.

$$\mathbf{F}_{i-1} = \begin{bmatrix} F'_{i-1} \\ F''_{i-1} \end{bmatrix} \qquad \mathbf{F}_{i} = \begin{bmatrix} F'_{i} \\ F''_{i} \end{bmatrix} \qquad \mathbf{F}_{i+1} = \begin{bmatrix} F'_{i+1} \\ F''_{i+1} \end{bmatrix} \tag{7.13}$$

In the case of draped tendon; a good estimate of the constant initial tendon force is given by

$$F_i = \frac{F_i' + F_i''}{2} \tag{7.14}$$

Whereas for a harped tendon an improved estimate is given by

$$F_i = \frac{1}{2}\left\{\left(\frac{F_{i-1}'' + F_i'}{2}\right) + \left(\frac{F_i'' + F_{i+1}'}{2}\right)\right\} \tag{7.15}$$

7.5. TIME DEPENDENT LOSSES; RELAXATION

The stress in a prestressing tendon held at a constant elongation decreases with time. This phenomenon is referred to as relaxation.

Based on their tests Magura, Sozen and Siess [78] showed that the relaxation of stress relieved wires or strands varied linearly with the log of time. They recommended the following equation to estimate the tendon stress after relaxation losses.

$$\frac{f_p}{f_{pi}} = 1 - \frac{\log t}{10}\left(\frac{f_{pi}}{f_{py}} - 0.55\right) \tag{7.16}$$

where f_{pi} is the initial stress in the tendon, f_{py} is the 0.1% offset yield stress and t is the time under load in hours and is not less than one hour. The ratio f_{pi} / f_{py} should not be less than 0.55. Note that no relaxation losses occur if $f_{pi} = 0.55 f_{py}$.

For low relaxation strand or prestressing bars, PCI committee on prestress losses [100] and the Ontario Highway Bridge Design Code [97] recommends the following modified version of Eq. 7.16.

$$\frac{f_p}{f_{pi}} = 1 - \frac{\log t}{45}\left(\frac{f_{pi}}{f_{py}} - 0.55\right) \tag{7.17}$$

The above equations are based on the assumption of constant strain. However, in the case of prestressed concrete bridges because of time dependent effects of creep and shrinkage in concrete the strain in prestressing steel varies with time. To get around this problem, Hernandez and Gamble [42] suggested a procedure based on the assumption that all stress

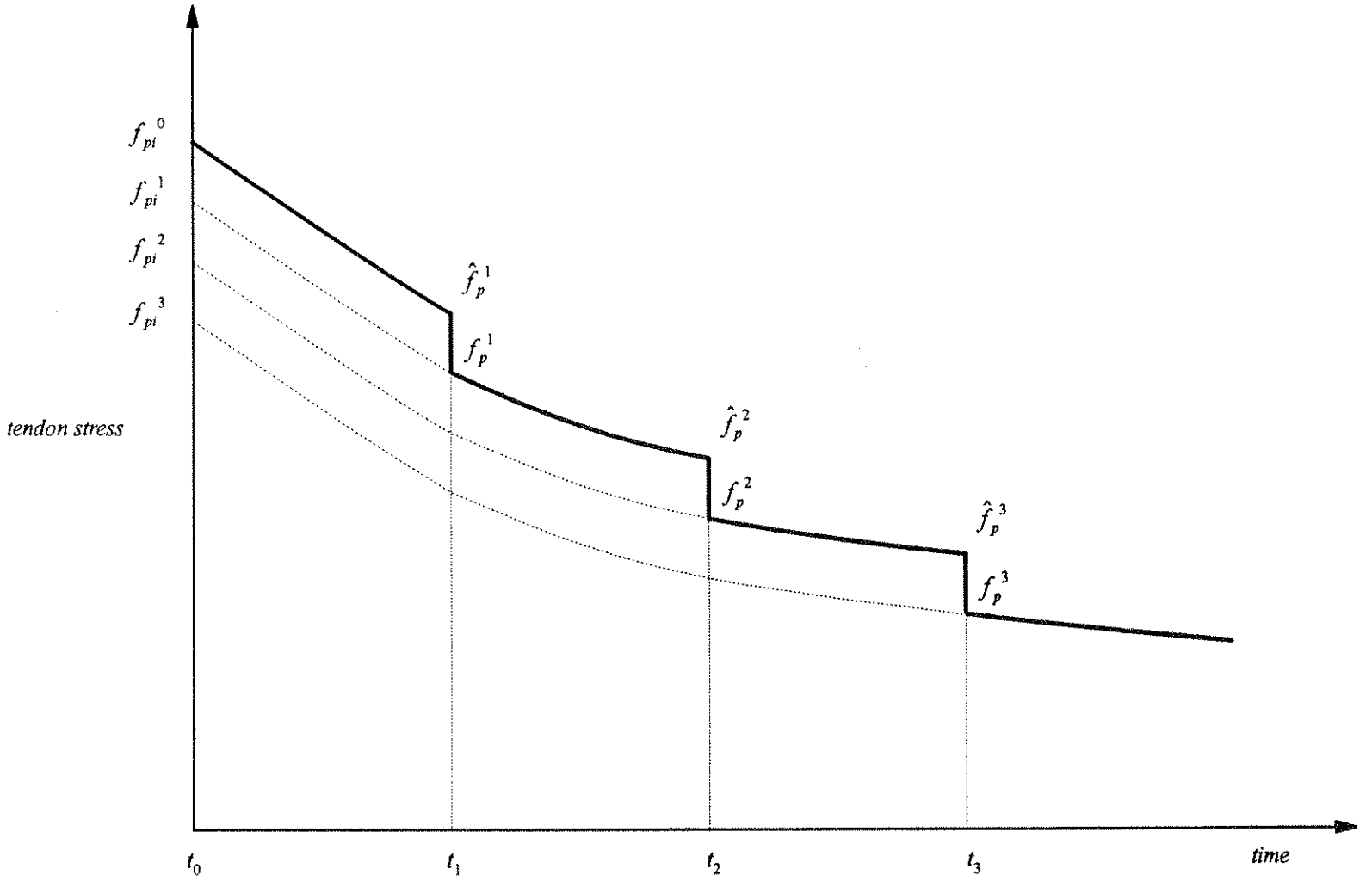

FIG. 7.11 TENDON STRESS RELAXATION UNDER VARIABLE STRAIN CONDITIONS. BASED ON A PROCEDURE SUGGESTED BY HERNANDEZ AND GAMBLE, 1975.

changes except relaxation are lumped at the end of time steps. This method is explained graphically in Fig. 7.11.

1. Time t_0; An initial stress of $f_{pi}^{\ o}$ is applied to the tendon .
2. Time t_1; Tendon stress is reduced to $\hat{f}_p^{\ 1}$ due to relaxation.

   $\hat{f}_p^{\ 1} = \lambda(t_1 - t_0, f_{pi}^{\ o})$
3. Time t_1; Tendon stress is reduced further to $f_p^{\ 1}$ due to external strains.
4. Calculate an initial fictitious stress denoted by $f_{pi}^{\ 1}$, which would have relaxed to $f_p^{\ 1}$ at time t_1. This is done by solving Eq. 7.16 which is quadratic in f_{pi}.
5. Time t_2; Tendon stress is reduced to $\hat{f}_p^{\ 2}$ due to relaxation.

   $\hat{f}_p^{\ 2} = \lambda(t_2 - t_0, f_{pi}^{\ 1})$

Steps 2 to 4 are repeated for each time step.

7.6. Material Constitutive Model

A bilinear strain hardening model, as shown in Fig. 7.12 may be used to approximate the stress-strain response of prestressed reinforcement. For strands and wires that do not exhibit a yield plateau, an equivalent yield stress which is defined as the stress at a strain of 1%, may be used instead.

The model used in the present study can also capture unload from and reload to the strain hardening branch. The slope of the unload branch is equal to that of the virgin elastic curve. The model is completely defined by σ_y the yield strength, ε_u the ultimate strain at failure, E the initial elastic modulus and E_{sh} the strain hardening modulus.

7.7. Formulation of Prestressing Tendon Element

As mentioned earlier each tendon is modeled as a series of piece-wise linear segments. Each tendon segment is assumed to behave as a pre-strained eccentric truss bar whose

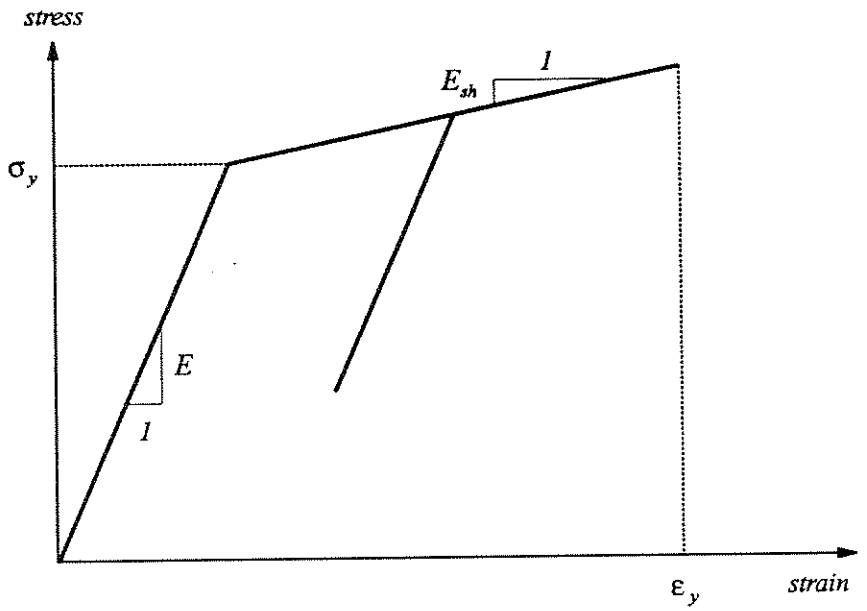

FIG. 7.12 BILINEAR STRAIN HARDENING MODEL

ends are rigidly connected to corresponding structure nodes, thereby allowing the tendon to contribute both load and stiffness to the structure, Fig. 7.13.

7.7.1. STIFFNESS MATRIX

Each tendon segment has one local degree of deformation freedom as shown in Fig. 7.14. The force deformation relationship in local coordinates is given by:

$$\mathbf{S}_V = \mathbf{K}_V \ \mathbf{v} \tag{7.18}$$

$$\mathbf{K}_V = \left(\frac{E_{tan} A_p}{L} \right) \tag{7.19}$$

where E_{tan} is the tangent modulus of elasticity, A_p is the area of cross section of prestressing steel and L is the length of the tendon segment.

The tendon segment has six degrees of displacement freedom, three at each end. The elastic stiffness $\mathbf{K}_T$ of the tendon segment in global coordinates is given by the following transformation.

$$\mathbf{K}_T = \mathbf{A}_{VT}{}^T \, \mathbf{K}_V \, \mathbf{A}_{VT} \tag{7.20}$$

Where $\mathbf{A}_{VT}$ (1x6) is the displacement transformation matrix from V to T coordinates.

$$\mathbf{A}_{VT} = \begin{bmatrix} -x & -y & -z & x & y & z \end{bmatrix} \tag{7.21}$$

and $(x \quad y \quad z)$ are the direction cosines of the tendon segment with respect to global coordinates.

The displacements of the tendon points are slaved to the corresponding structure nodes, the displacement transformation matrix $\mathbf{A}_{TQ}$ (6,12) is given as follows:

$$\mathbf{A}_{TQ} = \begin{bmatrix} \mathbf{D}_i & \mathbf{0} \\ \mathbf{0} & \mathbf{D}_j \end{bmatrix} \tag{7.22}$$

where $\mathbf{D}_i$ is (3x6) displacement transformation matrix relating the three translations of tendon point i to the six displacements of master node i and $\mathbf{D}_j$ is a similar matrix for end j. The general form of matrix $\mathbf{D}$ is as follows:

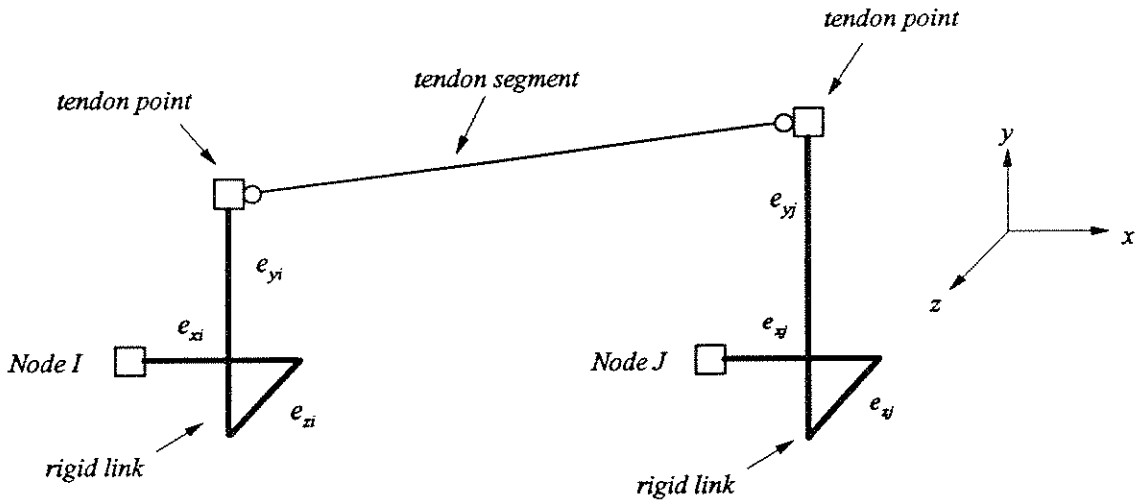

FIG. 7.13 TENDON SEGMENT ELEMENT; GEOMETRY.

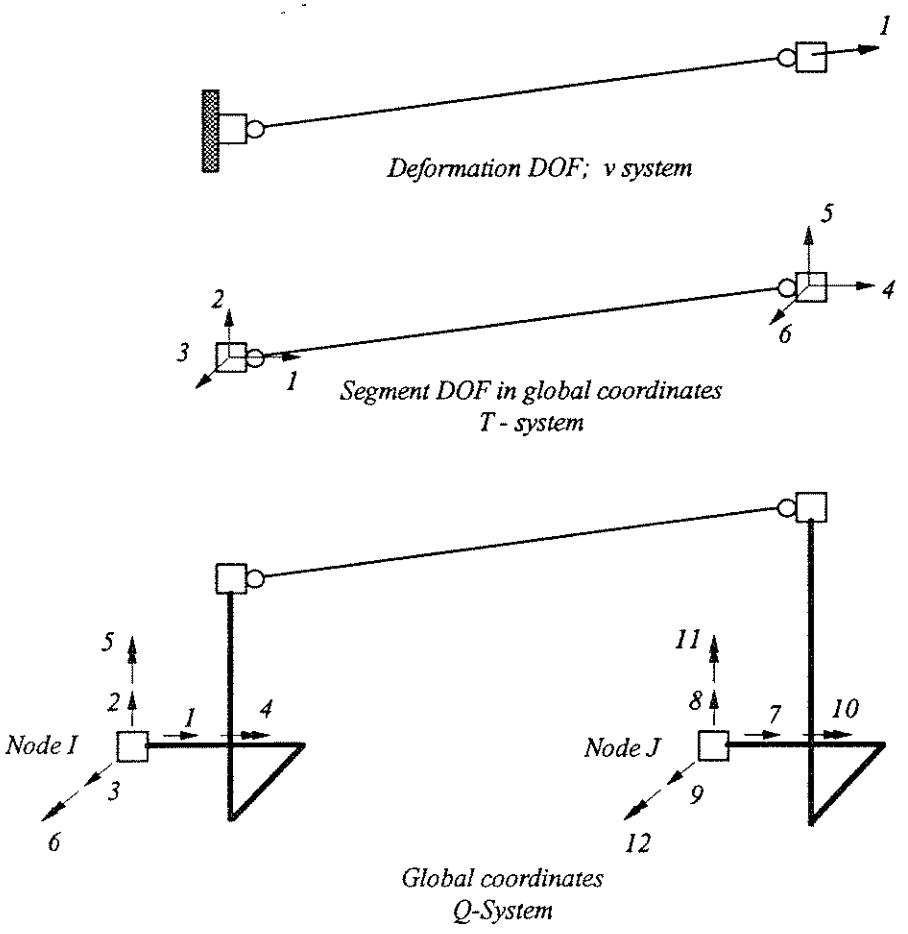

FIG. 7.14 TENDON SEGMENT ELEMENT; DEGREES OF FREEDOM.

$$\mathbf{D} = \begin{bmatrix} 1 & 0 & 0 & 0 & e_z & -e_y \\ 0 & 1 & 0 & -e_z & 0 & e_x \\ 0 & 0 & 1 & e_y & -e_x & 0 \end{bmatrix} \tag{7.23}$$

$$\begin{bmatrix} e_x \\ e_y \\ e_z \end{bmatrix} = \begin{bmatrix} x_t \\ y_t \\ z_t \end{bmatrix} - \begin{bmatrix} x_n \\ y_n \\ z_n \end{bmatrix} \tag{7.24}$$

where $(e_x \quad e_y \quad e_z)$ are the eccentricities of the tendon point with respect to the master node to which it is rigidly linked and $(x_t \quad y_t \quad z_t)$ and $(x_n \quad y_n \quad z_n)$ are the global position coordinates of the tendon point and the master node respectively.

The stiffness contribution of the tendon segment in global coordinates at the master nodes is given by:

$$\mathbf{K_Q} = \mathbf{A_{TQ}}^{\mathrm{T}}\, \mathbf{K_T}\, \mathbf{A_{TQ}} \tag{7.25}$$

7.7.2. Nodal Load Vector due to Prestress Forces

The internal load vector $\mathbf{S_Q}$ (12x1) of the tendon segment at the master nodes in the global coordinates is given by the following matrix transformation.

$$\mathbf{S_Q} = \mathbf{A_{TQ}}^{\mathrm{T}} \mathbf{A_{VQ}}^{\mathrm{T}} \mathbf{S_V} \tag{7.26}$$

The internal load vector is subtracted from the current load vector acting on the structure to account for the effect of prestressing force.

In the case of time dependent or nonlinear solution, internal load vector is evaluated at each step of the solution in order to keep track of the changes in tendon force due to the time dependent effects of creep and shrinkage of concrete and relaxation of prestressing of steel and due to any additional structure deformations. It is also utilized to determine the unbalanced nodal loads and hence judge the convergence of a nonlinear solution.

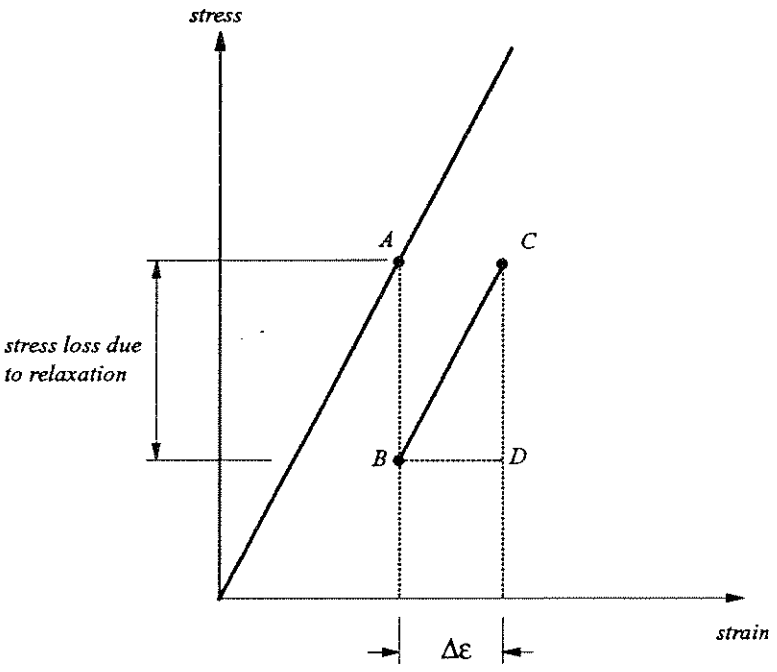

FIG. 7.15 STATE DETERMINATION PROCES
INCLUDING THE EFFECT OF RELAXATION

7.7.3. STATE DETERMINATION PROCEDURE

Given the pervious state of the tendon segment, namely stress, strain and material state code and a vector of displacement increments at the master nodes i and j, the process of finding the new state of the tendon segment is known as the state determination procedure.

1. Find Δv, the change in axial displacement of the tendon.
$$\Delta v = \mathbf{A}_{VT}\mathbf{A}_{VQ}\Delta q \tag{7.27}$$
2. The strain increment in the tendon segment is given by:
$$\Delta\varepsilon = \frac{\Delta v}{L} \tag{7.28}$$
3. Let the previous state of the tendon at the beginning of the time step be defined by point A on Fig. 7.15. Assume that the stress in the tendon has relaxed to point B and that length BD is equal to $\Delta\varepsilon$.
4. The new state of the tendon is defined by point C. Note that path BC is parallel to OA.

7.8. ANALYSIS EXAMPLE; TENDON STRESS RELAXATION

The numerical techniques discussed above were implemented in the computer program CALBRG developed as a part of this study. A 25 ft. long concrete beam was prestressed with a concentric stress relieved tendon at an age of 30 days. The beam was hinged at one end and had a roller support at the other end. The stress in the tendon changes due to relaxation and is tracked up to 1000 days. The results are shown in Fig. 7.16. The pertinent data are as follows:

Area of cross section of beam 400 in^2.

Compressive strength of concrete $f'_c = 4000\ psi$.

Area of cross section of tendon 1.0 in^2.

Yield strength of tendon $f_{py} = 230\ ksi$

Curvature friction coefficient $\mu = 0.15$

Wobble friction coefficient $K = .0005\ per\ ft$.

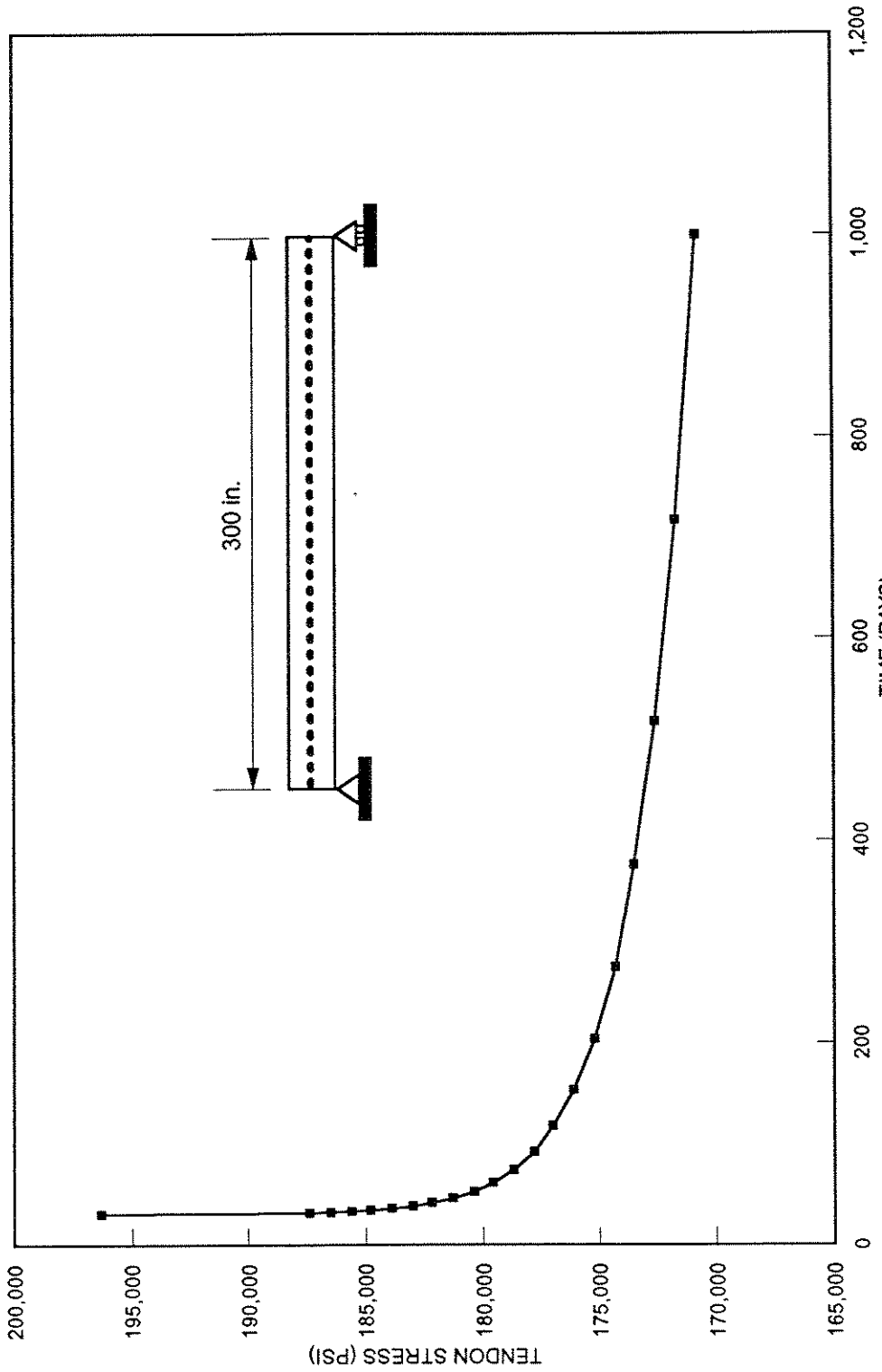

FIG. 7.16 RELAXATION OF PRESTRESSING TENDON WITH TIME; CALBRG

8. CABLE; PROPERTIES, STATICS AND GEOMETRY

8.1. BASIC TYPES OF CABLES

A definition of some of the terms used in this section are given below, Podolny [103].

- Cable: Any flexible tension member, consisting of one or more groups of wire strands or ropes.
- Wire: A single continuous length drawn from a cold rod.
- Strand: An arrangement of wires helically placed about a central wire to produce a symmetrical section.
- Rope: A number of strands helically wound around a core that is composed of a strand or a rope.

Several types of cables are available for use as stays in cable stayed bridges, Fig. 8.01. The selection of a particular type of cable depends on the mechanical properties desired, modulus of elasticity, ultimate tensile strength and durability, as well on the erection procedure, design of anchorages, etc.

8.1.1. PARALLEL-BAR CABLES

Parallel-bar cables are formed of steel bars or rods, parallel to each other, placed in a metal duct and kept in position by polyethylene spacers. The bars can slide in the longitudinal direction, thus allowing for individual tensioning of bars. After the stressing operation has

been carried out, cement grout is injected in the ducts for corrosion protection. Relatively mild steel is used in the manufacture of bars, which results in larger sections than those obtained with higher strength wires. This results in a reduction in stress variation and hence a higher factor of safety against fatigue failure. In addition, the low stress level results in a lower cable stiffness thus such bars can only be used in bridges where the dead load is predominant as compared to the live load. Large changes in load can produce significant changes in the stiffness of such cables, which is not desirable. Parallel bar cables manufactured by the firm of Dywidag were employed in the construction of Hoechst Bridge in West Germany.

8.1.2. PARALLEL-WIRE CABLES

Parallel-wire cables are made of high strength drawn steel and are placed in metal or polyethylene duct. The ducts are generally injected with cement grout after the stressing operation. A hexagon is considered to be the shape which provides the most compact grouping of wires. In addition, the shape is such that it is possible to maintain equal lengths of wires leading to a uniform stress in all wires. All wires are in a straight alignment and the elastic behavior of the cable approaches that of a single wire. These cables are manufactured by BBRV. In the BBRV process each stay consists of a bundle of 0.3 in. diameter wires, the number varying between 50 and 350. In actual operations, these can withstand forces of 300 to 2000 kips. They also have a satisfactory fatigue strength; the wires can withstand a stress variation of 60 ksi over two million cycles with a maximum stress of 110 ksi. It is of interest to note here that parallel wire cables were used by Roebling in the 19th century, who invented an ingenious method of fabricating them, which consisting of drawing a steel wire between two towers using a carriage like device which ran on previously stretched cables.

8.1.3. PARALLEL-STRAND CABLE

Such a cable consists of a group of parallel strands in a polyethylene duct. Each strand consists of seven twisted wires of 0.5 or 0.7 in., Walther [144]. When a strand is stressed, the wires are subjected to lateral stresses; this reduces the fatigue resistance of wires and increases their susceptibility to corrosion. However these problems have been overcome by recent advances and parallel-strand cables are available from a number of manufacturers.

8.1.4. LOCKED-COIL CABLES

The locked-coil cable consists of a central core of parallel circular wires, several inner layers of wedge or keystone shaped wires, and finally outer layers of Z or S shaped wires. The S sections overlap and from an almost water tight layer, hence the name locked coil cable. Units are thus obtained which consist of eight or nine layers of 0.18 in. diameter wires, reaching an ultimate load of 1350 to 2900 kips, Walther [144]. Ducts and grouting are unnecessary for such a system. The other advantages include greater flexibility which results in ease of placing and reduced anchorage space. However if proper care is not exercised during manufacture and installation, corrosion may set in, resulting in costly replacements which was the case with Maracaibo bridge in Venezuela.

8.2. MECHANICAL PROPERTIES

Some aspects of static and fatigue strength of different types of cables are discussed in the following sections.

8.2.1. STATIC STRENGTH

Typical stress-strain curves of structural rope and strand are shown in Fig. 8.02 , Irvine [45]. Due to different methods of manufacture the effective modulus of elasticity varies. Becasuse

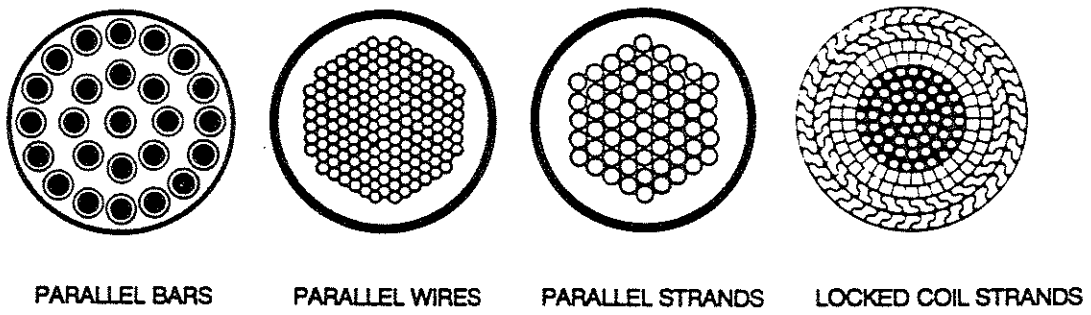

FIG. 8.01 VARIOUS TYPES OF CABLE STAYS.
Podolny, 1976

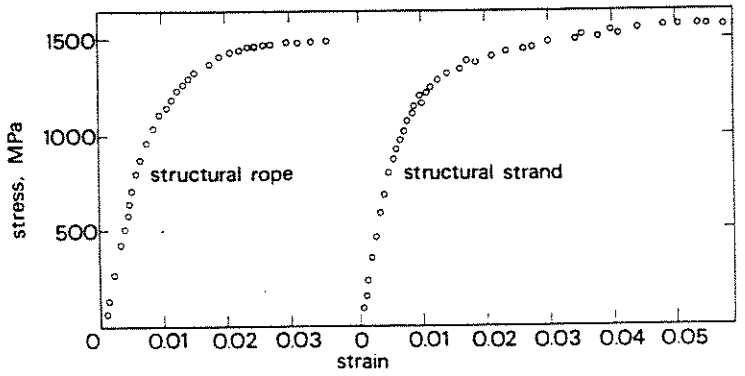

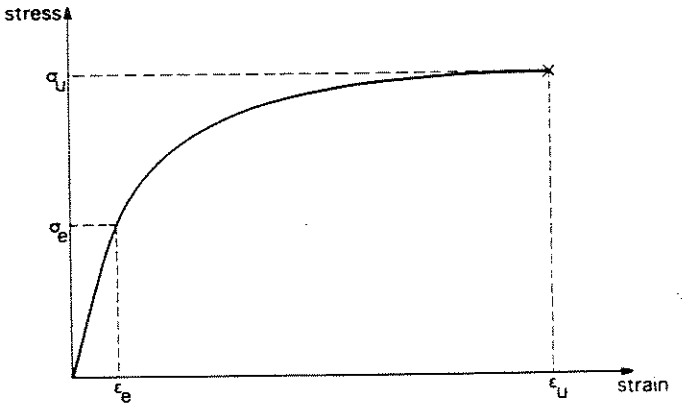

FIG. 8.02 TYPICAL STRESS-STRAIN CURVES FOR STRUCTURAL ROPE AND STRAND.
Irvine, 81

of the influence of helices, the rope has the smallest modulus, with an approximate value of E=20,000 ksi. This may be contrasted with 25,000 ksi for a structural strand and 30,000 ksi for a parallel wire strand.

An important prerequisite for structural ropes and strand is the pre-stretching process, which is usually carried out in the manufacturing plant. Pre-stretching may be defined as the application of a predetermined tension force to a finished strand or rope in order to remove the looseness inherent in the manufacturing process. In general, a pre-stretching load of about 55 % of the breaking load is applied.

Typically the elastic limit σ_e is reached at about 50 % of the ultimate tensile strength σ_u. Ultimate tensile strengths of about 220 ksi are regularly achieved with ultimate strains around 3 % for rope and 6 % for strand. Tests show that, in general, the strand is much stronger than the more flexible rope of the same size.

A safety factor of 3 is generally applied to the ultimate tensile stress, resulting in a working stress of about 70 ksi for a rope or a strand. A safety factor of 2.5, corresponding to a working stress of around 90 ksi, may be specified for pre-assembled parallel wire strands, which are commonly used in European cable stayed bridges, Podolny [103]. This same figure is typical for the cables of long span suspension bridges where the individual wires are spun and grouped into strands and these strands are bundled together before compaction and wrapping produces the final circular cross section.

The PTI manual [105], article 5.1, sets the following criteria for the allowable tensile stress values for cable-stays.

1. $.45 f_s'$ for AASHTO Group 1 loading.
2. $.50 f_s'$ for other AASHTO Group loadings.
3. $.56 f_s'$ during construction or stay replacement.

Where f_s' is the guaranteed ultimate tensile strength of the cable-stay.

8.2.2. FATIGUE STRENGTH

It is necessary to consider fatigue strength in the design of cables subject to pulsating loads. However, the fact that the cables are the main load carrying elements, with relatively large forces from the permanent loads and that the loads induced by the vehicular traffic are distributed by the stiffening girder, reduces to some extent the fatigue problem. The fatigue effects would not be significant in concrete cable stayed bridges carrying vehicular traffic because of the low value of live to dead load ratio. In contrast, for railway bridges, the fatigue effect will be dominating because of the larger ratio of live to dead load.

The fatigue resistance is represented by a Wohler curve showing the relationship between N the number of load cycles and the corresponding stress range $\Delta\sigma$. On a log-log scale the Wohler curve can be assumed to be composed of straight lines as shown in Fig. 8.03.

The Wohler curve for a parallel wire strand can be generated by using the equations recommended by Birkenmaier and Narayanan [13]. These are given below:

$$\log \Delta\sigma = -\frac{1}{4.5}\log N + 3.710 \qquad N \le 10^6 \qquad \Delta\sigma \ge 238\ MN/mm^2$$

$$\log \Delta\sigma = -\frac{1}{8.0}\log N + 3.127 \qquad N > 10^6 \qquad \Delta\sigma < 238\ MN/mm^2 \qquad (8.01)$$

These equations are plotted in Fig. 8.03.

The PTI manual [105], article 5.2, sets up detailed criteria for establishing allowable fatigue stress range values depending upon the cable type, the loading it is subjected to, the number of load cycles and whether it is installed in a redundant or non-redundant type of structure.

For example, for a strand conforming to ASTM A416 subjected to 2 million cycles of live load (AASHTO HS20 truck loading) and impact load (as defined by AASHTO Art. 3.8.2) and installed in a structure with multi load paths (a structure in which a single fracture in a member does not lead to collapse), the allowable fatigue stress range is 18 ksi.

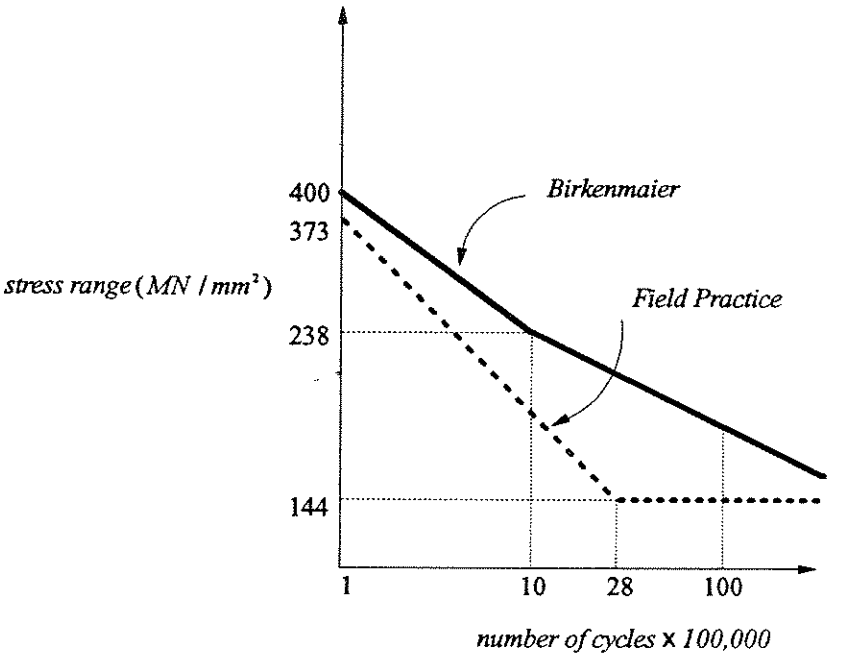

FIG. 8.03 WOHLER CURVES FOR PARALLEL WIRE CABLES.

Article 5.2 also recognizes the possibility of fatigue caused by existence of flexural stresses at the cable anchorage. These can be minimized by using special types of anchorages, Walther [144]. Any flexural stresses more than 3 ksi should be added to axial fatigue stress due to live and impact loading.

8.3. GEOMETRY AND STATICS OF A SUSPENDED CABLE

Historical accounts of investigations into geometry and statics of suspended cables date back to the fifteenth century. The geometric shape taken by a symmetrically suspended cable subject only to its self weight, known as the catenary, was discovered by Bernoulli and Leibnitz as far back as 1690. The solution of the elastic catenary was derived by Routh in 1896.

For the discussion presented in subsequent sections of this chapter, the author has made extensive use of the texts and papers by Gimsing [32], Irvine [44, 45], Möllman [90] and Walther [144].

Two different cases are considered:

1. A shallow cable with a parabolic profile.
2. The elastic catenary.

It is possible to show mathematically that the shallow cable is a limiting case of the elastic catenary. However, in the present study, each of the above mentioned cases along with its underlying assumptions, are discussed independently.

8.3.1. SHALLOW CABLE WITH A PARABOLIC PROFILE

A cable is considered to be shallow cable if the sag to span ratio is relatively small.

$$\frac{sag}{span} << 1$$

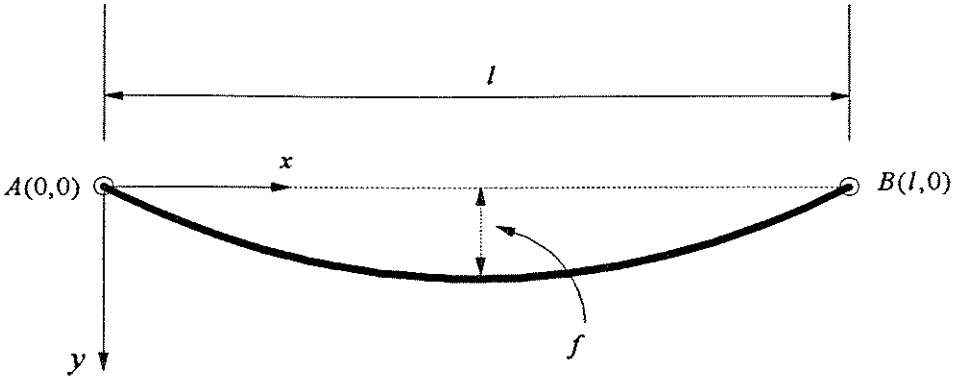

FIG. 8.04 (a) DEFINITION DIAGRAM.

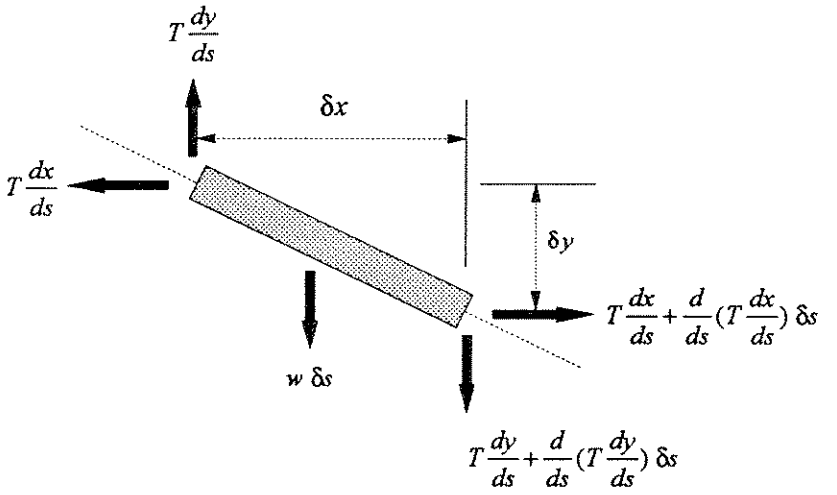

FIG. 8.04 (b) EQUILIBRIUM OF AN ELEMENT.

In general, if the sag to span ratio is less than 1 : 8 then the cable may be treated as a shallow cable. Shallow cables are used in many different types of structures such as cable-stayed bridges, guyed masts, suspension roofs, etc.

Consider a cable of uniform cross sectional area, hanging between two supports as shown in Fig. 8.04 (a); given the following data:

- Chord length of the cable l .
- Self weight of the cable per unit arc length w.
- Modulus of elasticity E.
- Area of cross section A.

It is required to find:

- Geometric shape of the cable.
- Tension in the cable.

The solution is based on the following assumptions:

1. The cable is perfectly flexible.
2. The cable material is linear elastic.
3. The load is applied along the arc length of the cable.
4. The cable is shallow.
5. The strains are small.

On the basis of assumptions 3 and 4, it can be approximated that the load is uniformly distributed along the horizontal projection of the cable, Möllman [90].

Refer to Fig. 8.04 (b). consider the vertical equilibrium of an element of the cable.

$$\frac{d}{ds}\left(T\frac{dy}{ds}\right)=w \tag{8.02}$$

Where T is the axial force in the cable and $\frac{dy}{ds}$ is the sine of the angle of inclination of the cable element to the horizontal. Similarly, if we consider the horizontal equilibrium of the cable element, the following equation is obtained.

$$T\frac{dx}{ds} = H \tag{8.03}$$

Where $\frac{dx}{ds}$ is the cosine of the angle of inclination and H is the horizontal component of the cable tension; since no longitudinal loads are acting on the cable, H is a constant.

Eq. 8.02 and 8.03 can be combined to yield Eq. 8.04.

$$H\frac{d^2y}{dx^2} = w\frac{ds}{dx} \tag{8.04}$$

For shallow cables the following equation is approximately satisfied.

$$\frac{ds}{dx} \approx 1 \tag{8.05}$$

thus Eq. [5.03] is reduced to:

$$H\frac{d^2y}{dx^2} = w \tag{8.06}$$

The boundary conditions at the cable supports are

$$x = 0 \qquad y = 0$$
$$x = l \qquad y = 0$$

Refer to Fig. 8.04 (b). The geometric constraint to be satisfied is

$$\left(\frac{dx}{ds}\right)^2 + \left(\frac{dy}{ds}\right)^2 = 1$$

$$\frac{ds}{dx} = \sqrt{1 + \left(\frac{dy}{dx}\right)^2} \tag{8.07}$$

A solution of Eq. 8.06 subject to the geometric constraints and boundary conditions given above, results in the following equation.

$$y = \frac{w}{2H}\left(x^2 - x\,l\right) \tag{8.08}$$

This is the equation of a parabola. The value of the sag at mid span f is given by:

$$f = \frac{w\,l^2}{8H} \tag{8.09}$$

The slope at any point of the cable is given by:

$$\frac{dy}{dx} = \frac{4f}{l}\left(\frac{2x}{l} - 1\right) \tag{8.10}$$

The total length of the cables between the supports is given by:

$$L_o = \int_0^l \sqrt{1 + \left(\frac{dy}{dx}\right)^2}\; dx \tag{8.11}$$

Substituting Eq. 8.10 into Eq. 8.11, using binomial expansion and integrating we have:

$$L_o = \int_0^l \sqrt{\left\{1 + \left[\frac{4f}{l}\left(\frac{2x}{l} - 1\right)\right]^2\right\}}\; dx$$

$$L_o = l\left[1 + \frac{8}{3}\left(\frac{f}{l}\right)^2 - \frac{32}{5}\left(\frac{f}{l}\right)^4 + \ldots.\right] \tag{8.12}$$

Ignoring fourth and higher powers of the ratio $\frac{f}{l}$ we have the following expression:

$$f = l\sqrt{\frac{3}{8}\left(\frac{L_o}{l} - 1\right)} \tag{8.13}$$

Thus given w, l and L_o it possible to find the mid span sag , the horizontal component of the axial force H and the parabolic profile of the cable, using the following sequence of steps.

1. Find the value of mid span sag f using Eq. 8.13.
2. Find the value of H using Eq. 8.09 .
3. Substitute the value of H in Eq. 8.08. This determines the cable profile.

8.3.2. ELASTIC CATENARY

Originally the solution of the symmetrically suspended elastic catenary is due to Routh [110]. More recently elastic catenary has been discussed in papers by O'Brien [96], Möllman [90], and Peyrot and Goulois [101, 102]. The catenary element developed in the present study is based on a discussion by Irvine [45].

Consider the cable shown in Fig. 8.05; given the following data:

- The unstrained length of the cable L_o.
- The weight per unit of the unstrained length w.
- The modulus of elasticity E.
- The area of cross section in the unstrained state A.
- The position of the end points of the cable $(0,0)$ and (l,h).

It is required to find:

- The geometric shape of the cable.
- The tension in the cable.
- The reactions at the support.

The solution is based on the following assumptions:

1. The cable is perfectly flexible.
2. The cable material is linear elastic.
3. The load is applied along the unstrained arc length of the cable.

To simplify the derivations, a Lagrangian approach is adopted. The Lagrangian coordinate is measured along the length of the cable from the origin to the point of interest on the cable. Consider a point having a Lagrangian coordinate s in the unstrained profile. When the load w is applied, this point moves to a new position on the strained profile of the cable. This position is defined by Cartesian coordinates x and z, and the Lagrangian coordinate p.

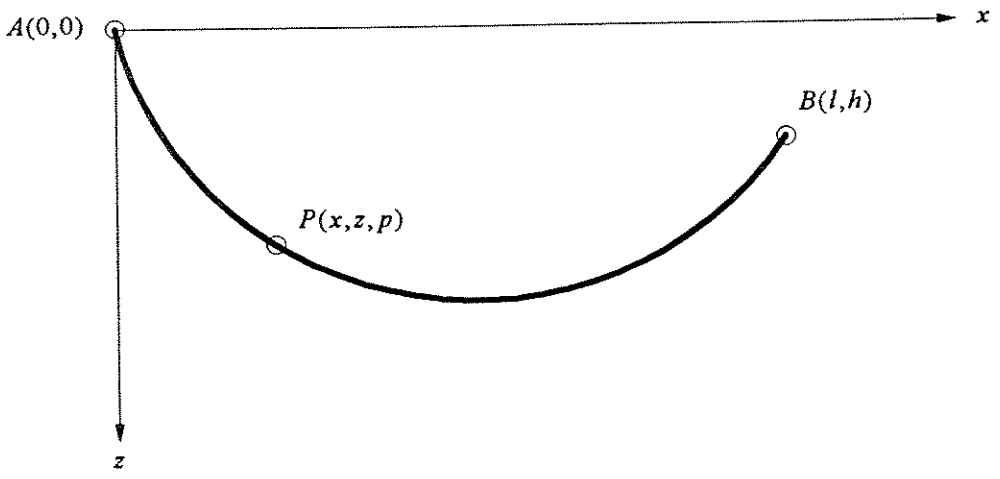

FIG. 8.05 COORDINATES FOR THE ELASTIC CATENARY.

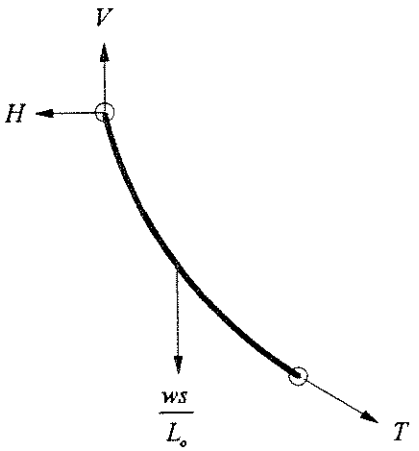

FIG. 8.06 FORCES ON A SEGMENT OF THE STRAINED CABLE PROFILE.

Refer to Fig. 8.06; Consider the equilibrium of an element of the cable.

$$T\frac{dx}{dp} = H$$

$$T\frac{dz}{dp} = V - W\frac{s}{L_o} \tag{8.14}$$

Where T is the tangential force in the cable, H is the constant horizontal component of the cable tension, V is the vertical reaction at the support.

The geometric condition is defined by the following equation

$$\left(\frac{dx}{dp}\right)^2 + \left(\frac{dz}{dp}\right)^2 = 1 \tag{8.15}$$

The material constitutive equation, based on assumption 2 stated above, may be expressed as

$$\sigma = E\left(\frac{dp - ds}{ds}\right)$$

$$T = EA\left(\frac{dp}{ds} - 1\right) \tag{8.16}$$

The boundary conditions at the cable supports A and B are

$$x = 0 \quad z = 0 \quad p = 0 \quad at \quad s = 0$$
$$x = L \quad z = h \quad p = L_s \quad at \quad s = L_o$$

Based on the above equations, we are in a position to derive expressions for the strained cable profile.

SOLUTION FOR CABLE TENSION

The force equilibrium equations (Eq. 8.14) are substituted in the geometric constraint equations (Eq. 8.15) to obtain the expression for cable tension

$$T(s) = \sqrt{H^2 + \left(V - W\frac{s}{L_o}\right)^2} \tag{8.17}$$

SOLUTION FOR THE STRAINED CABLE PROFILE

The derivative $\frac{dx}{ds}$ may be expressed as

$$\frac{dx}{ds} = \frac{dx}{dp}\frac{dp}{ds} \tag{8.18}$$

Substituting the value of $\frac{dx}{dp}$ from Eq. 8.14 and the value of $\frac{dp}{ds}$ from Eq. 8.16 into Eq. 8.17, we have

$$\frac{dx}{ds} = \frac{H}{EA} + \frac{H}{\sqrt{H^2 + \left(V - \frac{Ws}{L_o}\right)^2}} \tag{8.19}$$

Integrating and using the first of the boundary conditions, at end A of the cable, we have

$$x(s) = \frac{Hs}{EA} + \frac{HL_o}{W}\left[\sinh^{-1}\left(\frac{V}{H}\right) - \sinh^{-1}\left(\frac{V - \frac{Ws}{L_o}}{H}\right)\right] \tag{8.20}$$

Using a procedure similar to that given above we can get an expression for $z(s)$

$$z(s) = \frac{Ws}{EA}\left(\frac{V}{W} - \frac{s}{2L_o}\right) + \frac{HL_o}{W}\left[\sqrt{1 + \left(\frac{V}{H}\right)^2} - \sqrt{1 + \left(\frac{V - \frac{Ws}{L_o}}{H}\right)^2}\right] \tag{8.21}$$

SOLUTION FOR THE SUPPORT REACTIONS

By applying the boundary conditions at the end B of the cable to Eq. 8.20 and Eq. 8.21 we obtain

$$l = \frac{HL_o}{EA} + \frac{HL_o}{W}\left[\sinh^{-1}\left(\frac{V}{H}\right) - \sinh^{-1}\left(\frac{V - W}{H}\right)\right] \tag{8.22}$$

$$h = \frac{WL_o}{EA}\left(\frac{V}{W} - \frac{1}{2}\right) + \frac{HL_o}{W}\left[\sqrt{1+\left(\frac{V}{H}\right)^2} - \sqrt{1+\left(\frac{V-W}{H}\right)^2}\right] \tag{8.23}$$

Eq. 8.22 is a transcendental equation in H and V whereas Eq. 8.23 is an algebraic equation in these two quantities.

Hence the strained profile of the elastic catenary may be obtained as follows:

1. Solve Eq. 8.22 and Eq 8.23 simultaneously for H and V using an appropriate numerical method.
2. Use these values in Eq. 8.20 and Eq. 8.21 to evaluate $x(s)$ and $z(s)$.

9. CABLE-STAY ELEMENT

9.1. CONCEPTS AND THEORETICAL BACKGROUND

Shallow cables are defined as cables with a relatively small sag to span ratio. In general, if the sag to span ratio is less than 1:12 then the cable is considered to be a shallow cable and the cable shape may be approximated by a parabola instead of a catenary, Walther [144]. Such cables are used as structural elements in many engineering structures such as cable stayed bridges, guyed masts, suspension roofs, etc.

The static behavior of shallow cables has been investigated by a number of researchers. The formulation discussed below is originally due to Ernst [28] and has also been discussed by Gimsing [32] and several others.

Consider a symmetrically suspended cable, Fig. 9.01. It is desired to find a relation between the end displacement δ in the direction of the cable chord and the corresponding change in cable tension.

Let the cable have an area of cross section A, modulus of elasticity E, an unstrained length of L_o and a chord length of l.

Assume that the cable is subjected to a uniformly distributed load of w per unit chord length. The horizontal reactions at the supports A and B are both equal to H_1. From Eq. 8.12 the length of the cable is given by

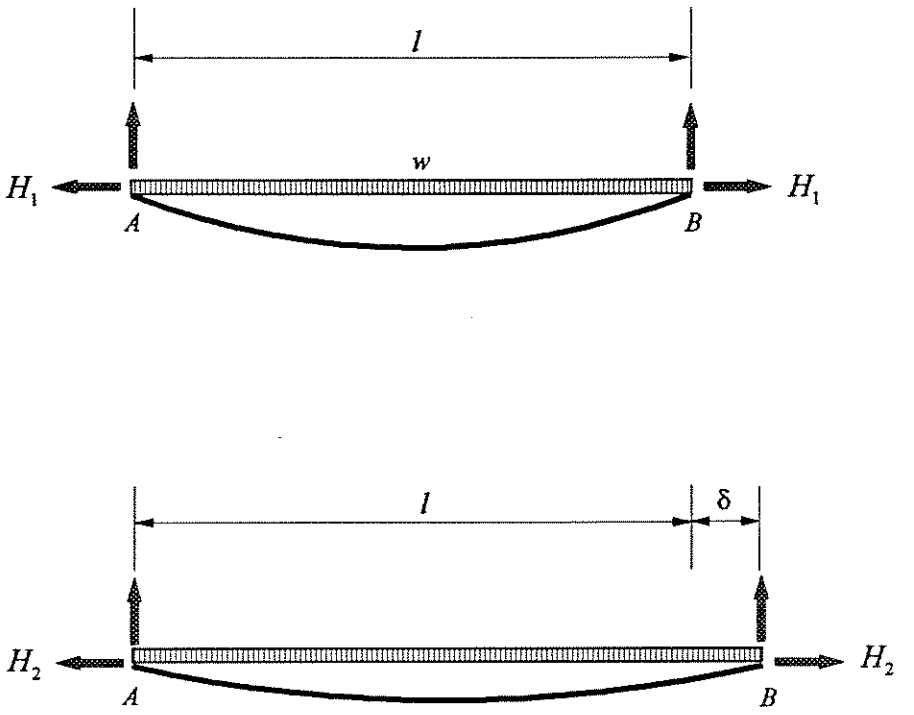

FIG. 9.01 ELASTIC CABLE STAY SUBJECT TO A UNIFORM LOAD *W* ALONG ITS CHORD LENGTH

$$L_1 \approx l + \frac{8}{3}\frac{f_1^2}{l} \tag{9.01}$$

where f_1 is cable sag and is given by

$$f_1 = \frac{wl^2}{8H_1}$$

The elastic elongation with respect to the original length L_o is given by

$$\Delta L_1 = \frac{H_1}{EA}\int_0^l \sqrt{\left[1+\left(\frac{dy}{dx}\right)^2\right]}\,dx$$

$$\Delta L_1 = \frac{wl^2}{2EA}\left(\frac{l}{4f_1}+\frac{4f_1}{3l}\right) \tag{9.02}$$

Let end B of the cable be given a small displacement in the direction of the chord as shown in Fig. 9.01. The new length of the cable and the elastic elongation are given by the following equations.

$$L_2 \approx (l+\delta) + \frac{8}{3}\frac{f_2^2}{(l+\delta)} \tag{9.03}$$

$$\Delta L_2 = \frac{w(l+\delta)^2}{2AE}\left[\frac{(l+\delta)}{4f_2}+\frac{4f_2}{3(l+\delta)}\right] \tag{9.04}$$

Geometric compatibility requires

$$L_2 - L_1 = \Delta L_2 - \Delta L_1$$

Assuming that $l+\delta \approx l$ and substituting the appropriate values from Eq. 9.01, Eq. 9.02, Eq. 9.03 and Eq. 9.04, and simplifying we have

$$\delta = \frac{l}{EA}(H_2 - H_1) + \frac{w^2l^3}{12EA}\left(\frac{1}{H_2}-\frac{1}{H_1}\right) + \frac{w^2l^3}{24}\left(\frac{1}{H_1^2}-\frac{1}{H_2^2}\right)$$

Substituting $\gamma = \frac{w}{A}$ $\sigma_1 = \frac{H_1}{A}$ $\sigma_2 = \frac{H_2}{A}$ we have

$$\frac{\delta}{l}=\frac{(\sigma_2-\sigma_1)}{E}+\frac{\gamma^2 l^2}{24}\left(\frac{1}{\sigma_1^{\,2}}-\frac{1}{\sigma_2^{\,2}}\right)+\frac{\gamma^2 l^2}{12E}\left(\frac{1}{\sigma_2}-\frac{1}{\sigma_1}\right) \tag{9.05}$$

The last term may be dropped without much loss of accuracy. The above equation forms the basis of the CALBRG shallow cable element, described at length in the next section. It has been established by a number of investigators that the parabola based stiffness equation performs satisfactorily for shallow cable-stays, Ernst [28], Walther [144], Möllman [90], Ghaffar [2], Seif [124].

9.2. Series Model for Cable-Stay Element

The axial stiffness of a cable-stay depends on two factors; the sag of the cable and deformation of the cable steel. The sag has a softening effect on the cable stiffness which results in a nonlinear axial force-displacement relationship. The cable has a relatively low stiffness for large values of sag; however as the sag decreases the cable stiffness increases and in the limit the behavior of the cable approaches that of a truss bar in tension.

The series model of the cable-stay element is based on a formulation similar to that discussed in section 9.1. However the derivation given below separates the effect of sag and elastic extension of cable steel and gives a better feel for the physical behavior of the shallow cable.

It is assumed that the cable has a parabolic profile. It is further postulated that the sag and elastic effects can be lumped into two different elements connected in series; thus the shallow cable element may be visualized as a cable having chord length l, area of cross section A and an infinite modulus of elasticity $E=\infty$, connected in series with an elastic truss bar of length l and having a modulus of elasticity and area of cross section equal to that of the actual cable. The force deformation relationship of each component is derived separately and subsequently used to obtain the stiffness of the series model.

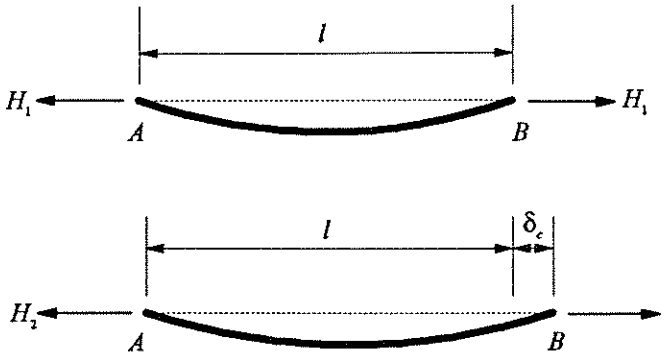

(a) INEXTENSIBLE STAY CABLE SUBJECT TO END DISPLACEMENT δ_c

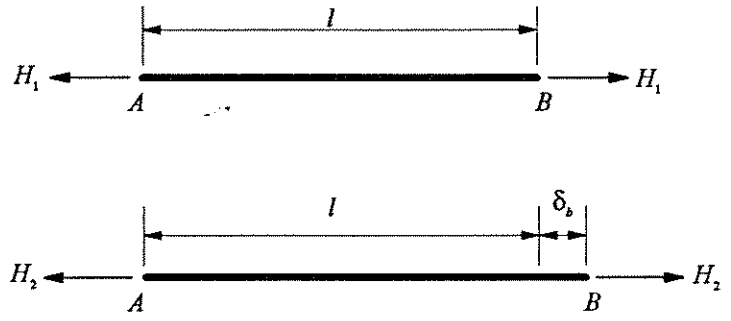

(b) ELASTIC TRUSS BAR SUBJECT TO END DISPLACEMENT δ_b

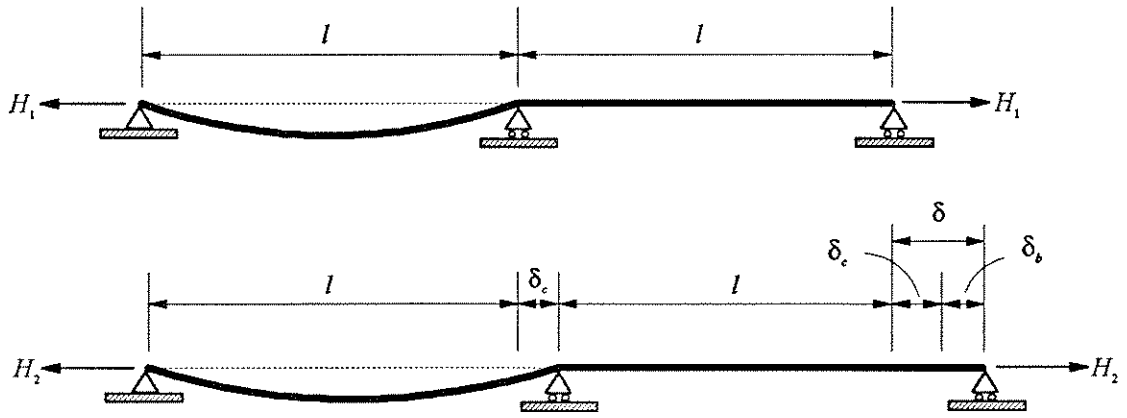

(c) SERIES MODEL FOR ELASTIC CABLE STAY

FIG. 9.02 COMBINED ELASTIC CABLE ELEMENT CONSISTING OF AN INEXTENSIBLE CABLE AND AN ELASTIC TRUSS BAR CONNECTED IN SERIES.

Consider the cable shown in the Fig. 9.02 (a). The unstrained length of the cable is L_o, chord length l and area of cross section is A. The cable is inextensible in the sense that it has a modulus of elasticity $E = \infty$. It is assumed that the cable has a parabolic profile. Hence the length of the cable as given by Eq. 8.12 is

$$L_o = l + \frac{8}{3}\frac{f_1^2}{l} \tag{9.06}$$

where $f_1 = \frac{wl^2}{8H_1}$.

Let the end of the cable be subjected to a displacement δ as shown in Fig. 9.02 (a). The cable is inextensible, it's length does not change and may be expressed as

$$L_o = (l+\delta) + \frac{8}{3}\frac{f_2^2}{(l+\delta)^2} \tag{9.07}$$

where $f_2 = \frac{w(l+\delta)^2}{8H_2}$

Subtracting Eq. 9.06 from 9.07, substituting the value of f_1 and f_2 and rearranging we have

$$\delta = \frac{w^2}{24}\left(\frac{l^3}{H_1^2} - \frac{(l+\delta)^3}{H_2^2}\right) \tag{9.08}$$

Since $\delta << l$ therefore it may be assumed that $l + \delta \approx l$ and Eq. 9.08 is reduced to

$$\delta = \frac{w^2 l^3}{24}\left(\frac{1}{H_1^2} - \frac{1}{H_2^2}\right) \tag{9.09}$$

Substituting $\sigma_1 = \frac{H_1}{A}$ $\sigma_2 = \frac{H_2}{A}$ $\gamma = \frac{w}{A}$ into Eq. 9.09 we have

$$\delta = \frac{\gamma^2 l^3}{24}\left(\frac{1}{\sigma_1^2} - \frac{1}{\sigma_2^2}\right) \tag{9.10}$$

For a cable whose chord is inclined at an angle ϕ to the horizontal, the sag creating transverse load has an intensity of $w\cos\phi$ as shown in Fig. 9.03. The deformational characteristics of the inclined cable will consequently be the same as those of a horizontal cable with the same chord length L but subjected to a transverse load of $w\cos\phi$. Thus for an inclined cable Eq. 9.10 is modified to

$$\delta = \frac{(\gamma\cos\phi)^2 l^3}{24}\left(\frac{1}{\sigma_1^{\,2}} - \frac{1}{\sigma_2^{\,2}}\right) \tag{9.11}$$

Consider the truss bar shown in the Fig. 9.02 (b). It has a length l, an area of cross section A and a modulus of elasticity E; which are equal to the chord length, area of cross section and modulus of elasticity of the cable respectively.

Let the initial axial force in the bar be H_1. Assume that the end of the bar is given an axial displacement δ. The force deformation relationship is given by

$$\delta = \frac{(H_2 - H_1)l}{AE}$$

$$\delta = \frac{(\sigma_2 - \sigma_1)l}{E} \tag{9.12}$$

Now consider the two elements connected in series as shown in Fig. 9.02 (c). As the element end force changes from H_1 to H_2, the end displacement δ is given by

$$\delta = \delta_c + \delta_b \tag{9.13}$$

where δ_c and δ_b are the individual elongations of the cable and the bar respectively when subjected to a stress change from σ_1 to σ_2. Substituting Eq. 9.11 and Eq. 9.12 into Eq. 9.13 we have

$$\frac{\delta}{l} = \frac{(\sigma_2 - \sigma_1)}{E} + \frac{(\gamma\cos\varphi)^2 l^2}{24}\left(\frac{1}{\sigma_1^{\,2}} - \frac{1}{\sigma_2^{\,2}}\right) \tag{9.14}$$

Note that this equation is similar to Eq. 9.05 except for the last term. As compared to the catenary equation, this is a relatively elegant and simple formula and is much more convenient to use.

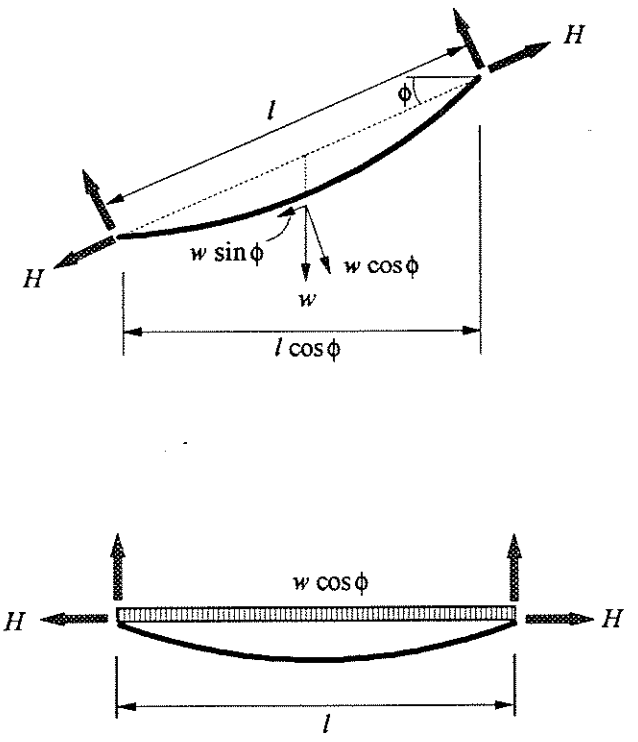

FIG. 9.03 INCLINED STAY CABLE AND EQUIVALENT HORIZONTAL STAY CABLE WITH EQUAL DEFORMATIONAL CHARACTERISTICS.

9.2.1. BASIC FORCE DISPLACEMENT RELATIONSHIP

Refer to Fig. 9.04, which shows a plot of the force deformation relationship of the shallow cable as defined by Eq. 9.14. The secant modulus is given by

$$E_{sec} = \frac{l(\sigma_2 - \sigma_1)}{\delta} \tag{9.15}$$

Substitute the value of $\frac{\delta}{l}$ from Eq. 9.14 into Eq. 9.15 . This yields

$$\frac{1}{E_{sec}} = \frac{1}{E} + \frac{(\gamma \cos\phi)^2 l^2}{24}\left(\frac{\sigma_1 + \sigma_2}{\sigma_1^2 \sigma_2^2}\right) \tag{9.16}$$

E_{sec} as defined by Eq. 9.16 is a modulus leading from state 1 (point A) to state 2 (point B) on the curve along a secant, hence the name secant modulus. Note that to determine the secant modulus, the cable stress in both condition 1 σ_1 and condition 2 σ_2 must be known. In most cases σ_2 is not known and has to be estimated; thereby resulting in an iterative solution.

Substituting $\sigma_2 = \sigma_1$ into Eq. 9.16, we get the tangent modulus equation.

$$\frac{1}{E_{tan}} = \frac{1}{E} + \frac{(\gamma \cos\phi)^2 l^2}{12\sigma_1^3}$$

$$E_{tan} = \frac{E}{1 + \frac{E(\gamma \cos\phi)^2 l^2}{12\sigma_1^3}} \tag{9.17}$$

According to Menn [86], the value of E_{tan} has a substantial influence on the overall stiffness of the structural system of a cable-stayed bridge. Decreasing E_{tan} reduces system stiffness and increases both first and second order moments. This reduces the stability of the system. Note that E_{tan} is a cubic function of stress σ_1; this indicates that the stress in the cables should be as high as possible. Menn [86] strongly recommends the use of high strength steel for cable-stays, especially for long span bridges.

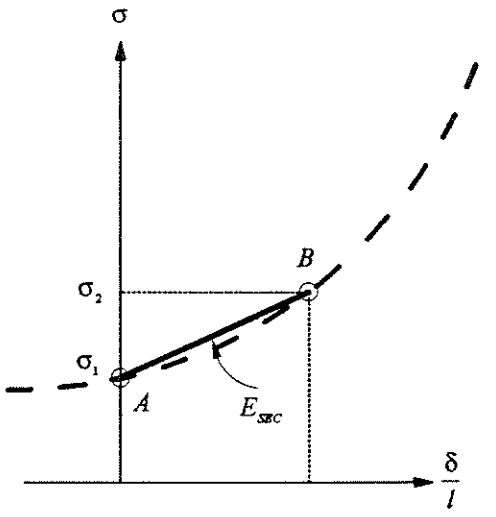

SECANT STIFFNESS

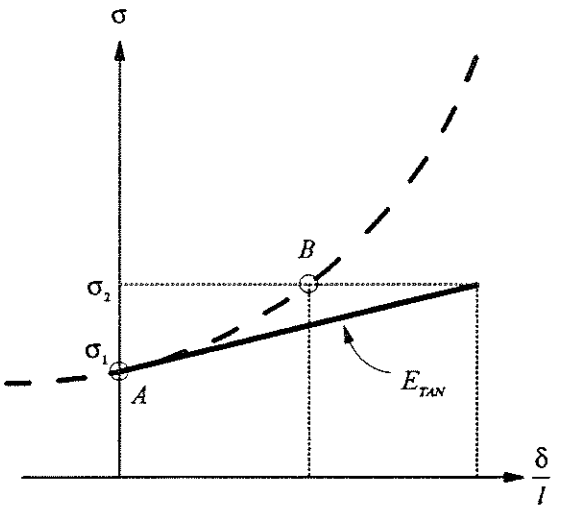

TANGENT STIFFNESS

FIG 9.04 LINEARIZED FORCE DISPLACEMENT RELATIONSHIPS
SECANT AND TANGENT STIFFNESS OF A CABLE STAY

CALBRG uses the tangent modulus for an initial estimate of cable stiffness; however the state determination process uses the nonlinear force deformation Eq. 9.14. Thus the solution is exact based on the inherent assumptions involved in the derivation of Eq. 9.14.

It is of interest to examine the procedure described by Ernst [28] to determine cable stress using a linear approximation of the force deformation relationship. The secant stiffness given by Eq. 9.16 may be expressed as:

$$E_{sec} = \frac{E}{1 + \frac{E(\gamma \cos\phi)^2 l^2}{24} \frac{(\sigma_1 + \sigma_2)}{(\sigma_1^2 + \sigma_2^2)}}$$

Let $\sigma_m = \frac{\sigma_1 + \sigma_2}{2}$ and $\mu = \frac{\sigma_1}{\sigma_2}$. We define a new variable $\bar{\sigma}$ such that

$$\bar{\sigma} = \left(\frac{2(\sigma_1^2 + \sigma_2^2)}{(\sigma_1 + \sigma_2)} \right)^{\frac{1}{3}}$$

$$= \left(\frac{16\mu^2}{(1+\mu)^4} \right)^{\frac{1}{3}} \sigma_m$$

Eq. 9.16 may be rewritten as follows:

$$E_{sec} = \frac{E}{1 + \frac{E(\gamma \cos\phi)^2 l^2}{12\bar{\sigma}^3}} \tag{9.18}$$

If the live load on the structure is small in relation to its dead load then the ratio $\mu \approx 1$. Also, if the approximate value of the average stress in the cables σ_m is known then $\bar{\sigma} \approx \sigma_m$ and hence a somewhat constant value of E_{sec} may be estimated from Eq. 9.18. This results in a linear force deformation relation and allows for linear elastic analysis wherein the cables are modeled as truss bars with the modulus of elasticity modified as described above.

9.2.2. Element Stiffness Matrix

The cable stay element developed in the previous section is shown in Fig. 9.05. The in-extensible cable, which models the sag effect, is shown as a zero length spring element with

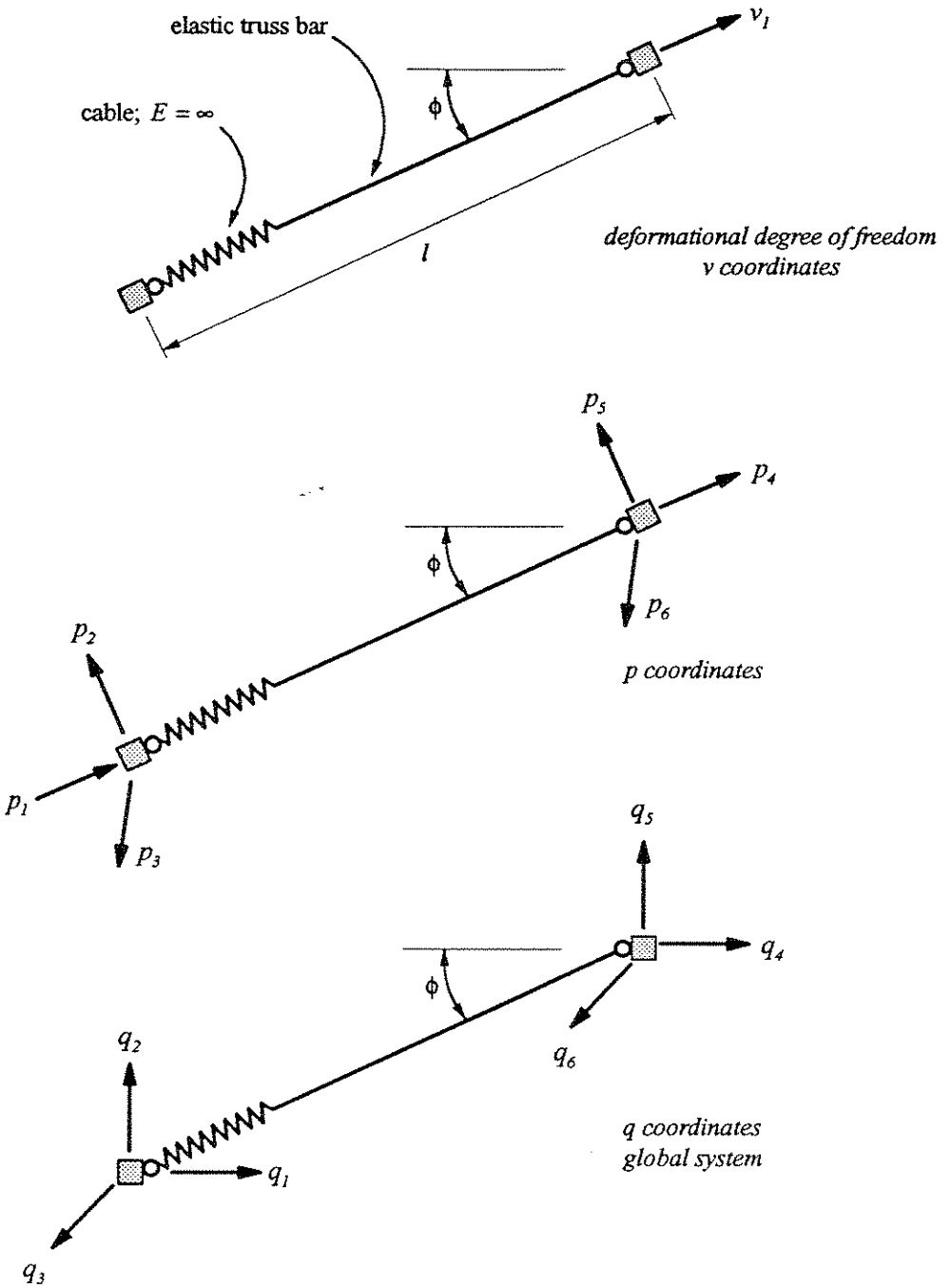

FIG. 9.05 CALBRG CABLE ELEMENT
LOCAL AND GLOBAL DEGREES OF FREEDOM

a nonlinear strain-displacement relationship. The local x-axis is defined by the two end nodes I and J; in the actual cable the local x-axis coincides with the chord of the cable. With reference to local coordinates, the element has one deformational degree of freedom. Thus the element stiffness in local coordinates is given by:

$$\mathbf{K}_{\mathrm{V}} = \frac{AE}{l}\left(\frac{1}{1+\dfrac{E\left(\gamma\cos\phi\right)^2 l^2}{12\sigma_l^2}}\right)$$

$$\mathbf{K}_{\mathrm{V}} = \frac{AE_{\tan}}{l} \tag{9.19}$$

Note that $E_{\tan}$ is the equivalent tangent modulus of elasticity as given by Eq. 9.17. The element has six degrees of displacement freedom, three at each end of the element (P coordinates) as shown in Fig. 9.05. The elastic stiffness in the P coordinates $\mathbf{K}_{\mathrm{Pe}}$ is given by the following equation.

$$\mathbf{K}_{\mathrm{Pe}} = \mathbf{A}_{\mathrm{VP}}{}^{\mathrm{T}}\,\mathbf{K}_{\mathrm{V}}\,\mathbf{A}_{\mathrm{VP}} \tag{9.20}$$

Where $\mathbf{A}_{\mathrm{VP}}$ (1x6) is the displacement transformation matrix from P to V coordinates.

$$\mathbf{A}_{\mathrm{VP}} = \begin{bmatrix} -1 & 0 & 0 & 1 & 0 & 0 \end{bmatrix} \tag{9.21}$$

The geometric stiffness matrix $\mathbf{K}_{\mathrm{Pg}}$ (6x6) for the element in P coordinates is given by:

$$\mathbf{K}_{\mathrm{Pg}} = \begin{bmatrix} 0 & 0 & 0 & 0 & 0 & 0 \\ 0 & 1 & 0 & 0 & -1 & 0 \\ 0 & 0 & 1 & 0 & 0 & -1 \\ 0 & 0 & 0 & 0 & 0 & 0 \\ 0 & -1 & 0 & 0 & 1 & 0 \\ 0 & 0 & -1 & 0 & 0 & 1 \end{bmatrix} \tag{9.22}$$

The complete element stiffness matrix in P coordinates is given by adding the elastic and the geometric stiffness matrix.

$$\mathbf{K}_{\mathrm{P}} = \mathbf{K}_{\mathrm{Pg}} + \mathbf{K}_{\mathrm{Pe}} \tag{9.23}$$

Hence the element end forces $\mathbf{S}_{\mathrm{P}}$ are related to the nodal displacements $\mathbf{V}_{\mathrm{P}}$ by the following equation.

$$\mathbf{S_P} = \mathbf{K_P}\ \mathbf{V_P}$$

$$\begin{pmatrix} P_1 \\ P_2 \\ P_3 \\ P_4 \\ P_5 \\ P_6 \end{pmatrix} = \left\{ \frac{AE_{\tan}}{l} \begin{pmatrix} 1 & 0 & 0 & -1 & 0 & 0 \\ 0 & 0 & 0 & 0 & 0 & 0 \\ 0 & 0 & 0 & 0 & 0 & 0 \\ -1 & 0 & 0 & 1 & 0 & 0 \\ 0 & 0 & 0 & 0 & 0 & 0 \\ 0 & 0 & 0 & 0 & 0 & 0 \end{pmatrix} + \frac{H}{l} \begin{pmatrix} 0 & 0 & 0 & 0 & 0 & 0 \\ 0 & 1 & 0 & 0 & -1 & 0 \\ 0 & 0 & 1 & 0 & 0 & -1 \\ 0 & 0 & 0 & 0 & 0 & 0 \\ 0 & -1 & 0 & 0 & 1 & 0 \\ 0 & 0 & -1 & 0 & 0 & 1 \end{pmatrix} \right\} \begin{pmatrix} p_1 \\ p_2 \\ p_3 \\ p_4 \\ p_5 \\ p_6 \end{pmatrix} \tag{9.24}$$

The global tangent stiffness matrix $\mathbf{K_Q}$ (6x6) can be obtained by transforming $\mathbf{K_P}$ (6x6) to global coordinates.

$$\mathbf{K_Q} = \mathbf{A_{PQ}}^{\mathrm{T}}\ \mathbf{K_P}\ \mathbf{A_{PQ}} \tag{9.25}$$

The displacement transformation matrix $\mathbf{A_{PQ}}$ (6x6) is expressed as

$$\mathbf{A_{PQ}} = \begin{bmatrix} \mathbf{D} & \mathbf{0} \\ \mathbf{0} & \mathbf{D} \end{bmatrix} \tag{9.26}$$

D (3x3) is a matrix of direction cosines; where the rows of the matrix D are the direction cosines of unit vectors $\bar{p}_1$, $\bar{p}_2$ and $\bar{p}_3$ respectively as referred to the global coordinates.

9.3. MATERIAL MODEL FOR CABLE-STAY STEEL

A bilinear strain hardening model is adopted for the cable stay steel. The model is shown in Fig. 9.06. It is completely defined by the following parameters.

σ_y, the yield stress of cable steel.

ε_y, the corresponding yield strain.

σ_u, the ultimate strain of the cable steel at failure.

ε_u, the corresponding ultimate strain at failure.

The model allows for loading and unloading from the strain hardening branch as shown in the figure. Note that this model cannot be used directly and has to be transformed into a stress versus apparent strain plot as described in the next section.

9.4. STATE DETERMINATION PROCEDURE

The algorithm used in CALBRG for the state determination for a nonlinear cable material is best explained by an example.

Assume that the cable steel has a bilinear strain hardening stress-strain curve of the type shown in Fig. 9.06. Further assume that the cable has a chord length l at the initial reference stress of σ_o and a weight density of γ. Let v denote the total axial displacement of the cable end with respect to the reference state.

For each cable element, generate the stress σ versus apparent strain $\hat{\varepsilon} = \frac{v}{l}$ curve. Refer to Fig. 9.07; the x-ordinates of σ_o, σ_y and σ_u are given by the following expressions respectively.

$$\hat{\varepsilon}_o = 0$$

$$\hat{\varepsilon}_y = \frac{v_y}{l} = \frac{\sigma_y - \sigma_o}{E} + \frac{\gamma^2 l^2}{24}\left(\frac{1}{\sigma_o^{\,2}} - \frac{1}{\sigma_y^{\,2}}\right)$$

$$\hat{\varepsilon}_u = \frac{v_u}{l} = \hat{\varepsilon}_y + \frac{\sigma_u - \sigma_y}{E_{sh}} + \frac{\gamma^2 l^2}{24}\left(\frac{1}{\sigma_y^{\,2}} - \frac{1}{\sigma_u^{\,2}}\right) \qquad (9.27)$$

Let the previous state of the cable be defined by the stress σ_1 and an apparent strain $\hat{\varepsilon}_1$ corresponding to an axial displacement of v_1. Now assume that an axial displacement increment of δ is imposed on the element. The current displacement and apparent strain are given by;

$$v_2 = v_1 + \delta$$

$$\hat{\varepsilon}_2 = \frac{v_2}{l}$$

It is required to find the new stress σ_2 in the cable. Compare the current apparent strain $\hat{\varepsilon}_2$ with the $\left[\hat{\varepsilon}_o \;\; \hat{\varepsilon}_1 \;\; \hat{\varepsilon}_y \;\; \hat{\varepsilon}_u\right]$ array. If $\hat{\varepsilon}_2$ is such that $\hat{\varepsilon}_1 < \hat{\varepsilon}_2 < \hat{\varepsilon}_y$ then the new value of stress σ_2 in the cable is given by the following equation.

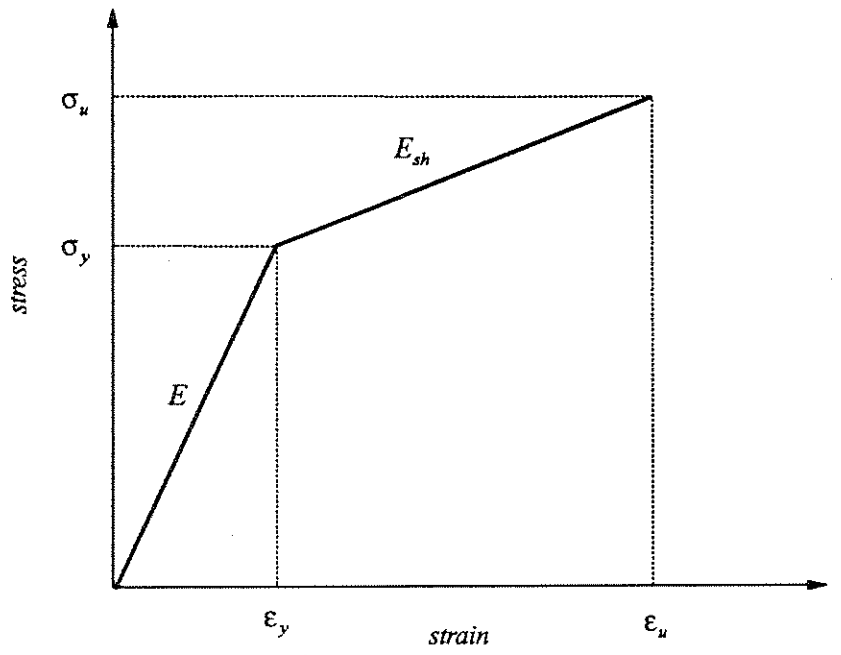

FIG 9.06 ASSUMED BILINEAR STRESS-STRAIN MODEL OF THE CABLE STEEL.

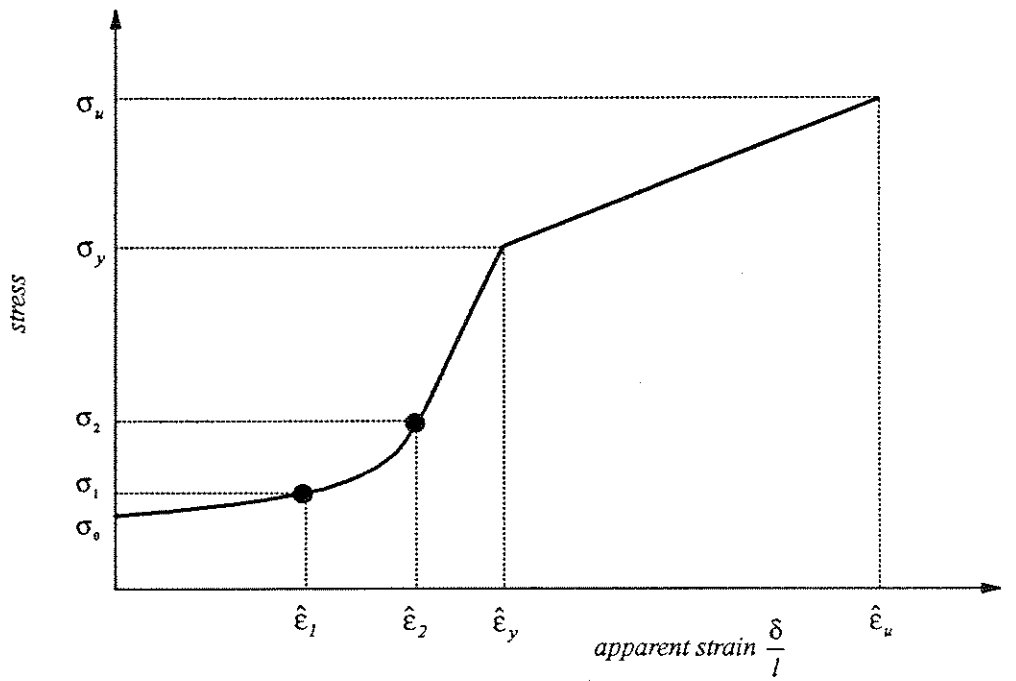

FIG. 9.07 STRESS VS APPARENT STRAIN PLOT OF THE CABLE STAY.

$$\frac{\delta}{l}=\frac{\sigma_2-\sigma_1}{E}+\frac{\gamma^2 l^2}{24}\left(\frac{1}{\sigma_1^{\,2}}-\frac{1}{\sigma_2^{\,2}}\right)$$

However, if $\hat{\varepsilon}_2$ is such that $\hat{\varepsilon}_y<\hat{\varepsilon}_2<\hat{\varepsilon}_u$ then the new cable stress σ_2 is given by the following equation.

$$\frac{v_2-v_y}{l}=\frac{\sigma_2-\sigma_y}{E_{sh}}+\frac{\gamma^2 l^2}{24}\left(\frac{1}{\sigma_y^{\,2}}-\frac{1}{\sigma_2^{\,2}}\right)$$

The above two equations are cubic in σ_2 and are solved by using the Newton-Raphson method or an alternate closed form solution suggested by the author; these are described in more detail in the following sections.

9.4.1. NEWTON-RAPHSON METHOD

Consider a cable of chord length l, area of cross section A and modulus of elasticity E. Let the element end axial force at the beginning of the step be $\sigma_1 A$. Now assume that at the end of the step the element end axial displacement increment is δ. The corresponding stress increment is given by:

$$\frac{\delta}{l}=\frac{(\sigma_2-\sigma_1)}{E}+\frac{\gamma^2 l^2}{24}\left(\frac{1}{\sigma_1^{\,2}}-\frac{1}{\sigma_2^{\,2}}\right) \tag{9.28}$$

This is an implicit equation in σ_2 and can be solved by using the Newton-Raphson method which is a well known numerical method for solving a root finding problem.

Transforming the Eq. 9.28 to the form $f(\sigma_2)=0$ and applying the Newton-Raphson technique we have the following iterative equation.

$$\sigma_{k+1}=\sigma_k-\frac{f(\sigma_k)}{f'(\sigma_k)} \tag{9.29}$$

where σ_k is an initial estimate of the total stress in the element and σ_{k+1} is an improved estimate of the same. The expressions for $f(\sigma_k)$ and its derivative $f'(\sigma_{k+1})$ are given below.

$$f(\sigma_k)=\sigma_k{}^3+\sigma_k{}^2\left(\frac{\gamma^2 l^3}{24\sigma_1{}^2}-\frac{\delta E}{l}-\sigma_1\right)-\frac{\gamma^2 l^2 E}{24}$$

$$f'(\sigma_k)=3\sigma_k{}^2+2\sigma_k\left(\frac{\gamma^2 l^3}{24\sigma_1{}^2}-\frac{\delta E}{l}-\sigma_1\right) \tag{9.30}$$

The iteration is stopped when the criteria set by the following equation is satisfied.

$$\frac{|\sigma_{k+1}-\sigma_k|}{|\sigma_k|}\le\kappa \tag{9.31}$$

where κ is the selected tolerance. The Newton Raphson algorithm was used by the author in the computer program NASCAB [1].

9.4.2. Closed Form Solution

The closed form solution is based on formulas given by Tuma [139] and verified against a solution generated by Maple V , a symbolic processor developed at University of Waterloo, Canada and provided with MathCad [82]. This solution is obviously more efficient as compared to Newton-Raphson and hence has been implemented in the computer program CALBRG developed as a part of this study. Transforming Eq. 9.28 to the form $f(\sigma)=0$, we have

$$\sigma_2{}^3+a\,\sigma_2{}^2+b=0 \tag{9.32}$$

where

$$a=-\sigma_1+\frac{\gamma^2 l^2 E}{24\sigma_1{}^2}-\frac{\delta E}{l}$$

$$b=\frac{\gamma^2 l^2 E}{24}$$

The three roots are as follows:

$$(\sigma_2)_1=u+v$$

$$(\sigma_2)_2=-\frac{u+v}{2}+\frac{u+v}{2}\sqrt{3}\;i$$

$$(\sigma_2)_2=-\frac{u+v}{2}-\frac{u+v}{2}\sqrt{3}\;i \tag{9.33}$$

where

$$u=\left(\frac{1}{2}b-\frac{1}{27}a^3+\frac{1}{18}\sqrt{3b}\sqrt{27b-4a^3}\right)^{\frac{1}{3}}-\frac{a}{6}$$

$$v=\left(\frac{1}{2}b-\frac{1}{27}a^3-\frac{1}{18}\sqrt{3b}\sqrt{27b-4a^3}\right)^{\frac{1}{3}}-\frac{a}{6}$$

If $D=27b-4a^3$, then depending on the value of D, one of the following conditions applies:

$D>0$ there are one real and two conjugate complex roots.

$D=0$ there are three real roots and at least two are equal.

$D<0$ there are three real and unequal roots.

The algorithm implemented in CALBRG selects a real positive root closest to the reference stress of the cable. A series of numerical experiments showed complete agreement with the results obtained by Newton-Raphson method.

9.5. Analysis Example

The analysis procedure described above was implemented in the computer program CALBRG. The results of a numerical example are presented in this section. A cable was loaded to failure and the force deformation relation was tracked through its elastic and yielding strain ranges up to the failure strain. The results are shown in Fig. 9.08. The pertinent cable data are as follows.

$$l=4000\ in \qquad A=7.75\ in^2 \qquad \gamma=2.84\times10^{-4}\ kips/in^2$$

The left end of the cable is fixed and the right end is subjected to controlled displacement increments. The initial tension in the cable was assumed to be $20\ kips$. At this point the cable has a relatively large sag and hence the stiffness is rather low as illustrated by Fig. 9.08.

Displacement was increased in steps of 2.5 inches from point A to point C. As the sag decreased, cable stiffness began to increase. At a displacement of about 30 inches, there

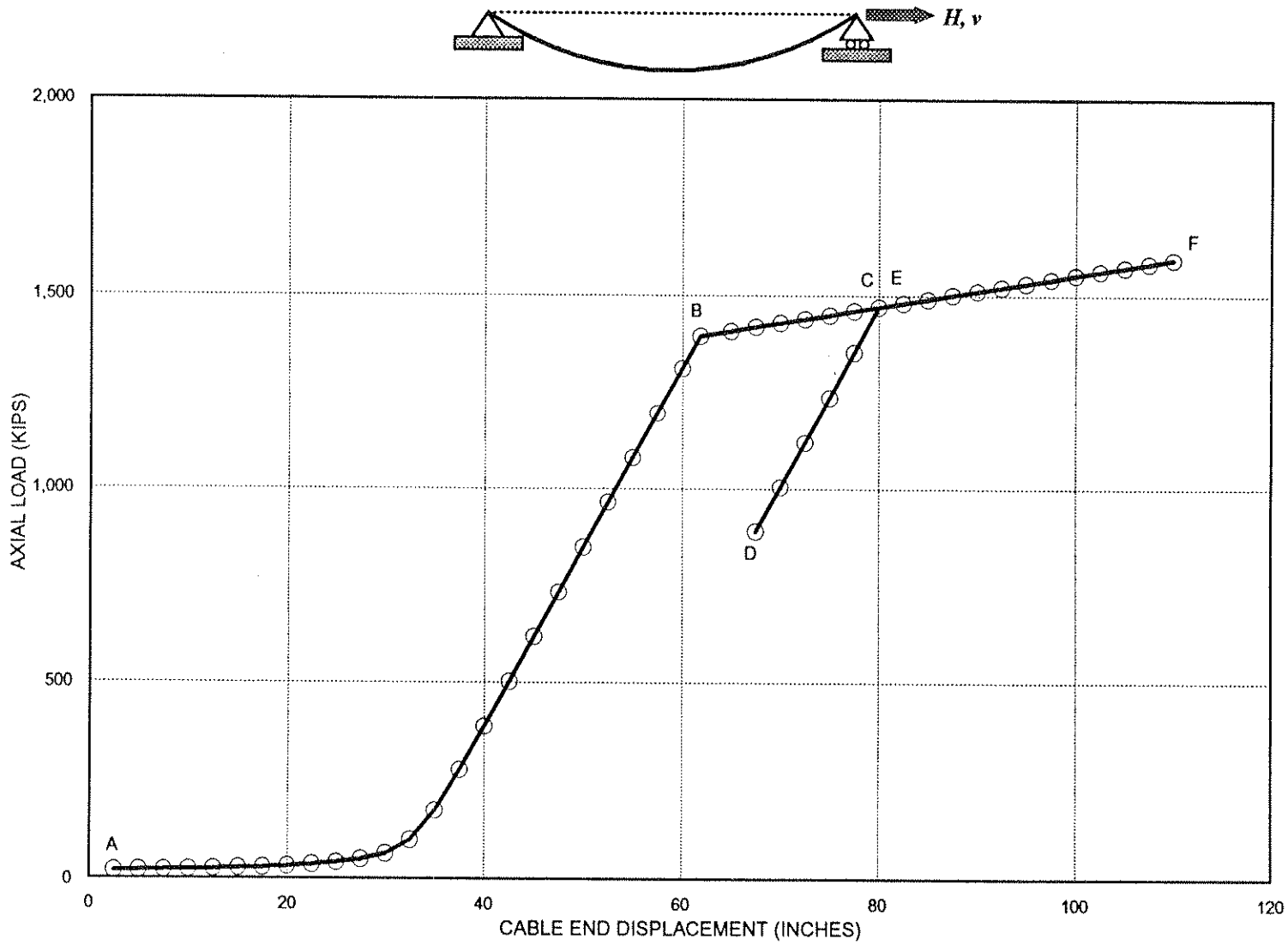

FIG. 9.08 CABLE STAY ELEMENT (SHALLOW CABLE); LOAD VS DISPLACEMENT PLOT

was a substantial increase in cable stiffness and it began to behave similar to a truss bar in tension.

At point B, corresponding to a displacement of about 60 inches the steel began to yield. From point B to C, the cable material went through strain hardening. At point C displacement was decreased and the cable began to unload. This continued till point D, from which point, the displacement was again incremented. The curve retraced its path and joined the virgin path at point E. The analysis was ultimately terminated at point F (not shown on the plot) close to the failure strain of the cable steel.

10. CATENARY ELEMENT

10.1. GENERAL

The catenary element, developed in the present study, is based explicitly on the differential equations describing the state of the elastic catenary and described earlier in section 8.3.2. This element is exact for a cable of linear elastic material which is suspended freely in space, subject only to a uniformly distributed load along its length and supported its end points. Moreover, this element can be used to model shallow cables used in cable-stayed bridges as well as large sag cables used in suspension bridges.

Engineering structures, which employ shallow cables, can be analyzed by modeling each cable as a series of linked truss bars or using special shallow cable elements such as that described in chapter 9, Abdel Ghaffar [2], Abbas [1]. However, when the cable sag is large and the structure can undergo large displacements, for example in mooring systems of ocean engineering structures, the multi-element modeling approach may require either a large number of iterations or may not converge at all. In such cases, it is advantageous to use a single element, based on the analytical expressions of the elastic catenary, to simulate the cable. Such approaches have been discussed by a number of researchers; O'Brien [96], Irvine [45], Peyrot et al. [102].

A major advantage of the catenary element, presented in this chapter, lies in the fact that a single element can successfully capture the response of the entire cable and it is not necessary to descritize it into smaller segments.

A state determination process, based on the two dimensional Newton-Raphson was developed in the present study and implemented in the computer program CALBRG. This algorithm was found to be very efficient and rapid convergence was obtained even for large displacements of the order of magnitude of the size of the structure.

Further, this element, when used in the environment of the computer program CALBRG, can be specially useful for the analysis of suspension bridges and the simulation of their construction sequence.

10.2. ELEMENT STIFFNESS

The derivation of the element stiffness matrix is based on the analytical expressions developed earlier in section 8.3.2 and Irvine [45].

Consider the cable shown in Fig. 10.01. The lower end of the cable is fixed. Let the upper end of the cable move through an infinitesimal displacement defined by the vector $\mathbf{dv}$:

$$\mathbf{dv} = \begin{bmatrix} dl \\ dh \end{bmatrix}$$

The corresponding changes in the element end forces are given by the vector $\mathbf{dS}$.

$$\mathbf{dS} = \begin{bmatrix} dH \\ dV \end{bmatrix}$$

Equations Eq. 8.22 and Eq. 8.23 may be expressed as functions of H and V

$$\begin{aligned} l &= f(H,V) \\ h &= g(H,V) \end{aligned} \qquad (10.01)$$

Also the total differentials of l and h may be expressed as

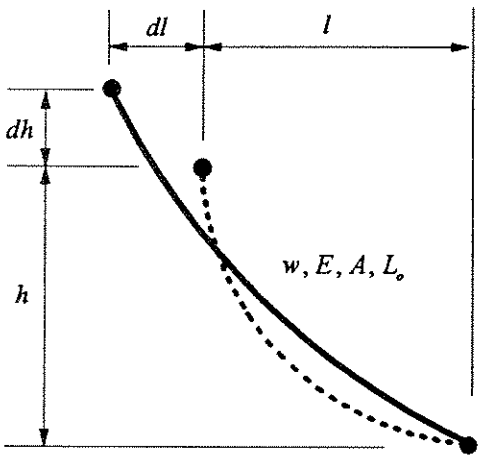

GEOMETRY

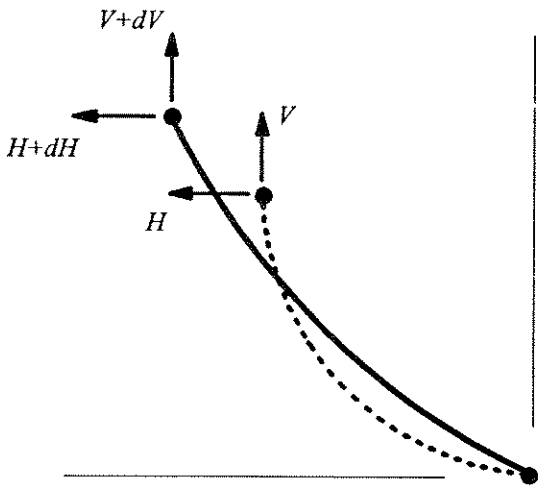

STATICS

FIG. 10.01 DEFINITION DIAGRAM; ELASTIC CATENARY

$$dl = \frac{\partial f}{\partial H} dH + \frac{\partial f}{\partial V} dV$$

$$dh = \frac{\partial g}{\partial H} dH + \frac{\partial g}{\partial V} dV \qquad (10.02)$$

In matrix notation

$$\begin{bmatrix} dl \\ dh \end{bmatrix} = \begin{bmatrix} \frac{\partial f}{\partial H} & \frac{\partial f}{\partial V} \\ \frac{\partial g}{\partial H} & \frac{\partial g}{\partial V} \end{bmatrix} \begin{bmatrix} dH \\ dV \end{bmatrix}$$

$$\mathbf{dv} = \mathbf{F}\ \mathbf{dS} \qquad (10.03)$$

where $\mathbf{F}$, the (2 x 2) Jacobian matrix is the flexibility matrix.

$$\mathbf{F} = \begin{bmatrix} \frac{\partial f}{\partial H} & \frac{\partial f}{\partial V} \\ \frac{\partial g}{\partial H} & \frac{\partial g}{\partial V} \end{bmatrix} = \begin{bmatrix} f_{11} & f_{12} \\ f_{21} & f_{22} \end{bmatrix}$$

The stiffness matrix $\mathbf{K}$ is the inverse of the flexibility matrix $\mathbf{F}$, therefore:

$$\mathbf{K} = \mathbf{F}^{-1} = \frac{1}{f_{11} f_{22} - f_{12} f_{21}} \begin{bmatrix} +f_{22} & -f_{12} \\ -f_{21} & +f_{11} \end{bmatrix} \qquad (10.04)$$

The flexibility influence coefficients are given by the following expressions:

$$f_{11} = \frac{L_o}{EA} + \frac{L_o}{W}\left[\sinh^{-1}\left(\frac{V}{H}\right) - \sinh^{-1}\left(\frac{V-W}{H}\right)\right] + \frac{L_o}{HW}\left[-\frac{V}{\eta} + \frac{V-W}{\xi}\right] \qquad (10.05)$$

$$f_{12} = \frac{L_o}{W}\left[\frac{1}{\eta} - \frac{1}{\xi}\right] \qquad (10.06)$$

$$f_{21} = \frac{L_o}{W}\left[\eta - \zeta\right] + \frac{L_o}{H^2 W}\left[-\frac{V^2}{\eta} + \frac{(V-W)^2}{\xi}\right] \qquad (10.07)$$

$$f_{22} = \frac{L_o}{EA} + \frac{L_o}{HW}\left[\frac{V}{\eta} + \frac{V-W}{\zeta}\right] \qquad (10.08)$$

where η and ξ are functions of the forces V and H and are defined as:

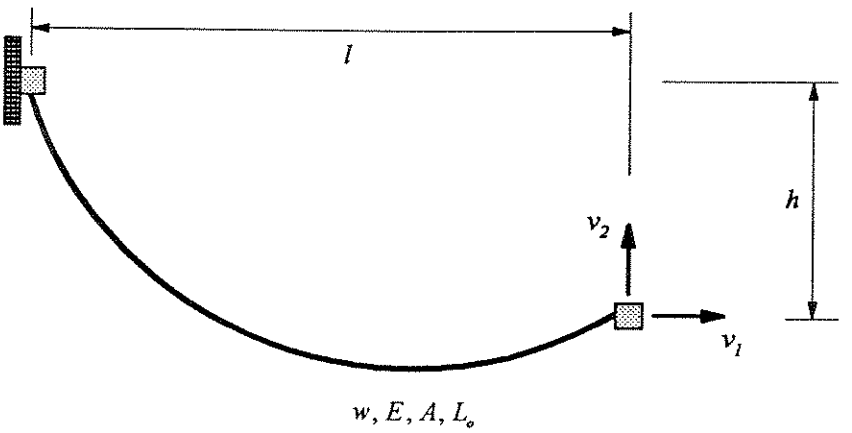

(a) Catenary; local degrees of freedom.

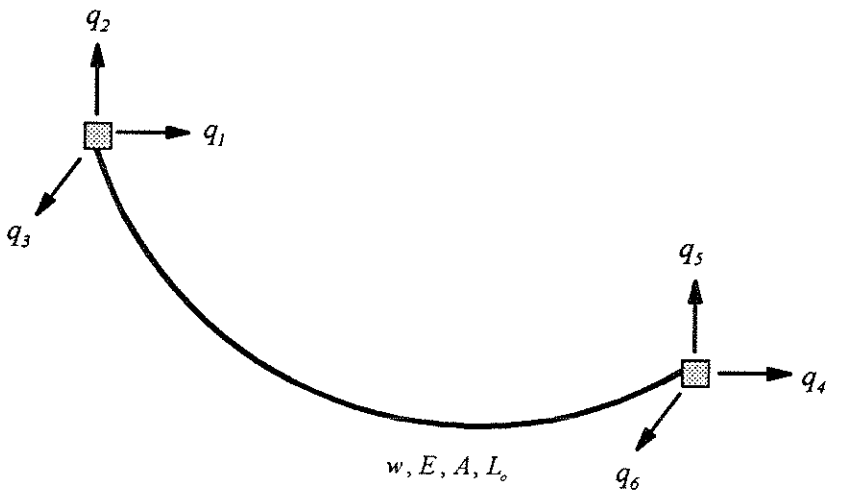

(b) Catenary; global coordinates

FIG. 10.02 CATENARY ELEMENT; DEGREES OF FREEDOM.

$$\eta = \sqrt{1+\left(\frac{V}{H}\right)^2} \qquad \xi = \sqrt{1+\left(\frac{V-W}{H}\right)^2}$$

Note that the flexibility matrix $\mathbf{F}$ and hence the stiffness matrix $\mathbf{K}$ are non symmetric. This creates a problem as most of the equation solving routines used in computer programs used for structural analysis are designed on the basis of a symmetric global structure stiffness matrix. One way to get around this problem is to set the off diagonal terms equal to their average

$$\hat{\mathbf{F}} = \begin{bmatrix} f_{11} & \hat{f} \\ \hat{f} & f_{22} \end{bmatrix} \tag{10.09}$$

where $\hat{f}$ is given by

$$\hat{f} = \frac{f_{12} + f_{21}}{2}$$

The modified flexibility matrix $\hat{\mathbf{F}}$ is used to generate a symmetric stiffness matrix $\hat{\mathbf{K}}$ (2x2) in the element local coordinates as shown in Fig. 10.02. This stiffness matrix is transformed to global coordinates, Fig. 10.02, and then assembled into structure stiffness matrix. This results in a reasonable estimate of the tangent stiffness of the structure; which is usually sufficient for the advancing phase of a nonlinear analysis. However, for the correcting phase the exact original matrices $\mathbf{F}$ and $\mathbf{K}$ are used.

10.3. STATE DETERMINATION PROCEDURE

Consider a cable with an unstrained length of L_o, modulus of elasticity E, area of cross section A and a uniform load w applied along the arc length of the cable; Fig. 10.03.

Assume that the initial state of a cable, which is completely defined by the following information, is known;

- Position of the end points of the cable defined by span l' and rise h'.
- Support reactions H' and V'.

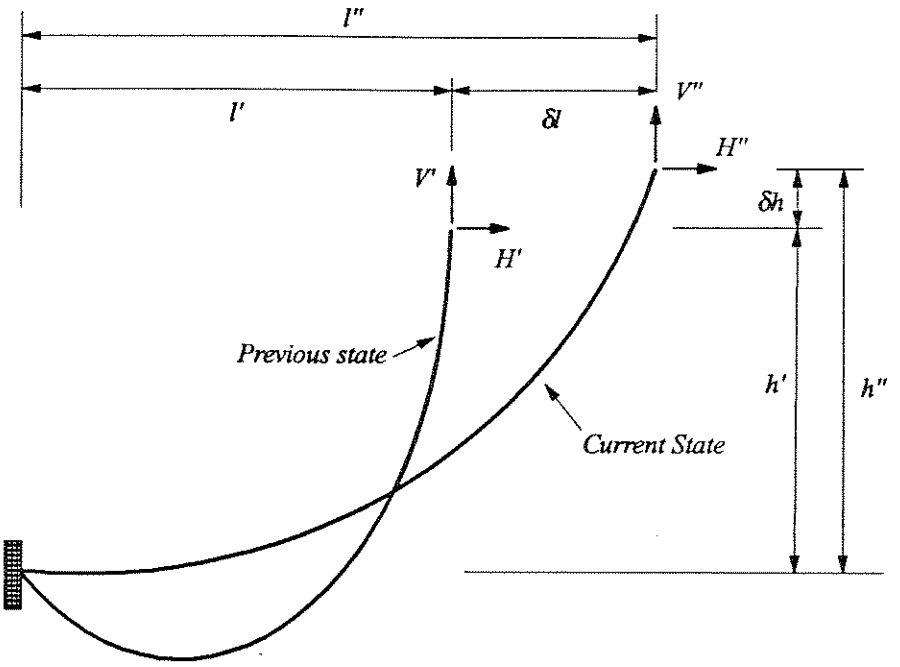

FIG. 10.03 STATE DETERMINATION PROCESS
CATENARY PROFILE IN THE PREVIOUS AND CURRENT STATE.

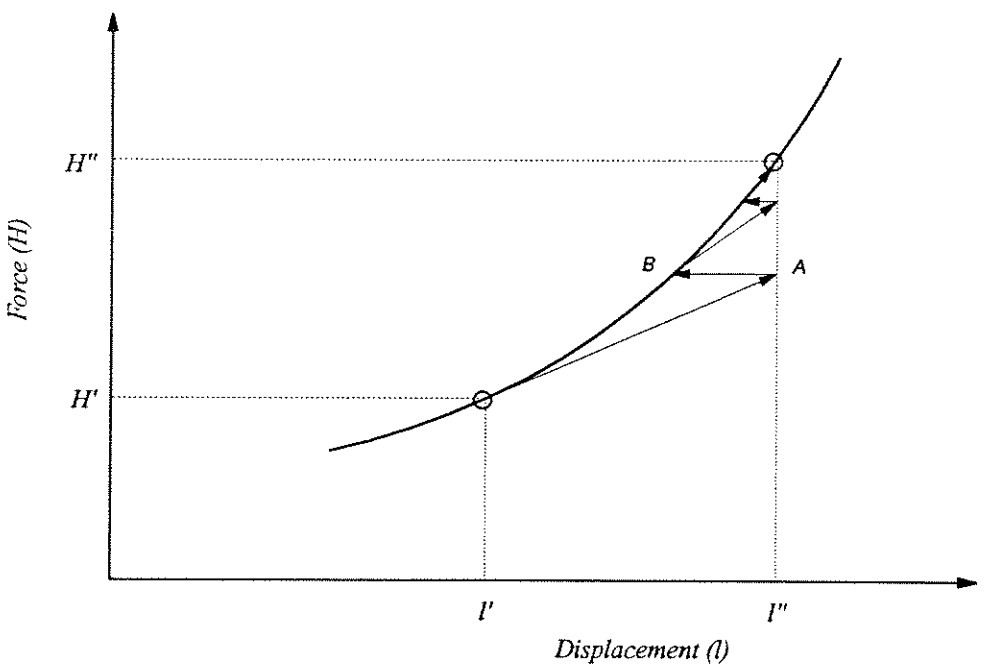

FIG. 10.04 STATE DETERMINATION PROCESS
FOR A GIVEN DISPLACEMENT INCREMENT.

Given the displacement increment $\delta \mathbf{v}$

$$\delta \mathbf{v} = \begin{bmatrix} \delta l \\ \delta h \end{bmatrix}$$

It is required to find the new state of the cable.

The new rise and span of the cable in the displaced state is given by:

$$\begin{bmatrix} l'' \\ h'' \end{bmatrix} = \begin{bmatrix} l' \\ h' \end{bmatrix} + \begin{bmatrix} dl \\ dh \end{bmatrix} \tag{10.10}$$

It is now required to find H'' and V''. Consider equations Eq. 8.22 and Eq. 8.23.

$$l = \frac{HL_o}{EA} + \frac{HL_o}{W}\left[\sinh^{-1}\left(\frac{V}{H}\right) - \sinh^{-1}\left(\frac{V-W}{H}\right)\right]$$

$$h = \frac{WL_o}{EA}\left(\frac{V}{W} - \frac{1}{2}\right) + \frac{HL_o}{W}\left[\sqrt{1+\left(\frac{V}{H}\right)^2} - \sqrt{1+\left(\frac{V-W}{H}\right)^2}\right]$$

These equations are implicit in the variables H and V and therefore it is not possible to find H'' and V'' directly. A two dimensional Newton's method for non linear systems as described by Burden and Faires [18] is employed for this purpose.

Equations Eq. 8.22 and Eq. 8.23 can be expressed as

$$\begin{bmatrix} f(H,V) - l \\ g(H,V) - h \end{bmatrix} = \begin{bmatrix} 0 \\ 0 \end{bmatrix}$$

$$\mathbf{P(S)} = \mathbf{0} \tag{10.11}$$

The iteration procedure is given by

$$\mathbf{S}_k = \mathbf{S}_{k-1} - \mathbf{F}_{k-1}^{-1}\ \mathbf{P}(\mathbf{S}_{k-1})$$

$$\begin{bmatrix} H \\ V \end{bmatrix}_k = \begin{bmatrix} H \\ V \end{bmatrix}_{k-1} - \begin{bmatrix} f_{11} & f_{12} \\ f_{21} & f_{22} \end{bmatrix}_{k-1}^{-1} \left\{ \begin{bmatrix} f(H,V) \\ g(H,V) \end{bmatrix}_{k-1} - \begin{bmatrix} l'' \\ h'' \end{bmatrix} \right\} \tag{10.12}$$

A graphical interpretation of this procedure is shown in Fig. 10.04. This method is generally expected to give quadratic convergence, provided that sufficiently accurate starting values are known. Iteration is stopped when the following criteria is satisfied:

$$\left\| \begin{matrix} H_k - H_{k-1} \\ V_k - V_{k-1} \end{matrix} \right\| \leq \varepsilon \tag{10.13}$$

where ε is a suitably selected tolerance. When starting a fresh analysis, it is recommended that the following may be used as stable start off values:

$$\begin{bmatrix} H \\ V \end{bmatrix}_0 = \begin{bmatrix} 1.\times 10^{-5} \\ .5 \times W \end{bmatrix} \tag{10.14}$$

A step by step algorithm, suitable for implementation in a computer program is described in the next section.

10.3.1. ALGORITHM FOR TWO DIMENSIONAL NEWTON'S METHOD

INPUT

- Unstrained length of the catenary L_o, modulus of elasticity E, area of cross section A, uniform load applied along arc length of the cable w and the state of the cable in reference state (l', h', H', V').
- Span l'' and rise h'' of the cable in the displaced state.
- Initial estimate of the cable end actions H_0 and V_0.
- Maximum number of iterations N.
- Solution tolerance ε

OUTPUT

- Approximate values of the cable end actions in the displaced state H'' and V''.

PROCEDURE

1. Set $k = 1$
2. While $k \leq N$ do steps 3 to 5
   3. Evaluate fresh estimate of cable end action

$$\begin{bmatrix} H \\ V \end{bmatrix}_k = \begin{bmatrix} H \\ V \end{bmatrix}_{k-1} - \begin{bmatrix} f_{11} & f_{12} \\ f_{21} & f_{22} \end{bmatrix}_{k-1}^{-1} \left\{ \begin{bmatrix} f(H,V) \\ g(H,V) \end{bmatrix}_{k-1} - \begin{bmatrix} l'' \\ h'' \end{bmatrix} \right\}$$

   4. Check if solution has converged.

$$\left\| \begin{matrix} H_k - H_{k-1} \\ V_k - V_{k-1} \end{matrix} \right\| \leq \varepsilon$$

   If solution has converged then output $\begin{bmatrix} H_k \\ V_k \end{bmatrix}$; procedure successful; stop.

   5. Set $k = k + 1$
6. Maximum number of iterations exceeded; procedure failed; stop.

10.4. ANALYSIS EXAMPLES

A series of numerical examples are presented to verify the proposed method of analysis and to establish the accuracy of the proposed catenary element.

The numerical examples were solved using the computer program CALBRG, which was developed as a part of the present study. Details about the structure and organization of the catenary element module are discussed in Chapter 11.

10.4.1. CATENARY SUBJECTED TO LARGE DISPLACEMENTS

This example has been adapted from a paper by Peyrot and Goulois [101]. Consider an elastic cable of unstrained length $L_o = 100$, area of cross section $A = 1.0$, modulus of elasticity $E = 29000$ and having a weight per unit length $w = 1.0$. The problem being addressed is that given the position coordinates of the two ends of the cable, find the cable

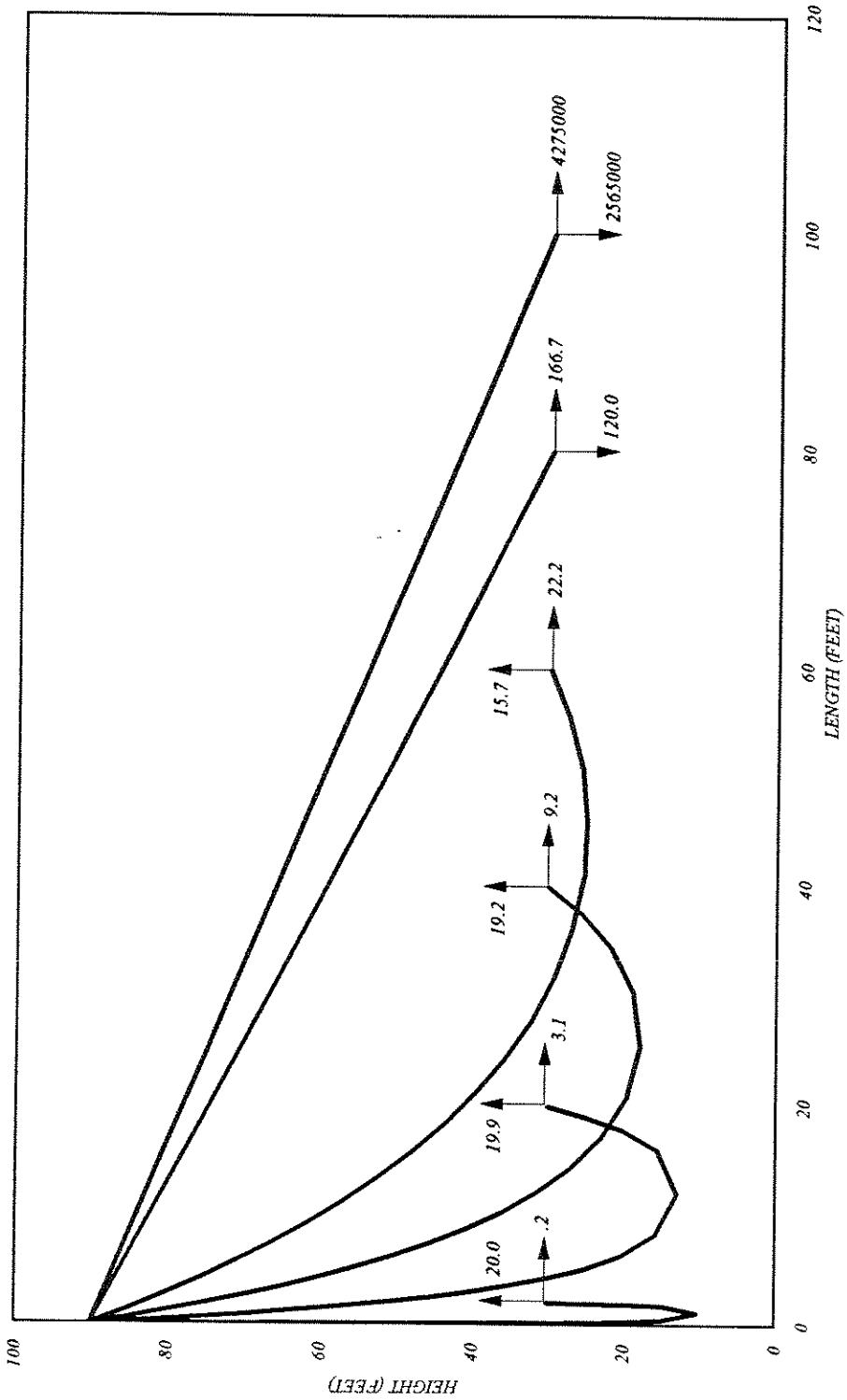

FIG. 10.05 CABLE PROFILE AND CORRESPONDING END FORCES.
EXAMPLE 10.4.1

profile and end reactions. For this particular example it is assumed that the left end I of the cable is fixed at coordinates (0,90), the right end J maintains a constant vertical elevation of 30 and is subjected to controlled horizontal displacement increments of 20 units each until it reaches the coordinates (100,30).

The entire cable is modeled as one catenary element and a displacement controlled solution strategy is employed. The resulting cable profiles are generated by the computer program; this is done by evaluating the position coordinates at each of 20 points along the cable length. The corresponding end reactions, which hold the cable in equilibrium are also shown in Fig. 10.05.

The results obtained by the author and Peyrot and Goulois [101] are given in the following table.

End Displacement.	Present Study		Peyrot and Goulois	
	H	V	H	V
0			0	20
2	.2	20		
20	3.1	19.9	3.1	19.9
40	9.2	19.2	9.2	19.2
60	22.2	15.7	22.2	15.7
80	166.7	-120	504	-328.8
100	4275000	2565000	4170000	-2511000

The results compare quite well except for the discrepancy at the end displacement of 80. Note that at this displacement the cable is just beginning to straighten out and the contribution of elastic stretch begins to increase and if the force tolerances to the nonlinear solution are not carefully chosen then substantial errors can appear in the solution.

This example illustrates that any conceivable shape of the catenary starting from the point when the right end of the cable is directly below the left support to the point where the cable is stretched taut can be easily handled by this algorithm.

10.4.2. LARGE DISPLACEMENT ANALYSIS OF A 3-D CABLE NET.

Fig. 10.06 shows the plan view of a cable net consisting of three cables with relatively large sags connected at node 2. The side elevation is shown in Fig. 10.07.

Cable No.	Node I	Node J	Length	A	w	E
1	1	2	580	1	1	29000
2	3	2	510	1	2	29000
3	4	2	510	1	2	29000

The cables are fixed at nodes 1, 3 and 4; whereas node 2 is free to move in the horizontal plane (X-Z plane) thereby resulting in a two degree of freedom structure. A load of 1000 units parallel to the Z axis is applied at node 2. A similar problem albeit with a vertical spring at node 2 was attempted by Peyrot and Goulois [101]. Cable data used in the present analysis is reproduced in the table below.

The structure is analyzed for two different load cases. In the first case it is required to find the cable geometry in space when node 2 is fixed against translation in X, Y, and Z directions and the cable net is subjected to its self weight only. This was accomplished by subjecting node 2 to a very small controlled displacement in the X direction. The resulting profile is shown in Fig. 10.06 and 10.07 by a solid line. A three dimensional view is shown in Fig. 10.08. The cable end actions at node 2 are shown in the following table.

Cable No.	Fxi	Fyi	Fzi	Fxj	Fyj	Fzj
1	-354.4	-101.1	0	354.4	681.1	0
2	1039	510	-778.9	-1039	510	778.9
3	1039	510	778.9	-1039	510	-778.9

Note that because of symmetry $\sum Fz = 0$ at node 2 and that each element individually satisfies equilibrium.

In the second case it is required to find the displaced shape of the cable net when node 2 is free to displace in the X-Y plane and a load of 1000 units, parallel to Y axis, is applied. This

FIG. 10.06 CABLE NET; PLAN VIEW.
EXAMPLE 10.4.2

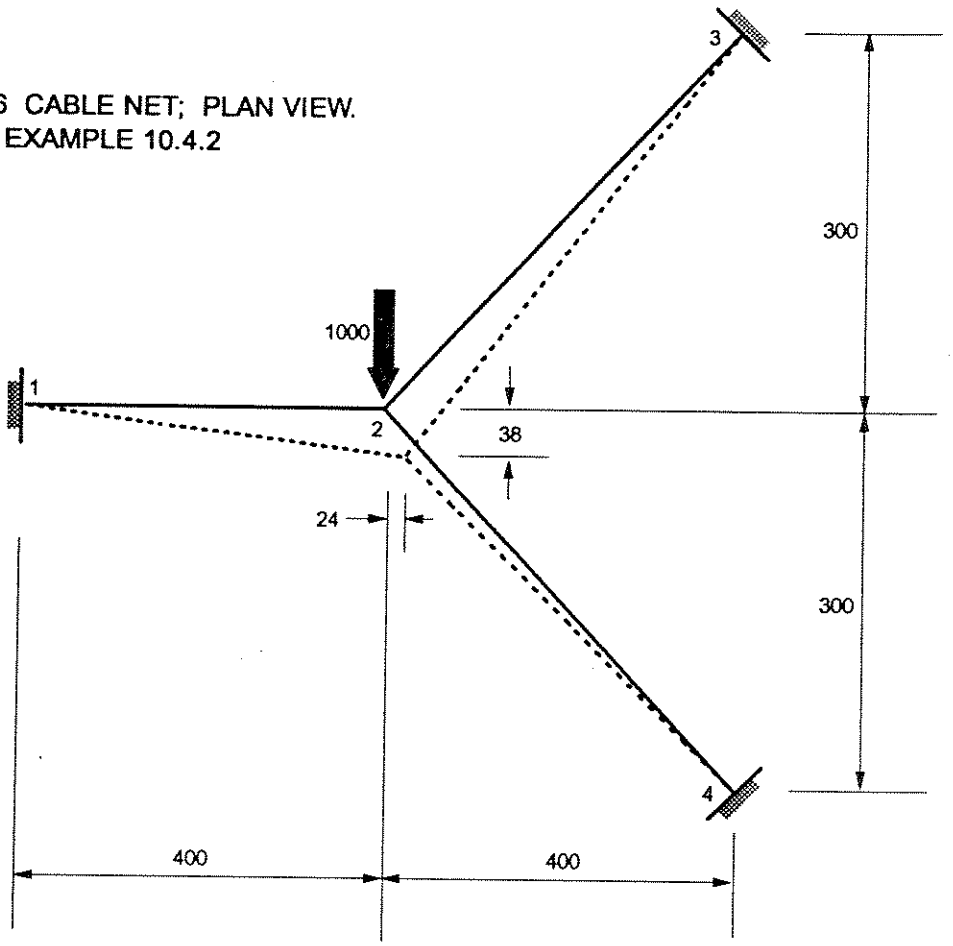

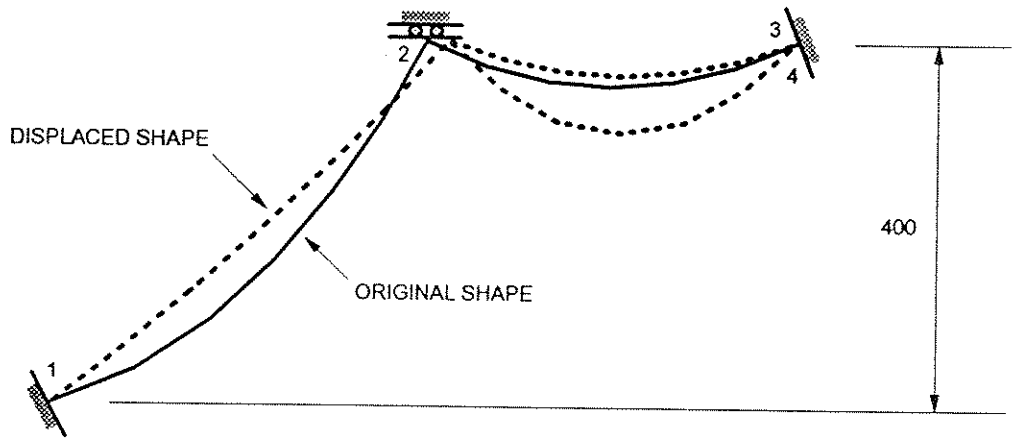

FIG. 10.07 CABLE NET; SIDE VIEW.
EXAMPLE 10.4.2

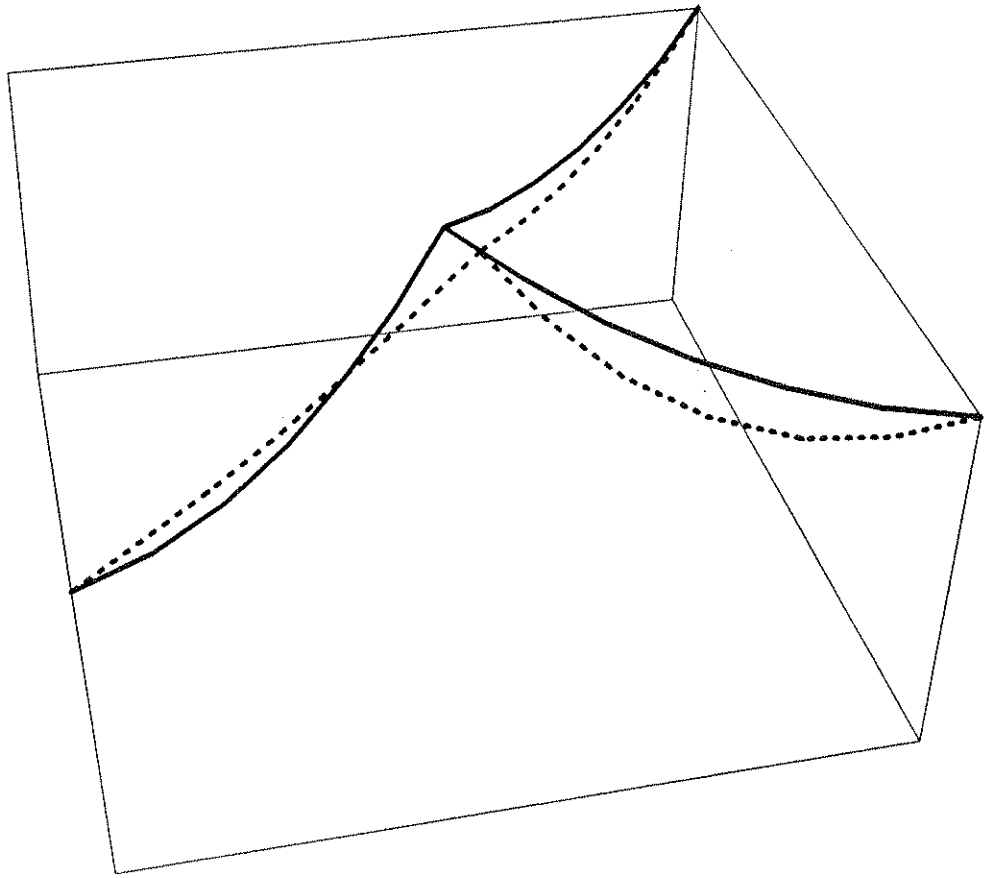

FIG. 10.8 THREE DIMENSIONAL VIEW OF THE CABLE NET; ORIGINAL AND DEFORMED GEOMETRY. EXAMPLE 10.4.2

shape of the displaced cable net is shown by the dotted line in Fig. 10.06, 10.07 and 10.08. Node 2 is displaced 38 units in the Z direction and 24 units in the X direction. Note the accompanied changes in the cable shape, the sag decreases in cables 2 and 3, and increases in cable 3. Cable end actions are shown in the table below.

Cable No.	Fxi	Fyi	Fzi	Fxj	Fyj	Fzj
1	-1748	-1367	158.5	1748	1947	-158.5
2	458.2	510	-318.6	-458.2	510	318.6
3	1289	510	1160	-1289	510	-1160

Note that $\sum Fz \approx 0$ and $\sum Fy \approx 0$ at node 2 and each element satisfies equilibrium within prescribed error tolerances.

10.4.3. CONSTRUCTION SEQUENCE OF A SUSPENSION BRIDGE

The following analyses of a catenary, which is similar to the central cable of the Golden Gate bridge, are based on the data given below, which was partly extracted from a report by Baron and Arikan, [8].

- Length of main span = 4200 feet
- No. of main cables = 2
- Cable sag = 472 feet
- Cable diameter = 3 feet
- Modulus of elasticity of cable steel = 3600000 kips/ft^2
- Total road width=60 feet
- Dead load center span = 22.8 kips/ft.

It was assumed that the dead load of the center span included the self weight of the cables; which at 7.1 kips/ft for the two cables is substantial. Note that the unstretched length of the catenary is not known. A series of analyses was carried out, employing the catenary element proposed in the present study.

1. The unstrained length of the catenary is not known; however the sag of the cable under full dead load is given. An iterative analysis was carried out and the unstrained length which would result in sag of 472 feet under full dead load was found to be 4329 feet. The consequent cable profile is shown in Fig. 10.09
2. Imposed dead load was removed and the cable was allowed to hang freely under its own self weight, Fig. 10.09.
3. The cable was subjected to a full dead load and a live load of 6 kips/ft; the live load was based on the assumption that 40 persons stand on each one foot length of the bridge and that each person weighs an average of 150 pounds.
4. Evaluate the dead load which will cause the cable to reach its yield stress of 160 ksi.

The results obtained are summarized in the following table. Note that the total load given in the table below is applied as uniformly distributed load along the length of a ***single*** cable.

Case	Total Load kips	Sag feet	Max. Stress ksi	Elastic Stretch feet
1	48000	472	57	9.3
2	15400	461	18	3.0
3	60500	476	72	11.6
4	269500	500	160	25.9

In the next set of analyses, the capability of the program CALBRG to perform construction sequence analysis was put to test. During the actual construction of the bridge deck segments were added starting from the towers and moved towards the mid span. However, it is of interest to examine the possibility of connecting the deck segments to the cable starting from the mid span and working towards the tower. In this example both the real and the hypothetical case are analyzed and the geometric shape of the cable is tracked as the construction proceeds.

For sake of simplicity, it was assumed that the total number of hanger cables is 11. The cable is first loaded to simulate the construction sequence from the tower to mid span. Fig. 10.10 shows a plot of the mid span sag versus the construction sequence. Note that at the start of the sequence the value of the mid span sag is 461 feet, as more segments are added the sag decreases to about 420 feet, with the addition of more segments close to mid span the sag begins to increase and finally at closure has a value of 472 feet.

In the second case, shown in Fig. 10.11 , the cable is loaded to simulate the construction sequence starting from the mid span and proceeding simultaneously towards both towers. Note that the sag first increases to about 498 feet and later decreases to its final value of 472 feet.

Note that despite the difference in the construction sequence, both solutions end up with the same final cable profile.

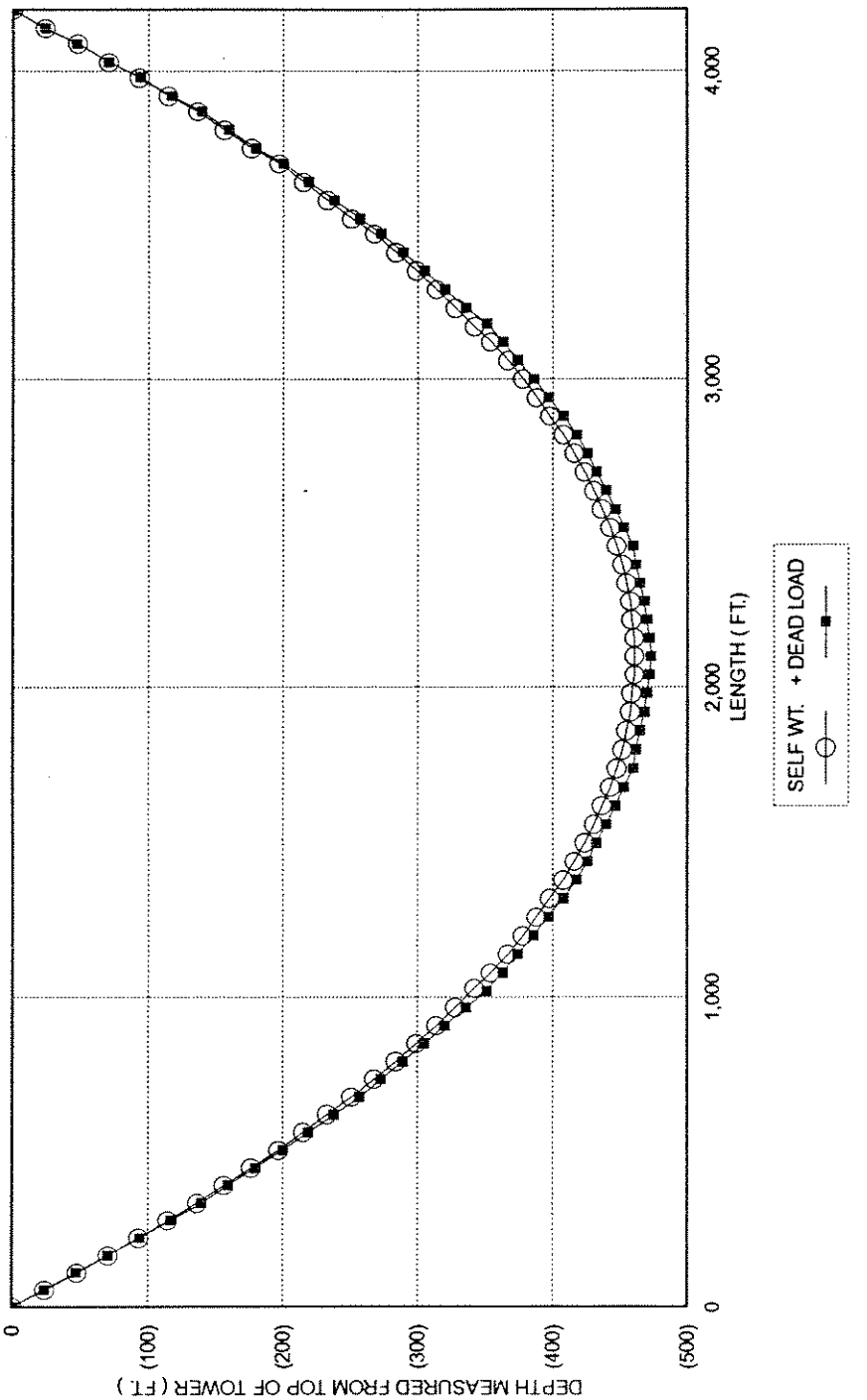

FIG. 10.09 GOLDEN GATE BRIDGE; CENTER SPAN
CABLE PROFILE UNDER SELF WEIGHT AND ADDED DEAD LOAD.
EXAMPLE 10.4.3

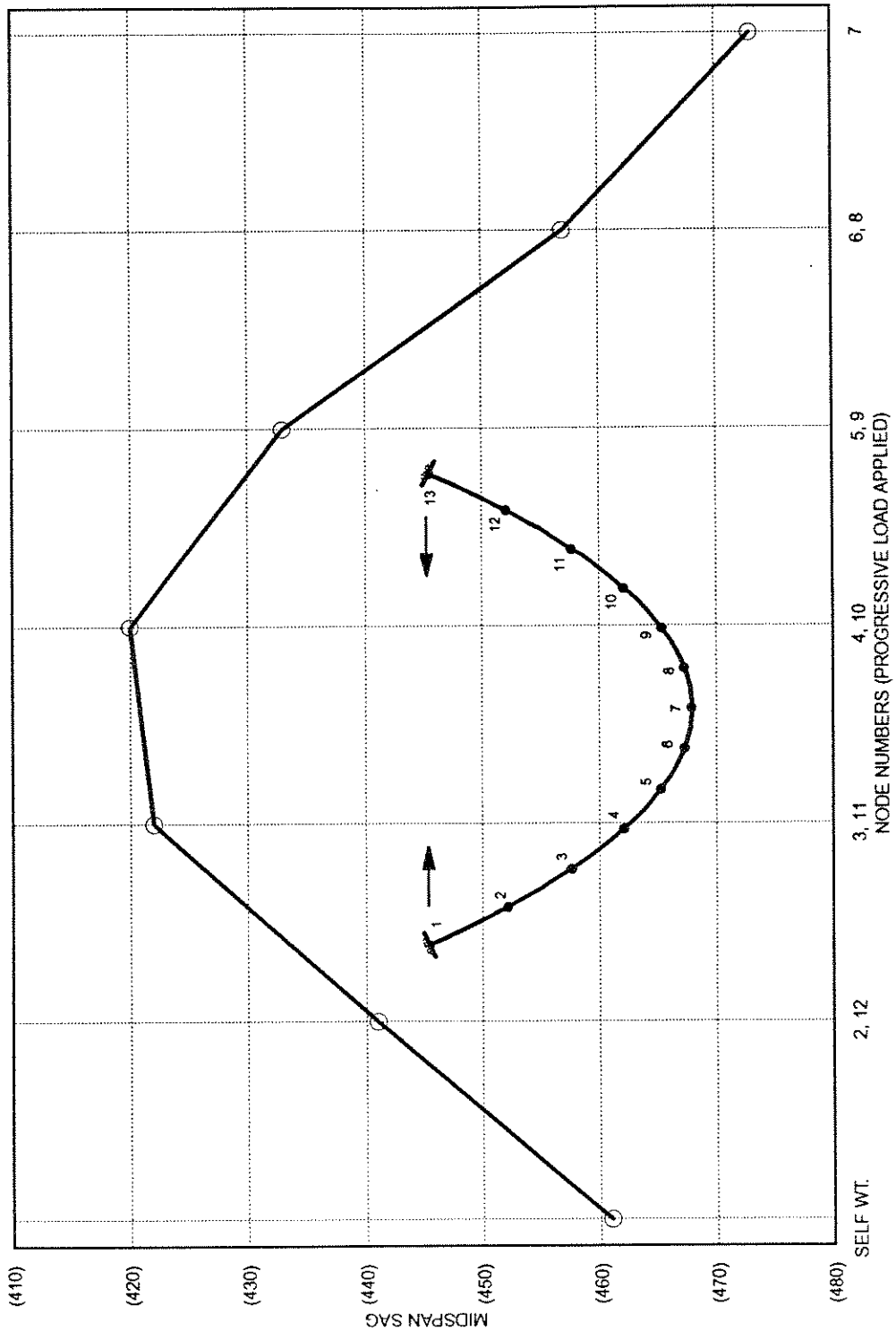

FIG. 10.10 GOLDEN GATE BRIDGE; CENTER SPAN
VARIATION IN MIDSPAN SAG AS CONSTRUCTION PROCEEDS FROM TOWERS TO MIDSPAN.
EXAMPLE 10.4.3

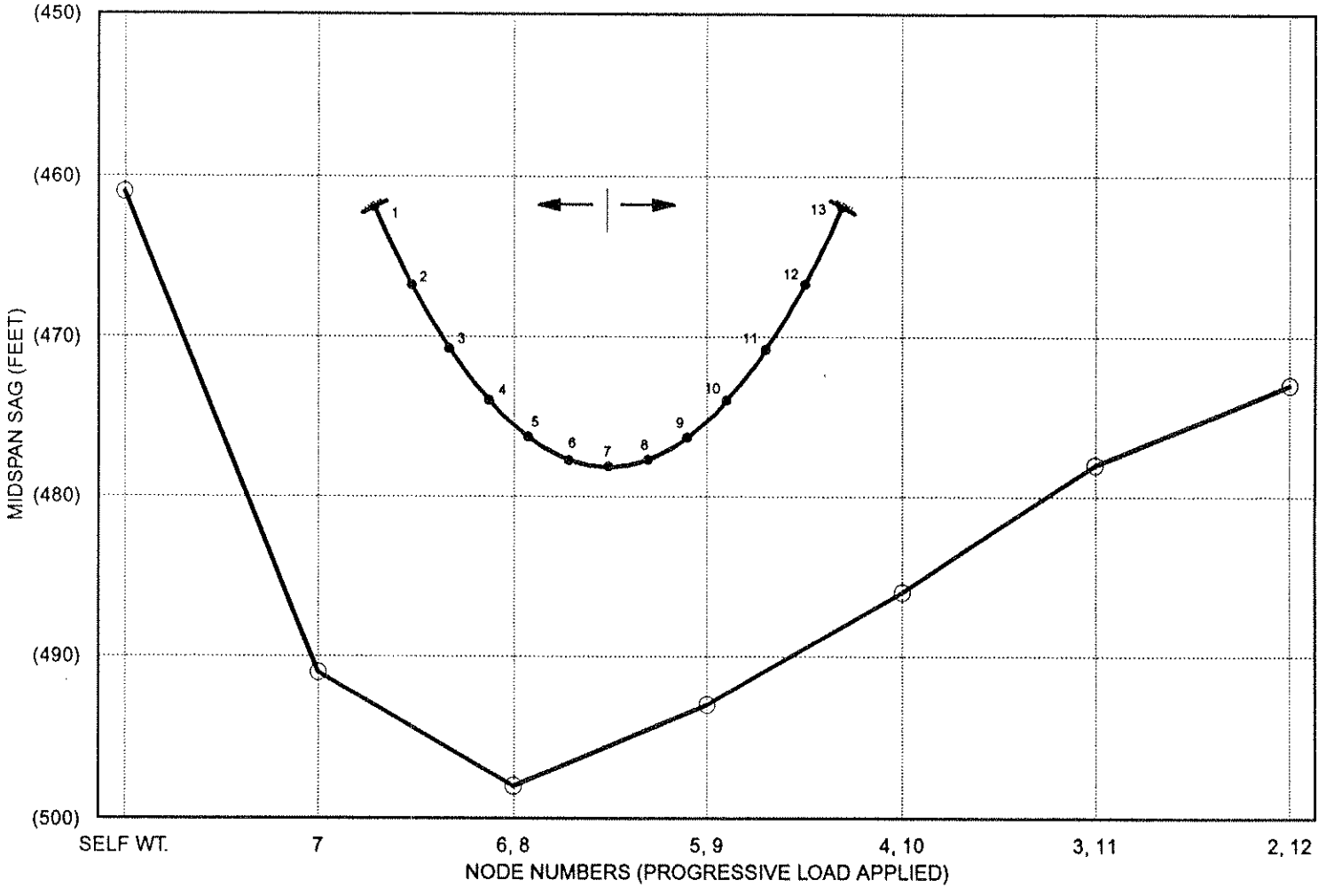

FIG. 10.11 GOLDEN GATE BRIDGE; CENTER SPAN
VARIATION IN MIDPSPAN SAG AS CONSTRUCTION PROCEEDS FROM MIDSPAN TO TOWERS.
EXAMPLE 10.4.3

10.4.4. LARGE DISPLACEMENT ANALYSIS OF A CATENARY

Two sets of analyses were carried out. In the first case, shown in Fig. 10.12, a cable structure consisting of two catenary elements was analyzed. Supports at A and C are fixed, the support at B is subjected to controlled vertical displacement increments. It is required to find the cable profiles at each step. Pertinent data for the two cables is given below:

Cable AB	*Chord length* $= 200$	$L_0 = 202$	$A = 1$	$w = 1$	$E = 29000$
Cable BC	*Chord length* $= 200$	$L_0 = 202$	$A = 1$	$w = 1$	$E = 29000$

Point B was then subjected to a controlled displacement increments of 8 units and the cable shape was generated at each step. Fig. 10.12 shows various cable profiles from ABC to AHC. Note that the solution procedure can successfully track the cable shape for both large (ABC) and small sag (AHC).

In the second case point B was set at the quarter span position and the cable data was set to the following values:

Cable AB	*Chord length* $= 100$	$L_0 = 101$	$A = 1$	$w = 1$	$E = 29000$
Cable BC	*Chord length* $= 300$	$L_0 = 303$	$A = 1$	$w = 1$	$E = 29000$

Point B was again subjected to controlled vertical displacement increments of 8 units each until the total displacement reached 40 units. The cable shape generated at each step is shown in Fig. 10.13. Note that only the vertical displacement of point B is controlled and it is free to translate horizontally; this is done to simulate a vertical external nodal load at point B. Also, note that as the cable sag decreases, point B tends to displace horizontally towards the near support A.

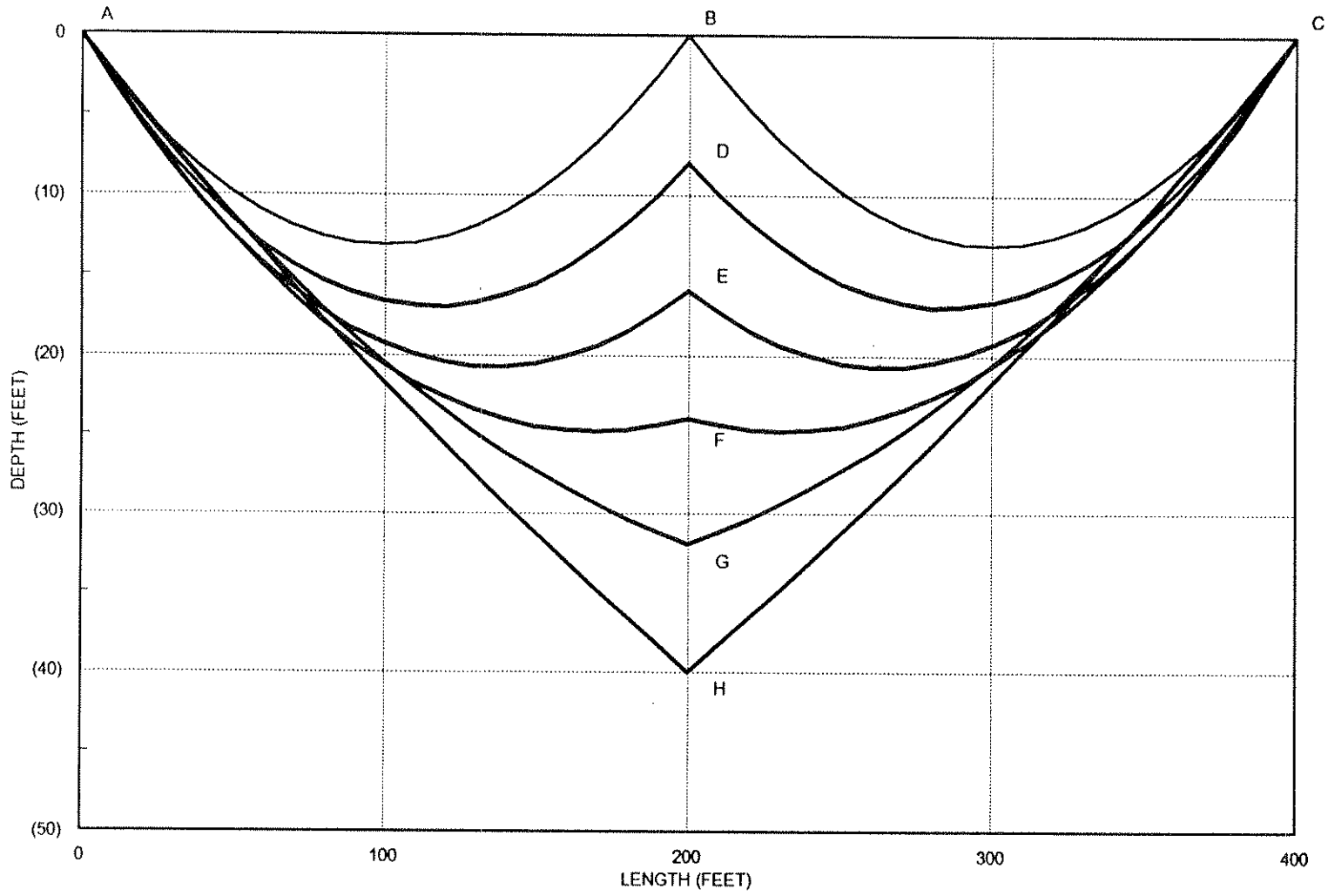

FIG. 10.12 CABLE PROFILE AS THE MIDSPAN SUPPORT IS SUBJECTED TO CONTROLLED VERTICAL DISPLACEMENTS. EXAMPLE 10.4.4

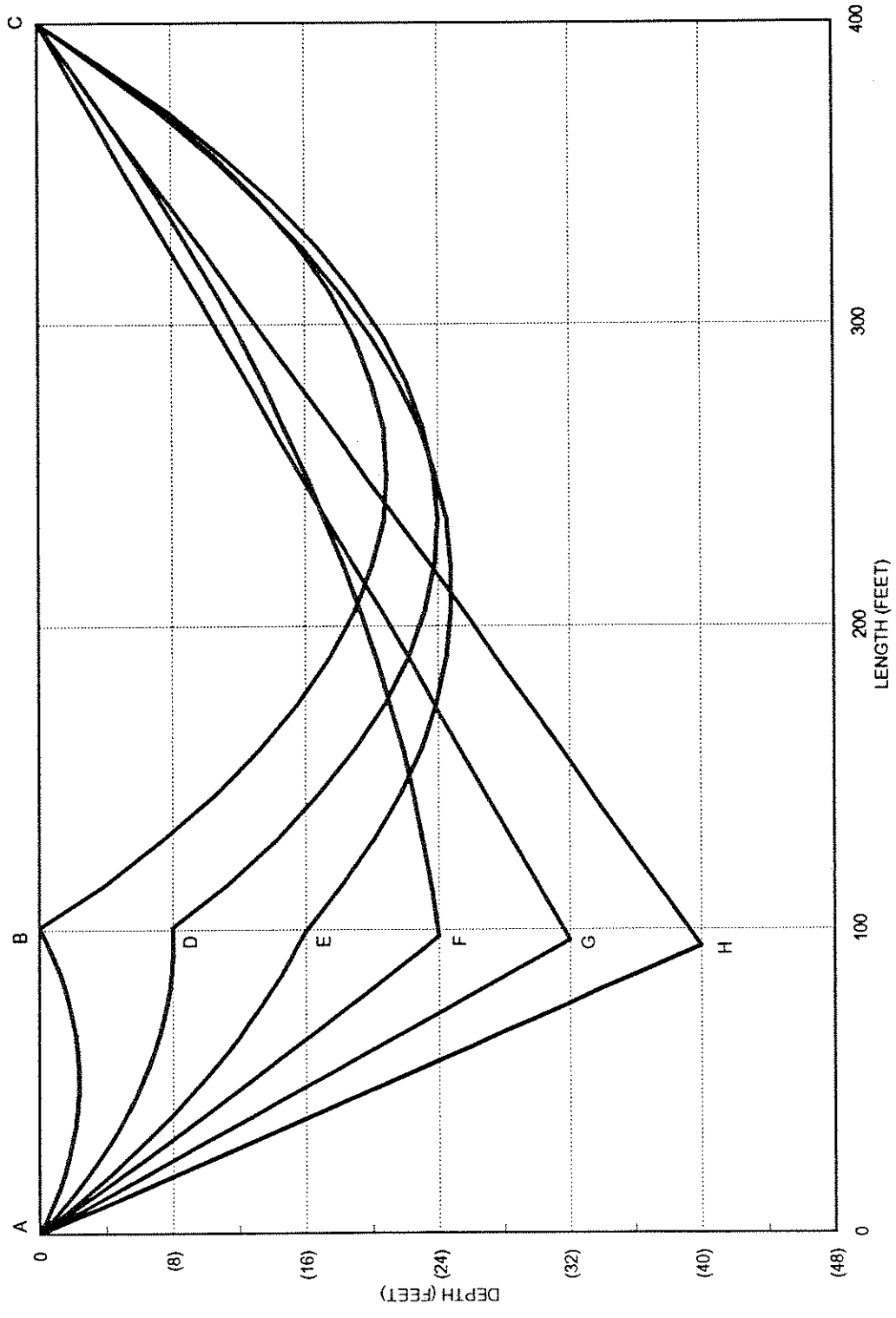

FIG. 10.13 CABLE PROFILE AS THE QUARTER SPAN SUPPORT IS SUBJECTED TO CONTROLLED VERTICAL DISPLACEMNETS.
EXAMPLE 10.4.4

10.4.5. ANALYSIS OF AN CABLE NET LAID OUT ON AN ORTHOGONAL GRID

Consider the cable net shown in Fig. 10.14. Given the initial position of the nodal points, unstrained lengths and the elastic properties of the individual cables, it is required to find the following:

1. The shape of the cable net under self weight.
2. The shape and the cable net when a load of 1000 units is applied to node 8.

It is assumed that initially all of the nodal points lie in the horizontal plane on a 40x40 grid. The cables are orthogonal to each other and all of them have the following common properties.

$$A = 1.0 \qquad w = 1.0 \qquad E = 29000 \qquad L_0 = 40$$

As shown in Fig. 10.14 nodes 1, 2, 3, 6, 7, 10, 11 and 12 are fixed whereas nodes 4, 5, 8 and 9 each have three translational degrees of freedom.

In the first analysis no external nodal load is applied and the cable net is allowed to take its natural shape in space under the action of its self weight. The resulting shape is shown by solid lines in a three dimensional plot in Fig. 10.15.

In the second analysis a load of 1000 units is applied to node 8. The shape of the cable net is changed dramatically; the resulting displacements are shown in the table below and in Fig. 10.15.

Node No.	Displacement (self weight)			Displacements (load at node 8)		
	X	Y	Z	X	Y	Z
4	-.007	-1.330	-.007	-.014	-1.631	.030
5	.007	-1.330	-.007	.004	-1.358	-.004
8	-.007	-1.330	.007	-.063	-3.175	.063
9	.007	-1.330	.007	-.030	-1.631	.014

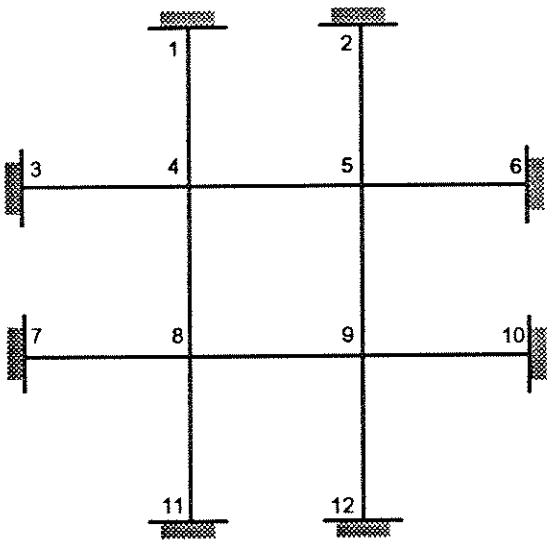

FIG. 10.14 PLAN OF CABLE NET (20 x 20 GRID); EXAMPLE 10.4.5

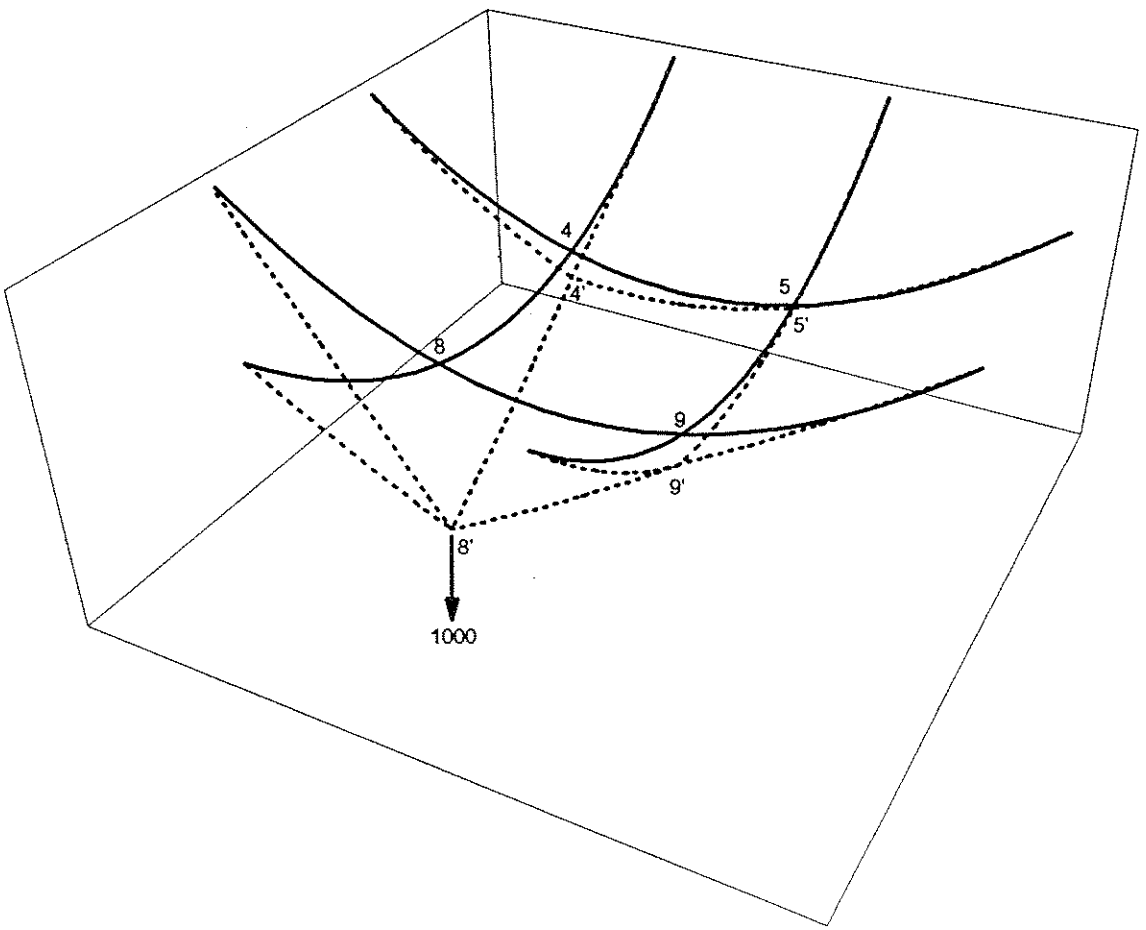

FIG. 10.15 THREE DIMENSIONAL VIEW OF CABLE NET.
EXAMPLE 10.4.5

11. THE COMPUTER PROGRAM "CALBRG"

11.1. GENERAL

The present study is the latest development in a long term research project on the nonlinear analysis of bridges conducted under the supervision of Prof. A. C. Scordelis at the University of California, Berkeley. A summary of this research is presented in several research publications by Scordelis [115, 116, 117].

Several computer programs were written in the course of the above mentioned research program. A brief summary of the more significant computer programs developed since 1977 is presented:

PCFRAME (KANG, 1977) [49]

This program provides an efficient numerical procedure for the material and geometric nonlinear analysis of planar reinforced and prestressed concrete frames including the time dependent effects due to load history, temperature history, creep, shrinkage and aging of concrete and relaxation of prestressing tendons. The analysis is capable of predicting the response of these structures through the elastic, cracking, inelastic and ultimate ranges at any given point in time. One dimensional frame elements, consisting of concrete and steel layers and linearized prestressing tendon segments, and having three degrees of displacement freedom at each node are used.

SEGAN (VAN ZYL, 1978) [141]

This program is capable of a linear elastic analysis of curved, segmentally erected, prestressed concrete box girder bridges. Time dependent effects such as creep and shrinkage, as well as environmental effects such as temperature and humidity, are accounted for. The deflection and stresses can be computed at any stage during construction or service life of the bridge. A skew ended finite element with eight degrees of freedom at each of its end nodes is used. Operations used in segmental construction, such as addition of segments, prestressing, changing of support conditions, application or removal of construction loads and prescribed displacements can be analyzed.

NOPARC (VAN GREUNEN, 1979) [140]

This program permits nonlinear material and geometric, time dependent analysis of reinforced and prestressed concrete slabs and panels of arbitrary boundary shape. Two dimensional flat triangular elements possessing both in plane membrane and bending stiffness are used; thickness is divided into a discrete number of concrete and reinforcing steel layers. External boundary spring elements can also be used. At each time step external gravity, surface and joint loads as well as temperature and shrinkage increments can be specified, thereby allowing for the analysis of slabs through various stages of service and ultimate load ranges.

NASHL (CHAN, 1982) [19]

This program was developed to trace the structural response of reinforced concrete shells with edge beams. Non-linearity as a result of tensile cracking, nonlinear behavior of concrete in compression, yielding of steel reinforcement, geometric non-linearity as a result of finite displacements; and the time dependent effects of creep and shrinkage are included in the analysis.

PCF3D (MARI, 1984) [80]

This program is capable of nonlinear material and geometric, time dependent analysis of three dimensional reinforced and prestressed frames. One dimensional finite elements having six degrees of displacement freedom at each end are used; the cross section is discretized into a finite number of concrete and steel filaments. The prestressing tendons are idealized by a series of straight line segments; prestressing losses such as friction, anchor slip and relaxation are accounted for internally in the program. This program may be thought of as a three dimensional version of PCFRAME.

SFRAME (KETCHUM, 1986) [53]

SFRAME permits a linear elastic, time dependent analysis of segmentally erected reinforced and prestressed concrete planar frames. One dimensional finite elements having three degrees of freedom at each end are used. Changes in structural configuration or loading can be incorporated in the analysis at any point in time. These include restraining and releasing boundary conditions, installing and removing frame elements, prestressing tendons and traveling form work. An improved creep model, based on refined integration over time is used. In addition, SFRAME uses improved programming techniques, such as an in-core database manager, user friendly free field input and improved portability, etc.

NAPBOX (CHOUDHURY, 1986) [20]

NAPBOX is capable of nonlinear material analysis of curved non-prismatic reinforced and prestressed concrete box girder bridges. Thin-walled beam theory and the finite element method are combined to develop a curved non-prismatic thin-walled box beam element. The cross section of the element is a rectangular single cell box with side cantilevers and the axis of the element is curved in plan. The macro element has three nodes along the longitudinal

axis; each node has eight displacement degrees of freedom, including transverse distortion and longitudinal warping of the cross section.

SPCFRAME (KANG, 1989) [50]

This has been developed by importing the nonlinear analysis capabilities of PCFRAME into the segmental analysis environment of SFRAME.

SPCF3D (KASTI, 1990) [51]

This program traces the nonlinear material and time dependent response of segmentally erected prestressed concrete composite three dimensional frame structures. It combines and augments the capabilities of two previous programs, SFRAME by Ketchum [53] and PCF3D by Mari [80]. The structural element used in the program has a cross section that is discretized into filaments and allows for composite segmental erection across its depth.

11.2. PRESENT STUDY; THE COMPUTER PROGRAM CALBRG

The program CALBRG is designed for the nonlinear material and geometric, time dependent analysis of segmentally erected, three dimensional cable stayed bridges. The program may be utilized for either reinforced and prestressed concrete or steel cable-stayed bridges. However the program is not limited to just cable stayed bridges; the element library is such that it may be used to analyze suspension bridges as well as segmentally erected box girder bridges.

The program is capable of tracing the response of the structure through various construction stages, including the time dependent effects of creep and shrinkage of concrete and relaxation of prestressing tendons. Creep integration schemes developed by Kabir [48] and Ketchum [53] are incorporated.

A number of segmental operations necessary for modeling construction operations involved in building a cable-stayed bridge are implemented in the program. The program can predict the forces and deformations in the structure induced by changes in structure configuration such as adding or removing deck or tower segments, installing and stressing of prestressing tendons having an arbitrary profile, installing and moving form travelers, installing, stressing, re-stressing or removing of cable-stays. Also boundary restraints may be added or released at any point in time

In addition the state of the structure can be predicted through various limit states as the concrete cracks, moves through the inelastic range to maximum compressive strength and through the strain softening range.

A nonlinear material constitutive relation is used for concrete and is based on the Kent-Park model [52] improved by Scott et al. [122]. Tension stiffening, based on formulation given by Vecchio and Collins [142] may also be included in the analysis. For steel, a bilinear strain hardening model is used; this model can capture unloading and reloading to the strain hardening branch and also approximates Bauschinger's effect.

Two different nonlinear solution strategies are available:

- Load Control Strategy.
- Displacement Control Strategy developed by Powell and Simons [107].

By adjusting the force tolerances the analyst has the option to choose a tangent or a constant stiffness iteration. In addition, the analyst has the option to use a path dependent or independent state determination scheme.

The equilibrium equations are solved by an efficient in-core solver based on the active column method developed by Wilson et al. [147], wherein only the non zero above diagonal terms of the stiffness matrix are stored in a compact one dimensional array along with an integer pointer array indicating each diagonal term.

11.3. STRUCTURE AND ORGANIZATION OF PROGRAM

The program was developed on an IBM PC compatible machine running an Intel 486 33 MHz processor. The program code is written using Microsoft FORTRAN version 5.1; this particular compiler was used because of its powerful debugging tools and the ability to generate executable files that can run under either DOS or OS/2 operating systems.

The present version of CALBRG is designed to operate under OS/2.1. This is primarily due to the fact that OS/2 allows a flat memory model, permits multi tasking, and in general, has better data handling capabilities.

The program is highly structured and organized into separate modules. The basic modules and their interaction is illustrated in a flow chart, Fig. 11.01. A brief description of the structure of each module and its functions is given in the following paragraphs:

CONTROL

The control module reads and interprets the input file. It directs the flow of the program through various modules.

CALSAP

The program CALBRG uses the CALSAP system, which is a set of utility subroutines developed by Wilson and Hoit [148], for several purposes which include:

- Input.
- In-core data Management.
- Out of core data Management.

The input routines are used to create a user friendly free format interface. All input takes the form of commands consisting of plain English keywords. These commands activate various

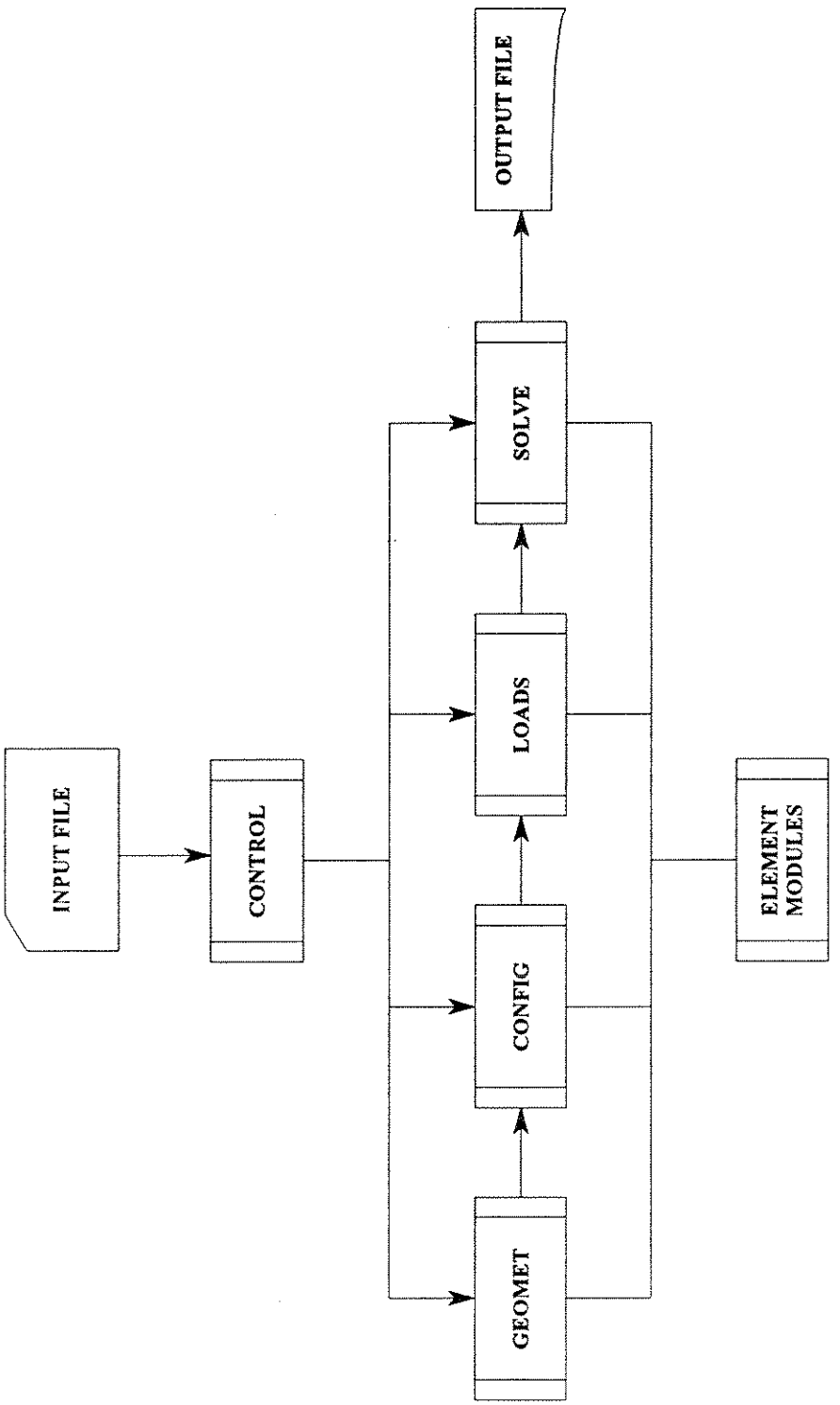

FIG. 11.01 ORGANIZATION OF THE MAIN MODULES IN CALBRG

modules of the program. The input data following a command is not formatted but simply separated by commas or blank spaces.

The in-core data base management routines implement a dynamic storage scheme, wherein a single array is partitioned to store all other data arrays. Each array is dynamically dimensioned to the size and precision required for each problem by using a set of pointers established in the control program. In this way no space is wasted on data storage. Because of this automatic storage scheme, it is not possible to establish absolute values for maximum numbers of material sets, nodes or elements. The total capacity of the program is controlled by the size of the array in the blank common which serves as the parent array for all other arrays. After the basic input data has been read, CALBRG will check that sufficient memory is available to solve the problem, if not an error message will be printed.

Out of core data management subroutines are used to create and manage disk files. At the end of each execution cycle, the program data is saved in a core file. This enables the analyst to restart a problem from a given state and is specially useful for nonlinear analysis.

TIMDEP

This module generates time dependent concrete properties and advances them to the solution module as necessary.

GEOMET

This module is used to define the geometry and material properties of the complete structure. This includes:

- Nodal position coordinates.
- Element connectivity.
- Element geometric properties.
- Material models.

For large analytical models the program has mesh generation capabilities.

In general, several elements have same material models and geometric properties. The program allows for the element to be connected to a particular material property set and geometry specification by indicating the property numbers on the element record. Thus the material and geometric properties need only be defined once.

CONFIG

This module manages segmental operations. The state of the structure at any given construction stage is defined through this module. The various operations managed by this module are as follows:

- Addition and removal of beam-column elements.
- Addition and stressing, re-stressing, and removal of cable elements.
- Addition and removal of catenary elements.
- Addition and stressing, re-stressing, and removal of prestressing tendons.
- Releasing and restraining of various boundary conditions.

LOAD

The module accepts the external nodal loads applied to the structure. A load pattern vector is defined which can be scaled using a pattern multiplier defined later in the solution module.

SOLVE

The SOLVE module allows for three different solution strategies each of which is managed by a sub-module:

- Load Control: Implements a step iterative type of solution strategy for non-linear equilibrium equations

- Displacement control: Implements a displacement controlled strategy, wherein the displacement of a selected degree of freedom is incremented gradually and the corresponding equilibrium configuration of the structure determined.
- Time step solver or time control: This module is used to trace the time dependent behavior of the structure at various construction stages in the time domain.

The environment of the solution can be conveniently controlled by setting several parameters and switches prior to invoking the SOLVE module. The following switches may be turned on or off as necessary.

- Material nonlinear solution.
- Geometry nonlinear solution.
- Include geometric stiffness.

This allows the analyst freedom in choosing the type of the analysis and to assess the effect of including material or geometric nonlinearity on the response of the structure being considered.

In addition, the solution environment includes convergence criteria consisting of maximum force and moment unbalances. When the maximum unbalance at the end of a solution step is less than the specified tolerance, the solution is assumed to have converged and the next step is initiated.

Moreover, the solution environment also includes specification of the creep integration scheme to be used in the case of time dependent analysis, and the level of detail to be output at the end of the solution.

11.3.1. ELEMENT MODULES

The program is designed to operate with an element library. New elements can be added easily, provided they conform to a pre-defined structure or template designed for a generic element. The typical structure of an element module is shown in Fig. 11.02.

The operation and functions of various routines are briefly described here. The prefix X identifies the element type.

X_INPUT

These subroutines are activated through the GEOMET module. These are used to read in data about the connectivity of the element, its geometric properties, and its material specification. This data is stored on random access disk files so that information about any required element can be accessed directly; this technique is useful for segmental operations where all elements are not active in the structure at a given instant of time.

X_CONFIG

These subroutines are activated through CONFIG module. These are used to initialize the state of the element prior to assembly in the main structure.

X_DBASE

These subroutines are used by different modules at different levels of solution. A client subroutine will request data or information from X_DBASE routines, which in turn grab the information from the appropriate in-core array or a disk file and place it in a common block.

The client subroutine either uses this data and discards it or updates it and returns to the X_DBASE routines to save for future use.

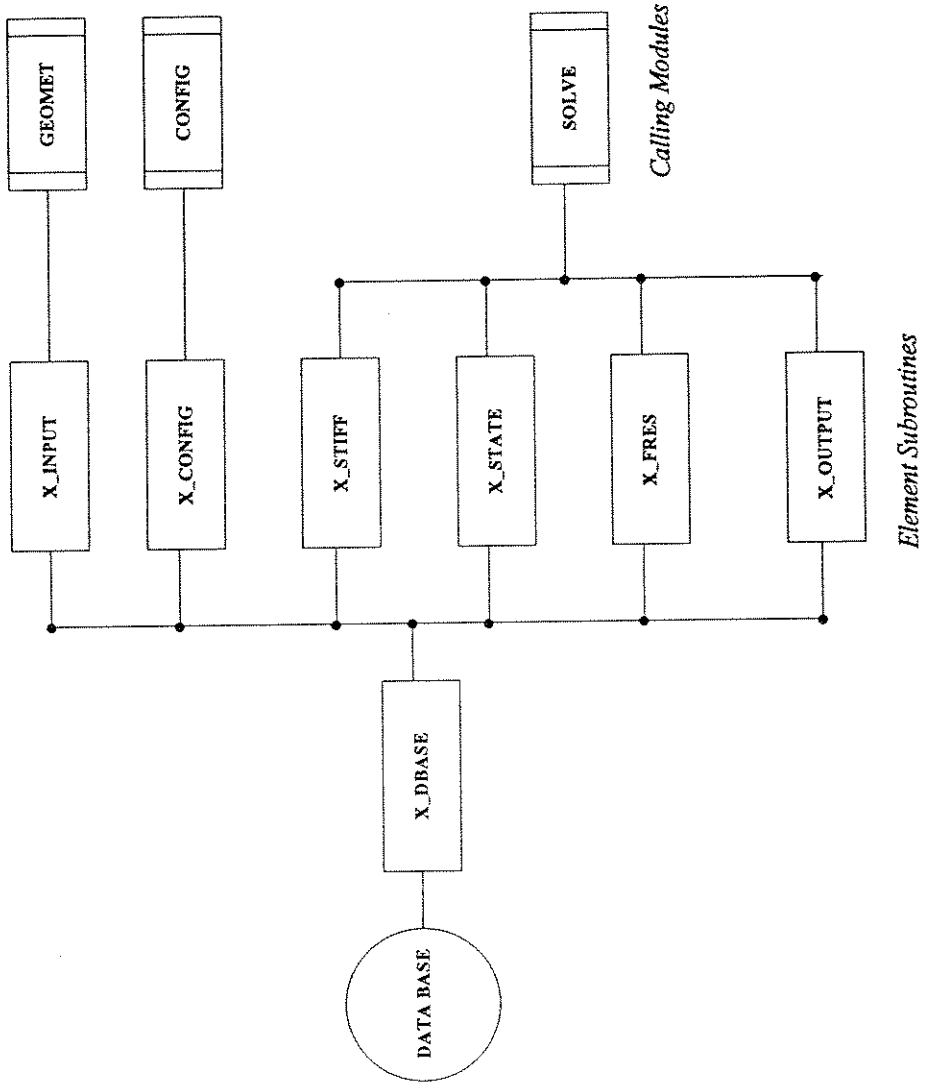

FIG. 11.02 THE TYPICAL STRUCTURE OF AN ELEMENT MODULE

The programmer can therefore concentrate on the algorithm itself, instead of writing tedious, repetitive code to access the data base.

X_STIFF

These subroutines are used by the SOLVE modules to generate the current element stiffness matrix. Depending upon the decision of the analyst, geometric stiffness may be included or excluded.

X_STATE

These subroutines, which are used in the state determination process, are called by the SOLVE module. In the course of a non linear solution, at the end of each solution step, the element end displacements are known. The X_STATE subroutines are used to translate these into increments in element internal forces or stresses. This is a very complex process and is the heart of non linear solution strategy. Most the programming effort as well as computer time is taken up by these routines.

X_FRES

These subroutines are used by SOLVE modules to determine the internal resisting forces at the ends of each element. This operation is required to estimate the unbalanced forces in a non linear analysis.

If the nonlinear geometry option is in force then the equilibrium of the structure is checked in deformed or displaced configuration.

X_OUTPUT

The output routines are used to manage the printout of results. Depending upon the type of switches set in the environment command, the detail in the print out varies; for example in the case of the frame element:

- At the lowest level, element fiber stresses and strain are printed.
- Section forces are printed out
- Element end forces and bending moments are printed out.

The X_OUTPUT subroutines simply access the data base and print out the results in an organized formatted form.

The frequency at which the output information is printed is controlled through the parameters set under the environment command. These may be:

- At the end of every iteration
- At the end of every load or displacement or time step.
- At the end of every solution.

11.3.2. ELEMENT LIBRARY

The elements presently available in the library include the following:

- Beam-Column Element.
- Prestressing Tendon Element
- Shallow Cable Element
- Catenary Element.

A brief description of each element is provided here for sake of completeness. Detailed descriptions may be found in Chapters 6, 7, 9 and 10.

BEAM-COLUMN ELEMENT

A fiber beam-column element is used to model the tower and deck segments in a cable-stayed bridge. The element has six degrees of freedom at each end. Multiple slices or control sections are defined at appropriately selected locations along the length of the element. The position of the intermediate slices is defined by the analyst in such a manner that it approximates the actual curvature variation of the element. The shape functions are updated as the state of the element changes.

The element is designed to capture ultimate load behavior of both concrete and steel members. Because of its formulation, a relatively longer element can be used instead of the usual fine mesh required to capture the spread of plasticity in the inelastic zones of the member.

In the case of a concrete element, the time dependent effects of creep and shrinkage are automatically included whenever the TIMECON module is invoked by the analyst.

PRESTRESSING TENDON ELEMENT

This element is used to model prestressing tendons having an arbitrary profile in space. If this profile conforms to a generic shape consisting of a series of parabolas and straight lines then it can be generated simply by defining certain parameters. Immediate prestress losses due to friction and anchor slip are accounted for. Time dependent stress loss due to relaxation of prestressing steel is automatically included whenever the TIMESOL module is activated by the analyst.

SHALLOW CABLE ELEMENT

Cables with a low sag to span ratio are modeled with this element which can therefore be used to simulate the stays in cable-stayed bridges.

A nonlinear material model is used for cable steel so that the cable behavior can be captured both in the elastic and in the inelastic range.

During segmental construction operations the cable tensions are often adjusted to correct the profile of the bridge deck. CALBRG can simulate this procedure and the cables can be set to any required tension at the desired construction stage.

CATENARY ELEMENT

The catenary element is a general purpose, elastic cable element, which may be used for both large and short sag cables. It is specially useful for modeling highly nonlinear large sag cables such as that used in mooring lines or suspension bridges. Only one element may be used to model an entire cable and discretization is not required. The solution is exact for an elastic catenary.

12. THE ANALYSIS OF A CURVED SEMICIRCULAR CABLE-STAYED FOOT BRIDGE

12.1. GENERAL

Ultimate load analysis of a semicircular foot bridge is presented in this section. The structural concept of this bridge, shown in Fig. 12.01, was originally proposed by Irvine [46], wherein a horizontal semicircular deck is supported by a system of cables connected to the top of an appropriately inclined tower. The geometry of this structure has been adapted from a paper by Loi, Mickleborough, Sharpe and Irvine [75].

Sharpe [126] has carried out a series of linear elastic analyses with SAP IV [9] to investigate the structural feasibility of this bridge. The modeling of the structural elements was based on Zung-An Lu's paper [76]; that is the cables were modeled as truss bar elements with the modulus of elasticity modified in accordance with Ernst's equation [28]. Note that Loi et al. [75] do not report any cable lengths or tensions in their paper and therefore any direct comparison with their results is not possible.

12.2. ANALYSIS MODEL

The analysis model is shown in Fig. 12.02. The bridge deck is shaped like a horse shoe with a total perimeter length equal to $455' - 11''$. The maximum vertical clearance between the deck and the road way is $20' - 10''$ which results in a slope of 1:8 in the direction of the road.

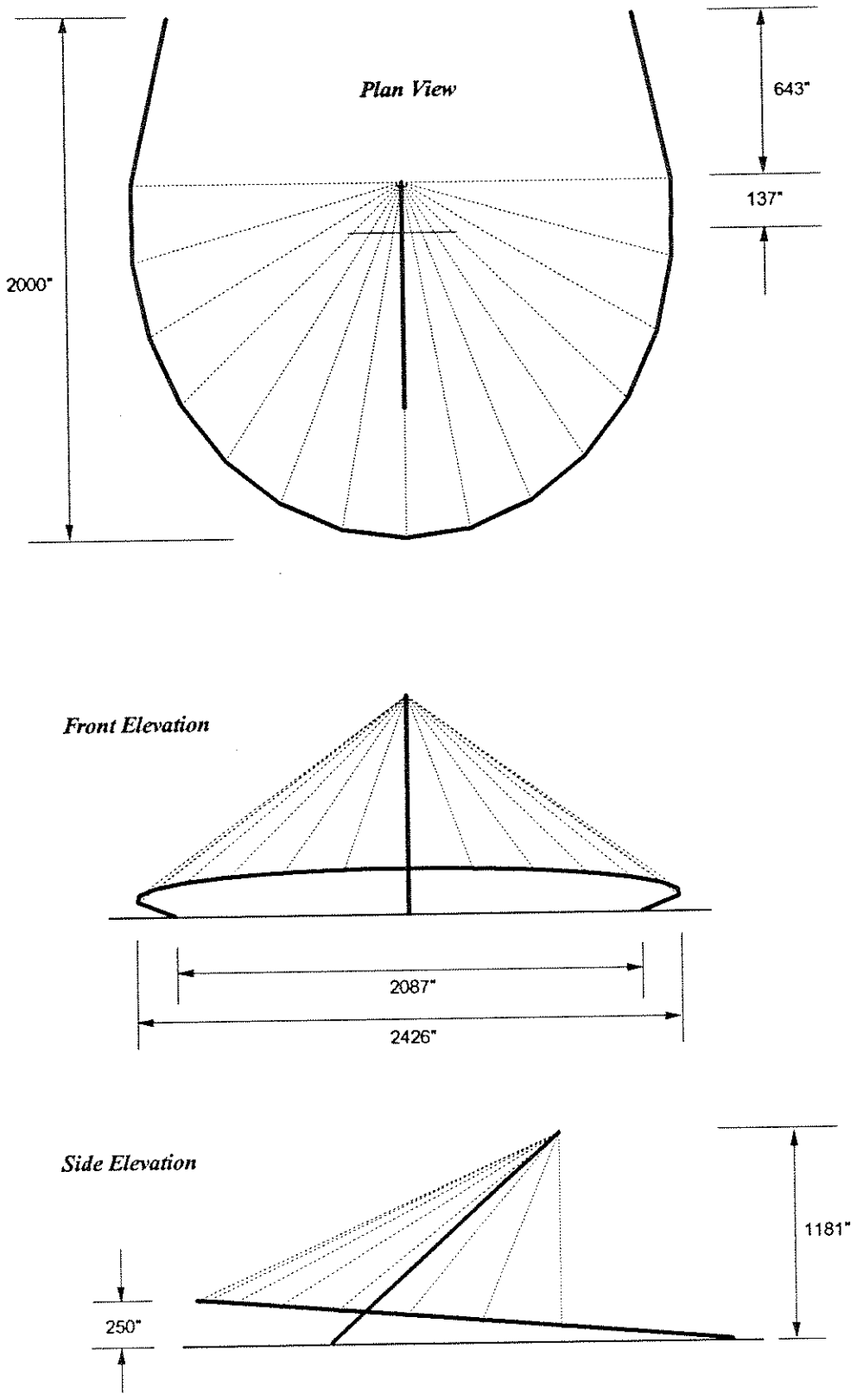

FIG. 12.01 GEOMETRY OF THE CURVED SEMICIRCULAR CABLE-STAYED BRIDGE.
Loi, Mickleborough, Sharpe and Irvine, 1987.

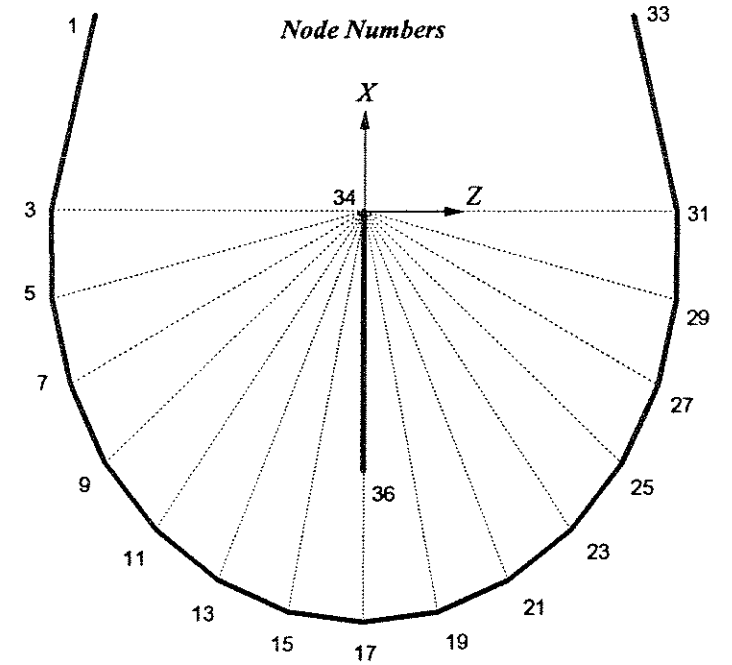

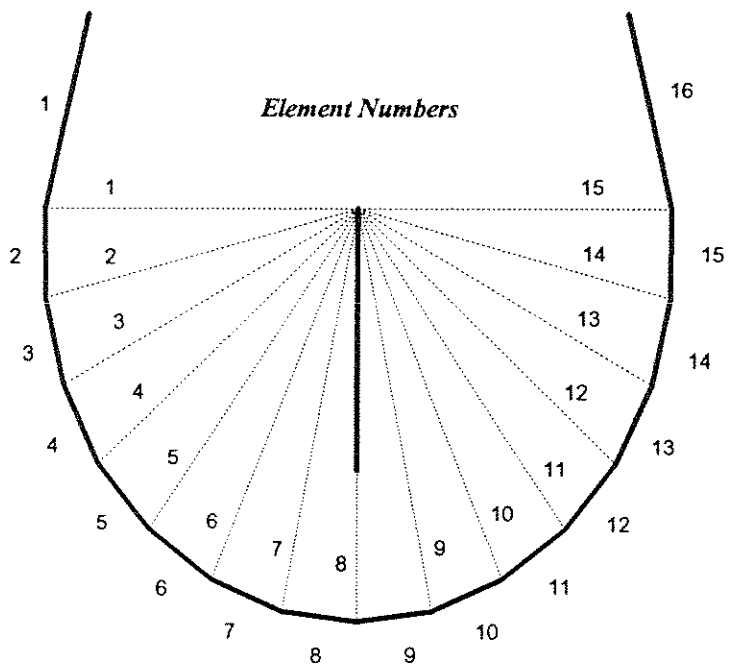

FIG. 12.02 ANALYSIS MODEL
NODE AND ELEMENT NUMBERS

The maximum width of the horse shoe, which is the diameter of the semicircle is equal to $203'-5''$. The deck consists of a tubular steel girder with a composite reinforced concrete foot path on top. At the abutments, the deck is free to rotate but the lateral and vertical translations are restrained.

The deck is supported by a set of cables arranged in a radial pattern; these are in turn hooked on to the top of a central steel tower. The tower has a vertical height of $98'-5''$ and is inclined at an angle of 54^{o} with the horizontal, it has a circular cross section and is fixed at the base to provide some degree of lateral stiffness. The inclination of the tower is designed to be collinear with the resultant of cable forces; thereby ensuring that the main structural action of the tower is in the axial direction. .

12.2.1. CABLES

The deck is supported by a total of 15 cables; each cable has a diameter of $1.4''$. A bilinear stress-strain curve is assumed for the cable-stay steel model. This model is defined by the following parameters:

$$f_y = 246\ ksi \quad \varepsilon_y = .00847 \quad f_u = 270\ ksi \quad \varepsilon_u = .0419$$

The cables are pre-tensioned to balance the dead load of the structure; that is the vertical component of the cable force at the deck anchorage is equal to the dead load of the deck segment or the tributary area of the deck. Loi et al. [75] do not report pretension values in their paper.

A set of pretension values were determined by the author on the basis of load balancing and is reported later in this section.

12.2.2. DECK

It is assumed that the steel used in the deck has a bilinear strain hardening material model. This model is defined completely by the following parameters.

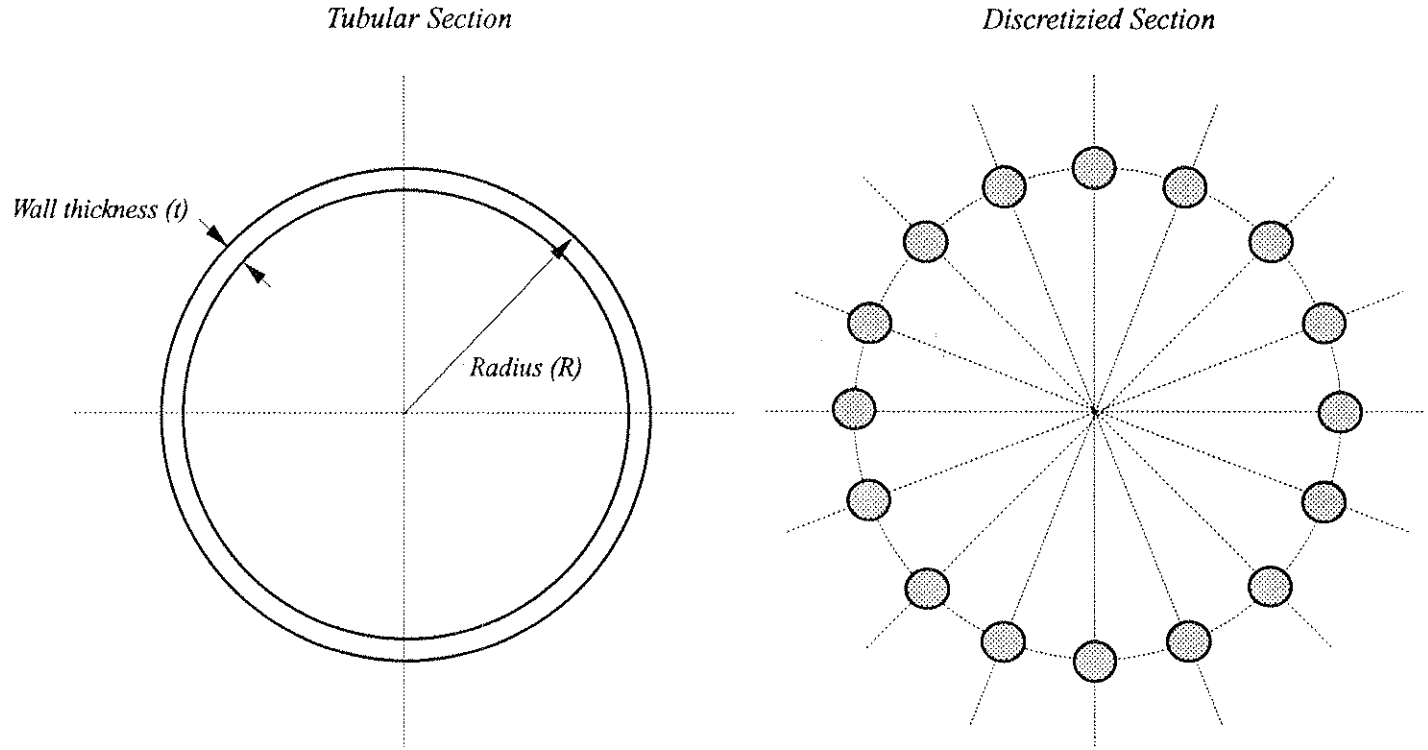

FIG. 12.03 SECTION DISCRETIZATION; TUBULAR SECTION

$$f_y = 60\ ksi \quad E_0 = 30000\ ksi \quad E_1 = 30\ ksi \quad \varepsilon_u = 0.12$$

where E_0 is the initial modulus, E_1 is the strain hardening modulus, f_y is the yield stress and ε_u is the ultimate strain at failure.

The deck has hollow circular cross section with a diameter of $71''$ and a wall thickness of $0.6''$. The cross section is descritized into 16 fibers, each having an area of 8.8 square inches and placed radially 22.5^o apart as shown in Fig. 12.03. The contribution of the reinforced concrete foot path is ignored for the purposes of this analysis.

12.2.3. TOWER

The tower has a hollow circular cross section with a diameter of $71''$ and a wall thickness of $0.8''$. It is fixed at the base and free to move at the top. The cross section is modeled as 16 fibers arranged in a radial pattern and placed 22.5^o apart. Each fiber has an area of 10.9 square inches.

The steel model is similar to that used for the deck.

12.2.4. LOAD PATTERN

The load pattern applied to deck nodes consists of deck and cable dead loads. For ultimate load analysis this pattern is gradually incremented until failure.

Node No.	Load (kips)
3	30
5	20
7	20
9	20
11	20
13	20
15	20
17	20

12.3. ANALYSIS

Two sets of analyses were carried out.

- Load balancing.
- Ultimate load analysis.

Nonlinear material and geometry was enforced for both analyses.

12.3.1. LOAD BALANCING

The first set of analyses was carried out to find the cable tensions to balance the dead load and produce a condition of zero deflection in the deck. To start off the analysis an initial set of pretensions was calculated based on the following equation:

$$T \sin \alpha = w \tag{12.01}$$

where T is the cable tension, α is the vertical angle subtended by the cable to the horizontal plane and w is the tributary dead load carried by the cable.

In general a state of zero deck deflection is not attained at the end of the first cycle of analysis and an iterative process is required. Cable tensions are adjusted depending on the degree of deck deflection and the next analysis is carried out until the desired deck profile is achieved.

In case of the foot bridge being considered, at the end of the first iteration with the cable tensions set to balance the dead loads, the maximum deflection was of the order of .07″. The resulting deck profile is shown in Fig. 12.04. No further iterations were carried out.

The cable tensions required to balance the dead load as set by Eq. 12.01 are given in the table below. Note that at the end of the analysis cable tensions had decreased (except for cables 1 and 15) because of transverse deflection of the top of the tower; see Fig. 12.05. In

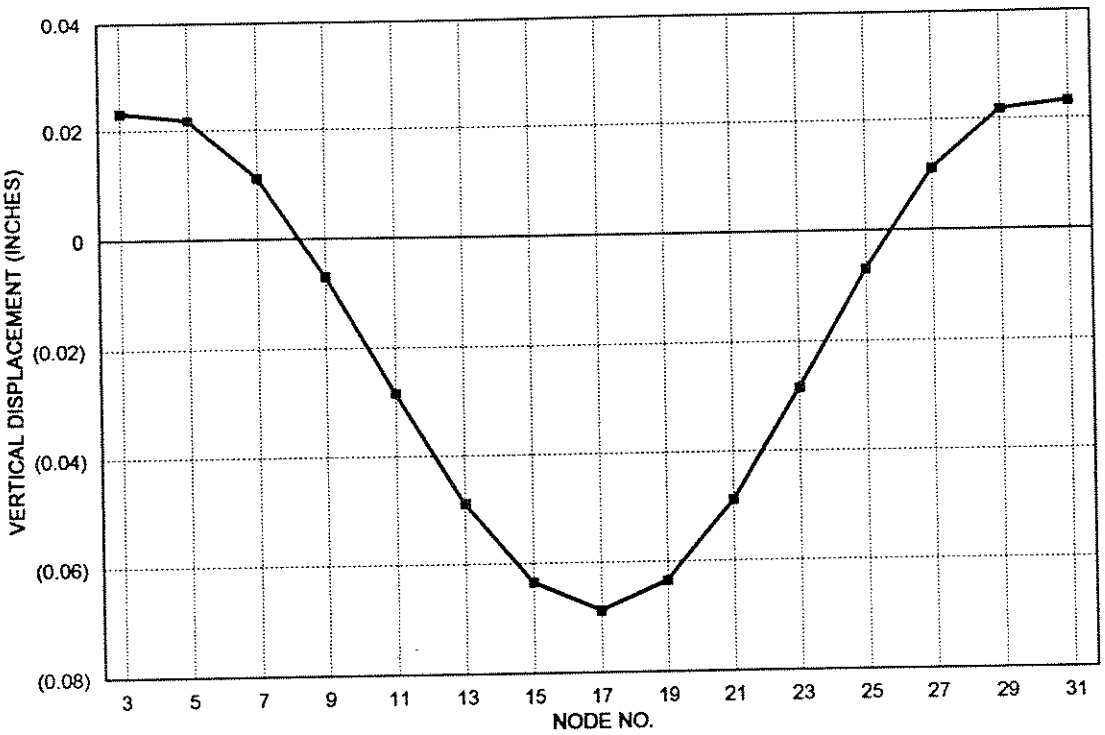

FIG. 12.04 VERTICAL DISPLACEMENT OF BRIDGE DECK SUBJECT TO DEAD LOADS

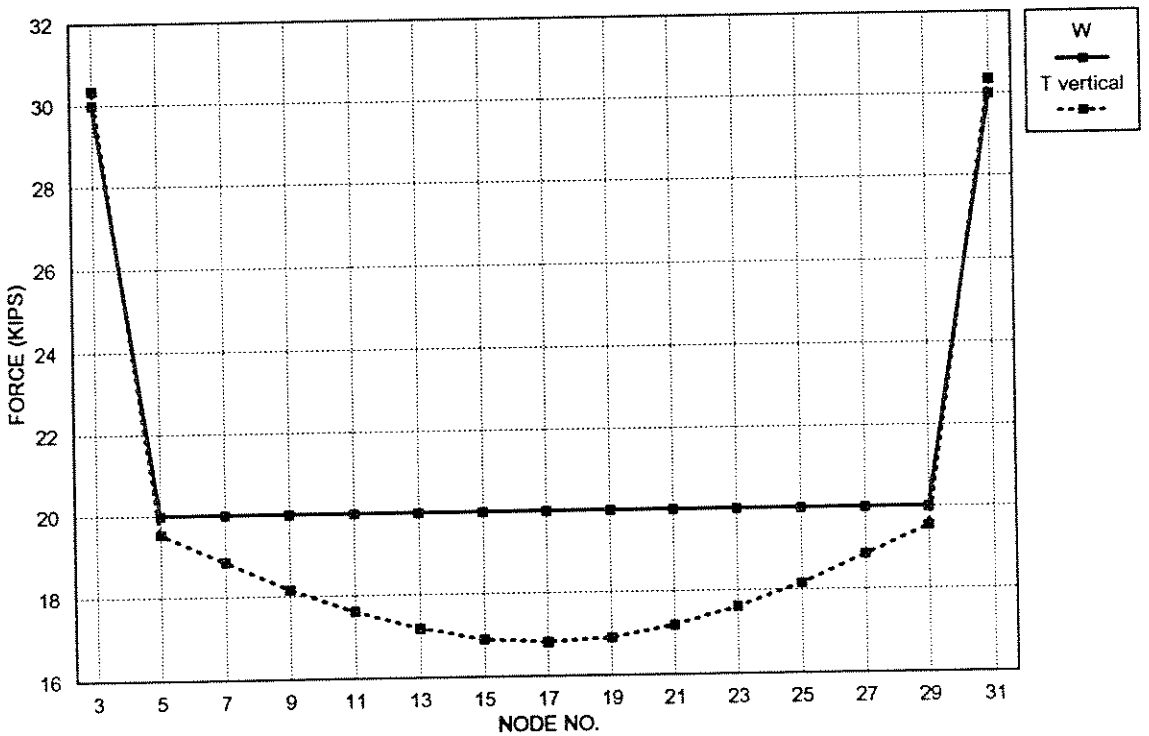

FIG. 12.05 CABLE TENSIONS SET FOR ZERO VERTICAL DEFLECTIONS VERTICAL COMPONENT OF CABLE FORCES VS DEAD LOAD

the case that this deflection was of considerable magnitude, cable tensions would have to be readjusted and a second analysis cycle required.

Cable No.	Tension (kips) Target	Tension (kips) Attained
1	44.7	45.2
2	30.8	30.1
3	31.9	30.0
4	32.9	29.9
5	33.9	29.8
6	34.7	29.8
7	35.2	29.7
8	35.4	29.7

12.3.2. ULTIMATE LOAD ANALYSIS

In the second analysis the structure was loaded to failure. The load pattern defined by the dead loads was maintained and a displacement controlled solution strategy was adopted.

The vertical displacement at node 17 (mid span) was selected as the controlled degree of freedom. This displacement was incremented gradually and the corresponding changes in the load pattern multiplier noted. A load versus displacement plot is shown in Fig. 12.06.

- The cables began to yield at about 12.5 times the dead load; at this point the vertical deflection at node 17 (mid span) was 30″.
- Further increments in the controlled displacement resulted in relatively smaller increments to the load applied to the structure.
- The structure failed at about 13.5 times the dead load; at this point the vertical deflection of node 17 (mid span) was 110″. The analysis results indicated that the failure occurred because the cables had reached their ultimate strain. Note that the structure has a yield ductility of about 3.7.

A comparison of cable forces at dead load and at failure is shown in Fig. 12.07. The reserve capacity of the cables is rather substantial. At the start of the analysis, the end cables,

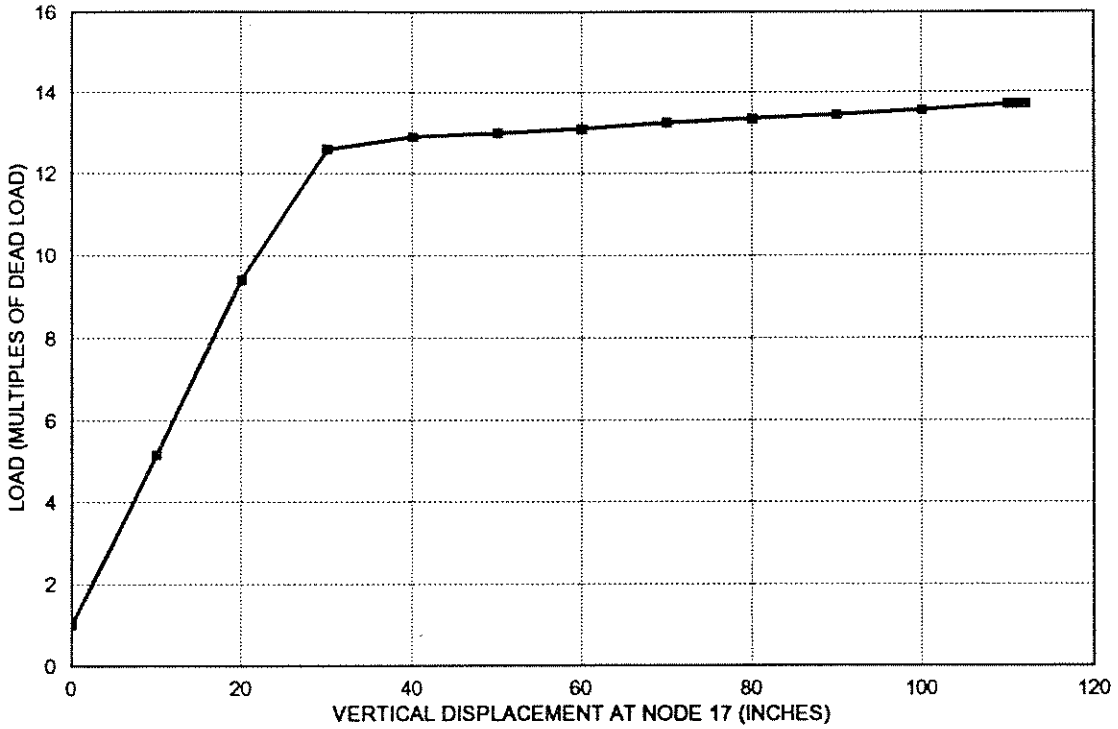

FIG. 12.06 ULTIMATE LOAD ANALYSIS
LOAD VS VERTICAL DISPLACEMENT AT MIDSPAN

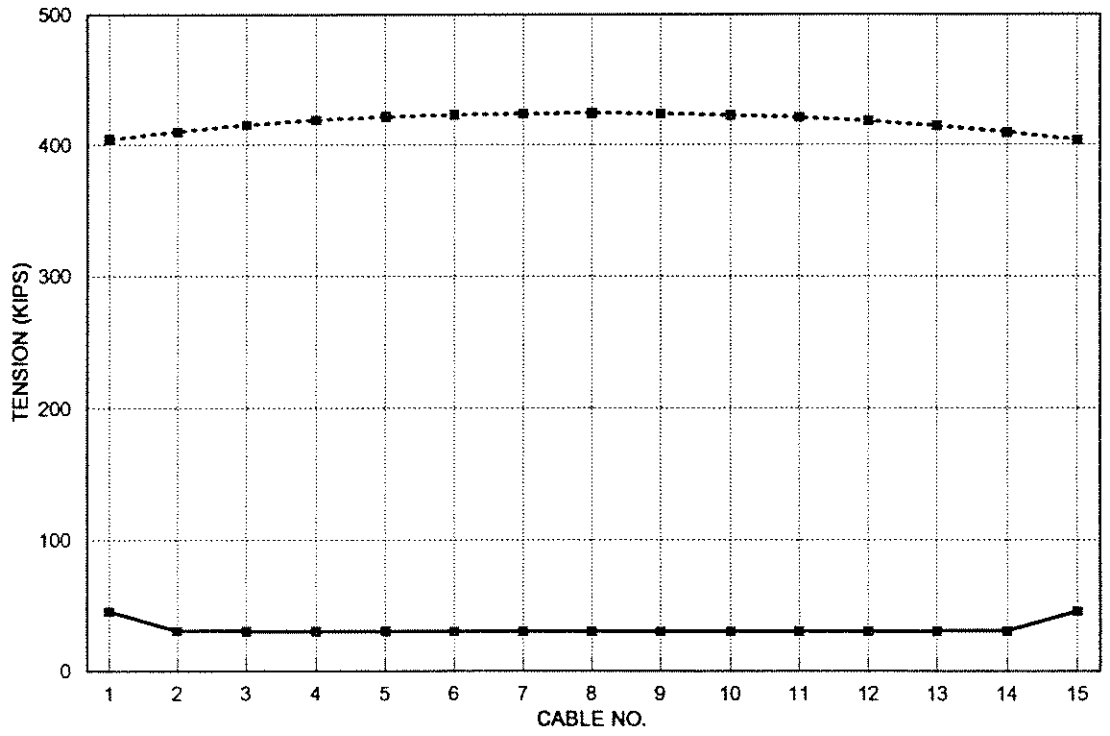

FIG. 12.07 CABLE FORCES AT DEAD LOAD AND AT ULTIMATE

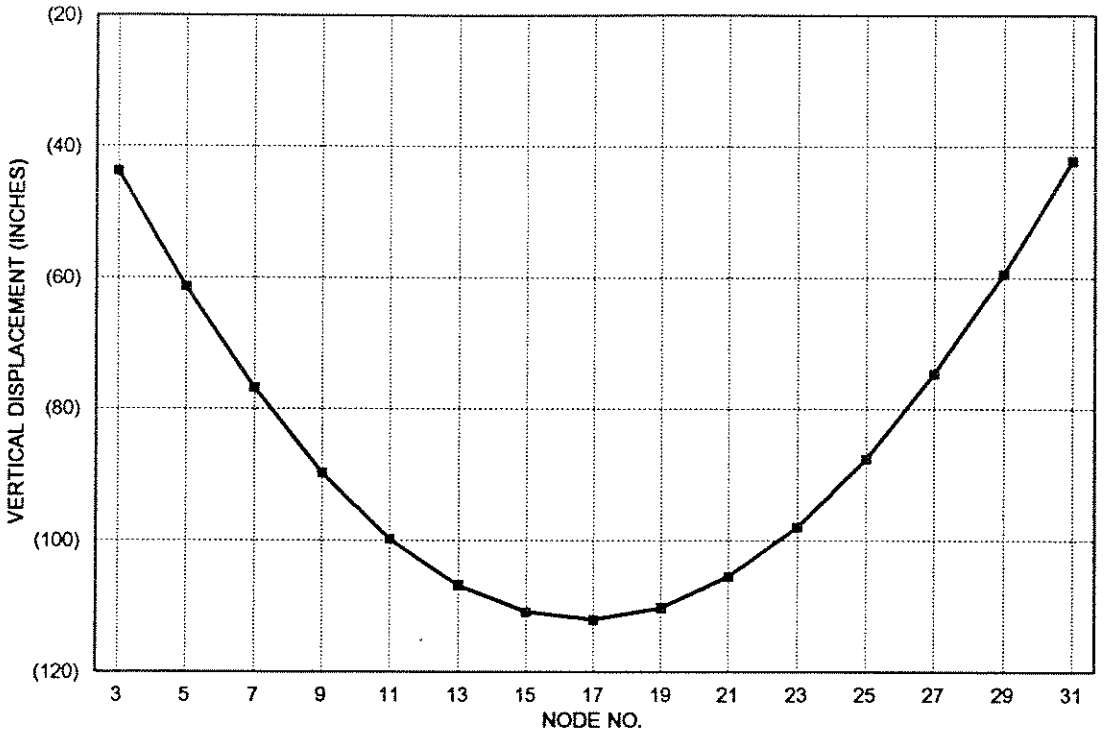

FIG. 12.08 VERTICAL DISPLACEMENT OF BRIDGE DECK AT ULTIMATE LOAD

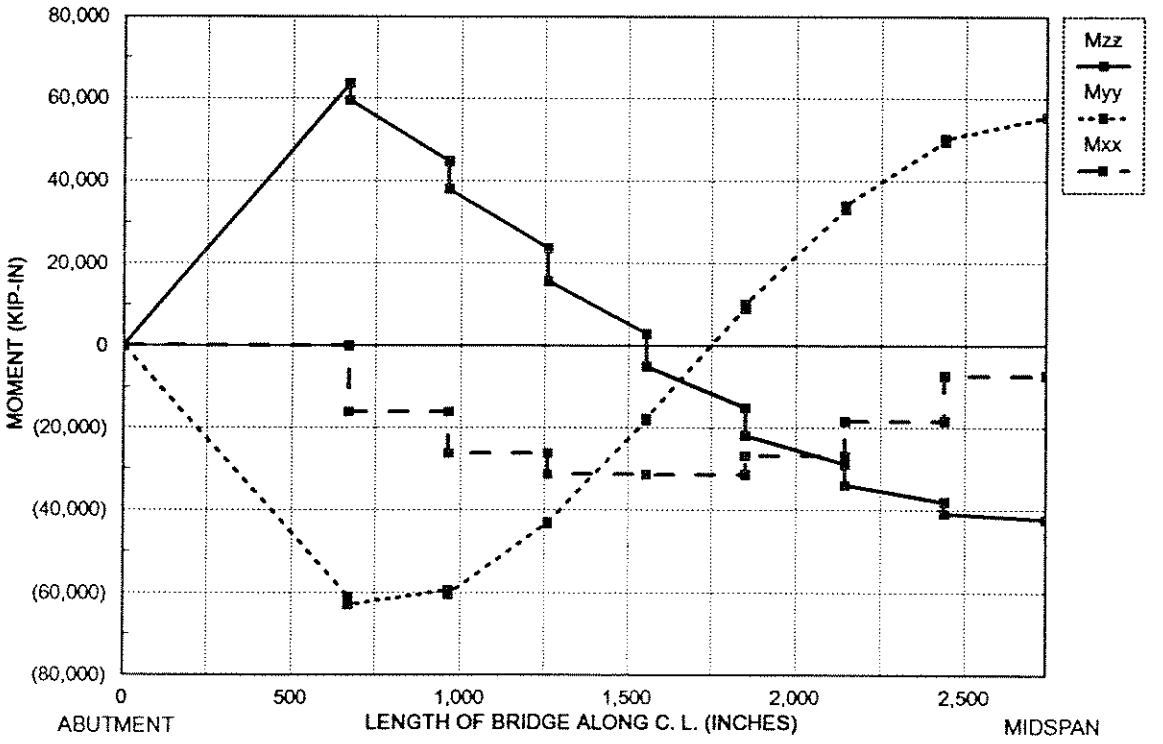

FIG. 12.09 VARIATION OF MOMENTS ALONG CENTER LINE OF BRIDGE DECK FROM ABUTMENT TO MIDSPAN

numbers 1 and 15 carry the heaviest load but at failure the mid span cable number 15 is the most heavily stressed and is the first to go.

Fig. 12.08 shows a plot of deck displacements in the vertical direction at failure. There is a parabolic variation of displacements with a maximum of $110''$ at node 17. Note that the variation in the displacements conforms to the change in the cable forces.

Fig. 12.09 shows plots of longitudinal (M_{zz}) and transverse (M_{yy}) bending moments and the torsional moments (M_{xx}) acting on the bridge deck. Maximum values of bending moments occur at node 3 and 17; corresponding maximum longitudinal fiber stresses at ultimate load are -28 ksi and -23 ksi respectively (tension +ve).

13. ANALYSIS OF A THREE DIMENSIONAL CURVED CABLE-STAYED STEEL BRIDGE

13.1. GENERAL

The Ruck-a-Chucky Bridge was designed to span across the middle fork of the American river over the reservoir created by the construction of Auburn dam near Sacramento in California. It is a 1300 ft span curved box girder bridge supported by cables which are anchored to the rocky walls of the gorge. The deck section has an overall width of 48 feet, a depth of 8 feet and a constant horizontal radius of curvature of 1500 feet as shown in Fig. 13.01. A three dimensional view of the bridge is shown in Fig. 13.02. However the bridge was never actually built as the construction of the dam and its allied projects were canceled due to environmental concerns.

The bridge was designed by T. Y. Lin International and Hanson Engineers and received a number of awards for design innovation and aesthetic sophistication from the Engineering and Architectural community at large. A number of papers and reports have been written on the design and analysis of the Ruck-a-chucky bridge, T. Y. Lin and Firmage [73], Zung-An Lu [76], Godden [34], Godden and Aslam [35], Shah [125].

Godden conducted seismic model studies of the bridge. A 1/200th scale model of the steel bridge (preliminary design) was built and tested over a shaking table for seismic response by subjecting it to a ground motion of increasing intensity. He reported that the primary

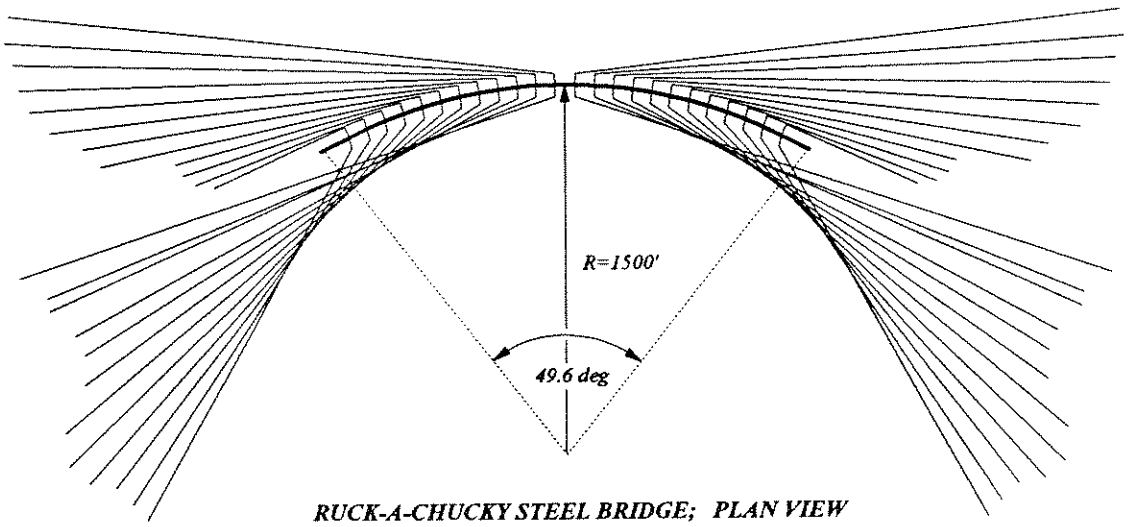

RUCK-A-CHUCKY STEEL BRIDGE; PLAN VIEW

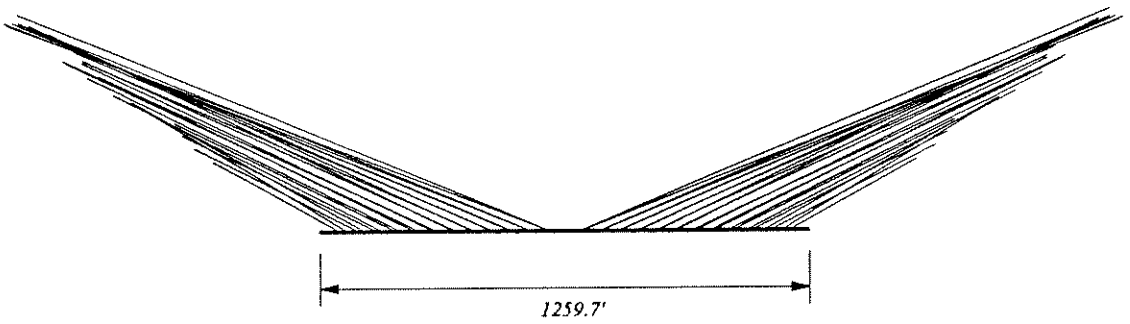

RUCK-A-CHUCKY STEEL BRIDGE; SIDE ELEVATION

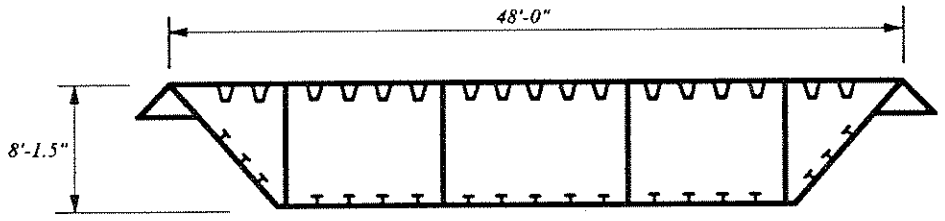

RUCK-A-CHUCKY STEEL BRIDGE; DECK CROSS SECTION

FIG. 13.01 RUCK-A-CHUCKY STEEL BRIDGE; GEOMETRY

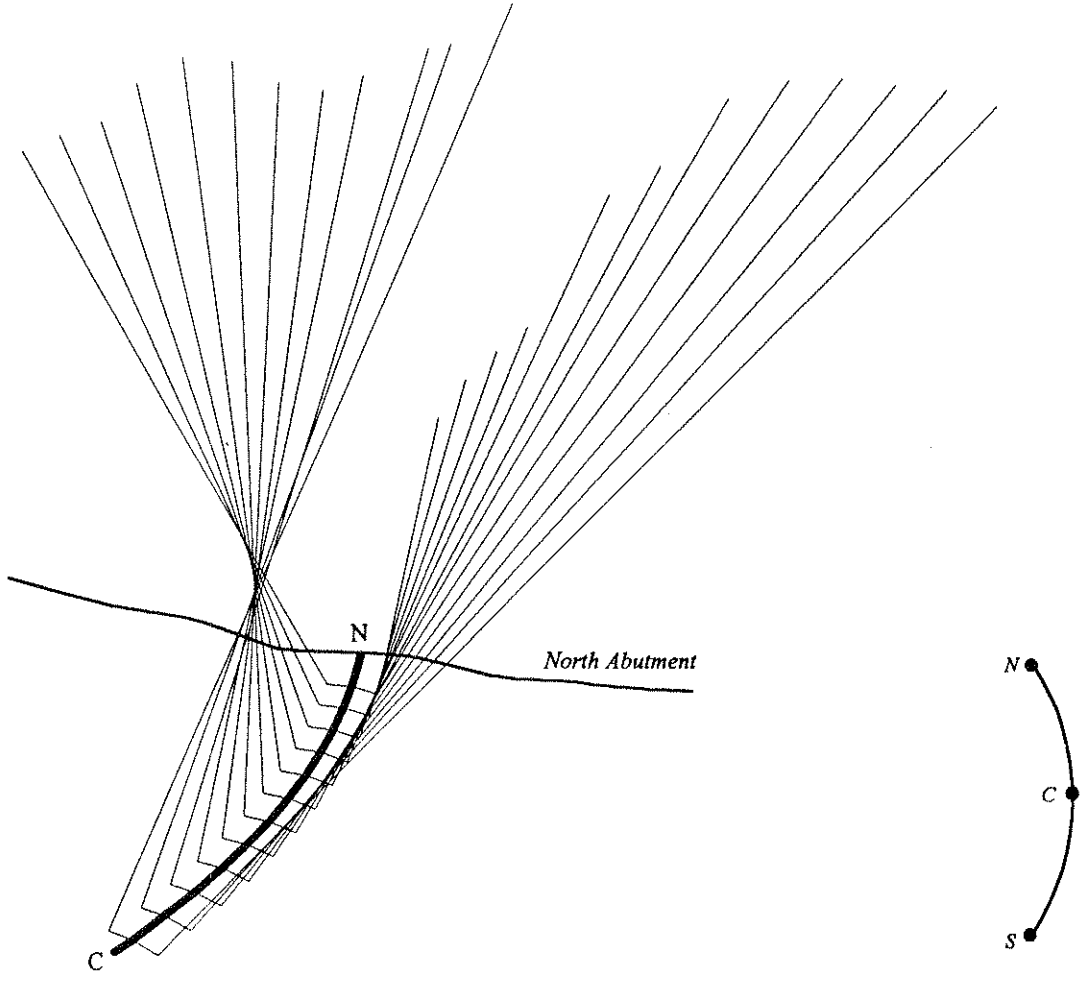

FIG. 13.02 RUCK-A-CHUCKY STEEL BRIDGE; 3D MODEL OF HALF SPAN.

response of the bridge was due to the vertical component of the ground motion and that all horizontal motion tests produced very small response. He concluded that the bridge will remain undamaged under any conceivable earthquake motion.

Zung-An Lu discussed the dynamic analysis of steel and concrete bridge (preliminary design). The bridge was analyzed as a linear elastic structure using the computer program SAP IV [9]. The cables supporting the deck were modeled as truss bars with a modified modulus of elasticity as described by Ernst [28] and the deck itself was modeled with beam column elements. The analysis results of the steel bridge were found to be in good agreement with the model testing done by Godden. According to Lu [76], comparison with model studies also indicated that use of truss bar type tension members instead of flexible cables did not appreciably affect the correctness of the analysis. As discussed in Chapter 8, this is true for most cable stayed bridges where the live loads are relatively small as compared to the dead load of the structure. In other cases, various researchers have reported that geometric non linearity of the cables may result in an increase of 10% to 15% in the deck moments, Seif [123].

The bridge structure analyzed in this study is based on the final design prepared by T. Y. Lin International [131] and therefore no direct comparisons can be made with the previous studies reported in the literature, Godden [34], Lu [76]. A number of assumptions were made as to the material and geometry of the bridge; these were made either because of a lack of pertinent data or to simplify the analysis model.

It was assumed that the bridge is symmetrical with respect to its center line in plan. However, the actual structure, as presented in the final design is not symmetrical because of the difference in locations of the cable anchor points on the gorge walls.

The problem was approached from the point of view of a designer who has completed a preliminary design using linear elastic analysis of the type described by Lu [76] and needs to evaluate cable forces both during the cantilever construction sequence and for the complete

bridge which would keep the bridge deck on a desired profile. A series of analyses were conducted using the computer program CALBRG which was developed in the present study. Nonlinear material and geometry was enforced in each analysis.

- Load balancing analysis to determine the cable tensions which would hold the completed bridge in the desired profile.
- Dis-assembly analysis wherein a completely built bridge with all the cables set to balanced tensions is taken apart segment by segment in a sequence which is reverse of the actual fabrication or assembly sequence. This results in a set of initial cable tensions; which is the tension to which a cable is set when the deck segment supported by that cable is first integrated in the structure..
- Assembly analysis to simulate the construction sequence. The leading cables in the cantilever construction sequence are set to the initial tensions extracted from the dis-assembly analysis. The bridge profile at each construction step and the corresponding cable tensions and moments in the bridge deck are obtained. These profiles and cable tensions may be compared with the actual construction in the field to verify that the structure is on the desired path and that the two halves of the bridge will indeed meet in the middle.
- Ultimate load analysis to find the failure mechanism and the load carried by the structure at failure. The structure was loaded incrementally with a load pattern corresponding to the dead load of the structure and its behavior tracked through the elastic and yielding ranges and finally to failure.

13.2. THE ANALYSIS MODEL

A plan of the analysis model is shown in Fig. 13.03 and 13.04. Because of the assumed symmetry in the structure only half of the bridge is modeled. The center line of the bridge

deck is a circular arc with a radius of 1501 ft. as shown in Fig 13.05. The center line of the roadway is offset from that of the bridge by 1 ft. and thus has a radius of 1500 ft. The bridge has an arc length of 1300 ft and subtends an angle of about 50 degrees at the center of the arc. The plane of symmetry divides the bridge into two halves, these will be subsequently referred to as the north and the south side of the bridge.

The deck consists of 27 box girder segments as shown in Fig. 13.05, there are 13 segments in each half span and one closure segment at the midspan. Each of the segments (except the abutment segments) is 50 ft. long. The segments adjacent to the abutment (N1 and S1) are 25 ft long and are assumed to be rigidly connected to the concrete abutment. The box girders have a uniform cross section with a depth of 8 ft as shown in Fig. 13.06.

The geometry of the bridge is defined with respect to a global coordinate system shown in Fig 13.05. The origin of the coordinate system is placed at midspan of the bridge on the center line of the road way; X and Z axes define the horizontal plane whereas Y is the vertical axis.

The deck is assumed to be fixed at the abutment support. The boundary conditions at midspan are established by structural symmetry; that is the deck is free to translate in the vertical plane and to rotate about its centroidal axis, the other three degrees of freedom are restrained. These conditions are summarized below.

Deck Boundary Conditions

	Dx	*Dy*	*Dz*	*Rxx*	*Ryy*	*Rzz*
abutment	*fixed*	*fixed*	*fixed*	*fixed*	*fixed*	*fixed*
midspan	*free*	*free*	*fixed*	*fixed*	*fixed*	*free*

The deck is supported by a total 48 cables which are anchored to the rocky sides of the gorge. Each cable has an identification mark such as 5-NO which signifies that the cable is connected to deck segment 5 in the north half of the span and is located outside of area bounded by the circular arc. The position coordinates of the cable anchor coordinates in the rock [131] are given in Table 13.1.

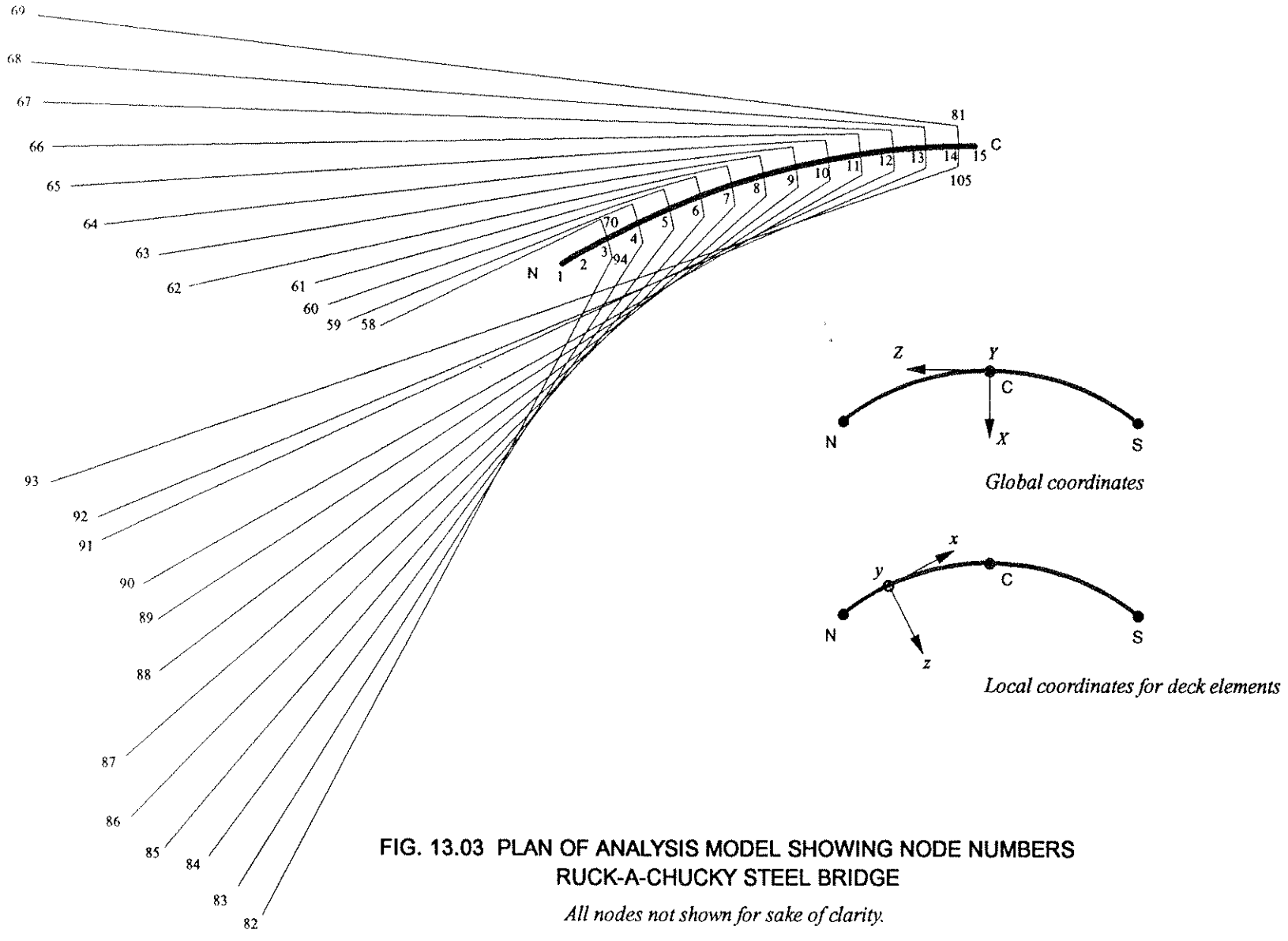

FIG. 13.03 PLAN OF ANALYSIS MODEL SHOWING NODE NUMBERS
RUCK-A-CHUCKY STEEL BRIDGE

All nodes not shown for sake of clarity.

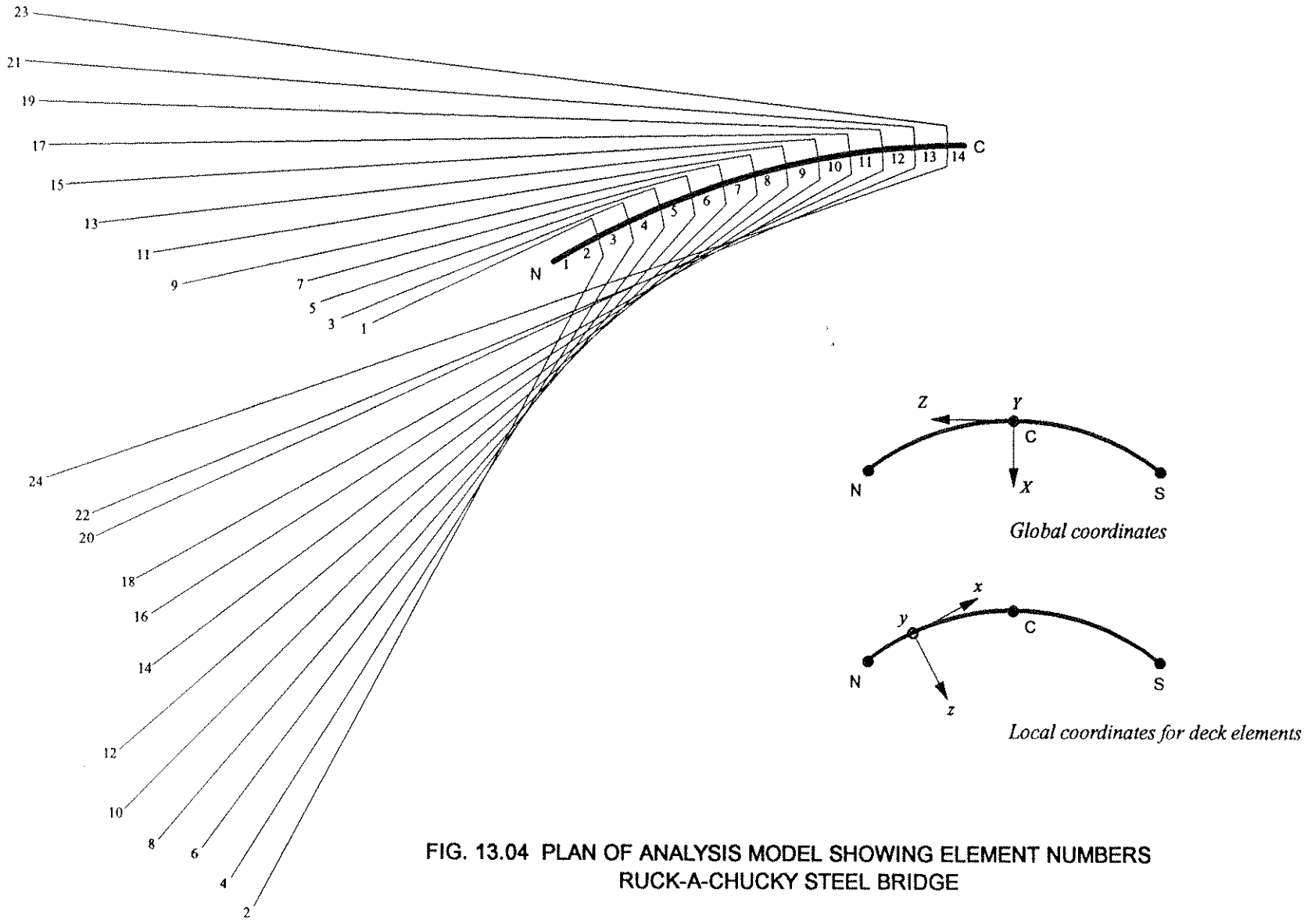

FIG. 13.04 PLAN OF ANALYSIS MODEL SHOWING ELEMENT NUMBERS
RUCK-A-CHUCKY STEEL BRIDGE

TABLE 13.01

COORDINATES OF CABLE ANCHORS AT NORTHERN ROCK WALL

CABLE NO.	*Node No.*	*X* *inches*	*Y* *inches*	*Z* *inches*
2NO	58	2521	1740	10912
3NO	59	2426	2088	11494
4NO	60	2231	2400	11862
5NO	61	1938	2712	12108
6NO	62	1994	3864	14411
7NO	63	1560	4200	14954
8NO	64	1141	4932	15960
9NO	65	614	5148	16567
10NO	66	59	5208	16899
11NO	67	-555	5208	17075
12NO	68	-1109	5196	17324
13NO	69	-1768	5136	17201
2NI	82	10726	3024	13026
3NI	83	10324	3240	13457
4NI	84	9913	3420	13998
5NI	85	9797	3852	14800
6NI	86	9376	4200	15435
7NI	87	8547	4260	15537
8NI	88	7354	4260	14923
9NI	89	6636	4260	14947
10NI	90	6145	4500	15230
11NI	91	5537	4848	15985
12NI	92	5217	4944	16061
13NI	93	4732	5412	16922

TABLE 13.02

STAY CABLES; AREA OF CROSS SECTION.

CABLE NO.	*ELEMENT NO.*	*NUMBER OF STRANDS*	*AREA in.²*
2NO	1	44 ø ½"	6.73
3NO	3	41 ø ½"	6.27
4NO	5	41 ø ½"	6.27
5NO	7	41 ø ½"	6.27
6NO	9	41 ø ½"	6.27
7NO	11	41 ø ½"	6.27
8NO	13	41 ø ½"	6.27
9NO	15	42 ø ½"	6.43
10NO	17	43 ø ½"	6.58
11NO	19	43 ø ½"	6.58
12NO	21	44 ø ½"	6.73
13NO	23	45 ø ½"	6.88
2NI	2	50 ø ½"	7.65
3NI	4	48 ø ½"	7.34
4NI	6	48 ø ½"	7.34
5NI	8	48 ø ½"	7.34
6NI	10	48 ø ½"	7.34
7NI	12	43 ø ½"	6.58
8NI	14	43 ø ½"	6.58
9NI	16	44 ø ½"	6.73
10NI	18	44 ø ½"	6.73
11NI	20	44 ø ½"	6.73
12NI	22	44 ø ½"	6.73
13NI	24	44 ø ½"	6.73

At the deck end, each cable is anchored to the leading edge of the segment that it supports. The cable-deck connection is assumed to be 36 in below the deck surface, 15 in from the leading edge and 24 in from the side of the segment as shown in Fig. 13.06.

As described earlier, the deck nodes lie on a circular arc and hence can be generated by the following equations.

$$x_k = R[1-\cos(\theta\, k)] - d \qquad (13.1)$$

$$z_k = R\sin(\theta\, k) \qquad (13.2)$$

where R=1501 ft, d=1 ft and θ =0.955 degrees which is the angle subtended by a 25 ft length of the bridge segment.

k=0 *for node number 15*

k=1, 3, 5,.....25 *for node number 14, 13, 12,.....2*

k=26 *for node number 1*

The x and z coordinates of the outer cable-deck anchor nodes may be generated by Eq. 13.01 and 13.02 with R=1525 ft, d=25 and θ =1.003 degrees.

k=1, 3, 5,.....23 *for node number 81, 80, 79,.....70*

Similarly, the inner cable-deck anchor coordinates can be obtained from Eq. 1.01 by setting R=1477 ft, d=23 ft and θ =1.003 degrees.

k=1, 3, 5,.....23 *for node number 105, 104, 103,.....94*

The formulation of the beam-column element used to model the deck segments allows for placing the longitudinal reference axis of the element at any arbitrary position of convenience to the analyst. Several choices exist for placing the longitudinal reference axis:

1. Along the centroidal axis of the deck section.
2. Along the shear center of the section.
3. At some convenient level.

When several members with centroidal axes and shear centers at various levels are connected together, such as in a grid idealization of a bridge deck, it is common practice to

place the grid at a convenient reference plane and to assume that the centroidal axes as well as shear centers for all members lie in the same plane. The results show good approximation of experimental results, Powell and Mondkar [106].

In the present case of the Ruck-a-Chucky Steel bridge, the longitudinal reference axis for deck elements was assumed to lie in the top surface of the deck along the center line of the bridge (case D).

The effect of the torsional moments, arising from the eccentricity of the transverse components of the cable tensions, with respect to the shear center, was considered. Because of the high torsional stiffness of the deck box girder, the effect of such loads was assumed to be negligible.

In order to judge the validity of the above assumption, the analyses were repeated with the longitudinal reference axis placed at the shear center (case S) and at the centroidal axis (case C). Note that the centroidal axis of the deck section lies at 42" below the deck surface, whereas the shear center lies at 33" inches below the deck surface. Three sets of analyses were carried out for each case; namely load balancing, dis-assembly, and ultimate load analysis.

The results obtained from case (S) and (C) were similar. Moreover, the differences between cases (S) and (C) as compared to case (D) were small. In the case of load balancing analysis, maximum vertical deflection increased from 1" to 1.2" whereas the maximum transverse displacement decreased from 0.8" to 0.6". Transverse and longitudinal bending moments were not affected. In the case of dis-assembly analysis, similar results were obtained for all three cases. Further, in the case of the ultimate load analysis, same results were obtained for all three cases.

13.2.1. STAY CABLES

The cables are modeled as shallow cable elements which are described earlier in Chapter 7. The cable stay steel is assumed to have a bilinear strain hardening material constitutive law defined by the following data.

$$\sigma_y = 245.76 \ ksi \qquad \varepsilon_y = .00847$$
$$\sigma_u = 270.00 \ ksi \qquad \varepsilon_u = .00419$$

The weight density of the cables is constant and is assumed to be

$$\gamma = 2.836 \times 10^{-4} \ kips / in^3$$

Note that the deck node of the cable is slaved to the segment node thereby reducing the number of equilibrium equations and resulting in a much more efficient solution. Each cable consists of a group of ½" diameter strands. Cable size (number of strands) and area of cross section are shown in Table 13.2.

13.2.2. DECK

The deck consists of a steel cellular box girder of uniform cross section as shown in Fig. 13.05. The steel used in the deck is grade 50, A572, [73].

The deck is modeled as fiber beam-column elements discussed in Chapter 8. Each element has 4 control sections, two at each end and at ¼ and ¾ of the element length. Each section is discretized into 40 steel fibers. The area and location of each fiber (Y and Z coordinates) are input to the computer program; see Appendix B.

The reference axis of each beam-column element is defined by the line connecting the I and J nodes and lies in the top surface of the deck along the center line of the bridge. It is very important to note that all bending moments and forces in the deck are reported with respect to the reference axis.

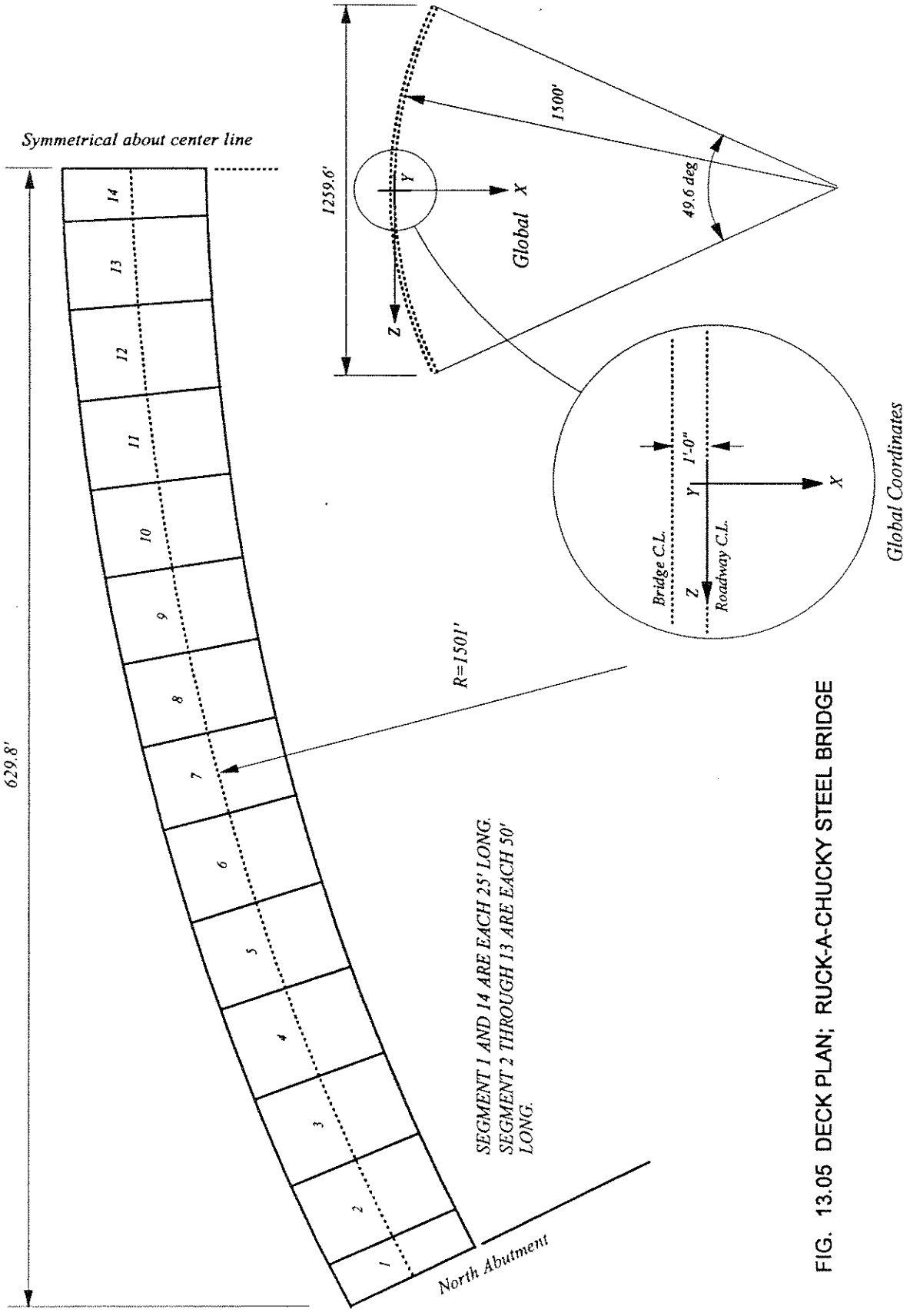

FIG. 13.05 DECK PLAN; RUCK-A-CHUCKY STEEL BRIDGE

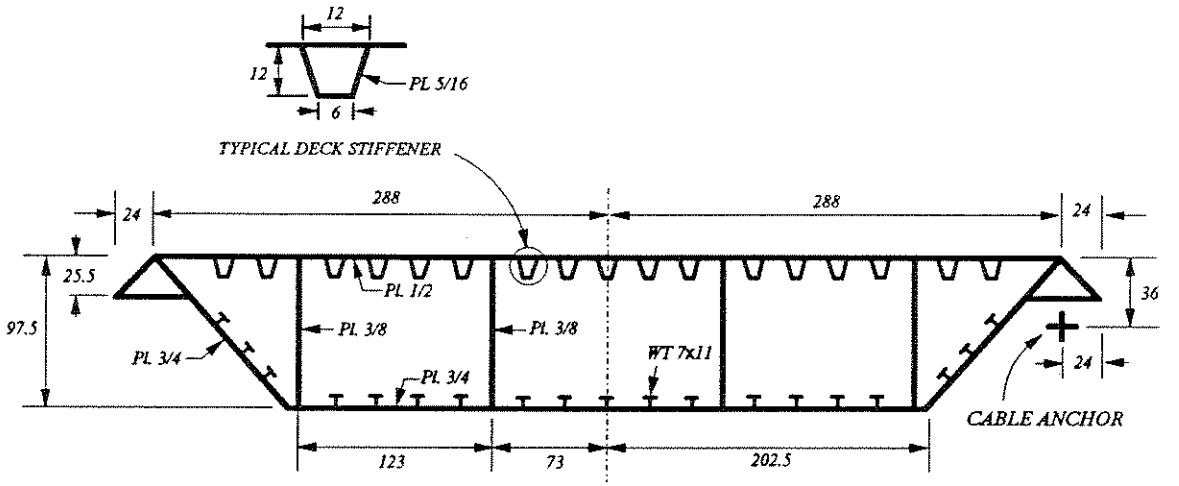

TYPICAL DECK ELEMENT SECTION

ALL DIMENSIONS IN INCHES

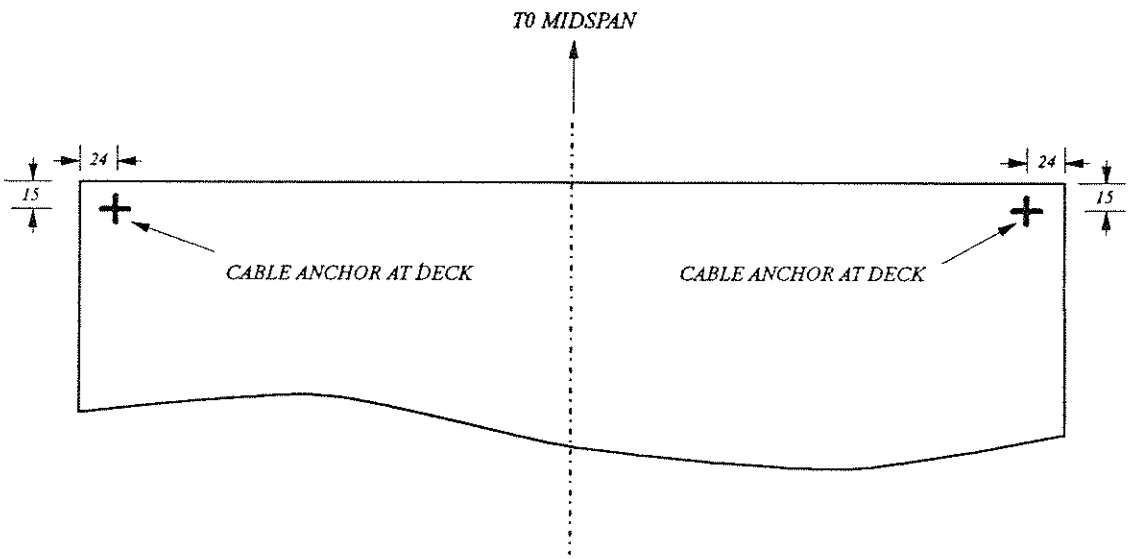

PLAN VIEW OF TYPICAL DECK ELEMENT

ALL DIMENSIONS IN INCHES

FIG. 13.06 TYPICAL DECK ELEMENT AND POSITION OF CABLE ANCHOR

A bilinear strain hardening steel model is assumed, pertinent data are as follows.

$\sigma_y = 50\ ksi \qquad E = 29000$

$E_{sh} = 100\ ksi \qquad \varepsilon_u = .20$

13.2.3. LOAD PATTERN

A dead load of 7.09 kips per ft along the length of the deck was assumed based on a value reported by Godden [34]. This load consists of the segment self weight and superimposed loads. The self weight includes the weight of the deck segment, transverse diaphragms, and splice plates whereas the superimposed load consists of the pavement and guard rail loads.

For long span bridges, AASHTO [129] requires a live load of 640 lbs per linear foot of the load lane. Live load effects are not considered directly in the present study.

The dead load pattern applied to the structure includes the dead loads from the bridge deck and the self weight of the cable-stays.

Structure Dead Loads

Node No.	*Load (kips)*
2	266
3	380
4	380
5	380
6	380
7	380
8	380
9	380
10	380
11	380
12	380
13	380
14	203

13.3. LOAD BALANCING ANALYSIS

For a two dimensional structure, cable tensions can be set directly to balance the applied load. However for a three dimensional structure the problem is more complex. Consider Fig. 13.07, which shows a plan view of a deck segment supported by two cables. The axial force in each cable can be resolved into three components:

1. Vertical component, $T\sin\theta$.
2. Tangential component, $T\cos\gamma$.
3. Radial component, $T\sin\gamma$.

where angles θ and γ are as defined in Fig. 13.07.

A number of conditions may be considered to evaluate a suitable set of values for the two cable tensions T_1 and T_2. The following four conditions were considered in this study.

1. The vertical components of the two cables must equal the weight of the segment.
$$T_1\sin\theta_1 + T_2\sin\theta_2 = W \tag{13.3}$$
2. The vertical components should be equal to each other to reduce torsion in the section.
$$T_1\sin\theta_1 - T_2\sin\theta_2 = 0 \tag{13.4}$$
3. The radial components should cancel out to reduce transverse bending.
$$T_1\sin\gamma_1 + T_2\sin\gamma_2 = 0 \tag{13.5}$$
4. The tangential components should be equal to each other to reduce transverse bending and to direct axial force along the center line of the bridge deck.
$$T_1\cos\gamma_1 - T_2\cos\gamma_2 = 0 \tag{13.6}$$

The four equations given above may be expressed as follows:

$$[\mathbf{A}]_{4\times2}\ [\mathbf{T}]_{2\times1} = [\mathbf{B}]_{4\times1} \tag{13.7}$$

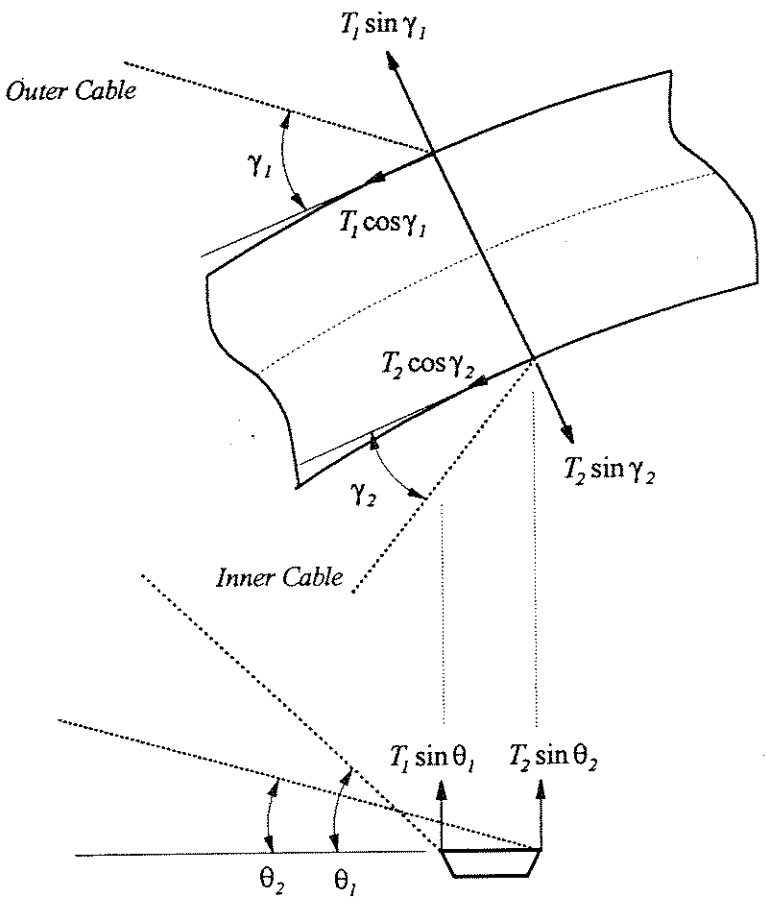

FIG. 13.07 CABLE TENSIONS; LOAD BALANCING

where

$$\mathbf{A}=\begin{pmatrix}\sin\theta_1 & \sin\theta_2\\ \sin\theta_1 & -\sin\theta_2\\ \sin\gamma_1 & \sin\gamma_2\\ \cos\gamma_1 & -\cos\gamma_2\end{pmatrix} \qquad \mathbf{B}=\begin{pmatrix}W\\ 0\\ 0\\ 0\end{pmatrix} \qquad \mathbf{T}=\begin{pmatrix}T_1\\ T_2\end{pmatrix}$$

Note that only two equations are necessary to find the value of T_1 and T_2. Eq. 13.3 must be satisfied and one or more of the remaining equations may be employed. For more than two conditions, a least squares approach is employed.

$$[\mathbf{T}]=\left[\mathbf{A}^{\mathrm{T}}\mathbf{A}\right]^{-1}\left[\mathbf{A}^{\mathrm{T}}\mathbf{B}\right] \tag{13.8}$$

One set of equations was solved for each segment. The forces thus obtained were used as input to the computer program CALBRG. The magnitude of deflections in the bridge deck under the action of these forces were used as criteria to select a suitable set of cable tension. The results were found to be unsatisfactory.

The number of conditions was reduced to three and then to two and various combinations were tried. Finally, it was found that conditions 1 and 4 gave the best results, that is the vertical component of the cable forces must balance the vertical load and the tangential components should be equal. These cable tensions were then adjusted slightly by iteration to bring the bridge to the desired profile and are reported in Table 13.3 and shown in Fig. 13.08. A comparison of segment dead loads versus the final cable tensions is shown in Fig. 13.09.

The resulting vertical and transverse displacements of the deck are shown in Fig. 13.10 and 13.11. Vertical displacement at mid span is less than 0.1 in. Maximum value of vertical displacement does not exceed 1 in. Maximum transverse displacement is of the order of 0.7 in and occurs at mid span.

Longitudinal bending moments in the deck are shown in Fig 13.12. Note that these moments are summed at the top edge of the section. The step in the bending moment diagram is due

to eccentricity of the cable forces as the cables are hooked to the deck 36 in. below the reference surface. Maximum bending moment occurs at the abutment section.

The distribution of transverse bending moments is shown in Fig. 13.13. The maximum value occurs at the abutment section and it is about 50 times larger than the longitudinal bending moment at that section. This is because of the fact that unlike vertical loads which are balanced by cable tensions, substantial unbalanced transverse forces exist in the system. These transverse forces are caused by the unbalance in the horizontal components of the cable forces acting on a deck segment.

The distribution of torsional and axial forces in the bridge deck is shown in Fig. 13.14 and 13.15. Most of the deck is subjected to compressive axial forces, the mid span closure segment is in tension, as might be expected.

Under balanced load conditions cable stresses vary from 80 ksi to 94 ksi, which is about 30 to 35% of the ultimate tensile strength of the cable (270 ksi). Note that the usual permissible stress for parallel strand cables is 50% of the ultimate tensile strength.

Maximum longitudinal stresses in the deck girder occur at the abutment section. Because of the heavy axial force at the abutment section all stresses are compressive. A summary of stresses at the abutment section is given below:

Top outer corner	*14 ksi*
Top inner corner	*5 ksi*
Bottom outer corner	*14 ksi*
Bottom inner corner	*9 ksi*

TABLE 13.03

CABLE TENSIONS

Cable No.	*Element No.*	*Balanced Tension (kips)*	*Adjusted Tension (kips)*
2NO	1	546.1	562.5
3NO	3	560.8	577.6
4NO	5	570.7	587.8
5NO	7	565.7	582.7
6NO	9	560.3	577.1
7NO	11	568.6	585.4
8NO	13	554.2	570.8
9No	15	573.1	590.3
10No	17	586.3	603.9
11NO	19	602.3	620.4
12NO	21	622.0	640.7
13NO	23	631.8	650.8
2NI	2	651.6	671.2
3NI	4	650.1	669.6
4NI	6	643.8	663.1
5NI	8	625.6	644.4
6NI	10	608.6	626.9
7NI	12	608.2	626.5
8NI	14	585.6	603.2
9NI	16	599.6	617.6
10NI	18	609.5	627.8
11NI	20	619.9	638.5
12NI	22	640.8	660.0
13NI	24	647.6	667.0

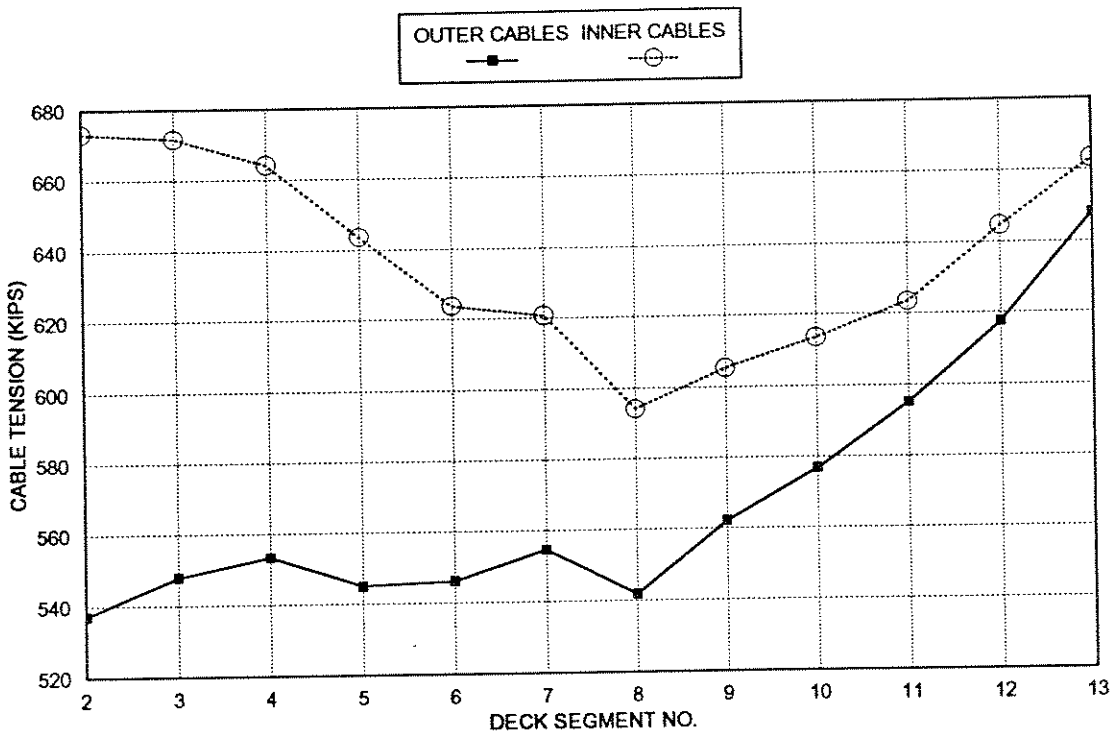

FIG. 13.08 CABLE FORCES; LOAD BALANCING ANALYSIS
RUCK-A-CHUCKY STEEL BRIDGE

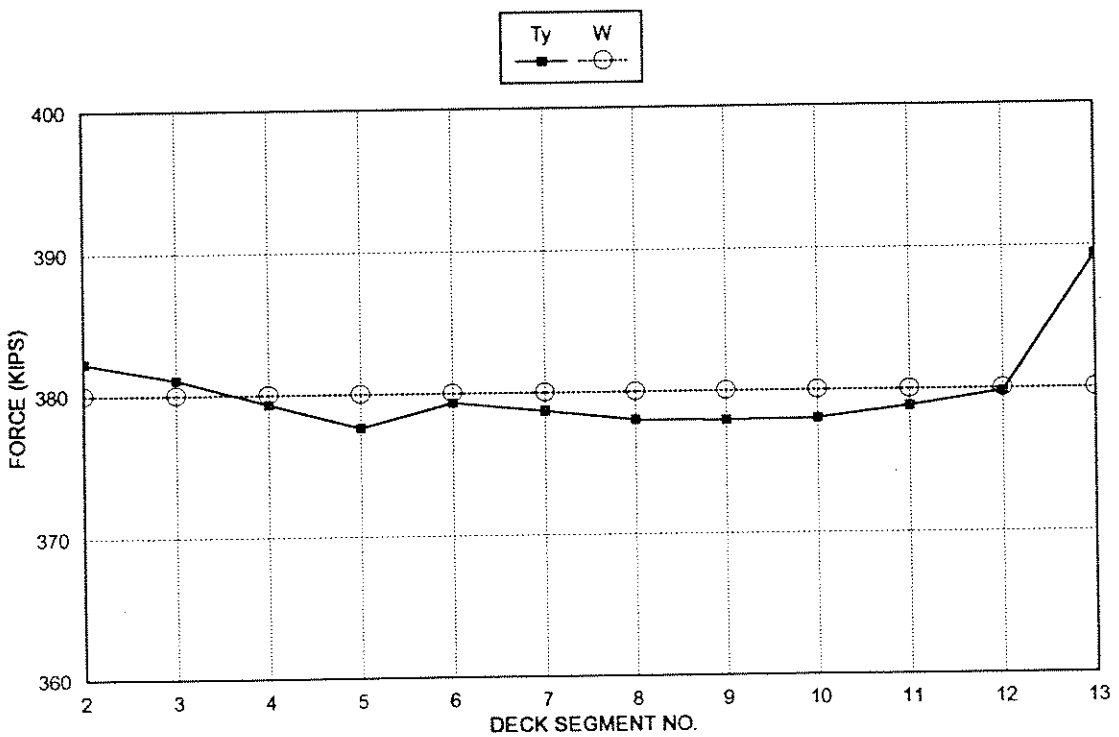

FIG. 13.09 VERTICAL COMPONENT OF CABLE FORCES AND SEGMENT LOADS
LOAD BALANCING ANALYSIS; RUCK-A-CHUCKY STEEL BRIDGE

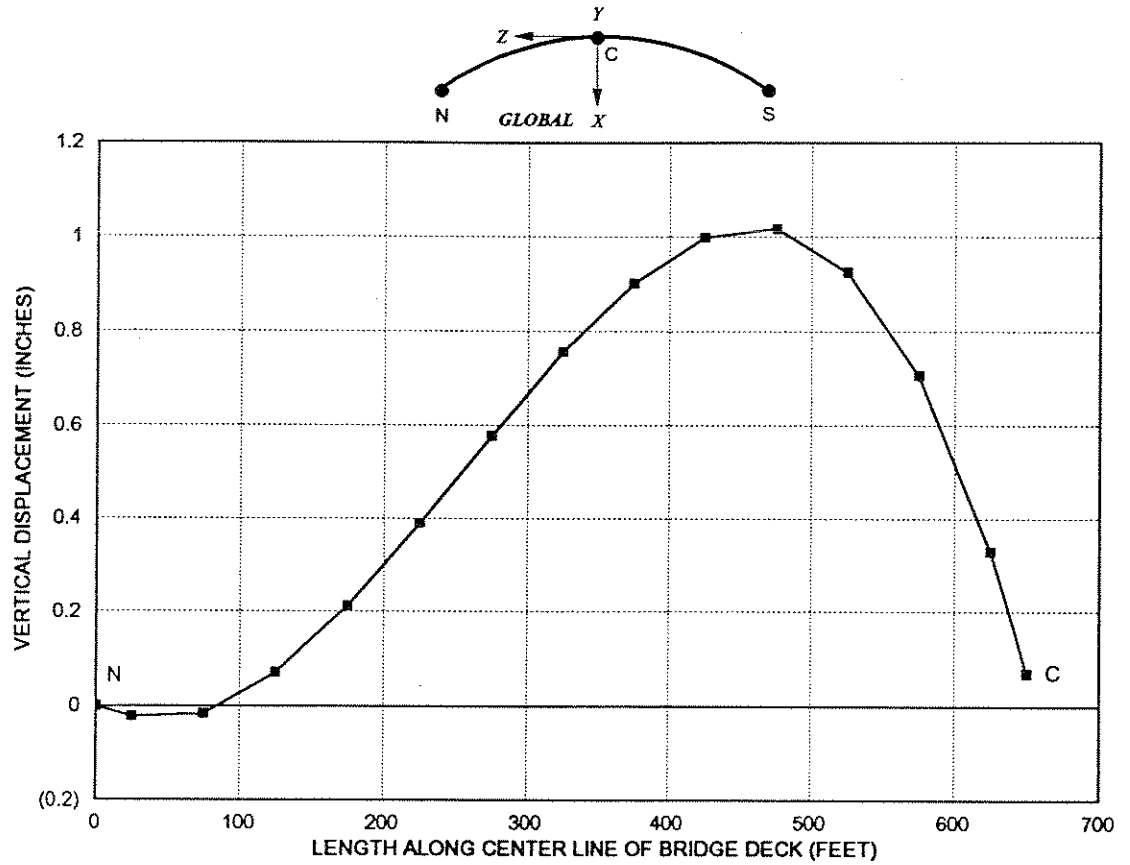

FIG. 13.10 VERTICAL DISPLACEMENTS (DY) OF THE BRIDGE DECK
LOAD BALANCING ANALYSIS; RUCK-A-CHUCKY STEEL BRIDGE

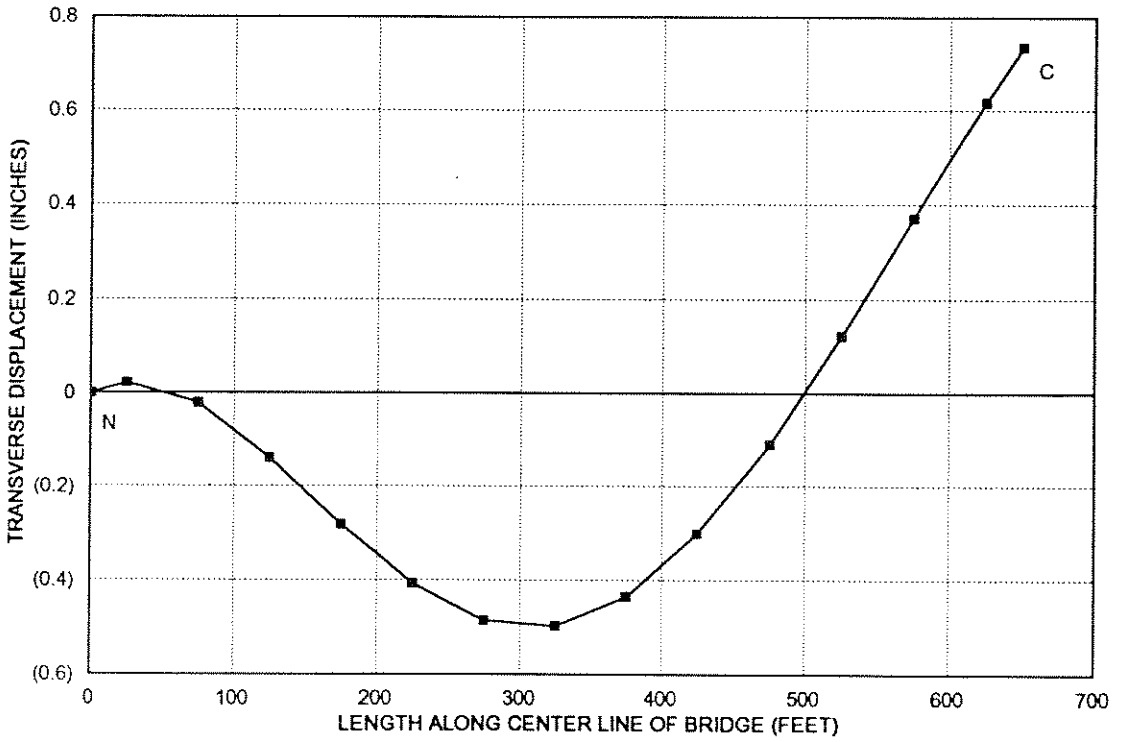

FIG. 13.11 TRANSVERSE DISPLACEMENTS (DX) OF THE BRIDGE DECK
LOAD BALANCING ANALYSIS; RUCK-A-CHUCKY STEEL BRIDGE

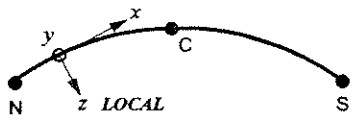

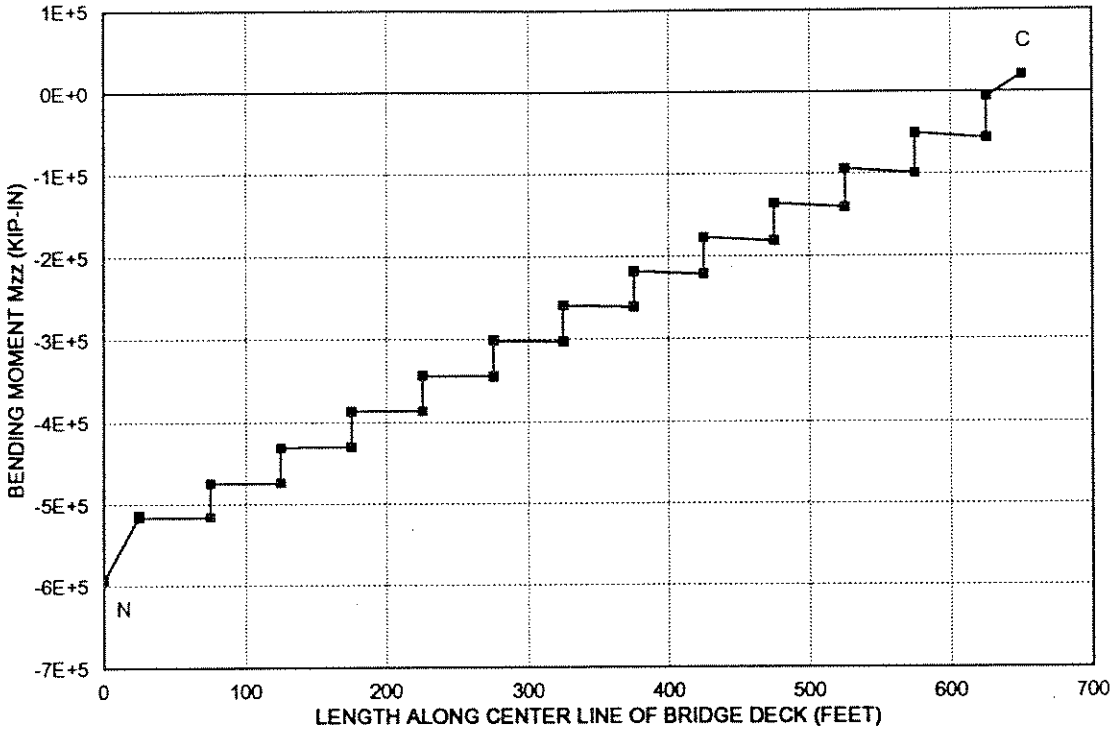

FIG. 13.12 LONGITUDINAL BENDING MOMENT Mzz IN THE BRIDGE DECK
LOAD BALANCING ANALYSIS; RUCK-A-CHUCKY STEEL BRIDGE

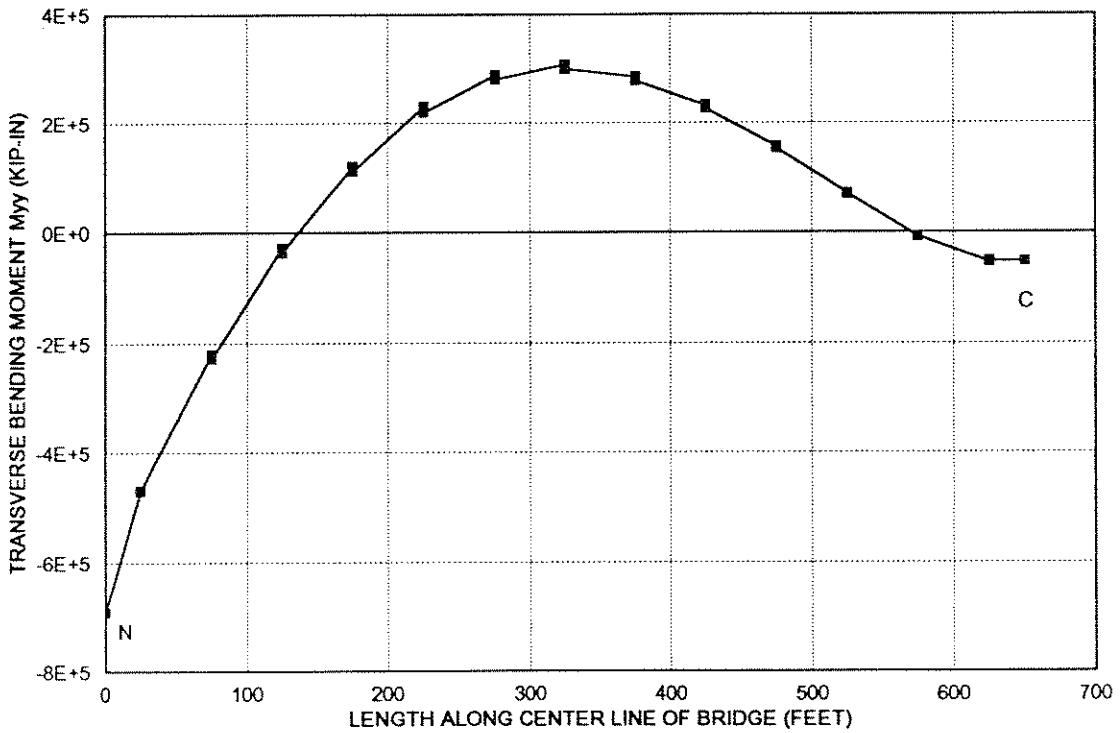

FIG. 13.13 TRANSVERSE BENDING MOMENT Myy IN THE BRIDGE DECK
LOAD BALANCING ANALYSIS; RUCK-A-CHUCKY STEEL BRIDGE

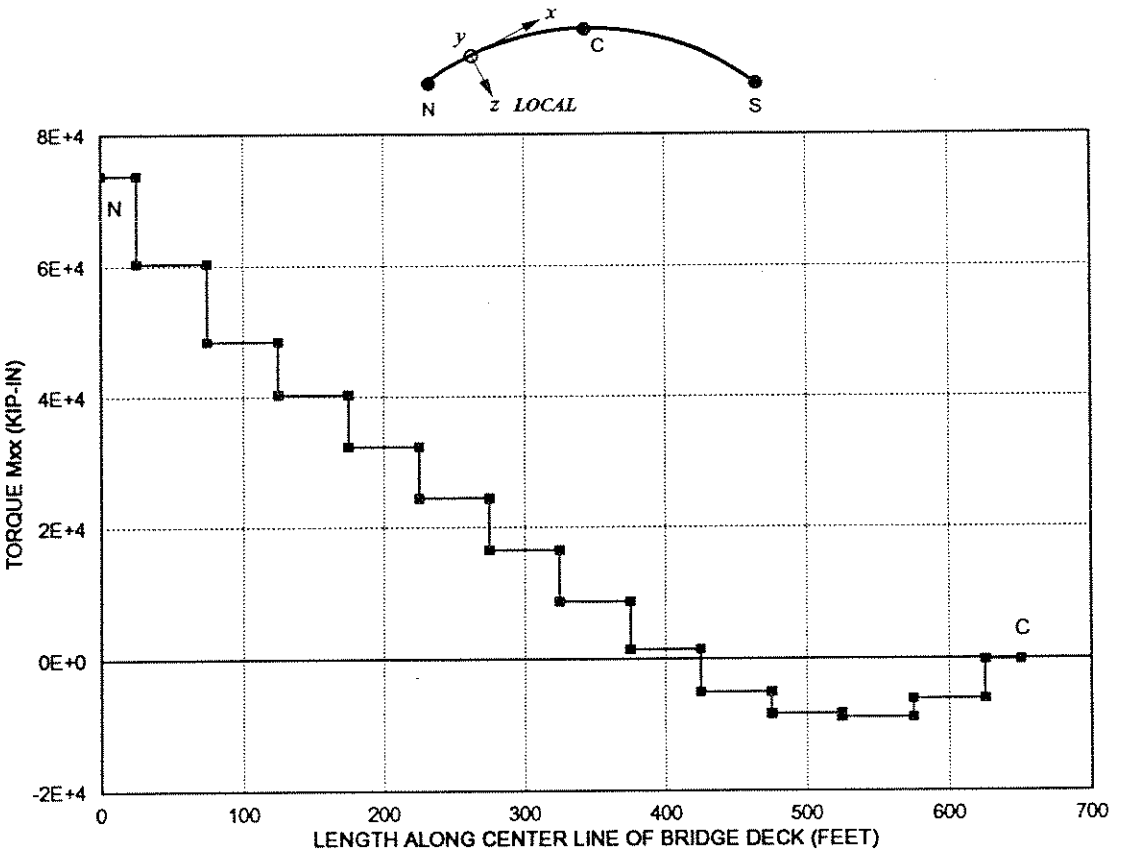

FIG. 13.14 TORQUE Mxx IN THE BRIDGE DECK
LOAD BALANCING ANALYSIS; RUCK-A-CHUCKY STEEL BRIDGE

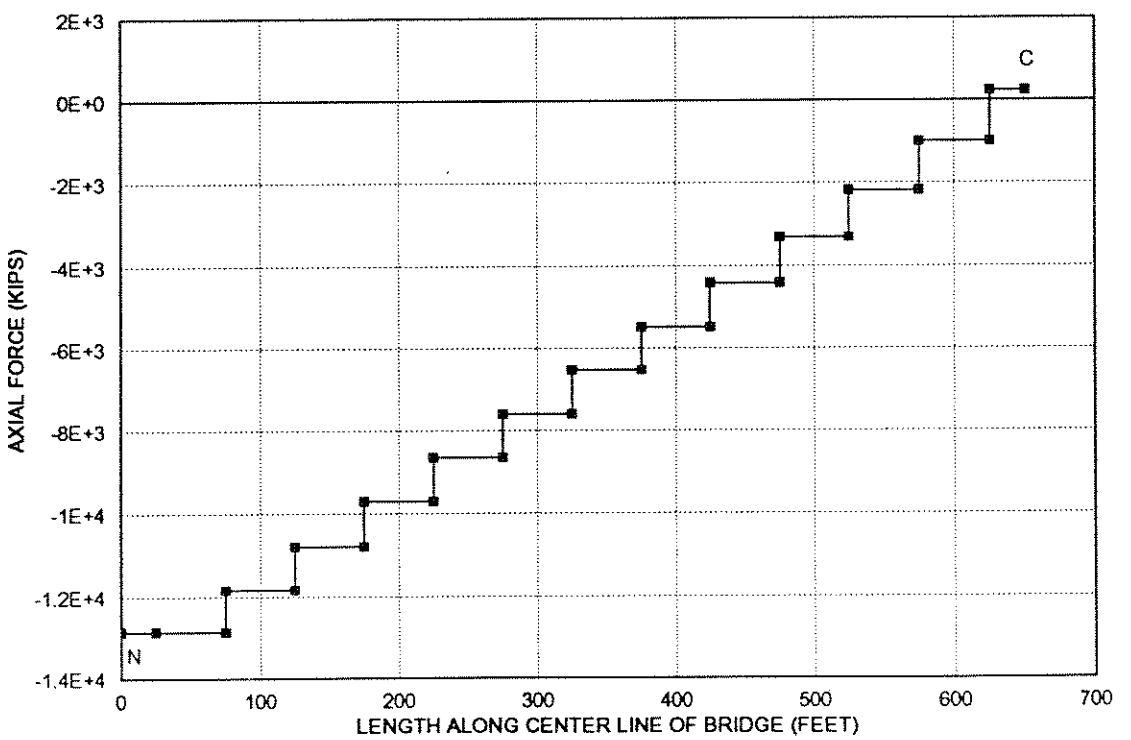

FIG. 13.15 AXIAL FORCE Fx IN THE BRIDGE DECK
LOAD BALANCING ANALYSIS; RUCK-A-CHUCKY STEEL BRIDGE

13.4. DIS-ASSEMBLY ANALYSIS

As described earlier, this analysis simulates the dis-assembly of a completed bridge structure sitting on the designed profile. The construction sequence for the steel bridge is based on a 15 day cycle. The entire bridge is completed in 195 days. The schedule is set out in Table 13.4.

The basic purpose of this type of analysis is get a set of cable forces which can be used in the fabrication of the structure in the field. A set of such initial tensions is shown in Table 13.5. The forces in the leading cables in the assumed cantilever erection sequence are shown in shaded cells and will be used later in the assembly analysis. The variation of cable forces during the dis-assembly procedure is shown in Fig. 13.16. Note that as more deck segments and their supporting cables are taken off the structure, the axial tension decreases in the remaining cables.

Fig. 13.17 and 13.18 show the vertical and transverse displacements of the deck along the centerline of the bridge at each step of the dis-assembly analysis. The line marked 14 shows the position of the structure when the bridge has been built up to segment 13 and cables 23 and 24 have been stressed. Note that cables 13 and 14 are not yet stressed to their full design tensions, this is so because it is desirable to keep the structure perfectly level and aligned with the other half of the bridge.

The dis-assembly analysis is started from this position of the structure. The line marked 13 shows the profile of the deck when segment 13 and cables 23 and 24 have been taken off. Note that the deck moves up about 30 inches and swings inwards towards the center of the bridge arc by 4 inches; this is due to the fact that the leading cable tensions are set to carry the entire load of one segment and at this stage only half of that is applied to the leading node. As the dis-assembly proceeds the structure continues to swing inwards but is held in check by the auxiliary cables, maximum transverse deflection of 7.5 inches occurs when segment 11 and its supporting cables are removed.

Thus we have a complete set of initial cable tensions and bridge profiles at various stages of construction. This data is of great use in the fabrication process of the bridge.

TABLE 13.04

CONSTRUCTION SCHEDULE

TIME DAYS	*ERECT SEGMENT NO.*	*STRESS CABLE NO.*	*REMOVE CABLE NO.*	*COMMENTS*
1	1			abutment
15	2	1, 2		
30	3	3, 4		
30		25		auxiliary cable
45	4	5, 6		
60	5	7, 8		
75	6	9, 10		
90	7	11, 12		
90		26		auxiliary cable
105	8	13, 14		
120	9	15, 16		
135	10	17, 18		
150	11	19, 20		
165	12	21, 22		
180	13	23, 24		
195	14			closure segment
195			25, 26	auxiliary cables

TABLE 13.05

CABLE FORCES (KIPS); DIS-ASSEMBLY ANALYSIS

Stay No.	*BRIDGE BUILT UP TO SEGMENT NO.*											
	13	*12*	*11*	*10*	*9*	*8*	*7*	*6*	*5*	*4*	*3*	*2*
1	537	549	551	552	552	551	548	547	543	542	545	554
2	673	670	666	663	660	658	656	653	654	656	661	667
3	548	561	561	560	557	551	544	540	535	536	547	
4	672	665	659	652	647	642	638	633	634	640	650	
5	554	565	563	559	552	542	530	524	519	524		
6	665	654	644	635	627	619	613	606	609	619		
7	546	551	546	539	528	514	497	491	488			
8	645	629	616	64	594	584	577	568	574			
9	547	543	537	529	517	503	488	485				
10	625	602	587	573	561	549	541	533				
11	556	541	534	524	511	496	481					
12	623	592	576	561	548	537	528					
13	543	516	507	496	481	468						
14	597	551	531	514	499	487						
15	564	522	514	504	492							
16	608	546	526	508	493							
17	579	522	515	507								
18	617	539	518	502								
19	598	526	521									
20	627	535	518									
21	620	535										
22	649	540										
23	334											
24	349											
25	12	14	15	17	18	19	19	21	19	18	16	
26	68	84	109	133	145	147	138					

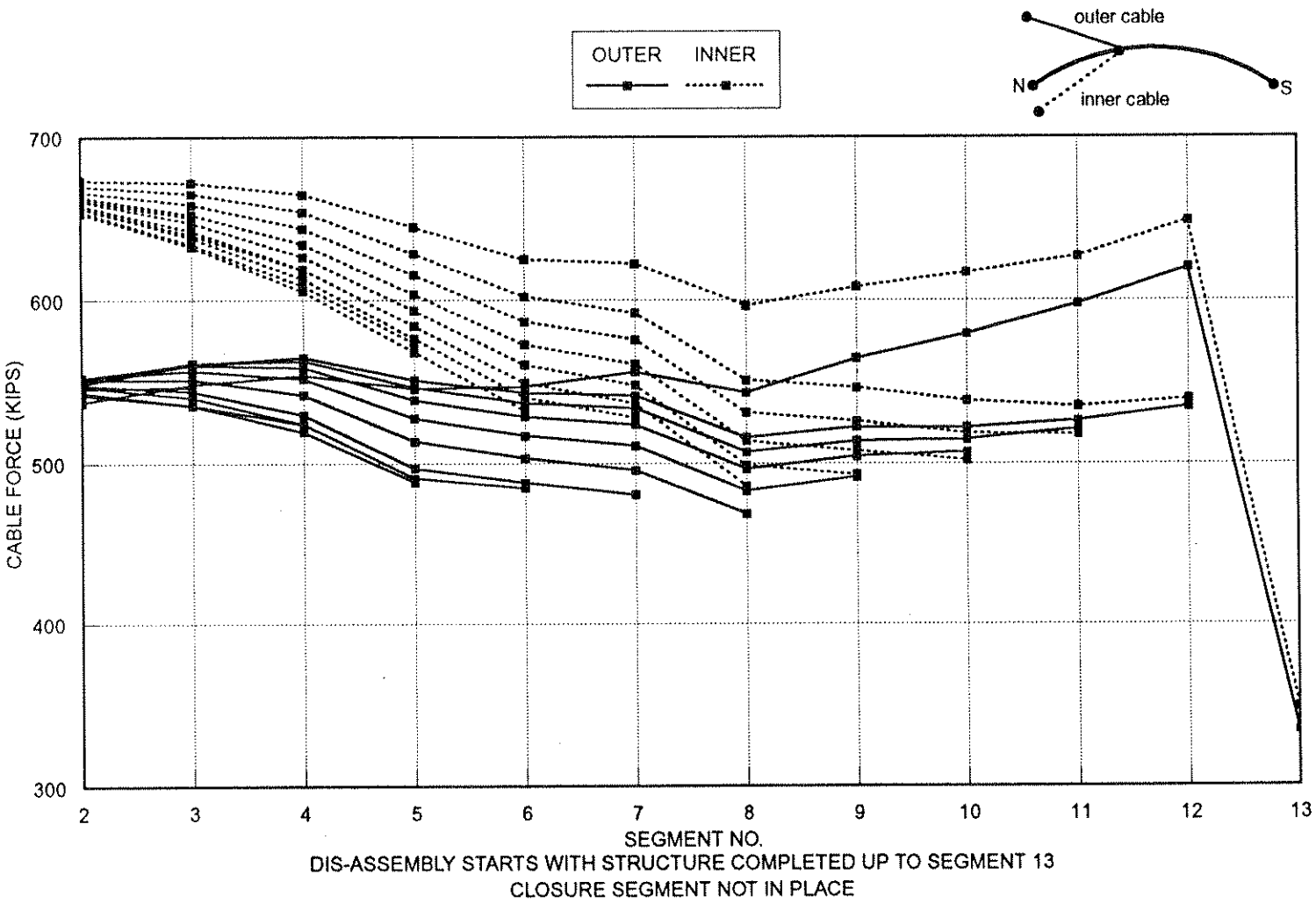

FIG. 13.16 CABLE FORCES; DIS-ASSEMBLY ANALYSIS
RUCK-A-CHUCKY STEEL BRIDGE

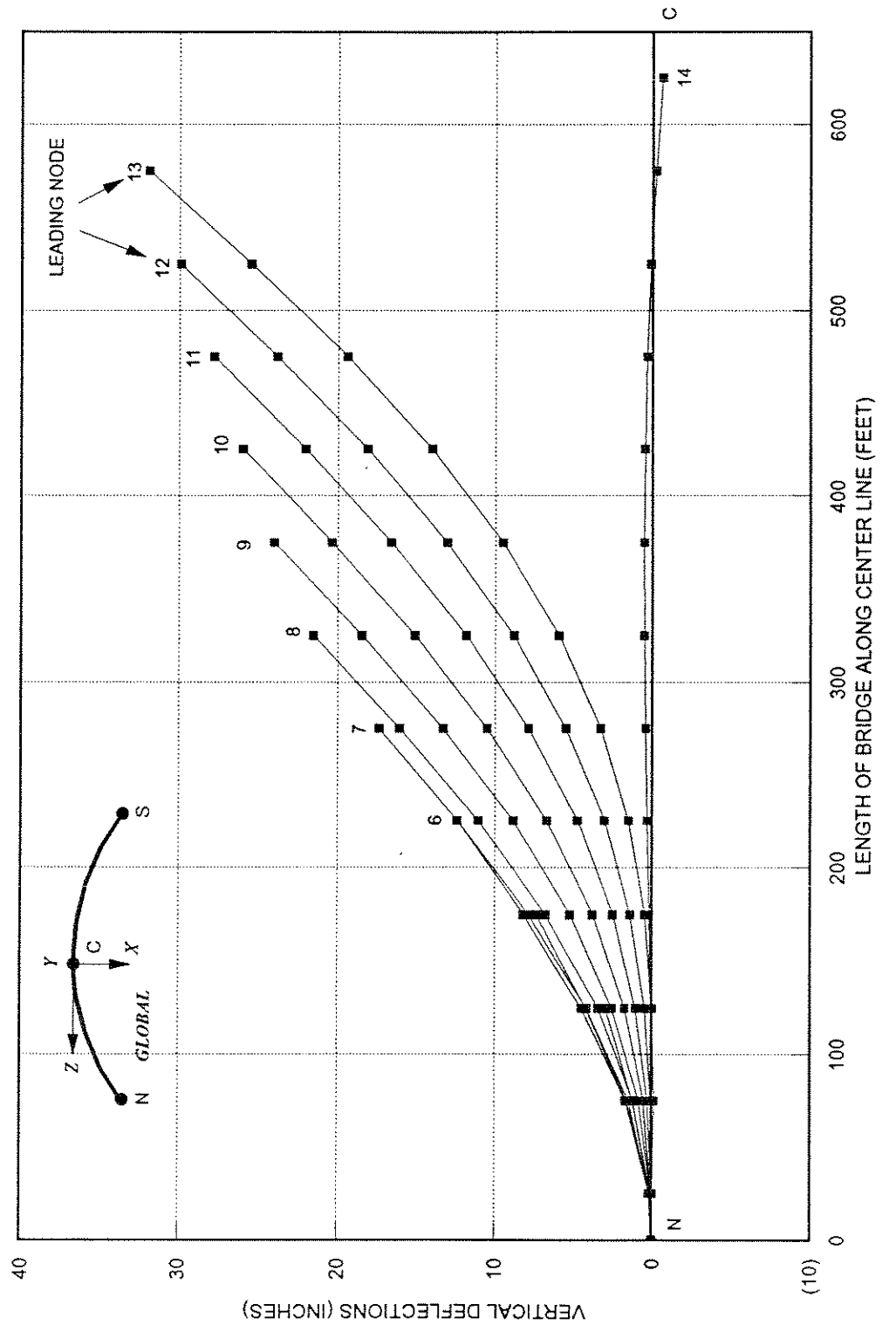

FIG. 13.17 VERTICAL DEFLECTIONS (DY); DIS-ASSEMBLY ANALYSIS
RUCK-A-CHUCKY STEEL BRIDGE

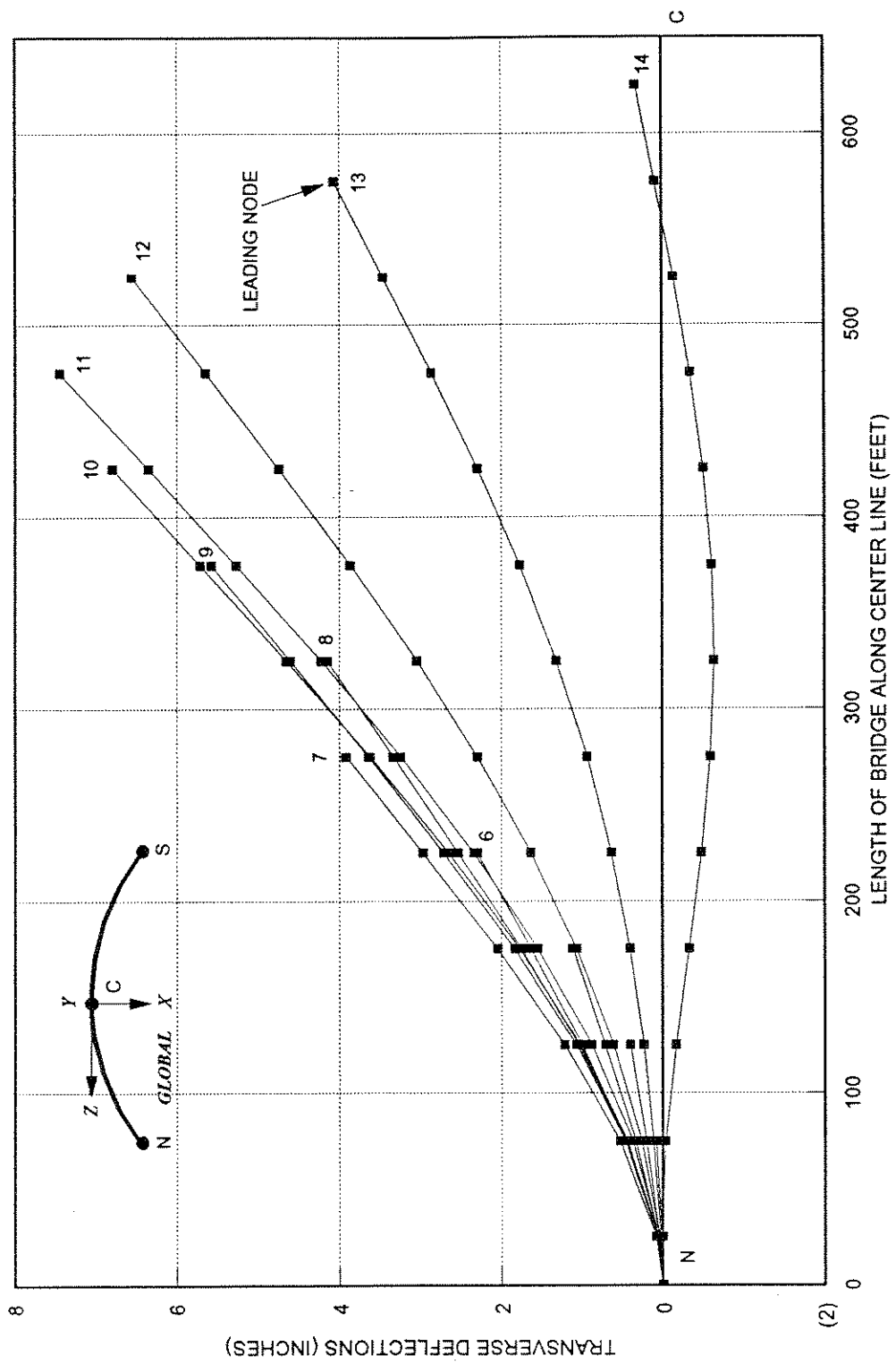

FIG. 13.18 TRANSVERSE DEFLECTIONS (DX); DIS-ASSEMBLY ANALYSIS
RUCK-A-CHUCKY STEEL BRIDGE

13.5. CONSTRUCTION SEQUENCE ANALYSIS

The construction sequence analysis was done essentially to verify the results of the disassembly analysis. Again the segmental analysis capabilities of the program CALBRG were utilized and the structure was assembled in accordance with the scheme discussed in the previous section. However in this case the closure segment 14 was installed, tensions in cables 23 and 24 adjusted to their full values and symmetry boundary conditions applied at node 15.

The resulting vertical and transverse profiles are shown in Fig. 13.19 and 13.20. As expected, these turned out be similar to those obtained by the disassembly analysis. Note that at completion, the vertical and horizontal displacements of the bridge deck are within ±2 in of the desired profile.

Fig. 13.21 shows tensions in the inner and outer cables at the completion of the construction. The forces in the inner cables are much higher close to the abutment as compared to the outer cables. This is due to the relatively shallow angle of rise of the inner cables, 16 degrees for the inner cables as opposed to 22 degrees for the outer cables. Towards the middle of the bridge the difference in the cable tensions decreases and the two plots tend to move closer.

EFFECT OF AUXILIARY CABLES

The purpose of horizontal auxiliary cables is to prevent excessive inward movement of the bridge deck during construction. In order to investigate the effectiveness of auxiliary cables, the bridge was assembled without the auxiliary cables and the consequent transverse and vertical deflections were compared with earlier analyses which included the use of auxiliary cables.

The two cases are compared in Fig. 13.22 and 13.23. If auxiliary cables are not used, the transverse deflections increase six times to about 6 in., whereas the vertical deflections increase from 0 to 4 in.

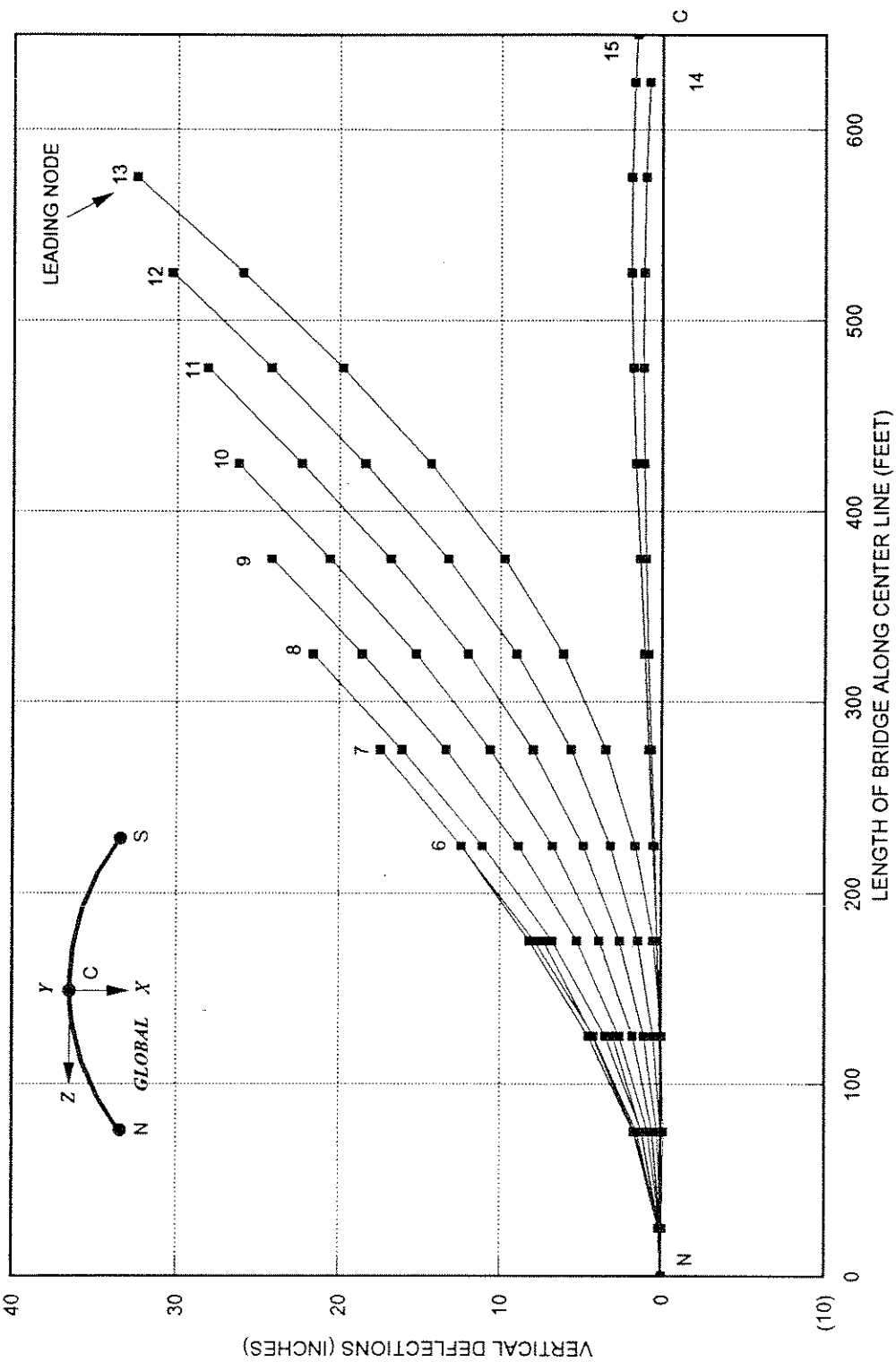

FIG. 13.19 VERTICAL DEFLECTIONS (DY); CONSTRUCTION SEQUENCE ANALYSIS
RUCK-A-CHUCKY STEEL BRIDGE

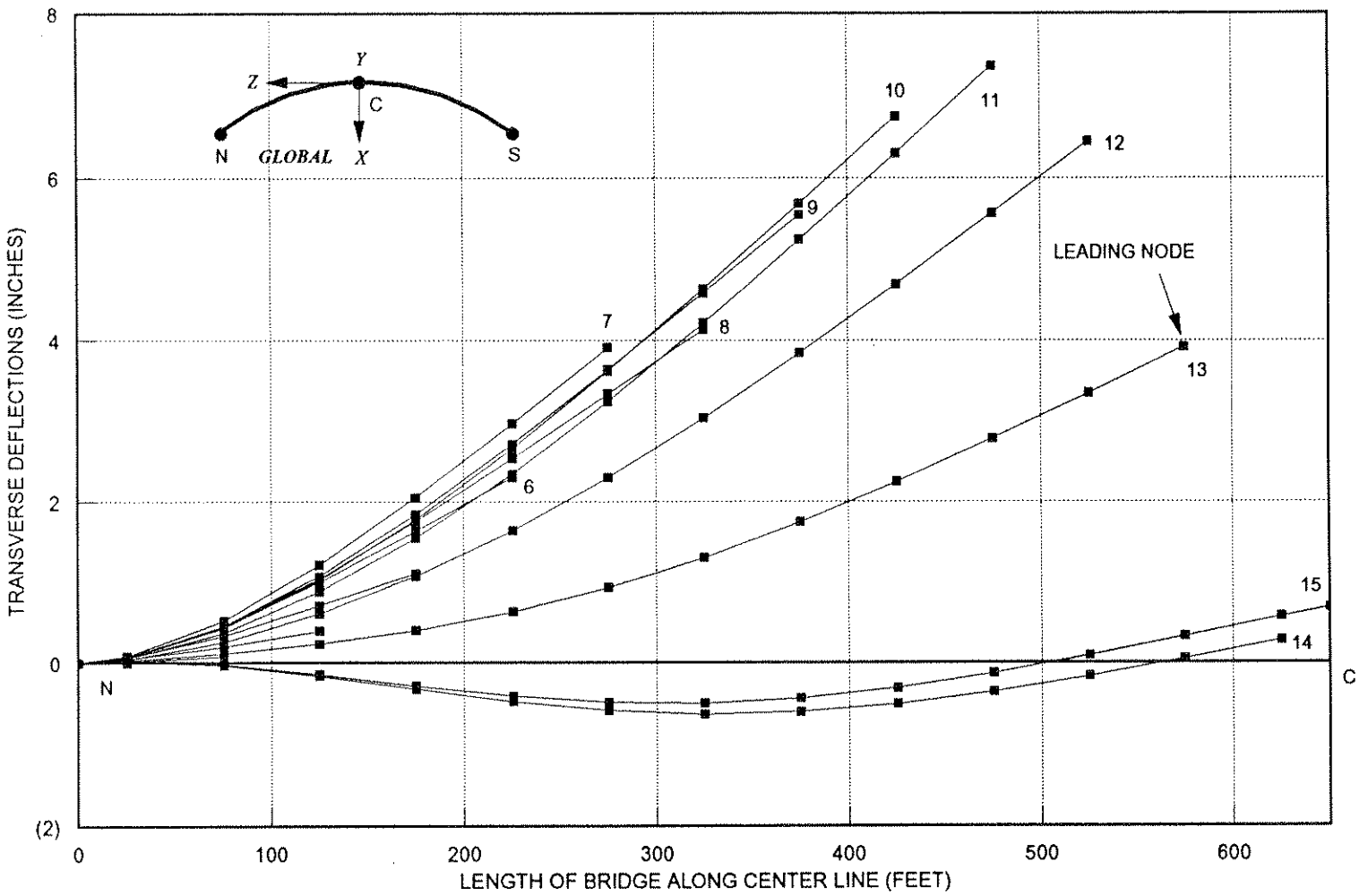

FIG. 13.20 TRANSVERSE DEFLECTIONS (DX); CONSTRUCTION SEQUENCE ANALYSIS
RUCK-A-CHUCKY STEEL BRIDGE

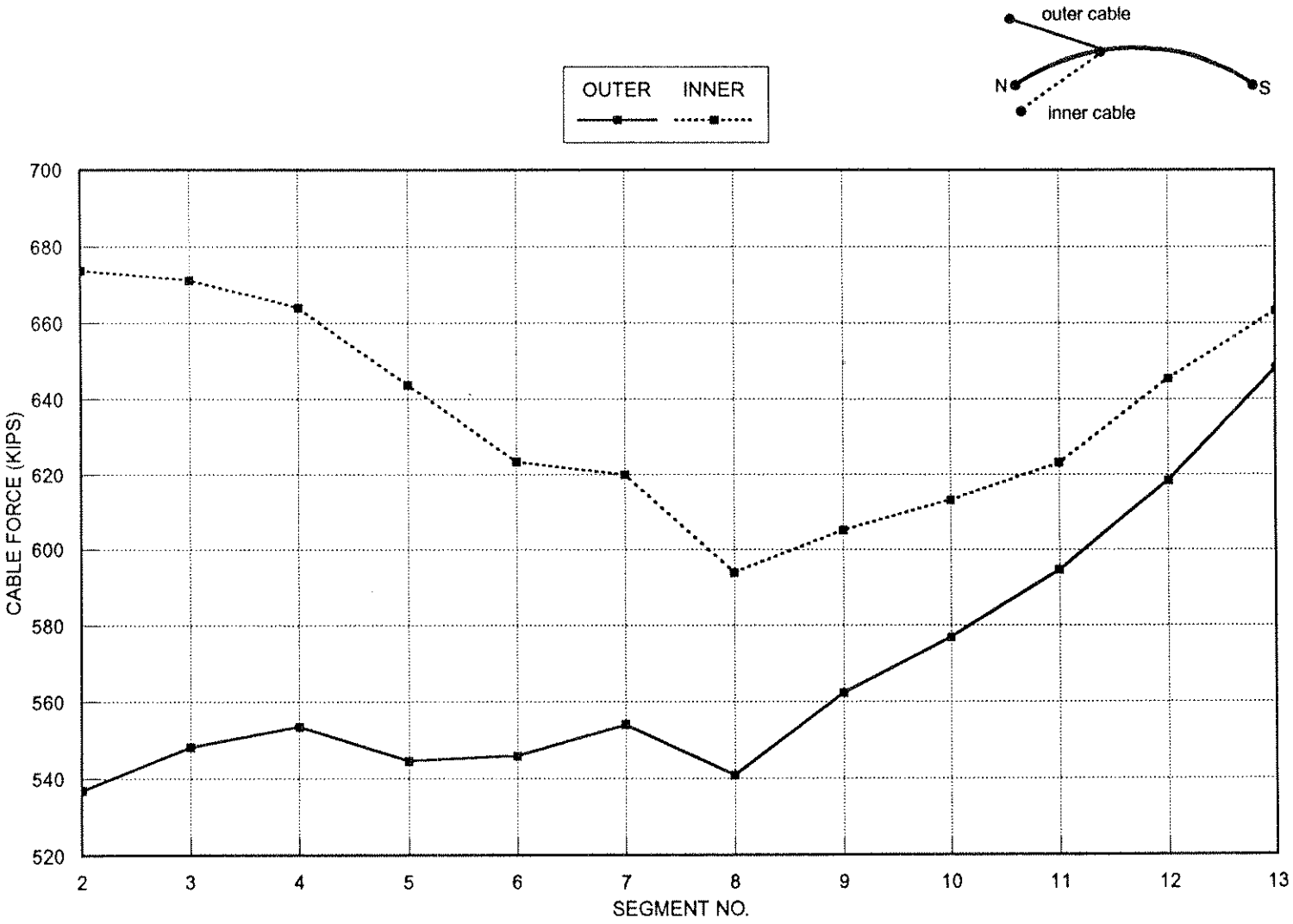

FIG. 13.21 CABLE FORCES AT CLOSURE; CONSTRUCTION SEQUENCE ANALYSIS
RUCK-A-CHUCKY STEEL BRIDGE

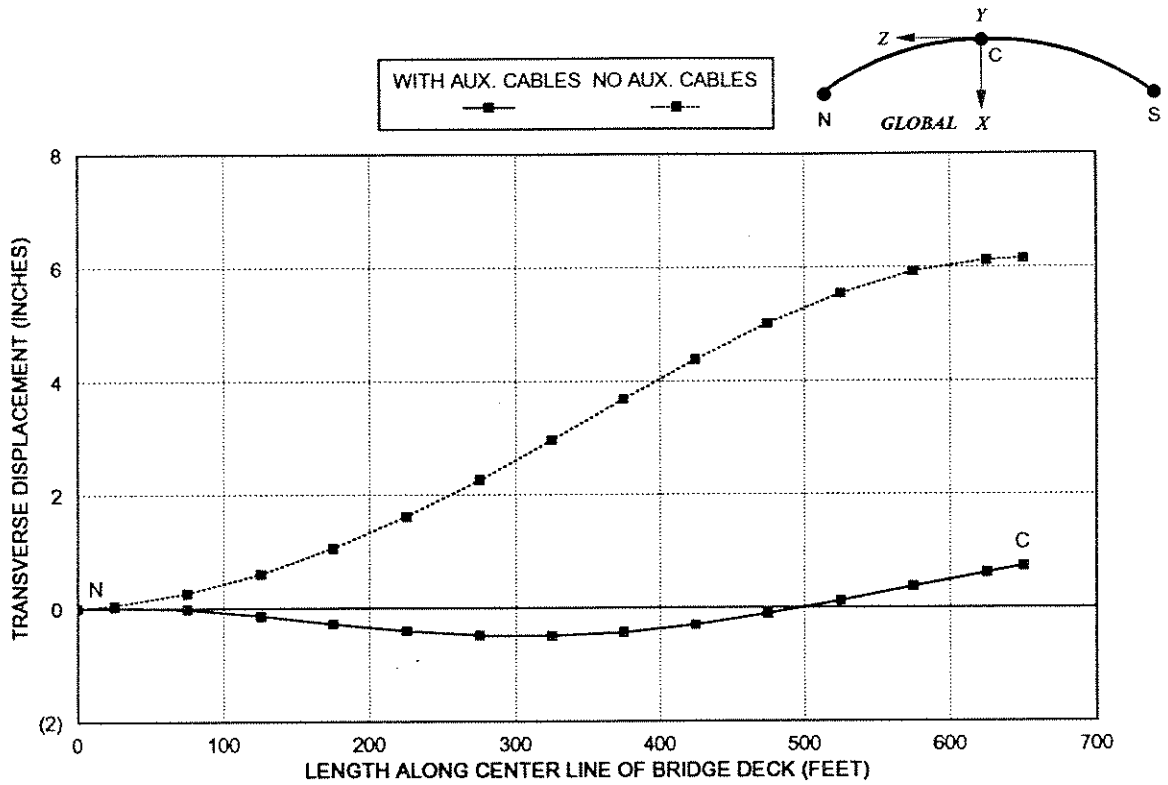

FIG. 13.22 TRANSVERSE DISPLACEMENTS (DX) OF THE BRIDGE DECK
EFFECT OF AUXILIARY CABLES; RUCK-A-CHUCKY STEEL BRIDGE

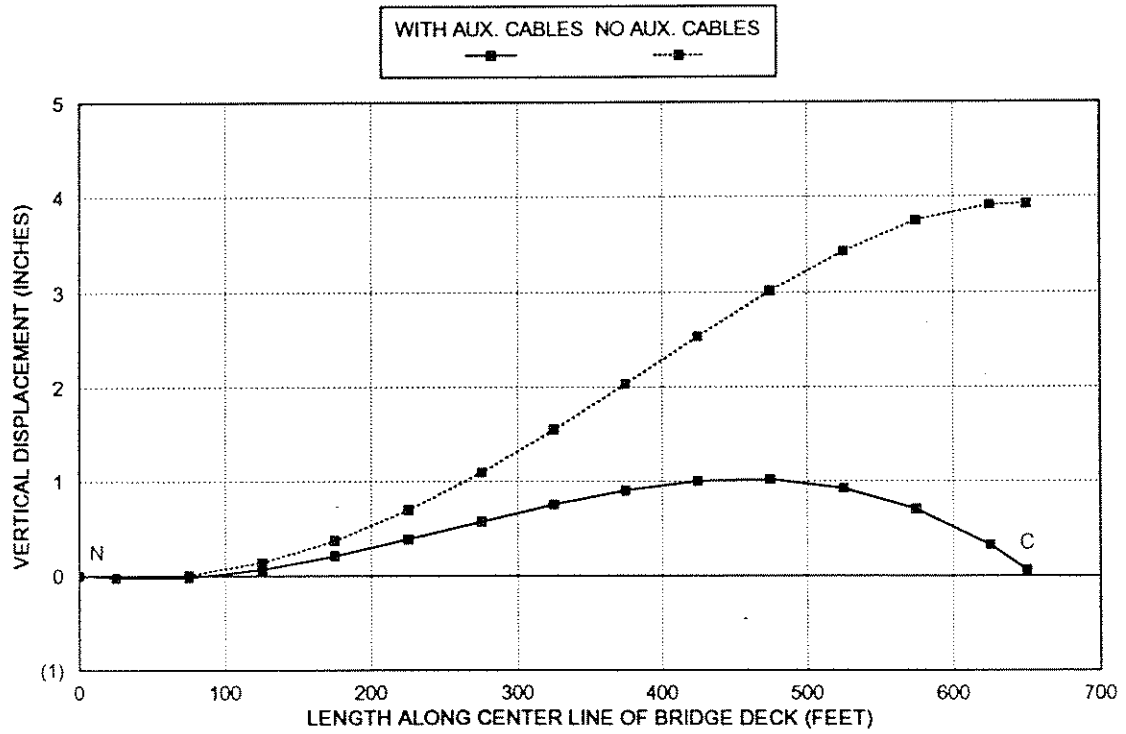

FIG. 13.23 VERTICAL DISPLACEMENTS (DY) OF THE BRIDGE DECK
EFFECT OF AUXILIARY CABLES; RUCK-A-CHUCKY STEEL BRIDGE

13.6. ULTIMATE LOAD ANALYSIS

Ultimate load analysis is carried out on the completed bridge. A load pattern corresponding to the dead load pattern is applied to the structure. A displacement controlled solution is carried out using the DISPCON algorithm implemented in the computer program CALBRG. The vertical displacement of the midspan node 15 is selected as the controlled degree of freedom. A displacement increment of 10 in is specified for each step and results are output after every 10 steps. Later, as the structure begins to yield the displacement increment is reduced.

Transverse displacements (Dx) of the midspan node 15 are plotted against the dead load multiplier in Fig 13.24. The plot shows that the structure yields gradually as the load is increased to 2.5 times the dead load; this point is marked A on the plot and corresponds to a transverse displacement of 3.5 ft. As the load is increased further the structure exhibits a substantially reduced stiffness until it reaches point B corresponding to a displacement of 5.9 ft. From this point onwards the curve becomes more or less flat and the structure continues to deform in a ductile manner without any substantial increase in the load until finally the load carrying capacity of the structure is exhausted at a transverse displacement (Dx) of about 18.8 ft. The failure load is about 2.6 times the dead load (2.6 D) of the structure. The average dead load (deck+cables) applied to the structure is 7.2 kips/ft. Assuming a live load of 640 lbs per ft. of load lane, as prescribed by AASHTO [129], the failure load is 1.4D+6.6L or D+8.8L.

The vertical displacements (Dy) show a similar trend, Fig. 13.25. The structure behaves linearly up to a displacement of 25 ft., at which point the steel deck yields at the abutment section under the combined action of biaxial moments and axial load. At a vertical displacement of 33 ft., some of the stay cables begin to yield and finally at a vertical displacement of 63 ft. the structure reaches its ultimate load carrying capacity.

The transverse displacements (Dx) of the bridge deck along the center line of the bridge are shown in Fig. 13.26. Vertical displacements (Dy) are shown in Fig. 13.27.

Fig. 13.28 shows a comparison of axial tensions in the inner and outer cables at dead and ultimate loads. Note that in general the cable forces increased to about 2.75 times their dead load tensions. However the inside cables close to the abutment did not follow the general trend; this is because of the relatively larger horizontal angle of these cables which tended to cancel out the net effect of the deck displacements.

Next we discuss the variation of moments and forces in the bridge deck; note that these are plotted at the level of the reference axis of the element in member local coordinates using beam sign convention. Plots are presented both at the dead load and at ultimate load to illustrate the physical behavior of the structure and changes in the distribution of moments.

Fig. 13.29 shows the variation of the longitudinal bending moment M_{zz} along the center line of the deck. At ultimate load, the peak value of M_{zz} of 2,500,000 occurs at the abutment section, which is more than 4 times the dead load value of M_{zz}. Under the action of the dead loads alone, M_{zz} has negative values through out the length of the bridge, whereas in the case of ultimate load, large positive bending moments M_{zz} exist over most of the bridge except for a small length near the abutment.

The transverse bending moments M_{yy} are plotted in Fig. 13.30. As the load increases from dead to ultimate, the moment at the abutment section changes from -690,000 k-in to +8,400,000 k-in which is an increase of more than 13 times. At the midspan section M_{yy} increase from a negligible value to 8,700,000 k-in.

Fig 13.31 shows the variation of torsion along the center line of the bridge deck. Although at ultimate load torsion increases substantially over its dead load value, it is much lower than the yield torque.

Fig. 13.32 shows a plot of the axial forces at dead load and at ultimate. When the bridge is completed only segment number 14, which is the closure segment, is in tension. At ultimate load most of the middle half of the structure is subjected to tension with a peak value at midspan of 15,000 kips whereas the compressive force at the abutment increases to 20,000 kips.

A detailed examination of the results output by CALBRG indicate that the abutment section was most severely strained. Fig. 13.33 shows fiber states at various section locations along the bridge center line at ultimate load. Fiber stress levels indicate that a plastic hinge had formed at the abutment section and that considerable yielding of fibers had occurred in the outer webs of the deck segments in the midspan zone.

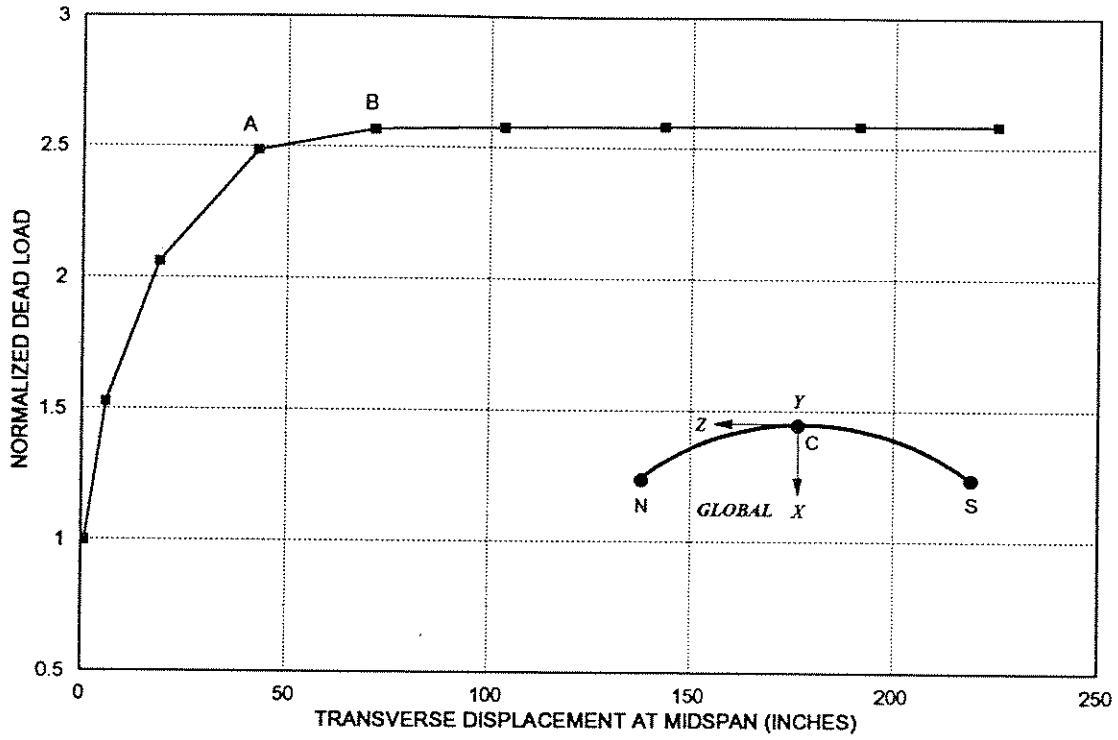

FIG. 13.24 TRANSVERSE DISPLACEMENT (DX) AT MIDSPAN VS NORMALIZED DEAD LOAD ULTIMATE LOAD ANALYSIS; RUCK-A-CHUCKY STEEL BRIDGE

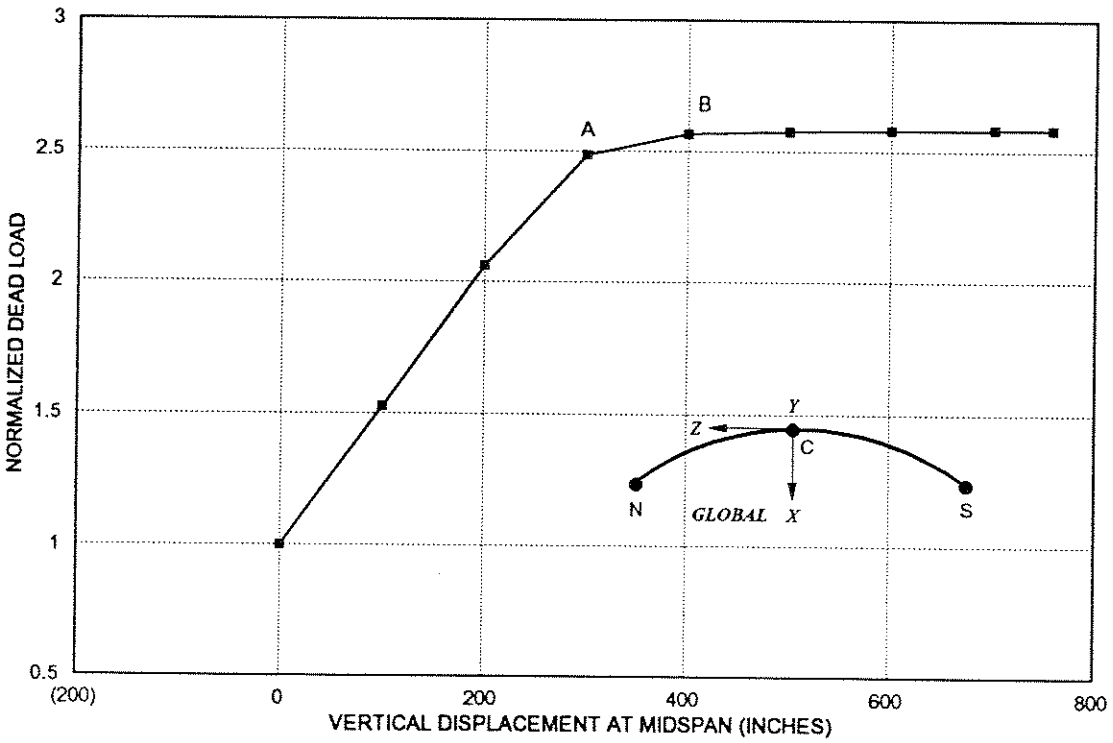

FIG. 13.25 VERTICAL DISPLACEMENT (DY) AT MIDSPAN VS NORMALIZED DEAD LOAD ULTIMATE LOAD ANALYSIS; RUCK-A-CHUCKY STEEL BRIDGE

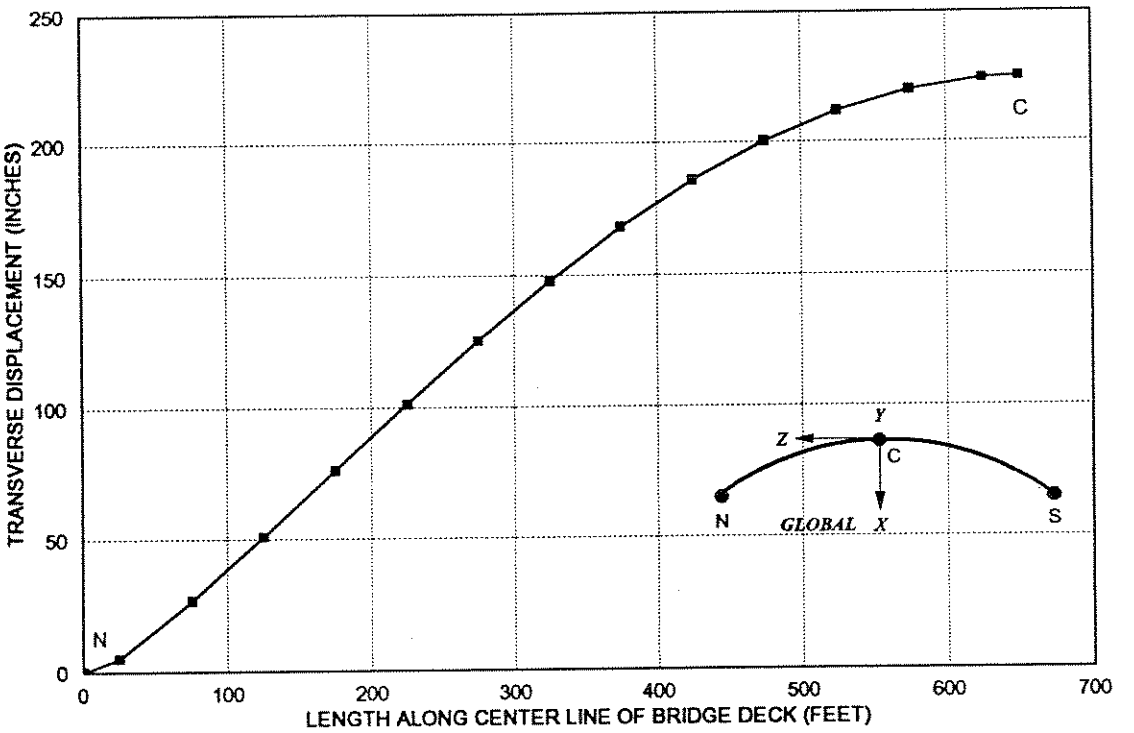

FIG. 13.26 TRANSVERSE DISPLACEMENTS (DX) OF THE BRIDGE DECK AT ULTIMATE LOAD
ULTIMATE LOAD ANALYSIS; RUCK-A-CHUCKY STEEL BRIDGE

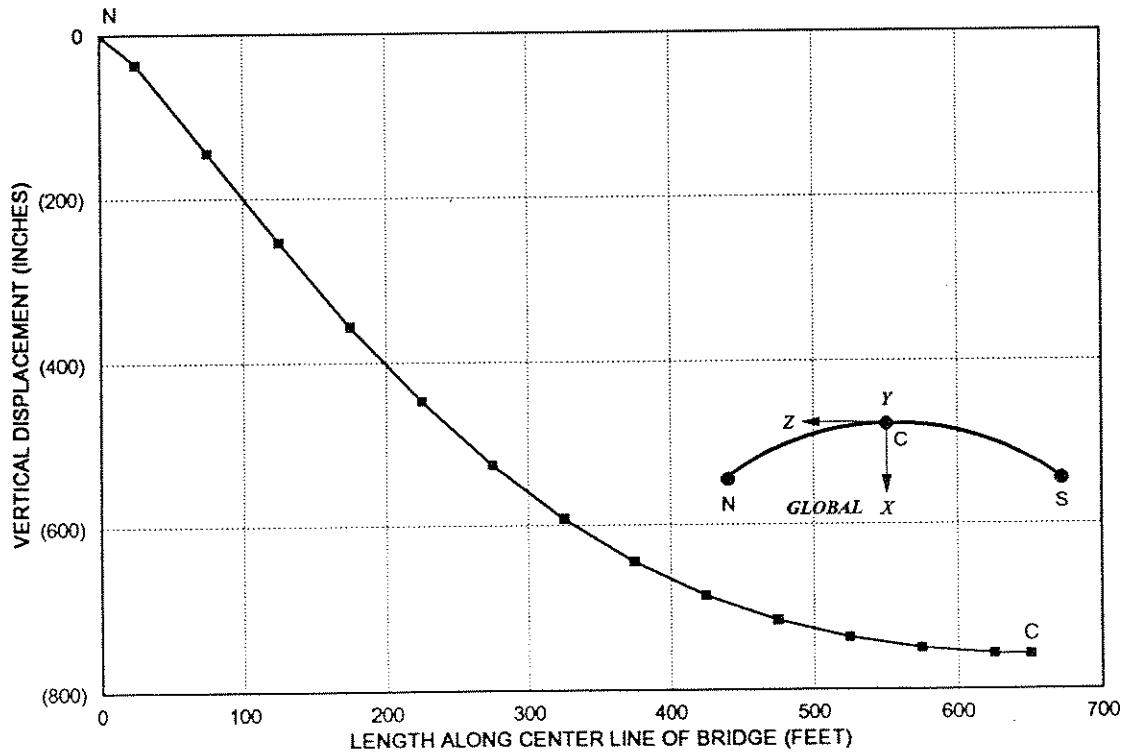

FIG. 13.27 VERTICAL DISPLACEMENTS (DY) OF THE BRIDGE DECK AT ULTIMATE LOAD
ULTIMATE LOAD ANALYSIS; RUCK-A-CHUCKY STEEL BRIDGE

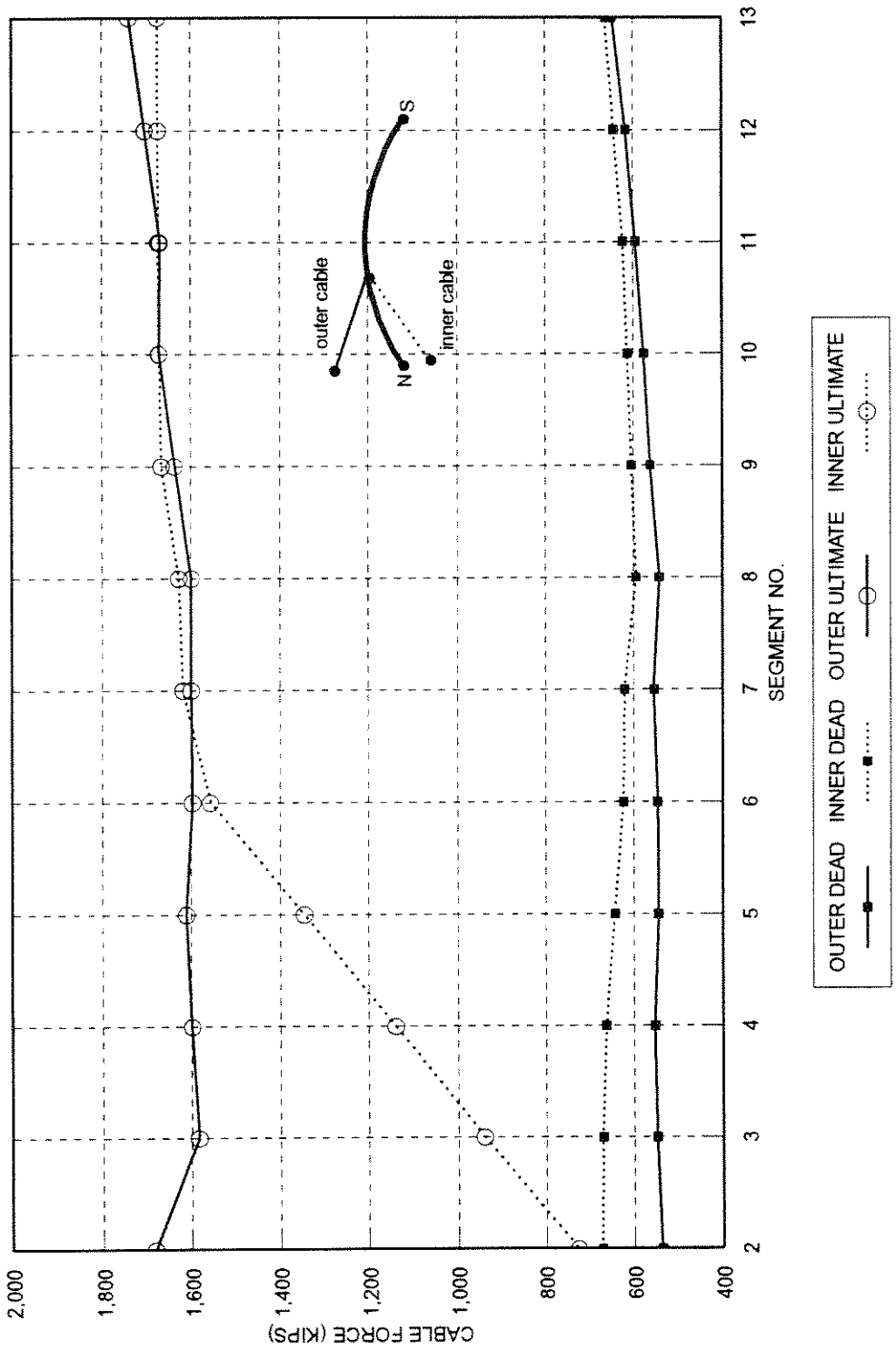

FIG. 13.28 CABLE FORCES AT DEAD AND ULTIMATE LOAD; ULTIMATE LOAD ANALYSIS
RUCK-A-CHUCKY STEEL BRIDGE

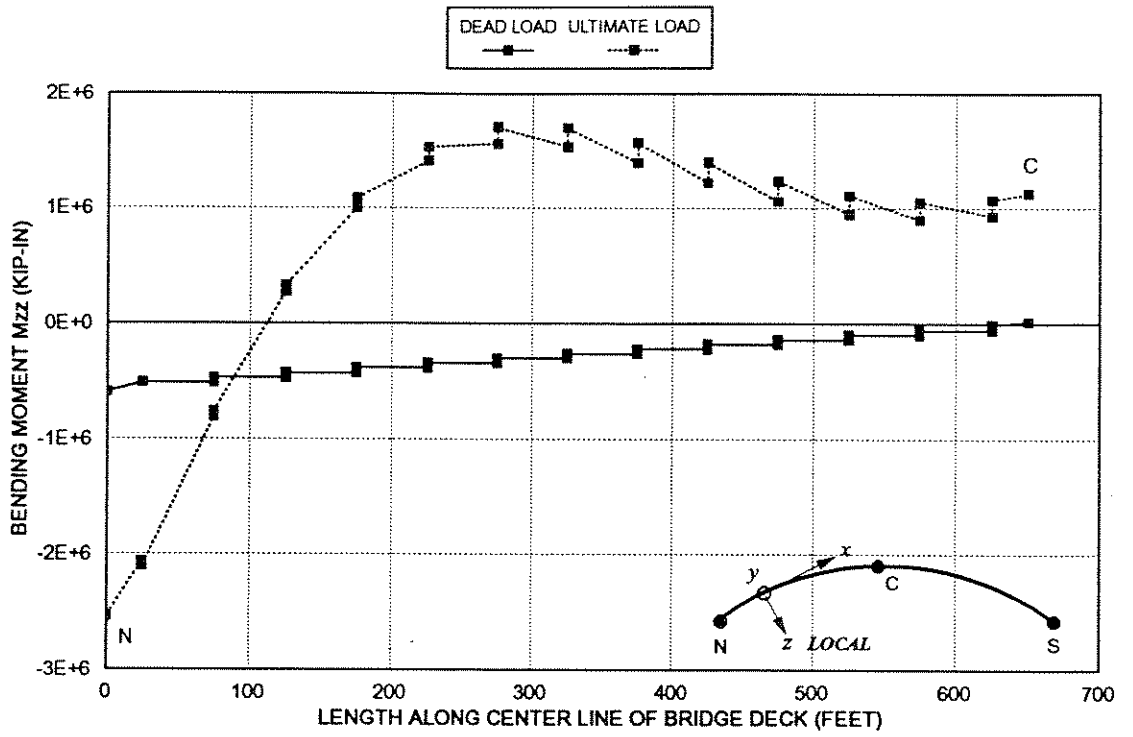

FIG. 13.29 LONGITUDINAL BENDING MOMENT Mzz IN THE BRIDGE DECK
AT DEAD AND ULTIMATE LOAD
ULTIMATE LOAD ANALYSIS; RUCK-A-CHUCKY STEEL BRIDGE

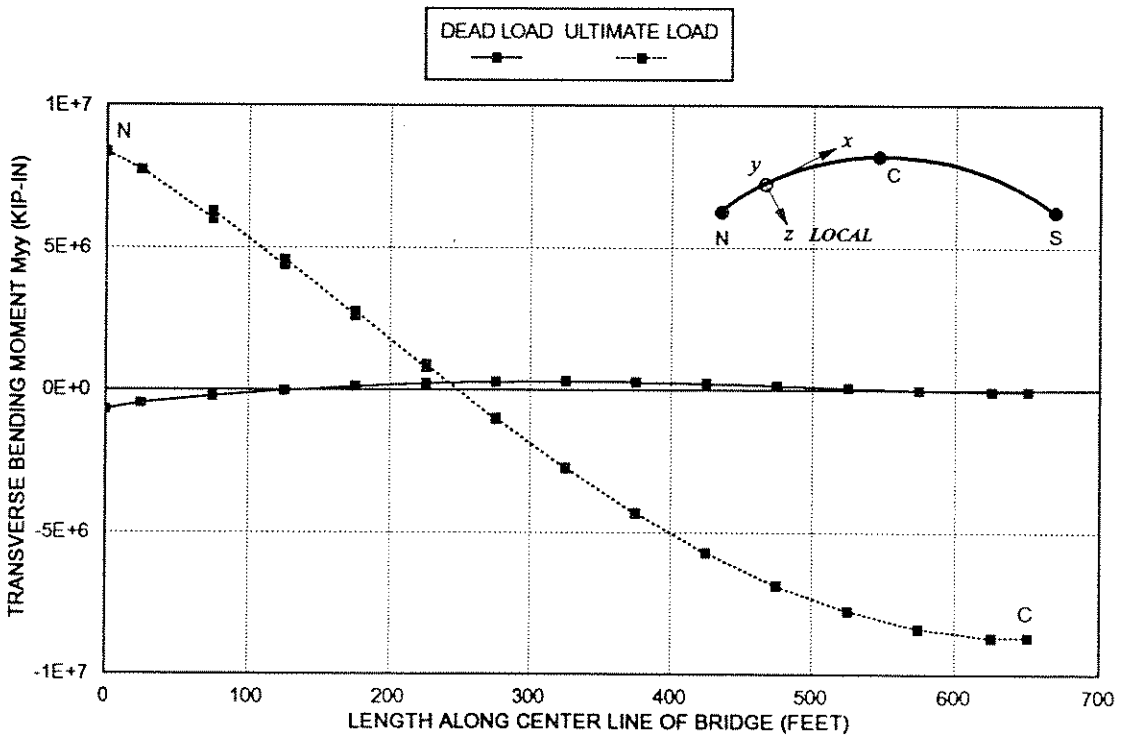

FIG. 13.30 TRANSVERSE BENDING MOMENT Myy IN THE BRIDGE DECK
AT DEAD AND ULTIMATE LOAD
ULTIMATE LOAD ANALYSIS; RUCK-A-CHUCKY STEEL BRIDGE

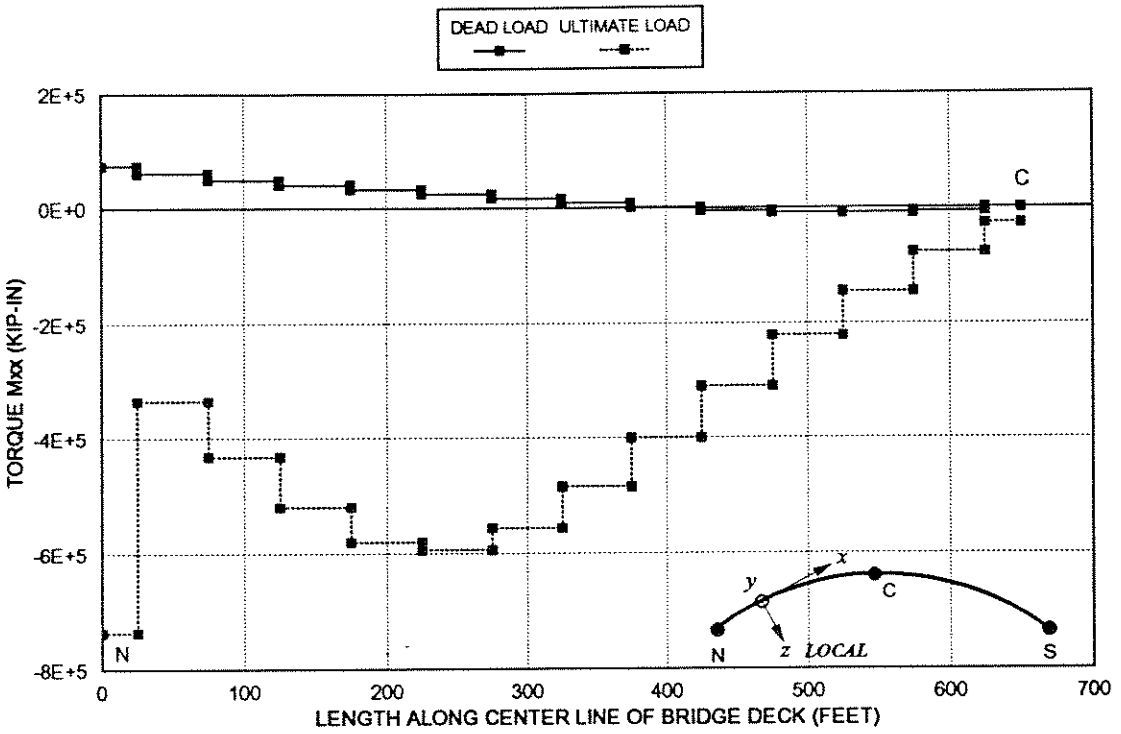

FIG. 13.31 TORQUE Mxx IN THE BRIDGE DECK; AT DEAD AND ULTIMATE LOAD ULTIMATE LOAD ANALYSIS; RUCK-A-CHUCKY STEEL BRIDGE

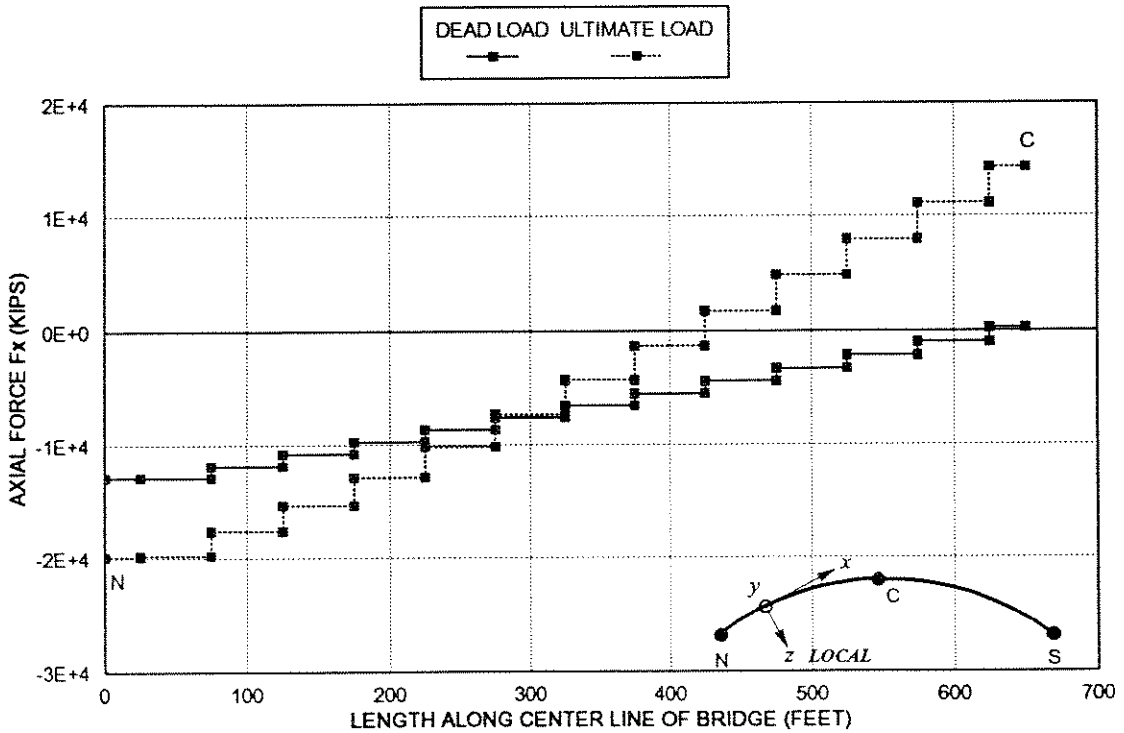

FIG. 13.32 AXIAL FORCE Fx IN THE BRIDGE DECK; AT DEAD AND ULTIMATE LOAD ULTIMATE LOAD ANALYSIS; RUCK-A-CHUCKY STEEL BRIDGE

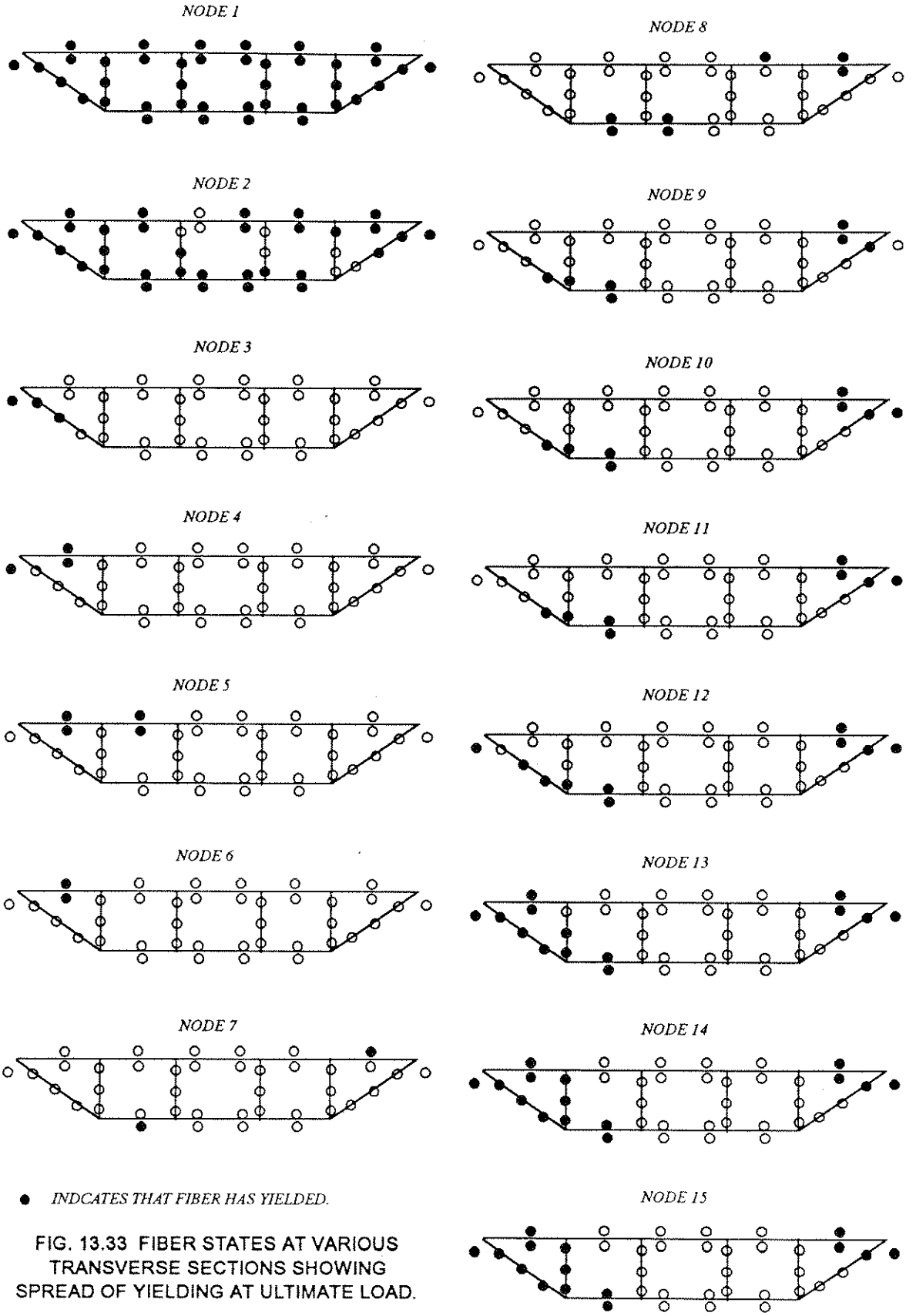

● *INDCATES THAT FIBER HAS YIELDED.*

FIG. 13.33 FIBER STATES AT VARIOUS TRANSVERSE SECTIONS SHOWING SPREAD OF YIELDING AT ULTIMATE LOAD.

14. ANALYSIS OF A THREE DIMENSIONAL CURVED CABLE-STAYED CONCRETE BRIDGE

14.1. GENERAL

The analysis of the Ruck-a-Chucky concrete bridge, designed by T.Y. Lin International, is presented in this chapter with the purpose of demonstrating the capabilities of the computer program CALBRG. This structure involves a higher degree of complexity as the number of deck segments and their supporting cables is almost twice that of the steel design. In addition, the analysis must also account for the effects of creep and shrinkage associated with concrete. Use of prestressing in the deck segments adjacent to abutments and in the midspan zone further complicates the analysis model.

A general layout of the structure and its geometry is shown in Fig. 14.01. The bridge has a length of 1300 feet between the hillsides. The deck has a vertical clearance of 55 feet at the high reservoir water level. A conventional bridge structure at this site would require several intermediate piers. However, piers were ruled out because of a water depth of 450 feet and canyon walls sloping at 40 degrees. This led the designers to the hanging arc concept, wherein the bridge deck does not require any piers and is entirely supported by cables which are anchored to the hillsides.

A simple cantilever construction sequence was recommended by the designers, T.Y. Lin International [131]. The bridge deck was to be extended from the abutment successively in

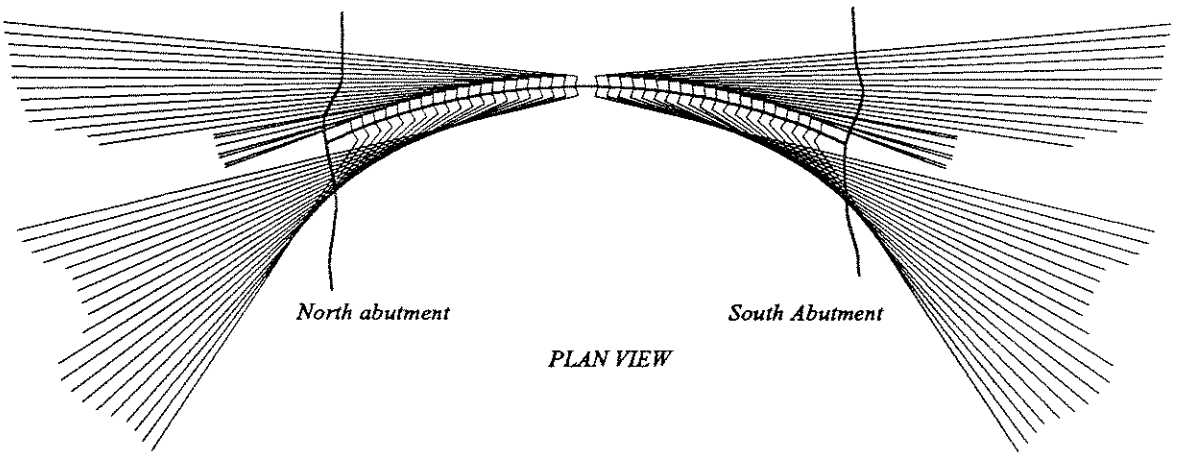

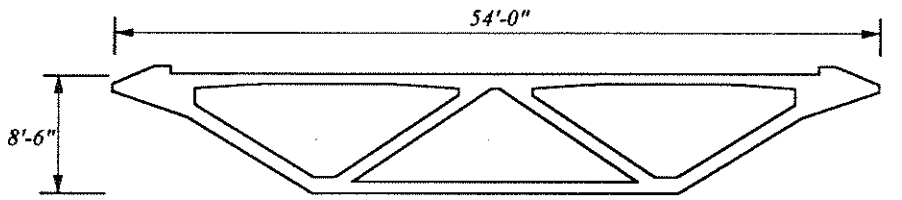

TYPICAL SECTION OF A DECK SEGMENT

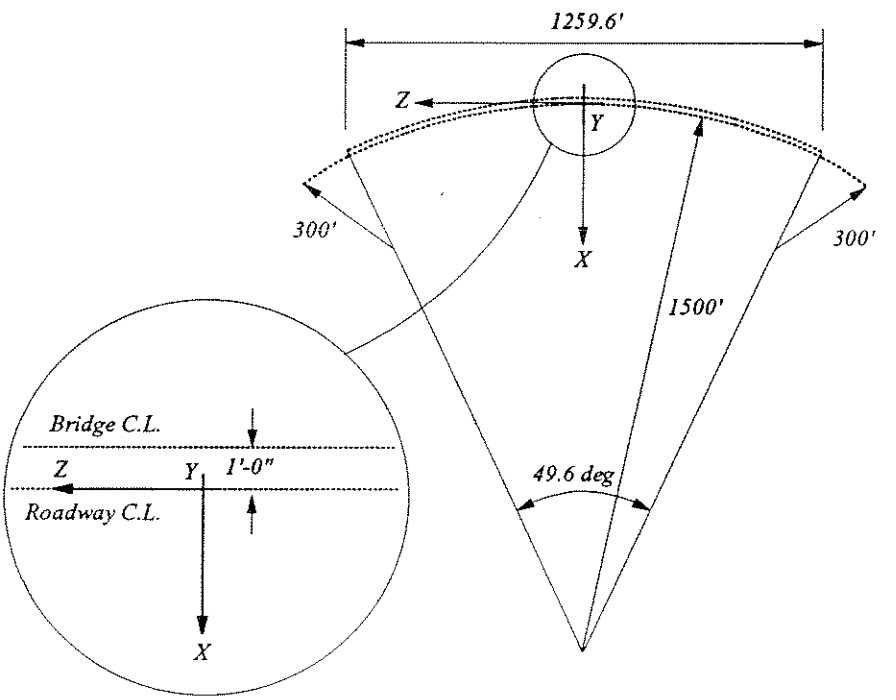

GLOBAL COORDINATES

FIG.14.01 LAYOUT AND GEOMETRY; RUCK-A-CHUCKY CONCRETE BRIDGE

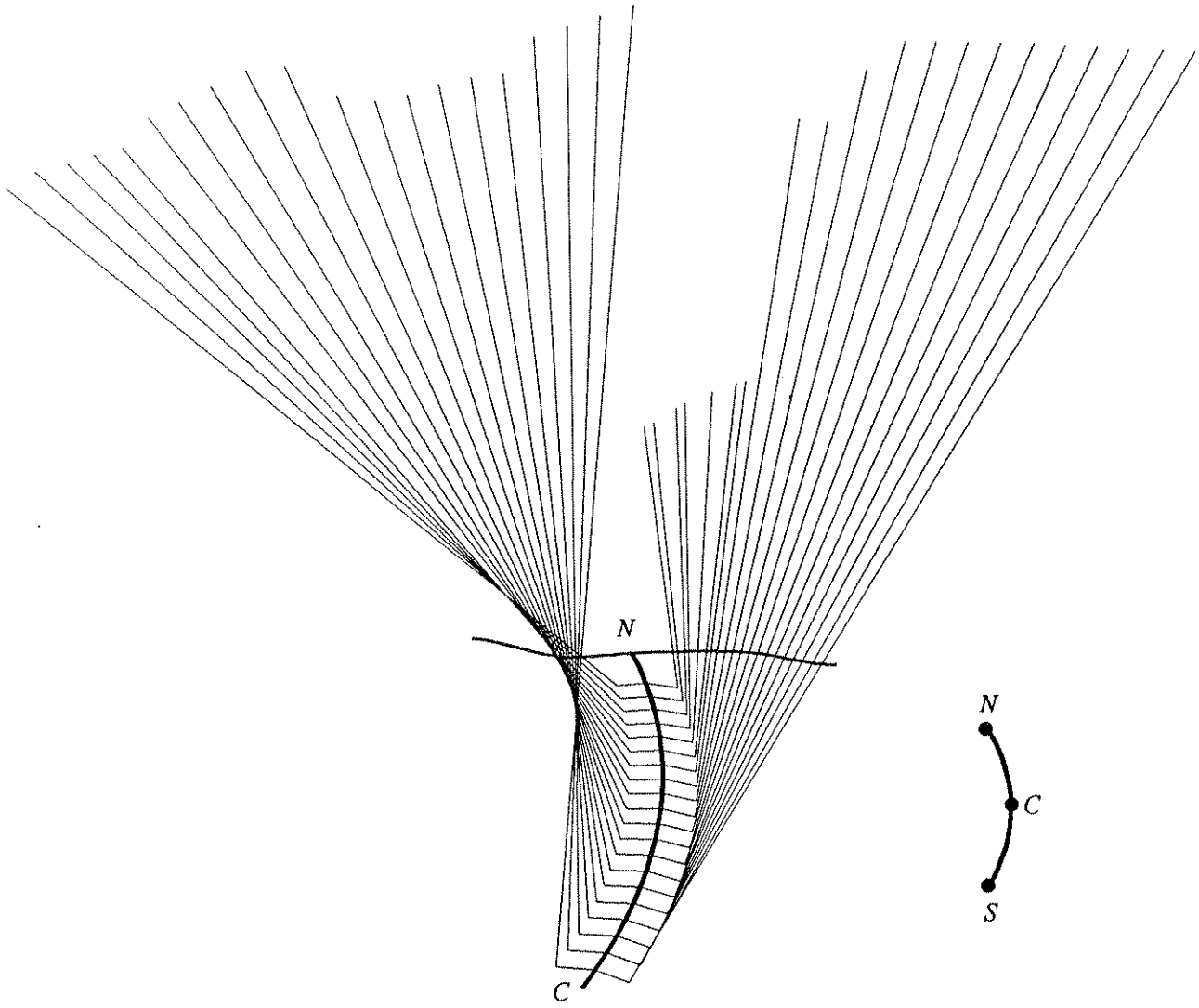

FIG. 14.02 3 D MODEL OF HALF SPAN; RUCK-A-CHUCKY CONCRETE BRIDGE

30 feet long, cast in place segments, using a movable steel erection truss. After each concrete segment has been cast and cured, its tip is connected to a pair of cables, which are, in turn, connected to pedestals about 400 feet above the deck level.

Prestressing was used in the deck near the abutments to allow for cantilever construction, and in the midspan zone to counter possible tensile forces that may arise due to live loads etc. In addition, time dependent effects of creep and shrinkage of concrete and relaxation of prestressing tendons take on special significance in the case of concrete bridge and must be accounted for in a construction sequence analysis as well as in the calculations of long term deflections.

14.2. THE ANALYSIS MODEL

A three dimensional analysis model of the Ruck-a-Chucky concrete bridge is shown in Fig. 14.02. The actual structure is not symmetric because of the difference in locations of cable-stay anchors on the north and south rock walls of the river gorge. However, in the present study, it is assumed for sake of simplicity, that the structure is symmetric about a vertical plane passing through the midspan of the bridge parallel to the direction of flow of the river.

The geometry of the bridge is defined with respect to a global coordinate system shown in Fig 14.01. The origin of the coordinate system is placed at midspan of the bridge on the center line of the road way; x and z axes define the horizontal plane whereas y is the vertical axis. The center line of the bridge deck is a circular arc with a radius of 1501 ft.. Note that the center line of the roadway is offset from that of the bridge by 1 ft. and thus has a radius of 1500 ft. The bridge has an arc length of 1340 ft. from abutment to abutment and subtends an angle of about 50 degrees at the center of the arc.

The bridge is modeled as an assemblage of fiber beam-column elements and shallow cable elements. A plan view of the analysis model showing node and element numbers is shown in Fig.14.03 and 14.04. The bridge has a total of 46 reinforced and prestressed concrete box

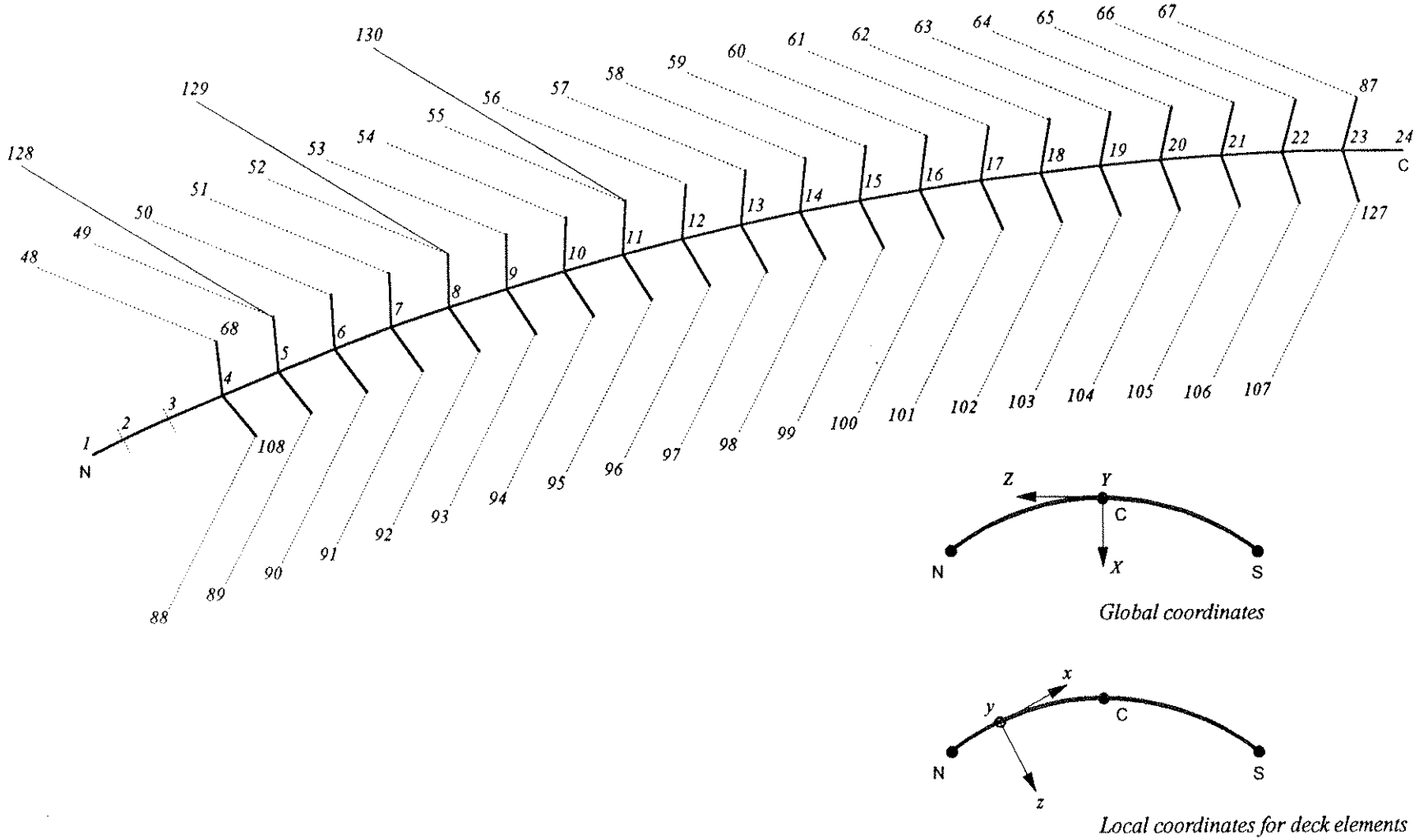

FIG. 14.03 PLAN SHOWING NODE NUMBERS; RUCK-A-CHUCKY CONCRETE BRIDGE

NOTE: ALL DECK ANCHOR NODES NOT SHOWN FOR CLARITY.

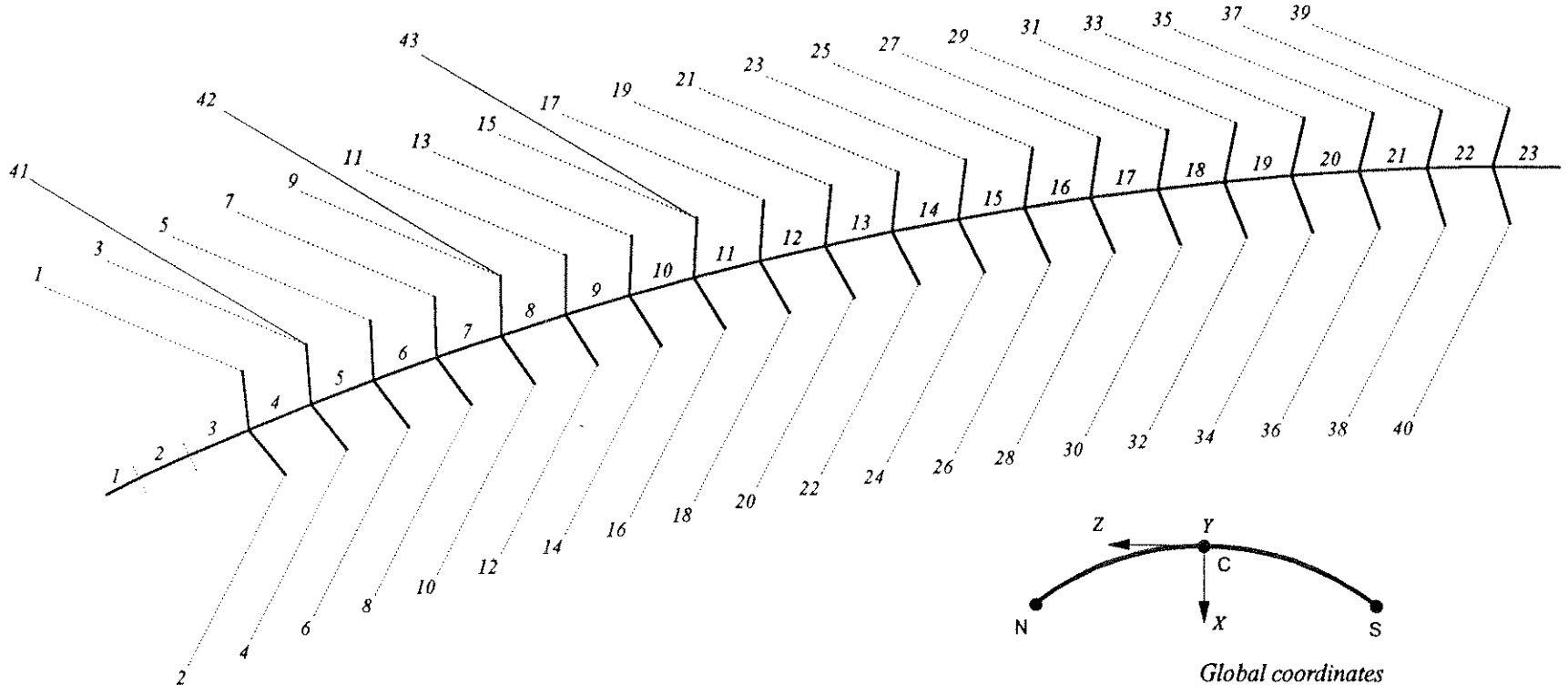

FIG. 14.04 PLAN SHOWING ELEMENT NUMBERS; RUCK-A-CHUCKY CONCRETE BRIDGE

girder deck segments, 23 in each half span as shown in Fig. 14.05. Segment No. 1 and 2, adjacent to the abutment are 20 feet long. The remaining segments No. 3 through 23 are each 30 feet long. The cross section of the deck is not uniform; five different types of cross sections labeled A through E are used as marked in Fig. 14.05. The dimensions of the concrete section and the steel reinforcement to be used in each case is shown in Figs. 14.06, 14.07, 14.08, 14.09, and 14.10.

The deck is assumed to be fixed at the abutment support. The boundary conditions at mid span are established by structural symmetry, that is the deck is free to translate in the vertical plane and to rotate about the bridge reference longitudinal axis, the other three degrees of freedom are restrained.

The deck boundary conditions are summarized as follows:

Deck Boundary Conditions

	Dx	*Dy*	*Dz*	*Rxx*	*Ryy*	*Rzz*
abutment	*fixed*	*fixed*	*fixed*	*fixed*	*fixed*	*fixed*
midspan	*free*	*free*	*fixed*	*fixed*	*fixed*	*free*

The deck is supported by a total of 80 cable-stays which are anchored to the rocky sides of the gorge. Each cable has an identification mark such as *5-NO* which signifies that the cable is connected to deck segment No. 5 in the north half of the span and is located outside of the area bounded by the circular arc. The position coordinates of the cable anchor coordinates in the rock [131] are given in the Table 14.01

At the deck end, each cable is anchored to the side of the segment that it supports. The cable-deck connection is assumed to be 4 in. below the deck surface, 24 in. from the side of the segment and 7.5 ft to 7.75 ft from the construction joint as shown in Fig. 14.11.

As described earlier, the deck nodes lie on a circular arc and hence can be generated by the following equation.

$$x_k = R[1 - \cos(\theta k + \alpha m)] - d \qquad (14.01)$$

TABLE 14.01

COORDINATES OF CABLE ANCHORS AT NORTHERN ROCK WALL

Cable outer	*Node No.*	*X inches*	*Y inches*	*Z inches*	*Cable inner*	*Node No.*	*X inches*	*Y inches*	*Z inches*
2NO	48	2502	1644	10774	*2NI*	86	11154	3048	12946
3NO	49	2412	1704	10806	*3NI*	87	10882	3252	13226
4NO	50	2207	1872	10961	*4NI*	88	10545	3348	13469
5NO	51	2115	1932	10988	*5NI*	89	10279	3444	13716
6NO	52	1846	2088	11056	*6NI*	90	10101	3468	14182
7NO	53	1607	2220	11112	*7NI*	91	9919	3804	14623
8NO	54	1513	2244	11130	*8NI*	92	9676	3960	15025
9NI	55	1832	4585	14540	*9NI*	93	9362	4140	15360
10NI	56	1586	4536	14898	*10NI*	94	9009	4320	15666
11NO	57	1387	4980	15860	*11NI*	95	8513	4416	15751
12NO	58	1127	5220	16604	*12NI*	96	7556	4236	15038
13NO	59	799	5220	16745	*13NI*	97	6996	4260	14855
14NO	60	467	5220	16878	*14NI*	98	6650	4344	15042
15NO	61	130	5220	17004	*15NI*	99	6292	4476	15186
16NO	62	-209	5220	17184	*16NI*	100	5937	4572	15349
17NO	63	-551	5220	17176	*17NI*	101	5597	4620	15530
18NO	64	-891	5220	17222	*18NI*	102	5435	4980	16220
19NO	65	-1233	5220	17263	*19NI*	103	5120	5100	16530
20NO	66	-1582	5220	17388	*20NI*	104	4795	5220	16829
21NO	67	-1917	5220	17432	*21NI*	105	4435	5364	17002

$$z_k = R\sin(\theta k + \alpha m) \tag{14.02}$$

where $R=1501\,ft.$, $d=1\,ft.$, $\theta=1.145$ *degrees* the angle subtended at the center of the arc by a 30 feet deck segment, and $\alpha=0.764$ *degrees* the angle subtended by a 20 feet long deck segment.

$k=0,1,.....21$ $\quad m=0$ *for node number 24, 23,.....3*

$k=21$ $\quad m=1$ *for node number 2*

The x and z coordinates of the outer cable-deck anchor nodes may be generated by the following equation.

$$x_k = R[1-\cos(\theta k + \beta)] - d \tag{14.03}$$

$$z_k = R\sin(\theta k + \beta) \tag{14.04}$$

where $R=1526\,ft.$, $d=26\,ft.$ and $\beta=0.855$ *degrees* which is the angle subtended at the center by an arc running from the anchor point to the leading edge of the segment.

$k=0,\ 1,.....19$ *for node number 87, 86,.....68*

Similarly, the inner cable-deck anchor coordinates can be obtained from Eq. 14.03 and 14.04 by setting $R=1476\,ft.$, $d=24\,ft.$ and $\beta=0.855$ *degrees.*

$k=0,\ 1,.....19$ *for node number 127, 126.....108*

14.2.1. STAY CABLES

The cables are modeled as shallow cable elements. The cable stay steel is assumed to have a bilinear strain hardening material constitutive law defined by the following data.

$\sigma_y = 245.76\ ksi$ $\quad \varepsilon_y = .00847$

$\sigma_u = 270.00\ ksi$ $\quad \varepsilon_u = .00419$

The weight density of the cables is assumed to be constant and is given by:

$$\gamma = 2.836\times10^{-4}\ kips/in^3$$

The deck node of the cable is slaved to the segment node thereby resulting in a much more efficient solution. Each cable consists of a group of ½" diameter strands. Cable size (number of strands) and area of cross section are shown in Table 14.02.

14.2.2. DECK

The deck consists of a light weight concrete box girder. The cross section of the deck varies along the length of the bridge. For the sake of simplicity, it is assumed that the cross section remains constant within each segment. This result in total of five different types of cross section labeled A through E. These sections are shown in Figs. 14.06, 14.07, 14.08, 14.09 and 14.10.

The deck is modeled as fiber beam-column elements. Two different types of beam-column elements are used.

1. Elements with two control sections, one at each end. These elements are used in those areas of the structure which are expected to stay elastic.
2. Elements with four control sections, one at each end and at $0.2\,l$ and $0.8\,l$, where l is the length of the element. These elements are used in those sections of the structure which are expected to yield or undergo plastic deformations.

The maximum number of concrete and steel fibers in any section is set at 50 and 24 respectively. Each different type of cross section is defined by the area and location of its constituent concrete and steel fibers. This information is listed in the input file used in the analysis of the concrete bridge and given in Appendix C.

Each element has a local reference x-axis which is defined by the straight line joining the left end node I with the right end node J. In this case each node is assumed to lie on the center line of the bridge at the top edge of the deck section. It is very important to note that all bending moments and forces in the deck are calculated and reported with respect to this axis.

TABLE 14.02

STAY CABLES; AREA OF CROSS SECTION.

Cable No. Outer	*Element No.*	*No. of Strands*	*Area in²*	*Cable No. Inner*	*Element No.*	*No. of Strands*	*Area in²*
2NO	1	55 ø ½	8.42	*2NI*	2	60 ø ½	9.18
3NO	3	53 ø ½	8.11	*3NI*	4	60 ø ½	9.18
4NO	5	48 ø ½	7.34	*4NI*	6	58 ø ½	8.87
5NO	7	47 ø ½	7.19	*5NI*	8	55 ø ½	8.41
6NO	9	47 ø ½	7.19	*6NI*	10	52 ø ½	7.96
7NO	11	41 ø ½	6.27	*7NI*	12	50 ø ½	7.65
8NO	13	41 ø ½	6.27	*8NI*	14	50 ø ½	7.65
9NO	15	34 ø ½	5.20	*9NI*	16	46 ø ½	7.04
10NO	17	35 ø ½	5.36	*10NI*	18	46 ø ½	7.04
11NO	19	36 ø ½	5.51	*11NI*	20	46 ø ½	7.04
12NO	21	37 ø ½	5.66	*12NI*	22	46 ø ½	7.04
13NO	23	38 ø ½	5.81	*13NI*	24	46 ø ½	7.04
14NO	25	40 ø ½	6.12	*14NI*	26	46 ø ½	7.04
15NO	27	41 ø ½	6.27	*15NI*	28	46 ø ½	7.04
16NO	29	42 ø ½	6.43	*16NI*	30	46 ø ½	7.04
17NO	31	43 ø ½	6.58	*17NI*	32	46 ø ½	7.04
18NO	33	44 ø ½	6.73	*18NI*	34	46 ø ½	7.04
19NO	35	45 ø ½	6.88	*19NI*	36	46 ø ½	7.04
20NO	37	46 ø ½	7.04	*20NI*	38	46 ø ½	7.04
21NO	39	48 ø ½	7.34	*21NI*	40	46 ø ½	7.04

Note: Strand diameter in inches.

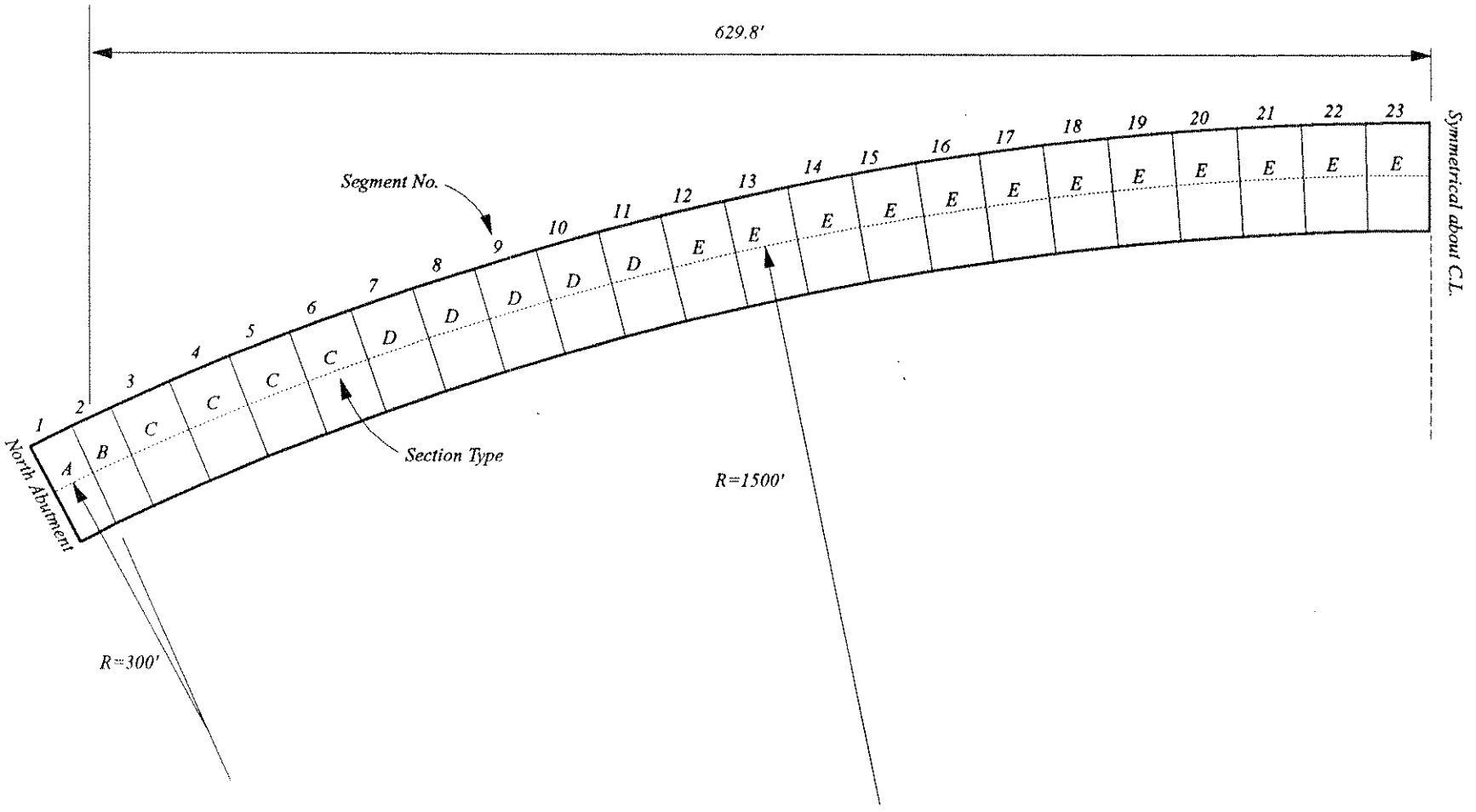

SEGMENT 1 AND 2 ARE EACH 20 FT. LONG ALONG BRIDGE C. L.
SEGMENT NO. 3 THROUGH 24 ARE EACH 30 FT. LONG ALONG BRIDGE C. L.

FIG. 14.05 DECK PLAN; RUCK-A-CHUCKY CONCRETE BRIDGE

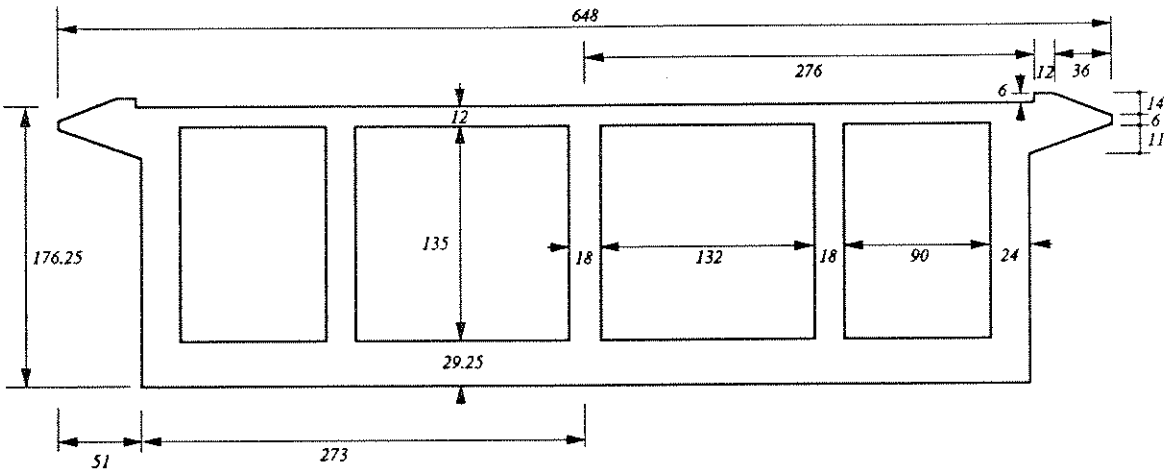

LONGITUDINAL STEEL REINFORCEMENT

Top Flange	*#7 @ 12" top & bottom*
Bottom Flange	*#7 @ 14" top & bottom*
Webs	*#5 @ 12" each face*

FIG 14.06 DECK CROSS SECTION TYPE A.

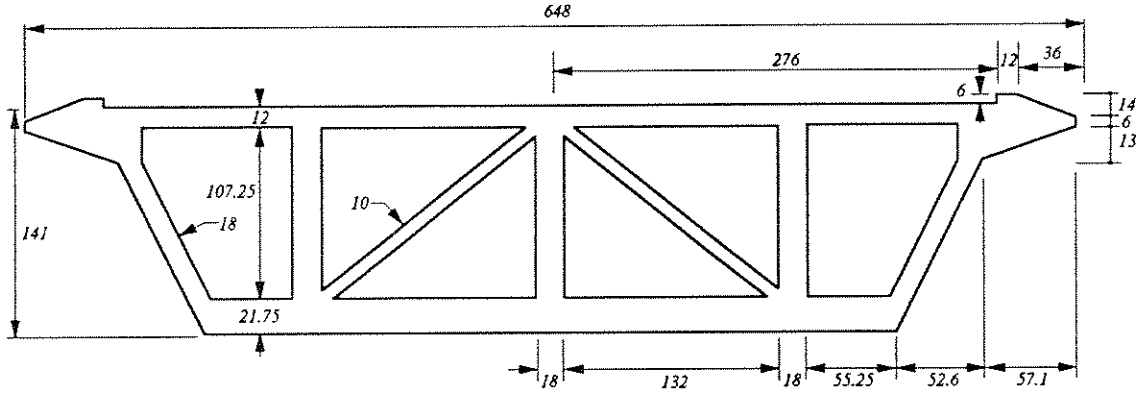

LONGITUDINAL STEEL REINFORCEMENT

Top Flange	*#8 @ 12" top & bottom*
Bottom Flange	*#7 @ 9" top & bottom*
Webs	*#5 @ 12" each face*

FIG 14.07 DECK CROSS SECTION; TYPE B.

All dimensions in inches.

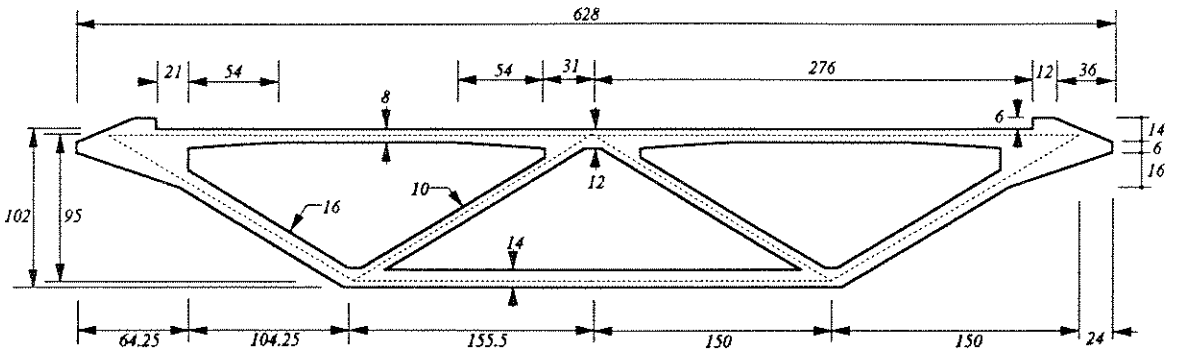

LONGITUDINAL STEEL REINFORCEMENT

Top Flange	*#8 @ 12" top & bottom*
Bottom Flange	*#8 @ 9" top & bottom*
Webs	*#8 @ 9" each face*
Edge Beams	*#8 - 21 bars*

FIG 14.08 DECK CROSS SECTION TYPE C.

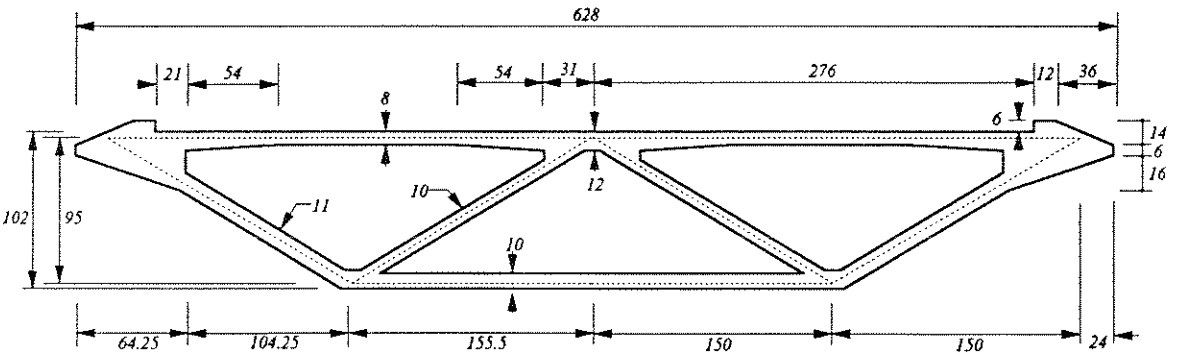

LONGITUDINAL STEEL REINFORCEMENT

Top Flange	*#6 @ 12" top & bottom*
Bottom Flange	*#6 @ 9" top & bottom*
Webs	*#6 @ 9" each face*
Edge Beams	*#8 - 21 bars*

FIG 14.09 DECK CROSS SECTION TYPE D.

All dimensions in inches.

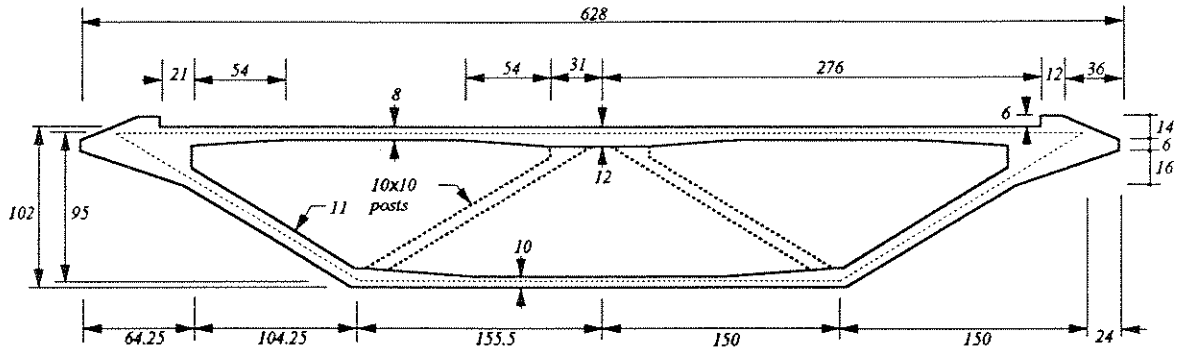

LONGITUDINAL STEEL REINFORCEMENT

Top Flange	*#4 @ 12" top & bottom*
Bottom Flange	*#4 @ 9" top & bottom*
Webs	*#4 @ 9" each face*
Edge Beams	*#8 - 21 bars*

FIG 14.10 DECK CROSS SECTION TYPE E.

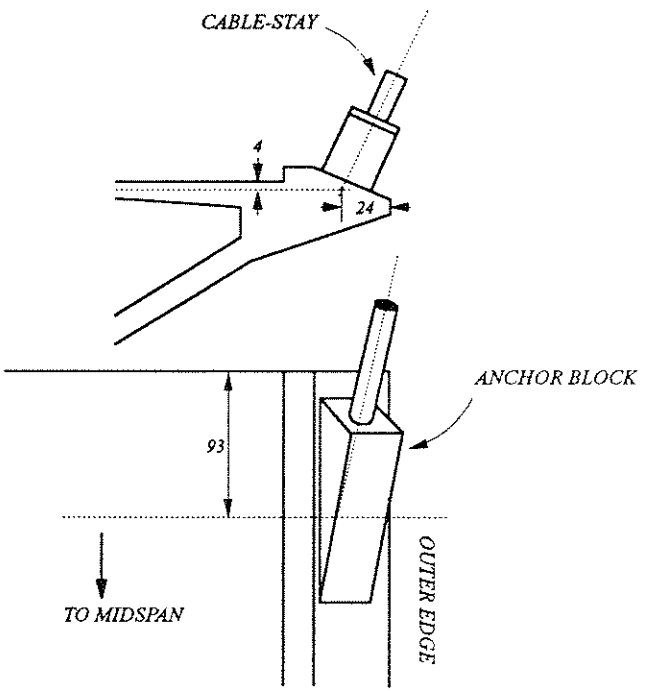

FIG. 14.11 CABLE CONNECTION AT DECK

All dimensions in inches.

14.2.3. CONCRETE MODEL

Modified Kent Park model, which is described earlier is used to simulate the uniaxial behavior of concrete. The model is defined by the following parameters:

$$f_c' = 5000 \ psi$$
$$\varepsilon_1 = 0.0064 \qquad \varepsilon_u = 0.0075$$

where ε_1 is the concrete strain at the end of the descending branch and ε_u is the ultimate strain at failure.

14.2.4. STEEL MODEL

A bilinear strain hardening steel model is assumed, pertinent data are as follows.

$$\sigma_y = 60{,}000 \ psi$$
$$E = 29{,}000{,}000 \ psi$$
$$E_{sh} = 290{,}000 \ psi$$
$$\varepsilon_u = .12$$

14.2.5. TORSION MODEL

The procedure for evaluation of parameters defining the torsion model is discussed in Chapter 3. Transverse (hoop) reinforcement in the deck section was assumed to be 0.88 in^2 @ 12". The torsion model used for each type of deck section is given below:

Torsion Parameters for Deck Sections

Section Type	T_{cr} *(lb.in.)*	α_{cr}	T_{yp} *(lb.in)*	α_{yp}	α_u
A	*1.6E+9*	*4.3E-6*	*8.7E+8*	*3.1E-5*	*.02*
B	*9.1E+8*	*4.7E-6*	*9.7E+8*	*3.6E-5*	*.02*
C	*4.3E+8*	*7.4E-6*	*5.7E+8*	*4.8E-5*	*.02*
D	*3.5E+8*	*6.6E-6*	*4.8E+8*	*5.1E-5*	*.02*
E	*3.2E+8*	*6.7E-6*	*3.6E+8*	*6.1E-5*	*.02*

14.2.6. PRESTRESSING

Prestressing is used to improve the service load behavior and to enhance the ultimate strength of the bridge structure. Post-tensioning is used at two locations in the Ruck-a-Chucky concrete bridge:

1. Near the abutment, tendons are laid out in the top flange of the deck, parallel to the center line of the bridge from segment 1 through 6 as shown in Fig. 14.12.
2. In the midspan zone, tendons are laid out in both the top and bottom flange of the deck, parallel to the center line of the bridge from segment 18 through 23 as shown in Fig. 14.13.

A low relaxation strand with an ultimate strength of $f_{pu} = 270\ ksi$ is used. A bilinear strain hardening model which approximates the modified Ramberg-Osgood function is employed for this analysis.

$$\sigma_y = 246{,}000\ psi$$
$$E = 29{,}000{,}000\ psi$$
$$E_{sh} = 716{,}000\ psi$$
$$\varepsilon_u = .042$$

Curvature and wobble coefficients to calculate stress loss due to friction are as follows:

$$\mu = .15$$
$$K = .0005\ per\ ft.$$

The geometry and the working force carried by the prestressing tendons is defined in the Table 14.03. Note that the position of the tendon in the cross section is defined with respect to an element local coordinate system, where x-axis is the longitudinal reference axis of the frame element and y-axis is perpendicular to it and lies in the IJK plane.

TABLE 14.03

ABUTMENT PRESTRESSING

Tendon No.	*Force kips*	*Area in.²*	*Anchor Node I*	*Anchor Node J*	*Y coord. in.*	*Z coord. in.*
1	600	3.7	1	3	-11	-258
2	600	3.7	1	3	-11	258
3	1850	11.3	1	4	-11	-286
4	300	1.8	1	4	-6	0
5	1850	11.3	1	4	-11	286
6	300	1.8	1	5	-11	-258
7	300	1.8	1	5	-6	0
8	300	1.8	1	5	-11	258
9	300	1.8	1	6	-11	-258
10	300	1.8	1	6	-6	0
11	300	1.8	1	6	-11	258
12	300	1.8	1	7	-11	-258
13	300	1.8	1	7	-6	0
14	300	1.8	1	7	-11	258

MID SPAN PRESTRESSING

Tendon No.	*Force kips*	*Area in.²*	*Anchor Node I*	*Anchor Node J*	*Y coord. in.*	*Z coord. in.*
1	300	1.8	18	24	-11	-261
2	300	1.8	18	24	-11	0
3	300	1.8	18	24	-11	-261
4	300	1.8	18	24	-95	-147
5	300	1.8	18	24	95	-147
6	300	1.8	19	24	-11	-261
7	300	1.8	19	24	-11	0
8	300	1.8	19	24	-11	-261
9	300	1.8	19	24	-95	-147
10	300	1.8	19	24	95	-147
11	300	1.8	20	24	-11	-261
12	300	1.8	20	24	-11	0
13	300	1.8	20	24	-11	-261
14	300	1.8	20	24	-95	-147
15	300	1.8	20	24	95	-147
16	300	1.8	21	24	-11	-261
17	300	1.8	21	24	-11	0
18	300	1.8	21	24	-11	-261
19	300	1.8	21	24	-95	-147
20	300	1.8	21	24	95	-147

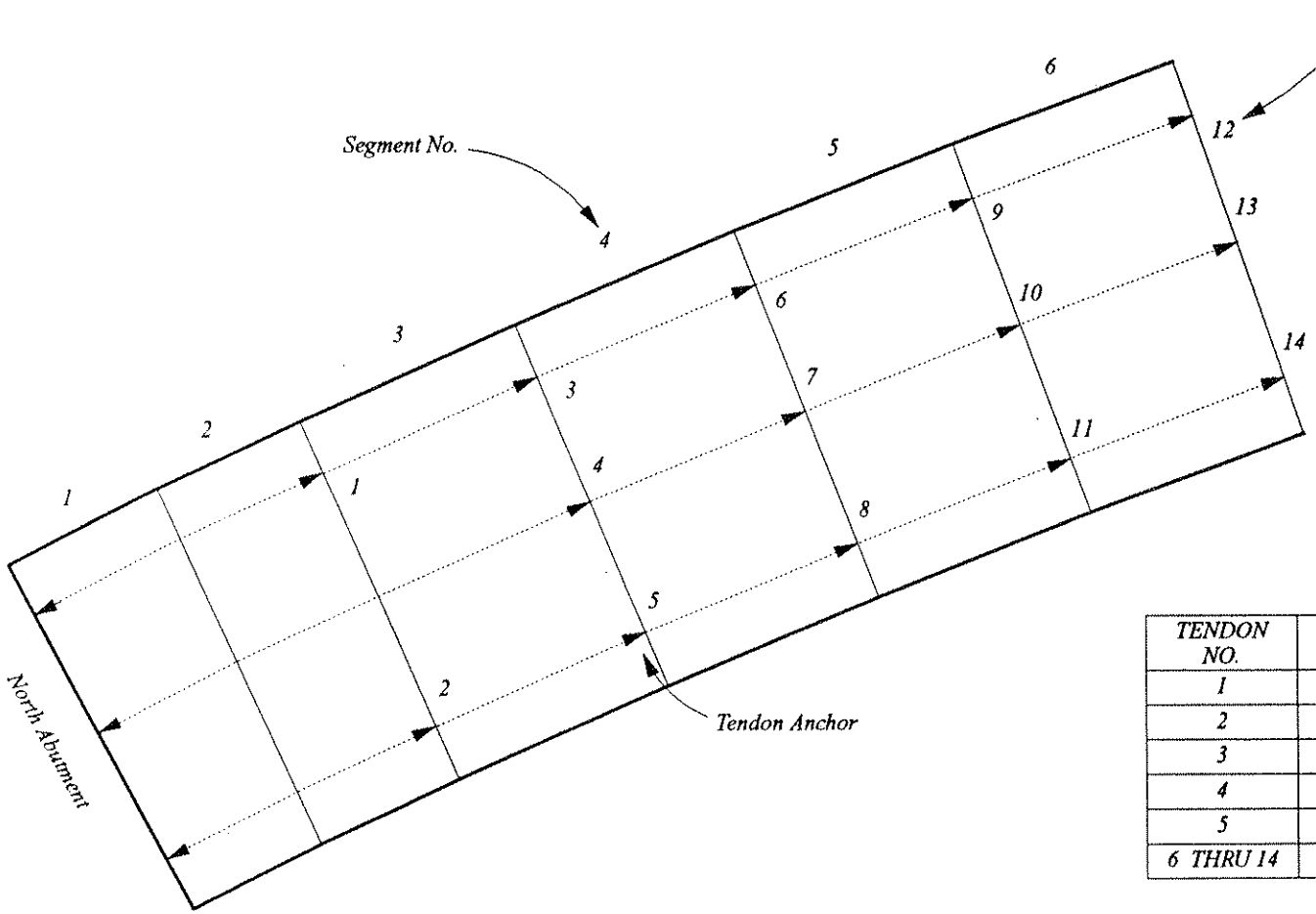

TENDON NO.	AREA (SQ. IN.)	FORCE (KIPS)
1	3.7	600
2	3.7	600
3	11.3	1850
4	1.8	300
5	11.3	1850
6 THRU 14	1.8	300

NOTE: ALL TENDONS ARE PLACED IN TOP DECK.

FIG. 14.12 PLAN OF ABUTMENT PRESTRESSING; RUCK-A-CHUCKY CONCRETE BRIDGE

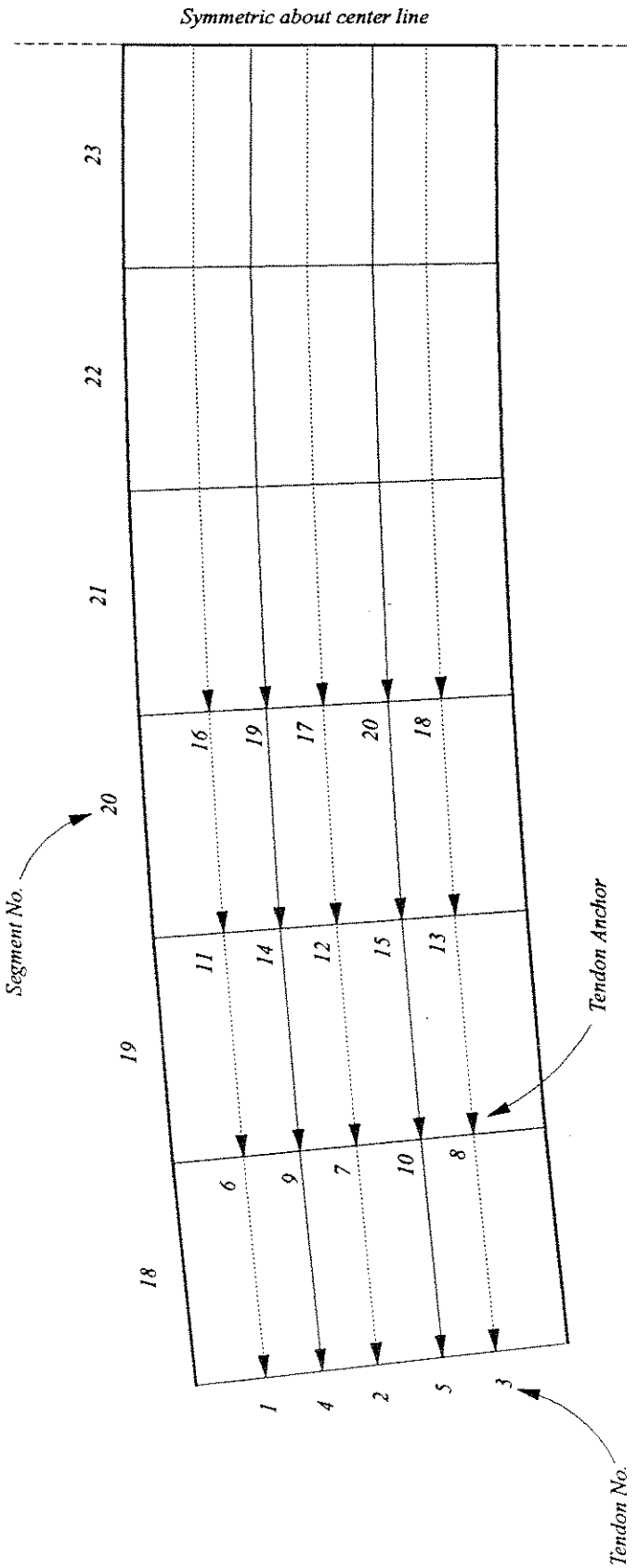

TENDON NO.	AREA (SQ. IN.)	FORCE (KIPS)
1 THRU 20	1.84	300

—— TENDON PLACED IN BOTTOM FLANGE

..... TENDON PLACED IN TOP FLANGE

FIG. 14.13 PLAN OF PRESTRESSING IN THE MIDSPAN ZONE
RUCK-A-CHUCKY CONCRETE BRIDGE

14.2.7. LOAD PATTERN

The dead load consists of two components.

1. Bridge deck self weight. The unit weight of light weight concrete is assumed to be 110 pcf. The deck dead load varies from 16 kips/ft. to 10 kips/ft. in the cable-stayed section of the bridge.
2. Cable self weight

The average dead load per unit length (deck+cables) applied to the structure is about 12.7 kips/ft.

For long span bridges, AASHTO [129] requires a live load of 640 lbs per linear foot of the load lane. Live load effects are not considered directly in the present study.

The dead load pattern applied to the structure is given below:

Structure Dead Loads

Node No.	*Load (kips)*	*Node No.*	*Load (kips)*
2	530	14	330
3	480	15	330
4	490	16	330
5	490	17	330
6	490	18	330
7	430	19	330
8	360	20	340
9	360	21	340
10	360	22	340
11	340	23	340
12	330	24	150
13	330		

14.3. LOAD BALANCING ANALYSIS

The purpose of the load balancing analysis is to find a set of cable tensions that support the bridge deck at the desired profile. In the case of the concrete bridge, the structure is analyzed at two distinct construction stages, which are as follows:

1. The structure is assumed to be complete up to segment no. 22, stay No. 37 and 38 are installed and tensioned. Auxiliary cables no. 41, 42 and 43 are in place. The closure segment is not yet installed. This allows for evaluation of cable tensions in the auxiliary cables.
2. The bridge is closed at midspan by adding segment no. 23 and its supporting cables No. 39 and 40. Auxiliary cables No. 41, 42 and 43 are removed and continuity tendons installed. This analysis yields the pretension in the permanent cable stays in the completed structure.

As done earlier in the case of the steel bridge, the initial balanced cable tensions were evaluated based on the following two conditions:

1. The vertical components of the two cables must equal the weight of the segment.
$$T_1 \sin\theta_1 + T_2 \sin\theta_2 = W \qquad (14.05)$$
2. The tangential components should be equal to each other to reduce transverse bending and to direct axial force along the center line of the bridge deck.
$$T_1 \cos\gamma_1 - T_2 \cos\gamma_2 = 0 \qquad (14.06)$$

The initial cable tensions were refined by iteration in order to minimize deck deflections and are reported in the Table 14.04.

The vertical displacements (Dy) of the deck under the action of the adjusted cable tensions are shown in Fig. 14.14. Maximum value of vertical displacement does not exceed ±0.8 in.

The transverse displacements (Dx) of the deck parallel to the global X-axis are shown in Fig. 14.15. Maximum transverse displacement is 0.9 in and occurs at mid span. This plot,

however, does not tell the whole story and is it is difficult to set up correspondence between this plot and the transverse bending moment diagram. A plan view of the displaced shape of the bridge deck with respect to its original position in space is shown in Fig. 14.16.

Balanced cable tensions are applied to the mathematical model as it occupies its original configuration in space. As the loads are applied the structure deforms and cable tensions change. Fig. 14.17 shows the effectiveness of load balancing in the displaced configuration; the sum of the vertical cable tensions at each deck node is compared with the dead load of the segment. The plot shows that near the abutment section, cable tensions are about 10% lower than the girder dead load; this is due to the fact that near the abutment, the girder carries a larger share of the load because of its higher stiffness. The plot shows excellent agreement in the middle half of the bridge.

The distribution of longitudinal bending moment, transverse bending moments torque and axial force along the length of the bridge deck is shown in Figs. 14.18, 14.19, 14.20, and 14.21 respectively.

Note that the bending moments and the axial force in the deck are reported at the level of the element reference axis, which in this case, passes through the top edge of the section. The step in the bending moment diagram is due to eccentricity of the cable forces with respect to the reference axis.

Refer to Fig. 14.21; note the increased compression caused by the prestressing in the midspan region of the bridge.

Under balanced load conditions cable stresses vary from 64 ksi to 86 ksi, which is about 24 to 32% of the ultimate tensile strength of the cable (270 ksi). Note that the usual permissible stress for parallel strand cables is 50% of the ultimate tensile strength.

Maximum longitudinal stresses in the deck girder occur at the abutment section. Because of the heavy axial force at the abutment section all stresses are compressive. A summary of stresses at the abutment section is given below:

Top outer corner	*1069 psi*
Top inner corner	*715 psi*
Bottom outer corner	*1417 psi*
Bottom inner corner	*1252 psi*

TABLE 14.04

CABLE TENSIONS; LOAD BALANCING ANALYSIS

Cable No.	*Element No.*	*Balanced Tension (kips)*	*Adjusted Tension (kips)*	*Cable No.*	*Element No.*	*Balanced Tension (kips)*	*Adjusted Tension (kips)*
2NO	1	702	653	*2NI*	2	851	791
3NO	3	712	662	*3NI*	4	846	787
4NO	5	716	666	*4NI*	6	834	776
5NO	7	643	598	*5NI*	8	738	686
6NO	9	549	511	*6NI*	10	618	575
7NO	11	541	503	*7NI*	12	600	558
8NO	13	556	517	*8NI*	14	609	566
9No	15	468	440	*9NI*	16	507	477
10No	17	469	441	*10NI*	18	504	474
11NO	19	473	485	*11NI*	20	504	517
12NO	21	481	493	*12NI*	22	508	521
13NO	23	488	500	*13NI*	24	512	525
14NO	25	498	510	*14NI*	26	519	532
15NO	27	506	519	*15NI*	28	525	538
16NO	29	516	529	*16NI*	30	533	546
17NO	31	526	547	*17NI*	32	542	564
18NO	33	546	568	*18NI*	34	561	583
19NO	35	556	581	*19NI*	36	569	595
20NO	37	567	593	*20NI*	38	579	605
21NO	39			*21NI*	40		
AUX.	41	10					
AUX.	42	15					
AUX.	43	25					

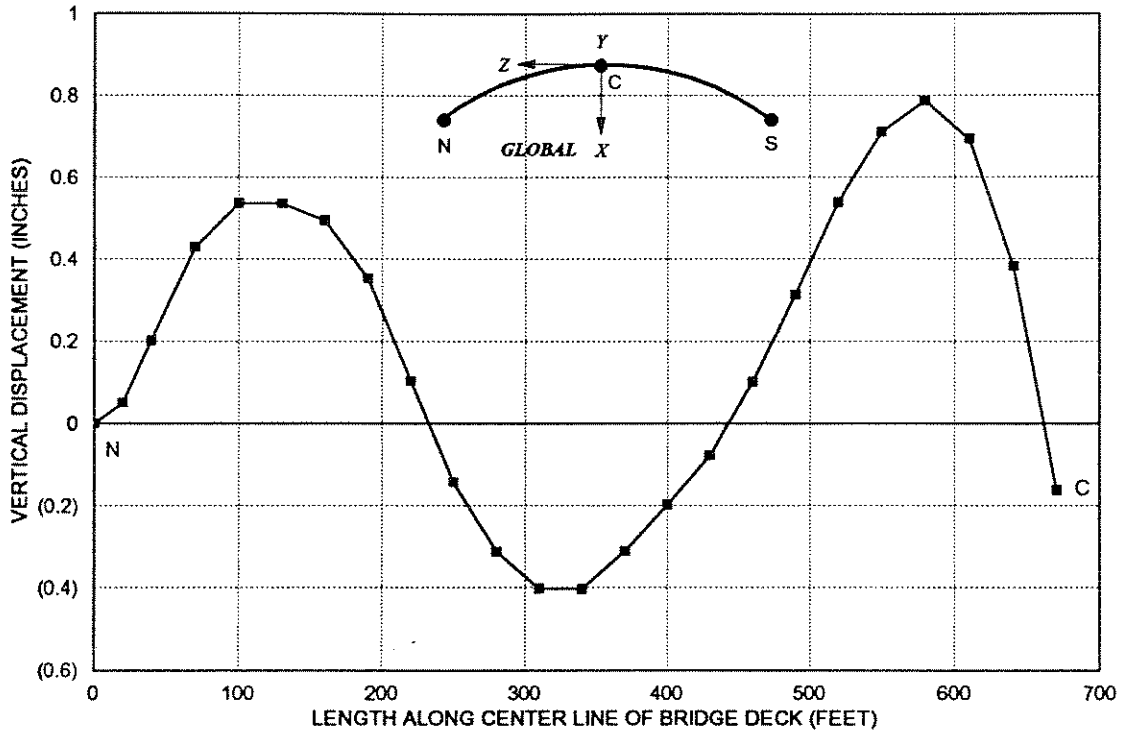

FIG. 14.14 VERTICAL DISPLACEMENTS (DY) OF THE BRIDGE DECK LOAD BALANCING ANALYSIS; RUCK-A-CHUCKY CONCRETE BRIDGE

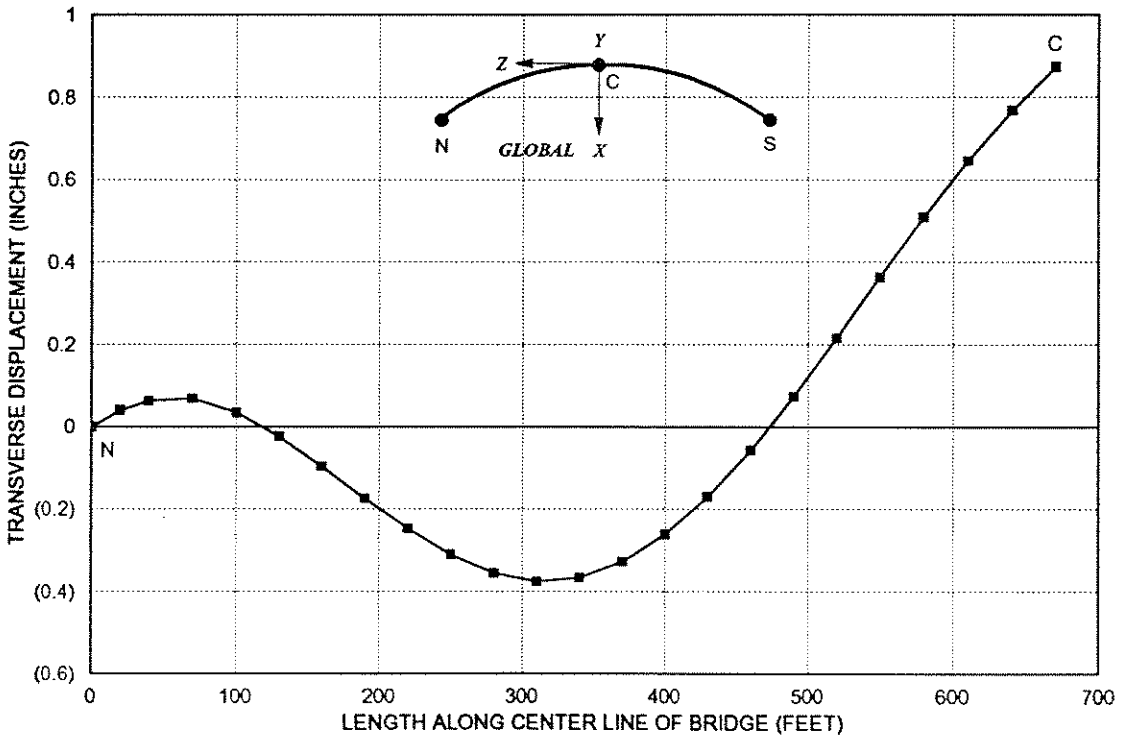

FIG. 14.15 TRANSVERSE DISPLACEMENTS (DX) OF THE BRIDGE DECK LOAD BALANCING ANALYSIS; RUCK-A-CHUCKY CONCRETE BRIDGE

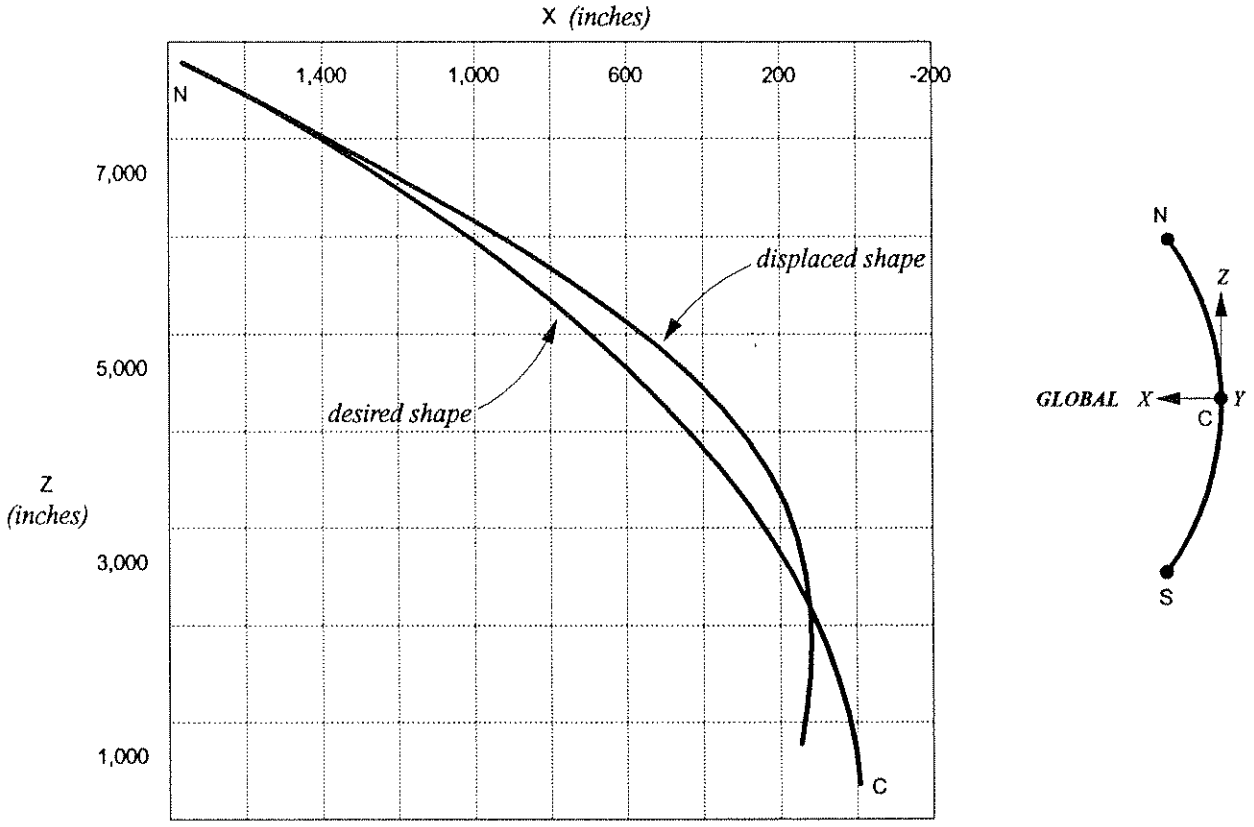

FIG. 14.16 DISPLACED SHAPE OF BRIDGE DECK; PLAN VIEW
DEFLECTIONS MAGNIFIED x 200
LOAD BALANCING ANALYSIS; RUCK-A-CHUCKY CONCRETE BRIDGE

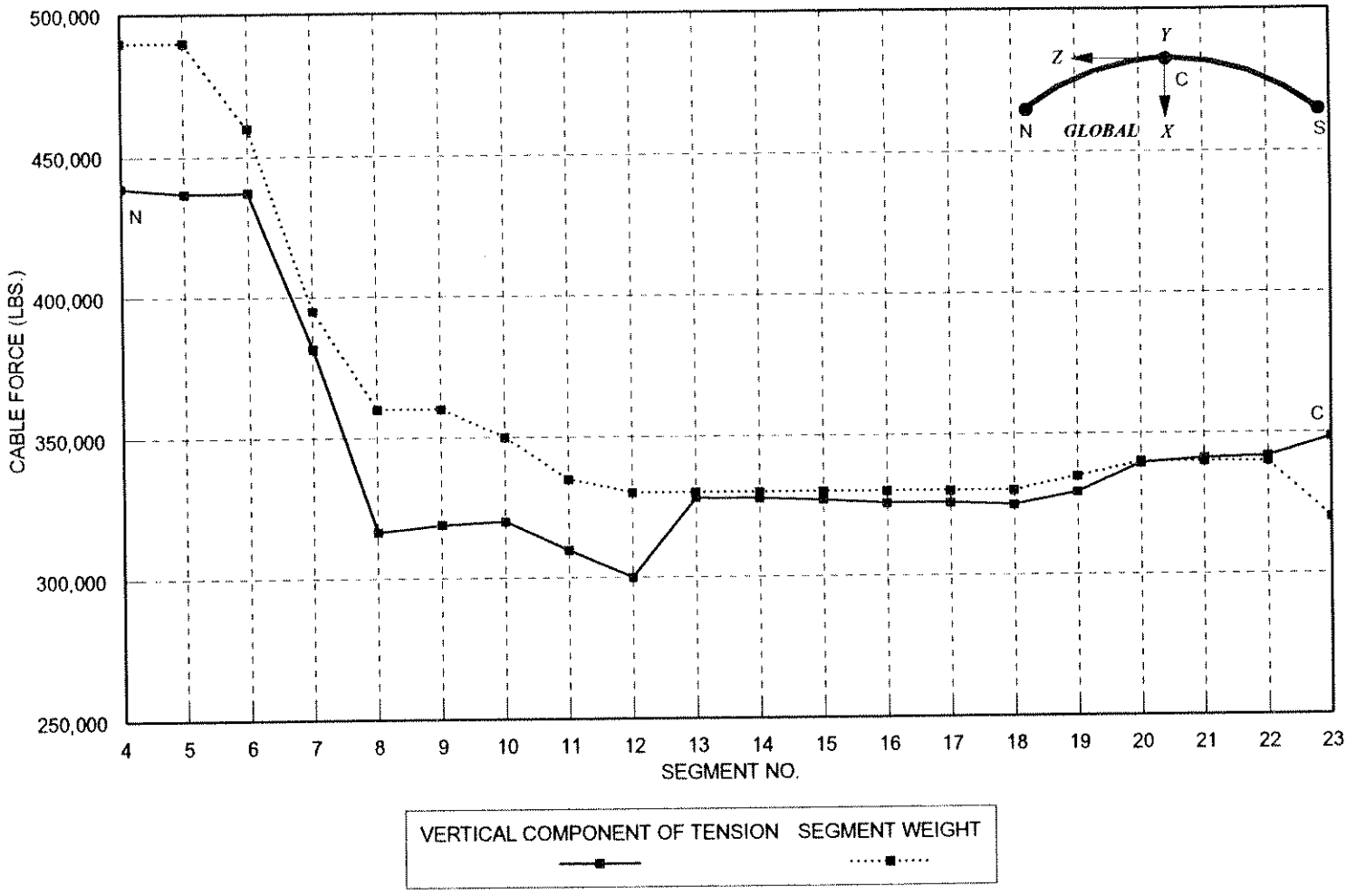

FIG. 14.17 VERTICAL COMPONENT OF CABLE TENSION VS SEGMENT WEIGHT; LOAD BALANCING ANALYSIS RUCK-A-CHUCKY CONCRETE BRIDGE

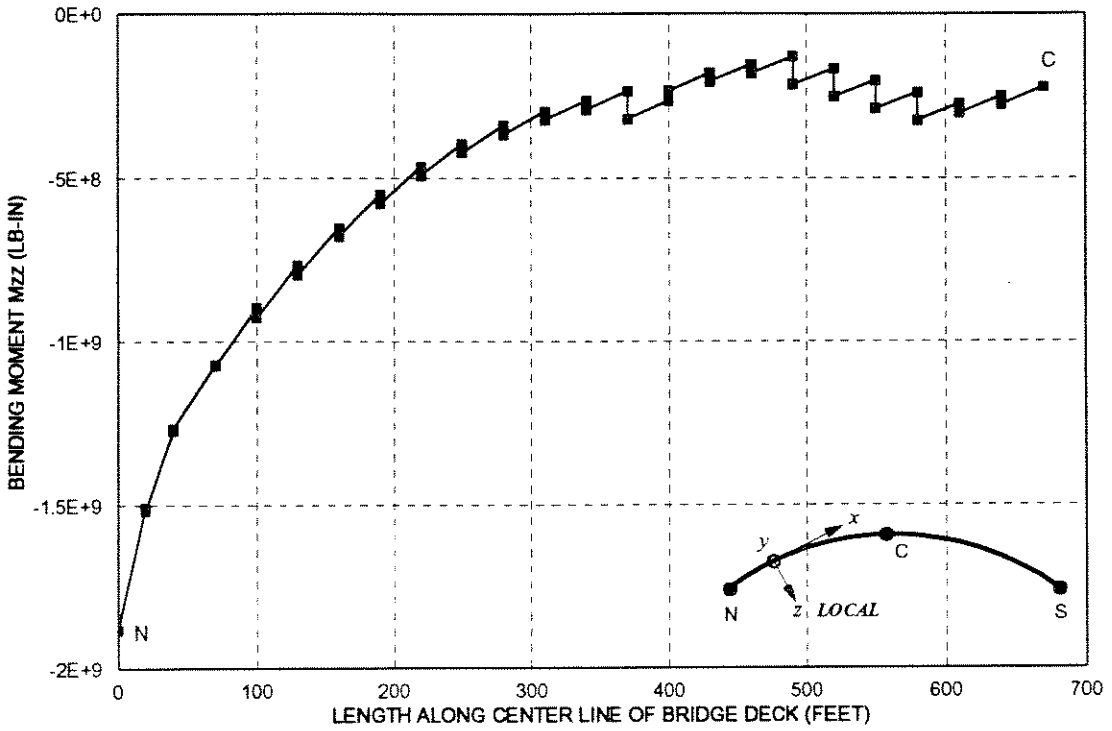

FIG. 14.18 LONGITUDINAL BENDING MOMENT Mzz IN THE BRIDGE DECK LOAD BALANCING ANALYSIS; RUCK-A-CHUCKY CONCRETE BRIDGE

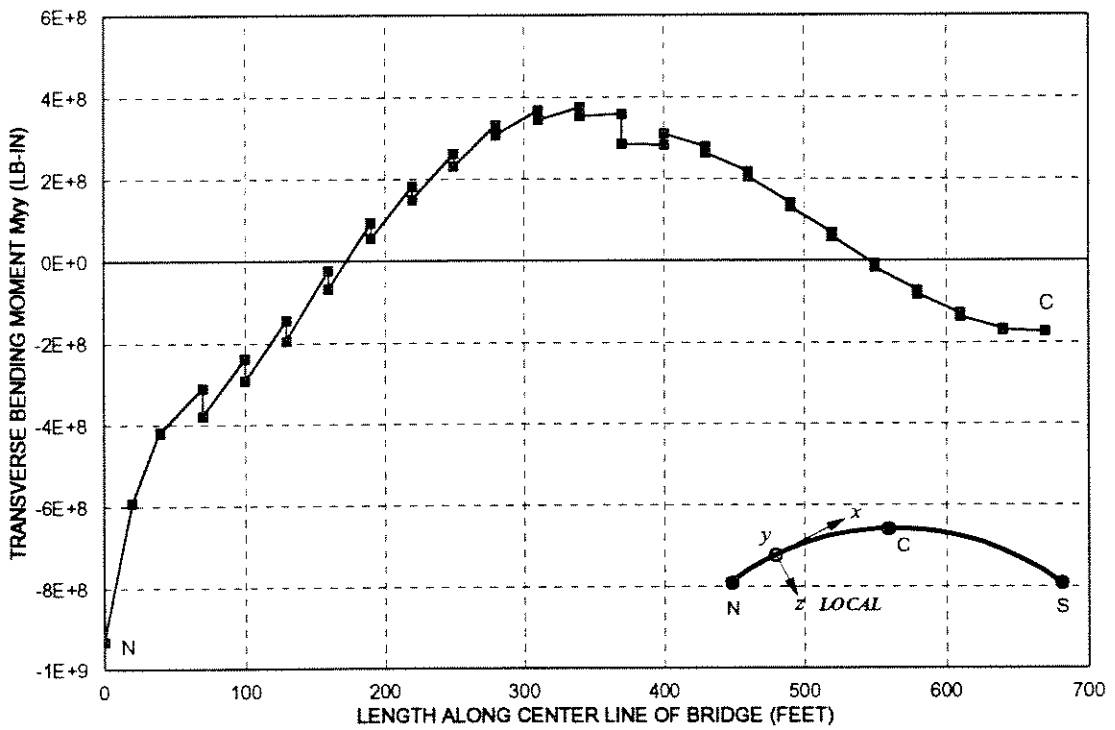

FIG. 14.19 TRANSVERSE BENDING MOMENT Myy IN THE BRIDGE DECK LOAD BALANCING ANALYSIS; RUCK-A-CHUCKY CONCRETE BRIDGE

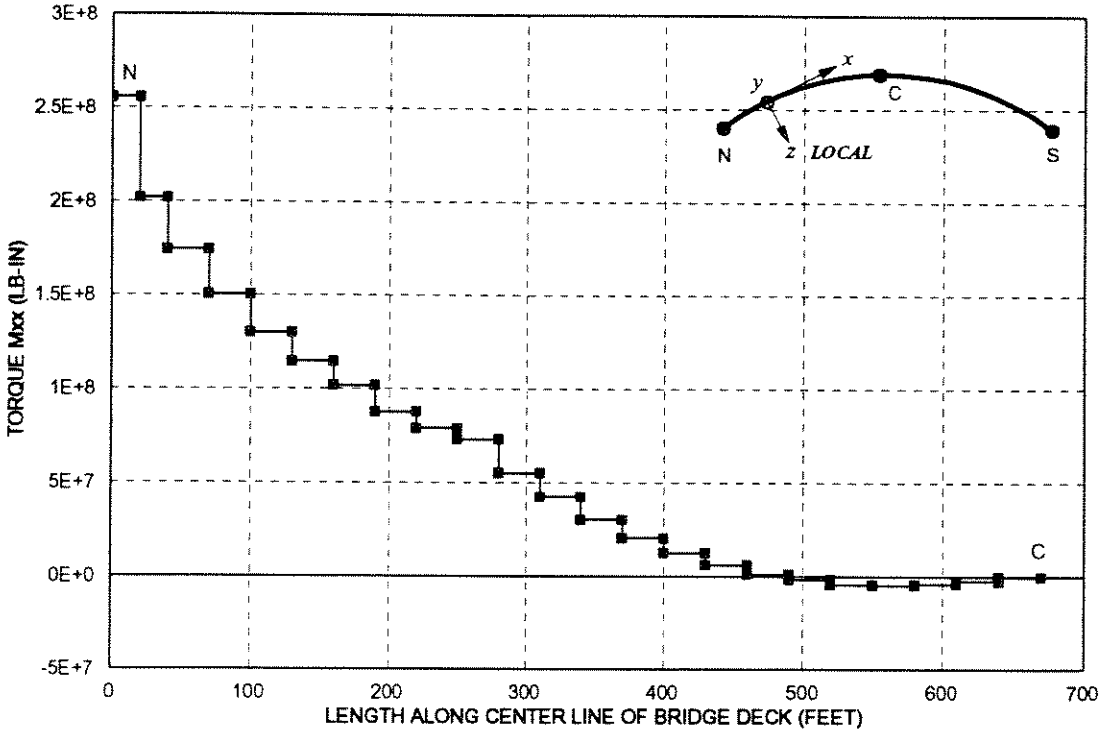

FIG. 14.20 TORQUE Mxx IN THE BRIDGE DECK
LOAD BALANCING ANALYSIS; RUCK-A-CHUCKY CONCRETE BRIDGE

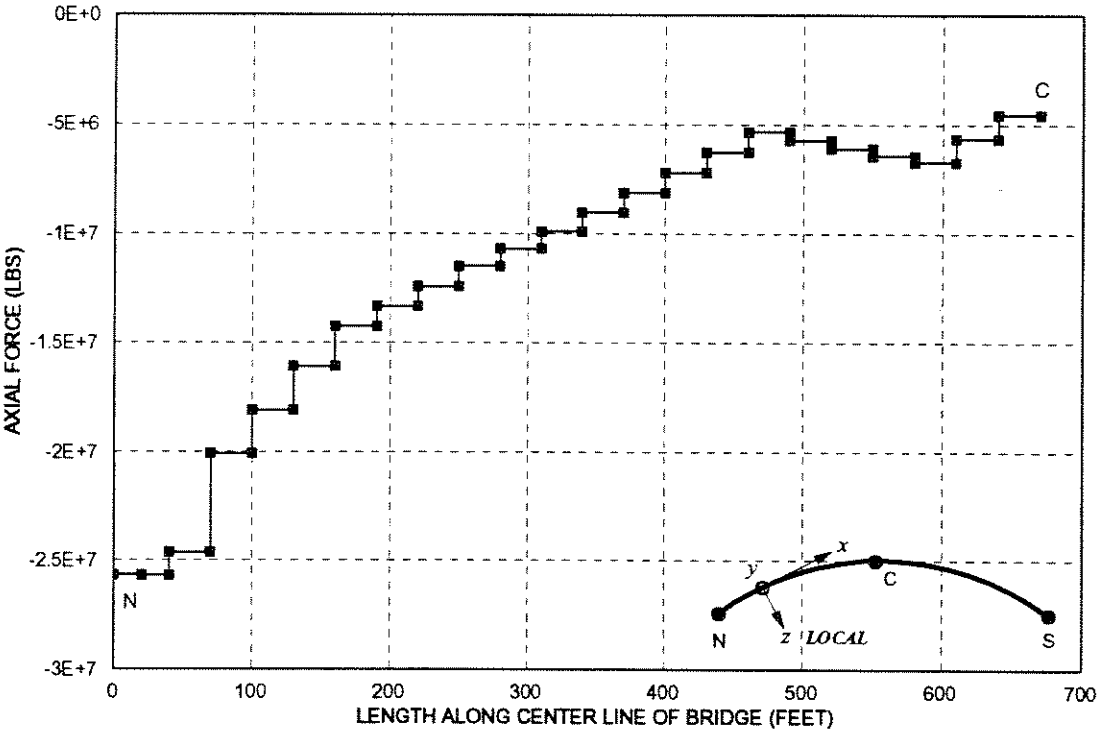

FIG. 14.21 AXIAL FORCE Fx IN THE BRIDGE DECK
LOAD BALANCING ANALYSIS; RUCK-A-CHUCKY CONCRETE BRIDGE

14.4. DIS-ASSEMBLY ANALYSIS

An assumed schedule for the construction sequence of the concrete bridge is given in the Table 14.05. The construction sequence is based on a 7 day cycle. The entire structure is erected in 154 days. Note that time dependent effects are not included in the dis-assembly analysis and appropriate corrections will be made later in the assembly analysis.

The summary of the cable tensions obtained from this analysis is presented in Table 14.06. These tensions will be subsequently used in the forward assembly analysis, discussed in the next section.

Fig. 14.22 and 14.23 show the vertical and transverse displacements of the bridge deck at various stages of dis-assembly. The plots are labeled in accordance with the following scheme.

a. Structure completed up to segment 22; auxiliary cables are in place. Cable tensions are set to values obtained in the load balancing analysis performed previously.
b. Segment 23 erected, symmetry boundary conditions imposed at node 24, midspan region prestressed and the construction of entire bridge completed.
c. Midspan prestressing tendons removed.
d. Midspan link released.
e. Segment 23 and cables removed.
f. Segment 22 and cables removed.

....

....

Segment 5 and cables removed.

Steps (a) and (b) are necessary so that the state of the completed structure corresponds exactly to that set out earlier in the load balancing analysis. The cable forces at stage (b),

with the auxiliary cables still on, are shown in Fig. 14.24. The dis-assembly commences from step (c) onwards.

The plots show some interesting aspects of the physical behavior of the structure. The maximum downward vertical deflection of the leading tip of the bridge during construction is about 4 in., whereas the maximum upward deflection is about 2 in. Also note the increase in vertical displacement due to prestressing in the midspan zone as shown by comparing plots (b) and (c) in Fig. 14.22.

Despite the fact that the transverse movement of the bridge is resisted by the temporary auxiliary cables, the structure tends to deflect inwards towards the center of the arc defined by the center line of the bridge . .However, maximum transverse deflection does not exceed 10 inches.

It is also interesting to note that at completion, both the transverse and vertical profile of the bridge as shown by plot (b), are within ±1 in. of the desired position, thereby establishing the fact that load balancing is indeed an effective tool in dealing with the design of cable stayed bridges.

TABLE 14.05

CONSTRUCTION SCHEDULE

Time (days)	*Cast Segment No.*	*Erect Segment No.*	*Stress Tendon No.*	*Stress Cable No.*	*Remove Cable No.*	*Comments*
0	1,2					Begin sequence
7	3	1,2	1,2			cantilever segments
14	4	3	3,4,5			
21	5	4	6,7,8	1,2		
28	6	5	9,10,11	3,4,41		
35	7	6	12,13,14	5,6		
42	8	7		7,8		
49	9	8		9,10,42		
56	10	9		11,12		
63	11	10		13,14		
70	12	11		15,16,43		
77	13	12		17,18		
84	14	13		19,20		
91	15	14		21,22		
98	16	15		23,24		
105	17	16		25,26		
112	18	17		27,28		
119	19	18		29,30		
126	20	19		31,32		
133	21	20		32,33		
140	22	21		33,34		
147	23	22		35,36		
154	24	23		37,38		
154		24		39,40		closure segment
154			15 - 34			midspan tendons
154					41,42,43	auxiliary cables

TABLE 14.06

DESIRED CABLE TENSIONS AT INSTALLATION

Cable No.	*Element No.*	*Tension (kips)*	*Cable No.*	*Element No.*	*Tension (kips)*
2NO	1	611	*2NI*	2	788
3NO	3	613	*3NI*	4	784
4NO	5	617	*4NI*	6	773
5NO	7	548	*5NI*	8	685
6N0	9	460	*6NI*	10	574
7NO	11	459	*7NI*	12	558
8NO	13	473	*8NI*	14	566
9NO	15	416	*9NI*	16	476
10NO	17	416	*10NI*	18	472
11NO	19	461	*11NI*	20	513
12NO	21	469	*12NI*	22	515
13NO	23	476	*13NI*	24	517
14NO	25	485	*14NI*	26	521
15NO	27	492	*15NI*	28	525
16NO	29	502	*16NI*	30	532
17NO	31	519	*17NI*	32	547
18NO	33	539	*18NI*	34	566
19NO	35	552	*19NI*	36	577
20NO	37	565	*20NI*	38	587
21NO	39	589	*21NI*	40	598
AUX	41	10			
AUX	42	16			
AUX	43	27			

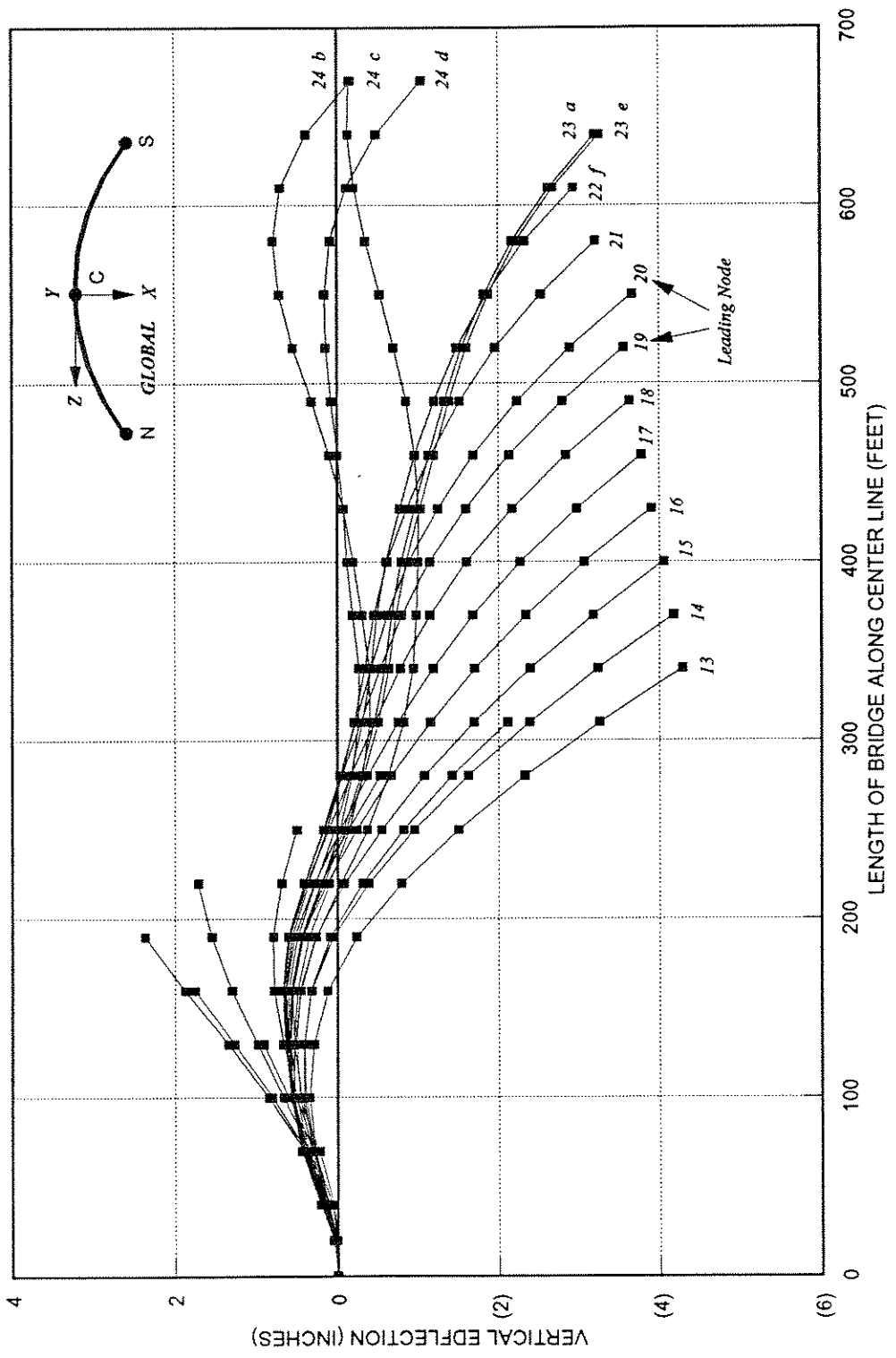

FIG. 14.22 VERTICAL DISPLACEMENTS (DY); DIS-ASSEMBLY ANALYSIS
RUCK-A-CHUCKY CONCRETE BRIDGE

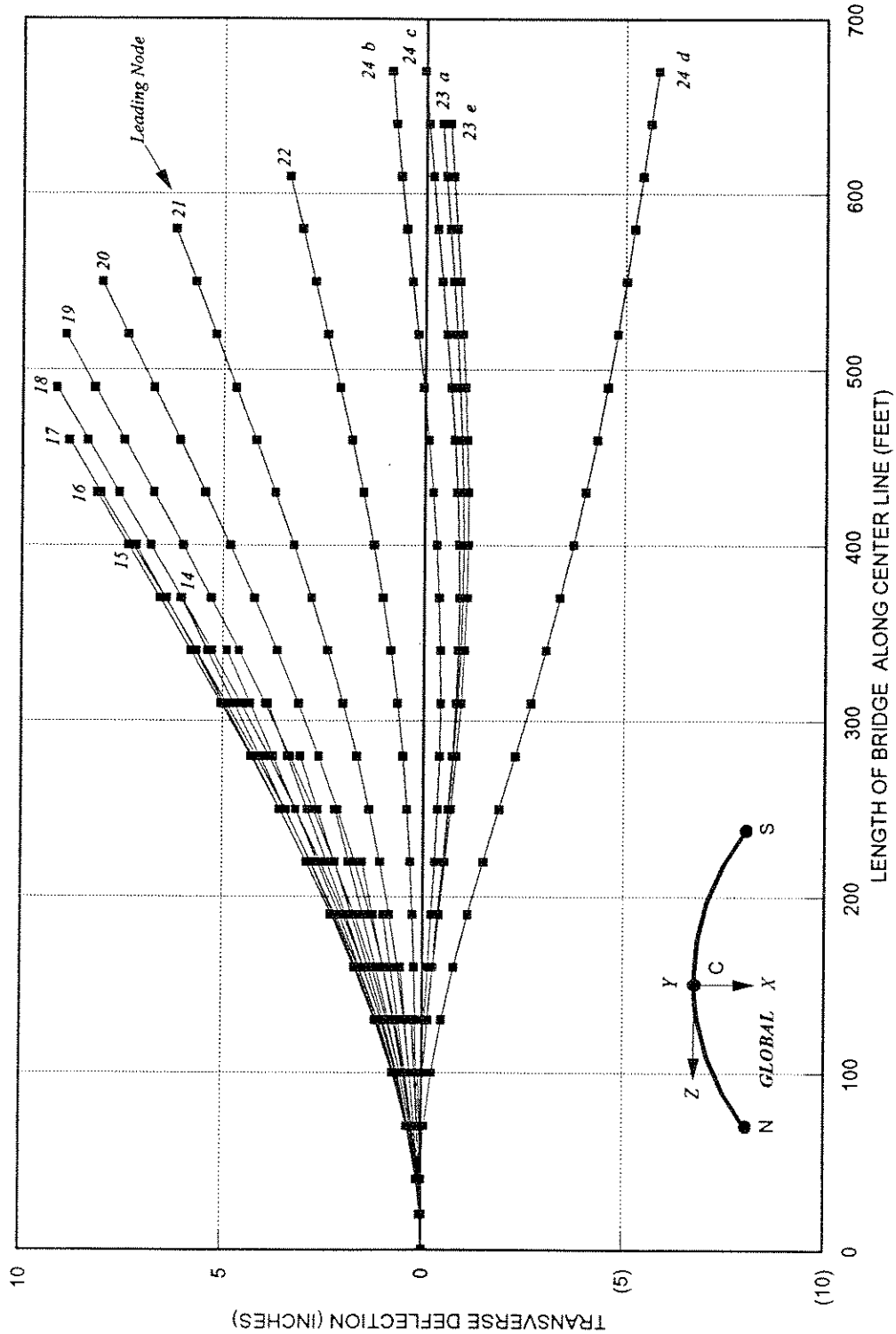

FIG. 14.23 TRANSVERSE DISPLACEMENTS (DX); DIS-ASSEMBLY ANALYSIS
RUCK-A-CHUCKY CONCRETE BRIDGE

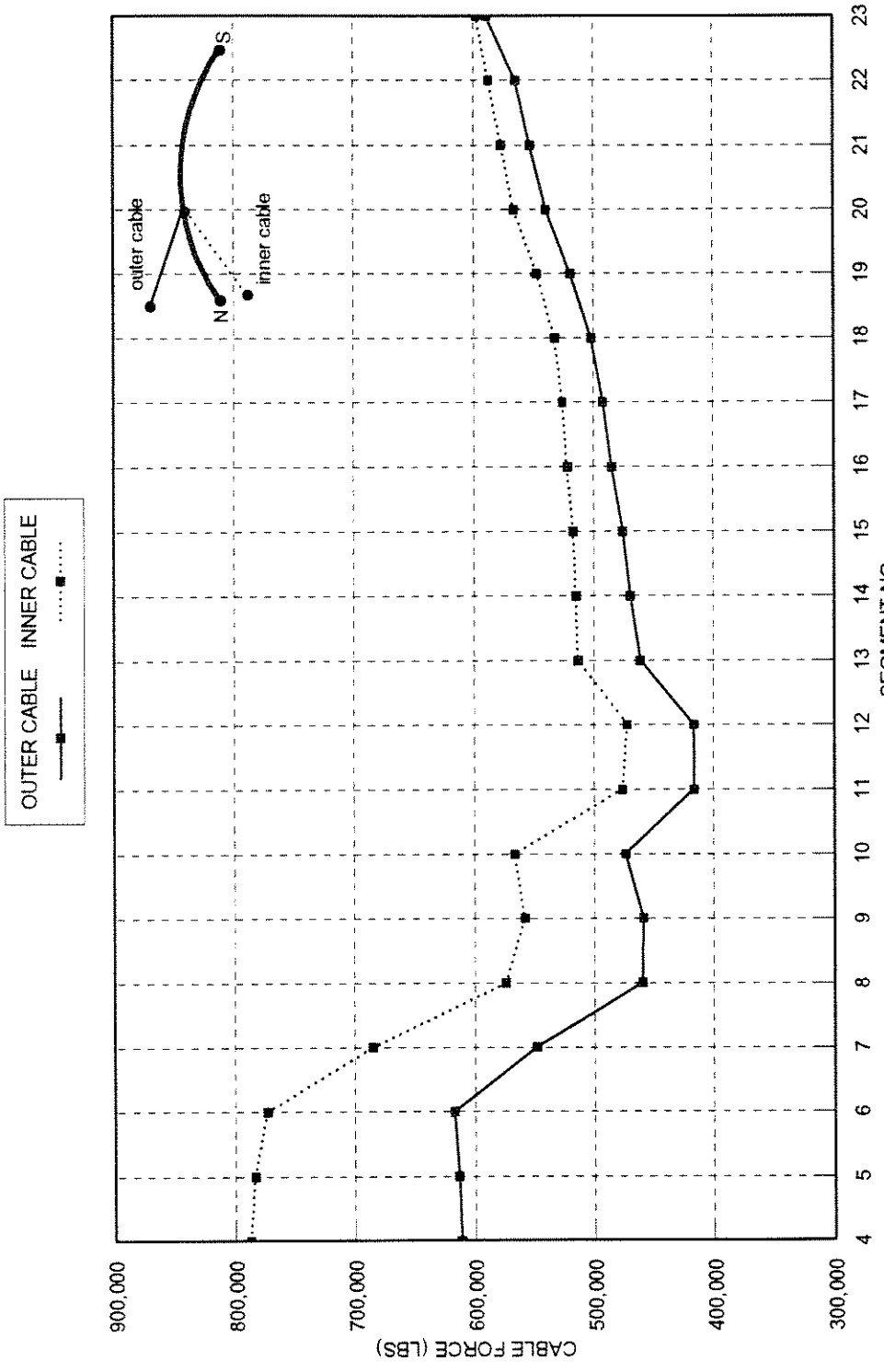

FIG. 14.24 CABLE FORCES AT CLOSURE; DIS-ASSEMBLY ANALYSIS
RUCK-A-CHUCKY CONCRETE BRIDGE

14.5. CONSTRUCTION SEQUENCE ANALYSIS

The forward assembly or the construction sequence analysis is performed using both the segmental and time dependent analysis capabilities of the computer program CALBRG.

The fabrication scheme discussed in the previous section was used for the forward assembly analysis. A typical solution step involves two analyses; for example consider the structural configuration at day 98. Refer to the construction schedule shown in Table 14.05; the two operations are as follows:

1. Install segment 15 (age 7 days) and cables 23 and 24. An instantaneous solution is obtained at this point.
2. Move forward in time to day 105. A time dependent analysis is carried out accounting for creep and shrinkage of concrete and relaxation of prestressing tendons.

This cycle is repeated until the entire structure is complete.

It is also required to determine the state of the structure after most of the creep and shrinkage has taken place and the state of the structure has somewhat stabilized. For this purpose the structure is subjected to a time dependent solution and the state of the structure is determined at the end of an arbitrarily chosen time period of 10000 days which is about 27 years.

Fig. 14.25 shows the vertical displacements (Dy) of the bridge at completion and at the end of 10000 days. At the completion of construction the structure deflects about 40 inches at mid span. This is clearly an unacceptable solution and measures to remedy this situation will be discussed later. The vertical deflections (Dy) do not change much with time because the deck is supported by cables at numerous points and the total cable force does not change with time.

The transverse deflections of the deck (Dx), shown in Fig. 14.26 are strongly influenced by the time dependent effects and increase from 5 inches at completion to about 20 inches after 10000 days. This is due to the relatively lower stiffness of the cable system in the transverse direction, hence allowing the deck girder to undergo time dependent deformations.

Fig. 14.27 shows a three dimensional view of the bridge, its shape at completion, and after 10000 days. The structure moves inwards and down with time.

The distribution of inner and outer cable tensions is shown in Fig. 14.28. Note that cable tensions increase in outer cables but decrease in the inner cables. Also the increase in tension in the outer cable at each node is equal to the decrease in tension in the inner cable at the same node in order to preserve equilibrium. In addition, the cable tensions tend to become equal to each as we move towards the mid span of the bridge.

The change in the distribution of longitudinal and transverse bending moments, torque, and axial force from completion to 10000 days is shown in Fig. 13.29, 13.30, 13.31, 13.32 respectively. Note that the transverse bending moment M_{yy} went through a substantial redistribution; the bending moment at the support changed from -1.5E+9 to +0.5E+9. This is due to a combination of changes in the transverse component of the cable tensions and to time dependent effects.

The deflections due to time dependent effects can be controlled in a number of ways.

1. Adjusting cable tensions before erecting the mid span closure segment.
2. Allowing the concrete segments to cure for a longer duration of time to reduce the effect of time dependent effects in the assembled structure.
3. Providing a camber in the structure against the time dependent effects such that after the time dependent displacements have occurred the structure moves into the desired position.

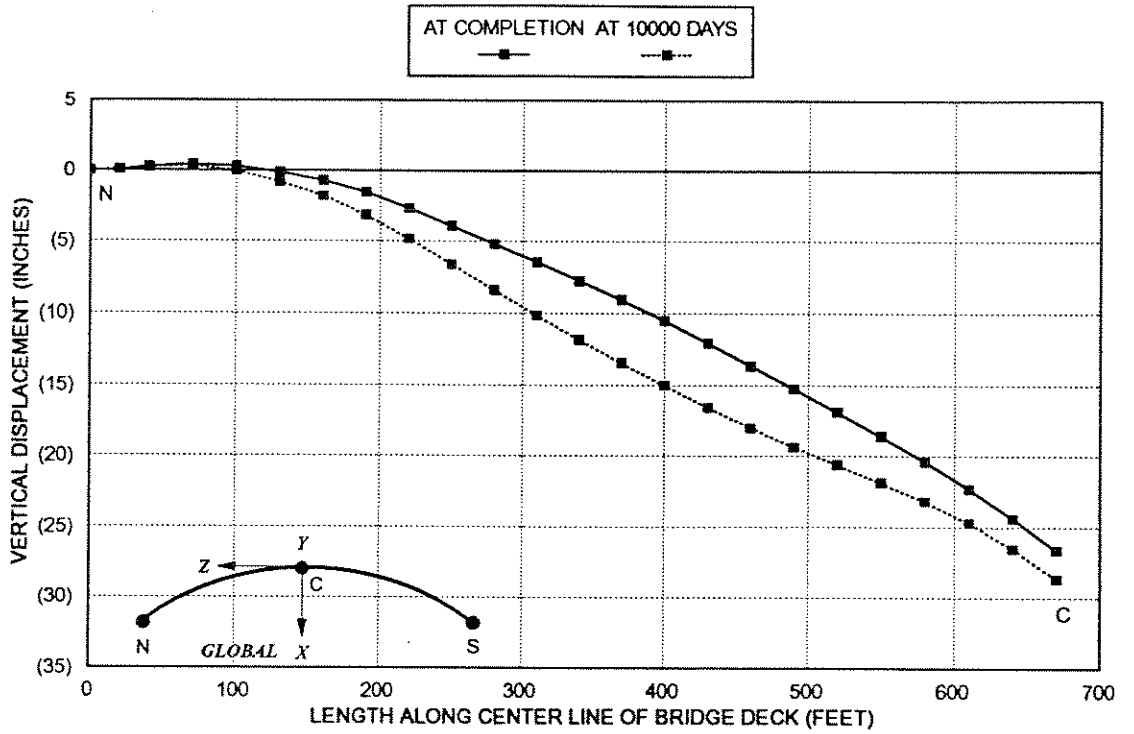

FIG. 14.25 VERTICAL DISPLACEMENTS (DY) OF THE BRIDGE DECK
TIME DEPENDENT ANALYSIS; RUCK-A-CHUCKY CONCRETE BRIDGE

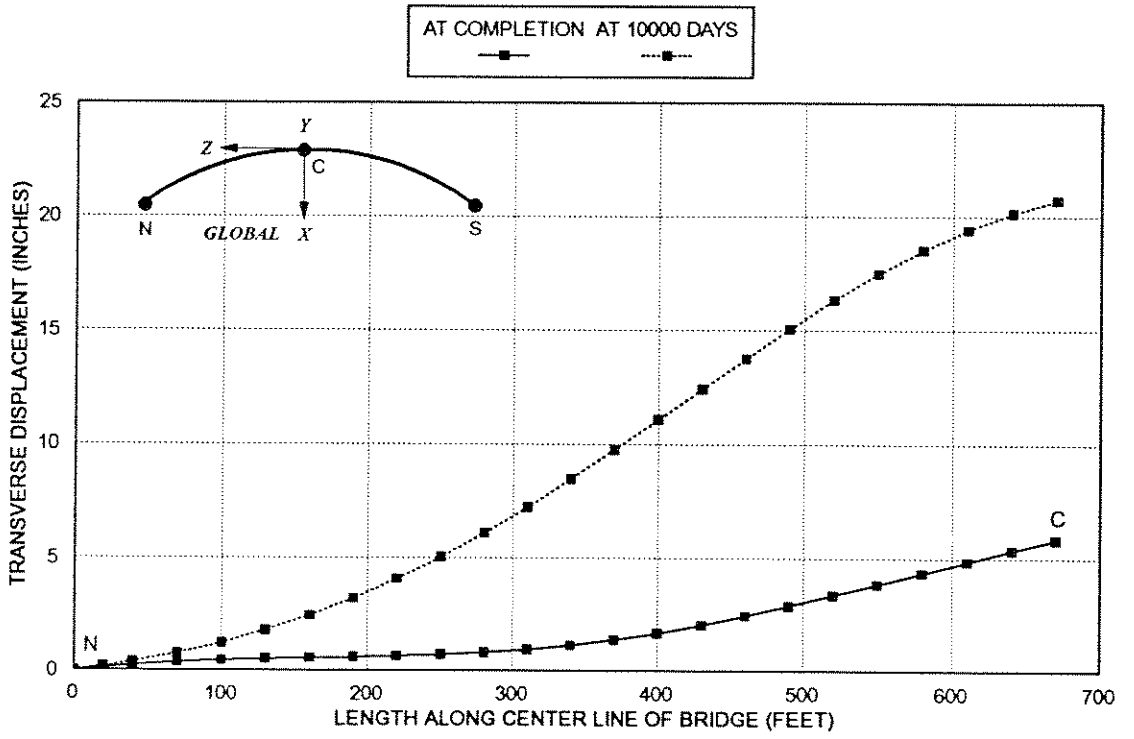

FIG. 14.26 TRANSVERSE DISPLACEMENTS (DX) OF THE BRIDGE DECK
TIME DEPENDENT ANALYSIS; RUCK-A-CHUCKY CONCRETE BRIDGE

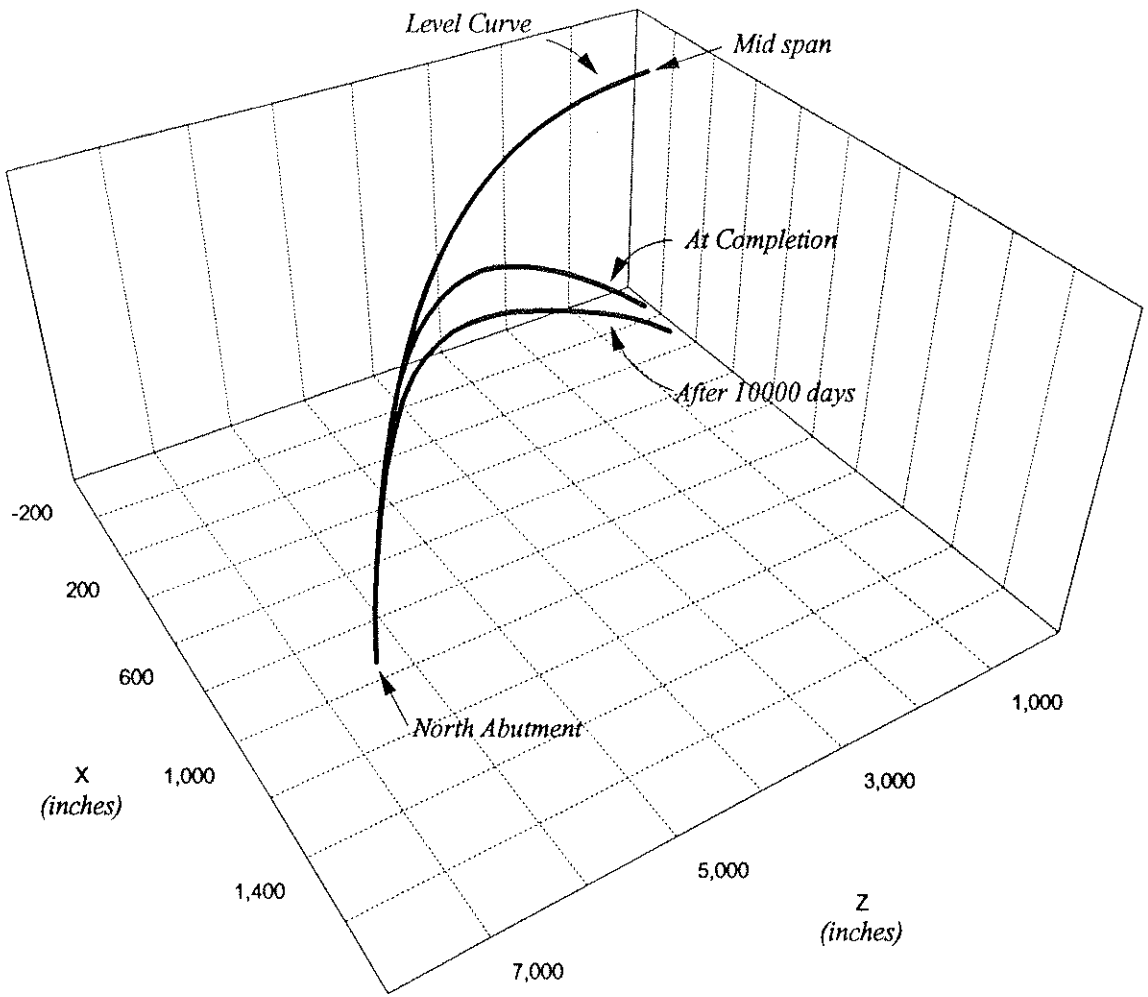

FIG.14.27 COMPARISON OF PROFILE AT COMPLETION AND AT 10000 DAYS
TIME DEPENDENT ANALYSIS; RUCK-A-CHUCKY CONCRETE BRIDGE

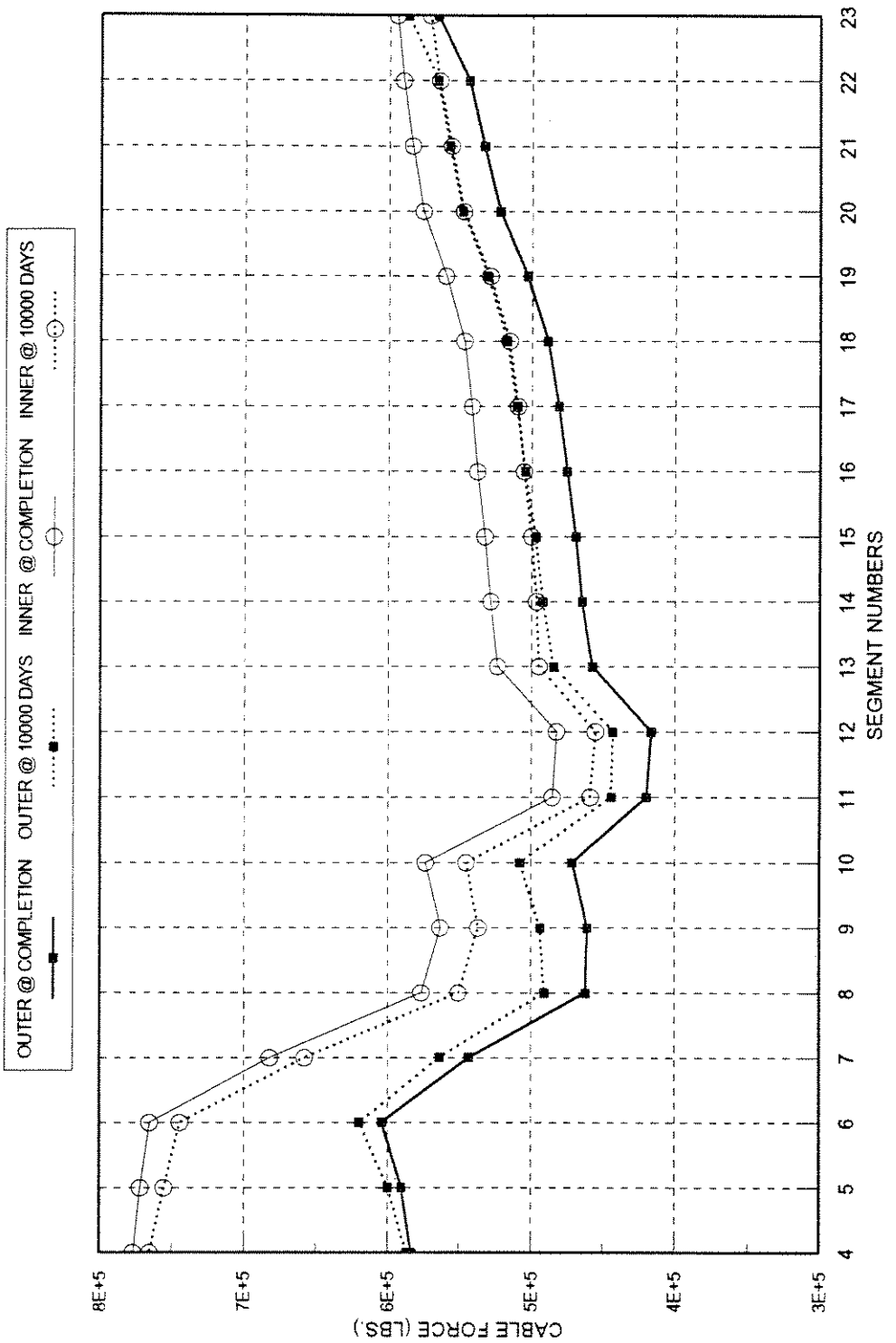

FIG. 14.28 CABLE TENSIONS AT COMPLETION AND AT 10000 DAYS
TIME DEPENDENT ANALYSIS; RUCK-A-CHUCKY CONCRETE BRIDGE

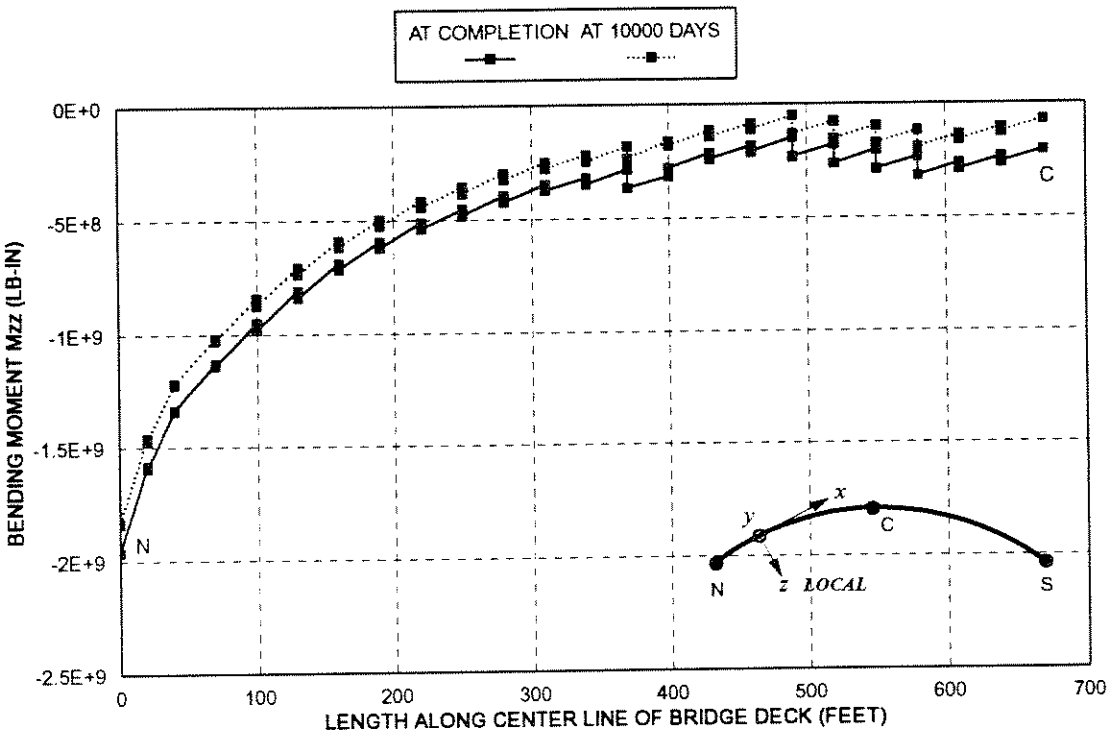

FIG. 14.29 LONGITUDINAL BENDING MOMENT Mzz IN THE BRIDGE DECK
TIME DEPENDENT ANALYSIS; RUCK-A-CHUCKY CONCRETE BRIDGE

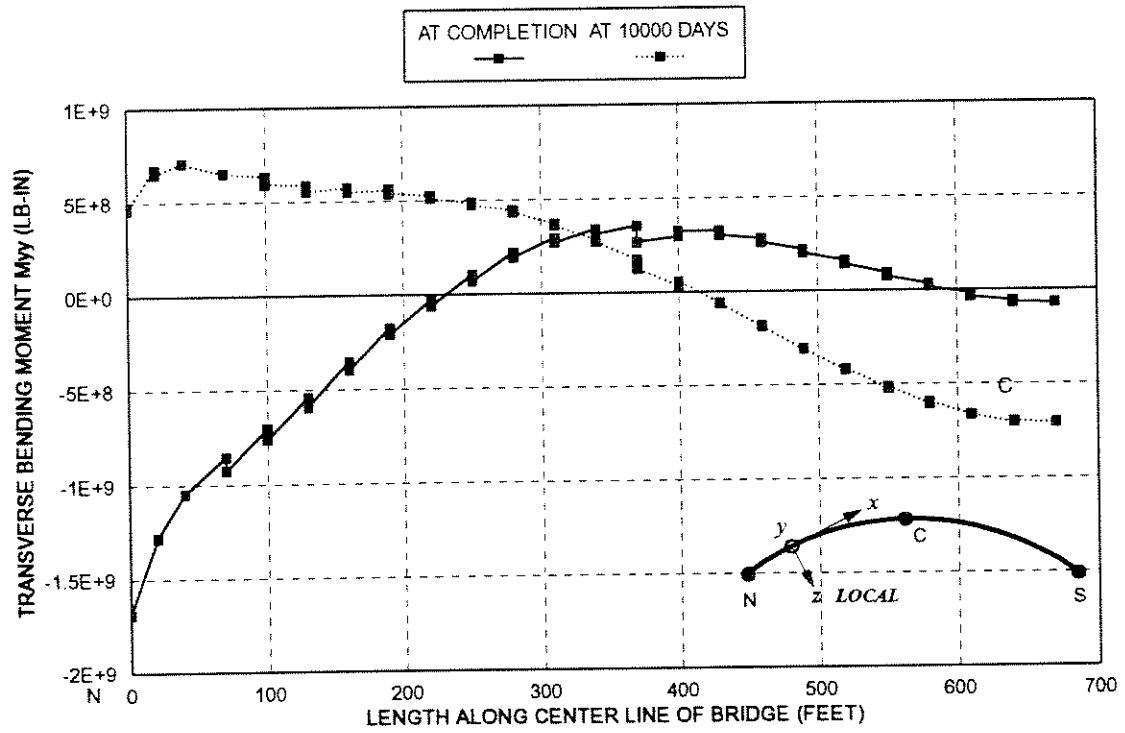

FIG. 14.30 TRANSVERSE BENDING MOMENT Myy IN THE BRIDGE DECK
TIME DEPENDENT ANALYSIS; RUCK-A-CHUCKY CONCRETE BRIDGE

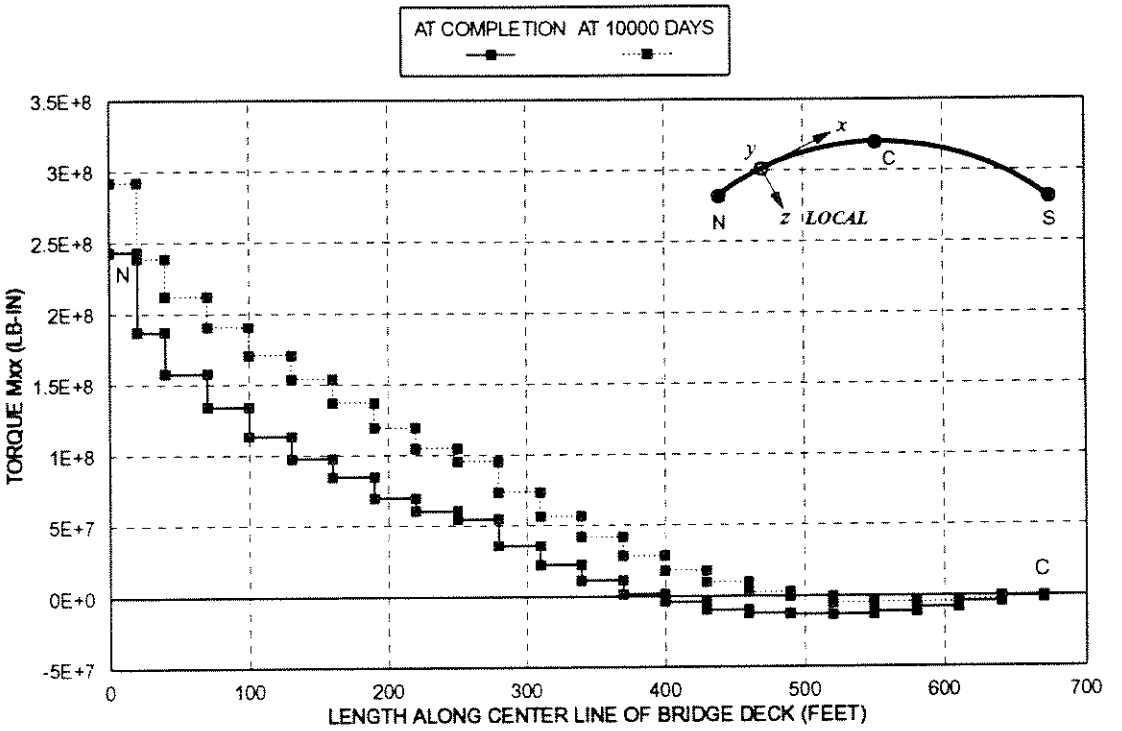

FIG. 14.31 TORQUE Mxx IN THE BRIDGE DECK
TIME DEPENDENT ANALYSIS; RUCK-A-CHUCKY CONCRETE BRIDGE

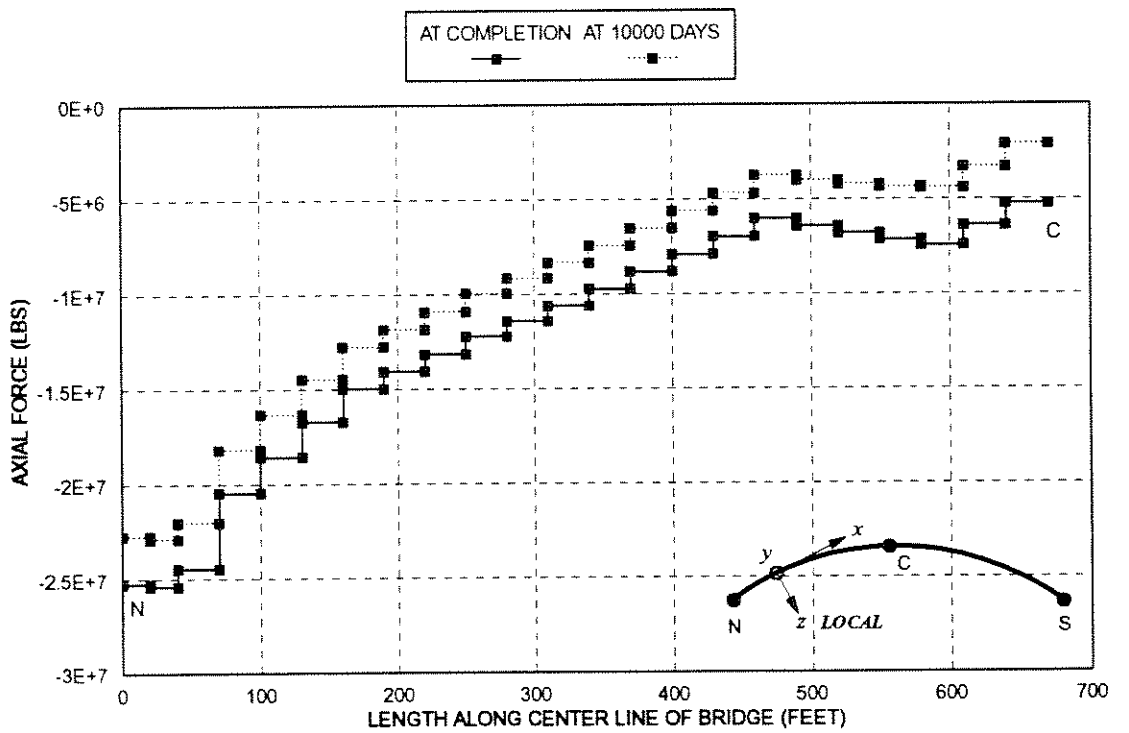

FIG. 14.32 AXIAL FORCE Fx IN THE BRIDGE DECK
TIME DEPENDENT ANALYSIS; RUCK-A-CHUCKY CONCRETE BRIDGE

14.6. ULTIMATE LOAD ANALYSIS

Ultimate load analysis is carried out on the completed bridge, built in a single step. All concrete is assumed to be 28 days old. Cable tensions are set to balance the dead loads and no auxiliary cables are used. Prestressing tendons at the abutment and in the midspan region are assumed to be active. Geometric and material nonlinearity is enforced. A load pattern corresponding to the distribution of dead loads is applied to the structure. The analysis employs both load and displacement control solution strategies.

The first step consists of applying the full dead load to the structure in a single step using load control. This load is balanced by the tension in the cable-stays. Analysis results show that at this stage the bridge deck is mostly uncracked. Maximum transverse deflection of 8 in. occurs at midspan. Vertical deflections are negligible.

The analysis is then continued using displacement control and the dead load pattern. The vertical displacement at node 24 is selected as the controlled degree of freedom. A displacement increment of 2.5 in. is specified for each step and results are output after every 4 steps.

The structure exhibits a strong nonlinearity in the transverse direction. However in the vertical direction the response is mostly linear. Fig. 14.33 shows the transverse displacements at the midspan of the bridge plotted against normalized dead load. The vertical displacements at the same point are shown in Fig. 14.34.

As the controlled vertical displacement at midspan is increased to 20 inches, the deck segments near the abutment begin to crack and there is a redistribution of forces in the bridge deck. This transition is shown by the softening of the structure between points A and B in Fig. 14.33 and is also obvious in Fig.14.43 and 14.44, which illustrate the evolution of forces and moments at the critical sections.

As the structure is loaded it continues to soften in the transverse direction. Note that for equal increments in the vertical displacements at the mid span, increasingly larger transverse displacements take place at each step. Finally the load carrying capacity of the structure is exhausted at point C which corresponds to a transverse displacement of 24 inches and a vertical displacement of 170 inches at the midspan. The failure load is about twice the dead load of the structure.

The linear behavior of the structure in the vertical direction can be attributed to two reasons.

1. Load is balanced by the cable-stays in the vertical direction as shown in Fig. 14.35, thereby reducing distress in the deck.
2. Large number of cable-stays, which remain mostly elastic.

In the transverse direction the deck has to absorb the increasing unbalanced horizontal components of the cable tensions by itself as the transverse stiffness of the supporting cable system is relatively low because of the following reasons:

1. The shallow horizontal angle of the outer cables.
2. Small contribution from the inner cables because the structure swings inwards as the load is increased.

A comparison of transverse displacements along the center line of the bridge deck at dead load and at ultimate is shown in Fig. 14.37. A similar plot for vertical displacements is shown in Fig. 14.38. Note that the deck segments in the midspan zone are much stiffer than the others because of the prestressing in that area and consequently behave somewhat like a rigid body.

Fig 14.36 compares the tension in the cable-stays at dead load and at ultimate. Cables near the abutment experience a relatively minor change in the axial tension because of the higher deck stiffness in that area. Cable No. 13, the outer cable on segment No. 10 under goes the largest change in axial tension from 520 kips to 1224 kips, however the corresponding maximum stress of 195 ksi at ultimate is still well below the yield limit of 246 ksi.

The variation of longitudinal and transverse bending moments, torque and axial force is shown in Figs. 9, 10, 11 and 12 respectively. The bending moments and axial force are calculated and plotted with respect to the reference axis of the element using the beam sign convention.

The longitudinal bending moment M_{zz} is shown in Fig. 14.39. This moment has a relatively small value in the midspan region, however, it increases rapidly near the abutment and has a peak value of 5,250,000 kip-in. at the abutment section. Note that ultimate load moment at the abutment is about 3 times the dead load moment.

The transverse bending moment M_{yy} shown in Fig. 14.40 has a relatively small value at the abutment but increases rapidly to a peak value of about 1,700,000 kip-in. in segment No. 8 , 9 and 10. Note that this increase in the transverse bending moment corresponds to the increase in the difference of axial tensions of the inner and outer cables as shown in Fig. 14.36. The transverse bending moment then changes sign and has a peak value of -1,400,000 kip-in. in the midspan segment No. 23.

Torsional moment at ultimate at the abutment is 3 times its dead load value, Fig. 14.41. A comparison of this plot with the yield capacities indicates that some torsional yielding may have occurred near the abutment; this will be examined later in this section.

The axial force picked up by the bridge deck is essentially the component of the cable force tangential to the deck, Fig. 14.42. As the cable tension increases, the axial force fed into the deck also increases. This induces compression in the bridge deck which increase from mid span to the abutment. At higher load levels some tension may be induced in the closure segment at midspan. However, in this particular case because of prestressing in the mid span zone, the higher cable tensions at ultimate merely manage to reduce the compression in the deck in that region. Absence of prestressing would have drastically reduced the load carrying capacity of the structure.

14.6.1. STATE OF THE STRUCTURE AT FAILURE

The computer program CALBRG produces a very detailed output that includes fiber stresses, strains and state codes. A thorough examination of this data at the ultimate state, identified the following information:

1. High fiber strains and yielding states exist in segment 3.
2. The torsional moment exceeds the cracking torque in segment 3.
3. The torsional moment exceeds the cracking torque in segment 4.
4. High fiber strains and yielding states exist in segment 23.

Fig. 14.43 shows the evolution of longitudinal moment M_{zz}, transverse moment M_{yy} and axial force F at section 1 of segment No. 3. Each quantity has been normalized with respect to its ultimate value, which is the moment or force acting alone, that would cause the section to fail. The plot shows that the dominating quantities are the longitudinal bending moment M_{zz} and the axial force F and that the presence of axial force enhances the ability of the section to carry the bending moment.

Fig. 14.44 shows a similar plot for the midspan section (section 4 of segment 23). Note that in this case the two bending moment namely M_{zz} and M_{yy} dominate the response of the section. The ratio $M_{zz}/(M_{zz})_{\max}$ reaches a maximum value of 0.65 at about 1.6 times the dead load and gradually decreases to 0.55 at ultimate load. Similarly the ratio $M_{yy}/(M_{yy})_{\max}$ reaches a value of 0.4 at 1.6 times the dead load and then gradually increases as more load is added to the structure. It is noteworthy here that in the absence of any appreciable axial load the following equation is approximately satisfied at or near the ultimate load.

$$\frac{M_{zz}}{(M_{zz})_{\max}} + \frac{M_{yy}}{(M_{yy})_{\max}} \cong 1$$

The analysis data further indicate that segment 3 begins to pick up stresses at relatively low load levels. This is perhaps due the fact that although segment 3 is the first relatively slender

segment at the end of the rather robust and heavily reinforced cantilever section, it is not supported by cable stays and instead the designer has relied on heavy prestressing in the top flange of the segment.

As the load on the structure is gradually increased, segment 3 near the abutment yields under the combined action of biaxial moments and axial load. This is followed by yielding of the deck at midspan (segment 23), predominantly due to the action of transverse bending moment M_{yy}. In addition to this, at about 1.6 times the dead load, the applied torque exceeded the cracking torque in segment No. 3 and 4 thereby reducing their torsional stiffness by a factor of approximately 17.

The failure load is about twice the dead load (2 D) of the structure. The average dead load (deck+cables) applied to the structure is 12.7 kips/ft. Assuming a live load of 640 lbs per ft. of load lane, as prescribed by AASHTO [129], the failure load is 1.4D+5.9L or D+9.9L.

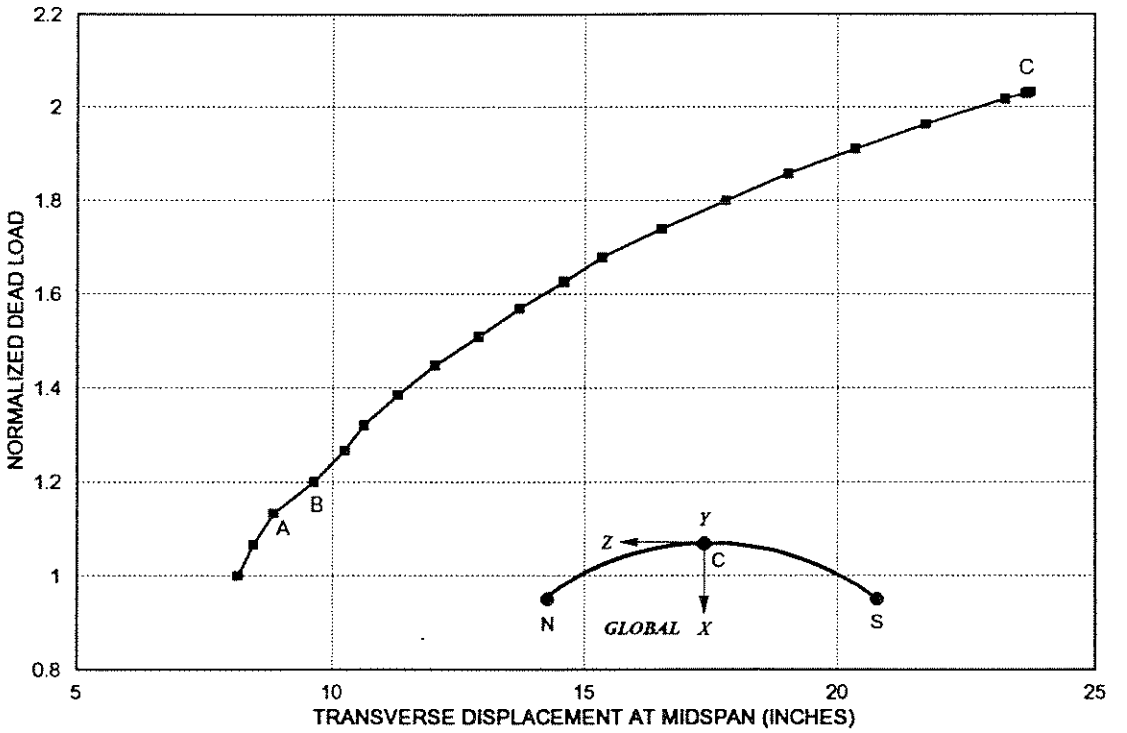

FIG. 14.33 TRANSVERSE DISPLACEMENT (DX) AT MIDSPAN VS NORMALIZED DEAD LOAD ULTIMATE LOAD ANALYSIS; RUCK-A-CHUCKY CONCRETE BRIDGE

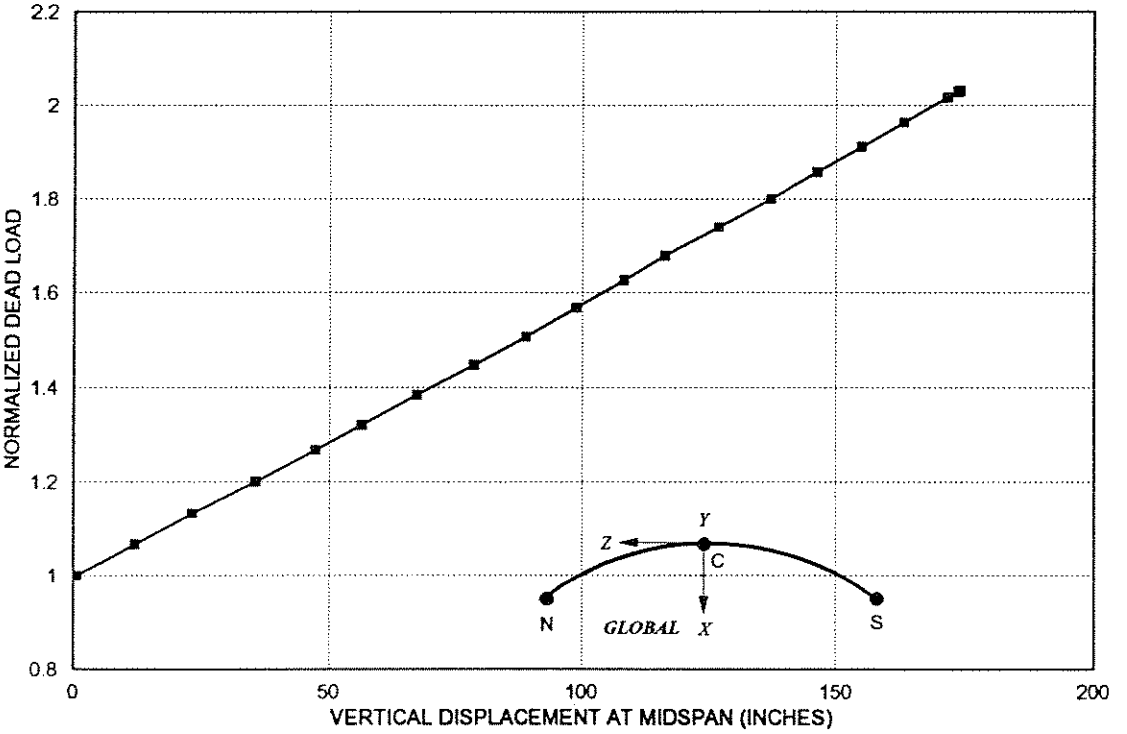

FIG. 14.34 VERTICAL DISPLACEMENT (DY) AT MIDSPAN VS NORMALIZED DEAD LOAD ULTIMATE LOAD ANALYSIS; RUCK-A-CHUCKY CONCRETE BRIDGE

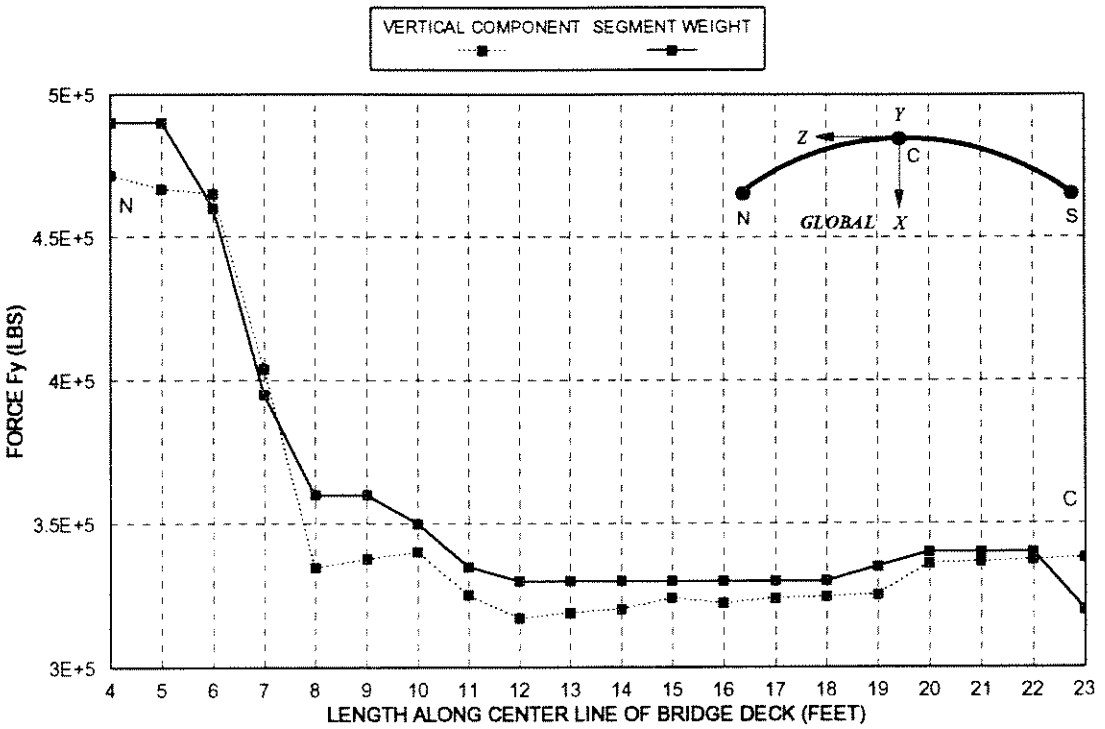

FIG. 14.35 VERTICAL COMPONENT OF CABLE FORCE (Fy) VS LOAD AT ULTIMATE
ULTIMATE LOAD ANALYSIS; RUCK-A-CHUCKY CONCRETE BRIDGE

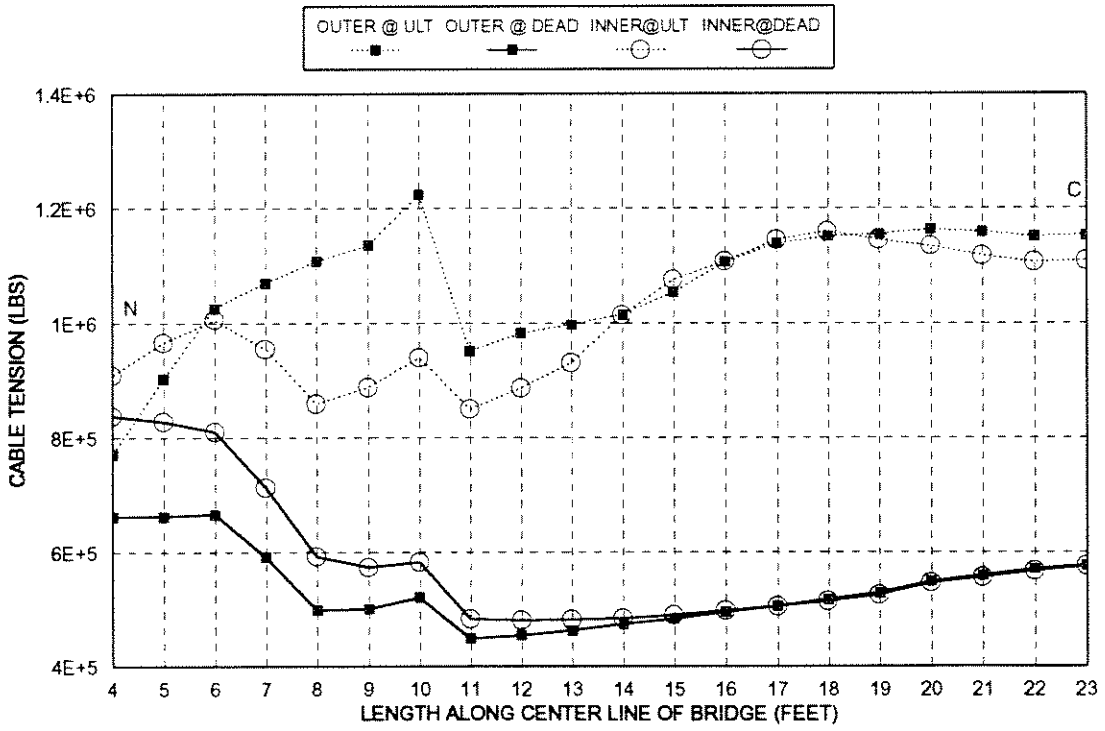

FIG. 14.36 COMPARISON OF CABLE TENSIONS AT DEAD AND ULTIMATE LOAD
ULTIMATE LOAD ANALYSIS; RUCK-A-CHUCKY CONCRETE BRIDGE

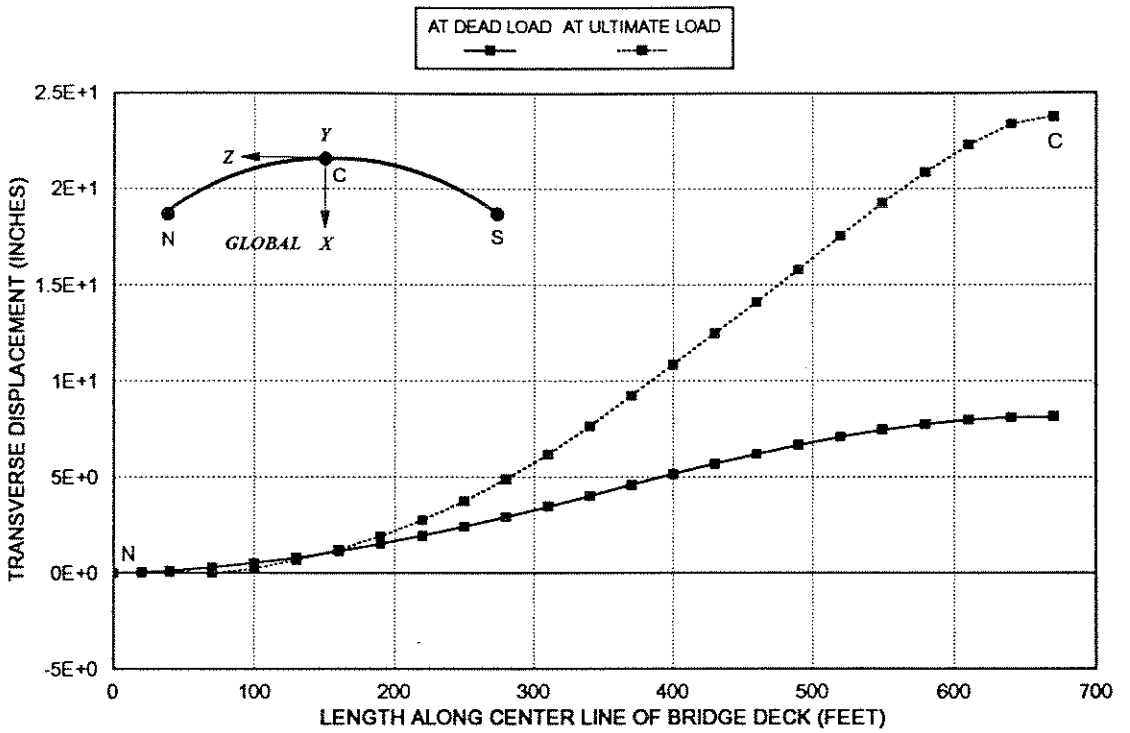

FIG. 14.37 TRANSVERSE DISPLACEMENTS (DX) OF THE BRIDGE DECK AT DEAD AND ULTIMATE LOAD ULTIMATE LOAD ANALYSIS; RUCK-A-CHUCKY CONCRETE BRIDGE

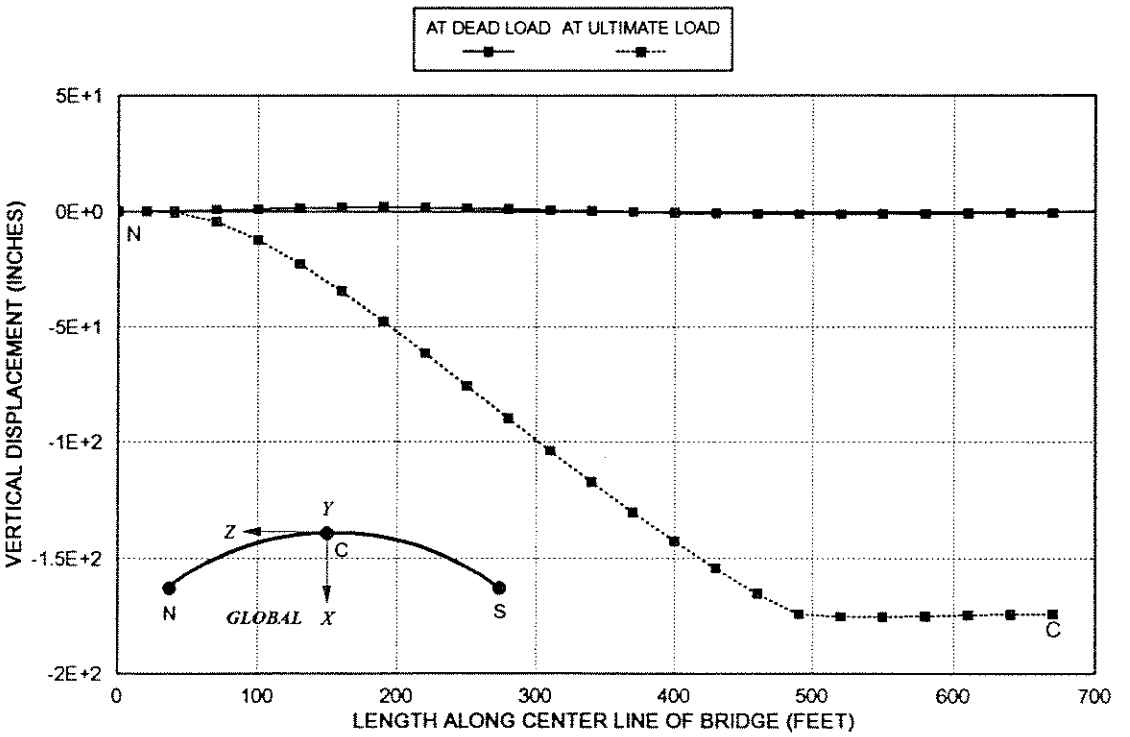

FIG. 14.38 VERTICAL DISPLACEMENTS (DY) OF THE BRIDGE DECK AT DEAD AND ULTIMATE LOAD ULTIMATE LOAD ANALYSIS; RUCK-A-CHUCKY CONCRETE BRIDGE

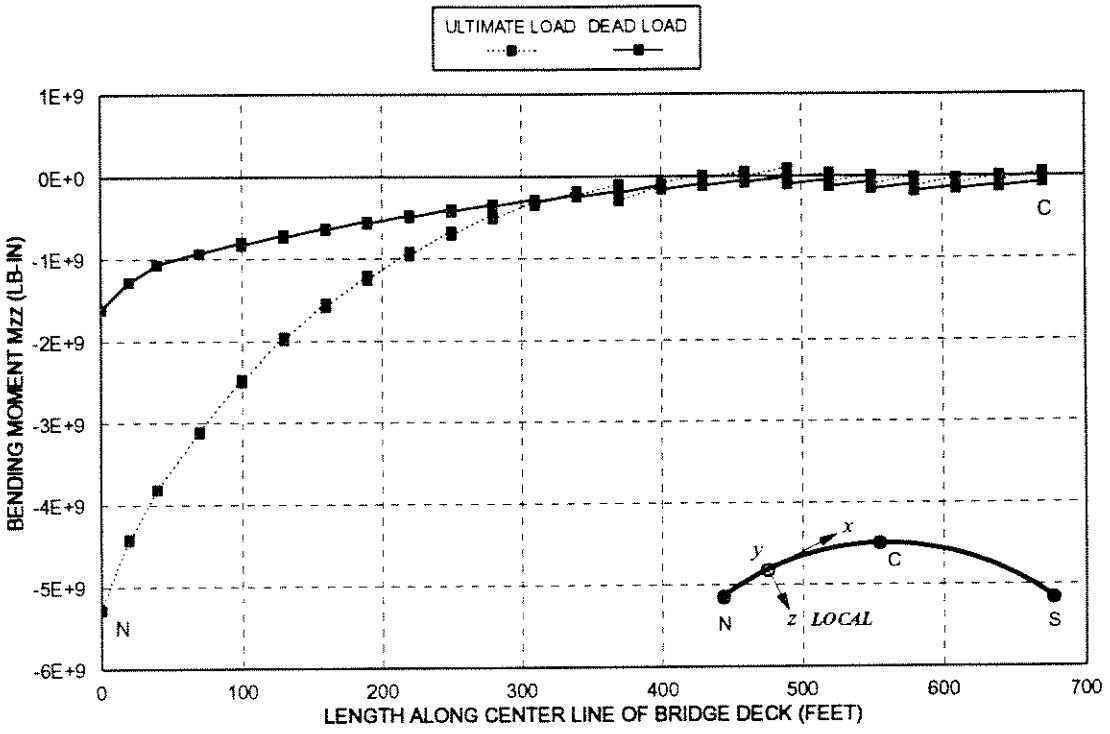

FIG. 14.39 LONGITUDINAL BENDING MOMENT Mzz IN THE BRIDGE DECK AT DEAD AND ULTIMATE LOAD; RUCK-A-CHUCKY CONCRETE BRIDGE

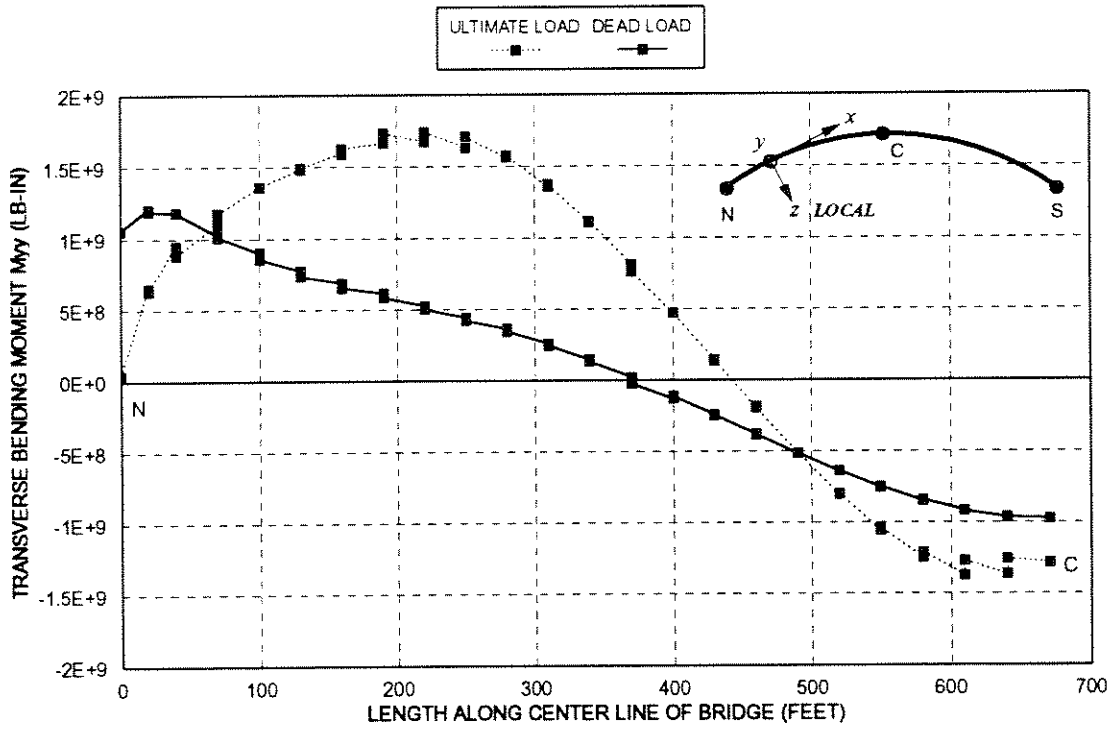

FIG. 14.40 TRANSVERSE BENDING MOMENT Myy IN THE BRIDGE DECK AT DEAD AND ULTIMATE LOAD; RUCK-A-CHUCKY CONCRETE BRIDGE

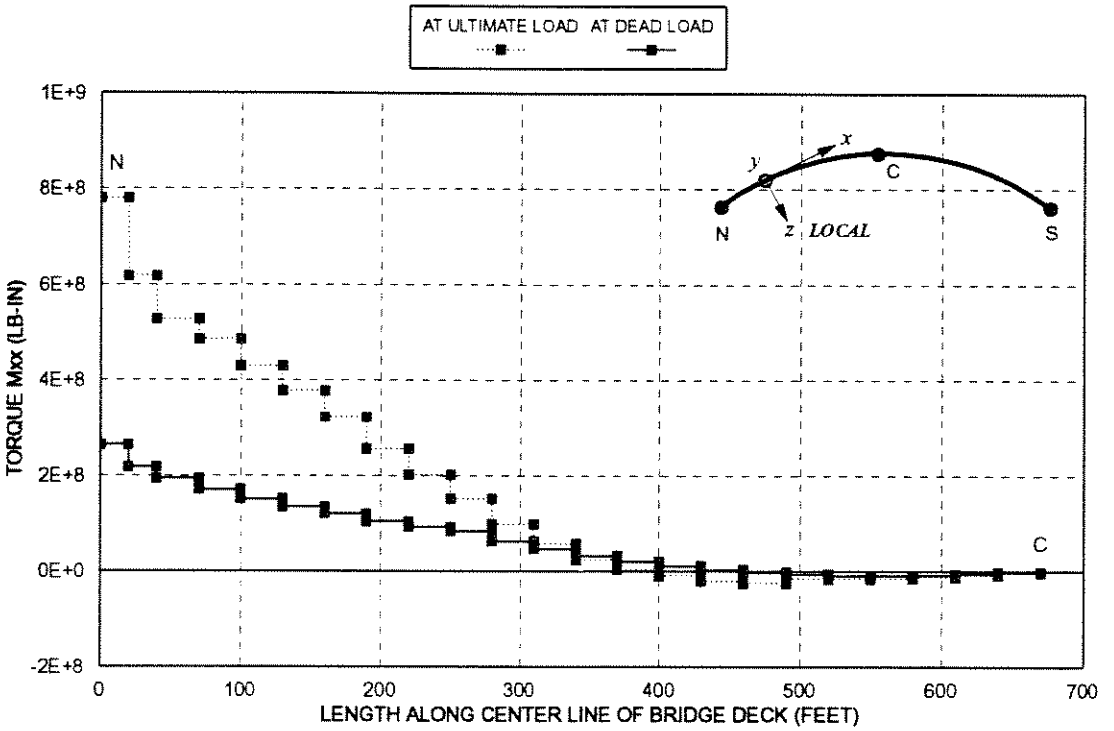

FIG. 14.41 TORQUE Mxx IN THE BRIDGE DECK; AT DEAD AND ULTIMATE LOAD
ULTIMATE LOAD ANALYSIS; RUCK-A-CHUCKY CONCRETE BRIDGE

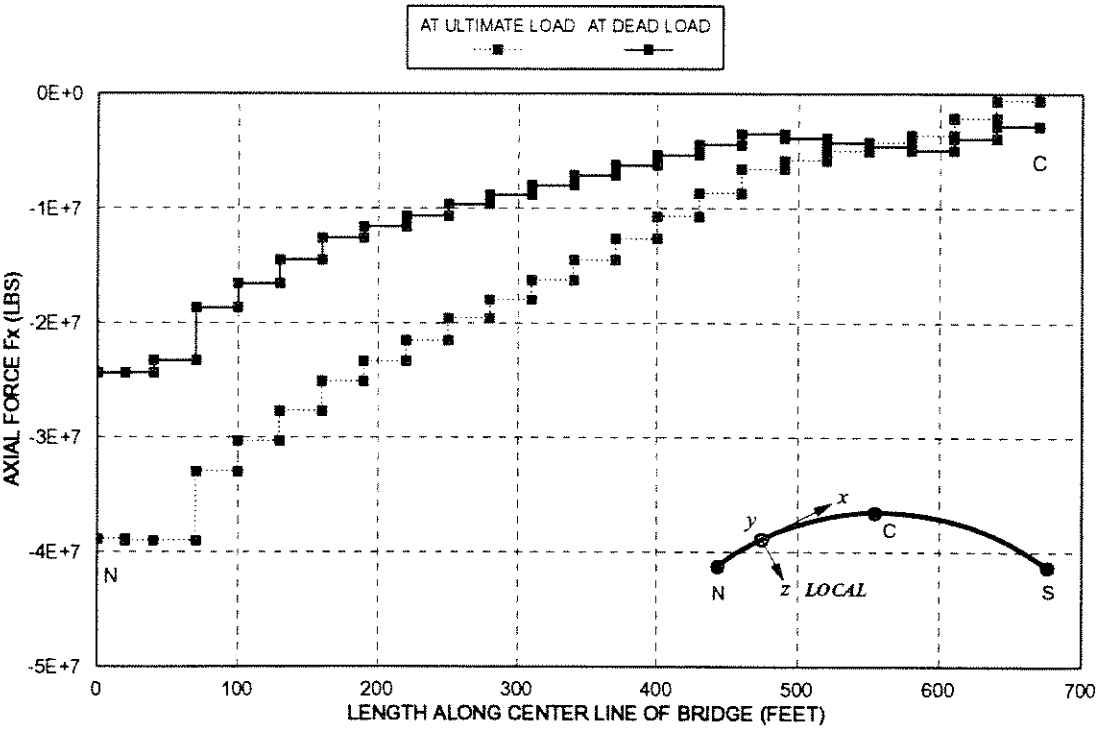

FIG. 14.42 AXIAL FORCE Fx IN THE BRIDGE DECK; AT DEAD AND ULTIMATE LOAD
ULTIMATE LOAD ANALYSIS; RUCK-A-CHUCKY CONCRETE BRIDGE

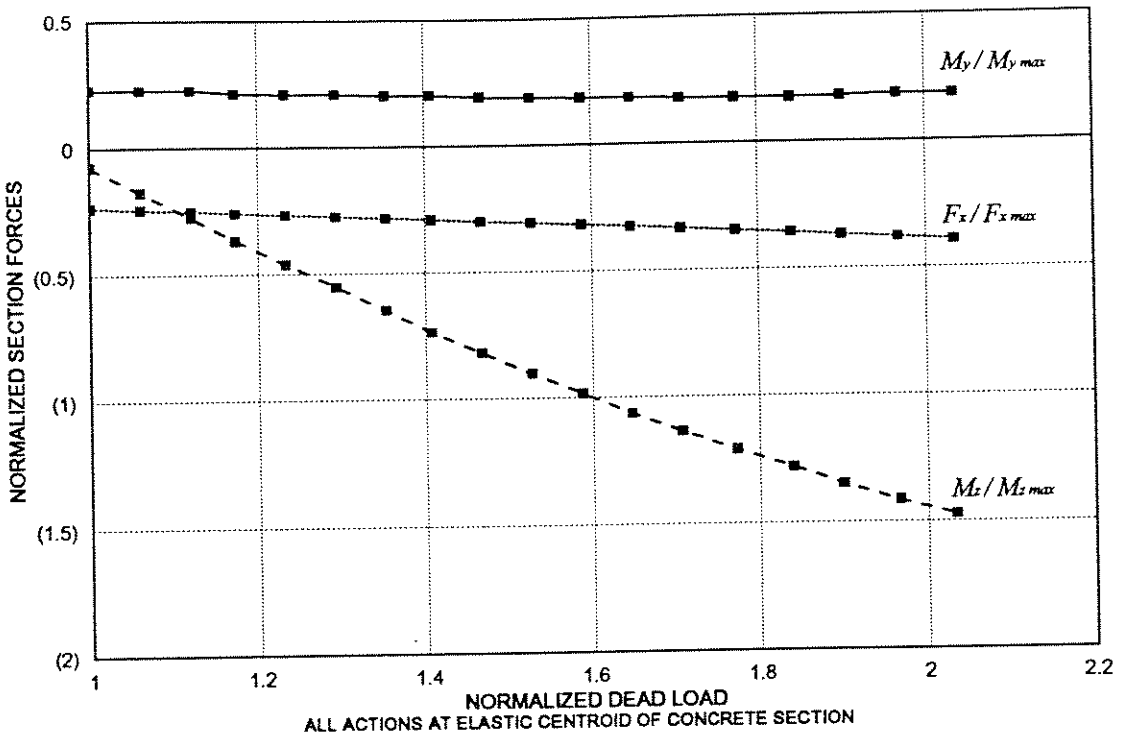

FIG. 14.43 EVOLUTION OF FORCES NEAR ABUTMENT; SLICE 1 OF BEAM 3
ULTIMATE LOAD ANALYSIS; RUCK-A-CHUCKY CONCRETE BRIDGE

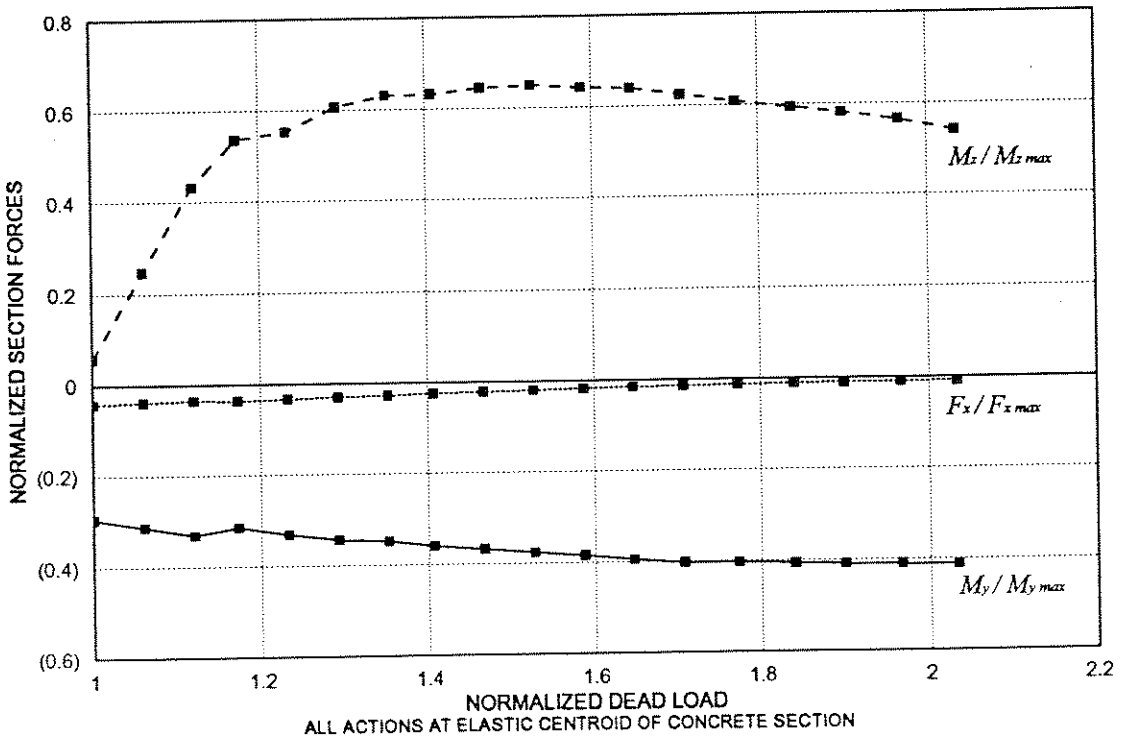

FIG. 14.44 EVOLUTION OF FORCES AT MIDSPAN SECTION; SLICE 4 OF BEAM 23
ULTIMATE LOAD ANALYSIS; RUCK-A-CHUCKY CONCRETE BRIDGE

15. SUMMARY AND CONCLUSIONS

15.1. SUMMARY

A numerical method of analysis has been developed to trace the response of segmentally erected, three dimensional, reinforced and prestressed concrete cable stayed bridges due to either immediate or sustained loads. The analysis incorporates the effects of both material and geometric nonlinearity. Time dependent effects due to load history, creep, shrinkage and aging of concrete and relaxation of stress in the prestressing steel are included in the analysis. The response of concrete structures can be tracked both before and after cracking, through the inelastic range and past the peak resistance through strain softening behavior.

This numerical procedure can predict the response of the changing structural configuration as it evolves progressively through different phases of cantilever construction of cables-stayed bridges. Any statically feasible construction sequence may be considered, including the installation or removal of deck or tower elements, placement and stressing of prestressing tendons, installation, stressing, restressing or removal of permanent or auxiliary cable-stays. In addition, boundary restraints may be added or released at any point in time.

Tower and deck segments are modeled with multi slice fiber beam-column elements with variable shape functions that are updated as the state of the element changes. The element has three translational and three rotational degrees of displacement freedom at each end. Material behavior is monitored at two or more slices or control sections. Each slice is further

divided into a number of sub elements or fibers. The location of the intermediate slices is selected so as to closely approximate the actual variation of curvature over the length of the element. Element stiffness matrix is obtained by integrating the contribution of all slices over the length of the element.

The material constitutive relationship is introduced at the fiber level. The stress-strain behavior of concrete under uniaxial loading is modeled by the modified Kent-Park relationship. Tension stiffening effects can also be included in the analysis. Variation of concrete strength with time is recognized. For steel a bilinear strain hardening model approximating the Bauschinger's effect is used.

Creep strain is evaluated using Kabir's algorithm [48]; this procedure is based on the principle of superposition and the use of a special form of creep compliance function which does not require the storage of entire stress history of the element. Refined creep integration schemes proposed by Ketchum [53] are also implemented.

Two different types of cable elements have been developed. The shallow cable element is used for modeling cables with a low sag to span ratio and is appropriate for the modeling of cable-stays. It is based on a series model in which one component simulates the elastic behavior of the cable and the second models the sag effect. The other element is a general cable element whose formulation is based on the differential equation of an elastic catenary. This element, which gives exact solutions for an elastic catenary, can be used for modeling large sag cables such as those used in the suspension bridges.

Prestressing steel tendons are modeled as a series of piece wise linear prestressing steel segments each of which spans a frame element. Each tendon segment is modeled as an eccentric truss bar. The displacements of segment ends are slaved to that of the corresponding end nodes of the host frame element. Initial stress losses due to friction and anchorage slip are accounted for.

For a time dependent analysis, the time domain is divided into a discrete number of intervals and a time step integration is performed during which the state of the structure is updated continuously as the solution progresses in the time domain. At each time step, the changes in structural configuration and loading are accounted for, and a direct stiffness solution based on the displacement method is performed.

Ultimate load analysis can be carried out by either load or displacement controlled solution strategies. The displacement control strategy is particularly useful for post buckling analyses and to track strain softening behavior of structures.

A complete analysis of both the concrete and steel design for the Ruck-a-Chucky Bridge [131] was performed to demonstrate the application of the numerical procedure to an actual design. This bridge is curved in plan and if built would span 1300 ft across the American River in California. The deck consists of a cellular box girder suspended on both edges by a set of cable-stays arranged in an aesthetically pleasing pattern and anchored to the rock walls of the valley. First, the bridge was analyzed to determine optimum cable tensions that will keep the bridge on the desired profile. Second, the structure was subjected to an dis-assembly analysis during which the completed structure was taken apart sequentially in order to determine the forces in the leading cables of the cantilever erection sequence. Third, the structure was forward assembled using the cable forces estimated from the prior analysis and corrected for time dependent effects. Finally an ultimate load analysis was carried out on the completed bridge to predict the maximum load that the structure could carry.

15.2. CONCLUSIONS

It has been demonstrated through numerical examples that the method of analysis developed in the present study can be used to predict the nonlinear response of concrete and steel bridge structures due to both immediate and sustained loads.

A special multi slice, variable shape function, fiber beam-column element perfected during the course of this study was compared with fixed shape function fiber elements developed in some previous studies. It was found that a *single* variable shape function element can be successfully used to model the inelastic behavior of long concrete members whereas *several* fixed shape function type elements were needed to solve the same problem with the same degree of accuracy.

The shallow sag cable element developed in the course of the present study was found to be computationally efficient and successfully predicted inelastic response as demonstrated in the case of the cable-stayed foot bridge designed by Loi et al. [75].

The elastic catenary element, also developed during the present study can be used to determine the highly nonlinear response of large sag cables such as those used in suspension bridges. This element can also be used in the analysis of cable nets as shown by several examples in Chapter 6

The behavior of cable-stayed bridges at or near the ultimate load, predicted using the numerical procedure developed in this study can easily pinpoint the weaker parts of the structure. Therefore, by increasing the strength of appropriately selected structural components, the designer can avoid any catastrophic modes of failure and ensure that the structure fails in a ductile manner.

For example, consider the cable-stayed footbridge designed by Irvine and Sharpe and analyzed for its ultimate strength by the author in Chapter 10. The analysis clearly demonstrated that the cable-stays were much weaker than the tubular steel deck and tower. Failure was initiated by the breaking of the mid span cable and spread very rapidly because of immediate overloading of adjacent cables. In this particular case the structure still had a very high factor of safety; however, in general, the cables should have sufficient reserve capacity to outlast other elements of the structure in order to avoid any possibility of progressive failure.

It has been further demonstrated through the example of cantilever construction of Ruck-a-Chucky Bridge that the present numerical method can successfully simulate segmental construction operations. The method was able to keep track of the changing state of forces and deformations in the structure as fresh deck segments are integrated into the bridge and the supporting cable-stays are installed and tensioned. The degree of complexity inherent in such an operation can be judged by the fact that the concrete used in each bridge segment may have been cast at a different age and therefore its strength may not be the same as that of the adjacent segments. Furthermore the rates at which creep and shrinkage strain develop also depends on the age of concrete.

The control of the bridge deck profile during the construction of the structure is accomplished by accurate prediction of displaced geometry of the bridge at each stage and careful monitoring of construction operations to ensure that they conform to guidelines set by the analyst. A mistake by either the designer or the builder will show up as misalignment with the target profile. This may be remedied by adjusting the tension in the cable stays or restressing prestressing tendons. The numerical procedure developed in the present study can be used to estimate the change in the pretension of the cable-stays for the required adjustment to the bridge profile.

In addition, the effect of maintenance or retrofit operations on the state of forces and deformations in the structure can also be assessed. For example, consider a damaged or corroded cable-stay replaced ten years after the construction of the bridge. Using the techniques developed in the present study, the bridge is built by numerically simulating the construction process. Next, the structure is brought to the current state by aging it 10 years while accounting for the effects of creep and shrinkage of concrete. At this stage the cable is removed and replaced with a new pretensioned cable and the fresh state of the structure is predicted. Moreover, all this can be accomplished in a single computer run.

Bridge structures can be rendered unserviceable because of excessive long term deflections. The procedures developed in the present study can successfully predict long term response of the structure under sustained loads as demonstrated by the example of the Ruck-a-Chucky Bridge.

15.3. RECOMMENDATIONS FOR FUTURE STUDIES

1. In the present study, torsion and flexural effects are assumed to be uncoupled and a parallel lumped plasticity model is used to simulate torsional plasticity. The possibility of an improved fiber element that can account for the interaction of torsion and flexure should be investigated.
2. The possibility of integrating the prestressing element with the fiber beam-column element should be explored.
3. The following extensions to the computer program CALBRG may be considered.
   - Add a stand alone interactive graphical post processor to simplify interpretation of copious data generated by a non linear program.
   - A second method of displacement control based on Crisfield's [25] arc length method with variable displacement steps should be incorporated allowing the analysis to capture both snap through and snap back phenomenon.
   - The fiber column element can be made more versatile by adding rigid end zones, end releases and variable cross section over its length.
   - The CEB-FIP (1990) and Bazant Panula (BPII) models for predicting concrete creep should be added to the existing two models.
   - An event to event scheme for non linear analysis should be added to the existing set of non linear solution strategies. This will allow the analyst to experiment with different strategies and use their respective strengths wherever warranted.

- The possibility of using high speed in-core storage as opposed to low speed disk storage for random access element files should be looked into.

4. In the case of fiber beam-column element further numerical studies should be carried out to optimize slice positions in the element and the results compared against experimental data.

5. Time dependent analysis of segmentally erected cable stayed bridges should be compared with experimental or field data to verify the accuracy of the numerical procedure implemented in the computer program.

6. Special connection elements to model the different kinds of bearings, connections and expansion joints used in cable stayed bridges should be studied and incorporated in the computer program CALBRG.

7. It is suggested that detailed parametric studies should be carried out with a view to establishing simple design rules that may be used as guidelines for preliminary design and proportioning of cable-stayed bridges.

16. REFERENCES

1 Abbas, S., Nonlinear Analysis of Segmentally Erected Reinforced and Prestressed Concrete Cable Stayed Bridges, Research Report (CE 299), Division of Structural Engineering, Mechanics and Materials, Department of Civil Engineering, University of California, Berkeley, October, 1990.

2 Abdel-Ghaffar, A. M., and Nazmy, A. S., Seismic Response Analysis of Cable-Stayed Bridges Subjected to Uniform and Multiple Support Excitations. Report No. 87-SM-1, Department Of Civil Engineering, Princeton University, Princeton, 1987.

3 ACI Committee 209, "Prediction of Creep, Shrinkage and Temperature Effects in Concrete Structures," ACI Special Publication SP-27, Paper SP 27-3, 1970.

4 Aldstedt, E., "Nonlinear Analysis of Reinforced Concrete Frames," Report No. 75-1, Division of Structural Mechanics, University of Trondheim, Norway, March, 1975.

5 Argyris, J. H., and Scharpf, D. W., "Large Deflection Analysis of Prestressed Networks." Journal of the Structural Division, ASCE, Vol. 98, No. ST3, March, 1972.

6 Baron, F., and Venkatesan, M. S., "Nonlinear Analysis of Cable and Truss Structures," Journal of Structural Division, ASCE, Vol. 97, No. ST2, Feb., 1971.

7 Baron, F. and Lien, Shen-Ying, "Analytical Studies of a Cable Stayed Girder Bridge," Computers and Structures, Vol. 3, Pergamon Press, New York, N. Y., 1977.

8 Baron, F., Arikan, M. and Hamati, R. E., The Effects of Seismic Disturbances on the Golden Gate Bridge, Report No. EERC 76-31, Earthquake Engineering Research Center, University of California, Berkeley, California, Nov., 1976.

9 Bathe, K. J., Wilson, E. L., and Peterson, F. E., SAP IV - A Structural Analysis Program for the Static and Dynamic Response of Linear Systems. Report No. EERC 73-11, Earthquake Engineering Research Center, University of California, Berkeley, California, 1974.

10 Batoz, J. L., and Dhatt, G., "Incremental Displacement Algorithms for Nonlinear Problems," International Journal for Numerical Methods in Engineering, Vol. 14, 1979.

11 Bazant, Z. P., and Wu, S. T., "Dirichlet Series Creep Function for Aging Concrete," Journal of the Engineering Mechanics Division, ASCE, Vol. 99, No. EM2, Proc. Paper 9645, April, 1973.

12 Billington, D. P., and Nazmy, A., History and Aesthetics in Cable Stayed Bridges. Private communication to A. C. Scordelis, 1988.

13 Birkenmaier, M., and Narayanan, R., "Fatigue Resistance of Large High Tensile Stay Tendons," Proceedings of the IABSE colloquium on Fatigue of Steel and Concrete Structures, Lausanne, 1982.

14 Branson, D. E., and Christiason, M. L., "Time Dependent Concrete Properties Related To Design," Symposium on Creep Shrinkage and Temperature Effects, ACI Special Publication SP-27, Detroit, 1971.

15 Bresler, B., and Selna, L. G., "Analysis of Time-Dependent Behavior of Reinforced Concrete Structures," ACI Symposium on Creep of Concrete, ACI Publication SP-9, 1964.

16 Bresler, B., Reinforced Concrete Engineering, Volume I, Wiley, New York, 1974.

17 Broyden, C. J., "Quasi-Newton or Modification Methods," Numerical Solution of Systems of Nonlinear Equations, G. Byrne and C. Hall, Academic Press, New York, 1973.

18 Burden, R. L., and Faires, J. D., Numerical Analysis, 4rth Edition, PWS-KENT Publishing Company, Boston, Massachusetts,1989.

19 Chan, E. C., Nonlinear Geometric, Material and Time Dependent Analysis of Reinforced Concrete Shells with Edge Beams, Ph.D. Thesis, Division of Structural Engineering and Structural Mechanics, Department of Civil Engineering, University of California, Berkeley, Report No. UCB/SESM-82/08, 1982.

20 Choudhury, D., Analysis of Curved Nonprismatic Reinforced and Prestressed Concrete Box Girder Bridges. Ph.D. Thesis, Division of Structural Engineering, Mechanics and Materials, Department of Civil Engineering, University of California, Berkeley, Report No. UCB/SEMM-86/13, 1986.

21 Clough, R., W., Benuska, K. L., and Wilson, E. L., "Inelastic Earth Quake Response of Tall Bulidings," Proceedings of the Third World Conference on Earthquake Engineering, Wellington, New Zealand, 1965.

22 Collins, M. P., and Mitchell, D., Prestressed Concrete Structures, Prentice Hall Inc., Englewood Cliffs, New Jersey, 1991.

23 Collins, M. P., and Lampert, P., "Redistribution of Moments at Cracking - The Key to Simpler Torsion Design?" American Concrete Institute, Special Publications, SP-35, "Analysis of Structural Systems for Torsion," March, 1971.

24 Corley, W. G., "Rotational Capacity of Reinforced Concrete Beams," Journal of Structural Division, ASCE, Vol. 92, No. ST-5, October, 1966.

25 Crisfield, M. A., "A Fast Incremental/Iterative Solution Procedure that Handles Snap-Through," Computers and Structures, Vol. 13, Pergamon Press, New York, N. Y., 1981.

26 de Saint-Venant, "Memoires presentes par divers savants a l'Academie des Sciences de l'Institut Imperial de France," Vol. 14 (Second Series), 1856.

27 Dennis, J. E., and More, J. J., "Quasi-Newton Methods, Motivation and Theory," SIAM Review, Vol. 19, No. 1, 1977.

28 Ernst, H. J., "Der E-Modul von Seilen unter Berücksichtigung des Durchhangers," Bauingenieur, 40 (2), 1965.

29 Fakhry, A., "Analysis of Cable-Stayed Bridges Supported by Flexible Towers", Journal of Structural Engineering, ASCE, Vol. 114, No. 12, December, 1988.

30 Fenwick, R. C., Influence of Creep and Shrinkage on Concrete Bridges, RRU Bulletin No. 28, Road Research Unit, National Roads Board, Wellington, New Zealand, 1974.

31 Gilbert, R. I., and Warner, R. F., "Tension Stiffening in Reinforced Concrete Slabs", Journal of Structural Division, ASCE, Vol. 104, No. ST12, December 1978.

32 Gimsing, N. J., Cable Supported Bridges, John Wiley & Sons, 1983.

33 Gimsing, N. J., "Multispan Stayed Girder Bridges," Journal of Structural Division, ASCE, Vol. 102, No. ST10, October, 1976.

34 Godden, W. G., "Seismic Model Studies of the Ruck-a-Chucky Bridge," University of California, Berkeley, California, July, 1977.

35 Godden, W. G., and Aslam, M., "Dynamic Model Studies of Ruck-a-Chucky Bridge," Journal of Structural Division, ASCE, Vol. 104, No. ST12, December, 1978.

36 Goto, Y., "Cracks formed in Concrete around Deformed Tension Bars," ACI Journal, Vol. 68, No. 4, April, 1971.

37 Grant, A., "Design and Construction of the East Huntington Bridge," PCI Journal, Vol. 32, No. 1, January-February, 1987.

38 Haisler, W. E., and Stricklin, J. A., "Displacement Incrementation In Nonlinear Structure Analysis by the Self Correcting Method," International Journal of Numerical Methods in Engineering, Vol. 11, 1977.

39 Hegab, H., "Energy Analysis of Cable-Stayed Bridges," Journal of Structural Engineering, ASCE, Vol. 112, No. 5, May, 1986.

40 Hellesland, J., and Scordelis, A. C., "Analysis of RC Bridge Columns under Imposed Deformations," Final Report, IABSE Colloquium on Advanced Mechanics of Reinforced Concrete, Delft, June, 1981.

41 Hellesland, J., Choudhury, D., and Scordelis, A. C., Nonlinear Analysis and Design of RC Bridge Columns Subjected to Imposed Deformations, Division of Structural Engineering and Structural Mechanics, Department of Civil Engineering, University of California, Berkeley, Report No. UCB/SESM-85/03, April, 1985.

42 Hernandez, H. D., and Gamble, W. L., Time Dependent Prestress Losses in Pretensioned Concrete Construction, Structural Research Series No. 417, Civil Engineering Studies, University of Illinois, Urbana, May, 1975.

43 Honshu-Shikoku Bridge Authority, "Tatara Bridge", Information brochure released by Honshu-Shikoku Bridge Authority, Japan. Undated.

44 Irvine, H. M., Studies in the Statics and Dynamics of Simple Cable Systems, C. E. Thesis, DYNL 108, California Institute of Technology, Pasadena, California, 1974.

45 Irvine, H. M., Cable Structures, The MIT Press, Cambridge, Massachusetts, 1981.

46 Irvine, H. M., "Notes on Structural Form in Cable Stayed Bridges," Proceedings of the International Conference on Cable Stayed Bridges, Bangkok, Thailand, 1987.

47 Kaba, S. A., and Mahin, S. A., Refined Modeling of Reinforced Concrete Columns for Seismic Analysis, Report No. EERC 84-03, Earthquake Engineering Research Center, University of California, Berkeley, California, April, 1984.

48 Kabir A. F., Nonlinear Analysis of Reinforced Concrete Panels, Slabs and Shells for Time Dependent Effects, Ph.D. Thesis, Division of Structural Engineering and Structural Mechanics, Department of Civil Engineering, University of California, Berkeley, Report No. UC-SESM 76-6, 1976.

49 Kang, Y. J., Nonlinear Geometric, Material and Time-Dependent Analysis of Prestressed Concrete Frames, Ph.D. Thesis, Division of Structural Engineering and Structural Mechanics, Department of Civil Engineering, University of California, Berkeley, Report No. UC-SESM 77-1, 1977.

50 Kang, Y. J., SPCFRAME - Computer Program for Nonlinear Segmental Analysis of Planar Prestressed Concrete Frames, Division of Structural Engineering, Mechanics and Materials, Department of Civil Engineering, University of California, Berkeley, Report No. UCB/SEMM-89/07, 1989.

51 Kasti, F. A., Nonlinear Material and Time Dependent Analysis of Segmentally Erected Reinforced and Prestressed Concrete Composite 3D Frame Structures, Ph.D. Thesis, Division of Structural Engineering, Mechanics and Materials, Department of Civil Engineering, University of California, Berkeley, Report No. UCB/SEMM-90/03, 1990.

52 Kent, D. C., and Park, R., "Flexural Members with Confined Concrete," Journal of the Structural Division, ASCE, Vol. 97, No. ST7, July 1971.

53 Ketchum, M. A., Redistribution of Stresses in Segmentally Erected Prestressed Concrete Bridges, Division of Structural Engineering and Structural Mechanics, University of California, Berkeley, Report No. UCB/SESM-86/07, 1986.

54 Knudson, W. C., Static and Dynamic Analysis of Cable-Net Structures, Ph.D. Thesis, Division of Structural Engineering and Structural Mechanics, Department of Civil Engineering, University of California, Berkeley, April, 1971.

55 Lai, S., Will, G. T., and Otani, S., "Model for Inelastic Biaxial Bending of Concrete Members," Journal of Structural Engineering, ASCE, Vol. 110, No. ST11, November, 1984.

56 Lampert, P, and Thurlimann, B., "Ultimate strength and Design of Reinforced Concrete Beams in Torsion and Bending," Publications, International Association of Bridge and Structural Engineering, Zurich, Vol. 31-I, 1971.

57 Lampert, P., Torsion und Beigung von Stahlbetonbalken (Torsion and Bending of Reinforced Concrete Beams), Bericht 27, Institute fur Baustatik, Zurich, January, 1970.

58 Lampert, P., "Postcracking Stiffness of Reinforced Concrete Beams in Torsion and Bending," American Concrete Institute, Special Publications, SP-35, "Analysis of Structural Systems for Torsion," March, 1971.

59 Lazar, B. E., "Stiffness Analysis of Cable-Stayed Bridges," Journal of Structural Divison, ASCE, Vol. 98, No. ST7, July, 1972.

60 Lazar, B. E. et al., "Load Balance Analysis of Cable-Stayed Bridges," Journal of Structural Division, ASCE, Vol. 98, No. ST8, August, 1972.

61 Leonhardt, F., and Zellner, W., Cable-stayed Bridges - Report on Latest Developments, Report submitted to the Canadian Structural Engineering Conference, Toronto, 1970.

62 Leonhardt, F., "Cable Stayed Bridges with Prestressed Concrete," PCI Journal, September-October, 1987.

63 Leonhardt, F.,, Brücken, Deutsche Verlags-Anstalt, 1982.

64 Leonhardt, F., Zellner, W., and Saul, R., Zwei Schrägseilbrücken für Eisenbahn und Strassenverkehr über den Rio Paraná, Stahlbau, 1979.

65 Leonhardt, F., Andra, W., and Wintergest, L., Kniebrucke Düsseldorf, Entwurf bearbeitung und Versuche. BetonVerlag GmbH, Düsseldorf, undated.

66 Leonhardt, F., Zur Entwicklung aerodynamisch stabiler Hängebrücken, Bautechnik 10, 11/1968.

67 Leonhardt, F., Latest developments of Cable-Stayed Bridges for Long Spans, Bygningsstatiske Meddelelser, Vol. 45, No. 4, 1974.

68 Leonhardt, F., and Zellner, W., "Cable Stayed Bridges," IABSE Surveys, S 13/80, Zurich, 1980.

69 Leonhardt, F., Zellner, W., and Svensson, H., "The Columbia River Bridge at Pasco-Kennewick, Washington, USA," Proceedings of the Eighth FIP Congress, May, 1978.

70 Lessig, N., Determination of the Load carrying capacity of Reinforced Concrete Elements with Rectangular Cross Section Subjected to Flexure and Torsion, Work 5, Institute Betona i Zhelezobetona, Moscow, 1959.

71 Lin, C. S., and Scordelis, A. C., "Nonlinear Analysis of Reinforced Concrete Shells of General Form," Journal of Structural Division, ASCE, Vol 101, No. ST3, March, 1975.

72 Lin, C. S., Nonlinear Analysis of Reinforced Concrete Slabs and Shells, Ph.D. Thesis, Division of Structural Engineering and Structural Mechanics, Department of Civil Engineering, University of California, Berkeley, Report No. UC-SESM 73-7, April, 1973.

73 Lin, T. Y., and Firmage, D. A., "The Design of the Ruck-a-Chucky Bridge," ASCE Convention and Exposition, Chicago, Illinois, October, 1978.

74 Linder, J., and Specht, M., "Bridge Design in Germany," Reports on Cooperative Research, Technische Universität Berlin and Massuchusetts Institute of Technology, 1983.

75 Loi, F. T., Mickleborough, N. C., Sharpe, P. R., and Irvine, H. M., "Investigation of a Cable Stayed Foot Bridge," Proceedings of the International Conference on Cable Stayed Bridges, Bangkok, Thailand, 1987.

76 Lu, Zung-An, "Dynamic Analysis of Cable Hung Ruck-a-Chucky Bridge," Journal of Structural Division, ASCE, Vol. 105, No. ST10, October, 1979.

77 MacGregor, J. G., Reinforced Concrete Mechanics and Design, Prentice Hall, Englewood Cliffs, New Jersey, 1988.

78 Magura, D., Sozen, M. A., and Siess, C. P., "A Study of Stress Relaxation in Prestressing Reinforcement," PCI Journal, Vol. 9, No. 2, Mar.-Apr., 1964.

79 Mahasuverachai, M., and Powell, G. H., Inelastic Analysis of Piping and Tubular Structures, Report No. EERC 82-27, Earthquake Engineering Research Center, University of California, Berkeley, California, November, 1982.

80 Mari, A. R., Nonlinear Geometric, Material, and Time-Dependent Analysis of Three Dimensional Reinforced Concrete Frames, Division of Structural Engineering and Structural Mechanics, Department of Civil Engineering, University of California, Berkeley, Report No. UCB/SESM-84/12, June, 1984.

81 Mark, K. M. S., and Roesset, J., M., "Nonlinear Dynamic Response of Reinforced Concrete Frames," Publication R76-38, Department of Civil Engineering, Massachusetts Institute of Technology, Cambridge, Massachusetts, August, 1976.

82 MATHCAD 3.0 (1991), Mathsoft Incorporated, Massachusetts, 1991.

83 Mathivat, J.,, The Cantilever Construction of Prestressed Concrete Bridges, John Wiley and Sons, New York, 1979.

84 Mattock, A. H., Discussion of "Rotational Capacity of Reinforced Concrete Beams," by Corley, W. G., Journal of the Structural Division, ASCE, Vol. 93, No. ST2, April, 1967.

85 Mattock, A. H., "Flexural Strength of Prestressed Concrete Sections by Programmable Calculator," PCI Journal, Vol. 24, No. 1, Jan.-Feb., 1979.

86 Menn, C., Prestressed Concrete Bridges. Birkhäuser Verlag. Boston, 1990.

87 Model Code for Concrete Structures, Bulletin d'Information, 124/125E, Comite Euro-International du Beton,, Federation Internationale de la Precontrainte, Paris, 1978.

88 Model Code for Concrete Structures, Bulletin d'Information, Comite Euro-International du Beton,, Federation Internationale de la Precontrainte, Paris, 1990.

89 Möllman, H., A Study in the Theory of suspension Structures. Copenhagen, 1965.

90 Möllman, H., "The Analysis of Shallow Cables." Byginingsstatiske Meddelelser, Volume 41. No. 3. 1970.

91 Mukaddam, M. A., and Bresler, B., "Behavior of Concrete under Variable Temperature and Loading," ACI Special Publication SP-34, 1972.

92 Naaman, A. E., Prestressed Concrete Analysis and Design, McGraw Hill, 1982.

93 Narayanan et al., "Bibliography on Cable-Stayed Bridges", Proceedings of the International Conference on Cable-Stayed Bridges, Bangkok, Thailand, November, 1987.

94 Ngo, D., and Scordelis, A. C., "Finite Element Analysis of Reinforced Concrete Beams," ACI Journal, Vol. 64, No. 3, March, 1967.

95 O'Brien, T., and Francis, A. J.,, "Cable Movements Under Two Dimensional Loads," Journal of Structural Division, ASCE, Vol. 90, No. ST3, June, 1964.

96 O'Brien, T., "General Solution of Suspended Cable Problems," Journal of Structural Division, ASCE, Vol. 93, No. ST1, Feburary, 1967.

97 OHBDC,, Ontario Highway Bridge Design Code, 2nd Ed., Ontario Ministry of Transportation and Communication, Toronto, 1983.

98 Otani, S., and Sozen, M. A., "Behavior of Multi-Story Reinforced Concrete Frames During Earthquakes," Civil Engineering Studies, Structural Research Series No. 392, University of Illinois, Urbana-Champaign, November, 1972.

99 Park, R., and Paulay, T., Reinforced Concrete Structures. A Wiley-Interscience Publication, John Wiley and Sons, 1975.

100 PCI Committee on Prestress Losses, "Recommendations for Estimating Prestress Losses," PCI Journal, July/August, 1975

101 Peyrot, A. H., and Goulois, A. M., "Analysis of Flexible Transmission Lines," Journal of Structural Division, ASCE, Vol. 104, No. ST5, 1978.

102 Peyrot, A. H., and Goulois, A. M., "Analysis of Cable Structures," Journal of Computers and Structures, Vol. 10, Pergamon Press, New York, N. Y., 1979.

103 Podolny, W., and Scalzi, J., Construction and Design of Cable-Stayed Bridges, 2nd Ed., John Wiley and Sons Inc., New York, 1976.

104 Post Tensioning Institute, Post Tensioning Manual, Post Tensioning Institute, Phoenix, Arizona, 1976.

105 Post Tensioning Institute, Recommendations for Stay-Cable Design, Testing and Installation, Post Tensioning Institute, Phoenix, Arizona, February, 1990.

106 Powell, G. and Mondkar, D. P., "CURVBRG: A Program for Analysis of Curved I-Girder Bridges," .Computers and Structures, Vol. 9, Pergamon Press, New York, N. Y., 1978.

107 Powell, G. and Simons, J., "Improved Iteration Strategy for Nonlinear Structures," International Journal of Numerical Methods in Engineering, Vol. 17, 1981.

108 Przemieniecki, J. S., Theory of Matrix Structure Analysis, McGraw-Hill, New York, 1967.

109 Riks, E., "An Incremental Approach to the Solution of Snapping and Buckling Problems," International Journal of Solids and Structures, Vol. 15, 1979.

110 Routh, E. J., Analytical Statics, Vol. 1, Cambridge University Press, Cambridge, 1891.

111 Scanlon, R. H., "Wind Stability Analysis and Commentary, Ruck-a-Chucky Bridge," United States Corps of Engineers, September, 1977.

112 Scanlon, A., Time Dependent Deflections of Reinforced Concrete Slabs. Ph.D. Thesis, Department of Civil Engineering, University of Alberta, Edmonton, Canada, December, 1971.

113 Schnobrich, W. C., "Behavior of Reinforced Concrete Predicted by Finite Element Method." Proceedings of the Second national Symposium on Computerized Structural Analysis and Design, George Washington University, Washington D. C., March, 1976.

114 Schreyer, H., and Masur, E., "Buckling of Shallow Arches," Journal of the Engineering Mechanics Division, ASCE, Vol. 92, No. EM4, August, 1966.

115 Scordelis, A. C., "Finite Element Analysis of Reinforced Concrete Structures," Proceedings of the Specialty Conference on Finite Element Methods in Civil Engineering. Montreal, June 1972.

116 Scordelis, A. C., "General Report - Basic Problems," Proceedings. IASS Symposium on Nonlinear Behavior of Reinforced Concrete Structures, Darmstadt, Germany, July, 1978.

117 Scordelis, A. C., "Finite Element Modeling of Reinforced Concrete Structures," Seminar on Finite Element Analysis of Reinforced Concrete Structures, University of Milan, June, 1978.

118 Scordelis, A. C., "Analytical Models for Nonlinear Material, Geometric, and Time-Dependent Effects," Proceedings, International Symposium on Nonlinearity and Continuity in Prestressed Concrete, Waterloo, Ontario, Canada, July, 1983.

119 Scordelis, A. C., "Computer Models for Nonlinear Analysis of Reinforced and Prestressed Concrete Structures," PCI Journal, Vol. 29, No. 6, Nov.-Dec., 1984.

120 Scordelis, A. C., Chan, E. C., Ketchum, M. A., and Van der Walt, P. P., "Computer Programs For Prestressed Concrete Box Girder Bridges," Structural Engineering and Structural Mechanics, Department of Civil Engineering, University of California, Berkeley, Report No. UCB/SESM-85/02, March, 1985.

121 Scordelis, A. C., "Recent Developments in Berkeley in Nonlinear Analysis of Prestressed Concrete Structures," Proceedings of the FIP Symposium, Jerusalem, Israel, September, 1988.

122 Scott, B. D., Park, R., and Priestly, M. J., "Stress Strain Behavior of Concrete Confined by Overlapping Hoops at Low and High Strain Rates," ACI Journal, Vol. 79, No. 1, Jan.-Feb., 1982.

123 Seif, S. P., Dilger, W. H., "Nonlinear Analysis and Collapse Load of P/C Cable-Stayed Bridges" Journal of Structural Engineering, ASCE, Vol. 116, No. 3, March, 1990.

124 Seif, S. P., Nonlinear Analysis and Ultimate Strength of Prestressed Concrete Cable-Stayed Bridges, Ph.D. Thesis, Department of Civil Engineering, University of Calgary, Alberta, Canada, May, 1986.

125 Shah, H., "Seismic Risk Analysis, Ruck-a-Chucky Bridge Site," Development of Response Spectra, Part II, Stanford University, Stanford, California, November, 1977.

126 Sharpe, P. R., The Analysis of a curved Cable Stayed Bridge Turning through 180 Degrees, M.Eng.Sc. Thesis, The University of New South Wales, Sydney, Australia, 1985.

127 Simons, J. W., Solution Strategies for Statically Loaded Nonlinear Structures. Ph.D. Thesis, Division of Structural Engineering and Structural Mechanics, Department of Civil Engineering, University of California, Berkeley, 1982.

128 Smerda, Z., and Kristek, V., Creep and Shrinkage of Concrete Elements and Structures, SNTL, Prague, 1988.

129 Standard Specifications for Highway Bridges, American Association of State Highway and Transportation Officials, Washington, D. C., 1981.

130 Suharwardy, M. I. H., and Pecknold, D. A., "Inelastic Response of Reinforced Concrete Columns Subjected to Two-Dimensional Earthquake Motions," Structural Research Series No. 455, Department of Civil Engineering, University of Illinois, Urbana-Champaign, October, 1978.

131 T. Y. Lin International, Ruck-a-Chucky Bridge - Reference Drawings, Private Communication to A. C. Scordelis, 1978.

132 Takayanagi, T., and Schnobrich, W. C., "Computed Behavior of Reinforced Concrete Coupled Shear Walls," Civil Engineering Studies, Structural Research Series No. 434, University of Illinois, Urbana-Champaign, December, 1976.

133 Tang, Man-Chung, "Analysis of Cable-Stayed Girder Bridges," Journal of Structural Division, ASCE, Vol. 97, No. ST5, May, 1971.

134 Tang, Man-Chung, "Design of Cable-Stayed Girder Bridges," Journal of Structural Division, ASCE, Vol. 98, No. ST8, August, 1972.

135 The Subcommittee on Cable-Stayed Bridges of the Committee on Long-Span Steel Bridges of the Committee on Metals of the Structural Division "Bibliography and Data on Cable-Stayed Bridges," Journal of Structural Division, Vol. 103, No. ST10, October, 1977.

136 The Task Committee on Cable-Suspended Structures of the Committee on Special Structures of the Committee on Metals of the Structural Division, "Tentative Recommendations for Cable-Stayed Bridge Structures," Journal of the Structural Division., ASCE, Vol. 103, No. ST5, May, 1977.

137 Timoshenko, S. P., and Goodier, J. N., Theory of Elasticity, 3rd Edition, McGraw-Hill Book Company, New York, 1970.

138 Troitsky, M. S., Cable Stayed Bridges, 2nd Edition, Van Nostrand Reinhold Company, New York, 1988.

139 Tuma, J. J., Engineering Mathematics Handbook, McGraw-HIll Book Company, New York, 1987.

140 Van Greunen, J., "Nonlinear Geometric, Material and Time Dependent Analysis of Reinforced and Prestressed Concrete Slabs and Panels," Ph.D. Thesis, Division of Structural Engineering and Structural Mechanics, Department of Civil Engineering, University of California, Berkeley, Report No. UC-SESM 79-3, 1979.

141 Van Zyl, S. F., "Analysis of Curved Segmentally Erected Prestressed Concrete Box Girder Bridges," Ph.D. Thesis, Division of Structural Engineering and Structural Mechanics, Department of Civil Engineering, University of California, Berkeley, Report No. UC-SESM 78-2, January, 1978.

142 Vecchio, F. J., and Collins, M. P., "The Modified Compression Field Theory for Reinforced Concrete Elements Subjected to Shear," ACI Journal, Vol. 83, No. 2, Mar.-Apr., 1986.

143 Volterra, V., "Sur les Equations Integro-Differentielles et Leurs Applications, Acta Mathematica," Stockholm, 1912.

144 Walther, R., Cable Stayed Bridges, Thomas Telford Ltd., London, England, 1988.

145 Warner, R. F., "Long Reinforced Concrete Columns in Biaxial Bending," IABSE Publications, Vol. 29-1, 1969.

146 Wegner, R., "Finite Element Models for Reinforced Concrete." Preprint, Proceedings of the US-Germany Symposium on Formulations and Computational Methods in Finite Element Analysis, Massachusetts Institute of Technology, Cambridge, August, 1976.

147 Wilson, E. L., Bathe, K. J., and Doherty, W. P., "Direct Solution of Large Systems of Linear Equations," Computers and Structures, Vol. 4, Pergamon Press, New York, N. Y., 1974.

148 Wilson, E. L., and Hoit, M. I.,, "A computer Adaptive language for the Development of Structural Analysis Programs," Computers and Structures, Vol. 19, Pergamon Press, New York, N. Y., 1984.

149 Zeris, C., and Mahin, S. A.,, "Analysis of Reinforced Concrete Beam-Columns Under Uniaxial Excitation." Journal of Structural Engineering, ASCE, Vol. 114, No. 4, April, 1988.

150 Zeris, C., Three Dimensional Nonlinear Response of Reinforced Concrete Buildings, Ph.D. Thesis, Division of Structural Engineering, Mechanics and Materials, Department of Civil Engineering, University of California, Berkeley, 1986.

151 Zienkiewicz, O. C., and Watson, M., "Some Creep Effects in Stress Analysis with Particular Reference to Concrete Pressure Vessels," Nuclear Engineering and Design, No. 4, 1966.

152 Zienkiewicz, O. C., and Taylor, R, L., The Finite Element Method, 4rth Edition, Volume 1 and 2, McGraw Hill Book Company (UK) Ltd., 1989.

APPENDIX A
COMPUTER PROGRAM CALBRG
SUMMARY OF COMMANDS

GENERAL

The program *CALBRG* is designed for nonlinear material, geometric and time-dependent analysis of segmentally erected three dimensional cable-stayed bridges. The program is written in *FORTRAN* and compiled using MicroSoft Fortran Compiler version 5.1. It must be run in an *OS2* environment, which is an operating system designed by the IBM corporation.

This appendix describes the command language used in the computer program *CALBRG*. Data input is based on the free field input routines of the *CALSAP* system developed by Wilson and Hoit [148].

Data is input to the program through an input file. The input file consists of a sequence of commands and sub-commands with appropriate arguments. The structure of a main command and its argument list is described as follows:

$$COMMAND\ [A=]n_1\ \ n_2\ n_3\ ....\ \ \{[B=n_1\ n_2\ n_3\ ....\ \ C=n_1\ n_2\ n_3\ ....]\}$$

The main command consists of a key word; six characters or longer, followed by a list of numerical data separated by spaces or commas. The data list is preceded by an identifier. The identifier consists of one or more characters and it is optional for the first list. Note that the optional arguments are enclosed in square brackets [ ]. Arguments that may be repeated

several times, if necessary, are enclosed in curly brackets { }. Values enclosed in standard brackets ( ) are the default values. Data lists must obey the following rules:

1. All numerical data is in free field format.
2. All items in a data list must be separated by a comma or one or more blanks.
3. A numerical data list without an identifier must be the first list on the line.
4. Simple arithmetical operations are possible when entering real number data. These statements are evaluated from left to right without operator hierarchy.
5. Certain characters have special meaning to the program. These are described in the ensuing list.
    - The exclamation point "!" is a special character used to delimit several command lines provided on one physical line.
    - The back slash "\" is a special character used for continuation of a command on the next physical line.
    - The semicolon ";" is a special character used to separate comments from the rest of input. All data on the right of the semicolon upto the end of the line are ignored by the program.

COMMAND STRUCTURE

The basic command structure used in the program *CALBRG* is shown in Fig. A.1. The commands may be standalone or head a subgroup of commands. The double wall boxes in Fig. A.1 indicate a parent command which has a family of subcommands.

Each command is described in a separate section according to the following scheme:

- Command syntax in Italics; this includes the command keyword followed by a tagged argument list.
- A tabular description of the argument list.
- A discussion of the scope of the command.

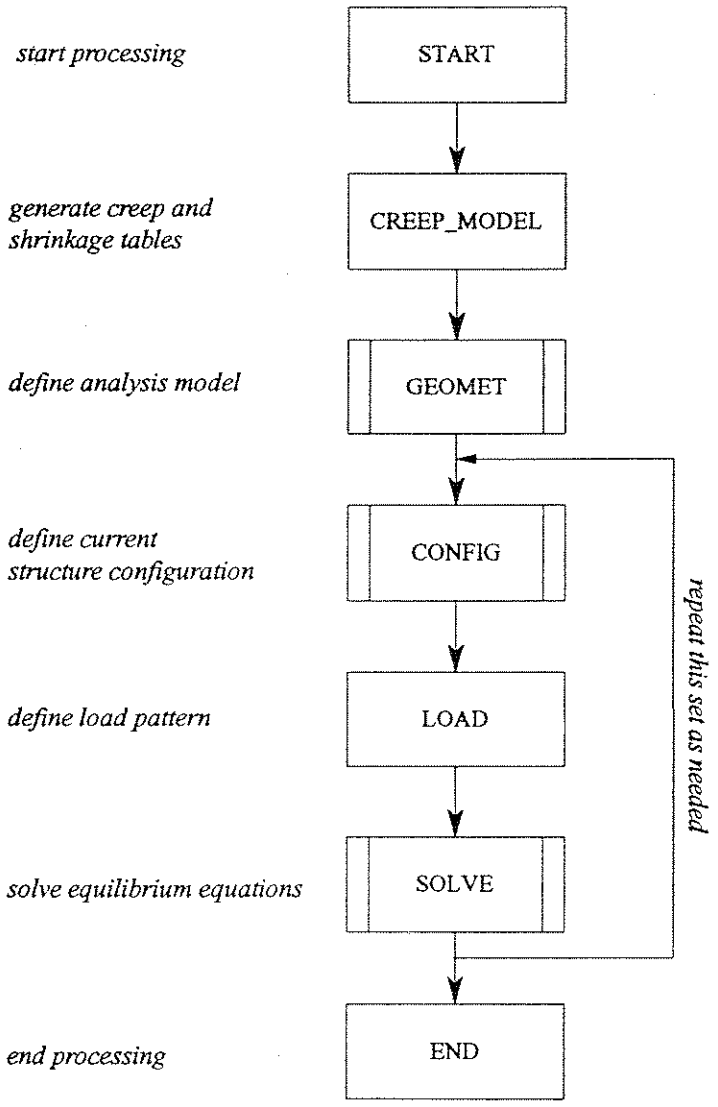

FIG. A.1 BASIC COMMAND STRUCTURE OF THE PROGRAM CALBRG.

1. START PROCESSING

START [R = kstart]

Identifier	*Variable*	*Description*
R	*kstart=0*	*start fresh analysis*
	kstart=1	*read data base, restart analysis*

This command starts program execution. *CALBRG* scans the input file for *Start* command. All commands preceding the *START* command are ignored and any subsequent commands are executed sequentially until the *END* command is encountered. If the *START* command is not found, program execution is stopped with an error message *"START command not found"*. At the end of analysis, the state of the structure is saved in a binary file *"alpha.cor"*, where *"alpha"* is the name of the input file.

To restart the program for subsequent analyses, a new input file is created with the desired command sequence. The new input file must have the same name as that of the original input file. The restart toggle *R* must be switched on, that is set equal to one. The program then reads the file *"alpha.cor"* to refresh the incore database and performs the required analysis. The output is appended to the file *"alpha.out"*. The process may be repeated any number of times. The restart capability is of great convenience for non-linear analysis, where intermediate results have to be examined in order to plan a stable strategy for any subsequent analyses.

2. PRINT PROBLEM TITLE

TITLE N=numline
{numline text lines here}

Identifier	*Variable*	*Description*
N	*numline*	*number of line in the problem title*

This command is used to print the problem title to the output file.

3. SET DEBUG TOGGLE

DEBUG

This command serves as a toggle switch for debugging information. When first encountered in an input file, it forces the program to produce copious debugging information. If used again in the subsequent input lines then it switches off debugging information. This allows for focused testing of program segments.

4. SET PAGE BREAKS

SET_PAGE

This command inserts page breaks in the output at the appropriate positions and enhances organization and readability of the output.

5. LIST IN-CORE ARRAYS

LDIR

This command produces a list of all the in-core arrays. The number and size of arrays stored in the database changes continuously. This command may be used any number of times to monitor the in-core database at various stages of solution. This command is meant for program maintenance or update operations and should not be used during regular problem solving.

6. TIME DEPENDENT PROPERTIES OF CONCRETE

The commands in this section are used to generate tables of shrinkage strain, elastic modulus and creep properties versus time. The values from these tables are used by the program in a time-dependent analysis of the structure. These commands must be used prior to the *GEOMET* command.

The data input for this section is organized as follows:

1. Input the total number of time-dependent models needed in the analysis.
2. For each model number:

- Input the basis used for generating creep curves.
    a. ACI
    b. CEB
    c. LAB
- If needed, default values used by the program for ACI and CEB models may be changed.
- If LAB data is used directly to define the basic creep curves, then the following information must be input.

a. Age at which concrete is loaded.
    b. Elastic modulus of concrete at age of loading.
    c. Shrinkage strain in concrete at age of loading.
    d. Observation times and creep strains at those times.

The first line is used to define the total number of creep models, maximum number of loading ages, observation times and retardation times. This data is used by the program to initialize arrays for storing data that will be generated by subsequent commands.

CREEP_MODEL N=ncpt T=na, nt, nr P=iprn

Identifier	*Variable*	*Description*
N	*ncpt*	*Total number of creep models*
T		*Time parameters*
	na (32)	*Loading ages in the table; maximum no. in any model*
	nt (32)	*Observation times in the table; maximum no. in any model*
	nr (4)	*Retardation times in the table; maximum no. in any model*
P	*iprn=0/1/2*	*Print code: echo input / parameter table / table & diagnostics*

The next line is used to define the basis used for generating the creep curves. Standard recommendation by ACI committee 209 or CEB-FIP may be used. If laboratory data is available then it may be used directly. If different from default values, the number of loading ages, observation times and retardation times may also be specified for the model being considered. The loading ages and observation times may be generated automatically by the program or directly input by the user.

{n M=model T=nat, ntt, nrt R=rt G=igen}

Identifier	*Variable*	*Description*
	n	*Creep model number*
M		*creep model is based on a specified code/lab data.*
	model=ACI	*ACI-209 recommendations*
	model=CEB	*CEB-FIP recommendations*
	model=CEB1	*CEB-FIP recommendations; one component*
	model=LAB	*Laboratory test data*
	nat (32)	*Loading ages in the table; for this creep model*
	ntt (32)	*Observation times in the table; for this creep model*
	nrt (4)	*Retardation times in the table; for this creep model*
R	*rt=(5)*	*smallest retardation time for this creep model*
G		*age and observation time generation flag*
	igen=(0)	*ages and observation times to generated by the program*
	igen=1	*ages and observation times to be input by the user*

If *model=ACI* and it is desired to change the default values used by the program then the following line is needed:

A=a B=b C=c D=d E=e F=f S=s W=w

Identifier	*Variable*	*Description*
A	*a=(4.000)*	*constant used in concrete strength equation; see Eq. A.1*
B	*b=(0.850)*	*constant used in concrete strength equation; see Eq. A.1*
C	*c=(1.250)*	*constant used in age function for creep; see Eq. A.2*
D	*d=(0.118)*	*constant used in age function for creep; see Eq. A.2*
E	*e=(1.000)*	*constant used in time function for shrinkage; see Eq. A.3*
F	*f=(50.00)*	*constant used in time function for shrinkage; see Eq. A.3*
S	*s=(7.000)*	*constant used in time function for shrinkage; see Eq. A.3*
W	*w=(150.0)*	*constant used in elastic modulus equation; see Eq. A.4*

The parameters a and b are used in the time function for strength, ACI-committee 209.

$$f_c^{'} = \frac{f_c^{'}(28)\,t}{a + bt} \tag{A.1}$$

The parameters c and d are used in the age function for creep.

$$K_\tau = C\tau^{-d} \tag{A.2}$$

The parameters e and s are used in the time function for shrinkage.

$$\varepsilon_s(t) = \varepsilon_s(\infty)\frac{(t-s)^e}{[f + (t-s)^e]} \tag{A.3}$$

The parameter w which is the unit weight of concrete is used in the time function for modulus of elasticity.

$$E(t) = 33(w)^{1.5}\sqrt{f_c^{'}(t)} \tag{A.4}$$

If *model=CEB* and it is desired to change the default values used by the program then the following line is needed:

H=humd U=thik D=temp

Identifier	*Variable*	*Description*
H	*humd=(70)*	*ambient relative humidity in percentage*
U	*thik=(30)*	*notional thickness in centimeters*
D	*temp=(20)*	*temperature in degrees centigrade*

If *model=ACI or CEB* and generation flag *G=1*, then the program will not generate loading ages and observation time and these must be input directly by the user as follows:

A=age(1) T=time(1), time(2),.....time(ntt)
A=age(2) T=time(1), time(2),.....time(ntt)
A=age(nat) T=time(1), time(2),.....time(ntt)

Identifier	*Variable*	*Description*
A	*age*	*loading age*
	nat	*total number of loading ages*
T	*time*	*Observation time*
	ntt	*total number of observation times*

If *model=LAB* then property tables are not generated by the program and have to be input directly by the user. Two lines are input for each loading age

A=age(1) E=emod S=shrn T=time(1), time(2),.....time(ntt)
C=crep(1), crep(2), time(ntt)
A=age(nat) E=emod S=shrn T=time(1), time(2),.....time(ntt)
C=crep(1), crep(2), time(ntt)

Identifier	*Variable*	*Description*
A	*age(a)*	*loading age (a)*
E	*emod*	*modulus of elasticity at age(a)*
S	*shrn*	*shrinkage strain at age(a)*
T	*time(t)*	*Observation time (t)*
C	*crep(t)*	*creep strain at time (t) for loading age (a)*

7. STRUCTURE DEFINITION

GEOMET

.....

END_GEOMET

This command group is used to define the complete structural model. This includes:

- Nodal coordinates.
- Material models.
- Element type, connectivity and material property numbers.

All temporary and permanent elements must be defined at this stage. Note that this command does not define the current analysis model; this is done separately by the *CONFIGURATION* command. The subcommand tree is shown in Fig. A.2. *FRAME, CABLE, CATENARY* and *TENDON* sub-commands are optional and should be used only when that element is to be used in a subsequent analysis. Each of the subcommands is discussed separately in the following sections.

7.1. NODAL COORDINATES

NODE

N=numnod

{ nodnum X=x_coord Y=y_coord Z=z_coord [G=node1,node2,ninc] }

Blank line

Identifier	*Variable*	*Description*
N	*numnod*	*total number of nodes in the structure*
	nodnum	*node number*
X	*x _coord*	*global x-coordinate of nodnum*
Y	*y_coord*	*global y-coordinate of nodnum*
Z	*z_coord*	*global z-coordinate of nodnum*
G	*node1*	*first node in the generation sequence; must be defined previously*
	node2	*last node in the generation sequence; must be defined previously*
	ninc	*node number increment in a linear generation scheme*

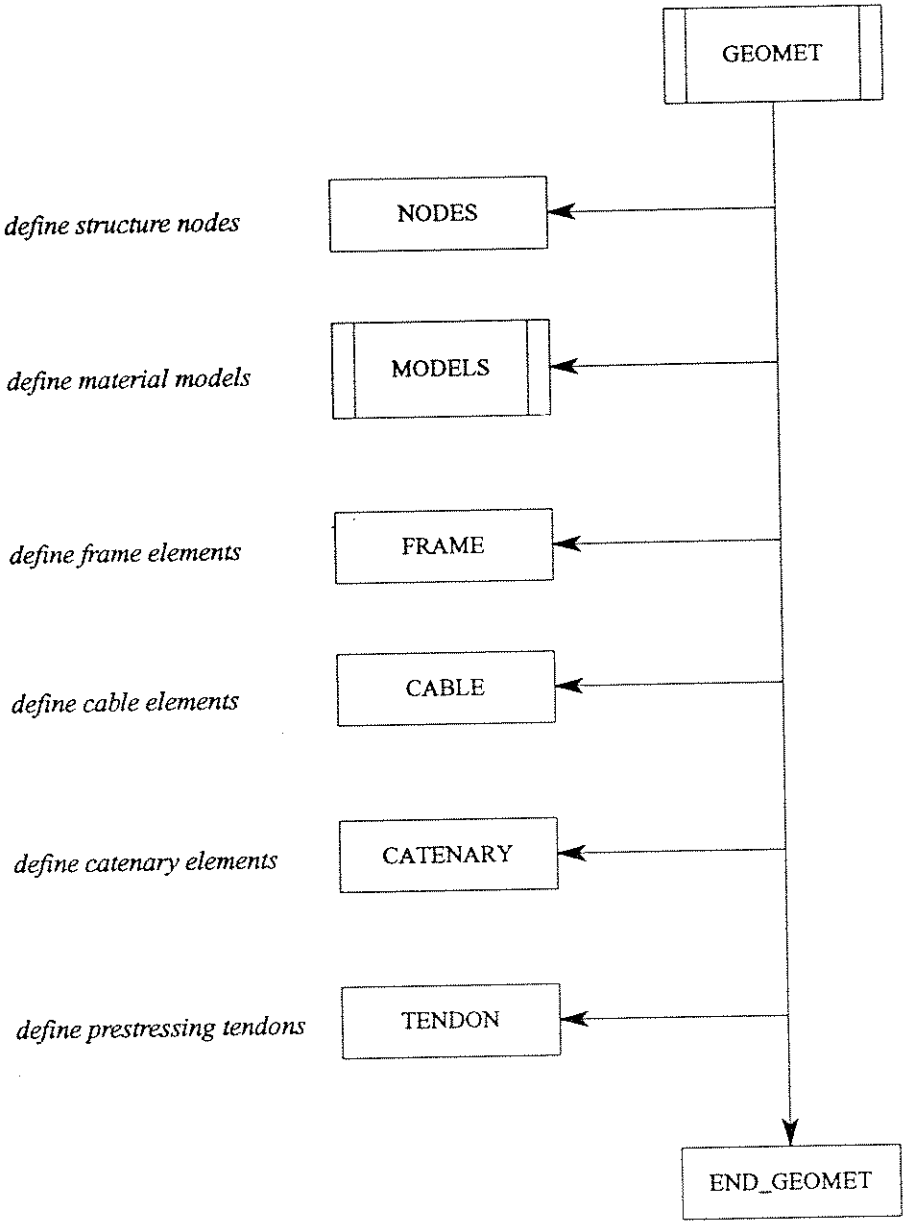

FIG. A.2 STRUCTURE DEFINITION; "GEOMET" AND ITS SUBCOMMANDS

This command is used to input the position of the nodal points. This is done by defining the Cartesian coordinates x, y, and z of each node as referred to a global coordinate system. Note that K nodes which specifies the orientation of the vertical axis of a beam element must also be specified in this section. A linear generation scheme is also incorporated. The first and the last node in the generation scheme must be previously defined; that is the lines defining these nodes in the input file must be above or to the left of generation parameters. The position coordinates of the intermediate nodes are then generated automatically by the program. The nodes may be defined in any order. This command sequence must be ended by a blank line.

7.2. MATERIAL MODELS

MODELS

[CONCRETE ()]

[STEEL ()]

[TORSION ()]

[CABLE ()]]

Blank line

The command group *MODELS* is used to define material constitutive models. Concrete, steel, and torsion models are defined for the frame element. Further, a steel model is defined for the cable element. All model definitions are optional and are required only when the corresponding element is to be used in the subsequent analysis. This group of commands must end with a blank line.

7.2.1. CONCRETE

CONCRETE NMOD=nmod

{mmod SIG0=sig0 EPS1=eps1 EPSU=epsu USHR=ultshr UCRP=ultcrp}

Identifier	*Variable*	*Description*
NMOD	*nmod*	*number of concrete models*
	mmod	*concrete model number*
SIG0	*sig0*	*maximum concrete compressive stress (-ve).*
EPS1	*eps1*	*concrete strain at end of descending branch (-ve).*
EPSU	*epsu*	*ultimate concrete compressive strain at crushing (-ve).*
USHR	*ultshr*	*ultimate shrinkage strain.*
UCRP	*ultcrp*	*ultimate creep coefficient.*

Modified Kent-Park model as described in Chapter 3, is used for concrete. If needed, more than one concrete model may be specified. The input parameters correspond to 28 day concrete strength. The model is automatically adjusted for age by the computer program.

If a material linear analysis is specified, the program transforms the nonlinear material model into a straight line with a slope equal to that of initial elastic modulus.

Tensile strength is assumed to be one tenth of the compressive strength. Tension stiffening is used if specified by the user (see *FRAME*). Ultimate shrinkage strain and ultimate creep coefficient are based on either laboratory results or as defined by ACI-209 and CEB-FIP.

7.2.2. STEEL

STEEL NMOD=nmod

{mmod SIGY=sigy EPSU=epsu EMOD0=emod0 EMOD1=emod1}

Identifier	*Variable*	*Description*
NMOD	*nmod*	*number of steel models*
	mmod	*steel model number*
SIGY	*sigy*	*yield stress (+ve)*
EPSU	*epsu*	*ultimate steel strain at failure (+ve)*
EMOD0	*emod0*	*initial modulus of elasticity (+ve)*
EMOD1	*emod1*	*strain hardening modulus (+ve)*

A bi-linear strain hardening material model is used for steel, as described in Chapter 3. If needed, more than one steel model may be specified. In case of a material linear analysis, the strain hardening branch is ignored and only the initial elastic modulus *EMOD0* is used to evaluate stress in the steel fibers.

7.2.3. TORSION

TORSION NMOD=nmod

{mmod TCR=tcr ACR=acr TYP=typ AYP=ayp AUT=aut}

Identifier	*Variable*	*Description*
NMOD	*nmod*	*number of torsion models*
	mmod	*torsion model number*
TCR	*tcr*	*torque at initial cracking of concrete section (+ve)*
ACR	*acr*	*twist at initial cracking of concrete section (+ve)*
TYP	*typ*	*torque at initial yield of concrete section (+ve)*
AYP	*ayp*	*twist at initial yield of concrete section (+ve)*
AUT	*aut*	*ultimate twist of concrete section at failure (+ve)*

A tri-linear torsion model is specified for beam-column elements. The evaluation of various parameters used in the torsion model are discussed in Chapter 3. Any number of torsion models may be specified. These models are later associated with specific frame elements using the torsion models number *mmod*.

7.2.4. CABLE

CABLE NMOD=nmod

{mmod SIGY=sigy EPSY=epsy SIGU=sigu EPSU=epsu}

Identifier	*Variable*	*Description*
NMOD	*nmod*	*number of cable steel models*
	mmod	*cable steel model number*
SIGY	*sigy*	*yield stress (+ve)*
EPSY	*epsy*	*yield strain at failure (+ve)*
SIGU	*sigu*	*ultimate stress at failure (+ve)*
EPSU	*epsu*	*ultimate strain at failure (+ve)*

This command is used to specify the material model for cable-stay steel. A bilinear strain hardening steel model is used. This model is then used to construct an apparent stress-strain model for each cable stay which accounts for the effect of cable sag on the end displacement of a cable-stay and is discussed in detail in Chapter 9.

7.3. FRAME ELEMENTS

This command structure in this section, which defines the fiber beam-column elements used in the structure, is organized as follows:

1. Maximum number of section types, concrete and steel fibers are defined.
2. Each section is defined separately. Fiber properties are either generated or input directly.
3. Element flexibility models are defined. These define the number and location of control sections in an element.
4. Element model patterns are defined. Each pattern consists of an element flexibility model, section type, concrete model, steel model, torsion model and creep model.
5. Individual frame elements are defined either directly or by using a generation scheme. A frame element is completely defined by node numbers I, J and K, where I and J are element end nodes and K defines the orientation of the vertical axis of the element, and the model pattern number to be associated with the element.

First, the total number of different section types, and maximum number of concrete and steel fibers used in any section are set. This information is used to prepare incore database to receive element data.

FRAME

NSEC=nsec MAXC=maxc MAXS=maxs P=iprn

Identifier	*Variable*	*Description*
NSEC	*nsec*	*total number of different sections*
MAXC	*maxc*	*maximum number of concrete fibers in any section*
MAXS	*maxs*	*maximum number of steel fiber in any section*
P	*iprn=0*	*do not print fiber geometry information*
	iprn=1	*print fiber geometry information*

Each individual section is defined separately. The next line is used to input the section number and the total number of concrete and steel fibers in that section.

MSEC=msec NCF=ncf NSF=nsf

Identifier	*Variable*	*Description*
MSEC	*msec*	*section number*
NCF	*ncf*	*number of concrete fibers*
NSF	*nsf*	*number of steel fibers*

Next, the geometry of concrete fibers in element section being considered is input. Each fiber is completely defined by its y and z coordinates with respect to the element local axes and its area of cross section. A tension stiffening switch is provided for each fiber, allowing the analyst to specify use of tension stiffening model for concrete fibers in the vicinity of steel bars. Fiber data may be input directly or may be generated. Only section shapes that can be divided into rectangles can be generated; other shapes must be input directly. Each rectangle is defined by the y and z coordinates of its four corners and the number of fibers along its width and height. Note that even if there are no concrete fibers in the section, a blank line must be inserted in the input file. This indicates to the program to start looking for steel fiber data.

{AC=ac Z=z_coord Y=y_coord T=t_stiff}

[{CW=z_width CH=y_height A=bot_r B=bot_l C=top_l T=t_stiff}]

Blank Line

Identifier	*Variable*	*Description*
AC	*ac*	*area of concrete fiber*
Z	*z_coord*	*local Z coordinate of concrete fiber.*
Y	*y_coord*	*local Y coordinate of concrete fiber*
T	*t_stiff=0*	*tension stiffening switched off*
	t_stiff=1	*tension stiffening switched on*
CW	*z_width*	*number of concrete fibers in width (Z) of the selected rectangle*
CH	*y_height*	*number of concrete fibers in height (Y) of the rectangle*
A	*bot_r*	*(z,y) coordinates of the bottom right corner of the rectangle*
B	*bot_l*	*(z,y) coordinates of the bottom left corner of the rectangle*
C	*top_l*	*(z,y) coordinates of the top right corner of the rectangle*

Next, the same process is repeated for steel fibers in the section.

{AS=as Z=z_coord Y=y_coord}

[{SW= SH=.. A= B= C=.. }]

Blank Line

Identifier	*Variable*	*Description*
AS	*as*	*area of steel fiber*
Z	*z_coord*	*local Z coordinate of steel fiber*
Y	*y_coord*	*local Y coordinate of steel fiber*
CW	*z_width*	*number of steel fibers in width (Z) of the selected rectangle*
CH	*y_height*	*number of steel fibers in height (Y) of the rectangle*
A	*bot_r*	*(z,y) coordinates of the bottom right corner of the rectangle*
B	*bot_l*	*(z,y) coordinates of the bottom left corner of the rectangle*
C	*top_l*	*(z,y) coordinates of the top right corner of the rectangle*

A number of different element flexibility models may be designed depending on the number and location of control sections in the element. This allows the analyst to build and use elements of varying complexity, which if used appropriately, can result in considerable saving of computational effort.

NELM=nelm MAXX=maxx

{melm NUMX=numx XCRD=x_crd(1), ... x_crd(6)}

Identifier	*Variable*	*Description*
NELM	*nelm*	*Total no. of element flexibility models* *Each has different number of control sections*
MAXX	*maxx*	*maximum no. of control sections in any model*
	melm	*element flexibility model number*
NUMX	*numx*	*number of control sections*
XCRD	*x_crd(1)=0*	*position of first control section expressed as a ratio of section's local x-coordinate and element length*
	x_crd( )	*position of an intermediate control section*
	x_crd( )=1	*position of last control section; maximum six allowed*

The next line is used to build model combinations. The component models, namely concrete, steel, torsion, creep and element flexibility models are combined to create a pattern. This pattern is later associated with individual frame elements.

NMDL=nmdl

{mmdl MSEC=sec MCON=con MSTL=stl MTOR=tor MCRP=crp MELM=elm}

Identifier	*Variable*	*Description*
NMDL	*nmdl*	*number of element models*
	mmdl	*element model number*
MSEC	*sec*	*section model number*
MCON	*con*	*concrete model number*
MSTL	*stl*	*steel model number*
MTOR	*tor*	*torsion model number*
MCRP	*crp*	*creep model number*
MELM	*elm*	*element flexibility model number*

The following lines are used to define frame element connectivity and to specify an element property pattern number *mmdl* which associates each frame element with a set of material and flexibility models specified earlier.

NFRM=nfrm

{mfrm, node_I, node_J, node_K mmdl G=nadd,ninc,iinc,jinc,kinc}

Blank Line

Identifier	*Variable*	*Description*
NFRM	*nfrm*	*total number of frame elements*
	mfrm	*frame element number*
	node_I	*node number of I node*
	node_J	*node number of J node*
	node_K	*node number of K node*
	mmdl	*element model number*
G		*generation parameters*
	nadd	*number of frame elements to be generated with the same mmdl*
	ninc	*element number increment*
	iinc	*I node increment*
	jinc	*J node increment*
	kinc	*K node increment*

7.4. CABLE ELEMENTS

This section is used to specify connectivity, material and geometric properties of cable-stay elements. The organization is as follows:

1. Define cable section property sets. These properties include the area of cross section of the cable and its weight density.
2. Define cable elements. Input cable end node numbers and the section and material model number associated with that element.

CABLE

NSEC=nsec

{msec AREA=area DENSITY=density}

Identifier	*Variable*	*Description*
NSEC	*nsec*	*number of section types*
	msec	*section number*
AREA	*area*	*area of cross section*
DENSITY	*density*	*weight density of cable material*

NCBL=ncbl

{mcbl, node_I, node_J SECNUM=msec MATNUM=mmat G=nadd,ninc,iinc}

Blank Line

Identifier	*Variable*	*Description*
NCBL	*ncbl*	*total number of cable elements*
	mcbl	*cable element number*
	node_I	*node number of I node*
	node_J	*node number of J node*
SECNUM	*msec*	*section type number*
MATNUM	*mmat*	*material model number*
G		*generation parameters*
	nadd	*number of cable elements to be generated with same msec*
	ninc	*element number increment*
	iinc	*I node increment*
	jinc	*J node increment*

7.5. CATENARY ELEMENTS

This section is used to specify connectivity, material and geometric properties of catenary elements. The organization is as follows:

1. Define section property sets. These properties include the area of cross section of the cable, elastic modulus of the cable material and its weight density.
2. Define catenary elements. Input end node numbers and the section property set number associated with each catenary element.

Note that at the present time, CALBRG allows only linear material models for catenary elements.

CATENARY

NSEC=nsec

{msec AREA=area WEIGHT=weight EMOD=emod}

Identifier	*Variable*	*Description*
NSEC	*nsec*	*number of section types*
	msec	*section number*
AREA	*area*	*area of cross section*
WEIGHT	*weight*	*weight per unit length of the catenary*
EMOD	*emod*	*modulus of elasticity of catenary steel*

NCAT=ncat

{mcat, node_I, node_J MSEC=msec G=nadd,ninc,iinc}

Blank Line

Identifier	***Variable***	***Description***
NCAT	*ncat*	*total number of catenary elements*
	mcat	*catenary element number*
	node_I	*node number of I node*
	node_J	*node number of J node*
MSEC	*msec*	*section type number*
G		*generation parameters*
	nadd	*number of catenary elements to be generated with same msec*
	ninc	*element number increment*
	iinc	*I node increment*
	jinc	*J node increment*

7.6. PRESTRESSING TENDONS

The command is used to specify and generate the geometry of all prestressing tendons used in the structure. Each tendon is divided into spans, where a span is defined as a portion of the tendon which has a standard geometric profile that can be generated. Each span is subdivided into tendon segments. The tendon is thus modeled as a series of piece wise linear tendon segments. Structurally each tendon segment is modeled as an eccentric truss bar, its ends rigidly connected to the corresponding nodes of the host frame element.

Tendon point coordinates are defined with respect to a local coordinate system. These coordinates may be input directly by defining the local coordinates of each tendon point or

they may be generated. Standard geometric profiles, which consist of a combination of parabolas may be generated by defining a set of parameters. In the case of a three dimensional structure, these generation parameters must be defined both in the x-y and x-z plane. Tendon point coordinates are written in tabular form to the output file for later verification.

The command sequence used in this section is as follows:

1. Define tendon stress loss property sets.
2. Start tendon definition.

   For each tendon:

   - Input number of spans in the tendon, steel model and stress loss property set associated with that tendon.

     For each span:

     - Define structure nodes that fall in the span.
     - Input tendon point coordinates directly

       or

     - Use parametric generation schemes for

       (a) Linear profiles.

       (b) Standard geometric profiles consisting of series of parabolas.

The next lines define tendon properties used to calculate loss of prestress due to friction between the tendon and the duct, and relaxation of prestressing steel. Any number of property sets may be defined.

TENDON
NPRP=nprp
{mprp FYLD=fyld RCOF=rcof CCOF=ccof WCOF=wcof}

Identifier	*Variable*	*Description*
NPRP	*nprp*	*number of property sets*
	mprp	*property set number*
FYLD	*fyld*	*yield stress of tendon steel*
RCOF	*rcof*	*relaxation coefficient*
CCOF	*ccof*	*coefficient of curvature friction*
WCOF	*wcof*	*coefficient of wobble friction*

The following lines define the number of spans *nspn* in tendon number *mtdn*. Each prestressing tendon is associated with a stress loss property set and a material model.

NTDN=ntdn
mtdn NSPN=nspn MSTL=mstl MPRP=mprp AREA=area

Identifier	*Variable*	*Description*
NTDN	*ntdn*	*total number of tendons*
	mtdn	*tendon number*
NSPN	*nspn*	*span number*
MSTL	*mstl*	*steel model number; input under MODELS command*
MPRP	*mprp*	*property set number*
AREA	*area*	*area of cross section*

Each span in the tendon is defined independently. Span numbers must be provided in an ascending order starting with span no. 1.

For each span, the number of structure nodes that fall within that span are input and the local coordinates system that will be used to input tendon point coordinates is established. This coordinate system is usually defined by the *I, J* and *K* nodes of the host frame element.

The structure nodes inside the span may be either generated or listed in order from left to right of span.

mspn NNIS=nnis [G=nfirst, nlast, ninc] CSYS=I, J, K
[L=n1, n2, nn]

Identifier	*Variable*	*Description*
	mspn	*span number*
NNIS	*nnis*	*number of nodes in span*
G		*generation parameters: use only if L will not be used*
	nfirst	*first node number*
	nlast	*last node number*
	ninc	*node number increment*
CSYS		
	I	*reference coordinate system*
	J	*I node of CSYS*
	K	*J node of CSYS*
		K node of CSYS
L		*List of node numbers in span; use only if G not used*

Use next line for direct input of tendon points in the span. Repeat *nnis* times.

{mnod YL=y_coord ZL=z_coord}

Identifier	*Variable*	*Description*
	mnod	*node number*
YL	*y_coord*	*y coordinate in the local reference system defined by CSYS*
ZL	*z_coord*	*z coordinate in the local reference system defined by CSYS*

Use followoing lines for linear generation of tendon point coordinates in the span

YL=yle, yre
ZL=zle, zre

Identifier	*Variable*	*Description*
YL		*y coordinates in the local reference system defined by CSYS*
	yle	*y coordinate at the left end of span*
	yre	*y coordinate at the right end of span*
ZL		*z coordinates in the local reference system defined by CSYS*
	zle	*z coordinate at the left end of span*
	zre	*z coordinate at the right end of span*

The next lines are used for generation of tendon points lying on a standard geometric profile defined by a series of parabolas as described in Chapter 7.

XYP=rli,rlp,rri YL=yle,ylp,yre

XZP=rli,rlpp,rri ZL=zle,zlp,zre

Identifier	*Variable*	*Description*
XYP		*parameters for generation of parabola in XY plane*
	rli	*(distance b/w left inflection point & left end)/(element length)*
	rlp	*(distance b/w low point & left end)/(element length)*
	rri	*(distance b/w right inflection point & right end)/(element length)*
YL		*y coordinates in the local reference system defined by CSYS*
	yle	*y coordinate at the left end of span*
	ylp	*y coordinate of the low point in span*
	yre	*y coordinate at the right end of span*
XZP		*parameters for generation of parabola in XZ plane*
	rli	*(distance b/w left inflection point & left end)/(element length)*
	rlp	*(distance b/w low point & left end)/(element length)*
	rri	*(distance b/w right inflection point & right end)/(element length)*
ZL		*z coordinates in the local reference system defined by CSYS*
	zle	*z coordinate at the left end of span*
	zlp	*y coordinate of the low point in span*
	zre	*z coordinate at the right end of span*

7.7. EXIT STRUCTURE DEFINITION

END_GEOMETRY

This command indicates the end of command group *GEOMETRY*, and returns control of program to the main routine.

8. CHANGE STRUCTURE CONFIGURATION

CONFIGURATION

.....

END_CONFIGURATION

This command group is used to define, modify or change the analysis model. Frame elements, cast at various dates, may be added or removed. Stay cables and pre-stressing tendons may be stressed, restressed or removed. Large sag catenary cables may be installed or removed. Boundary restraints may be imposed or released. It is, however essential that the resulting model be statically feasible.

The sub-command tree is shown in Fig. A.3. All the sub-commands in this category are optional and are used only as needed, to build or modify, the analysis model. Each of the sub-commands is described in detail in the following sections.

8.1. ADD FRAME ELEMENT

ADD_FRAME F=mfrm TCAST=day [G=nelm,ninc]

Identifier	*Variable*	*Description*
F	*mfrm*	*frame element number*
TCAST	*day*	*the time at which element was cast in days*
G		*generation parameters*
	nelm	*number of elements to be generated*
	ninc	*element number increment*

This command is used to add reinforced concrete or steel frame elements to the current analysis model. In the case of concrete elements, the analyst must specify the casting time; this is compared with the time at which the analysis is desired and appropriate adjustments made to the material model.

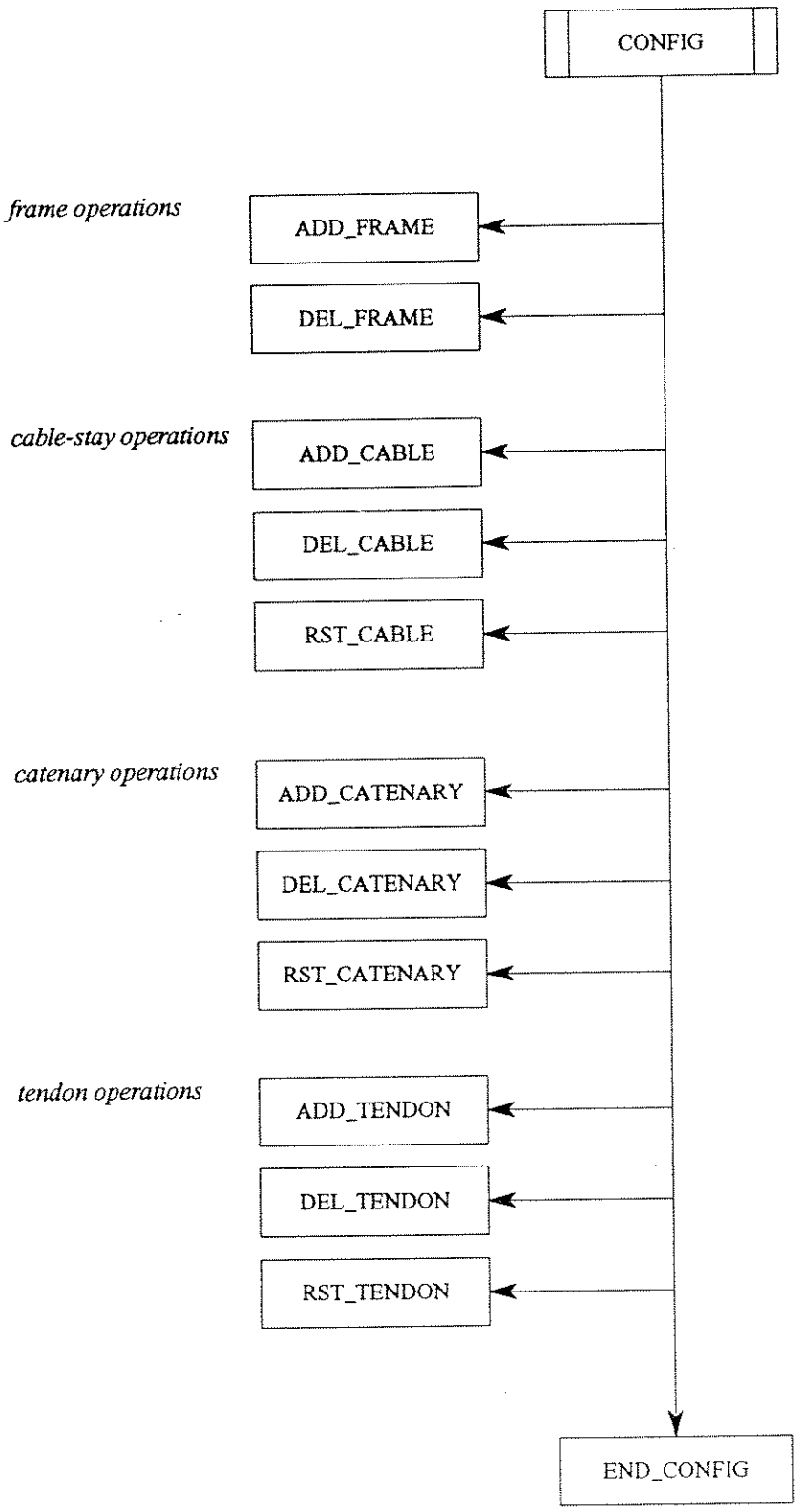

FIG. A.3 SEGMENTAL CONSTRUCTION OPERATIONS
"CONFIG" AND ITS SUBCOMMANDS

8.2. REMOVE FRAME ELEMENT

DEL_FRAME F=mfrm

Identifier	*Variable*	*Description*
F	*mfrm*	*frame element number*

This command is used to remove frame elements from the existing analysis model. It is specially useful to remove temporary frame elements such as those used to model false work or temporary supports to the structure. In the present study this command is used to perform a dis-assembly analysis on a three dimensional cable-stayed bridge. This is done to determine the correct tension in the leading cable-stays at the time of their initial installation, during a cantilever construction sequence.

Note that this command can only be used on an element previously installed in the structure with the *ADD_FRAME* command.

8.3. ADD PRESTRESSING TENDON

ADD_TENDON P=mtdn SA=sig_l [SB=sig_r] DA=anc_l [DB=anc_r] [G=nelm,ninc]

Identifier	*Variable*	*Description*
P	*mtdn*	*tendon element number*
SA	*sig_l*	*Jacking stress at left end of tendon*
SB	*sig_r*	*Jacking stress at right end of tendon*
DA	*anc_l*	*Anchor set at left end of tendon*
DB	*anc_r*	*Anchor set at right end of tendon*
G		*generation parameters*
	nelm	*number of elements to be generated*
	ninc	*element number increment*

This command is used to add prestressing tendons to previously defined frame elements. The jacking stress and anchor set at one or both ends must be specified.

8.4. REMOVE PRESTRESSING TENDON

DEL_TENDON P=mtdn [G=nelm,ninc]

Identifier	*Variable*	*Description*
P	*mtdn*	*tendon element number*
G		*generation parameters*
	nelm	*number of elements to be generated*
	ninc	*element number increment*

The above command is used to remove existing tendons from the analysis model. For example, it may be used to remove tendons used to temporarily hold precast segments in place during cantilever construction operations.

8.5. RESTRESS PRESTRESSING TENDON

RST_TENDON P=mtdn SA=sig_l SB=sig_r DA=anc_l DB=anc_r [G=nelm,ninc]

Identifier	*Variable*	*Description*
P	*mtdn*	*tendon element number*
SA	*sig_l*	*Jacking stress at left end of tendon*
SB	*sig_r*	*Jacking stress at right end of tendon*
DA	*anc_l*	*Anchor set at left end of tendon*
DB	*anc_r*	*Anchor set at right end of tendon*
G		*generation parameters*
	nelm	*number of elements to be generated*
	ninc	*element number increment*

This command is used to change the stress level in an existing prestressing tendon.

8.6. ADD CABLE-STAY

ADD_CABLE C=mcbl TENSION=fini [G=nelm,ninc]

Identifier	*Variable*	*Description*
C	*mcbl*	*cable element number*
TENSION	*fini*	*initial cable force*
G		*generation parameters*
	nelm	*number of elements to be generated*
	ninc	*element number increment*

This command is used to install a cable-stay into the structure and set it to the desired tension. The cable is installed with the two end nodes held rigidly in place; the cable length corresponding to the design tension is automatically calculated by the program and written to the output file. During the analysis the two end nodes undergo displacements and hence the cable tension changes slightly.

8.7. REMOVE CABLE-STAY

DEL_CABLE C=mcbl

Identifier	*Variable*	*Description*
C	*mcbl*	*cable element number*

This command is used to remove auxiliary cable stays commonly used in the construction of cable-stayed bridges. It may also be employed in a dis-assembly analysis in which a completed structure sitting on a desired profile is taken apart to find initial tensions in the cable-stays.

8.8. RESTRESS CABLE-STAY

RST_CABLE C=mcbl TENSION=fini [G=nelm,ninc]

Identifier	*Variable*	*Description*
C	*mcbl*	*cable element number*
TENSION	*fini*	*initial cable force*
G		*generation parameters*
	nelm	*number of elements to be generated*
	ninc	*element number increment*

This command is used to restress existing cable-stays in the structure. It is frequently used in cantilever construction operations. When the cables are first installed, they usually carry half the segment load. When the next segment is added, the cable tensions must be increased to compensate for the higher load. This command may also be used to adjust cable tensions before casting the closure joint in a cable-stayed bridge in order to align the two halves of the structure. Note that this command can only be used on a previously installed cable.

8.9. ADD CATENARY ELEMENT

ADD_CATENARY R=mcat L=elen [G=nelm,ninc]

Identifier	*Variable*	*Description*
R	*mcat*	*catenary element number*
L	*elen*	*un-stressed length of catenary*
G		*generation parameters*
	nelm	*number of elements to be generated*
	ninc	*element number increment*

This command is used to install a catenary element in the structure. The unstressed length of the element must be specified by the analyst. Note that only linear elastic material models are allowed for the large sag catenary element.

8.10. REMOVE CATENARY ELEMENT

DEL_CATENARY R=mcat

Identifier	*Variable*	*Description*
R	*mcat*	*catenary element number*

This command is used to remove existing catenary elements from the structure.

8.11. CHANGE TENSION IN A CATENARY ELEMENT

RST_CATENARY R=mcat L=elen [G=nelm,ninc]

Identifier	*Variable*	*Description*
R	*mcat*	*catenary element number*
L	*elen*	*changed un-stressed length of catenary*
G		*generation parameters*
	nelm	*number of elements to be generated*
	ninc	*element number increment*

The above command is used to change the tension in an existing catenary element. A new unstressed length is specified for the element.

8.12. CHANGE RESTRAINTS

RESTRAINTS

[nodnum R=x, y, z, xx, yy, zz [G=nadd,ninc]]

Blank Line

Identifier	*Variable*	*Description*
	nodnum	*boundary conditions will be modified for this node number*
R		*restraint codes; 0 is free, 1 is locked.*
	x	*translation in global x direction*
	y	*translation in global y direction*
	z	*translation in global z direction*
	xx	*rotation about global x axis*
	yy	*rotation about global y axis*
	zz	*rotation about global z axis*
G		*generation parameters*
	nadd	*number of additional restraints to be generated*
	ninc	*node number increment*

The *RESTRAINTS* command is used to specify boundary conditions for the structure. These conditions may be changed to correspond to the construction operations or at any other time during the life of the structure. When a degree of freedom which was previously free to move, is locked with the *RESTRAINTS* command, it is fixed at its current displacement. On the other hand, when a degree of freedom which was previously locked, is released with the *RESTRAINTS* command, it is free to displace.

8.13. EXIT CHANGE STRUCTURE PHASE

END_CONFIGURATION

This command signifies the end of command group *CONFIGURATION*, and returns control of program to the main routine.

9. DEFINE LOAD PATTERN

LOAD

{nodnum F=x, y, z, xx, yy, zz {G=nadd, ninc}}

Blank Line

Identifier	*Variable*	*Description*
	nodnum	*load applied at this node number*
F		*defines load pattern applied to nodnum*
	x	*load applied in global x direction*
	y	*load applied in global y direction*
	z	*load applied in global z direction*
	xx	*moment applied about global x axis*
	yy	*moment applied about global y axis*
	zz	*moment applied about global z axis*
G		*generation parameters*
	nadd	*number of additional nodes with similar pattern to be generated*
	ninc	*node number increment*

This command is used to define a load pattern. The load pattern is later multiplied by a *"load pattern multiplier"* specified under the *SOLVE* subcommand. This command may be used as many times as desired. All loadings remain in effect until they are removed by the application of equal and opposite loading. All external loads are defined with respect to the global coordinate axes. The total current loads applied to the structure are stored internally by the program and printed out at every solution step.

10. DEFINE SOLUTION ENVIRONMENT

ENVIRONMENT

NONLMAT=mat	***PATHDEP=path***	***NONLGMT=gmt***	***KGEOMET=kgmt***
PCODE_M=mcode	***PCODE_S=scode***	***PCODE_F=fcode***	
TOLR_FI=ftol_i	***TOLR_FL=ftol_l***	***TOLR_FK=ftol_k***	
TOLR_MI=mtol_i	***TOLR_ML=mtol_l***	***TOLR_MK=mtol_k***	
SEC_EQM=keqm	***NUMIT_S=numit_s***	***NSTEP_S=nstep_s***	
TOLR_ST=stol	***INTTYPE=ityp***		

Identifier	*Variable*	*Description*
NONLMAT	*mat=1/0*	*material non-linearity switch; on/off*
PATHDEP	*path=1/0*	*path dependence switch; on/off*
NONLGMT	*gmt=1/0*	*geometric non-linearity switch; on/off*
KGEOMET	*kgmt=1/0*	*include geometric stiffness switch; on/off*
PCODE_M	*mcode=3/2/1*	*print member forces at end of: each iteration / each step / at end*
PCODE_S	*scode=1/0*	*print section forces switch; on/off*
PCODE_F	*fcode=1/0*	*print fiber stresses switch; on/off*
TOLR_FI	*ftol_i*	*force tolerance of intermediate solution steps*
TOLR_FL	*ftol_l*	*force tolerance for last solution step*
TOLR_FK	*ftol_k*	*force tolerance for stiffness matrix update*
TOLR_MI	*mtol_i*	*moment tolerance of intermediate solution steps*
TOLR_ML	*mtol_l*	*moment tolerance for last solution step*
SEC_EQM	*keqm=1/0*	*enforce equilibrium at internal slices in the frame element; on/off*
NUMIT_S	*numit_s*	*max. number of iterations in the slice NR iterations*
NSTEP_S	*nstep_s*	*number of steps that the slice unbalanced load is divided into.*
TOLR_MK	*mtol_k*	*moment tolerance for stiffness matrix update*
TOLR_ST	*stol*	*stress tolerance for creep solution convergence*
INTTYPE	*ityp=1/2/3*	*time step integration type*

This command is used to set the solution environment for solving the nonlinear equilibrium equations and must be specified before the *SOLVE* group of commands.

The first line following the *ENVIRONMENT* command is used to set the material and geometric nonlinearity switches. The analyst has the option to include or exclude the element geometric stiffness matrix and may select either path dependent or independent state determination schemes.

The second line is used to control the frequency and detail of output generated by the program. The third and fourth lines are used to set force and moment tolerances for non-linear solution. Refresh rate of stiffness matrix may be adjusted by controlling it through a specified force tolerance.

The fourth line is used to enforce slice equilibrium at internal sections in a beam column element. This activates a special numerical procedure designed to predict the behavior of a structure past the point of maximum resistance and overcome the usual numerical problems associated with strain softening.

The last line is used to set the stress tolerances used in a time dependent solution. The creep integration method is also specified in this line; the analyst has a choice of three different procedures:

1. Constant stress and constant variation of material parameters over the time step.
2. Linear variation of stress and constant material parameters over the time step.
3. Linear variation of both stress and material properties over the time step.

This *ENVIRONMENT* command may be repeated as many times as needed.

11. SET CURRENT TIME

SET_TIME TCUR=tcur

Identifier	*Variable*	*Description*
TCUR	*tcur*	*current time in days*

This command sets the current time. This is used to evaluate time dependent properties of various elements. Any construction operations carried out in a subsequent change *CONFIGURATION* command are implemented at *TCUR*. This command must be used for both time step solutions and instantaneous solutions.

Note that the value of *TCUR* is also changed by the *SOLVE-TIMECON* command wherein *TCUR* is incremented in steps to *TEND* (the time when solution ends).

12. SOLVE EQUILIBRIUM EQUATIONS

SOLVE

.....

END_SOLVE

This command group is used to determine the equilibrium state of the analysis model subjected to the load pattern defined earlier and/or time dependent effects. The basic structure of the command group is shown in Fig. A.4. Three different solution strategies are available:

1. Load control method.
2. Displacement control method.
3. Time step method.

The first two methods may be used to obtain instantaneous solutions whereas the last is used for time dependent solutions involving creep and shrinkage of concrete. This command group may be repeated any number of times.

12.1. LOAD CONTROLLED SOLUTION STRATEGY

LOAD_CONTROL

XFPTN=xfptn NUMSTEP=nstep NUMIT_I=nit_i NUMIT_L=nit_l

Identifier	*Variable*	*Description*
XFPTN	*xfptn*	*load pattern multiplier*
NUMSTEP	*nstep*	*(XFPTN x load pattern) applied to structure NUMSTEP times*
NUMIT_I	*nit_i*	*maximum number of iterations allowed for intermediate steps*
NUMIT_L	*nit_l*	*maximum number of iterations allowed for final step*

The load pattern vector defined earlier under the *LOADS* command is multiplied by *XFPTN* the load pattern multiplier, the resulting load is applied to the structure and a solution obtained. This process is repeated *NUMSTEP* times. Newton-Raphson method is used to solve the nonlinear equilibrium equations at each load step. The computation time and degree of

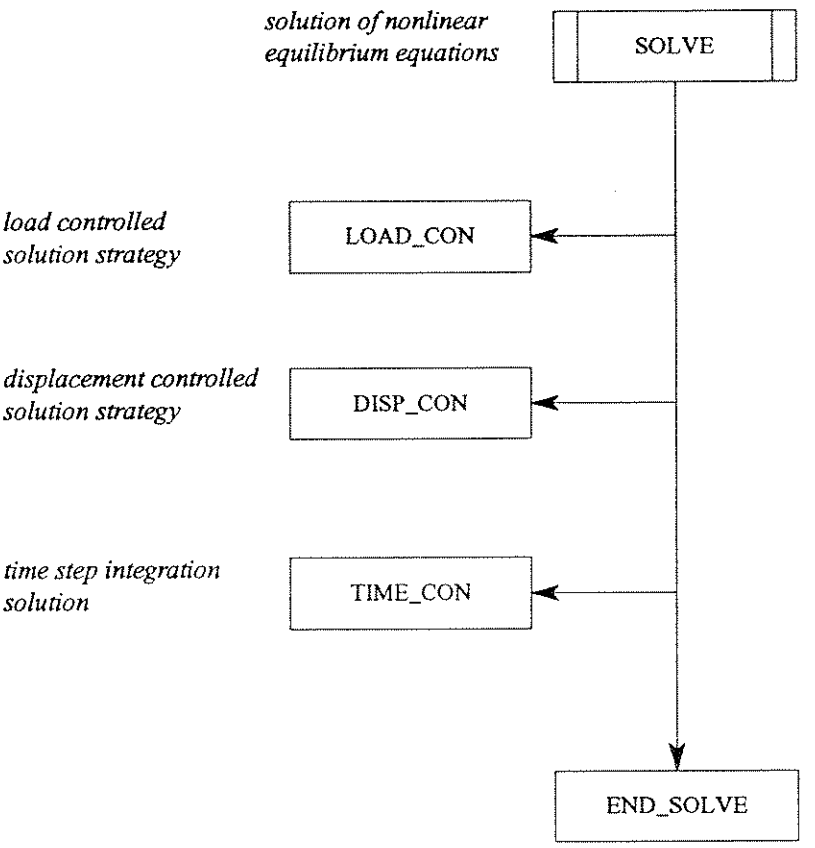

FIG. A.4 SOLUTION OF NONLINEAR EQUILIBRIUM EQUATIONS "SOLVE" AND ITS SUBCOMMANDS

accuracy of the solution can be controlled by adjusting convergence tolerances and number of iterations allowed for intermediate and final solution steps.

12.2. DISPLACEMENT CONTROLLED SOLUTION STRATEGY

DISP_CONTROL
NUMNODE=nnod NUMDISP=ndisp
DISPMAG=disp NUMSTEP=nstep NUMIT_I=nit_i NUMIT_L=nit_l

Identifier	*Variable*	*Description*
NUMNOD	*nnod*	*node number; being subjected to displacement control*
NUMDISP	*ndisp=1,2...6*	*displacement being controlled*
DISPMAG	*disp*	*magnitude of controlled displacement*
NUMSTEP	*nstep*	*DISPMAG repeated NUMSTEP times*
NUMIT_I	*nit_i*	*maximum number of iterations allowed for intermediate steps*
NUMIT_L	*nit_l*	*maximum number of iterations allowed for final step*

This command is used to activate the displacement control solution strategy. The displacement of the selected degree of freedom is incremented by *DISPMAG,* and the corresponding load vector which would hold the structure in equilibrium, is obtained. This process is repeated *NUMSTEP* number of times. The number of iterations allowed during the intermediate and the final solution steps may also be specified.

The displacement control method is very effective for snap-through type of problems as well as structures exhibiting strain softening behavior.

12.3. TIME STEP INTEGRATION

TIME_CONTROL

TEND=tend NUMSTEP=nstep NUMIT_I=nit_i NUMIT_L=nit_l

Identifier	*Variable*	*Description*
NUMNOD	*nnod*	*node number; being subjected to displacement control*
TEND	*tend*	*time at end of solution*
NUMSTEP	*nstep*	*(TCUR-TEND) is divided log-linearly into NUMSTEPs*
NUMIT_I	*nit_i*	*maximum number of iterations allowed for intermediate steps*
NUMIT_L	*nit_l*	*maximum number of iterations allowed for final step*

This command is used for a time dependent analysis of reinforced and prestressed concrete structures. The time domain, which spans from time TCUR to time TEND is divided into log-linear time steps, and a solution is obtained at each time step. Increments of creep and shrinkage strains in concrete and change in the prestressing tendon stress due to relaxation losses is accounted for during each time step. Creep strain increments are evaluated using one of three integration methods described earlier. Any external load is applied to the structure during the first time step.

For a cantilever construction sequences, it is recommended that an instantaneous solution may be obtained whenever new structural elements are added or external loads applied to the structure. This is done by setting *TEND=TCUR*. The structure is then allowed to age using a time dependent solution until the next cycle of element addition. The process is repeated as many times as needed.

12.4. EXIT SOLVER

END_SOLVE

This command is used to exit the *SOLVE* group of commands, and returns control of the program to main module.

13. END PROCESSING

END

The execution of CALBRG is stopped; incore information is saved in a database file named *"alpha.cor"*, where *"alpha"* is the name of the input file. Control is returned to OS2.

APPENDIX B
RUCK-A-CHUCKY STEEL BRIDGE
INPUT FILE FOR COMPUTER PROGRAM CALBRG
LOAD BALANCING ANALYSIS

```
START r=0
:
TITLE  n=2
RUCK-A-CHUCKY STEEL BRIDGE.
LOAD BALANCING ANALYSIS:

GEOMETRY
node
n=109
1     z=7563     x=1653     y= 0.      : deck nodes
2     z=7290     x=1529
3     z=6737     x=1295
4     z=6176     x=1080
5     z=5609     x=884
6     z=5035     x=706
7     z=4456     x=548
8     z=3872     x=409
9     z=3284     x=290
10    z=2692     x=190
11    z=2097     x=110
12    z=1499     x=51
13    z=900      x=11
14    z=300      x=-10
15    z=0        x=-12
30    z=7563     x=1653     y=1000     : deck k nodes
31    z=7290     x=1529
32    z=6737     x=1295
33    z=6176     x=1080
34    z=5609     x=884
35    z=5035     x=706
36    z=4456     x=548
37    z=3872     x=409
38    z=3284     x=290
39    z=2692     x=190
40    z=2097     x=110
41    z=1499     x=51
42    z=900      x=11
43    z=300      x=-10
58    z=10912    x=2521     y=1740     :outer rock anchor
59    z=11494    x=2456     y=2088
60    z=11862    x=2231     y=2400
61    z=12108    x=1938     y=2712
62    z=14411    x=1994     y=3864
63    z=14954    x=1560     y=4200
64    z=15960    x=1141     y=4932
65    z=16567    x=614      y=5148
66    z=16899    x=59       y=5208
67    z=17075    x=-555     y=5208
68    z=17324    x=-1109    y=5196
69    z=17201    x=-1768    y=5136
70    z=6859     x=1034     y=-36      : outer deck anchors
71    z=6289     x=815
72    z=5713     x=615
73    z=5131     x=434
74    z=4542     x=273
75    z=3949     x=131
76    z=3351     x=10
77    z=2750     x=-92
78    z=2145     x=-174
79    z=1538     x=-235
80    z=930      x=-276
81    z=320      x=-297
82    z=13026    x=10726    y=3024     : inner rock anchors
83    z=13457    x=10324    y=3240
84    z=13998    x=9913     y=3420
85    z=14800    x=9797     y=3852
86    z=15435    x=9376     y=4200
87    z=15537    x=8547     y=4260
88    z=14923    x=7354     y=4260
89    z=14947    x=6636     y=4260
90    z=15230    x=6145     y=4500
91    z=15985    x=5537     y=4848
```

```
92    z=16061    x=5217     y=4944
93    z=16922    x=4732     y=5412
94    z=6643     x=1568     y=-36      : inner deck anchors
95    z=6091     x=1356
96    z=5533     x=1162
97    z=4969     x=987
98    z=4399     x=831
99    z=3825     x=694
100   z=3246     x=576
101   z=2663     x=477
102   z=2078     x=398
103   z=1490     x=339
104   z=901      x=299
105   z=310      x=279
106   z=7563     x=429      y=-36      : auxiliary cables
107   z=7563     x=-3483    y=-36
108   z=6289     x=815      y=-36
109   z=3949     x=131      y=-36

MODELS
steel nmod=1
1 sigy=50 epsu=.20 emod0=29000 emod1=100.869
torsion nmod=1
1 tcr=2.2e+6 acr=8.3e-5 typ=3.5e+6 ayp=.02 aut=.02
CABLE nmod=1
1 sigy=245.760 epsy=.00847 sigu=270 epsu=.0419

FRAME
nsec=1 maxc=0 maxs=40 p=1
msec=1 ncf=0 nsf=40

as=48      y=-.25     z=-48
as=48      y=-.25     z=-144
as=48      y=-.25     z=-240
as=29      y=-3.1     z=-48
as=29      y=-3.1     z=-144
as=29      y=-3.1     z=-240
as=12.2    y=-16.3    z=-73
as=12.2    y=-16.3    z=-196
as=35.7    y=-16.3    z=-275
as=62.3    y=-20.1    z=-293
as=12.2    y=-48.8    z=-73
as=12.2    y=-48.8    z=-196
as=35.7    y=-48.8    z=-246.5
as=12.2    y=-81.3    z=-73
as=12.2    y=-81.3    z=-196
as=35.7    y=-81.3    z=-218
as=10.6    y=-91.5    z=-50.6
as=10.6    y=-91.5    z=-151.9
as=76      y=-97.1    z=-50.6
as=76      y=-97.1    z=-151.9
as=48      y=-.25     z=48
as=48      y=-.25     z=144
as=48      y=-.25     z=240
as=29      y=-3.1     z=48
as=29      y=-3.1     z=144
as=29      y=-3.1     z=240
as=12.2    y=-16.3    z=73
as=12.2    y=-16.3    z=196
as=35.7    y=-16.3    z=275
as=62.3    y=-20.1    z=293
as=12.2    y=-48.8    z=73
as=12.2    y=-48.8    z=196
as=35.7    y=-48.8    z=246.5
as=12.2    y=-81.3    z=73
as=12.2    y=-81.3    z=196
as=35.7    y=-81.3    z=218
as=10.6    y=-91.5    z=50.6
```

```
as=10.6     y=-91.5     z=151.9
as=76       y=-97.1     z=50.6
as=76       y=-97.1     z=151.9

nelm=1  maxx=4
1  numx=4  xcrd=0.,.25,.75,1.
nmdl=1
1  msec=1  mcon=1  mstl=1  mtor=1  mcrp=1  melm=1
nfrm=14
1,  1,  2,  30    mmdl=1    g=13,1,1,1,1

CABLE
nsec=24
1       area= 6.73      density=.490/1728
3       area= 6.27
5       area= 6.27
7       area= 6.27
9       area= 6.27
11      area= 6.27
13      area= 6.27
15      area= 6.43
17      area= 6.58
19      area= 6.58
21      area= 6.73
23      area= 6.88
2       area= 7.65
4       area= 7.34
6       area= 7.34
8       area= 7.34
10      area= 7.34
12      area= 6.58
14      area= 6.58
16      area= 6.73
18      area= 6.73
20      area= 6.73
22      area= 6.73
24      area= 6.73
ncbl=26
1,58, 70        mj=3        secnum=1    matnum=1
3,59, 71        mj=4        secnum=3
5,60, 72        mj=5        secnum=5
7,61, 73        mj=6        secnum=7
9,62, 74        mj=7        secnum=9
11,63, 75       mj=8        secnum=11
13,64, 76       mj=9        secnum=13
15,65, 77       mj=10       secnum=15
17,66, 78       mj=11       secnum=17
19,67, 79       mj=12       secnum=19
21,68, 80       mj=13       secnum=21
23,69, 81       mj=14       secnum=23
2,82, 94        mj=3        secnum=2
4,83, 95        mj=4        secnum=4
6,84, 96        mj=5        secnum=6
8,85, 97        mj=6        secnum=8
10,86, 98       mj=7        secnum=10
12,87, 99       mj=8        secnum=12
14,88,100       mj=9        secnum=14
16,89,101       mj=10       secnum=16
18,90,102       mj=11       secnum=18
20,91,103       mj=12       secnum=20
22,92,104       mj=13       secnum=22
24,93,105       mj=14       secnum=24
25,106,108      mj=4        secnum=24
26,107,109      mj=8        secnum=24

END_GEOMETRY
:
SET_TIME tcur=30
:
CONFIGURATION
add_frame F=1   g=12,1
```

```
add_cable c=1   tension=546.1*1.03
add_cable c=2   tension=651.6*1.03
add_cable c=3   tension=560.8*1.03
add_cable c=4   tension=650.1*1.03
add_cable c=5   tension=570.7*1.03
add_cable c=6   tension=643.8*1.03
add_cable c=7   tension=565.7*1.03
add_cable c=8   tension=625.6*1.03
add_cable c=9   tension=560.3*1.03
add_cable c=10  tension=608.6*1.03
add_cable c=11  tension=568.6*1.03
add_cable c=12  tension=608.2*1.03
add_cable c=13  tension=554.2*1.03
add_cable c=14  tension=585.6*1.03
add_cable c=15  tension=573.1*1.03
add_cable c=16  tension=599.6*1.03
add_cable c=17  tension=586.3*1.03
add_cable c=18  tension=609.5*1.03
add_cable c=19  tension=602.3*1.03
add_cable c=20  tension=619.9*1.03
add_cable c=21  tension=622.0*1.03
add_cable c=22  tension=640.8*1.03
add_cable c=23  tension=337.5*1.03
add_cable c=24  tension=346.0*1.03
add_cable c=25  tension=15
add_cable c=26  tension=80

restraints
1               r=1,1,1,1,1,1
58              r=1,1,1,1,1,1  g=11,1
82              r=1,1,1,1,1,1  g=11,1
106             r=1,1,1,1,1,1  g=1,1

END_CONFIGURATION
:
LOAD
2       f=0,-266
3       f=0,-380
4       f=0,-380
5       f=0,-380
6       f=0,-380
7       f=0,-380
8       f=0,-380
9       f=0,-380
10      f=0,-380
11      f=0,-380
12      f=0,-380
13      f=0,-380
14      f=0,-203

:
ENVIRONMENT
nonlmat=1       pathdep=0       nonlgmt=1       kgeomet=1
pcode_m=2       pcode_s=0       pcode_f=0
tolr_fi=1       tolr_fl=1       tolr_fk=1
tolr_mi=1       tolr_ml=1       tolr_mk=1
sec_eqm=0       numit_s=10      nstep_s=1
tolr_st=1.      inttype=1
:
SOLVE
LOAD_CONTROL
xfptn=1   numstep=1     numit_i=20    numit_l=20
END_SOLVE
: ----------------------------------------------------------------
: add segment 14; remove cables 25 & 26
: ----------------------------------------------------------------
CONFIGURATION
add_frame F=14
rst_cable c=23  tension=631.8*1.03
rst_cable c=24  tension=647.6*1.03
del_cable c=25
del_cable c=26
```

```
restraints
15          r=0,0,1,1,1,0

END_CONFIGURATION
:
LOAD
14      f=0,-88.5
15      f=0,-88.5

:
SOLVE
LOAD_CONTROL
xfptn=1    numstep=1      numit_i=20     numit_l=20
END_SOLVE
END
```

APPENDIX C
RUCK-A-CHUCKY CONCRETE BRIDGE
INPUT FILE FOR COMPUTER PROGRAM CALBRG
CONSTRUCTION SEQUENCE ANALYSIS

```
START r=0
:
TITLE  n=2
ANALYSIS OF RUCK-A-CHUCKY CONCRETE BRIDGE.
CONSTRUCTION SEQUENCE ANALYSIS
:
CREEP_MODEL  n=1 p=1
1 m=aci  w=110
:
GEOMETRY
node
n=130
1    z=7777    x=1761    y= 0.     :deck segment nodes
2    z=7563    x=1653
3    z=7345    x=1553
4    z=7014    x=1410
5    z=6681    x=1273
6    z=6345    x=1143
7    z=6007    x=1019
8    z=5666    x=902     y=1
9    z=5323    x=793     y=2
10   z=4978    x=690     y=4
11   z=4631    x=593     y=5
12   z=4282    x=504     y=6
13   z=3931    x=422     y=8
14   z=3578    x=347     y=9
15   z=3225    x=279     y=11
16   z=2870    x=218     y=12
17   z=2514    x=164     y=14
18   z=2156    x=118     y=15
19   z=1798    x=78      y=17
20   z=1439    x=46      y=18
21   z=1080    x=20      y=20
22   z=720     x=2       y=22
23   z=360     x=-8      y=24
24   z=0       x=-12     y=26
25   z=7777    x=1761    y= 1000.  :deck segment k nodes
26   z=7563    x=1653
27   z=7345    x=1553
28   z=7014    x=1410
29   z=6681    x=1273
30   z=6345    x=1143
31   z=6007    x=1019
32   z=5666    x=902
33   z=5323    x=793
34   z=4978    x=690
35   z=4631    x=593
36   z=4282    x=504
37   z=3931    x=422
38   z=4578    x=347
39   z=3225    x=279
40   z=2870    x=218
41   z=2514    x=164
42   z=2156    x=118
43   z=1798    x=78
44   z=1439    x=46
45   z=1080    x=20
46   z=720     x=2
47   z=360     x=-8
48   z=10774   x=2502    y=1644    :outer rock anchors
49   z=10806   x=2412    y=1704
50   z=10961   x=2207    y=1872
51   z=10988   x=2115    y=1932
52   z=11056   x=1846    y=2088
53   z=11112   x=1607    y=2220
54   z=11130   x=1513    y=2244
55   z=14540   x=1832    y=4585
56   z=14898   x=1586    y=4536
57   z=15860   x=1387    y=4980
58   z=16604   x=1127    y=5220
59   z=16745   x=799     y=5220
60   z=16878   x=467     y=5220
```

61 z=17004 x=130 y=5220
62 z=17184 x=-209 y=5220
63 z=17176 x=-551 y=5220
64 z=17222 x=-891 y=5220
65 z=17263 x=-1233 y=5220
66 z=17388 x=-1582 y=5220
67 z=17432 x=-1917 y=5220
68 z=7045 x=1098 y=-4 :outer deck anchors
69 z=6706 x=960
70 z=6364 x=829
71 z=6019 x=705
72 z=5672 x=589 y=-3
73 z=5323 x=479 y=-2
74 z=4971 x=376 y=0
75 z=4618 x=280 y=1
76 z=4262 x=191 y=2
77 z=3905 x=109 y=4
78 z=3547 x=35 y=5
79 z=3187 x=-33 y=7
80 z=2826 x=-93 y=8
81 z=2463 x=-146 y=10
82 z=2100 x=-191 y=11
83 z=1736 x=-230 y=13
84 z=1371 x=-261 y=14
85 z=1005 x=-284 y=16
86 z=639 x=-301 y=18
87 z=273 x=-310 y=20
88 z=12946 x=11154 y=3048 :inner rock anchors
89 z=13226 x=10882 y=3252
90 z=13469 x=10545 y=3348
91 z=13716 x=10279 y=3444
92 z=14182 x=10101 y=3468
93 z=14623 x=9919 y=3804
94 z=15025 x=9676 y=3960
95 z=15360 x=9362 y=4140
96 z=15666 x=9009 y=4320
97 z=15751 x=8513 y=4416
98 z=15038 x=7556 y=4236
99 z=14855 x=6996 y=4260
100 z=15042 x=6650 y=4344
101 z=15186 x=6292 y=4476
102 z=15349 x=5937 y=4572
103 z=15530 x=5597 y=4620
104 z=16220 x=5435 y=4980
105 z=16530 x=5120 y=5100
106 z=16829 x=4795 y=5220
107 z=17002 x=4435 y=5364
108 z=6814 x=1651 y=-4 :inner deck anchors
109 z=6486 x=1518
110 z=6155 x=1392
111 z=5822 x=1272
112 z=5486 x=1159 y=-3
113 z=5148 x=1053 y=-2
114 z=4808 x=953 y=0
115 z=4466 x=860 y=1
116 z=4123 x=775 y=2
117 z=3777 x=695 y=4
118 z=3431 x=623 y=5
119 z=3082 x=558 y=7
120 z=2733 x=500 y=8
121 z=2382 x=449 y=10
122 z=2031 x=405 y=11
123 z=1679 x=368 y=13
124 z=1326 x=338 y=14
125 z=972 x=315 y=16
126 z=618 x=299 y=18
127 z=264 x=290 y=20
128 z=7600 x=66 y=-4 :auxiliary cables
129 z=7600 x=-1339 y=-3
130 z=7600 x=-2702 y=1

MODELS

```
concrete nmod=1
1 sig0=-5000 eps1=-.0064 epsu=-.0075 ushr=-.0008 ucrp=2.35
steel nmod=2
1 sigy=60000     epsu=.12    emod0=29E+6 emod1=29E+4
2 sigy=246000    epsu=.042   emod0=29E+6 emod1=716E+3
torsion nmod=5
1 tcr=1.6e+9    acr=4.3e-6 typ=8.7e+8    ayp=3.1e-5  aut=.02
2 tcr=9.1e+8    acr=4.7e-6 typ=9.7e+8    ayp=3.6e-5  aut=.02
3 tcr=4.3e+8    acr=7.4e-6 typ=5.7e+8    ayp=4.8e-5  aut=.02
4 tcr=3.5e+8    acr=6.6e-6 typ=4.8e+8    ayp=5.1e-5  aut=.02
5 tcr=3.2e+8    acr=6.7e-6 typ=3.6e+8    ayp=6.1e-5  aut=.02
CABLE nmod=1
1 sigy=245760  epsy=.00847  sigu=270000  epsu=.0419

FRAME
nsec=5  maxc=50 maxs=24 p=1
msec=1  ncf=44  nsf=20              :station 4 to 5
ac=546      y=-6.0      z=-22.8
ac=546      y=-6.0      z=-68.3
ac=546      y=-6.0      z=-113.8
ac=546      y=-6.0      z=-159.3
ac=546      y=-6.0      z=-204.8
ac=546      y=-6.0      z=-250.3
ac=956      y=-12.8     z=-290.0
ac=405      y=-34.5     z=-4.5
ac=810      y=-34.5     z=-150.0
ac=1080     y=-34.5     z=-261.0
ac=405      y=-79.5     z=-4.5
ac=810      y=-79.5     z=-150.0
ac=1080     y=-79.5     z=-261.0
ac=405      y=-124.5    z=-4.5
ac=810      y=-124.5    z=-150.0
ac=1080     y=-124.5    z=-261.0
ac=1331     y=-161.6    z=-250.3
ac=1331     y=-161.6    z=-204.8
ac=1331     y=-161.6    z=-159.3
ac=1331     y=-161.6    z=-113.8
ac=1331     y=-161.6    z=-68.3
ac=1331     y=-161.6    z=-22.8
ac=546      y=-6.0      z=22.8
ac=546      y=-6.0      z=68.3
ac=546      y=-6.0      z=113.8
ac=546      y=-6.0      z=159.3
ac=546      y=-6.0      z=204.8
ac=546      y=-6.0      z=250.3
ac=956      y=-12.8     z=290.0
ac=405      y=-34.5     z=4.5
ac=810      y=-34.5     z=150.0
ac=1080     y=-34.5     z=261.0
ac=405      y=-79.5     z=4.5
ac=810      y=-79.5     z=150.0
ac=1080     y=-79.5     z=261.0
ac=405      y=-124.5    z=4.5
ac=810      y=-124.5    z=150.0
ac=1080     y=-124.5    z=261.0
ac=1331     y=-161.6    z=250.3
ac=1331     y=-161.6    z=204.8
ac=1331     y=-161.6    z=159.3
ac=1331     y=-161.6    z=113.8
ac=1331     y=-161.6    z=68.3
ac=1331     y=-161.6    z=22.8

as=8.1      y=-6.0      z=-40.5
as=8.1      y=-6.0      z=-121.5
as=8.1      y=-6.0      z=-202.5
as=8.1      y=-6.0      z=-283.5
as=4.0      y=-83.8     z=-4.5
```

as=8.0 y=-83.8 z=-150.0
as=8.0 y=-83.8 z=-261.0
as=7.3 y=-161.6 z=-43.5
as=7.3 y=-161.6 z=-130.5
as=7.3 y=-161.6 z=-217.5
as=8.1 y=-6.0 z=40.5
as=8.1 y=-6.0 z=121.5
as=8.1 y=-6.0 z=202.5
as=8.1 y=-6.0 z=283.5
as=4.0 y=-83.8 z=4.5
as=8.0 y=-83.8 z=150.0
as=8.0 y=-83.8 z=261.0
as=7.3 y=-161.6 z=43.5
as=7.3 y=-161.6 z=130.5
as=7.3 y=-161.6 z=217.5

msec=2 ncf=44 nsf=20 :station 5 to 6
ac=534 y=-6.0 z=-22.2
ac=534 y=-6.0 z=-66.7
ac=534 y=-6.0 z=-111.2
ac=534 y=-6.0 z=-155.7
ac=534 y=-6.0 z=-200.1
ac=534 y=-6.0 z=-244.6
ac=1128 y=-13.8 z=-285.9
ac=482 y=-38.8 z=-4.5
ac=850 y=-38.8 z=-42.0
ac=965 y=-38.8 z=-150.0
ac=1080 y=-39.9 z=-253.7
ac=482 y=-92.4 z=-4.5
ac=850 y=-92.4 z=-108.0
ac=965 y=-92.4 z=-150.0
ac=1080 y=-93.6 z=-227.4
ac=776. y=-130.1 z=-17.9
ac=776. y=-130.1 z=-53.6
ac=776. y=-130.1 z=-89.3
ac=776. y=-130.1 z=-125.0
ac=776. y=-130.1 z=-160.7
ac=776. y=-130.1 z=-196.4
ac=534 y=-6.0 z=22.2
ac=534 y=-6.0 z=66.7
ac=534 y=-6.0 z=111.2
ac=534 y=-6.0 z=155.7
ac=534 y=-6.0 z=200.1
ac=534 y=-6.0 z=244.6
ac=1128 y=-13.8 z=285.9
ac=482 y=-38.8 z=4.5
ac=850 y=-38.8 z=42.0
ac=965 y=-38.8 z=150.0
ac=1080 y=-39.9 z=253.7
ac=482 y=-92.4 z=4.5
ac=850 y=-92.4 z=108.0
ac=965 y=-92.4 z=150.0
ac=1080 y=-93.6 z=227.4
ac=776. y=-130.1 z=17.9
ac=776.5 y=-130.1 z=53.6
ac=776 y=-130.1 z=89.3
ac=776. y=-130.1 z=125.0
ac=776. y=-130.1 z=160.7
ac=776. y=-130.1 z=196.4

as=10.7 y=-6.0 z=-40.5
as=10 y=-6.0 z=-121.5
as=10.7 y=-6.0 z=-202.5
as=10.7 y=-6.0 z=-283.5
as=6.4 y=-68.1 z=-4.5
as=10.0 y=-68.1 z=-75.0

as=6.4 y=-68.1 z=-150.0
as=10.0 y=-68.1 z=-244.5
as=8.4 y=-130.1 z=-53.5
as=8.4 y=-130.1 z=-160.5
as=10.7 y=-6.0 z=40.5
as=10.7 y=-6.0 z=121.5
as=10.7 y=-6.0 z=202.5
as=10.7 y=-6.0 z=283.5
as=6.4 y=-68.1 z=4.5
as=10.0 y=-68.1 z=75.0
as=6.4 y=-68.1 z=150.0
as=10.0 y=-68.1 z=244.5
as=8.4 y=-130.1 z=53.5
as=8.4 y=-130.1 z=160.5

msec=3 ncf=50 nsf=24 :station 6 thru 10
ac=375 y=-6.0 z=-15.6
ac=297 y=-5.5 z=-44.4
ac=243 y=-4.5 z=-71.3
ac=309 y=-4.0 z=-104.6
ac=309 y=-4.0 z=-143.1
ac=309 y=-4.0 z=-181.7
ac=243 y=-4.5 z=-203.4
ac=297 y=-5.5 z=-230.3
ac=294 y=-7.0 z=-253.9
ac=240 y=-4.0 z=-270.4
ac=468 y=-6.9 z=-291.2
ac=234 y=-18.3 z=-288.4
ac=174 y=-21.3 z=-270.2
ac=431 y=-24.4 z=-253.1
ac=470 y=-26.3 z=-25
ac=470 y=-51.0 z=-75
ac=470 y=-75.7 z=-125
ac=781 y=-42.4 z=-237.5
ac=781 y=-64.4 z=-202.5
ac=781 y=-86.4 z=-167.5
ac=504 y=-95.0 z=-142.0
ac=504 y=-95.0 z=-106.0
ac=364 y=-95.0 z=-65.0
ac=364 y=-95.0 z=-39.0
ac=364 y=-95.0 z=-13.0
ac=375 y=-6.0 z=15.6
ac=297 y=-5.5 z=44.4
ac=243 y=-4.5 z=71.3
ac=309 y=-4.0 z=104.6
ac=309 y=-4.0 z=143.1
ac=309 y=-4.0 z=181.7
ac=243 y=-4.5 z=203.4
ac=297 y=-5.5 z=230.3
ac=294 y=-7.0 z=253.9
ac=240 y=-4.0 z=270.4
ac=468 y=-6.9 z=291.2
ac=234 y=-18.3 z=288.4
ac=174 y=-21.3 z=270.2
ac=431 y=-24.4 z=253.1
ac=470 y=-26.3 z=25
ac=470 y=-51.0 z=75
ac=470 y=-75.7 z=125
ac=781 y=-42.4 z=237.5
ac=781 y=-64.4 z=202.5
ac=781 y=-86.4 z=167.5
ac=504 y=-95.0 z=142.0
ac=504 y=-95.0 z=106.0
ac=364 y=-95.0 z=65.0
ac=364 y=-95.0 z=39.0
ac=364 y=-95.0 z=13.0

as=8.5 y=-4.0 z=-32.4
as=8.5 y=-4.0 z=-97.2
as=8.5 y=-4.0 z=-162.0
as=8.5 y=-4.0 z=-226.8
as=8.5 y=-4.0 z=-291.6
as=10.2 y=-19.2 z=-275.0
as=10.2 y=-49.5 z=-225.0
as=10.2 y=-79.8 z=-175.0
as=4.6 y=-27.8 z=-37.5
as=4.6 y=-75.3 z=-112.5
as=13.2 y=-95.0 z=-112.5
as=13.2 y=-95.0 z=-37.5
as=8.5 y=-4.0 z=32.4
as=8.5 y=-4.0 z=97.2
as=8.5 y=-4.0 z=162.0
as=8.5 y=-4.0 z=226.8
as=8.5 y=-4.0 z=291.6
as=10.2 y=-19.2 z=275.0
as=10.2 y=-49.5 z=225.0
as=10.2 y=-79.8 z=175.0
as=4.6 y=-27.8 z=37.5
as=4.6 y=-75.3 z=112.5
as=13.2 y=-95.0 z=112.5
as=13.2 y=-95.0 z=37.5

msec=4 ncf=44 nsf=20 :station 10 thru 14
ac=375 y=-6.0 z=-15.6
ac=297 y=-5.5 z=-44.4
ac=243 y=-4.5 z=-71.3
ac=309 y=-4.0 z=-104.6
ac=309 y=-4.0 z=-143.1
ac=309 y=-4.0 z=-181.7
ac=243 y=-4.5 z=-203.4
ac=297 y=-5.5 z=-230.3
ac=294 y=-7.0 z=-253.9
ac=240 y=-4.0 z=-270.4
ac=468 y=-6.9 z=-291.2
ac=234 y=-18.3 z=-288.4
ac=174 y=-21.3 z=-270.2
ac=431 y=-24.4 z=-253.1
ac=534 y=-43.5 z=-261.9
ac=534 y=-65.5 z=-227.2
ac=534 y=-87.5 z=-192.4
ac=360 y=-97.0 z=-142.0
ac=360 y=-97.0 z=-106.0
ac=260 y=-97.0 z=-65.0
ac=260 y=-97.0 z=-39.0
ac=260 y=-97.0 z=-13.0
ac=375 y=-6.0 z=15.6
ac=297 y=-5.5 z=44.4
ac=243 y=-4.5 z=71.3
ac=309 y=-4.0 z=104.6
ac=309 y=-4.0 z=143.1
ac=309 y=-4.0 z=181.7
ac=243 y=-4.5 z=203.4
ac=297 y=-5.5 z=230.3
ac=294 y=-7.0 z=253.9
ac=240 y=-4.0 z=270.4
ac=468 y=-6.9 z=291.2
ac=234 y=-18.3 z=288.4
ac=174 y=-21.3 z=270.2
ac=431 y=-24.4 z=253.1
ac=534 y=-43.5 z=261.9
ac=534 y=-65.5 z=227.2
ac=534 y=-87.5 z=192.4

ac=360 y=-97.0 z=142.0
ac=360 y=-97.0 z=106.0
ac=260 y=-97.0 z=65.0
ac=260 y=-97.0 z=39.0
ac=260 y=-97.0 z=13.0

as=6.2 y=-4.0 z=-42.5
as=6.2 y=-4.0 z=-127.5
as=6.2 y=-4.0 z=-212.5
as=8.3 y=-4.0 z=-272.3
as=8.3 y=-4.0 z=-306.8
as=5.8 y=-19.5 z=-275.0
as=5.8 y=-50.5 z=-225.0
as=5.8 y=-81.5 z=-175.0
as=7.4 y=-97.0 z=-112.5
as=7.4 y=-97.0 z=-37.5
as=6.2 y=-4.0 z=42.5
as=6.2 y=-4.0 z=127.5
as=6.2 y=-4.0 z=212.5
as=8.3 y=-4.0 z=272.3
as=8.3 y=-4.0 z=306.8
as=5.8 y=-19.5 z=275.0
as=5.8 y=-50.5 z=225.0
as=5.8 y=-81.5 z=175.0
as=7.4 y=-97.0 z=112.5
as=7.4 y=-97.0 z=37.5

msec=5 ncf=44 nsf=20 :station 14 thru 27
ac=375 y=-6.0 z=-15.6
ac=297 y=-5.5 z=-44.4
ac=243 y=-4.5 z=-71.3
ac=309 y=-4.0 z=-104.6
ac=309 y=-4.0 z=-143.1
ac=309 y=-4.0 z=-181.7
ac=243 y=-4.5 z=-203.4
ac=297 y=-5.5 z=-230.3
ac=294 y=-7.0 z=-253.9
ac=240 y=-4.0 z=-270.4
ac=468 y=-6.9 z=-291.2
ac=234 y=-18.3 z=-288.4
ac=174 y=-21.3 z=-270.2
ac=431 y=-24.4 z=-253.1
ac=428 y=-51.6 z=-234.4
ac=428 y=-72.9 z=-200.7
ac=428 y=-94.2 z=-166.9
ac=378 y=-99.7 z=-132.9
ac=270 y=-98.2 z=-97.2
ac=156 y=-99.0 z=-65.0
ac=156 y=-99.0 z=-39.0
ac=156 y=-99.0 z=-13.0
ac=375 y=-6.0 z=15.6
ac=297 y=-5.5 z=44.4
ac=243 y=-4.5 z=71.3
ac=309 y=-4.0 z=104.6
ac=309 y=-4.0 z=143.1
ac=309 y=-4.0 z=181.7
ac=243 y=-4.5 z=203.4
ac=297 y=-5.5 z=230.3
ac=294 y=-7.0 z=253.9
ac=240 y=-4.0 z=270.4
ac=468 y=-6.9 z=291.2
ac=234 y=-18.3 z=288.4
ac=174 y=-21.3 z=270.2
ac=431 y=-24.4 z=253.1
ac=428 y=-51.6 z=234.4
ac=428 y=-72.9 z=200.7

ac=428 y=-94.2 z=166.9
ac=378 y=-99.7 z=132.9
ac=270 y=-98.2 z=97.2
ac=156 y=-99.0 z=65.0
ac=156 y=-99.0 z=39.0
ac=156 y=-99.0 z=13.0

as=2.8 y=-4.0 z=-42.5
as=2.8 y=-4.0 z=-127.5
as=2.8 y=-4.0 z=-212.5
as=8.3 y=-4.0 z=-272.3
as=8.3 y=-4.0 z=-306.8
as=2.6 y=-19.8 z=-275.0
as=2.6 y=-51.5 z=-225.0
as=2.6 y=-83.2 z=-175.0
as=3.4 y=-99.0 z=-112.5
as=3.4 y=-99.0 z=-37.5
as=2.8 y=-4.0 z=42.5
as=2.8 y=-4.0 z=127.5
as=2.8 y=-4.0 z=212.5
as=8.3 y=-4.0 z=272.3
as=8.3 y=-4.0 z=306.8
as=2.6 y=-19.8 z=275.0
as=2.6 y=-51.5 z=225.0
as=2.6 y=-83.2 z=175.0
as=3.4 y=-99.0 z=112.5
as=3.4 y=-99.0 z=37.5

nelm=1 maxx=4
1 numx=4 xcrd=0.,.2,.8,1.
nmdl=5
1 msec=1 mcon=1 mstl=1 mtor=1 mcrp=1 melm=1
2 msec=2 mcon=1 mstl=1 mtor=2 mcrp=1 melm=1
3 msec=3 mcon=1 mstl=1 mtor=3 mcrp=1 melm=1
4 msec=4 mcon=1 mstl=1 mtor=4 mcrp=1 melm=1
5 msec=5 mcon=1 mstl=1 mtor=5 mcrp=1 melm=1
nfrm=23
1, 1, 2, 25 mmdl=1
2, 2, 3, 26 mmdl=2
3, 3, 4, 27 mmdl=3 g=3,1,1,1,1
7, 7, 8, 31 mmdl=4 g=3,1,1,1,1
11,11,12, 35 mmdl=5 g=12,1,1,1,1

CABLE
nsec=43
1 area= 8.42 density=490/1728
3 area= 8.11
5 area= 7.34
7 area= 7.19
9 area= 7.19
11 area= 6.27
13 area= 6.27
15 area= 5.20
17 area= 5.36
19 area= 5.51
21 area= 5.66
23 area= 5.81
25 area= 6.12
27 area= 6.27
29 area= 6.43
31 area= 6.58
33 area= 6.73
35 area= 6.88
37 area= 7.04
39 area= 7.34
2 area= 9.18
4 area= 9.18
6 area= 8.87
8 area= 8.41

```
10     area= 7.96
12     area= 7.65
14     area= 7.65
16     area= 7.04
18     area= 7.04
20     area= 7.04
22     area= 7.04
24     area= 7.04
26     area= 7.04
28     area= 7.04
30     area= 7.04
32     area= 7.04
34     area= 7.04
36     area= 7.04
38     area= 7.04
40     area= 7.04
41     area= 7.04
42     area= 7.04
43     area= 7.04
ncbl=43
1,48, 68        mj=4      secnum= 1   matnum=1
3,49, 69        mj=5      secnum= 3
5,50, 70        mj=6      secnum= 5
7,51, 71        mj=7      secnum= 7
9,52, 72        mj=8      secnum= 9
11,53, 73       mj=9      secnum=11
13,54, 74       mj=10     secnum=13
15,55, 75       mj=11     secnum=15
17,56, 76       mj=12     secnum=17
19,57, 77       mj=13     secnum=19
21,58, 78       mj=14     secnum=21
23,59, 79       mj=15     secnum=23
25,60, 80       mj=16     secnum=25
27,61, 81       mj=17     secnum=27
29,62, 82       mj=18     secnum=29
31,63, 83       mj=19     secnum=31
33,64, 84       mj=20     secnum=33
35,65, 85       mj=21     secnum=35
37,66, 86       mj=22     secnum=37
39,67, 87       mj=23     secnum=39
2,88,108        mj=4      secnum= 2
4,89,109        mj=5      secnum= 4
6,90,110        mj=6      secnum= 6
8,91,111        mj=7      secnum= 8
10,92,112       mj=8      secnum=10
12,93,113       mj=9      secnum=12
14,94,114       mj=10     secnum=14
16,95,115       mj=11     secnum=16
18,96,116       mj=12     secnum=18
20,97,117       mj=13     secnum=20
22,98,118       mj=14     secnum=22
24,99,119       mj=15     secnum=24
26,100,120      mj=16     secnum=26
28,101,121      mj=17     secnum=28
30,102,122      mj=18     secnum=30
32,103,123      mj=19     secnum=32
34,104,124      mj=20     secnum=34
36,105,125      mj=21     secnum=36
38,106,126      mj=22     secnum=38
40,107,127      mj=23     secnum=40
41,128,5                  secnum=41
42,129,8                  secnum=42
43,130,11                 secnum=43

TENDON
nprp=1
1 fyld=243000 rcof=45 ccof=.15 wcof=.0005/12
ntdn=34
 1 nspn=2  mstl=2  mprp=1  area=3.67
   1 nnis=2  g=1,2,1  csys=1,2,25
     1      yl=-11     zl=-258
     2      yl=-11     zl=-258
```

```
  2 nnis=2  g=2,3,1  csys=2,3,26
    1     yl=-11     zl=-258
    2     yl=-11     zl=-258
2 nspn=2  mstl=2  mprp=1  area=3.67
  1 nnis=2  g=1,2,1  csys=1,2,25
    1     yl=-11     zl=258
    2     yl=-11     zl=258
  2 nnis=2  g=2,3,1  csys=2,3,26
    1     yl=-11     zl=258
    2     yl=-11     zl=258
3 nspn=3  mstl=2  mprp=1  area=11.32
  1 nnis=2  g=1,2,1  csys=1,2,25
    1     yl=-11     zl=-286
    2     yl=-11     zl=-286
  2 nnis=2  g=2,3,1  csys=2,3,26
    1     yl=-11     zl=-286
    2     yl=-11     zl=-286
  3 nnis=2  g=3,4,1  csys=3,4,27
    1     yl=-11     zl=-286
    2     yl=-11     zl=-286
4 nspn=3  mstl=2  mprp=1  area=1.84
  1 nnis=2  g=1,2,1  csys=1,2,25
    1     yl=-6      zl=0
    2     yl=-6      zl=0
  2 nnis=2  g=2,3,1  csys=2,3,26
    1     yl=-6      zl=0
    2     yl=-6      zl=0
  3 nnis=2  g=3,4,1  csys=3,4,27
    1     yl=-6      zl=0
    2     yl=-6      zl=0
5 nspn=3  mstl=2  mprp=1  area=11.32
  1 nnis=2  g=1,2,1  csys=1,2,25
    1     yl=-11     zl=286
    2     yl=-11     zl=286
  2 nnis=2  g=2,3,1  csys=2,3,26
    1     yl=-11     zl=286
    2     yl=-11     zl=286
  3 nnis=2  g=3,4,1  csys=3,4,27
    1     yl=-11     zl=286
    2     yl=-11     zl=286
6 nspn=4  mstl=2  mprp=1  area=1.84
  1 nnis=2  g=1,2,1  csys=1,2,25
    1     yl=-11     zl=-258
    2     yl=-11     zl=-258
  2 nnis=2  g=2,3,1  csys=2,3,26
    1     yl=-11     zl=-258
    2     yl=-11     zl=-258
  3 nnis=2  g=3,4,1  csys=3,4,27
    1     yl=-11     zl=-258
    2     yl=-11     zl=-258
  4 nnis=2  g=4,5,1  csys=4,5,28
    1     yl=-11     zl=-258
    2     yl=-11     zl=-258
7 nspn=4  mstl=2  mprp=1  area=1.84
  1 nnis=2  g=1,2,1  csys=1,2,25
    1     yl=-6      zl=0
    2     yl=-6      zl=0
  2 nnis=2  g=2,3,1  csys=2,3,26
    1     yl=-6      zl=0
    2     yl=-6      zl=0
  3 nnis=2  g=3,4,1  csys=3,4,27
    1     yl=-6      zl=0
    2     yl=-6      zl=0
  4 nnis=2  g=4,5,1  csys=4,5,28
    1     yl=-6      zl=0
    2     yl=-6      zl=0
8 nspn=4  mstl=2  mprp=1  area=1.84
  1 nnis=2  g=1,2,1  csys=1,2,25
    1     yl=-11     zl=258
    2     yl=-11     zl=258
  2 nnis=2  g=2,3,1  csys=2,3,26
    1     yl=-11     zl=258
```

```
   2      yl=-11     zl=258
  3 nnis=2   g=3,4,1  csys=3,4,27
   1      yl=-11     zl=258
   2      yl=-11     zl=258
  4 nnis=2   g=4,5,1  csys=4,5,28
   1      yl=-11     zl=258
   2      yl=-11     zl=258
 9  nspn=5   mstl=2   mprp=1   area=1.84
  1 nnis=2   g=1,2,1  csys=1,2,25
   1      yl=-11     zl=-258
   2      yl=-11     zl=-258
  2 nnis=2   g=2,3,1  csys=2,3,26
   1      yl=-11     zl=-258
   2      yl=-11     zl=-258
  3 nnis=2   g=3,4,1  csys=3,4,27
   1      yl=-11     zl=-258
   2      yl=-11     zl=-258
  4 nnis=2   g=4,5,1  csys=4,5,28
   1      yl=-11     zl=-258
   2      yl=-11     zl=-258
  5 nnis=2   g=5,6,1  csys=5,6,29
   1      yl=-11     zl=-258
   2      yl=-11     zl=-258
 10  nspn=5   mstl=2   mprp=1   area=1.84
  1 nnis=2   g=1,2,1  csys=1,2,25
   1      yl=-6      zl=0
   2      yl=-6      zl=0
  2 nnis=2   g=2,3,1  csys=2,3,26
   1      yl=-6      zl=0
   2      yl=-6      zl=0
  3 nnis=2   g=3,4,1  csys=3,4,27
   1      yl=-6      zl=0
   2      yl=-6      zl=0
  4 nnis=2   g=4,5,1  csys=4,5,28
   1      yl=-6      zl=0
   2      yl=-6      zl=0
  5 nnis=2   g=5,6,1  csys=5,6,29
   1      yl=-6      zl=0
   2      yl=-6      zl=0
 11  nspn=5   mstl=2   mprp=1   area=1.84
  1 nnis=2   g=1,2,1  csys=1,2,25
   1      yl=-11     zl=258
   2      yl=-11     zl=258
  2 nnis=2   g=2,3,1  csys=2,3,26
   1      yl=-11     zl=258
   2      yl=-11     zl=258
  3 nnis=2   g=3,4,1  csys=3,4,27
   1      yl=-11     zl=258
   2      yl=-11     zl=258
  4 nnis=2   g=4,5,1  csys=4,5,28
   1      yl=-11     zl=258
   2      yl=-11     zl=258
  5 nnis=2   g=5,6,1  csys=5,6,29
   1      yl=-11     zl=258
   2      yl=-11     zl=258
 12  nspn=6   mstl=2   mprp=1   area=1.84
  1 nnis=2   g=1,2,1  csys=1,2,25
   1      yl=-11     zl=-258
   2      yl=-11     zl=-258
  2 nnis=2   g=2,3,1  csys=2,3,26
   1      yl=-11     zl=-258
   2      yl=-11     zl=-258
  3 nnis=2   g=3,4,1  csys=3,4,27
   1      yl=-11     zl=-258
   2      yl=-11     zl=-258
  4 nnis=2   g=4,5,1  csys=4,5,28
   1      yl=-11     zl=-258
   2      yl=-11     zl=-258
  5 nnis=2   g=5,6,1  csys=5,6,29
   1      yl=-11     zl=-258
   2      yl=-11     zl=-258
  6 nnis=2   g=6,7,1  csys=6,7,30
```

```
    1      yl=-11     zl=-258
    2      yl=-11     zl=-258
 13  nspn=6   mstl=2   mprp=1   area=1.84
   1 nnis=2   g=1,2,1   csys=1,2,25
    1      yl=-6      zl=0
    2      yl=-6      zl=0
   2 nnis=2   g=2,3,1   csys=2,3,26
    1      yl=-6      zl=0
    2      yl=-6      zl=0
   3 nnis=2   g=3,4,1   csys=3,4,27
    1      yl=-6      zl=0
    2      yl=-6      zl=0
   4 nnis=2   g=4,5,1   csys=4,5,28
    1      yl=-6      zl=0
    2      yl=-6      zl=0
   5 nnis=2   g=5,6,1   csys=5,6,29
    1      yl=-6      zl=0
    2      yl=-6      zl=0
   6 nnis=2   g=6,7,1   csys=6,7,30
    1      yl=-6      zl=0
    2      yl=-6      zl=0
 14  nspn=6   mstl=2   mprp=1   area=1.84
   1 nnis=2   g=1,2,1   csys=1,2,25
    1      yl=-11     zl=258
    2      yl=-11     zl=258
   2 nnis=2   g=2,3,1   csys=2,3,26
    1      yl=-11     zl=258
    2      yl=-11     zl=258
   3 nnis=2   g=3,4,1   csys=3,4,27
    1      yl=-11     zl=258
    2      yl=-11     zl=258
   4 nnis=2   g=4,5,1   csys=4,5,28
    1      yl=-11     zl=258
    2      yl=-11     zl=258
   5 nnis=2   g=5,6,1   csys=5,6,29
    1      yl=-11     zl=258
    2      yl=-11     zl=258
   6 nnis=2   g=6,7,1   csys=6,7,30
    1      yl=-11     zl=258
    2      yl=-11     zl=258
 15  nspn=6   mstl=2   mprp=1   area=1.84
   1 nnis=2   g=18,19,1   csys=18,19,42
    1      yl=-11     zl=-261
    2      yl=-11     zl=-261
   2 nnis=2   g=19,20,1   csys=19,20,43
    1      yl=-11     zl=-261
    2      yl=-11     zl=-261
   3 nnis=2   g=20,21,1   csys=20,21,44
    1      yl=-11     zl=-261
    2      yl=-11     zl=-261
   4 nnis=2   g=21,22,1   csys=21,22,45
    1      yl=-11     zl=-261
    2      yl=-11     zl=-261
   5 nnis=2   g=22,23,1   csys=22,23,46
    1      yl=-11     zl=-261
    2      yl=-11     zl=-261
   6 nnis=2   g=23,24,1   csys=23,24,47
    1      yl=-11     zl=-261
    2      yl=-11     zl=-261
 16  nspn=6   mstl=2   mprp=1   area=1.84
   1 nnis=2   g=18,19,1   csys=18,19,42
    1      yl=-6      zl=0
    2      yl=-6      zl=0
   2 nnis=2   g=19,20,1   csys=19,20,43
    1      yl=-6      zl=0
    2      yl=-6      zl=0
   3 nnis=2   g=20,21,1   csys=20,21,44
    1      yl=-6      zl=0
    2      yl=-6      zl=0
   4 nnis=2   g=21,22,1   csys=21,22,45
    1      yl=-6      zl=0
    2      yl=-6      zl=0
```

```
 5 nnis=2  g=22,23,1  csys=22,23,46
  1     yl=-6       zl=0
  2     yl=-6       zl=0
 6 nnis=2  g=23,24,1  csys=23,24,47
  1     yl=-6       zl=0
  2     yl=-6       zl=0
17  nspn=6  mstl=2  mprp=1  area=1.84
 1 nnis=2  g=18,19,1  csys=18,19,42
  1     yl=-11      zl=261
  2     yl=-11      zl=261
 2 nnis=2  g=19,20,1  csys=19,20,43
  1     yl=-11      zl=261
  2     yl=-11      zl=261
 3 nnis=2  g=20,21,1  csys=20,21,44
  1     yl=-11      zl=261
  2     yl=-11      zl=261
 4 nnis=2  g=21,22,1  csys=21,22,45
  1     yl=-11      zl=261
  2     yl=-11      zl=261
 5 nnis=2  g=22,23,1  csys=22,23,46
  1     yl=-11      zl=261
  2     yl=-11      zl=261
 6 nnis=2  g=23,24,1  csys=23,24,47
  1     yl=-11      zl=261
  2     yl=-11      zl=261
18  nspn=6  mstl=2  mprp=1  area=1.84
 1 nnis=2  g=18,19,1  csys=18,19,42
  1     yl=-95      zl=-147
  2     yl=-95      zl=-147
 2 nnis=2  g=19,20,1  csys=19,20,43
  1     yl=-95      zl=-147
  2     yl=-95      zl=-147
 3 nnis=2  g=20,21,1  csys=20,21,44
  1     yl=-95      zl=-147
  2     yl=-95      zl=-147
 4 nnis=2  g=21,22,1  csys=21,22,45
  1     yl=-95      zl=-147
  2     yl=-95      zl=-147
 5 nnis=2  g=22,23,1  csys=22,23,46
  1     yl=-95      zl=-147
  2     yl=-95      zl=-147
 6 nnis=2  g=23,24,1  csys=23,24,47
  1     yl=-95      zl=-147
  2     yl=-95      zl=-147
19  nspn=6  mstl=2  mprp=1  area=1.84
 1 nnis=2  g=18,19,1  csys=18,19,42
  1     yl=-95      zl=147
  2     yl=-95      zl=147
 2 nnis=2  g=19,20,1  csys=19,20,43
  1     yl=-95      zl=147
  2     yl=-95      zl=147
 3 nnis=2  g=20,21,1  csys=20,21,44
  1     yl=-95      zl=147
  2     yl=-95      zl=147
 4 nnis=2  g=21,22,1  csys=21,22,45
  1     yl=-95      zl=147
  2     yl=-95      zl=147
 5 nnis=2  g=22,23,1  csys=22,23,46
  1     yl=-95      zl=147
  2     yl=-95      zl=147
 6 nnis=2  g=23,24,1  csys=23,24,47
  1     yl=-95      zl=147
  2     yl=-95      zl=147
20  nspn=5  mstl=2  mprp=1  area=1.84
 1 nnis=2  g=19,20,1  csys=19,20,43
  1     yl=-11      zl=-261
  2     yl=-11      zl=-261
 2 nnis=2  g=20,21,1  csys=20,21,44
  1     yl=-11      zl=-261
  2     yl=-11      zl=-261
 3 nnis=2  g=21,22,1  csys=21,22,45
  1     yl=-11      zl=-261
```

```
    2      yl=-11       zl=-261
  4 nnis=2  g=22,23,1  csys=22,23,46
    1      yl=-11       zl=-261
    2      yl=-11       zl=-261
  5 nnis=2  g=23,24,1  csys=23,24,47
    1      yl=-11       zl=-261
    2      yl=-11       zl=-261
21  nspn=5  mstl=2  mprp=1  area=1.84
  1 nnis=2  g=19,20,1  csys=19,20,43
    1      yl=-6        zl=0
    2      yl=-6        zl=0
  2 nnis=2  g=20,21,1  csys=20,21,44
    1      yl=-6        zl=0
    2      yl=-6        zl=0
  3 nnis=2  g=21,22,1  csys=21,22,45
    1      yl=-6        zl=0
    2      yl=-6        zl=0
  4 nnis=2  g=22,23,1  csys=22,23,46
    1      yl=-6        zl=0
    2      yl=-6        zl=0
  5 nnis=2  g=23,24,1  csys=23,24,47
    1      yl=-6        zl=0
    2      yl=-6        zl=0
22  nspn=5  mstl=2  mprp=1  area=1.84
  1 nnis=2  g=19,20,1  csys=19,20,43
    1      yl=-11       zl=261
    2      yl=-11       zl=261
  2 nnis=2  g=20,21,1  csys=20,21,44
    1      yl=-11       zl=261
    2      yl=-11       zl=261
  3 nnis=2  g=21,22,1  csys=21,22,45
    1      yl=-11       zl=261
    2      yl=-11       zl=261
  4 nnis=2  g=22,23,1  csys=22,23,46
    1      yl=-11       zl=261
    2      yl=-11       zl=261
  5 nnis=2  g=23,24,1  csys=23,24,47
    1      yl=-11       zl=261
    2      yl=-11       zl=261
23  nspn=5  mstl=2  mprp=1  area=1.84
  1 nnis=2  g=19,20,1  csys=19,20,43
    1      yl=-95       zl=-147
    2      yl=-95       zl=-147
  2 nnis=2  g=20,21,1  csys=20,21,44
    1      yl=-95       zl=-147
    2      yl=-95       zl=-147
  3 nnis=2  g=21,22,1  csys=21,22,45
    1      yl=-95       zl=-147
    2      yl=-95       zl=-147
  4 nnis=2  g=22,23,1  csys=22,23,46
    1      yl=-95       zl=-147
    2      yl=-95       zl=-147
  5 nnis=2  g=23,24,1  csys=23,24,47
    1      yl=-95       zl=-147
    2      yl=-95       zl=-147
24  nspn=5  mstl=2  mprp=1  area=1.84
  1 nnis=2  g=19,20,1  csys=19,20,43
    1      yl=-95       zl=147
    2      yl=-95       zl=147
  2 nnis=2  g=20,21,1  csys=20,21,44
    1      yl=-95       zl=147
    2      yl=-95       zl=147
  3 nnis=2  g=21,22,1  csys=21,22,45
    1      yl=-95       zl=147
    2      yl=-95       zl=147
  4 nnis=2  g=22,23,1  csys=22,23,46
    1      yl=-95       zl=147
    2      yl=-95       zl=147
  5 nnis=2  g=23,24,1  csys=23,24,47
    1      yl=-95       zl=147
    2      yl=-95       zl=147
25  nspn=4  mstl=2  mprp=1  area=1.84
```

```
  1 nnis=2  g=20,21,1  csys=20,21,44
    1     yl=-11      zl=-261
    2     yl=-11      zl=-261
  2 nnis=2  g=21,22,1  csys=21,22,45
    1     yl=-11      zl=-261
    2     yl=-11      zl=-261
  3 nnis=2  g=22,23,1  csys=22,23,46
    1     yl=-11      zl=-261
    2     yl=-11      zl=-261
  4 nnis=2  g=23,24,1  csys=23,24,47
    1     yl=-11      zl=-261
    2     yl=-11      zl=-261
26 nspn=4  mstl=2  mprp=1  area=1.84
  1 nnis=2  g=20,21,1  csys=20,21,44
    1     yl=-6       zl=0
    2     yl=-6       zl=0
  2 nnis=2  g=21,22,1  csys=21,22,45
    1     yl=-6       zl=0
    2     yl=-6       zl=0
  3 nnis=2  g=22,23,1  csys=22,23,46
    1     yl=-6       zl=0
    2     yl=-6       zl=0
  4 nnis=2  g=23,24,1  csys=23,24,47
    1     yl=-6       zl=0
    2     yl=-6       zl=0
27 nspn=4  mstl=2  mprp=1  area=1.84
  1 nnis=2  g=20,21,1  csys=20,21,44
    1     yl=-11      zl=261
    2     yl=-11      zl=261
  2 nnis=2  g=21,22,1  csys=21,22,45
    1     yl=-11      zl=261
    2     yl=-11      zl=261
  3 nnis=2  g=22,23,1  csys=22,23,46
    1     yl=-11      zl=261
    2     yl=-11      zl=261
  4 nnis=2  g=23,24,1  csys=23,24,47
    1     yl=-11      zl=261
    2     yl=-11      zl=261
28 nspn=4  mstl=2  mprp=1  area=1.84
  1 nnis=2  g=20,21,1  csys=20,21,44
    1     yl=-95      zl=-147
    2     yl=-95      zl=-147
  2 nnis=2  g=21,22,1  csys=21,22,45
    1     yl=-95      zl=-147
    2     yl=-95      zl=-147
  3 nnis=2  g=22,23,1  csys=22,23,46
    1     yl=-95      zl=-147
    2     yl=-95      zl=-147
  4 nnis=2  g=23,24,1  csys=23,24,47
    1     yl=-95      zl=-147
    2     yl=-95      zl=-147
29 nspn=4  mstl=2  mprp=1  area=1.84
  1 nnis=2  g=20,21,1  csys=20,21,44
    1     yl=-95      zl=147
    2     yl=-95      zl=147
  2 nnis=2  g=21,22,1  csys=21,22,45
    1     yl=-95      zl=147
    2     yl=-95      zl=147
  3 nnis=2  g=22,23,1  csys=22,23,46
    1     yl=-95      zl=147
    2     yl=-95      zl=147
  4 nnis=2  g=23,24,1  csys=23,24,47
    1     yl=-95      zl=147
    2     yl=-95      zl=147
30 nspn=3  mstl=2  mprp=1  area=1.84
  1 nnis=2  g=21,22,1  csys=21,22,45
    1     yl=-11      zl=-261
    2     yl=-11      zl=-261
  2 nnis=2  g=22,23,1  csys=22,23,46
    1     yl=-11      zl=-261
    2     yl=-11      zl=-261
  3 nnis=2  g=23,24,1  csys=23,24,47
```

```
    1      yl=-11       zl=-261
    2      yl=-11       zl=-261
31  nspn=3   mstl=2   mprp=1   area=1.84
   1 nnis=2   g=21,22,1  csys=21,22,45
    1      yl=-6        zl=0
    2      yl=-6        zl=0
   2 nnis=2   g=22,23,1  csys=22,23,46
    1      yl=-6        zl=0
    2      yl=-6        zl=0
   3 nnis=2   g=23,24,1  csys=23,24,47
    1      yl=-6        zl=0
    2      yl=-6        zl=0
32  nspn=3   mstl=2   mprp=1   area=1.84
   1 nnis=2   g=21,22,1  csys=21,22,45
    1      yl=-11       zl=261
    2      yl=-11       zl=261
   2 nnis=2   g=22,23,1  csys=22,23,46
    1      yl=-11       zl=261
    2      yl=-11       zl=261
   3 nnis=2   g=23,24,1  csys=23,24,47
    1      yl=-11       zl=261
    2      yl=-11       zl=261
33  nspn=3   mstl=2   mprp=1   area=1.84
   1 nnis=2   g=21,22,1  csys=21,22,45
    1      yl=-95       zl=-147
    2      yl=-95       zl=-147
   2 nnis=2   g=22,23,1  csys=22,23,46
    1      yl=-95       zl=-147
    2      yl=-95       zl=-147
   3 nnis=2   g=23,24,1  csys=23,24,47
    1      yl=-95       zl=-147
    2      yl=-95       zl=-147
34  nspn=3   mstl=2   mprp=1   area=1.84
   1 nnis=2   g=21,22,1  csys=21,22,45
    1      yl=-95       zl=147
    2      yl=-95       zl=147
   2 nnis=2   g=22,23,1  csys=22,23,46
    1      yl=-95       zl=147
    2      yl=-95       zl=147
   3 nnis=2   g=23,24,1  csys=23,24,47
    1      yl=-95       zl=147
    2      yl=-95       zl=147

END_GEOMETRY
:
ENVIRONMENT
nonlmat=1        pathdep=0        nonlgmt=1        kgeomet=1
pcode_m=2        pcode_s=0        pcode_f=0
tolr_fi=10       tolr_fl=10       tolr_fk=10
tolr_mi=100      tolr_ml=100      tolr_mk=100
sec_eqm=0        numit_s=10       nstep_s=100
tolr_st=10.      inttype=1
:


SET_TIME tcur=7
:-------------------------------------------------------------------
: stress segment 1, 2. Cast segment 3                    day 7
:-------------------------------------------------------------------
CONFIGURATION
add_frame F=1   tcast=0
add_frame F=2   tcast=0
add_tendon p=1  sa=0     sb=164E+3  da=.0   db=.25
add_tendon p=2  sa=0     sb=164E+3  da=.0   db=.25

restraints
1          r=1,1,1,1,1,1

END_CONFIGURATION
:
LOAD
 2  f=0,-530E+3
```

```
 3   f=0,-480E+3/2

:
SOLVE
TIME_CONTROL
tend=7.       numstep=1      numit_i=50     numit_l=50
END_SOLVE


:-------------------------------------------------------------------
: stress segment 3. Cast segment 4                          day 14
:-------------------------------------------------------------------
SOLVE
TIME_CONTROL
tend=14.      numstep=1      numit_i=50     numit_l=50
END_SOLVE

CONFIGURATION
add_frame F=3    tcast=7
add_tendon p=3   sa=0     sb=164E+3  da=.0   db=.25
add_tendon p=4   sa=0     sb=164E+3  da=.0   db=.25
add_tendon p=5   sa=0     sb=164E+3  da=.0   db=.25

END_CONFIGURATION
:
LOAD
 3   f=0,-480E+3/2
 4   f=0,-490E+3/2

:
SOLVE
TIME_CONTROL
tend=14.      numstep=1      numit_i=50     numit_l=50
END_SOLVE

:-------------------------------------------------------------------
```

```
: stress segment 4. Cast segment 5                          day 21
:-------------------------------------------------------------------
SOLVE
TIME_CONTROL
tend=21.      numstep=1      numit_i=50     numit_l=50
END_SOLVE

CONFIGURATION
restraints
48            r=1,1,1,1,1,1
88            r=1,1,1,1,1,1

add_frame F=4    tcast=15
add_tendon p=6   sa=0     sb=164E+3     da=.0   db=.25
add_tendon p=7   sa=0     sb=164E+3     da=.0   db=.25
add_tendon p=8   sa=0     sb=164E+3     da=.0   db=.25
add_cable c=1    tension=643100
add_cable c=2    tension=788900


END_CONFIGURATION
:
LOAD
 4   f=0,-490E+3/2
 5   f=0,-490E+3/2

:
SOLVE
TIME_CONTROL
tend=21.      numstep=1      numit_i=50     numit_l=50
END_SOLVE
:-------------------------------------------------------------------
: stress segment 5. Cast segment 6                          day 28
:-------------------------------------------------------------------
SOLVE
TIME_CONTROL
```

```
tend=28.      numstep=1     numit_i=50    numit_l=50
END_SOLVE

CONFIGURATION
restraints
49          r=1,1,1,1,1,1
89          r=1,1,1,1,1,1
128         r=1,1,1,1,1,1

add_frame F=5   tcast=21
add_tendon p=9  sa=0   sb=164E+3    da=.0  db=.25
add_tendon p=10 sa=0   sb=164E+3    da=.0  db=.25
add_tendon p=11 sa=0   sb=164E+3    da=.0  db=.25
add_cable c=3   tension=646000
add_cable c=4   tension=780000
add_cable c=41  tension=10930


END_CONFIGURATION
:
LOAD
 5  f=0,-490E+3/2
 6  f=0,-490E+3/2

:
SOLVE
TIME_CONTROL
tend=28.      numstep=1     numit_i=50    numit_l=50
END_SOLVE
:-------------------------------------------------------------
: stress segment 6. Cast segment 7                  day 35
:-------------------------------------------------------------
SOLVE
TIME_CONTROL
tend=35.      numstep=1     numit_i=50    numit_l=50
END_SOLVE
```

```
CONFIGURATION
restraints
50          r=1,1,1,1,1,1
90          r=1,1,1,1,1,1

add_frame F=6   tcast=28
add_tendon p=12 sa=0   sb=164E+3    da=.0  db=.25
add_tendon p=13 sa=0   sb=164E+3    da=.0  db=.25
add_tendon p=14 sa=0   sb=164E+3    da=.0  db=.25
add_cable c=5   tension=646E+3
add_cable c=6   tension=765E+3

END_CONFIGURATION
:
LOAD
 6  f=0,-490E+3/2
 7  f=0,-430E+3/2

:
SOLVE
TIME_CONTROL
tend=35.      numstep=1     numit_i=50    numit_l=50
END_SOLVE

:-------------------------------------------------------------
: stress segment 7. Cast segment 8                  day 42
:-------------------------------------------------------------
SOLVE
TIME_CONTROL
tend=42.      numstep=1     numit_i=50    numit_l=50
END_SOLVE

CONFIGURATION
restraints
51          r=1,1,1,1,1,1
```

```
91          r=1,1,1,1,1,1

add_frame F=7    tcast=35
add_cable c=7   tension=568E+3
add_cable c=8   tension=667E+3

END_CONFIGURATION
:
LOAD
 7  f=0,-430E+3/2
 8  f=0,-360E+3/2

:
SOLVE
TIME_CONTROL
tend=42.       numstep=1      numit_i=50     numit_l=50
END_SOLVE

:-------------------------------------------------------------------
: stress segment 8. Cast segment 9                          day 49
:-------------------------------------------------------------------
SOLVE
TIME_CONTROL
tend=49.       numstep=1      numit_i=50     numit_l=50
END_SOLVE

CONFIGURATION
restraints
52          r=1,1,1,1,1,1
92          r=1,1,1,1,1,1
129         r=1,1,1,1,1,1

add_frame F=8    tcast=42
add_cable c=9   tension=478E+3
add_cable c=10  tension=552E+3
add_cable c=42  tension=15300

END_CONFIGURATION
:
LOAD
 8  f=0,-360E+3/2
 9  f=0,-360E+3/2

:
SOLVE
TIME_CONTROL
tend=49.       numstep=1      numit_i=50     numit_l=50
END_SOLVE

:-------------------------------------------------------------------
: stress segment 9. Cast segment 10                         day 56
:-------------------------------------------------------------------
SOLVE
TIME_CONTROL
tend=56.       numstep=1      numit_i=50     numit_l=50
END_SOLVE

CONFIGURATION
restraints
53          r=1,1,1,1,1,1
93          r=1,1,1,1,1,1

add_frame F=9    tcast=49
add_cable c=11  tension=487E+3
add_cable c=12  tension=536E+3

END_CONFIGURATION
:
LOAD
 9  f=0,-360E+3/2
 10  f=0,-360E+3/2
```

```
:
SOLVE
TIME_CONTROL
tend=56.      numstep=1     numit_i=50    numit_l=50
END_SOLVE
:-------------------------------------------------------------------
: stress segment 10. Cast segment 11                    day 63
:-------------------------------------------------------------------
SOLVE
TIME_CONTROL
tend=63.      numstep=1     numit_i=50    numit_l=50
END_SOLVE

CONFIGURATION
restraints
54          r=1,1,1,1,1,1
94          r=1,1,1,1,1,1

add_frame F=10   tcast=56
add_cable c=13  tension=517E+3
add_cable c=14  tension=547E+3

END_CONFIGURATION
:
LOAD
10   f=0,-360E+3/2
11   f=0,-340E+3/2

:
SOLVE
TIME_CONTROL
tend=63.      numstep=1     numit_i=50    numit_l=50
END_SOLVE

:-------------------------------------------------------------------
: stress segment 11. Cast segment 12                    day 70
:-------------------------------------------------------------------
SOLVE
TIME_CONTROL
tend=70.      numstep=1     numit_i=50    numit_l=50
END_SOLVE

CONFIGURATION
restraints
55          r=1,1,1,1,1,1
95          r=1,1,1,1,1,1
130         r=1,1,1,1,1,1

add_frame F=11   tcast=63
add_cable c=15  tension=447E+3
add_cable c=16  tension=460E+3
add_cable c=43  tension=26580

END_CONFIGURATION
:
LOAD
11   f=0,-340E+3/2
12   f=0,-330E+3/2

:
SOLVE
TIME_CONTROL
tend=70.      numstep=1     numit_i=50    numit_l=50
END_SOLVE

:-------------------------------------------------------------------
: stress segment 12. Cast segment 13                    day 77
:-------------------------------------------------------------------
SOLVE
TIME_CONTROL
tend=77.      numstep=1     numit_i=50    numit_l=50
END_SOLVE
```

```
CONFIGURATION
restraints
56          r=1,1,1,1,1,1
96          r=1,1,1,1,1,1

add_frame F=12   tcast=70
add_cable c=17  tension=457E+3
add_cable c=18  tension=462E+3

END_CONFIGURATION
:
LOAD
12   f=0,-330E+3/2
13   f=0,-330E+3/2

:
SOLVE
TIME_CONTROL
tend=77.       numstep=1      numit_i=50     numit_l=50
END_SOLVE
:-------------------------------------------------------------------
: stress segment 13. Cast segment 14                    day 84
:-------------------------------------------------------------------
SOLVE
TIME_CONTROL
tend=84.       numstep=1      numit_i=50     numit_l=50
END_SOLVE

CONFIGURATION
restraints
57          r=1,1,1,1,1,1
97          r=1,1,1,1,1,1

add_frame F=13   tcast=77
add_cable c=19  tension=511E+3
add_cable c=20  tension=510E+3

END_CONFIGURATION
:
LOAD
13   f=0,-330E+3/2
14   f=0,-330E+3/2

:
SOLVE
TIME_CONTROL
tend=84.       numstep=1      numit_i=50     numit_l=50
END_SOLVE

:-------------------------------------------------------------------
: stress segment 14. Cast segment 15                    day 91
:-------------------------------------------------------------------
SOLVE
TIME_CONTROL
tend=91.       numstep=1      numit_i=50     numit_l=50
END_SOLVE

CONFIGURATION
restraints
58          r=1,1,1,1,1,1
98          r=1,1,1,1,1,1

add_frame F=14   tcast=84
add_cable c=21  tension=519E+3
add_cable c=22  tension=511E+3

END_CONFIGURATION
:
LOAD
14   f=0,-330E+3/2
15   f=0,-330E+3/2
```

```
:
SOLVE
TIME_CONTROL
tend=91.      numstep=1     numit_i=50    numit_l=50
END_SOLVE

:-------------------------------------------------------------------
: stress segment 15. Cast segment 16                    day 98
:-------------------------------------------------------------------
SOLVE
TIME_CONTROL
tend=98.      numstep=1     numit_i=50    numit_l=50
END_SOLVE

CONFIGURATION
restraints
59          r=1,1,1,1,1,1
99          r=1,1,1,1,1,1

add_frame F=15   tcast=91
add_cable c=23  tension=526E+3
add_cable c=24  tension=513E+3

END_CONFIGURATION
:
LOAD
15  f=0,-330E+3/2
16  f=0,-330E+3/2

:
SOLVE
TIME_CONTROL
tend=98.      numstep=1     numit_i=50    numit_l=50
END_SOLVE
```

```
:-------------------------------------------------------------------
: stress segment 16. Cast segment 17                    day 105
:-------------------------------------------------------------------
SOLVE
TIME_CONTROL
tend=105      numstep=1     numit_i=50    numit_l=50
END_SOLVE

CONFIGURATION
restraints
60          r=1,1,1,1,1,1
100          r=1,1,1,1,1,1

add_frame F=16   tcast=98
add_cable c=25  tension=536E+3
add_cable c=26  tension=518E+3

END_CONFIGURATION
:
LOAD
16  f=0,-330E+3/2
17  f=0,-330E+3/2

:
SOLVE
TIME_CONTROL
tend=105      numstep=1     numit_i=50    numit_l=50
END_SOLVE

:-------------------------------------------------------------------
: stress segment 17. Cast segment 18                    day 112
:-------------------------------------------------------------------
SOLVE
TIME_CONTROL
tend=112      numstep=1     numit_i=50    numit_l=50
END_SOLVE
```

```
CONFIGURATION
restraints
61          r=1,1,1,1,1,1
101         r=1,1,1,1,1,1

add_frame F=17   tcast=105
add_cable c=27  tension=544E+3
add_cable c=28  tension=524E+3

END_CONFIGURATION
:
LOAD
17  f=0,-330E+3/2
18  f=0,-330E+3/2

:
SOLVE
TIME_CONTROL
tend=112      numstep=1     numit_i=50    numit_l=50
END_SOLVE

:-------------------------------------------------------------------
: stress segment 18. Cast segment 19                    day 119
:-------------------------------------------------------------------
SOLVE
TIME_CONTROL
tend=119      numstep=1     numit_i=50    numit_l=50
END_SOLVE

CONFIGURATION
restraints
62          r=1,1,1,1,1,1
102         r=1,1,1,1,1,1

add_frame F=18   tcast=112
add_cable c=29  tension=552E+3
add_cable c=30  tension=533E+3

END_CONFIGURATION
:
LOAD
18  f=0,-330E+3/2
19  f=0,-330E+3/2

:
SOLVE
TIME_CONTROL
tend=119      numstep=1     numit_i=50    numit_l=50
END_SOLVE

:-------------------------------------------------------------------
: stress segment 19. Cast segment 20                    day 126
:-------------------------------------------------------------------
SOLVE
TIME_CONTROL
tend=126      numstep=1     numit_i=50    numit_l=50
END_SOLVE

CONFIGURATION
restraints
63          r=1,1,1,1,1,1
103         r=1,1,1,1,1,1

add_frame F=19   tcast=119
add_cable c=31  tension=566E+3
add_cable c=32  tension=551E+3

END_CONFIGURATION
:
LOAD
19  f=0,-330E+3/2
```

```
20   f=0,-340E+3/2

:
SOLVE
TIME_CONTROL
tend=126        numstep=1       numit_i=50     numit_l=50
END_SOLVE

:-------------------------------------------------------------------
: stress segment 20. Cast segment 21                    day 133
:-------------------------------------------------------------------
SOLVE
TIME_CONTROL
tend=133        numstep=1       numit_i=50     numit_l=50
END_SOLVE

CONFIGURATION
restraints
64              r=1,1,1,1,1,1
104             r=1,1,1,1,1,1

add_frame F=20   tcast=126
add_cable c=33  tension=583E+3
add_cable c=34  tension=574E+3

END_CONFIGURATION
:
LOAD
20   f=0,-340E+3/2
21   f=0,-340E+3/2

:
SOLVE
TIME_CONTROL
tend=133        numstep=1       numit_i=50     numit_l=50
END_SOLVE
```

```
:-------------------------------------------------------------------
: stress segment 21. Cast segment 22                    day 140
:-------------------------------------------------------------------
SOLVE
TIME_CONTROL
tend=140        numstep=1       numit_i=50     numit_l=50
END_SOLVE

CONFIGURATION
restraints
65              r=1,1,1,1,1,1
105             r=1,1,1,1,1,1

add_frame F=21   tcast=133
add_cable c=35  tension=586E+3
add_cable c=36  tension=586E+3

END_CONFIGURATION
:
LOAD
21   f=0,-340E+3/2
22   f=0,-340E+3/2

:
SOLVE
TIME_CONTROL
tend=140        numstep=1       numit_i=50     numit_l=50
END_SOLVE

:-------------------------------------------------------------------
: stress segment 22. Cast segment 23                    day 147
:-------------------------------------------------------------------
SOLVE
TIME_CONTROL
tend=147        numstep=1       numit_i=50     numit_l=50
```

```
END_SOLVE

CONFIGURATION
restraints
66          r=1,1,1,1,1,1
106         r=1,1,1,1,1,1

add_frame F=22   tcast=140
add_cable c=37  tension=585E+3
add_cable c=38  tension=597E+3

END_CONFIGURATION
:
LOAD
22   f=0,-340E+3/2
23   f=0,-340E+3/2

:
SOLVE
TIME_CONTROL
tend=147       numstep=1      numit_i=50     numit_l=50
END_SOLVE

:-------------------------------------------------------------------
: stress segment 23.                                    day 154
:-------------------------------------------------------------------
SOLVE
TIME_CONTROL
tend=154       numstep=1      numit_i=50     numit_l=50
END_SOLVE

CONFIGURATION
restraints
67          r=1,1,1,1,1,1
107         r=1,1,1,1,1,1

add_frame F=23   tcast=147
add_cable c=39  tension=594E+3
add_cable c=40  tension=607E+3


END_CONFIGURATION
:
LOAD
23   f=0,-340E+3/2
24   f=0,-150E+3

:
SOLVE
TIME_CONTROL
tend=154       numstep=1      numit_i=50     numit_l=50
END_SOLVE

:-------------------------------------------------------------------
: close link                                            day 154
:-------------------------------------------------------------------
:START R=1

CONFIGURATION
restraints
24          r=0,0,1,1,1,0

END_CONFIGURATION
:
LOAD
24   f=0

:
SOLVE
TIME_CONTROL
tend=154       numstep=1      numit_i=50     numit_l=50
END_SOLVE
```

```
:-------------------------------------------------------------------
: add continuity tendons                                  day 154
:-------------------------------------------------------------------
CONFIGURATION
add_tendon p=15  sa=164E+3  sb=0      da=.25  db=.0   g=19,1

END_CONFIGURATION
:
LOAD
24   f=0

:
SOLVE
TIME_CONTROL
tend=154       numstep=1      numit_i=50     numit_l=50
END_SOLVE

:-------------------------------------------------------------------
: remove aux stays                                        day 154
:-------------------------------------------------------------------
CONFIGURATION
del_cable  c=41
del_cable  c=42
del_cable  c=43

END_CONFIGURATION
:
LOAD
24   f=0

:
SOLVE
TIME_CONTROL
tend=154       numstep=1      numit_i=50     numit_l=50
END_SOLVE

END
```